

Volume II

Technical  
Studies and Results

Final  
Report

September 1974

**A Feasibility Study of  
Unmanned Rendezvous  
and Docking in  
Mars Orbit**



**MARTIN MARIETTA**

MCR 74-244

Contract JPL 953746

A FEASIBILITY STUDY  
OF  
UNMANNED RENDEZVOUS AND DOCKING  
IN MARS ORBIT

Final Report

Volume II

TECHNICAL STUDIES AND RESULTS

July 1974

Approved

  
\_\_\_\_\_  
J. R. Mellin  
Technical Director

  
\_\_\_\_\_  
W. T. Scofield  
Program Manager



This report was performed for the Jet Propulsion Laboratory,  
California Institute of Technology, sponsored by the National  
Aeronautics and Space Administration under Contract NAS7-100.

MARTIN MARIETTA CORPORATION  
DENVER DIVISION  
Denver, Colorado 80201

## FOREWORD

This is Volume II of the Final Report on a Feasibility Study of Unmanned Rendezvous and Docking in Mars Orbit, conducted by the Martin Marietta Corporation, Denver Division.

This study was performed for the Jet Propulsion Laboratory, California Institute of Technology, under contract 953746, and was conducted during the period November 1973 through June 1974. Mr. J. W. Moore of JPL was the Technical Manager of the study which was sponsored by the National Aeronautics and Space Administration.

This Final Report consists of two volumes as follows:

Volume I - Summary

Volume II - Technical Studies and Results

### ACKNOWLEDGEMENT

Martin Marietta wishes to recognize the contributions of the following individuals to this study:

Jesse W. Moore of the Jet Propulsion Laboratory, Technical Representative of the Contracting Officer, for management and direction.

Donald Udlock of the Jet Propulsion Laboratory for supplying data on JPL studies concerning solid rocket motor sterilization.

Daniel H. Herman, Director Advanced Planetary Programs, NASA Headquarters, for general guidance and support.

## ABSTRACT

The technical feasibility of achieving automatic rendezvous and docking in Mars orbit as a part of a surface sample return mission was investigated based on using as much existing Viking '75 Orbiter and Lander hardware as possible. Both 1981 and 1983/84 mission opportunities were considered. The principal result of the study was the definition of a three stage 290 kg Mars Ascent Vehicle (MAV) capable of accepting a 1 kg sample, injecting itself into a 2200 km circular orbit, and rendezvousing with an orbiting spacecraft carrying an Earth Return Vehicle.

The modifications necessary to convert a Viking '75 Orbiter to the sample return mission orbiter are defined. These consist primarily of propulsion system changes and the addition of a rendezvous radar sensor. Required modifications to the Viking Lander are also described; the major ones being the addition of a MAV erector/launcher mechanism and thermal control canopy on the existing equipment platform and converting the terminal descent propulsion to a pressure regulated system.

Digital computer simulations of dispersed MAV ascent and orbit injection and circularization were performed to establish the conditions at start of terminal rendezvous. Flight control laws were then established which would be preprogrammed into the orbiter's computer to effect final closing and docking of the two vehicles in the presence of dispersed as well as nominal conditions at start of rendezvous.

Conclusions are that with state of the art systems plus limited application of new developments in areas where feasibility has already been demonstrated, e.g., solid rocket motor sterilization, it is possible to land a small ascent vehicle capable of automatically ascending and rendezvousing with a modified Viking '75 orbiter spacecraft. The mission can be flown in 1981 or 1983/84, but a dual launch or a larger launch vehicle than the Viking Titan III Centaur, or the use of space storable propellants for Mars orbit injection, would be required in the 1983/84 opportunity.

TABLE OF CONTENTS

	<u>Page</u>
Foreword	ii
Acknowledgement	iii
Abstract	iv
Table of Contents	v thru ix
List of Figures	x thru xiii
List of Tables	xiv thru xvi
Glossary	xvii thru xviii
List of Symbols	xix thru xxi
I OBJECTIVES, GUIDELINES AND STUDY RESULTS . . . . .	I-1
A. Objectives . . . . .	I-2 thru I-3
B. Guidelines . . . . .	I-4 thru I-5
C. Study Results . . . . .	I-6 thru I-13
II MISSION ANALYSIS . . . . .	II-1
A. Launch Energy Requirements . . . . .	II-1 thru II-4
B. Direct Entry Mission Description . . . . .	II-5 thru II-12
C. Tradeoffs in Mission Baseline Definition . . . . .	II-13 thru II-26
D. Mission Analysis Summary . . . . .	II-27 thru II-29
References . . . . .	II-30

	<u>Page</u>
III NAVIGATION ASPECTS OF ASCENT, RENDEZVOUS AND DOCKING . . .	III-1
A. Navigation Results for Mission Phases . . . . .	III-3 thru III-22
B. Navigation Sensitivity Studies . . . . .	III-23 thru III-39
C. Assessment of Navigation Feasibility . . . . .	III-40
References . . . . .	III-41
IV GUIDANCE AND CONTROL ASPECTS OF ASCENT, RENDEZVOUS AND DOCKING . . . . .	IV-1
A. Requirements . . . . .	IV-2 thru IV-3
B. MAV Launch, Ascent and Orbiter Operations . . . . .	IV-4 thru IV-12
C. Terminal Rendezvous . . . . .	IV-13 thru IV-27
D. Docking Phase . . . . .	IV-28 thru IV-30
E. G&C Hardware Implementation . . . . .	IV-31 thru IV-37
F. Spin Stabilized vs Three-Axis Stabilized MAV . . . . .	IV-38 thru IV-40
G. Technology Assessment . . . . .	IV-41
References . . . . .	IV-42
V RADAR SENSOR DESIGN FOR RENDEZVOUS AND DOCKING . . . . .	V-1
A. Requirements . . . . .	V-1 thru V-2
B. Selected Sensor Characteristics . . . . .	V-3 thru V-19
C. Sensor System Calculations . . . . .	V-20 thru V-30
D. Sensor System Comparisons and Cost Considerations . . . . .	V-31 thru V-34

	<u>Page</u>
E. Rendezvous Sensor Reliability and Failure Mode Operation . . . . .	V-35 thru V-41
F. New Technology Development Requirements . . . . .	V-42 thru V-44
VI SPACECRAFT SYSTEM DESIGN . . . . .	VI-1
A. Mars Ascent Vehicle Tradeoff and System Design Summary . . . . .	VI-1 thru VI-15
B. Lander System Design . . . . .	VI-16 thru VI-29
C. Orbiter System Design . . . . .	VI-30 thru VI-39
D. Earth Return Vehicle Candidates . . . . .	VI-40 thru VI-42
E. Total Spacecraft Mass Distribution and Margin Considerations . . . . .	VI-43 thru VI-46
F. Failure Modes and Backup Provisions . . . . .	VI-47
G. Tradeoff Considerations Relative to Keeping the Orbiter and ERV Mated During the 400-Day Parking Orbit at Mars . . . . .	VI-47 thru VI-48
H. Feasibility of Providing for Lander Survival After MAV Launch . . . . .	VI-49
I. Impact of the 1983/84 Mission Opportunity . . . . .	VI-49 thru VI-51
VII SUBSYSTEM DEFINITION FOR ALL MISSION PHASES . . . . .	VII-1
A. Communications . . . . .	VII-1 thru VII-30
B. Power . . . . .	VII-31 thru VII-42
C. Propulsion . . . . .	VII-43 thru VII-69

	<u>Page</u>
D. Thermal Control . . . . .	VII-70 thru VII-77
E. Aerodynamics . . . . .	VII-78 thru VII-87
F. Structure . . . . .	VII-88 thru VII-91
VIII <b>M</b> ISSION PROFILE/OPERATIONS . . . . .	VIII-1
A. 1981 Detailed Mission Timeline . . . . .	VIII-1 thru VIII-13
B. Mission Opportunity Dependent Quantities . . . . .	VIII-14
IX <b>E</b> ARTH ENTRY CAPSULE STUDY . . . . .	IX-1
A. Task Description . . . . .	IX-1
B. Guidelines . . . . .	IX-2
C. Configuration Tradeoffs . . . . .	IX-3 thru IX-5
D. Sequence of Events . . . . .	IX-6 thru IX-8
E. Description of Baseline Capsule . . . . .	IX-9 thru IX-28
F. Sample-Protection-Only Capsule Design . . . . .	IX-29 thru IX-30
G. 5-kg Sample Capsule Design . . . . .	IX-31 thru IX-32
H. Enhanced Probability of Success Capsule Design . . . . .	IX-33 thru IX-36
References . . . . .	IX-37
X <b>T</b> ECHNOLOGY AND PROGRAMMATIC ASSESSMENT	X-1
A. Technology Development Required . . . . .	X-1 thru X-6
B. Concerns Requiring Further Study . . . . .	X-6

APPENDIX A	SCIENCE CONSULTANTS' RECOMMENDATIONS - MSSR SEMINAR (Denver, Colorado; May 9, 1974) . . . . .	A-1 thru A-3
APPENDIX B	DESCRIPTION OF ASCENT TO RENDEZVOUS SIMULATION . . .	B-1 thru B-13
APPENDIX C	RENDEZVOUS DIGITAL COMPUTER PROGRAM . . . . .	C-1 thru C-5
APPENDIX D	ADDITIONAL RENDEZVOUS STUDY RESULTS . . . . .	D-1 thru D-11
APPENDIX E	RENDEZVOUS SENSOR ERROR CALCULATIONS . . . . .	E-1 thru E-10
APPENDIX F	1 kg SAMPLE MAV DETAIL MASS DERIVATION . . . . .	F-1 thru F-4
APPENDIX G	BIOTA TRANSFER . . . . .	G-1 thru G-6
APPENDIX H	ALTERNATIVE MAV BIOPROPELLANT STAGE . . . . .	H-1 thru H-6
APPENDIX I	STERILIZABLE SOLID PROPELLANTS FOR MAV . . . . .	I-1 thru I-10
APPENDIX J	THRUSTER SIZING AND PROPELLANT CONSUMPTION . . . . .	J-1 thru J-4

LIST OF FIGURES

<u>Figure</u>		<u>Page</u>
I-1	MSSR Mission Sequence - Mars Rendezvous Mode . . . . .	I-1
I-2	MSSR Mission Sequence - Mars Rendezvous Mode-- Dual Launch--Direct Entry . . . . .	I-8
I-3	MSSR Mission Sequence - Mars Rendezvous Mode-- Dual Launch--Out of Orbit Entry . . . . .	I-9
I-4	Earth Entry Capsule Recovery Sequence . . . . .	I-12
II-1	Mars Approach and Lander Trajectory - Direct Entry .	II-6
II-2	MOI Profile . . . . .	II-7
II-3	Mars Ascent Vehicle Trajectory . . . . .	II-9
II-4	TEI (Earth Return) Profile for 1981 MSSR . . . . .	II-10
II-5	Earth Return Landing Accessibility . . . . .	II-12
II-6	Capture Orbit Stability . . . . .	II-15
II-7	Landed weight Capability . . . . .	II-17
II-8	Landing Site Accessibility . . . . .	II-18
II-9	Mars Ascent Vehicle - Staging Considerations . . . . .	II-20
II-10	Landed Weight vs Rendezvous Orbit Altitude for 1981.	II-23
II-11	MAV Performance Design Trade for 1981 . . . . .	II-25
II-12	Alternative Mission Concepts and Design Impact (1981)	II-29
III-1	Mission Phase #1 - Orbiter Capture to MAV Ascent . .	III-4
III-2	Approach Geometry . . . . .	III-5
III-3	Mission Phase #2 - MAV Ascent to Circularization Trim . . . . .	III-9
III-4	Mission Phase #3 - Orbiter Periapsis Change to Orbiter Circularization to First Occultation Exit . . . . .	III-13
III-5	Mission Phase #4 - First Occultation Exit to Start of Circular Trim . . . . .	III-17
III-6	Multi-vehicle $\Delta$ VLB1 . . . . .	III-18
III-7	Mission Phase #5 - Circular Trim Sequence Through 10th Occultation Exit . . . . .	III-20
III-8	"Knowledge" Data Type Deimos/Stars - Single Camera .	III-24
III-9	Approach O.D.: DSN vs DSN + Optional . . . . .	III-25
III-10	Comparison of Orbiter Maneuvers . . . . .	III-37

<u>Figure</u>	<u>Page</u>
IV-1 MAV Pitch Angle and Dynamic Pressure vs Time of Flight	IV-5
IV-2 MAV Launch, Ascent, and Earth Acquisition . . . . .	IV-6
IV-3 MAV Orbital Maneuvers . . . . .	IV-10
IV-4 Terminal Rendezvous and Docking Phases . . . . .	IV-12
IV-5 Proportional Navigation . . . . .	IV-16
IV-6 Rendezvous Propellant Efficiency . . . . .	IV-17
IV-7 Axial Thrust Control Curves - Nominal Case . . . . .	IV-19
IV-8 Rendezvous Trajectory (Rotating Coordinates) - Nominal Case . . . . .	IV-20
IV-9 Range, Range Rate and LOS Rate vs Rendezvous Time - Nominal Case . . . . .	IV-21
IV-10 Axial Thrust Control Curves - 3-Sigma Dispersed Case	IV-22
IV-11 Rendezvous Trajectory (Rotating Coordinates) - 3-Sigma Dispersed Case . . . . .	IV-23
IV-12 Rendezvous Trajectory (Out-of-Plane) - 3-Sigma Dispersed Case . . . . .	IV-24
IV-13 Range, Range Rate, LOS Rate vs Rendezvous Time - 3-Sigma Dispersed Case . . . . .	IV-25
IV-14 Docking Phase . . . . .	IV-29
IV-15 Orbiter G&C System Mechanization . . . . .	IV-34
IV-16 MAV G&C System Mechanization . . . . .	IV-35
V-1 Orbiter Rendezvous and Command System--Simplified Block Diagram . . . . .	V-4
V-2 Orbiter Rendezvous and Command System--System Antenna	V-5
V-3 Antenna Near-Field Amplitude and Phase Distributions	V-6
V-4 Composite Signal Spectrum . . . . .	V-10
V-5 Orbiter Rendezvous and Command System--System Block Diagram . . . . .	V-11
V-6 Multi-mode Spiral Feed . . . . .	V-12
V-7 MAV Angle Tracking Dual-Ratio Transponder--System Antenna . . . . .	V-14
V-8 MAV Antenna Gain Reduction and Sidelobe Level vs Blockage Ratio . . . . .	V-16
V-9 MAV Dual-Ratio Transponder Block Diagram . . . . .	V-17
V-10 Input Signal Levels vs Range . . . . .	V-22
V-11 S/N Ratio vs Range . . . . .	V-25
V-12 Range Error vs Range . . . . .	V-27
V-13 Radar Detection Probability Curves . . . . .	V-40
VI-1 Mars Ascent Vehicle . . . . .	VI-5
VI-2 MAV Stage III Equipment Accommodations . . . . .	VI-8

<u>Figure</u>		<u>Page</u>
VI-3	Sample Canister Concept . . . . .	VI-10
VI-4	Impact of Increasing Sample Size from 1.0 kg to 5.0 kg . . . . .	VI-12
VI-5	MAV Impact on Viking Lander Capsule . . . . .	VI-17
VI-6	Lander Modifications . . . . .	VI-19
VI-7	URDMO/Viking Landed Weight Relations . . . . .	VI-23
VI-8	Sample Acquisition Operation . . . . .	VI-29
VI-9	MSSR Elements in Earth Launch Arrangement . . . . .	VI-31
VI-10	Sample Transfer and Contamination Control . . . . .	VI-35
VI-11	Sample Canister Sealing Concept . . . . .	VI-36
VI-12	Earth Return Vehicle (ERV) Contamination Considerations . . . . .	VI-37
VI-13	Alternative Sample Transfer Concept . . . . .	VI-39
VI-14	Alternative Margin Allocations . . . . .	VI-46
VII-1	Geometries for Orbiter Phase of a 1981 URDMO Mission . . . . .	VII-4
VII-2	Proposed MAV Telecommunications Block Diagram . . . . .	VII-5
VII-3	Proposed Orbiter/MAV Communications . . . . .	VII-8
VII-4	Lander Telecommunications Block Diagram . . . . .	VII-20
VII-5	MAV Power Subsystem . . . . .	VII-33
VII-6	Lander Deorbit Coast Energy Allocation . . . . .	VII-36
VII-7	Lander Power Profile . . . . .	VII-37
VII-8	MAV Power Profile . . . . .	VII-39
VII-9	20-Watt RTG Program . . . . .	VII-42
VII-10	MAV Propulsion System . . . . .	VII-46
VII-11	Typical Propulsion System Mass Fractions . . . . .	VII-50
VII-12	MAV Solid Propellant Motor Characteristics . . . . .	VII-51
VII-13	MAV Stage III Propulsion System . . . . .	VII-57
VII-14	VO'75 Propulsion Subsystem . . . . .	VII-60
VII-15	Orbiter Propulsion System . . . . .	VII-62
VII-16	Orbiter Auxiliary Propulsion System Schematic . . . . .	VII-65
VII-17	Terminal Propulsion System . . . . .	VII-69
VII-18	Mars Surface Thermal Environment . . . . .	VII-72
VII-19	Current Baseline Concept for MAV Thermal Control on Mars Surface . . . . .	VII-74
VII-20	MAV Thermal Control During Orbital Operations . . . . .	VII-76
VII-21	Sample Container Thermal Control - Docking through Earth Entry . . . . .	VII-77
VII-22	Aerodynamic Coefficients for the MAV . . . . .	VII-80
VII-23	Aerodynamic Heating and Heat Protection Options During MAV Ascent . . . . .	VII-82

<u>Figure</u>		<u>Page</u>
VII-24	Aerodynamic Heating Distribution for the MAV Nose Cone	VII-83
VII-25	Center of Pressure Variation with Mach Number . . . . .	VII-84
VII-26	Pitch Damping Coefficient Functions . . . . .	VII-86
VII-27	Pitch Damping Coefficient Functions . . . . .	VII-88
VII-28	Earth Launched Payload . . . . .	VII-90
IX-1	Candidate Earth Entry Capsule . . . . .	IX-4
IX-2	Earth Entry Capsule Recovery Sequence . . . . .	IX-7
IX-3	Earth Entry Capsule (1 kg Sample) . . . . .	IX-10
IX-4	Earth Entry Capsule . . . . .	IX-11
IX-5	28 kg Earth Entry Capsule Key Subsystems . . . . .	IX-13
IX-6	Typical Convective & Radiative Heating Rate Histories for the Earth Entry Capsule . . . . .	IX-17
IX-7	Earth Entry Capsule Heat Shield Performance . . . . .	IX-18
IX-8	Earth Entry Capsule Descent Velocity Profile . . . . .	IX-20
IX-9	Entry Capsule Deceleration as a Function of Entry Angle	IX-21
IX-10	Earth Entry Capsule Electrical Functional Diagram . .	IX-24
IX-11	Impact Limiter Requirements - Earth Entry Capsule . .	IX-27
IX-12	Earth Entry Capsule Design - Structural Considerations	IX-28
IX-13	Earth Entry Capsule (Canister Survivability Only) . .	IX-30
IX-14	Earth Entry Capsule (5 kg Sample) . . . . .	IX-32

LIST OF TABLES

<u>Table</u>		<u>Page</u>
I-1	MSSR Science Guidelines . . . . .	I-5
II-1	MSSR Launch/Encounter Space . . . . .	II-3
II-2	1981 and 1983/4 Opportunity Comparison for Direct Entry Mode . . . . .	II-4
II-3	Earth Return Window for a 1981 MSSR . . . . .	II-11
II-4	Typical Weight Distribution for a 1981 MSSR . . . . .	II-22
III-1	Representative Control and Knowledge Uncertainties Expressed in B-plane System . . . . .	III-6
III-2	Lander Deflection Summary . . . . .	III-7
III-3	Orbiter $\Delta V_{STAT}$ Summary . . . . .	III-7
III-4	Capture Orbit Dispersions . . . . .	III-8
III-5	Capture Orbit O.D. (1 $\sigma$ Uncertainties) . . . . .	III-8
III-6	Ascent Dispersions (P=2.58 hrs, $h_A=2200$ km) . . . . .	III-11
III-7	O.D. Accuracies for Baseline Analysis . . . . .	III-12
III-8	MAV $\Delta V_{STAT}$ . . . . .	III-12
III-9	Post-Circularization Dispersions . . . . .	III-15
III-10	Dispersion Ellipse At First Occultation Exit ( $\phi_o = 2^\circ$ ) . . . . .	III-15
III-11	Line-of-Sight Error At First Occultation Exit. . . . .	III-16
III-12	Relative State Accuracies At DLVI Update . . . . .	III-19
III-13	Pointing Accuracy at $\Delta VLBI$ Update . . . . .	III-19
III-14	Trim $\Delta V_{STAT}$ . . . . .	III-22
III-15	Dispersion Ellipse At 10th Occultation Exit . . . . .	III-22
III-16	$\Delta VLBI$ vs Conventional Doppler . . . . .	III-29
III-17	Prediction Capability for $h_p = 2200$ Circular . . . . .	III-31
III-18	Prediction Capability for $h_p = 1725$ Circular . . . . .	III-32
III-19	MAV Orbit Determination Accuracies . . . . .	III-33
III-20	MAV $\Delta V_{STAT}$ Sensitivity . . . . .	III-35
III-21	Orbiter Trim $\Delta V_{STAT}$ Sensitivity . . . . .	III-35
III-22	Dispersion Ellipse Sensitivity . . . . .	III-35
III-23	Sensitivity of Pointing Accuracy to Gravity Field Errors . . . . .	III-35
III-24	Sensitivity of $\Delta V_{STAT}$ to Initial Rendezvous Errors . . . . .	III-38

<u>Table</u>	<u>Page</u>
IV-1 Launch Phase Error Source . . . . .	IV-7
IV-2 Launch Phase Errors . . . . .	IV-8
IV-3 Three-Axis Stabilized MAV . . . . .	IV-36
IV-4 Attributes of Three-Axis vs Spin Stabilized MAV . .	IV-39
IV-5 Spin Stabilized MAV . . . . .	IV-40
IV-6 Guidance and Control Components (Typical) . . . . .	IV-41
V-1 MAV Transponder Mass . . . . .	V-19
V-2 Rendezvous Radar Error Summary . . . . .	V-29
V-3 CW Rendezvous Radar Sensor Characteristics . . . . .	V-32
V-4 Comparison of Apollo and URDMO Rendezvous Sensors .	V-33
V-5 New Technology Development Requirements . . . . .	V-44
VI-1 1981 MAV Mass Properties . . . . .	VI-7
VI-2 1 kg vs 5 kg MAV Mass Comparisons . . . . .	VI-13
VI-3 Launcher and Thermal Canopy Mass . . . . .	VI-21
VI-4 Lander Mass Derivation . . . . .	VI-22
VI-5 Results of Flat Landings Study . . . . .	VI-25
VI-6 Results of Nominal Descent Rate Landings on 20° Slopes . . . . .	VI-26
VI-7 Results of Max. Horizontal Velocity Landings on Steep Slopes . . . . .	VI-27
VI-8 Derivation of Modified VO'75 Orbiter for the MSSR Mission . . . . .	VI-33
VI-9 Candidate ERV Mass Summaries Based on Modified Pioneer Venus Spacecraft . . . . .	VI-42
VI-10 $\Delta V$ Budget in m/sec . . . . .	VI-43
VI-11 Orbiting System Mass Derivation . . . . .	VI-44
VI-12 Determination of In-Orbit Margin for the Baseline Configuration . . . . .	VI-45
VI-13 Failure Modes and Backup Provisions . . . . .	VI-48
VI-14 Requirements and Feasibility of Lander Survival After MAV Launch . . . . .	VI-50
VII-1 MAV Telecommunications Functional Requirements . . .	VII-3
VII-2 MAV Telecommunications Weight and Power Estimates .	VII-6
VII-3 MAV-to-Earth Communications Link with MAV in Orbit .	VII-9
VII-4 Earth-to-MAV Command Link with MAV in Orbit . . . .	VII-10
VII-5 Telecommunications Design Control Table - Turn Around Ranging with MAV-to-Orbiter Telemetry . . . .	VII-11 thru VII-13

<u>Table</u>	<u>Page</u>
VII-6 Telecommunications Design Control Table - MAV-to-Orbiter Command and Ranging Uplink . . . . .	VII-14
VII-7 MAV Measurement List . . . . .	VII-16
VII-8 URDMO System Frequency Allocations . . . . .	VII-17
VII-9 Lander Telecommunications Functional Requirements .	VII-19
VII-10 Lander Telecommunications Physical Properties . . .	VII-22
VII-11 Lander-to-Earth Telemetry Design Control Table - Surface Operations . . . . .	VII-23
VII-12 Earth-to-Lander Command Design Control Table - Surface Operations . . . . .	VII-24
VII-13 Telecommunications Design Control Table - Planetary Ranging with Downlink Telemetry (Lander) . . . . .	VII-25 thru VII-27
VII-14 Lander Telecommunications Performance . . . . .	VII-27
VII-15 Lander/MAV Equipment Operating Sequence for Surface Operations . . . . .	VII-28
VII-16 MAV Telecommunications Link Margins . . . . .	VII-30
VII-17 Orbiter Power Allocation . . . . .	VII-34
VII-18 Orbiter Energy Requirements and Margins During Maneuvers . . . . .	VII-35
VII-19 MAV Power Utilization . . . . .	VII-38
VII-20 URDMO Propulsion Requirements . . . . .	VII-44
VII-21 MAV Propulsion System Characteristics . . . . .	VII-47
VII-22 MAV Stage III Propulsion System Duty Cycle . . . . .	VII-54
VIII-1 MSSR Mission Detailed Timeline . . . . .	VIII-2 thru VIII-12
IX-1 Baseline Earth Entry Capsule Mass Distribution Estimate (1 kg Sample) . . . . .	IX-14
IX-2 Critical Entry Environment Results for the Earth Entry Capsule . . . . .	IX-16
IX-3 Physical Properties of the EEC Electrical System . .	IX-25
IX-4 Cost Trends as a Function of Probability of Successful Sample Recovery . . . . .	IX-34
X-1 Technology Assessment . . . . .	X-2

## GLOSSARY

ACS	Attitude Control System
AZL	Azimuth of MAV Ascent Vehicle
CC	Control Computer
CIRC	Orbiter Circularization Maneuver
CMOS	Complementary Metal Oxide Semiconductors
CST	Coast Time Between MAV 1st and 2nd Stage Ascent burns
DSN	Deep Space Net
DVM	Magnitude of $\Delta V$
EEC	Earth Entry Capsule
ERV	Earth Return Vehicle
FOV	Field of View
H/S	Heat Shield
G&C	Guidance and Control
GCSC	Guidance Control and Sequencing Computer
HGA	High Gain Antenna
LATL	Landing Sight Latitude
LONG	Landing Sight Longitude
LOS	Line of Sight
LSI	Large Scale Integrated (Circuit)
LVMP	Launch Vehicle Mission Peculiarities
MIC	Microwave Integrated Circuits
MAV	Mars Ascent Vehicle
MNOS	Metallized Nitride On Silicon
MOI	Mars Orbit Insertion
MOR	Mars Orbital Rendezvous

MSSR	Mars Surface Sample Return
PCM	Pulse Core Modulation
PSK	Pulse Shift Keying
PM	Phase Modulation
PN	Proportional Navigation
PROM	Permanent Read Only Memory
KAM	Random Access Memory
RCS	Reaction Control System
RF	Radio Frequency
RR	Rendezvous Radar
RECIRC	MAV Post Circularization Trim
S/A	Safe/Arm (Device)
SCR	Silicon Controlled Rectifier
STEM	Storable Tubular Extendible Member
TEI	Trans-Earth Injection
TR	Terminal Rendezvous
TR1	Terminal Rendezvous Initiation
THR	Orbiter Thrust
URDMO	Unmanned Rendezvous and Docking in Mars Orbit

## LIST OF SYMBOLS

$\alpha$	right ascension of thrust direction
$\beta$	declination of thrust direction
$B$	ballistic coefficient $m/C_D A$
$\gamma$	flight path angle
$\gamma_E$	flight path angle at entry
$\Delta V$	delta velocity (vehicle velocity change)
$\Delta V_C$	closing $\Delta V$ (for start of terminal rendezvous)
$\Delta V_H$	$\Delta V$ for Hohmann transfer
$\Delta V_{LBI}$	differential very long baseline interferometry
$\Delta V_{MOI}$	velocity change for MOI
$\Delta V_{PC}$	velocity change for plane change
$\Delta V_{STAT}$	statistical $\Delta V$
$\Delta V_T$	terminal $\Delta V$ (total $\Delta V$ used in rendezvous control law burns)
$\Delta$	change
$\Delta V_1, \Delta V_2, \Delta V_3$	orbiter trim maneuvers, control law burns
$\Delta \gamma_{STAT}$	statistical flight path angle variation from nominal
$\theta$	angle traversed in terminal rendezvous (transfer angle)
$\theta_{AIM}$	angle between B-vector and $\vec{T}$ -axis
$\theta_{MI}$	angle between B-ellipse minor axis and T axis
$\theta_o$	initial launch ramp angle
$\theta_s$	cone half angle
$\dot{\theta}$	constant pitch rate after launch
$\mu$	gravitational constant
$\sigma_{BMIN}$	standard deviation of B-vector magnitude along minor axis of B-ellipse
$\sigma_x, \sigma_y, \sigma_z$	standard deviations of position (Cartesian components)
$\sigma_{\dot{x}}, \sigma_{\dot{y}}, \sigma_{\dot{z}}$	standard deviations of velocity (Cartesian components)

$\sigma_u, \sigma_v, \sigma_w$	standard deviations of position (orbit plane components)
$\sigma_{\dot{u}}, \sigma_{\dot{v}}, \sigma_{\dot{w}}$	standard deviations of velocity (orbit plane components)
$\sigma_{\rho_p}$	standard deviation in projected relative velocity
$\phi_0$	initial phase angle at o.e.
$\dot{\phi}$	phase angle catch up rate
$Q$	longitude of ascending node
$\omega$	argument of periapsis, LOS rate
$A$	base area or reference area (in ballistic coefficient)
$a$	semi-major axis
B-plane	plane perpendicular to VHE vector
B-vector	center of planet to B-plane impact point
$b_p$	projection of baseline vector
$C_D$	aerodynamic drag coefficient (in ballistic coefficient)
$D_0$	parachute diameter (deflated)
$E$	covariance matrix of launch errors
$e$	eccentricity
HP	orbiter periapsis altitude adjust maneuver
$h_p$	periapsis attitude
$h_a$	apoapsis attitude
$i$	inclination
$M$	injection sensitivity matrix
$m$	mass (in ballistic coefficient)
O.D.	Orbit Determination
o.e.	occultation exit
$P$	period
$P_{INJ}$	covariance matrix of injection dispersions

$P_{ORB}$	period of orbiter orbit
$P_{MAV}$	period of MAV orbit
$P_{phase}$	period of phasing orbit
$R$	range
$\dot{R}$	range rate
$R_A$	actual MAV position vector
$R_E$	radius of earth entry
$R_N$	entry capsule nose radius
$R_{SB}$	entry capsule base radius
$r_{EM}$	Earth-Mars distance
$\vec{R}, \vec{S}, \vec{T}$	coordinate axes for B-plane coordinates: S along VHE, T in ecliptic, R completes landed system
$\delta t_{12}, \delta t_{23}$	times between trim maneuvers #1, #2 and #2, #3
TA	true anomaly
$T_1$	thrust of stage #1
$T_2$	thrust of stage #2
t	time
$t_B$	burn time
$t_{B1}$	time of stage #1 burn
$t_{B2}$	time of stage #2 burn
$t_R$	time for rendezvous
$v_E$	entry velocity
VHF	hyperbolic excess velocity
$v_\infty$	hyperbolic excess velocity
$W_p$	propellant weight
X	generic designation for position
$\dot{X}$	generic designation for velocity

## I OBJECTIVES, GUIDELINES AND STUDY RESULTS

The scientific value of bringing a Mars surface sample back to Earth for careful analysis is far greater than casual thinking may lead one to believe. At Mars, where wind, volcanism, meteor impact, and probably water, have worked over millions of years to distribute surface material, much can be learned from a single sample about the history and evolution of the entire planet, if the investigating methods are sophisticated and precise enough. Techniques now exist for geochemical, petrological, organic and biological analysis of a small sample, that have been proven on both terrestrial and lunar materials to be immensely powerful.

These techniques involve meticulous sample preparation and extremely accurate measurement. Moreover, many of the analysis procedures require a flexible sequence of examination where the results of one step dictate the approach to be taken to the next.

Scientific workers in this field seem to express a near uniform conviction that to attempt to duplicate this accuracy, flexibility and reliability of Earth laboratory facilities in remotely operated instruments, sent to the surface of Mars, would be infeasible, both technically and economically.

Therefore, if the scientific value of a Mars Surface Sample Return (MSSR) mission is established, what are the key elements in a decision to mount such a mission? There are three important questions to be answered:

- 1) Is the mission technically feasible with current or predicted state-of-the art?
- 2) Can any potential back contamination of the Earth's biosphere by Martian biota be prevented or controlled?
- 3) Can the mission be performed within projected NASA budget levels?

## A. OBJECTIVES

The purpose of this study, as directed by the JPL Technical Manager, Mr. J. W. Moore, was to examine the first question listed above: is MSSR technically feasible? Emphasis was to be on the feasibility of unmanned rendezvous and docking.

Assuming that flights between Earth and Mars, Mars orbital operations, and Mars landings will have been proven by previous Mariner and Viking '75 missions, the question narrows somewhat to the feasibility of mission sequences peculiar to MSR. These involve the ascent of the sample from the Mars surface, the return to Earth, and recovery of the sample into safe keeping for analysis. One of the most attractive methods for performing these specialized MSSR sequences is the Mars orbital rendezvous mode. In this mode, which is similar to the approach taken in Apollo, the vehicle that will carry the sample from Mars back to Earth is not sent to the surface but is kept in orbit about Mars. A much smaller Mars Ascent Vehicle (MAV) is landed and subsequently ascends, participates in a rendezvous with the orbiting spacecraft, and transfers the sample to the Earth Return Vehicle (ERV). The MOR mode makes control of back contamination easier, and reduces the size (and probably the cost) of some of the spacecraft elements. Most important to the issue of program cost, the MOR mode allows the use of modified versions of existing spacecraft to carry out the mission.

However, the MOR mode does pose some question of feasibility in the execution of unmanned, partly automatic, rendezvous, docking and sample transfer at Mars.

The primary thrust of this study then was to examine the feasibility of unmanned rendezvous and docking in Mars orbit. Hopefully these results will be a useful input to the NASA decision making process on the MSSR mission.

The study tasks, outlined in the contract statement of work, focused on the feasibility of unmanned rendezvous and docking in Mars orbit. However, other parts of the mission were to be examined also to make certain that approaches taken to implement rendezvous were compatible with a technically feasible and cost-effective total spacecraft and mission

**design. The specific contract tasks were:**

- a. Mission Analysis**
- b. Spacecraft Tradeoffs and Design**
- c. Rendezvous and Docking**
- d. Sample Transfer**
- e. Mission Profile/Operations**
- f. Mars Sample Return Earth Entry Capsule Study**
- g. Technology and Programmatic Assessment**

## B. GUIDELINES

A number of technical and programmatic guidelines were suggested by the JPL Technical Manager to focus the study effort. They included the following ground rules:

1. The 1981 and 1983/84 Mars mission opportunities were to be considered.
2. Mars planetary quarantine requirements were to be recognized in the spacecraft and mission designs.
3. Maximum use of existing hardware, experience and facilities was desired. The Mars lander was to be a Viking-class vehicle.
4. Sample size was to cover the range from 0.2 to 5.0 kg.
5. Sample acquisition, processing, environmental control and transfer for Earth return were the only science-related functions to be studied for the mission.

To support the definition of the science requirements on the acquisition and handling of the sample, a one-day science work shop was held in Denver on May 9, 1974 as an adjunct to this study. The attendees included recognized scientists in the Apollo lunar sample analysis programs and other scientists with extensive experience in planetary exploration missions.

Appendix A summarizes the results of this meeting and lists the attendees. Table I-1 outlines the major science guidelines followed in the study.

Table I-1 MSSR Science Guidelines

Sample Use	Sample Amount (per site)	Sample Type	Sample Site	Sample Control
Inorganic Analysis	100 grams	Sieved to 2-10 mm Size; Surface & Trench	Mouth of Stream Bed	Sealed; Temp. < Mars Surf. Max.
Organic Analyses	200 grams	Fines; Surface & Trench		Sealed; Temp. < Mars Surf. Max.
Biological Analyses	200 grams	Fines; Surface		Sealed; Temp. < 0°C
Pathogenicity	300 grams			
Reserve	200 grams			

## C. STUDY RESULTS

The major result of the study was the definition of a baseline MSSR mission, using the MOR mode, within which tradeoff studies were performed and feasibility tested.

Figure I-1 identifies the hardware elements of the baseline mission and the functions they perform.

Before describing the baseline concept, it should be pointed out that this configuration is only one of several attractive options that will meet the objectives and guidelines of this study. The principal choices come in the method of delivering the spacecraft to Mars. In the baseline concept a single launch of a Titan IIIE Centaur injects a spacecraft consisting of an orbiter, a lander and an Earth Return Vehicle (ERV) to Mars. The lander separates prior to Mars encounter and performs a direct entry landing without going into orbit. The orbiter then carries the ERV into orbit to participate in the rendezvous.

In Figure I-2 a dual launch concept is shown in which the same spacecraft elements are divided between two Titan IIIE/Centaur launch vehicles. The lander is carried to Mars by a simple cruise module that flies on by the planet after the direct entry capsule is separated. The orbiter functions the same as in the baseline.

Figure I-3 shows another and perhaps more attractive dual launch option in which the lander is carried into orbit by a second orbiter. This allows surveillance and certification of the landing site prior to a commitment to land and permits the use of the by then Viking-proven out of orbit landing technique.

Both dual launch options permit greater launch vehicle weight margins and provide clean interfaces for possible international cooperation missions. This extra weight margin can be carried into the critical, landing ascent and rendezvous phases if a somewhat more extensively modified Viking-class lander and an orbiter are used (at higher cost).

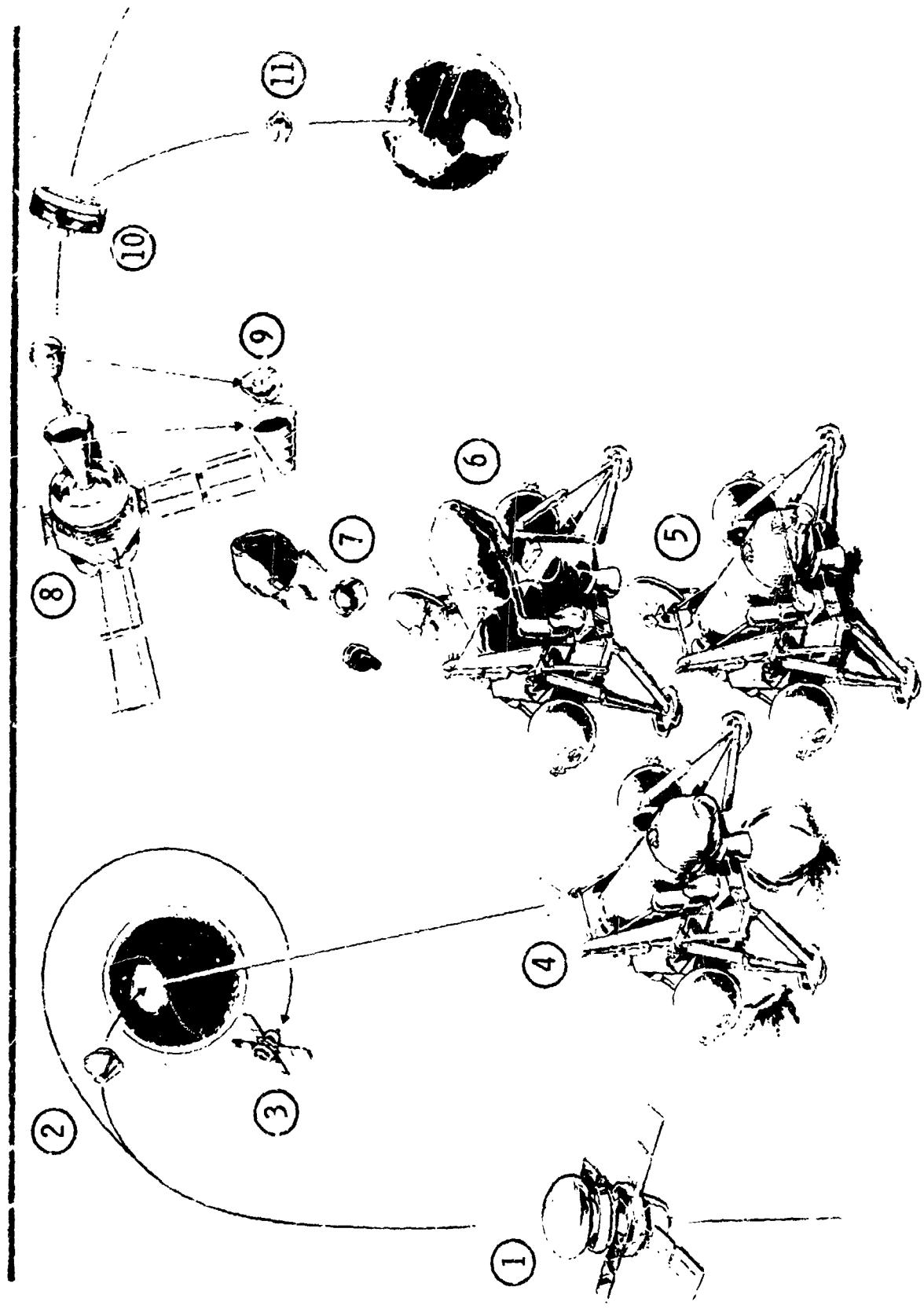


Figure I-1 MSSR Mission Sequence - Mars Rendezvous Mode

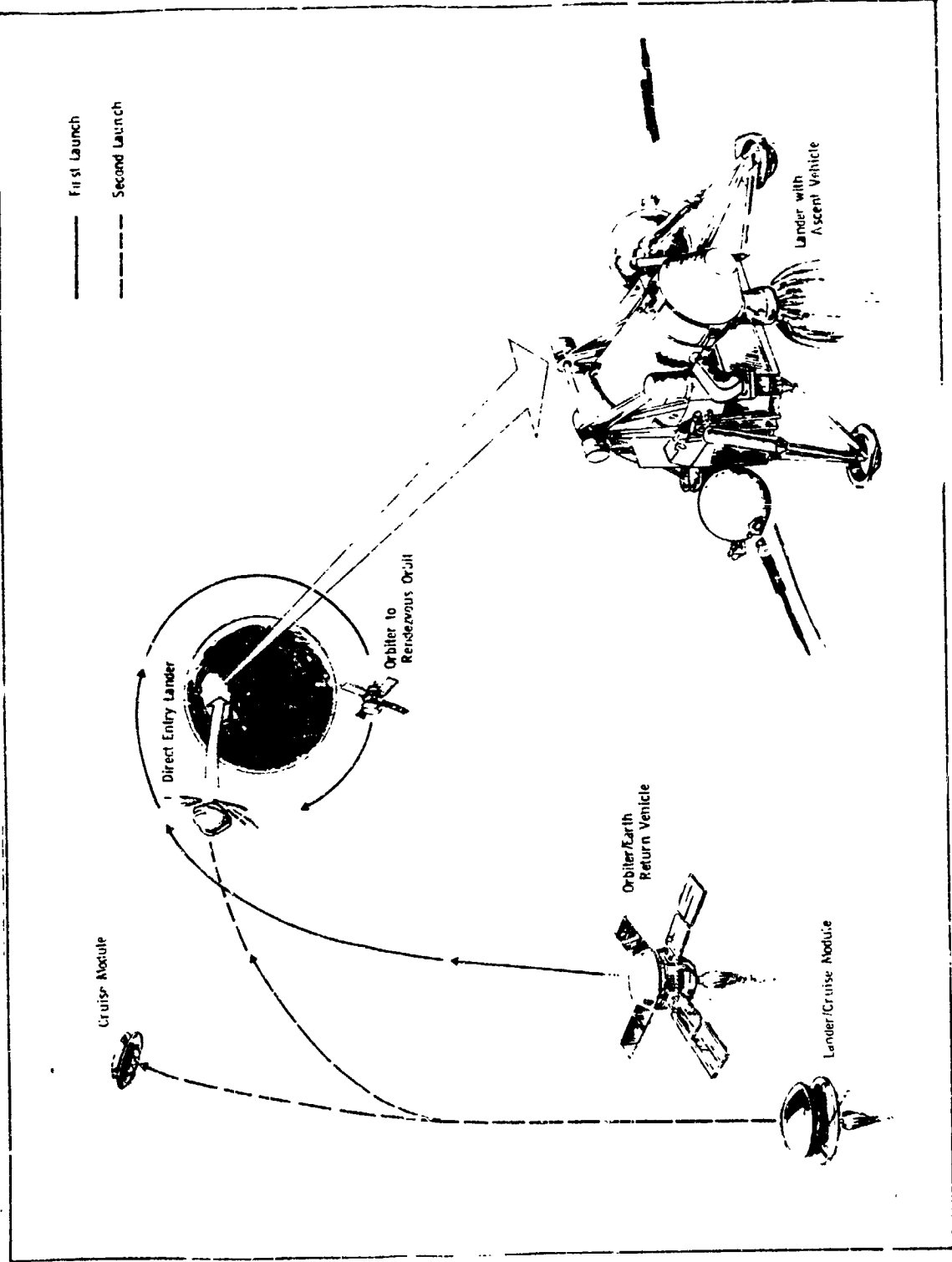


Figure I-2 MSSR Mission Sequence - Mars Rendezvous Mode--Dual Launch--Direct Entry

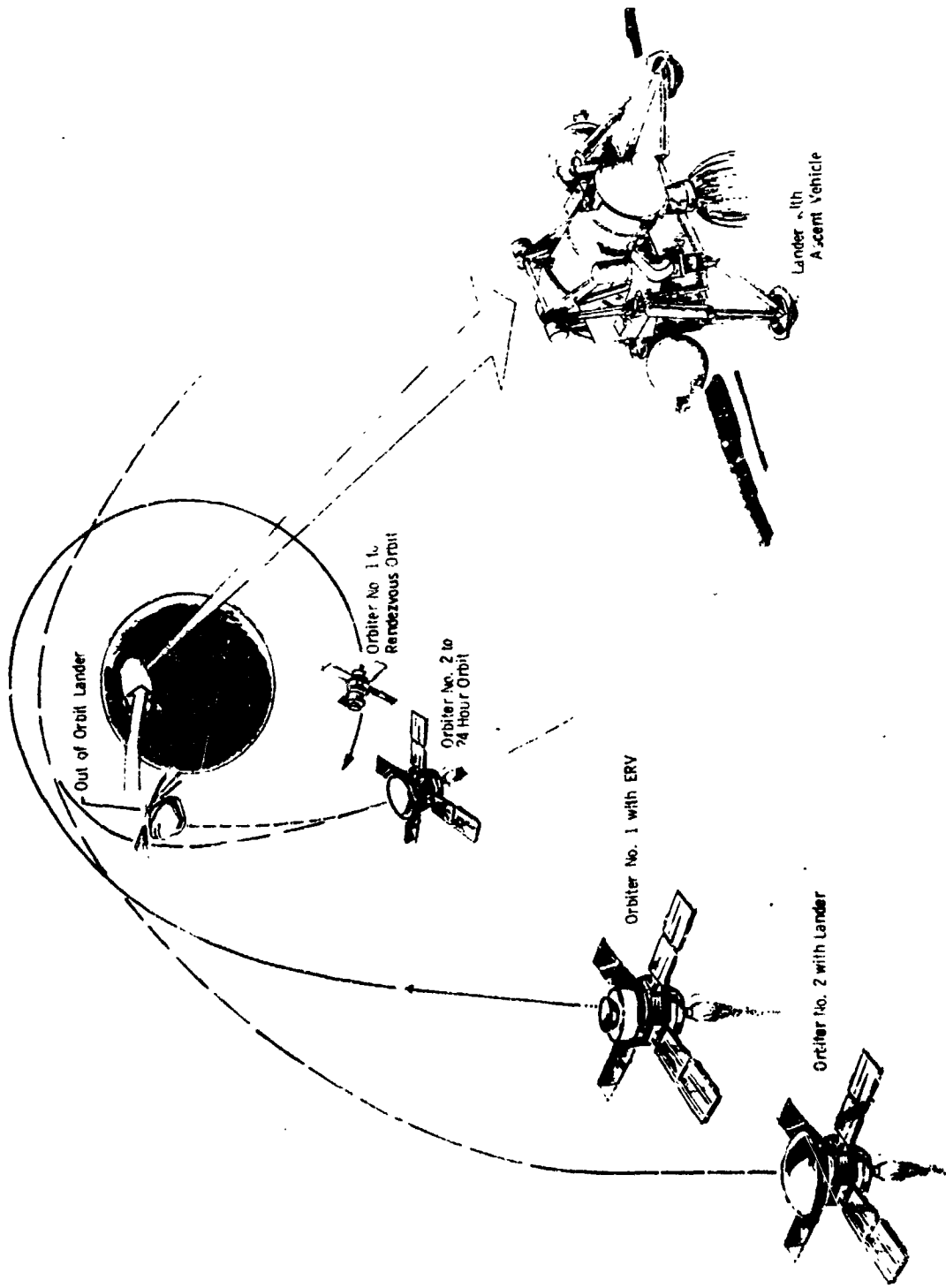


Figure I-3 MSSR Mission Sequence - Mars Rendezvous Mode--Dual Launch--Out of Orbit Entry

Returning to the baseline mission in Figure I-1, the lander capsule, having separated from the orbiter, touches down on the surface a little over four hours later. The lander configuration is a basic Viking '75 capsule modified to carry the Mars Ascent Vehicle as shown in Step 4. The MAV weighs 290 kg. The lander is stripped of unneeded subsystems and its terminal propulsion system converted from a blow-down to a fully pressurized feed system to provide most of the increased landed weight capability compared to Viking '75.

The lander remains on the surface for 11 days during which time the sample is collected and stowed, the position and orientation are updated through Earth-based tracking and telemetry and the proper launch azimuth and elevation are calculated at Earth.

The sample, baselined at 1 kg in this study, is loaded in a sealable canister mounted in the nose of the MAV.

Upon receiving the launch instructions from Earth, the MAV is launched to an initial orbit of 100 x 2200 km altitude. The MAV is a three stage (two solid and one liquid) three axis stabilized vehicle incorporating comparatively simple subsystems. After the second stage injects into the initial orbit, the third stage becomes a maneuvering satellite. It weighs 41 kg and is capable of being tracked from Earth, being commanded to perform orbital maneuvers, and participating in a semi-passive way in the subsequent rendezvous with the orbiter.

After the MAV third stage is tracked to determine its initial orbit, it is commanded to circularize at 2200 km altitude into the rendezvous orbit. The orbiter then is commanded to maneuver from its initial capture orbit of 1000 x 100,000 km altitude, to a circular orbit of 2250 km altitude.

Up to this point the only series of maneuvers not performed under Earth control have been the MAV ascent to 100 km and injection into the initial orbit. The MAV and orbiter are brought into close proximity thereafter with DSN tracking providing position information before and after each maneuver. Conventional DSN doppler tracking can determine the position of each vehicle to an accuracy of 3 km and the velocity to 1.5 mps.

Another data type, known as  $\Delta$ VLBI can be used to determine the relative positions between the two vehicles to an accuracy of 0.3 km and relative velocities to 0.15 mps.  $\Delta$ VLBI uses a double differenced very long baseline interferometry technique and will be developed and proven for the Pioneer Venus mission that will fly in 1978.

By using these powerful tracking tools the orbiter can be brought to an accurately known position relative to the MAV for the initiation of the automatic terminal rendezvous

The orbiter will carry an S-band rendezvous radar unit that will lock on the MAV transponder to control the terminal rendezvous. The same MAV transponder is thus used for both Earth tracking and rendezvous participation.

The orbiter employs a series of propulsion maneuvers controlled by the range, range-rate, and line of sight rotation information generated by the rendezvous radar, to bring it to a position approximately 30 m away from the MAV.

At this point the sample canister is extended from the nose of the MAV as shown in Step 8 of Figure I-1, and the orbiter closes at 0.3 mps, under accurate pointing control, until docking and sample transfer are accomplished.

The MAV and the docking guide cone are discarded (Step 9) and the ERV, now containing the sample, is ready for the return to Earth.

In the baseline mission the ERV must wait in Mars orbit for approximately 400 days before the planetary geometry is established for injection to the return trajectory.

The total mission duration, for the 1981 opportunity, from Earth launch to Earth recovery of the sample is approximately 1050 days.

Figure I-4 illustrates the sequence occurring at Earth to recover the sample in this baseline mission. The direct Earth entry mode is shown. This involves the separation of an Earth entry capsule from the ERV that decelerates with a heat shield and parachute and is air snatched or landed on the surface.

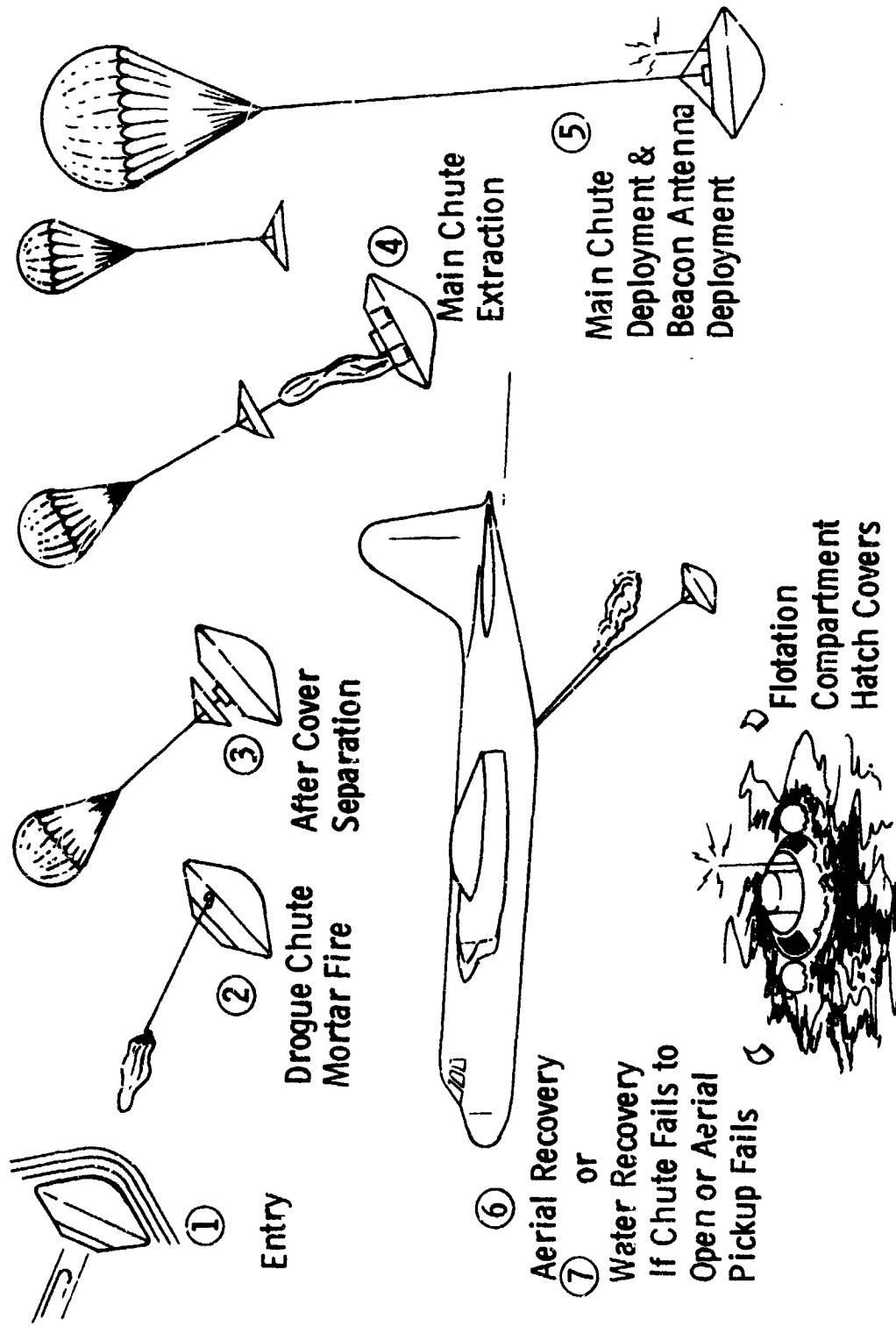


Figure I-4 Earth Entry Capsule Recovery Sequence

The general result of the analyses and trade studies conducted on this baseline MSSR mission concept is the conclusion that the mission can be performed as described, using technology that, for the most part, exists today, and, in many cases, using spacecraft and subsystems that will have been developed and proven in other programs.

## II MISSION ANALYSIS

Mission analysis for MSSR has dealt primarily with the definition and optimization of performance characteristics of the various mission phases. For this study, an underlying premise of constrained launch vehicle capability (specifically, single launch Titan IIIE/Centaur) has served to force the design toward the maximization of all available performance, minimization of weight allocations whenever possible, and to deletion of Viking '75 spacecraft components and operations not essential to the sample return objective. Given this background, the baseline mission design evolved toward a direct entry landing of the Lander/MAV, with an Orbiter/ERV inserting into an initial capture orbit of high eccentricity, transferring later to a 2200 km rendezvous orbit. Analysis of ascent profiles for the MAV led to selection of a three-stage vehicle, solid-solid-liquid, as the most efficient method to deliver a payload to rendezvous orbit.

This section develops performance and trajectory details of the baseline mission selected for the 1981 Mars opportunity, presents the trades critical to shaping that baseline, and examines the possibilities which exist for alternative mission strategies with different launch vehicle assumptions or mission opportunities.

### A. LAUNCH ENERGY REQUIREMENTS

The general thrust of the performance analysis was directed toward provision of sufficient weight allocation to the systems directly involved with landing, ascent, and rendezvous, within a structure of Viking-derived spacecraft elements. Earlier in-house sizing of the MSSR mission indicated that the 1981 opportunity would be severely weight limited, with the 1983/84 period being even more restricted. The current study concluded early that given the constraint of a single Titan/Centaur launch, orbit insertion of the entire spacecraft mass plus lander for an out-of-orbit descent would require major redevelopment of existing systems. Landing instead from a direct entry approach required 15% less launch weight, 33% less orbit insertion propulsion, and led to a performance situation compatible with mission feasibility. Direct entry landing is therefore carried through the baseline development, while it is recognized that real-time site certification would not be possible, and that accepting either dual launch or Shuttle performance could reopen the out-of-orbit mission.

In Table II-1 are presented the pertinent trajectory and representative performance parameters for 20-day launch periods defined for both opportunities. Launch/encounter space has been optimized toward a design which includes deflection of a Lander/MAV (1374 kg typical) prior to orbit insertion, with a subsequent burn into a highly eccentric initial capture orbit. Following initial capture, the orbit is trimmed to a final circular rendezvous orbit with a maneuver sequence to be discussed later.

Table II-1 indicates the performance loss associated with a 1983/84 opportunity, in terms of a mission baselined for feasibility in 1981. Minimum non-propulsive weight delivered to a 2200 km rendezvous orbit decreases from 904 kg in 1981 to 739 kg in 1983/84. Given the weight-critical nature of even the 1981 mission, an identical MSSR in 1983/84 would require either a higher performance launch vehicle and increased orbiter propellant, or the substitution of space-storable orbit insertion propulsion for the conventional system adequate in 1981. The mission description which follows therefore considers the 1981 opportunity as prime, and all referenced performance and navigation analyses are appropriate for that case.

As a more specific comparison of the two opportunities, Table II-2 presents weight and performance figures for both cases, sized for the worst end of their respective launch windows. The first column reflects the 1981 MSSR baseline, with earth storable (VO) propulsion, and a MAV sized at 289 kg liftoff weight. Here an orbited weight margin of 134 kg exists using full launch vehicle capability. For 1983 launch vehicle injected weight capability is reduced to 4354 kg, and the second column indicates that a baseline comparable to that defined for 1981 would exceed injected weight capability (even with orbited weight margin reduced to zero), requiring a higher performance launch system. In the third column, space storable insertion propulsion is substituted for the VO '75 system, and using full launch vehicle capability this essentially restores the original baseline performance.

Table II-1 MSSR Launch/Encounter Space

1981 MSSR

Day	Launch	Arrival	$C_3$ (km/sec) <sup>2</sup>	Injected Weight (kg)	$\theta$ (deg)	Vhp (km/sec)	Useful Orbits* Weight (kg) to 2200 km
1	11-17-81	9-15-82	10.60	4185	221	3.06	907
10	11-26-81	9-21-82	9.41	4273	216	3.05	940
20	12-6-81	10-4-82	9.08	4244	213	3.15	904

1983/84 MSSR

Day	Launch	Arrival	$C_3$ (km/sec) <sup>2</sup>	Injected Weight (kg)	$\theta$ (deg)	Vhp (km/sec)	Useful Orbits* Weight (kg) to 2200 km
1	12-23-83	9-29-84	12.61	4045	221	3.53	739
10	1-1-84	10-7-84	11.35	4132	216	3.57	754
20	1-11-84	10-17-84	10.55	4189	213	3.69	739

\*1374 kg associated with VLC/MAV is not orbited

Table II-2 1981 and 1983/4 Opportunity Comparison for Direct Entry Mode

	<u>1981 E/S*</u>	<u>1983 E/S**</u>	<u>1983 S/S*</u>
MAV at Liftoff	289 kg	289 kg	289 kg
Entry Velocity	18981 fps	20021 fps	20021 fps
Lander/MAV Separation	1285 kg	1296 kg	1296 kg
Vhp	3.15 km/s	3.69 km/s	3.69 km/s
S/C Wt at MOI	2818 kg	3022 kg	2752 kg
Propellant Wt	1593 kg	1881 kg	1460 kg
Stretch Rel. VO'75	+15%	+34%	+4%
Orbited Wt Margin	134 kg	0	129 kg
C <sub>3</sub>	9.08 km <sup>2</sup> /s <sup>2</sup>	10.55 km <sup>2</sup> /s <sup>2</sup>	10.55 km <sup>2</sup> /s <sup>2</sup>
Launch Weight	4409 kg	4624 kg	4354 kg

\* Sized to Titan IIIE/Centaur Capability

\*\* Exceeds Launch Vehicle Capability

## B. DIRECT ENTRY MISSION DESCRIPTION

### 1. Approach and Nominal MOI

The 1981 MSSR baseline mission involves deflection of the Lander/MAV configuration four hours prior to MOI, leaving only the Orbiter/ERV mass to be inserted into an orbit about Mars. Figure II-1 shows the sequence in a pictorial. From the point of deflection, the Lander/MAV begins its trajectory which reaches the "entry interface" of sensible Mars atmosphere at 243.8 km (800,000 ft) above the mean surface radius. At the interface, relative velocity is 5.785 km/sec (18981 fps), with a range of flight path angles from  $-17.6^\circ$  to  $-21.6^\circ$  for a  $4^\circ$  corridor. Following a final descent very similar to that planned for VO '75, the MAV is landed, collects a surface sample storing it within its third stage, and approximately eleven days after MOI performs its critical ascent to rendezvous. MAV weight at liftoff is 290 kg, including its 1 kg of Mars surface material.

Meanwhile, the MOI sequence begins with an initial impulse which transfers the 2618 kg spacecraft to a capture orbit of 1000 by 100,000 km altitude, of 105 hour period. The full MOI transfer sequence is illustrated in Figure II-2. The capture orbit serves as a waiting orbit while surface operations take place, and during this period the actual trajectory of descent, location of landing site, and trajectory of ascent are determined by DSN tracking. These operations occur over an eleven day period, and at that time the Orbiter/ERV resumes its transfer. Any necessary plane change is executed at apoapsis of the initial ellipse, one pass before the second impulse which raises periapsis to 50 km above the nominal MAV orbit of 2200 km circular. This ellipse is then trimmed in apoapsis altitude to 2250 by 5904 km, an intermediate step before final circularization at 2250 km. The 2250 by 5904 km step is required to establish the proper time phasing between MAV and orbiter, so that at orbiter circularization the orbiter leads the MAV by  $44^\circ$  central angle. After nine revs in this phasing orbit, both vehicles are positioned to begin terminal rendezvous.

### 2. MAV Ascent and Circularization

Ascent from the Mars surface is accomplished by a staged launch system of three separate propulsive units. These stages each perform a critical

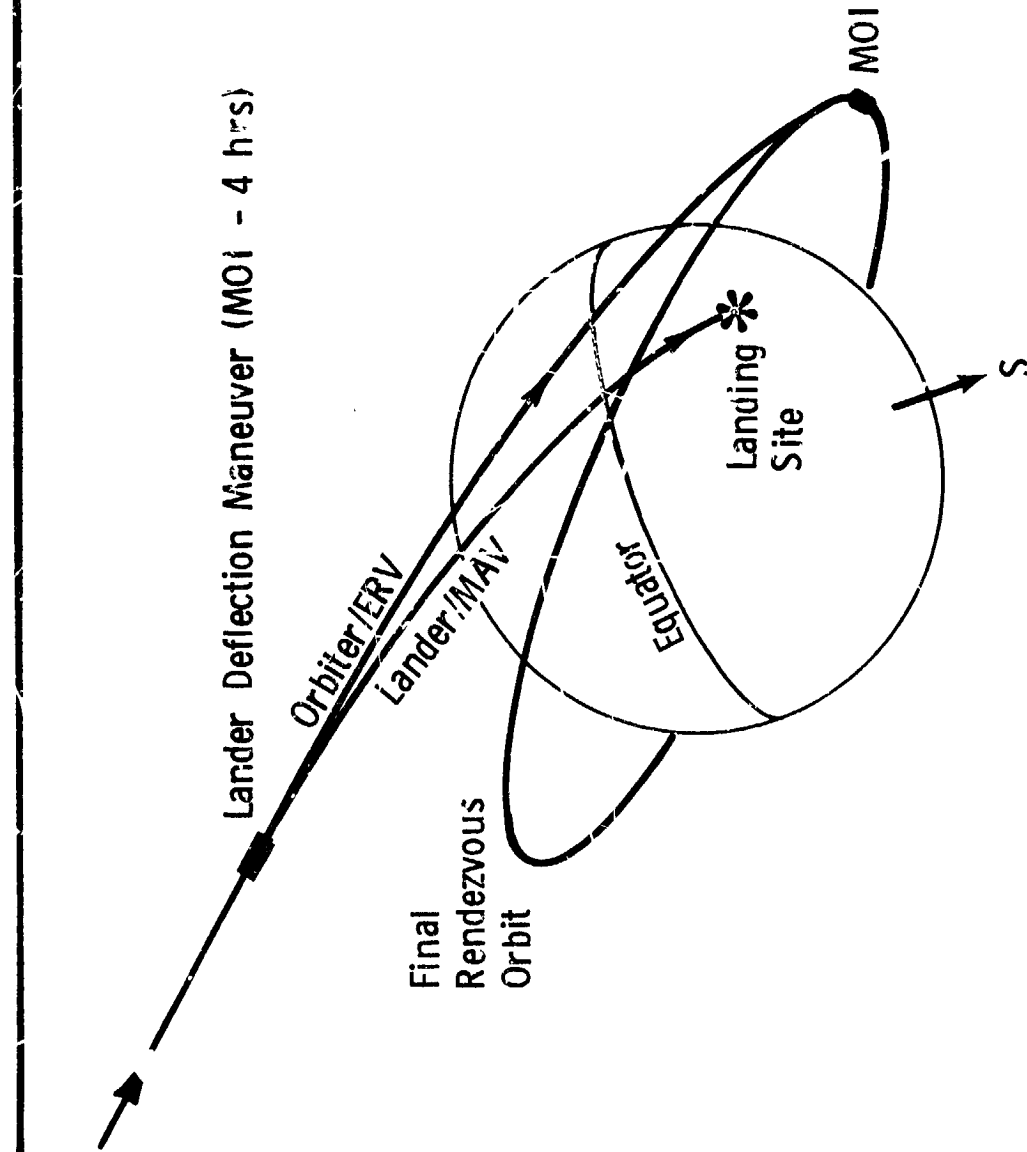


Figure II-1 Mars Approach and Lander Trajectory - Direct Entry

$V_{hp} = 3.15 \text{ km/sec}$

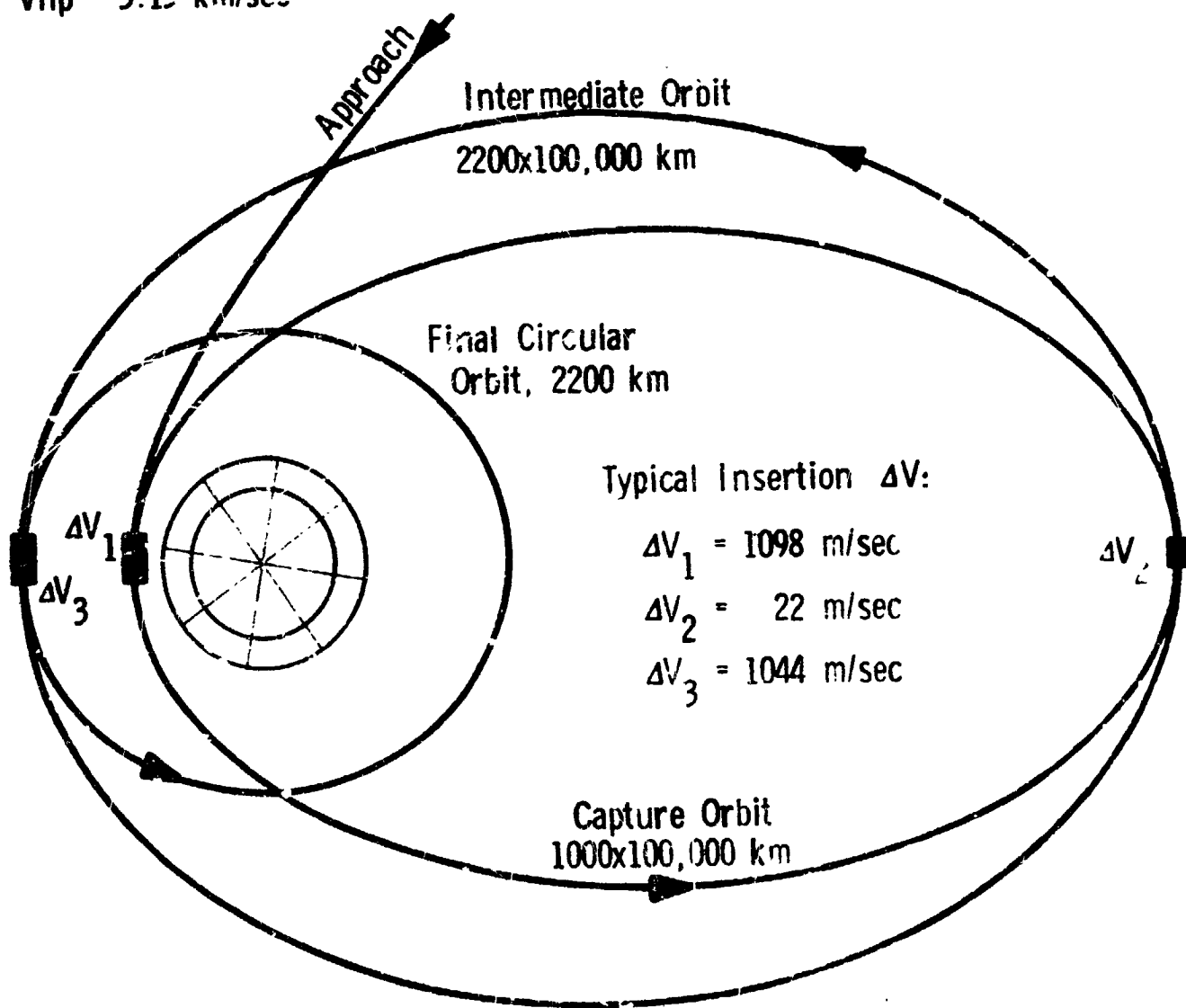


Figure II-2 MOI Profile

impulse in the ascent to rendezvous orbit. The sequence of trajectory transfers proposed for the MAV is illustrated in Figure II-3. The initial MAV stage is a solid rocket engine, designed for 6672 n (1500 lbf) thrust and 285 sec specific impulse, with an associated mass fraction of 0.88. This stage launches the entire MAV liftoff weight of 290 kg on a ballistic trajectory that reaches an altitude of 100 km. Launch orientation is inclined to a ramp angle of  $57^\circ$ , or  $33^\circ$  from local vertical. First stage burn duration is 54 seconds (generating a  $\Delta V = 1.654$  km/sec), and following the cutoff and jettison of this stage, the upper stages coast for 217 seconds to reach 100 km. There stage two performs a postgrade burn of 2.530 km/sec, 34 sec duration, to achieve a closed orbit of 100 by 2200 km. This stage is also solid rocket, with performance characteristics the same as stage one. During the coast to apoapsis which follows, stage two is jettisoned and at apoapsis the final MAV stage executes a circularization burn of 341 km/sec to achieve the 2200 km rendezvous orbit. The third stage, with a mass of about 40 kg, consists of a restartable liquid propulsion system of 200 n thrust, 235 sec specific impulse, with a prepulsion mass of 22.5 kg. From this circular orbit the MAV and Orbiter/ERV begin the trims which ultimately lead to rendezvous, docking, and sample transfer.

Details of specific pitch profiles during the burn sequence are discussed in a later section on Guidance and Control. The simulations done for performance optimization considered all burns approximated a gravity turn, with angle of attack driven to zero.

### 3. Earth Return Profile

After the Mars surface operations are completed and ascent, rendezvous, and docking have been successfully performed, the Orbiter/ERV continues in a parking orbit for about 420 days, awaiting the opening of the Earth return window in November, 1983. Prior to executing the return trans-Earth injection (TEI) sequence, the orbiter and ERV separate. Then follows the multi-impulse transfer from the parking orbit to the return hyperbola, executed by the ERV in a similar, but reverse, manner as the MOI. The return sequence is illustrated in Figure II-4. An initial burn transfers to an ellipse nominally 2200 by 100,000 km. At apoapsis of this orbit, any required plane change would probably be performed, along with a small impulse to lower

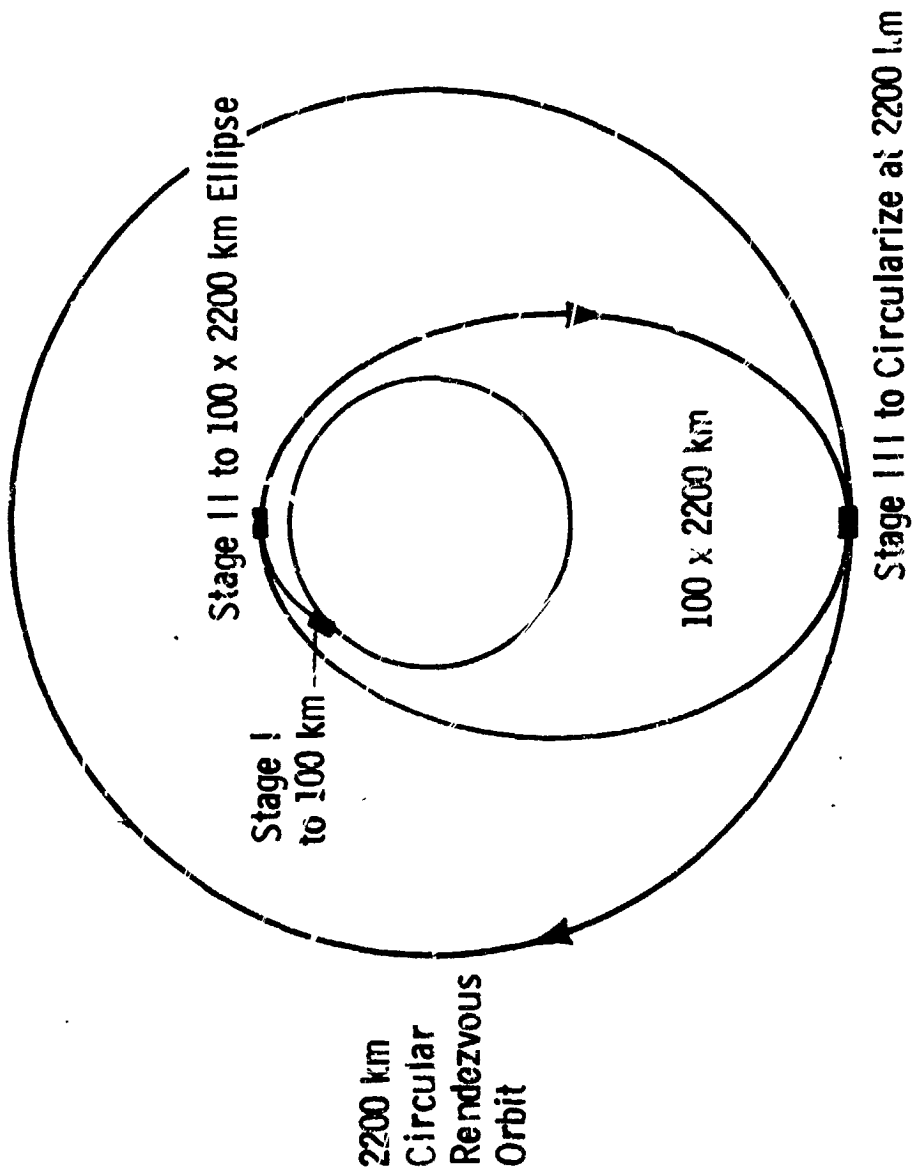


Figure II-3 Mars Ascent Vehicle Trajectory

$$C_3 = 5.42 \text{ km}^2/\text{sec}^2$$

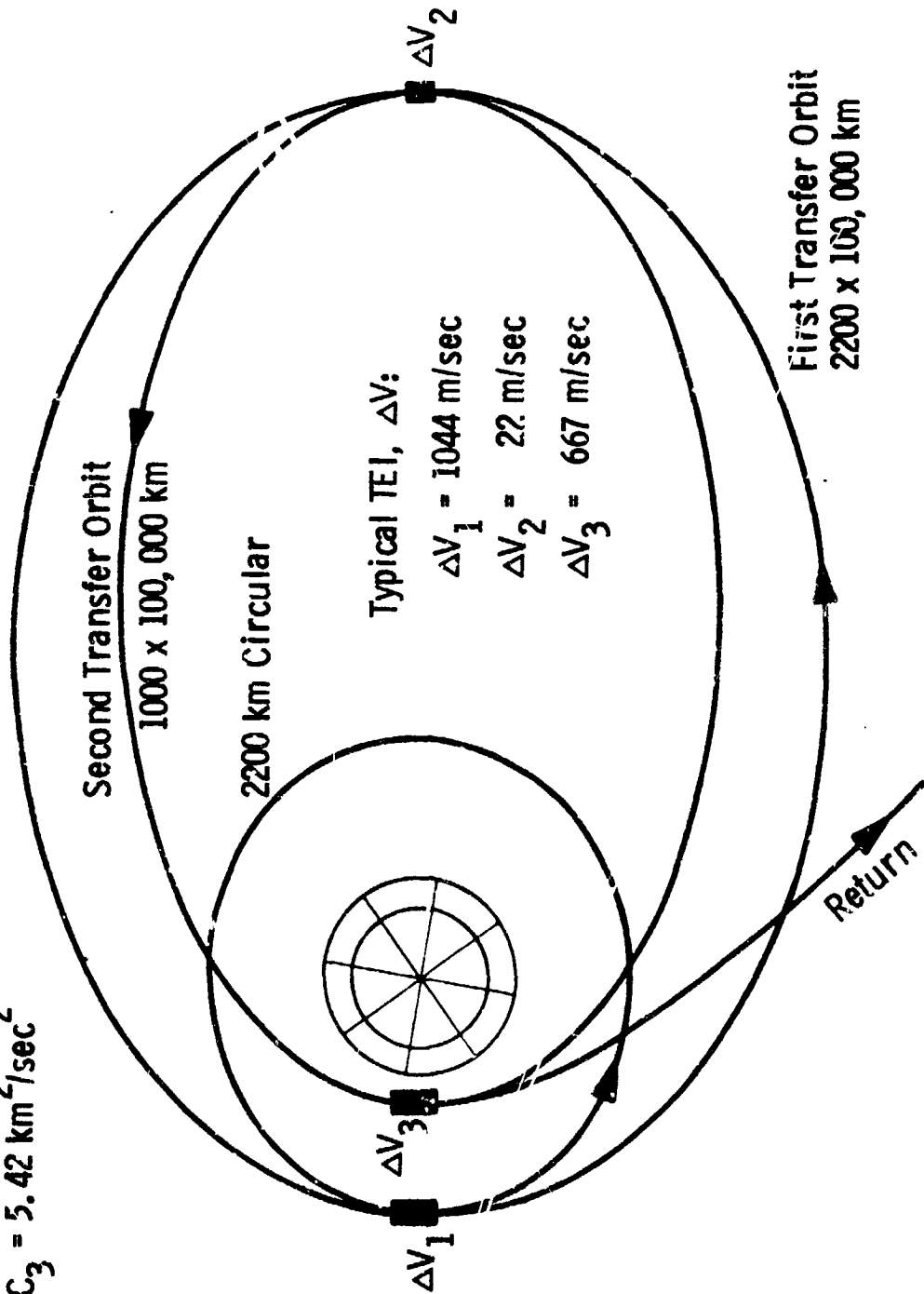


Figure II-4 TEI (Earth Return) Profile for 1981 MSSK

periapsis to 1000 km. Near periapsis of the 1000 by 100,000 km orbit, the final burn is executed to transfer the ERV to the return hyperbola.

For the 1981 MSSR opportunity, the return window proposed is presented in Table II-3. A 20-day period has been defined for November 1983, with Earth arrival occurring in September-October 1984. Given the Earth entry conditions associated with the return leg, a first estimate of landing site accessibility for direct entry landing has been determined, and is shown in Figure II-5. With  $V_{he}$  equal to 5.5 km/sec, latitude accessibility extends from near the North pole to 40°S, depending upon the approach aimpoint selected. Timing the entry appropriately gains access to any Earth longitude. Greenland is noted to show its possibility as an MSSR landing location.

Table II-3. Earth Return Window for a 1981 MSSR

Mars Launch Date	Earth Arrival Date	$C_3$ (km/sec) <sup>2</sup>	Trip Time (days)	$V_{he}$ (km/sec)
11-15-83	9-26-84	5.44	316	5.34
11-24-83	9-30-84	5.42	311	5.52
12-4-83	10-4-84	5.44	305	5.69

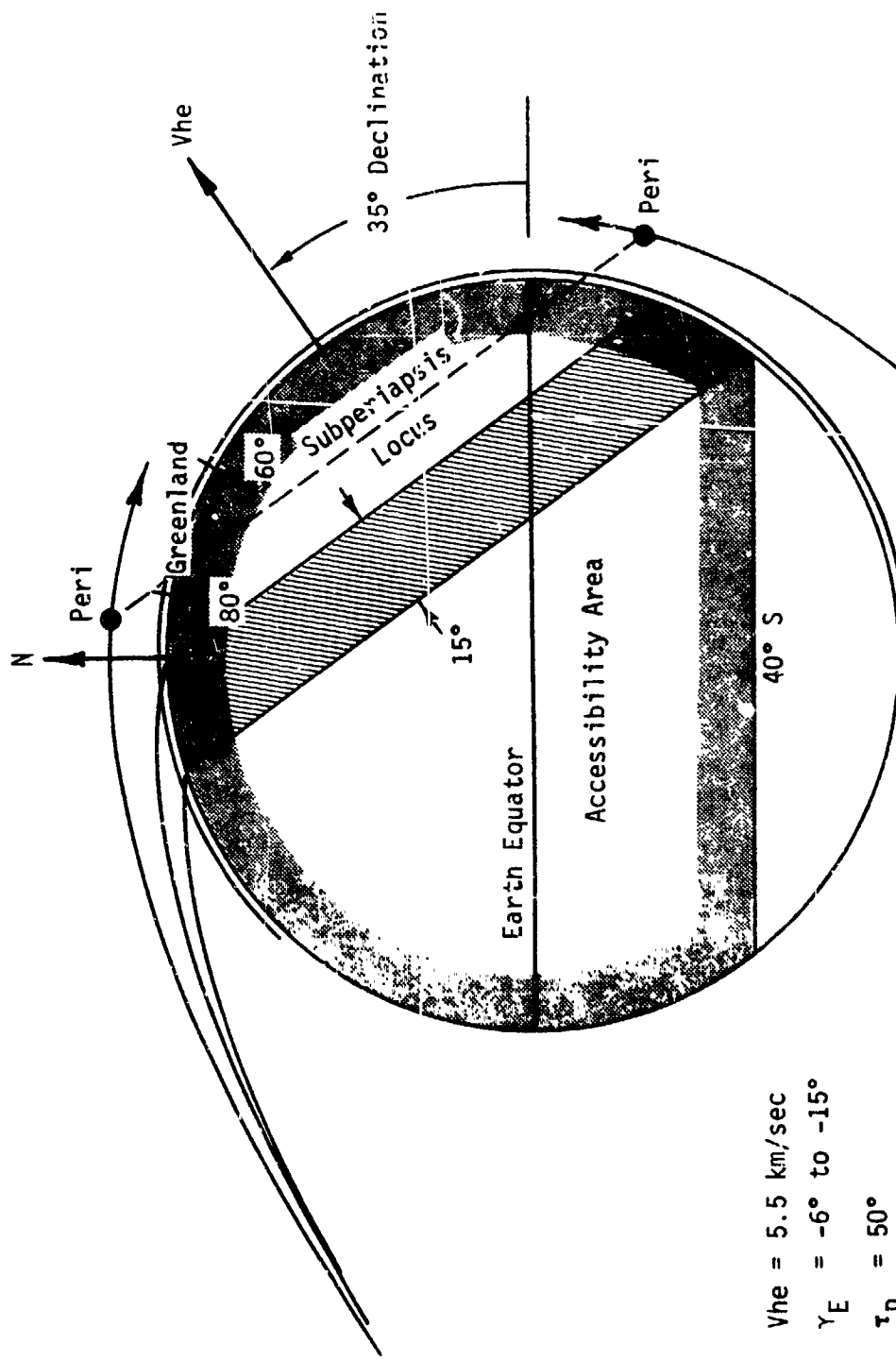


Figure II-5 Earth Return Landing Accessibility

## C. TRADEOFFS IN MISSION BASELINE DEFINITION

### 1. MOI and Capture Orbit Selection

In the context of extracting all available mission performance, toward the goal of enhancing weight allocations for ascent and rendezvous systems, Mars orbit insertion (MOI) was designed to offer both an energy-efficient orbital transfer and compatibility with rendezvous navigation. The sequence selected has been illustrated in Figure II-2, where the final transfer objective is a relatively low circular orbit. Use of a multiple-impulse transfer yields the desired performance and degree of flexibility.

An initial impulse ( $\Delta V_1$ ) achieves the primary capture at Mars into an orbit of 1000 km periapsis altitude, 0.9185 eccentricity, and 105 hour period. This capture orbit is held for about eleven days while landing and surface operations are performed, followed by MAV ascent and establishment of its circular rendezvous orbit. After orbit determination has resolved the actual MAV trajectory, the MOI sequence resumes, with the orbiter raising its periapsis ( $\Delta V_2$ ) to match the achieved MAV altitude. Plane of the orbit adjustments would be made from this highly eccentric ellipse. Finally, the orbiter trims apoapsis to the circular rendezvous altitude ( $\Delta V_3$ ), through one or a series of steps as required for proper time phasing of orbiter and MAV at final encounter. Additionally, it should be noted that a provision of extra  $\Delta V$  budget, totally 258 m/s, was made to account for midcourse corrections, finite burn loss, statistical  $\Delta V$ , and allocations for rendezvous and orbit trims.

Details of this sequence and its relation to navigation and rendezvous are further addressed in the section entitled "Navigation Aspects." From a purely performance standpoint, this approach is of value in moderating burn time durations and reducing burn loss. The only major concern existed in the area of Mars quarantine constraints, which would require that the initial capture orbit be stable for about 40 years. Before developing that condition, some mention must first be made of the philosophy behind the selection of orbit orientation for this baseline. In order to avoid a serious mismatch in orbital geometry at the opening of the Earth return window (about 14 months after MOI) an approach aim point was selected to achieve that particular inclination which contained not only the incoming,

but also the Mars-departure-to-Earth, Vhp asymptotes. The scheme is intended to reduce plane change requirements for return to a level no greater than that needed for minor trims. This select inclination ranges between  $42^{\circ}$  and  $45^{\circ}$  for the 1981 MSSR (defined in the Mars equatorial-vernal equinox system). For that capture orbit definition, with elements listed in the legend of Figure II-6, a periapsis altitude history is presented over a five-year period. Beginning with the design periapsis altitude of 1000 km, periapsis exhibits a rather orderly tendency to long term growth, a pattern which does continue throughout the period of quarantine concern. The stability analysis was performed with the aid of the lifetime program, ORBHIST (Ref. II-1).

## 2. Direct Entry Landing Trades

As definition of the 1981 direct entry baseline progressed, the requirement to modify the lander to contend with higher entry velocities and increased landed weights emerged as a principal control of the design. These modifications of the nominal Viking Lander spacecraft involved a number of systems, but none are considered radical departures from the basic vehicle. First, to partially compensate for the added weight of the MAV, nearly all systems superfluous to the basic objective of sample return were stripped from the lander. Second, to counter the increased aerodynamic loads with high direct entry velocities, the aeroshell and heat shield were allowed to grow in mass and thickness sufficiently to offset those conditions. Finally, the terminal descent propulsion was redesigned from a "blowdown" system to a pressure regulated propellant system, affording higher average thrust levels, shorter burn time, and hence more time and altitude for the parachutes to assist the descent.

Other departures from the nominal Viking mission plan involved trajectory constraints and considered atmosphere models. For the MSSR mission, a reduction of the terrain height uncertainty from 10,000 ft. to zero was accepted. Also assumed was the use of a mean Mars atmospheric model, rather than a spread of models. Both assumptions were considered more reasonable in view of the improved knowledge expected to be gained from the 1975/76 landing.

Given that background, the relationship between what nonpropulsive dry weight could be landed for varying system weights at entry interface

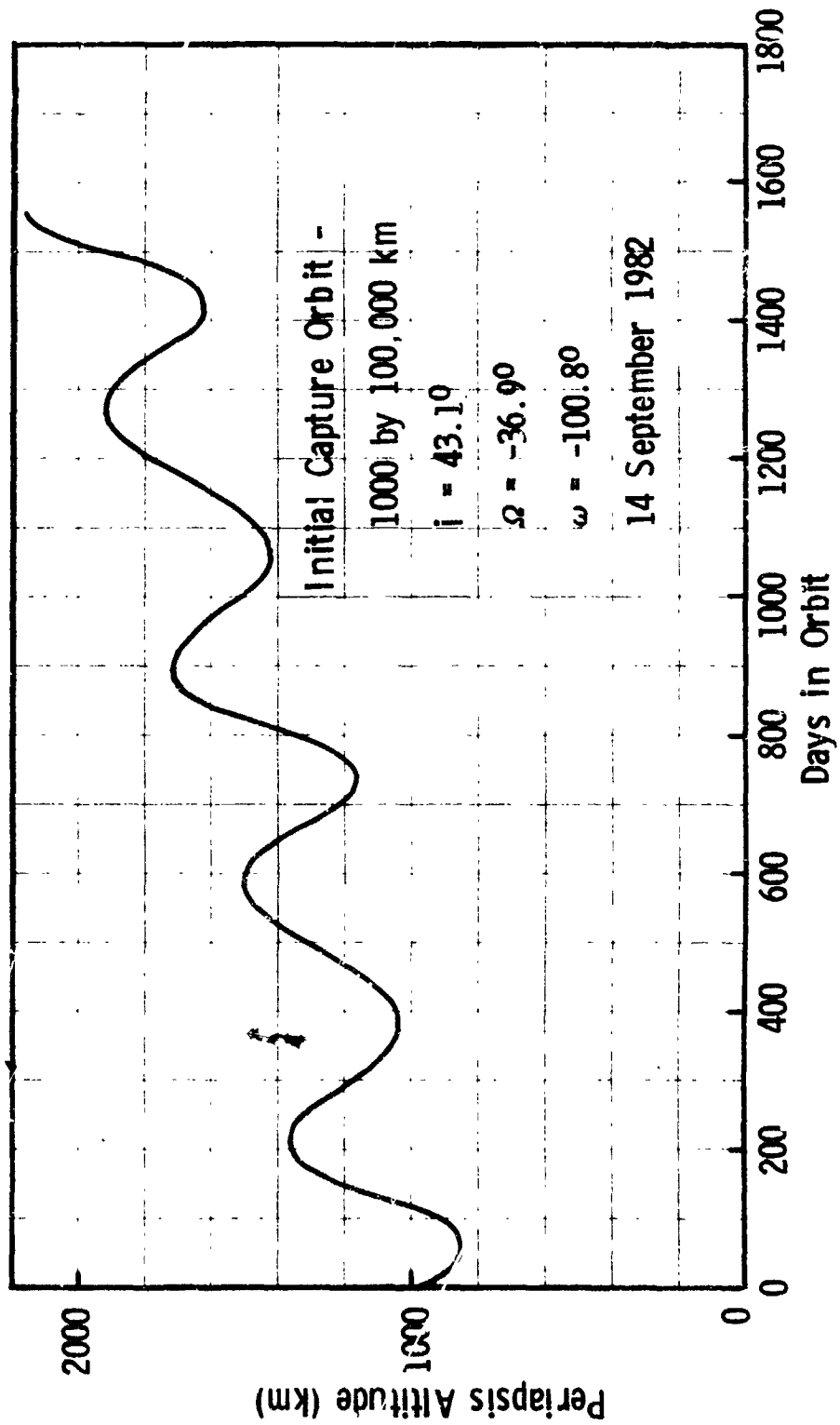


Figure II-6 Capture Orbit Stability

was developed, and is presented in Figure II-7. Entry corridor widths of  $2^\circ$  and  $4^\circ$  are compared by the two upper curves of the figure. With the wider corridor ( $4^\circ$ ) fixed to  $-17.6^\circ$  on the shallow end by the skipout constraint, steeper design conditions require a heavier aeroshell and, relative to the  $2^\circ$  corridor, reduce landed weight potential by 20 kg. Yet navigation analysis has indicated that onboard optical navigation would be necessary to achieve the narrow  $2^\circ$  corridor, while DSN tracking is adequate for  $4^\circ$ . Since inclusion of the optical system weight would diminish the increase in landed weight deriving from a shallower entry and add to the modifications required, the  $4^\circ$  corridor was accepted as a reference.

The lower curve in Figure II-7 is included only to illustrate the performance gain accruing from the pressure regulated lander propulsion system. Where "Lander Limits" are denoted, this refers to the maximum entry weight for which the descent thrust level and parachute deployment altitudes are acceptable.

An important characteristic of the direct entry landing mode for MSSR is the limited range of landing site accessibility available if the asymptote containment principle discussed earlier is accepted. Figure II-8 illustrates the situation for the select inclination (aimpoint) design, and for an unrestricted aimpoint case. A representative Vhp declination is chosen, with the periapsis locus noted by the dashed line. If inclination is restricted to the unique value of  $43^\circ$  dictated by containment, the  $4^\circ$  entry corridor maps into a  $5^\circ$  landing strip (arc) on the Mars surface, extending in latitude only from  $37^\circ\text{S}$  to  $39^\circ\text{S}$ . Adjusting the exact encounter time would allow this strip to be rotated  $360^\circ$  in longitude about the planet, while still providing only limited accessibility.

If inclination is not restricted by containment, only by the Vhp declination, then rotation of the incoming trajectory about the Vhp vector allows the  $5^\circ$  landing arc to be likewise rotated. This provides potential access to all latitudes between  $50^\circ\text{N}$  and  $85^\circ\text{S}$ , and again by timing encounter all longitudes can be accessed. This assessment of site accessibility is strictly shaped by the performance aspects of the 1981 MSSR Earth to Mars trajectory, and does not incorporate constraints which may arise from other design areas. Certain inclinations, for example, may require the

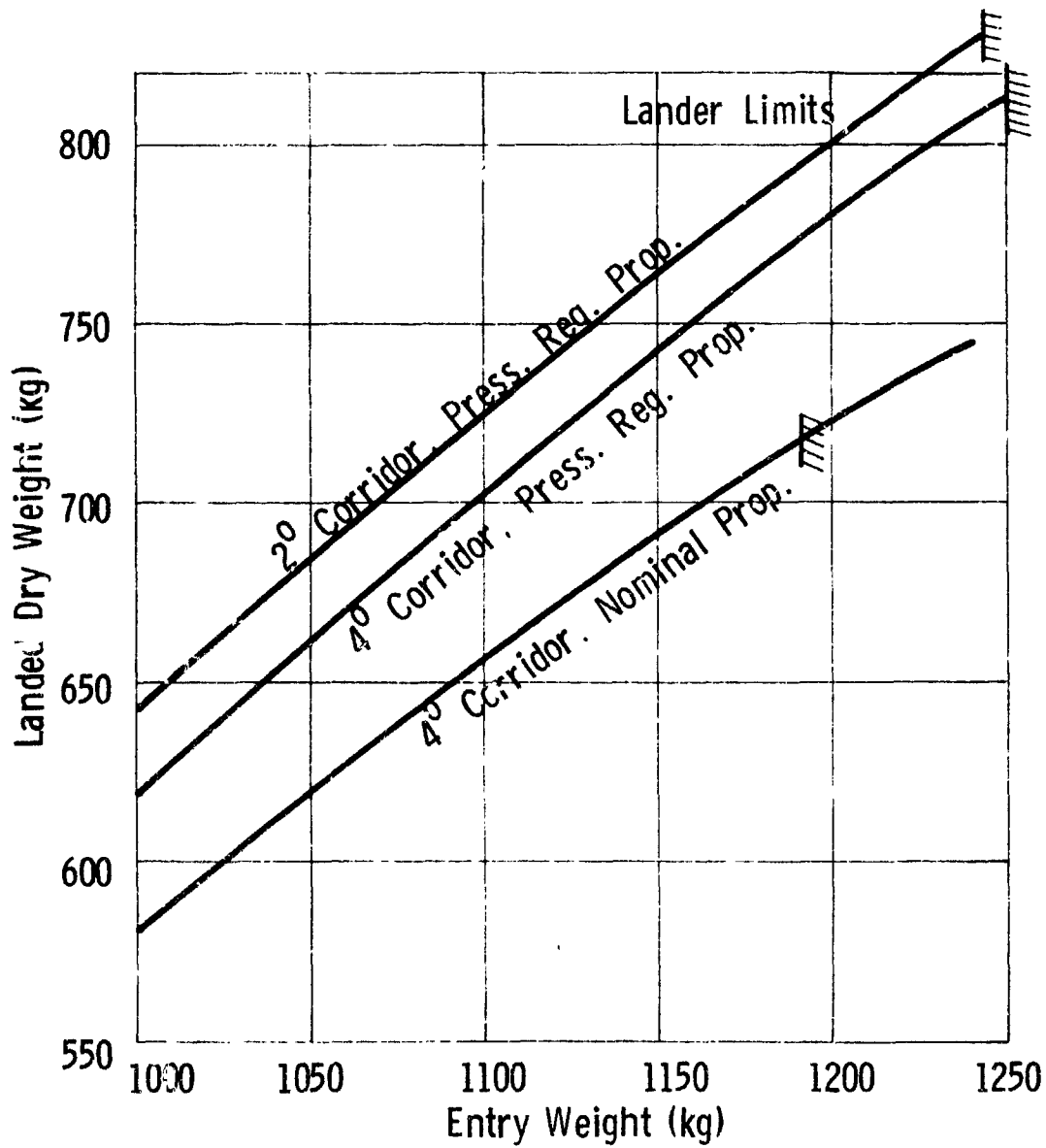


Figure II-7 Landed Weight Capability

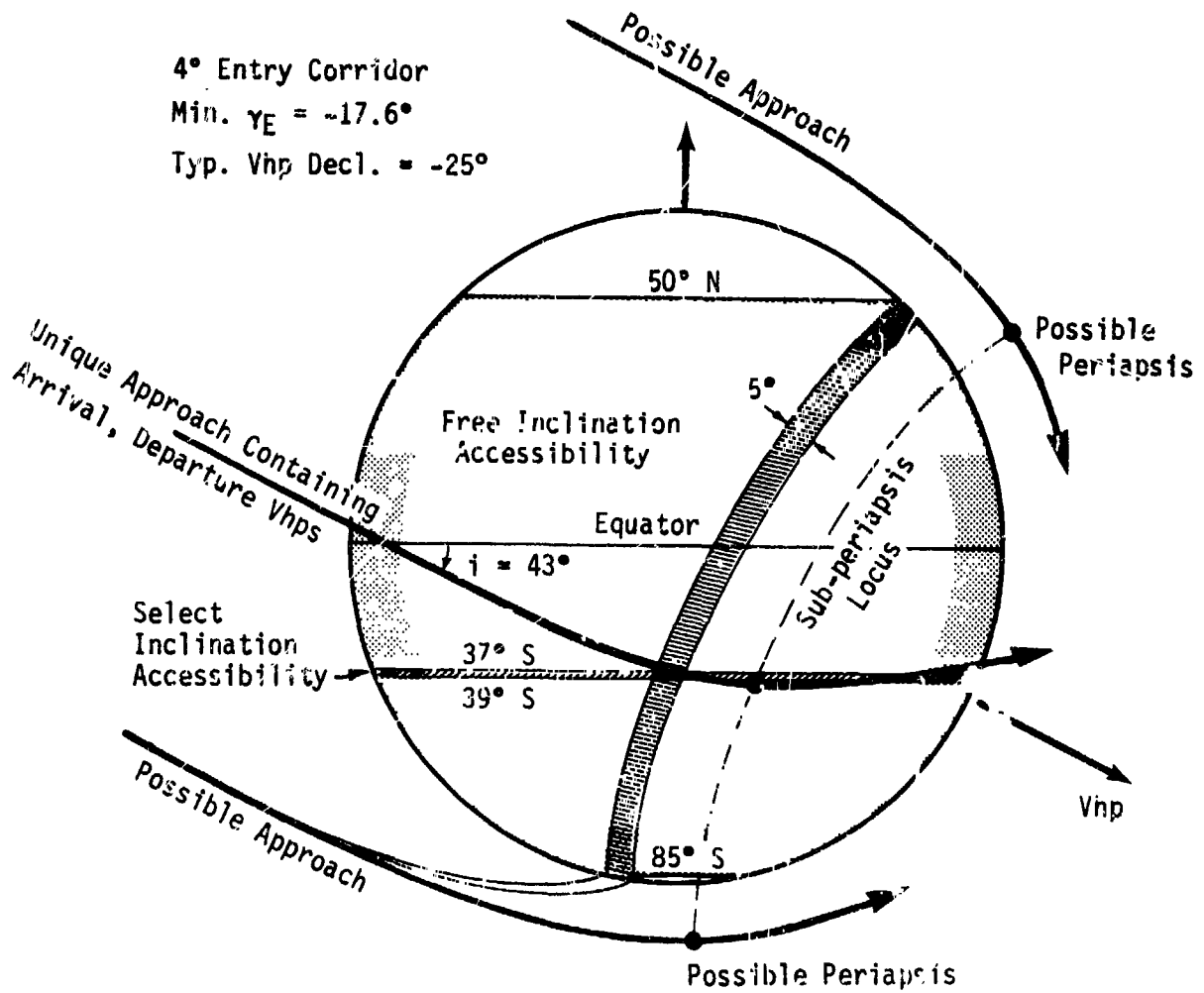


Figure II-8 Landing Site Accessibility

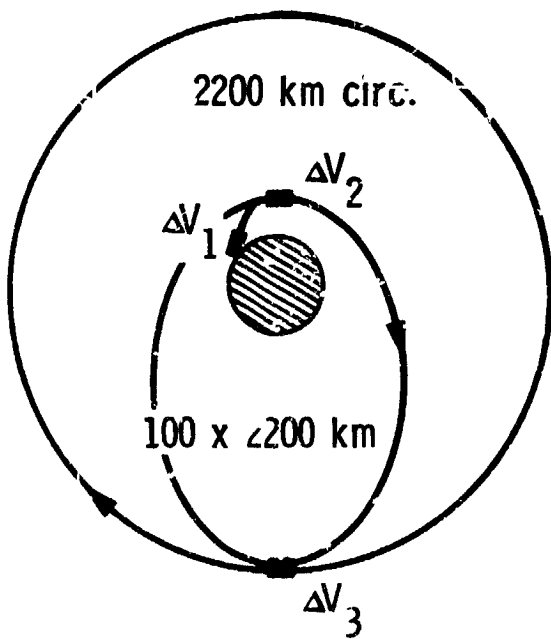
ERV to execute large plane change maneuvers in order to transfer to the return hyperbola. Without asymptote containment, this possibility exists to some degree for all aimpoint orientations and would need to be further examined to assess the impact on ERV design for particular landing sites. Dividing any large plane change requirement between TEI and MOI should also be examined for the complete analysis of site accessibility and system impact.

### 3. Mars Ascent Profile Selection

An integral part of the 1981 MSSR design development involves the selection of an efficient, reliable MAV ascent profile. Specifically treated is the question of how to deliver the most non-propulsive payload to a circular orbit of some altitude compatible with rendezvous, given a MAV which is constrained in size and weight by the external dimensions and performance of a minimally modified Viking Lander.

Of many possible approaches to the design of the ascent trajectory and staging philosophy for this situation, three options were examined in depth, i.e., analytically simulated and optimized by computer methods using the general optimization program POST (Ref. II-2). Figure II-9 illustrates two different ascent trajectory schemes, each designed to reach a final orbit of 2200 km circular. The first pictorial represents a "Hohmann Ascent" sequence, composed of three burns to three conics - 1) an initial boost to a ballistic trajectory that coasts to 100 km, 2) an impulse at 100 km to establish an elliptic orbit with a 2200 km apoapsis, and 3) a final circularization burn at apoapsis to achieve 2200 km circular. The sequence readily lends itself to a staged MAV of two or three propulsive units. This ascent profile was then evaluated for a three-stage MAV configuration, staged propulsion being solid-solid-liquid. A restartable final stage was necessary for the MAV to perform its rendezvous function. Solid stages were used due to their relatively easy adaptation to a staged, impulsive, fixed  $\Delta V$  application. (Solid performance assumed as follows:  $I_{sp} = 285$  sec, mass fraction = .88, thrust = 6672 n. Liquid performance:  $I_{sp} = 235$  sec, mass fraction = .4, thrust = 200 n.) A two-stage MAV configuration was also considered, staging being solid-liquid. In this case the solid stage executed the initial boost to 100 km, with the liquid

### Hohmann Ascent



### Steep Ascent

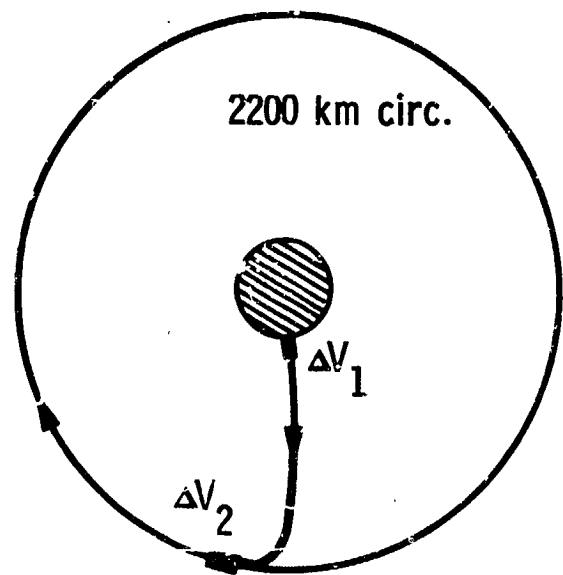


Figure II-9 Mars Ascent Vehicle - Staging Considerations

stage performing all remaining impulses. (Solid performance as before. Liquid performance:  $I_{sp} = 295$  sec, mass fraction = 0.7, thrust = 6672 n.) Each system was optimized in terms of trajectory profile and mass distribution, for a controlled liftoff MAV weight of 250 kg with identical terminal flight path conditions (2200 km circular). With performance measured by non-propulsive payload weight delivered to rendezvous orbit (including surface sample plus all supporting subsystems), the three-stage MAV achieved a payload of 18 kg, while the two-stage configuration achieved only 7 kg.

The second pictorial in Figure II-9 illustrates the third option considered. Here a two-stage MAV with performance similar to the above two-stage configuration is treated, but the initial solid stage boosts the vehicle directly to rendezvous altitude. At that point the second, liquid stage performs circularization. Optimization of this alternative trajectory profile for a 250 kg MAV disclosed a payload potential similar to the two-stage "Hohmann Ascent", of 8 kg, still far below that achieved by the three-stage MAV.

The obvious performance superiority of the three-stage, "Hohmann Ascent" concept led to the incorporation of this design as an important part of the baseline. Interaction of this approach with rendezvous navigation and integration of the ascent vehicle with the Viking Lander will be discussed later.

#### 4. Rendezvous Orbit Selection and MAV Sizing

All performance aspects of the various mission phases which have been described to this point set the stage for what is the primary design trade of the 1981 direct entry MSSR baseline. From what is available in terms of launch weight for the 1981 opportunity, certain relatively inflexible weight allocations must be assigned to various systems such as the orbiter bus (530 kg), the ERV (261 kg), the basic dry lander (446 kg) excluding the MAV, and to vehicle adapters and launch vehicle peculiarities. A typical allocation is listed in Table II-4. The remaining reservoir of weight can then be distributed, within limits, between the orbiter propulsion system and the total Lander/MAV complex. It is this distribution which lends itself to performance optimization, and serves to control MAV sizing and selection of the rendezvous orbit altitude.

Table II-4. Typical Weight Distribution for a 1981 MSSR

Launch Weight	4409 kg	
Adapters, Bioshield, LVMP	306	
Spacecraft at MOI	2878	
Orbiter Bus	530	
ERV	261	
Orbited Weight Margin	134	} $\Sigma = 3327$
Propellant	1631	
Prop Inerts	262	
Lander/MAV at Separation	1285	
Expendables (all)	509	
Basic Dry Lander	446	
MAV	290	
Launcher	40	

Since the critical objective of this approach to MSSR involves bringing together the MAV and Orbiter/ERV in a coincident orbit, that orbit must be selected which places the most reasonable demands on each vehicle given their respective complexities, enhances the likelihood of mission success, and ideally maximizes the payload weight which is delivered from the surface. Drawing from the given weight reservoir, as that weight is increasingly allocated to enhance the orbiter propulsion system, lower rendezvous orbit altitudes become possible. Although the Lander/MAV weight allocation is correspondingly reduced, the lower rendezvous orbit eases requirements on MAV ascent propulsion. On the other hand, distributing more weight to the Lander/MAV could possibly yield a more reasonably sized Mars launch system which could deliver a larger payload to a higher rendezvous orbit.

The nature of this trade is illustrated by Figure II-10. In the upper curve labeled "Entry Weight" can be seen the quantified effect of trading weight between the Lander/MAV and orbiter propulsion (trading MAV weight against orbit altitude). Curves below "Entry Weight" translate the landing spacecraft through entry to weight on the surface. Subtracting the

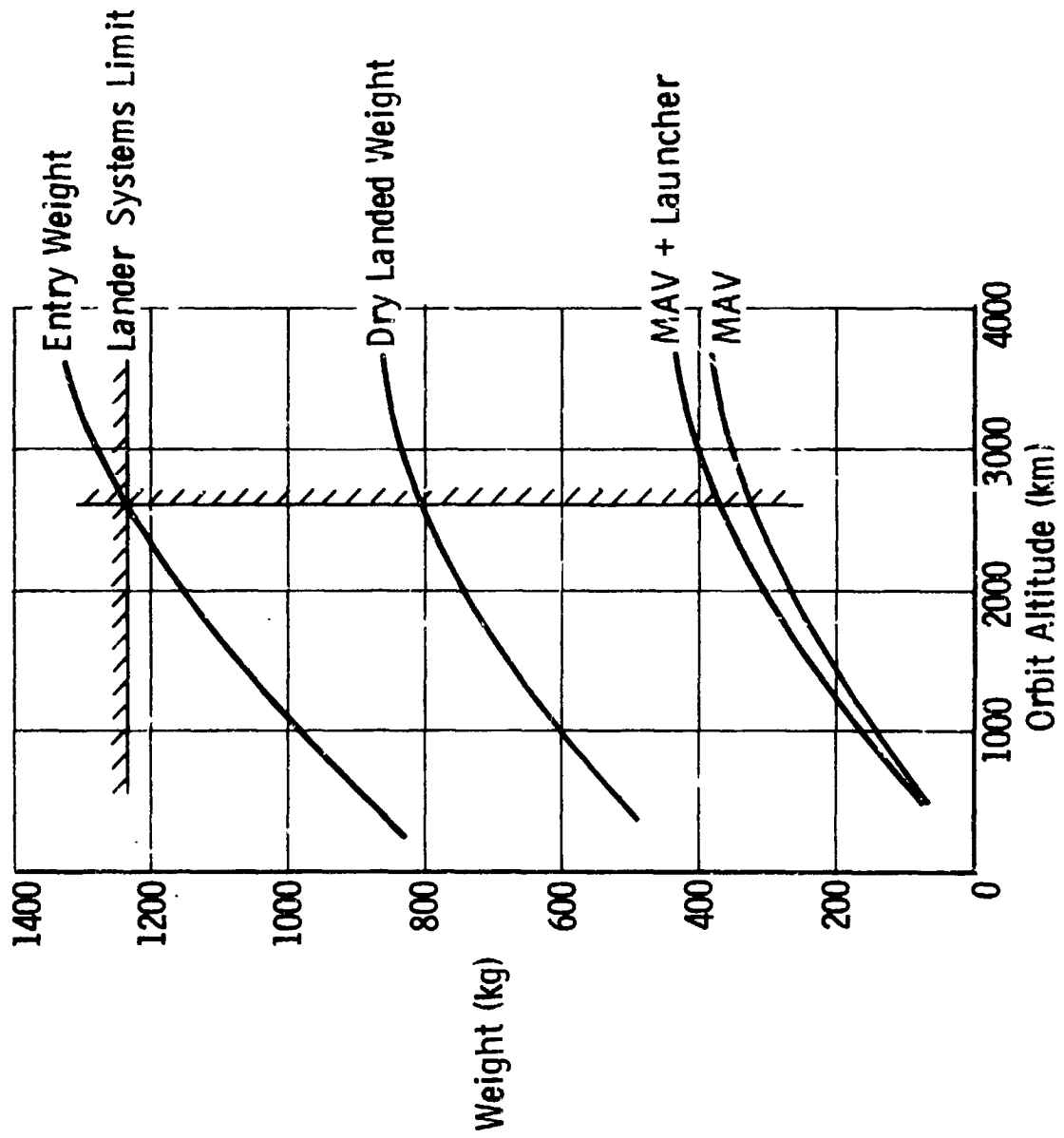


Figure II-10 Landed Weight vs Rendezvous Orbit Altitude for 1981

446 kg basic lander from "Dry Landed Weight" leads to weight available for the MAV and its launch mechanism, of which about 88% can be assigned to the MAV alone.

Limits to this design trade exist on both ends. A maximum weight for the Lander/MAV at entry of 1250 kg, derived from lander system limits mentioned earlier, bounds the MAV to a maximum of 325 kg. Orbit altitude is in turn constrained to values above 1500 km, a condition which reflects the lowest orbit from which the ERV propulsion (in the 263 kg ERV preliminary design) can effect a return-to-Earth. These bounds are better illustrated by Figure II-11, which summarizes all basic elements of the trade. (It should be mentioned here that this plot is representative of the analysis involved in MSSR performance optimization, and although it may differ in small degree from the most recent weight derivations, the analysis itself and derived conclusions for 1981 remain valid.)

In Figure II-11 the curve "Performance Limit" represents possible combinations of MAV weight and rendezvous orbit altitude resulting from the distribution of all available weight in the "reservoir". Points on this curve use full mission capability. Points above the curve are possible and would provide weight margin, while points below the curve cannot be achieved. The "ERV Limit" establishes a 1500 km minimum orbit altitude, and the "Landed Weight Limit" bounds MAV weight to values under 325 kg. If full mission performance is exploited, the range of possible design solutions would extend from a "light MAV" of 215 kg with rendezvous at 1500 km, to the "heavy MAV" of 325 kg and rendezvous at 2600 km.

Remaining to be resolved, then, in some way to evaluate this range of possibilities, to converge on an optimum. Drawing from the analyses of MAV ascent profiles discussed earlier, the sensitivities of final stage payload weight to both MAV liftoff weight and desired orbit altitude could be approximated for the three-stage configuration. These sensitivities were found to be greatly influenced by the assumptions made for the propulsion mass fractions and other inert weight requirements, but nevertheless allow deductions to be made for the specific optimization problem. Sensitivity of Stage III non-propulsive payload to liftoff weight is about

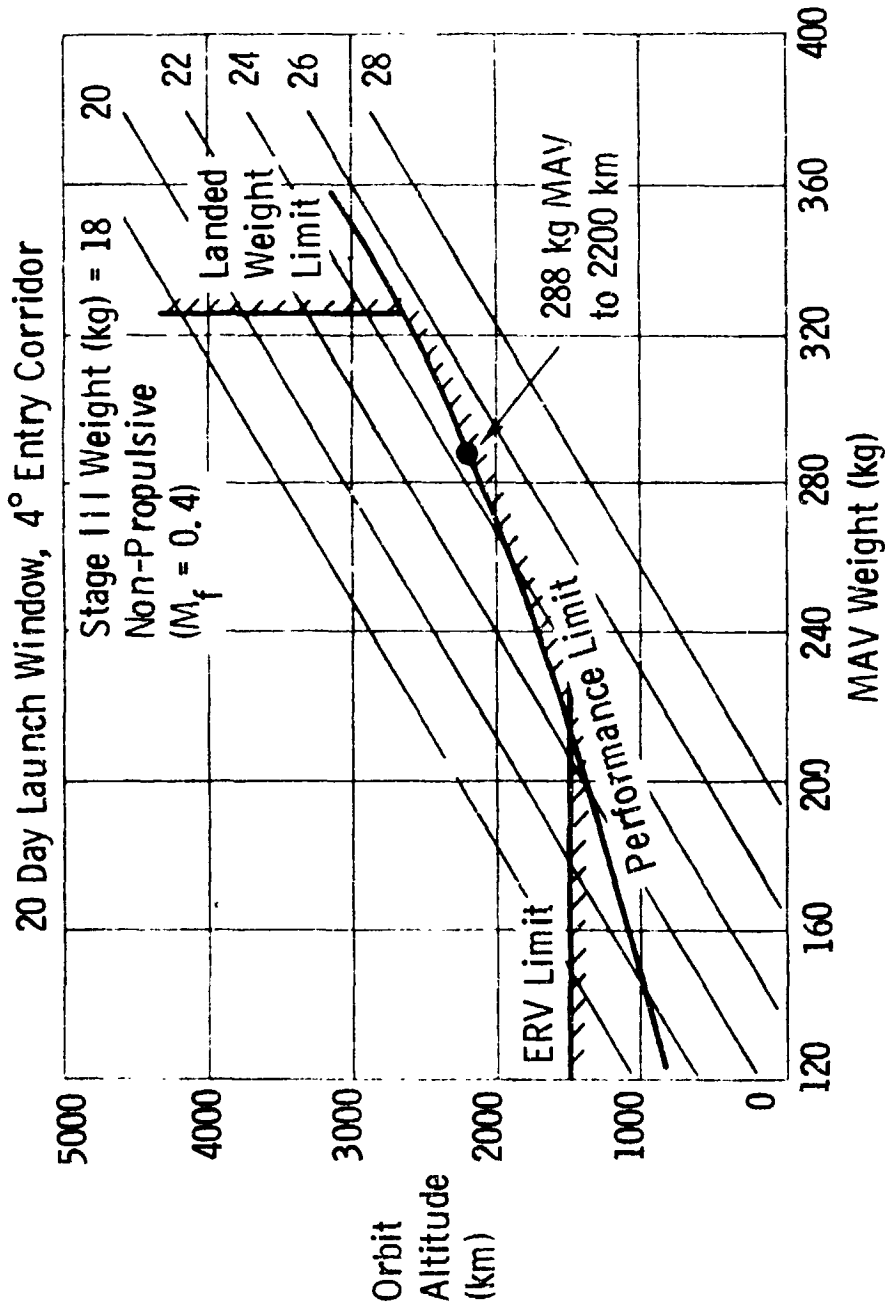


Figure II-11 MAV Performance Design Trade for 1981

+0.07 kg/kg, and of payload to orbit altitude about -0.005 kg/km. A one kilogram increase in non-propulsive payload could therefore be gained by either a 14 kg increase in MAV liftoff weight, or by a 200 km reduction in rendezvous orbit altitude.

Using these sensitivities, a linear approximation of payload "contours" has been superimposed over the design curves in Figure II-11. The resulting relationship of the performance curve with payload potential indicates payload is maximized for the "heavy MAV" solution. From purely a performance view, the optimal choice for the MAV weight vs. altitude trade would be the 325 kg MAV to 2600 km, bumping the lander systems boundary, and achieving 25 kg payload.

At this juncture of the study, factors involved with configuration integration intervened. The size of the larger MAV with respect to the external Viking Lander dimensions presented somewhat difficult integration problems. Noting from Figure II-11 the relative flatness of payload with respect to MAV weight at the heavy end of the performance curve suggested that a backoff position, with reduced MAV weight (and size), would yield only a small compromise in final payload. Given this interplay of performance and configuration analyses, a compromise design evolved. MAV containment within the lander could be demonstrated for a MAV weight of 288 kg, which, using full mission performance, would correspond to a 2200 km rendezvous orbit. Loss in payload potential for this compromise position would be only 1 kilogram, from 25 kg to 24 kg, which was considered acceptable. This mission scenario, of a three-stage MAV sized to about 288 kg, with rendezvous occurring in a 2200 km circular orbit following a Hohmann ascent, was therefore accepted as the reference for the MSSR feasibility assessment of orbital rendezvous and docking.

Specific mass figures quoted in this section for MAV stages are especially for MAV third stage payload are representative of system design characteristics assumed for the performance analysis. Since these system characteristics evolved continually during the course of our study, direct mass comparisons with other chapters, particularly Chapter VI, will show slightly lower vehicle masses for the final MSSR spacecraft design.

#### D. MISSION ANALYSIS SUMMARY

The baseline mission suggested for a 1981 MSSR involving rendezvous and docking in Mars orbit, when constrained to a single launch Titan IIIE/Centaur, includes the direct entry landing of a Mars Ascent Vehicle. Modifications to the '75 Viking Lander are required to accommodate the MAV, but these mods appear to be of a reasonable nature. An Orbiter/ERV configuration inserts, by way of a multiple-impulse transfer, into a final circular rendezvous orbit of 2200 km altitude. After sample acquisition, the MAV begins its ascent sequence. In three stages, the MAV first boosts to 100 km on a parabolic trajectory. A second stage then burns to achieve a 100 by 2200 km ellipse. At apoapsis of that orbit, the third stage (liquid propulsion) executes a circularization burn to achieve the rendezvous orbit.

From this point rendezvous, docking, and sample transfer are accomplished following a series of phasing orbits. The MAV is jettisoned and the Orbiter/ERV continue in parking orbit until the Earth return window opens in November 1983. Then the ERV and Orbiter separate, and the ERV begins a multiple-impulse Trans-Earth Insertion to the return hyperbola, in a manner approximately the reverse of MOI. In October 1984, Earth is encountered, and the Earth Entry capsule is separated from the ERV for its final descent through the Earth's atmosphere.

## E. ALTERNATIVE MISSION CONCEPTS

Three mission options for Mars sample return in 1981 are illustrated and compared in Figure II-12. The first option requires either dual Titan IIIE/Centaur launches, or the availability of a Shuttle launch. One Viking-derived spacecraft essentially follows the VO '75 mission plan, but delivers out-of-orbit a lander modified to carry a MAV. A second Viking-derived spacecraft carries an Earth Return Vehicle (ERV) into the final rendezvous orbit required to mate the MAV and ERV for rendezvous, docking, and sample transfer. Orbiter propulsion growth for both spacecraft is about 5% beyond nominal Viking. In the second mission option illustrated, all spacecraft elements (orbiter, ERV, Lander/MAV) are carried first into a four-day orbit from which the landing is accomplished. Orbiter and ERV then transfer to the rendezvous orbit. This scenario requires the heaviest single spacecraft, and depends upon Shuttle launch performance. The third option, our presented baseline, derives from the performance capability of a single Titan IIIE/Centaur launch. Landing is performed from a direct entry trajectory at Mars, and the Orbiter/ERV insert into the final rendezvous orbit after a multi-impulse transfer. Orbiter propulsion growth is about 15% above nominal Viking. This system is essentially a modified VO '75 spacecraft. To fully exploit the greater launch weight available with the first two options, requiring dual Titan IIIE/Centaur launch or Shuttle, both the Mars Lander and Mars entry vehicle would require modifications to the Viking '75 derived systems considerably greater than those identified in this study.

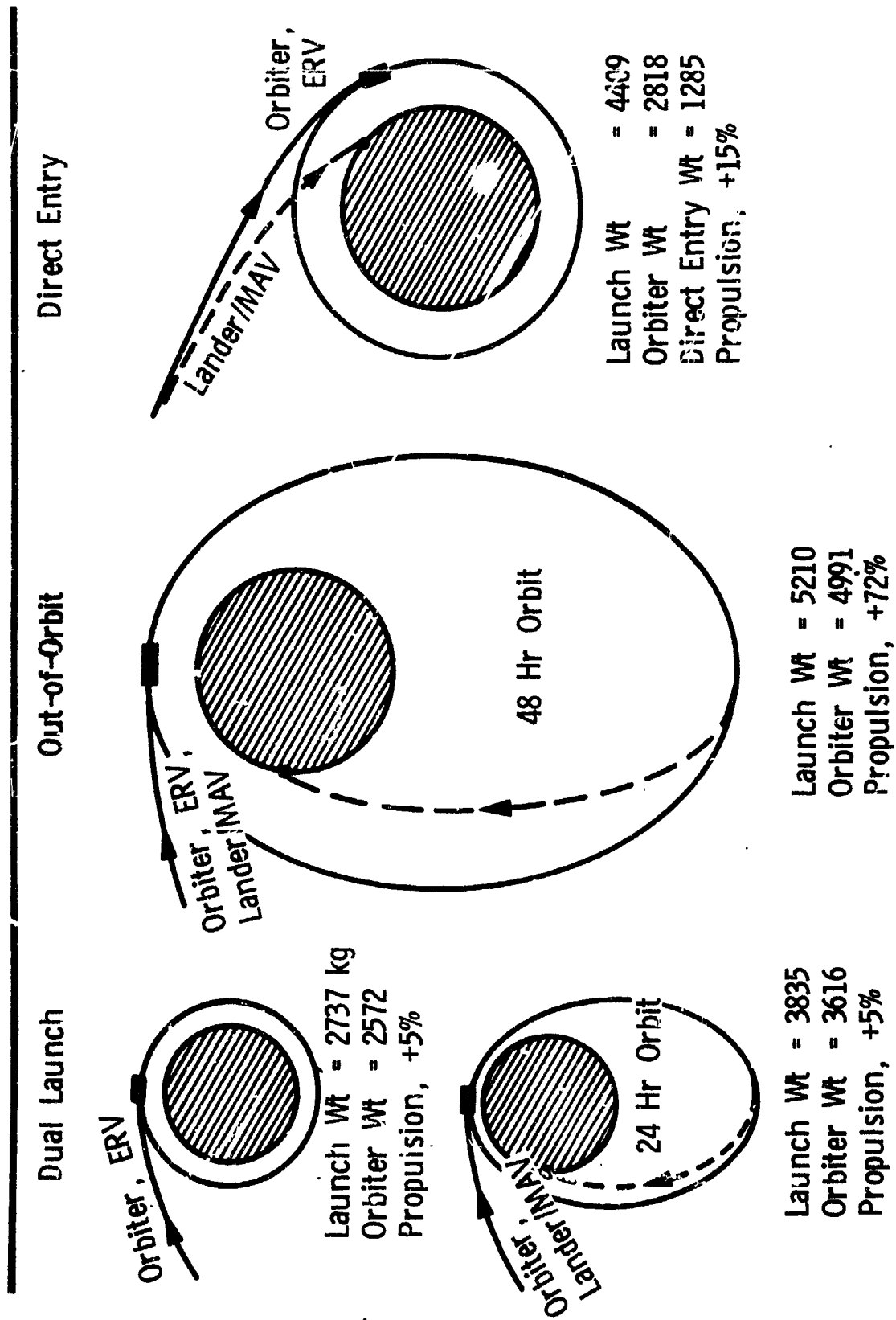


Figure II-12 Alternative Mission Concepts and Design Impact (1981)

## REFERENCES

- II-1. Vogt, E. D., "Science and Mission Analysis for Planetary Exploration," Final Report for Task D-23R, Appendix G, December 1973.
- II-2. Brauer, G. L., Cornick, D. E., et al, "Program to Optimize Simulated Trajectories (POST)", Final Report for Contract No. NAS1-12165, for LRC, NASA, October, 1973.

### III NAVIGATION ASPECTS OF ASCENT, RENDEZVOUS AND DOCKING

The MSSR mission described herein utilizes a so-called "slow" rendezvous profile as opposed to a "fast" direct ascent-to-rendezvous mode. The slow rendezvous is considered more reliable and can be performed with a relatively simple open loop guidance and control package for MAV ascent. Once the MAV has circularized, it assumes a passive role as far as orbital maneuvers are concerned. Only the Orbiter is active in the rendezvous sequence from then on. The Orbiter activity is composed of two phases: an initial Earth-controlled phase and an automatic terminal phase. The Orbiter is maneuvered under Earth control until conditions for terminal rendezvous initiation are satisfied--then the automatic system takes command.

The initial rendezvous segment has a coarse phasing adjustment provided by the maneuver designated "Orbiter phasing" and a fine phasing adjustment resulting from the "circular trim sequence." Very accurate "knowledge" of the MAV/Orbiter relative state (position and velocity) is required to target the circular trim sequence. This information is provided by sequential filtering of multi-vehicle Differential Very Long Baseline Interferometric (AVLBI) data. To obtain this type of data both vehicles must be simultaneously visible to the DSN. This is the function of the "Orbiter phasing" maneuver. In the study the latter maneuver is computed with orbit estimates derived from conventional Doppler range rate data.

This section of the final report deals with the navigation aspects of the MSSR mission as a whole and particularly with the initial Earth-controlled portion of the rendezvous.

The reference mission was simulated by Monte Carlo methods in order to test the mission design and maneuver strategies for trajectories dispersed by random maneuver execution and orbit determination (O.E.) error. The limiting effect of these errors on the "controllability" of the MAV/Orbiter relative state at a fixed MAV orbital position was examined. These dispersions in the actual state from the reference are generally referred to as "control" dispersions because they measure the ability to control the state to the reference. On the other hand, deviations in the estimate of state from the actual state are referred to as knowledge dispersions. In addition to relative state dispersions other simulation outputs of particular interest

are orbital dispersions, pointing errors and the statistical  $\Delta V$  quantities (denoted as  $\Delta V_{stat}$ ). The latter is defined as the amount by which the 99 percentile  $\Delta V$  exceeds the nominal  $\Delta V$ . This quantity is then the amount of  $\Delta V$  which must be budgeted above nominal so that 99% of the time there will be enough  $\Delta V$  to perform the mission. The ultimate success of the Earth-controlled portion of the mission will hinge on the simultaneous acceptability of (1)  $\Delta V_{stat}$  loads, (2) dispersions at terminal rendezvous initiation (TRI) and (3) orbiter trajectories for planetary quarantine. Part A of this chapter will present navigation analysis results for five mission segments defined below; Part B reports on the sensitivity of mission performance to navigation techniques and parameters; and Part C provides an assessment of overall MSSR mission feasibility from a navigation standpoint.

## A. NAVIGATION RESULTS FOR MISSION PHASES

The MSSR mission, from Mars encounter to terminal rendezvous initiation, is for simplicity divided into 5 segments or phases. These are: 1) Orbiter Capture to MAV Ascent, 2) MAV Ascent to MAV Circularization Trim, 3) Orbiter Periapsis Change to Orbiter Circularization to First Occultation Exit, 4) First Occultation Exit to Start of Circular Trim Sequence and 5) Circular Trim Sequence through 10th Occultation Exit. Each mission phase is first described in conjunction with a figure having key events numerically called out. A brief discussion explaining the mission design and key parameters precedes the presentation of results for that mission phase.

### 1. Mission Phase #1 - Orbiter Capture to MAV Ascent

#### Description. (See Figure III-1)

#1) The orbiter performs a fixed attitude Mars Orbit Insertion (MOI) maneuver targeted to achieve an orbit with semi-major axis  $a = 53893.4$  km (nominally the 1000 x 100,000 km capture orbit). This requires a finite burn of  $\Delta V_{MOI} = 1116$  m/s. The Lander touches down near periapsis.

#2) The Orbiter state vector is updated on Earth, based on approximately 1-1/2 orbits of conventional DSN Doppler data.

#3) The Orbiter performs a coarse plane change maneuver  $\Delta V_{pc}$ , if required, to contain the outgoing hyperbolic excess velocity vector (VHE). This occurs at the 2nd apoapsis.

#4) Final determination of orientation of Orbiter plane of motion prior to MAV liftoff. Based on a 1 orbit of conventional DSN Doppler data.

#5) MAV liftoff when Orbiter at 3rd apoapsis.

Discussion. The approach tracking period and deflection maneuver time are shown in Figure III-2. Tracking data from E-30d to E-10d is used to target the last midcourse correction at E-10d. The orbit determination (O.D.) accuracy at this time limits the orbit control capability for deflection and MOI maneuvers. Tracking data for determination of the deflection maneuver is taken from E-30d to E-18h since 12 hours are required for O.D. processing and maneuver computation.

State accuracies at this time point represent the knowledge available to target deflection. Tracking down to E-12h may be used to target the MOI

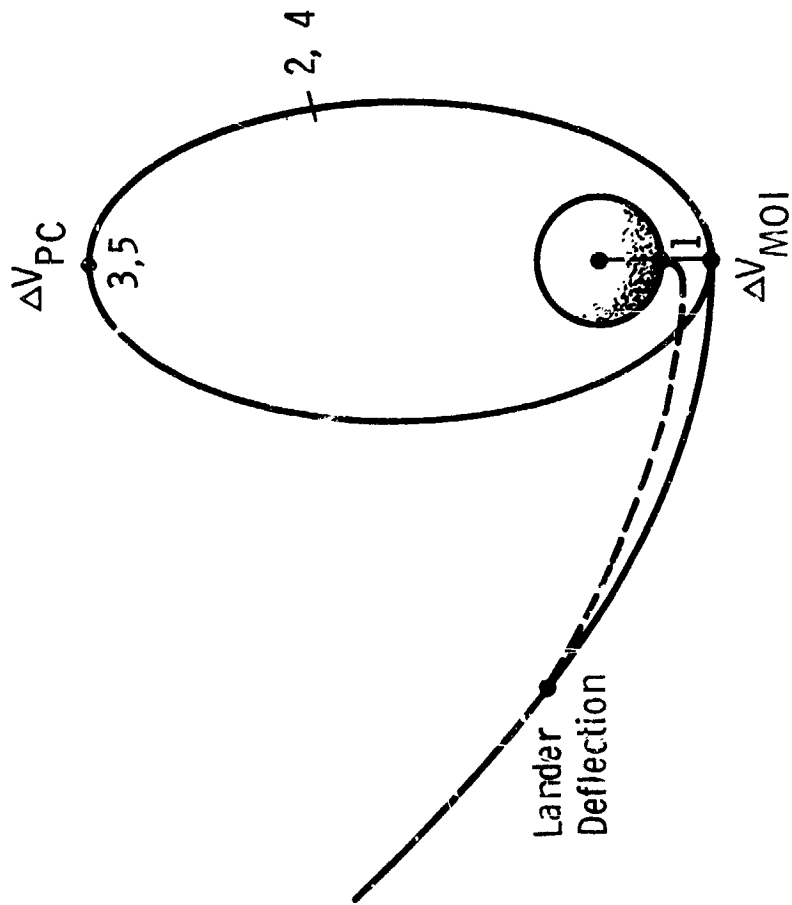
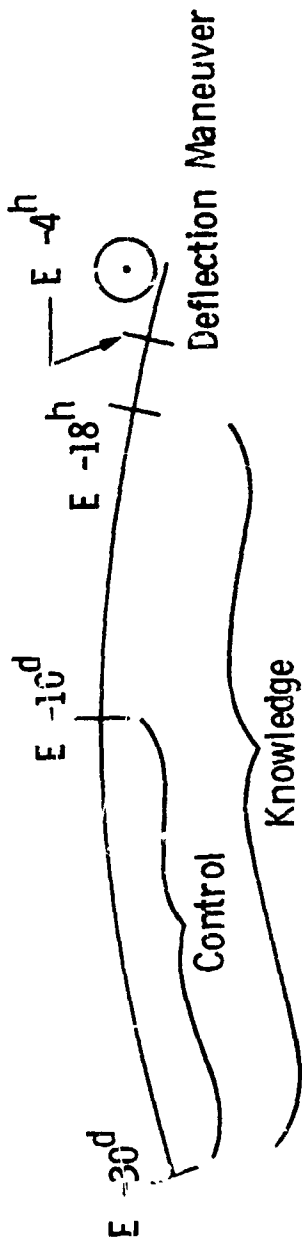


Figure III-1 Mission Phase #1 - Orbiter Capture to MAV Ascent



B Plane Error Ellipse

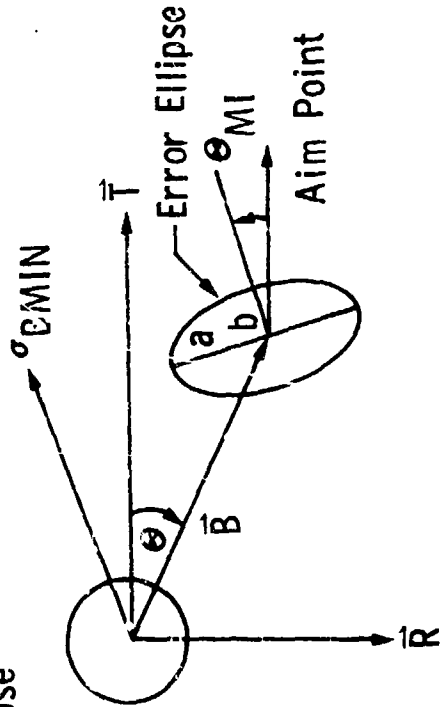


Figure III-2 Approach Geometry

maneuver. Statistics of state dispersions are represented by the B-plane error ellipse centered at the nominal B (impact) vector. The orientation of this ellipse is specified by the angle  $\theta_{MI}$ . Note that the smallest dispersions in the B-vector magnitude occur when the B-vector is oriented along the ellipse minor axis (b). This approach  $\theta_{AIM}$  (i.e.  $\theta_{AIM} = \theta_{MI}$ ) will therefore yield the smallest entry flight-path-angle ( $\gamma$ ) dispersions. A Monte Carlo simulation of the deflection maneuver computation and execution was used to determine entry control capability. A separate simulation was used to determine the  $\Delta V_{STAT}$  requirement for the Orbiter maneuver sequence through circularization. These include MOI, periapsis altitude adjust (HP) and circularization (CIRC). The dispersed approach periapsis altitude, unaltered by MOI, is assumed to be adjusted back to nominal (2250 km) prior to circularizing at that altitude. As will be seen later this is an approximation to the actual maneuver strategy.

The computation was performed assuming only encounter control and knowledge uncertainties and maneuver execution error. B-plane control and knowledge statistics are as shown in Table III-1. An optimal set of MOI burn controls ( $\alpha$ ,  $\beta$ ,  $t_B$ , TA) is computed based on the pre-encounter state estimate for each dispersed Monte Carlo case. The actual state is then integrated through the burn to produce the capture orbit. A similar technique is used to target the circularization burn except for this computation no knowledge error is assumed (i.e. estimate = actual state). Statistics of total  $\Delta V$  are computed for the three maneuvers and  $\Delta V_{STAT}$  output as the 99 percentile sample less the nominal  $\Delta V$ .

Table III-1 Representative Control and Knowledge Uncertainties Expressed in B-plane System

Control: $\delta X_A = X_A - X_E$			
Knowledge: $\Delta X_E = X_E - X_A$			
	$\sigma_{B \cdot R}$	$\sigma_{B \cdot T}$	$\theta_{SMAA}$
Knowledge	210. km	60. km	90°
Control	227. km	101. km	97°

Results. Tables III-2 through III-5 contain results for Mission Phase #1. As shown in Table III-2, a 25 km B-plane control and knowledge ellipse semi-minor axis (sized by Mars ephemeris error) allows for a .88° corridor

width. Here it is assumed that the approach B-vector lies along the minor axis direction. The 4-hour deflection time was set by Lander power considerations.

Table III-2 Lander Deflection Summary

Deflection Time	Nominal Maneuver	$\Delta\gamma_{STAT}$	$\Delta V_{STAT}$
4 hours (Range = 53500 km)	83.9 m/s	.88°	1.6 m/s

The total Orbiter fuel budget required to perform MOI, raising of periaxis and circularization is 2192.3 m/s, made up in part by a  $\Delta V_{STAT}$  component of 37.5 m/s (Table III-3). The total Orbiter  $\Delta V_{STAT}$  load will be 37.5 m/s plus the  $\Delta V$  requirement for the circular trim sequence used to "catch" the MAV. The MOI  $\Delta V_{STAT}$  is due primarily to positive dispersions in the approach hp. If the MOI strategy targeted to the nominal  $h_a$  instead of the nominal semi-major axis it would be possible to reduce  $\Delta V_{STAT}$  for the CIRC maneuver to the execution error level.

Table III-3 Orbiter  $\Delta V_{STAT}$  Summary

	Nominal $\Delta V$	$\Delta V_{STAT}$
MOI	1115.9 m/s	28.7 m/s
HP	22.0 m/s	6.1 m/s
CIRC	1054.4 m/s	22.0 m/s
Total	2192.3 m/s	37.5 m/s

Table III-4 presents ninety-nine percentile (99%) capture orbit dispersions for representative E-plane uncertainties. Capture orbit  $h_p$  dispersions are corrected by the HP maneuver whereas period variations are accounted for implicitly in the phasing orbit computation. Inclination and nodal errors affect the time and azimuth of MAV ascent. Since  $h_p$  will not be dispersed down by more than 200 or 300 km, the orbit stays well out of the sensible atmosphere and has been shown to satisfy planetary quarantine requirements. Capture orbit O.D. results are found in Table III-5. Systematic error parameters considered in the analysis are correlated station locations (at the 3m, 5m, 15m level), and Mariner 9 defined Mars gravity field uncertainties. Results are extremely good when data is discarded on either side of periapsis.

Table III-4 Capture Orbit Dispersions

	Nominal	99%	99% Δ
Period	106.4 hrs.	$\frac{-132.8 \text{ hrs.}}{83.0 \text{ hrs.}}$	$\frac{+26.4 \text{ hrs.}}{-23.4 \text{ hrs.}}$
$h_p$	1000 km	$\frac{1394.0 \text{ km}}{762.9 \text{ km}}$	$\frac{+394.0 \text{ km}}{-237.1 \text{ km}}$
$\Omega$	$323.3^\circ$	$\frac{-327.6 \text{ deg.}}{319.7 \text{ deg.}}$	$\frac{+4.3 \text{ deg.}}{-3.6 \text{ deg.}}$
$i$	$42.5^\circ$	$\frac{-45.4 \text{ deg.}}{40.0 \text{ deg.}}$	$\frac{+2.9 \text{ deg.}}{-2.5 \text{ deg.}}$

Table III-5 Capture Orbit O.D. (1σ Uncertainties)

Period	HP	INC	$\Omega$	$\omega$	T ≠ TP
10.0 sec	.08 km	.003°	.004°	.003°	9.6 sec

2. Mission Phase 2 - MAV Ascent to MAV Circularization Trim

Description. (See Figure III-3)

#6) The two MAV solid rocket stages inject the liquid third state into a 100 x 2200 km orbit (period = 2.58 hours). Liftoff is at an initial ramp angle  $\theta_0$ . A constant pitch rate  $\dot{\theta}$  is initiated after 2 seconds of thrust to approximate the gravity turn pitch profiles.

#7) After 8 orbits of conventional Doppler tracking by the DSN the MAV injected orbit and circularization maneuver are computed. Since 12 hours are allowed for computation time the maneuver is not loaded onboard the MAV until the 12th orbit.

#8) The circularization burn is performed (nominal  $\Delta V_{CIRC} = 337.3 \text{ m/s}$ ) at 12th apoapsis.

#9) Another state vector update and trim  $\Delta V$  (RECIRC) is computed after 4 more orbits of conventional Doppler.

#10) The 2nd attempt to circularize the orbit is made at the next apoapsis.

#11) Final MAV update, based on 4 more orbits of data required for Orbiter periapsis adjust maneuver.

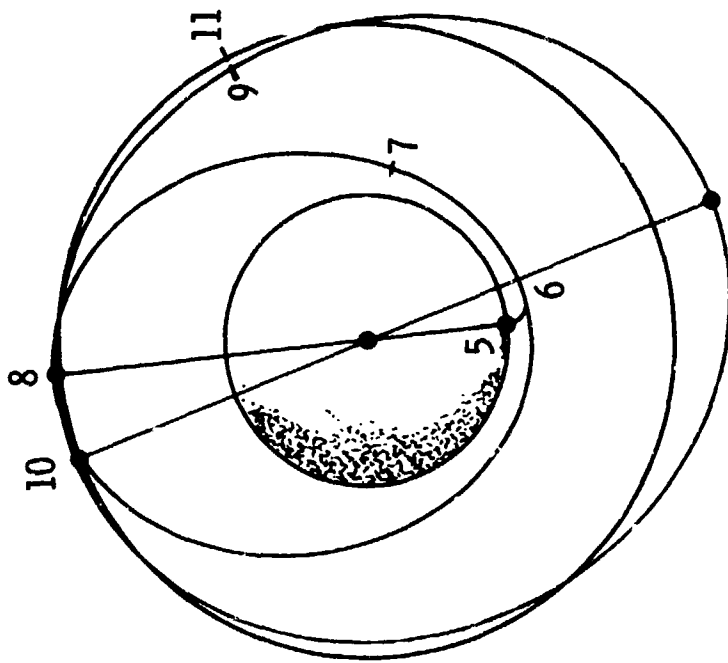


Figure III-3 Mission Phase #2 - MAV Ascent to Circularization Trim

Discussion. Since the ascent is executed open loop according to a pre-programmed pitch profile there is no on-board sensed estimate of state from which guidance corrections are computed. The injected state will only be dispersed by actual (control) deviations in pre-launch computed parameters such as landing site position ( $\delta\text{LONG}$ ,  $\delta\text{LATL}$ ,  $\delta\text{ALT}$ ), launch azimuth ( $\delta\text{AZL}$ ), initial ramp angle ( $\delta\theta_0$ ), constant pitch rate ( $\delta\theta$ ), liftoff weight ( $\delta\text{WT}$ ), burn times ( $\delta t_{B1}$ ,  $\delta t_{B2}$ ), thrusts ( $\delta T_1$ ,  $\delta T_2$ ) and coast time ( $\delta t_{\text{CST}}$ ). The sensitivity of the Cartesian injected state to each of these error sources was derived by flying the ascent with the 1 $\sigma$  perturbed values. The sensitivity matrix M, where

$M = \frac{\partial X}{\partial e}$  (6 x 12) was used to form a covariance matrix for injected state deviations according to

$$P_{\text{INJ}} = M E M^T \quad \text{where} \quad (1)$$

E is the covariance matrix of launch parameter control deviations. E is not diagonal since burn time and thrust are correlated -.98. The underlying assumption implying the validity of equation (1) is that any dispersed state,  $\delta X$ , resulting from a combination of launch errors,  $\delta e$ , may be represented according to

$$\delta X = M \delta e \quad \text{i.e. linearity holds.}$$

On each Monte Carlo pass through the Ascent-to-TRI simulation the matrix  $P_{\text{INJ}}$  was used to construct a random sample of injected state error. This was then added to the nominal Cartesian state to form a random actual injected state. After Earth-based O.D. is accomplished the MAV will be commanded to circularize (by firing at apoapsis) at whatever apoapsis altitude it happened to be injected into from launch. This maneuver can be computed rather coarsely since the MAV has only to lift itself out of the gravity well to where the O.D. situation improves for the final trim. The MAV is assumed capable of executing as accurately as the Orbiter. The Orbiter execution accuracy is as specified by the Viking Orbiter Design Handbook (Ref. III-1). Uncertainties correspond to the Viking Orbiter specifications and not to the mission requirements on system design (MRSD). The 1 $\sigma$  pointing misalignment is computed from

$$\sigma_{\alpha} = \left[ (.0023)^2 + (.1/\text{DVM})^2 \right]^{1/2} \quad (2)$$

and the  $\Delta V$  magnitude error (or burn time error) is given by

$$\sigma_{t_B} = \left[ (.027)^2 + (.001 \text{ DVM})^2 \right]^{1/2} \text{ MASS/THR} \quad (3)$$

In equation (2) DVM is commanded  $\Delta V$  magnitude in m/sec where in equation (3) DVM is the same quantity in km/sec.

Results. The major sources of error affecting an equatorial ascent trajectory are found in Table III-6 along with their separate (1 $\sigma$ ) effects on period ( $\delta P$ ) and apoapsis altitude ( $\delta h_A$ ).

Table III-6 Ascent Dispersions ( $P=2.58$  hrs,  $h_A=2200$  km)

	$\delta \text{LATL}$	$\delta \text{LONG}$	$\delta \text{ALT}$	$\delta \text{AZL}$	$\delta \theta_0$	$\delta \theta$
$\delta P$ (hrs)	0.	- 0.07	+ 0.06	0.	0.025	0.035
$\delta h_A$ (km)	0.	-158.8	+126.5	0.	+56.6	+80.2

	$\delta \text{WT}$	$\delta \tau_{B1}$	$\delta T_1$	$\delta t_{\text{CST}}$	$\delta t_{B2}$	$\delta T_2$
$\delta P$ (hrs)	- 0.03	+ 0.31	+ 0.31	0.	+ 0.14	+ 0.14
$\delta h_A$ (km)	-71.8	+707.8	+725.5	0.	+327.7	+330.2

Landing site errors are for the case where only landing footprint and gyrocompassing are used to fix the landing site position. When S-band ranging to the Lander is used to solve for the landing site position the location errors are reduced so that their effect is more comparable to that of ramp angle, pitch rate and liftoff weight. Burn time errors and corresponding thrust errors cancel because they are highly negatively correlated. Coast time error (controlled by on-board clock) has negligible effect on ascent. The  $\delta h_A$  dispersions due to all these error sources fall in the interval  $-462 \text{ km} < \delta h_A < 425. \text{ km}$ . The periapsis dispersions correspond to a MAV orbital lifetime of  $> 30$  days.

Table III-7 presents O.D. results for the  $100 \times 2200$  km and  $2200 \times 2200$  km orbits with a 2nd order gravity field (i.e. only uncertainties to 2nd order corrupted state estimates). The effect of drag and higher order harmonic terms is discussed in the navigation sensitivity section. Uncertainties in the harmonic coefficients were taken from Mariner 9 results (Ref. III-2).

Table III-7 O.D. Accuracies for Baseline Analysis

	$\sigma_x$ (km)	$\sigma_y$ (km)	$\sigma_z$ (km)	$\sigma_{\dot{x}}$ (m/s)	$\sigma_{\dot{y}}$ (m/s)	$\sigma_{\dot{z}}$ (m/s)
Ascent Orbit	1.1	2.3	2.1	.6	1.0	1.3
Circular Orbit	.8	1.3	1.3	.2	1.2	1.0

Table III-8 presents  $\Delta V_{STAT}$  results for the MAV. The effect of maneuver execution error on the circularization burn is removed by the "recircularization (RECIRC)" trim. The total MAV  $\Delta V_{STAT}$  is 41.6 m/s.

Table III-8 MAV  $\Delta V_{STAT}$

	Nominal $\Delta V$	99% $\Delta V$	$\Delta V_{STAT}$
CIRC	337.3 m/s	376.6 m/s	39.3 m/s
RECIRC	0.	17.9 m/s	17.9 m/s
Total	337.3 m/s	378.9 m/s	41.6 m/s

### 3. Mission Phase #3 - Orbiter Periapsis Change to Orbiter Circularization to First Occultation Exit

#### Description. (See Figure III-4)

#12) Orbiter state update (based on 1 orbit of conventional Doppler). This Orbiter estimate and the latest MAV estimate are used to compute an Orbiter maneuver which will raise the Orbiter periapsis altitude to 50 km above the MAV circular altitude.

#13) The Orbiter raises periapsis on the 4th apoapsis ( $\Delta V_{NOM} = 22$  m/s for  $h_A = 2250$  km).

#14) Orbiter state vector update based on 1-1/2 orbits of conventional Doppler data.

#15) Orbiter intermediate phasing burn ( $\Delta V_{NOM} = 720.6$  m/s) and MAV orbital position at this time.

#16) Orbiter state updated based on 4 orbits of conventional Doppler. An additional 4 orbits is spent in the phasing orbit while the state and circularization maneuver computations are being made.

#17) Orbiter circularization ( $\Delta V_{NOM} = 318.5$  m/s) is targeted to achieve a semi-major axis equal to the estimated radius of periapsis.

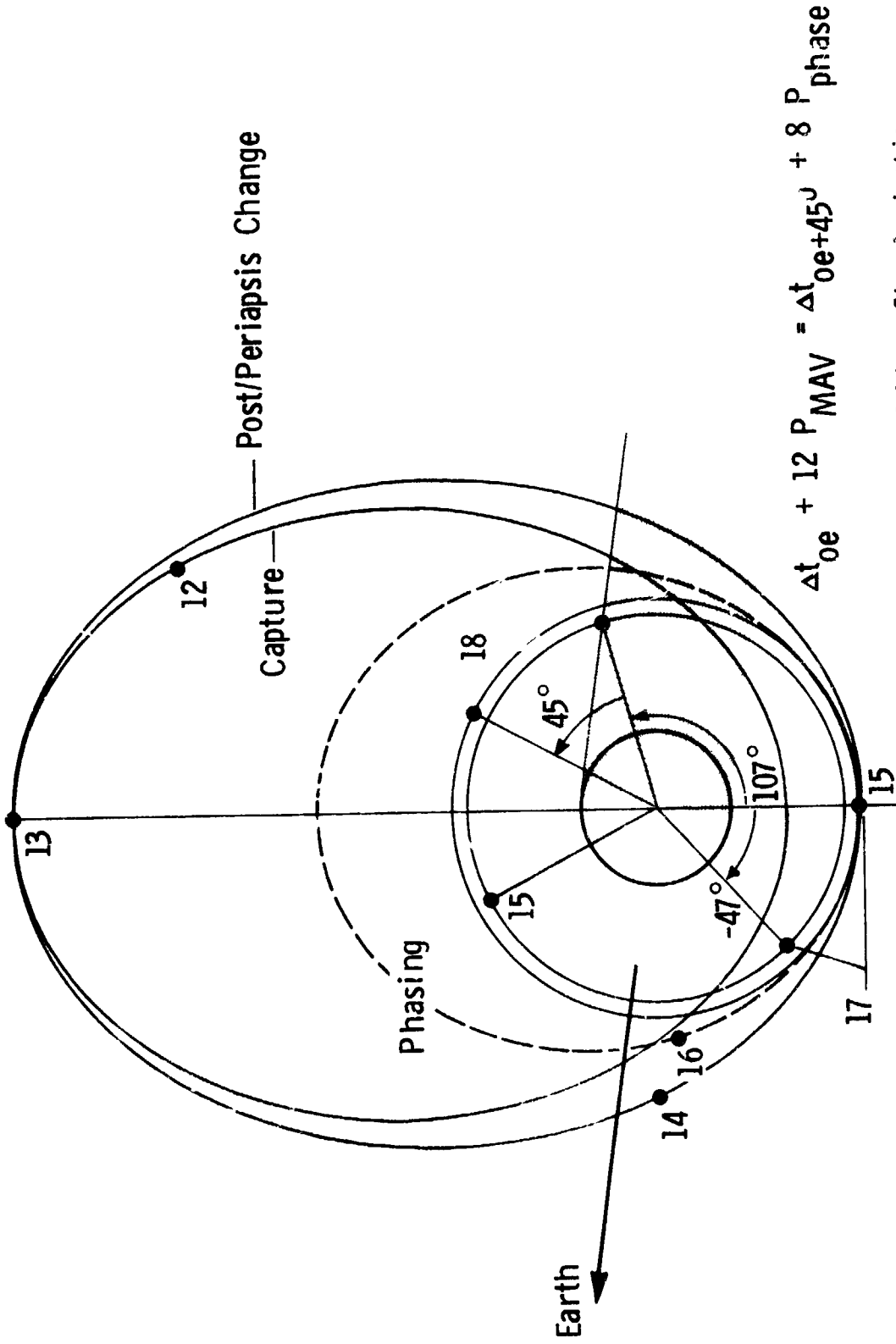


Figure III-4 Mission Phase #3 - Orbiter Periapsis Change to Orbiter Circularization to First Occultation Exit

#18) As a result of the phasing orbit period calculation a  $45^\circ$  phase angle is established between Orbiter and MAV when the MAV exits from the Earth occultation zone for the first time after Orbiter circularization.

Discussion. After the Orbiter has circularized, to a radius 50 km greater than the MAV radius, the plan is to very accurately determine the relative state of the two vehicles, using an Earth-based simultaneous data type, and then to trim up the Orbiter trajectory to set the initial conditions for the automatic terminal rendezvous sequence. Simultaneous Earth coverage must be guaranteed for 4 orbits and 4 orbits are spent computing the trim sequence. The trim sequence is executed in 1 orbit so that a total of 9 MAV orbits after the 1st MAV occultation exit are required to set up the TRI conditions. The time of the 10th MAV occultation exit is taken to be the TRI time. At TRI a  $2^\circ$  MAV/Orbiter phase angle is desired (determined from terminal rendezvous analysis). This being the case the desired phase angle (or Orbiter lead angle) at the 1st MAV occultation exit is given by

$$\dot{\phi}_o = 9 \dot{\phi} + 2^\circ \quad \text{where} \quad (4)$$

$$\dot{\phi} = 360 (P_{ORB} - P_{MAV}) / P_{ORB} \quad (5)$$

Equation (4) results since the orbiter "slips" in lead angle by an amount  $\dot{\phi}$  every MAV orbit. Once  $\dot{\phi}_o$  is known the period of the phasing orbit may be computed from

$$8 P_{\text{phase}} + \Delta t_{oe} + \phi_o = \Delta t_{oe} + 12 P_{MAV} \quad (6)$$

Equation (6) is for a minimum time spent in the phasing orbit--namely 8 revolutions. The quantity  $\Delta t_{oe}$  is the time required by the MAV to move from its orbital true anomaly at the time of the Orbiter phasing maneuver to the occultation exit (o.e.) true anomaly. Likewise  $\Delta t_{oe+\phi_o}$  is the time required by the Orbiter to go from circularization true anomaly to the true anomaly of o.e. plus  $\phi_o$ . Note that for each MAV injected radius a new  $\dot{\phi}_o$  and phasing orbit period is computed. The nominal  $P_{\text{phase}} = 5.5$  hours with  $h_A = 5904$  km.

Results. The major source of error limiting the accuracy with which  $\dot{\phi}_o$  may be set is the execution error in the Orbiter circularization maneuver. Table III-9 shows the post-circularization dispersions for a  $1\sigma$  perturbation

in execution errors  $\delta TA$  (true anomaly),  $\delta\alpha$ ,  $\delta\beta$  (pointing angles) and  $\delta t_B$  (burn time). These sensitivities are for a worst case insertion--namely directly from the high capture orbit.

Table III-9 Post-Circularization Dispersions

	$\delta a$	$\delta e$	$\delta i$	$\delta \omega$	$\delta \Omega$	$\delta TA$
$\delta TA$	0.1 km	-3.1(-4)	0.	-22.1°	0.0°	22.5°
$\delta\alpha$	0.2 km	-2.4(-4)	-0.02°	-29.9°	-0.2°	30.0°
$\delta\beta$	0.2 km	1.2(-3)	-0.02°	20.3°	-0.2°	-20.1°
$\delta t_B$	-5.3 km	-1.2(-3)	0.	4.2°	0.0°	-4.2°

It is assumed that the phasing is perfect prior to circularization. Note from Table III-9 that the primary execution error is burn time. (This is the case even with in-flight calibration of the accelerometers prior to each maneuver.) Note also that the argument of periapsis ( $\omega$ ) and the true anomaly (TA) change greatly while the sum of the two is relatively constant. For this reason all Orbiter maneuvers after circularization occur at nominal  $\omega + TA$ . The question arises as to what relative state control dispersions would result at the 1st MAV occultation exit if the 2<sup>o</sup> TRI conditions were targeted for immediately without waiting for the additional Earth tracking (i.e. instead of targeting for  $\phi_0$ ). Table III-10 presents these results in the MAV, u, v, w coordinate system defined as follows:

$$u = R_A / |R_A|; \quad w = R_A \times V_A / |R_A \times V_A|; \quad v = w \times u \quad \text{where}$$

$R_A$ ,  $V_A$  are the actual MAV position and velocity vectors respectively.

Table III-10 Dispersion Ellipse At First Occultation Exit ( $\phi_0 = 2^\circ$ )

$3 \sigma_u = 25.8 \text{ km}$	$3 \sigma_{\dot{u}} = 60.8 \text{ m/s}$
$3 \sigma_v = 108.2 \text{ km}$	$3 \sigma_{\dot{v}} = 9.5 \text{ m/s}$
$3 \sigma_w = 27.7 \text{ km}$	$3 \sigma_{\dot{w}} = 5.8 \text{ m/s}$

This ellipsoid places the vehicles within rendezvous radar range; however, the pointing knowledge error (Table III-11) precludes the pre-circularization computation of look angles which will produce a line-of-sight (LOS) within the radar beamwidth ( $20^\circ$ ).

Table III-11 Line-of-Sight Error At  
First Occultation Exit

	6- LOS Error
In-Plane	24 <sup>o</sup>
Out-of-Plane	.2 <sup>o</sup>

4. Mission Phase #4 - First Occultation Exit to Start of Circular  
Trim Sequence

Description. (See Figure III-5)

#19) The simultaneous solution for Orbiter and MAV states is available at -135<sup>o</sup> true anomaly on the 7th orbit as shown. The O.D. solution is based on conventional Doppler data on the Orbiter and multi-vehicle  $\Delta$ VLBI (DLBI) data on both vehicles. The updated states are used to compute a 3 maneuver circular trim-sequence ( $\Delta V_1, \Delta V_2, \Delta V_3$ ) which corrects phasing error and radius error during the next Orbiter revolution. The 3 maneuvers ( $\Delta V$  components and maneuver times) are loaded in the Orbiter memory at this time.

Discussion. The multi-vehicle  $\Delta$ VLBI data type results from Very Long Baseline Interferometry on two coherent vehicle sources. The technique depends on counting interference fringes for a specified time period--the fringe rate being proportional to a component of the relative velocity vector. The data type may also be thought of as being the symmetric double difference of range changes of two spacecraft measured from two Earth-based tracking stations (Figure III-6). In this analysis it is modeled as a measure of the component of relative velocity along the projection of the baseline vector in a plane perpendicular to the Earth-Mars line. The inherent measurement noise is given by

$$\sigma_{\Delta VLBI} = (b_p / r_{EM}) \sigma_{\dot{\rho}} = .034 \text{ mm/s}$$

since  $\sigma_{\dot{\rho}}$ , the uncertainty in projected velocity, is computed to be 2 m/s. (For a 1<sup>c</sup> fringe resolution the projected relative velocity uncertainty is  $10 t^{-1}$  where  $t$  = fringe integration time, see Ref. III-3). The relative state error covariance matrix resulting from the sequential filtering of four orbits (1 hr/orbit) of  $\Delta$ VLBI data was computed. In this calculation the only source of error was data noise. This matrix was used to compute random samples of relative state knowledge error ( $\Delta XY_E$ ) at the  $\Delta$ VLBI update

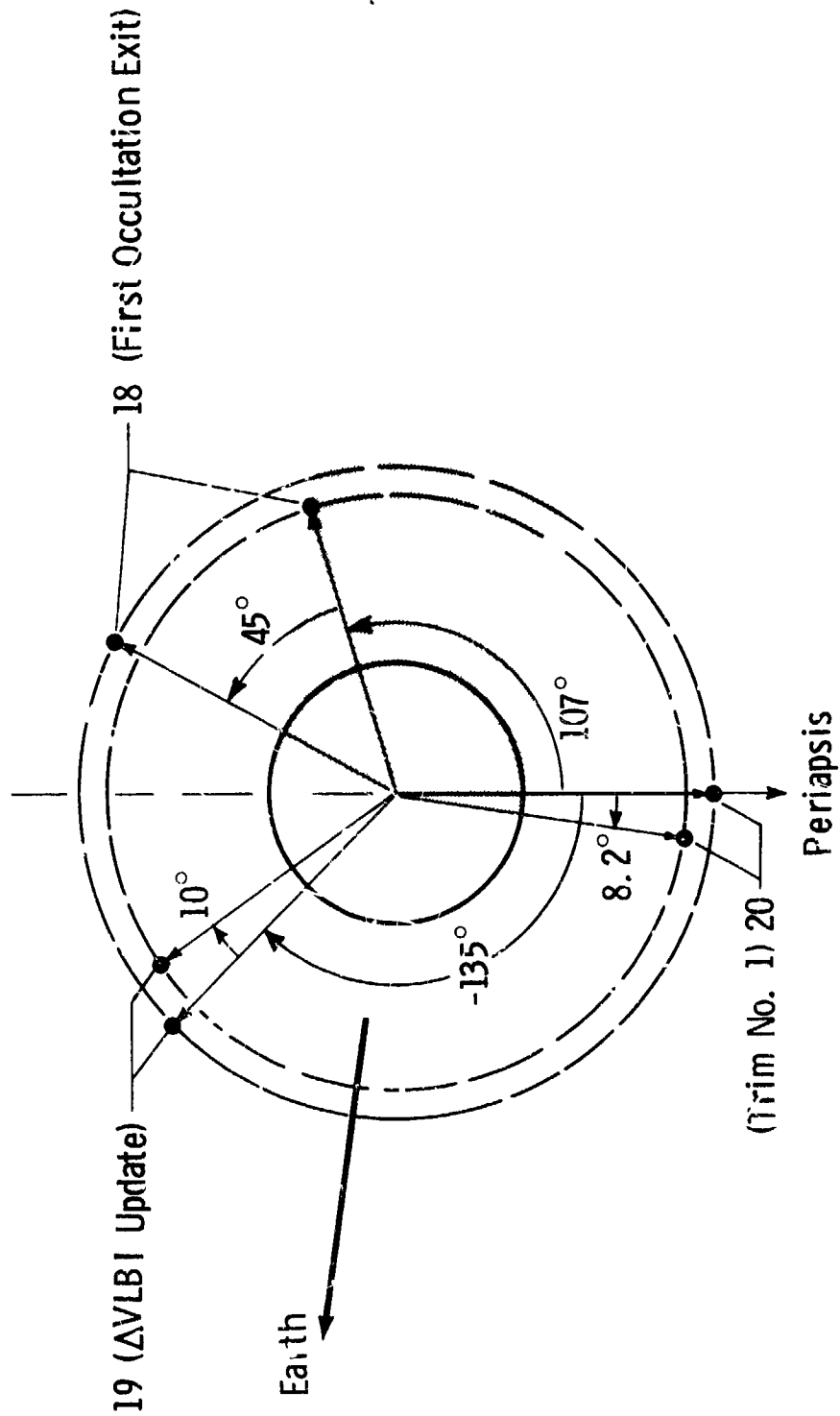
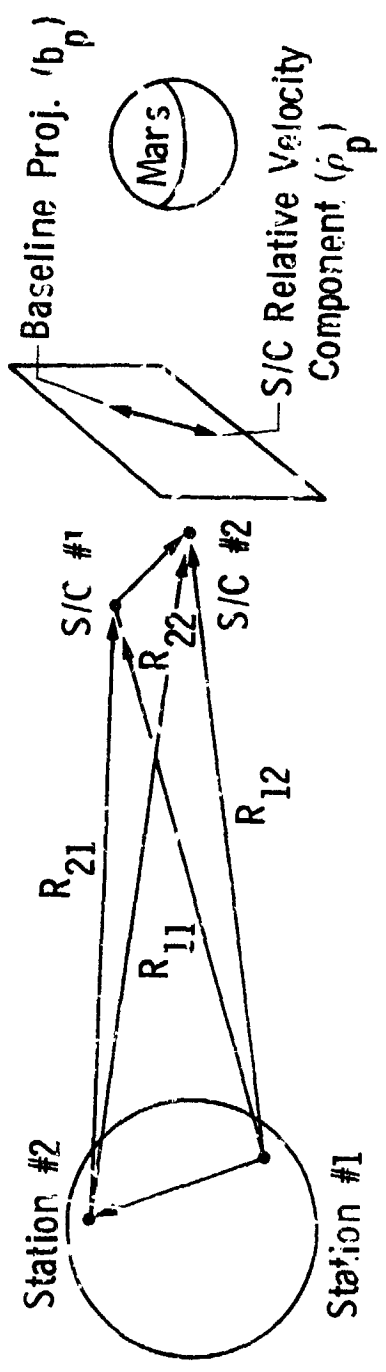


Figure III-5 Mission Phase #4 - First Occultation Exit to Start of Circular Trim



31-111

$$\sigma_{\Delta VLBI} = (b_p / r_{EM}) \sigma_{\dot{\rho}_p} = .034 \text{ m.m/s}$$

$$\sigma_{\dot{\rho}_p} = 2 \text{ m/s for a 5 sec Fringe Integration Time}$$

Figure III-6 Multi-vehicle  $\Delta VLBI$

time. The Orbiter estimate was computed initially and then the MAV estimate was formed by adding on the relative state estimate, i.e.

$$Y_E = Y_A + \Delta Y_E \quad \text{for the Orbiter}$$

$$Y_E - X_E = XY_E = XY_A + \Delta XY_E \quad \text{for the relative state, and}$$

$$X_E = Y_E - XY_E \quad \text{for the MAV.}$$

Results. Relative state accuracies (knowledge) after four orbits of  $\Delta VLEI$  data processing and four orbits of prediction are shown in Table III-12.

Table III-12 Relative State Accuracies  
At DLBI Update

$\sigma_u = 0.6 \text{ km}$	$\sigma_{\dot{u}} = 0.14 \text{ m/s}$
$\sigma_r = 0.29 \text{ km}$	$\sigma_{\dot{v}} = 0.03 \text{ m/s}$
$\sigma_w = 0.08 \text{ km}$	$\sigma_{\dot{w}} = 0.04 \text{ m/s}$

(The velocity accuracy is comparable to the quoted wind speed determination accuracy of Ref. III-4, i.e., tens of centimeters/sec.) These O.D. uncertainties allow the computation of intervehicular look angles to the accuracy specified in Table III-13, i.e., the estimated IOS will be off the actual IOS by the stated amounts. Of particular importance is the actual pointing accuracy after the 3rd circular trim maneuver. This must be sufficient to allow Orbiter radar acquisition of the MAV at that time.

Table III-13 Pointing Accuracy  
at  $\Delta VLEI$  Update

$6\sigma$ In-Plane	$= 0.06^\circ$
$6\sigma$ Out-of-Plane	$= 0.01^\circ$

#### 5. Mission Phase #5 - Circular Trim Sequence through 10th Occultation Exit

Description. (See Figure III-7.)

#20) When  $\theta + TA = (\theta + TA)_{NOM}$ , corresponding to the nominal position of periapsis, the Orbiter performs the first of the circular trim maneuvers  $\Delta V_1$ .

#21) After a fixed time  $\delta t_1$  later the 2nd trim maneuver is performed (nominally  $180^\circ$  from the first maneuver) to null radius error  $\delta r$ .

$$\delta t_1 + \delta t_2 = \delta t$$

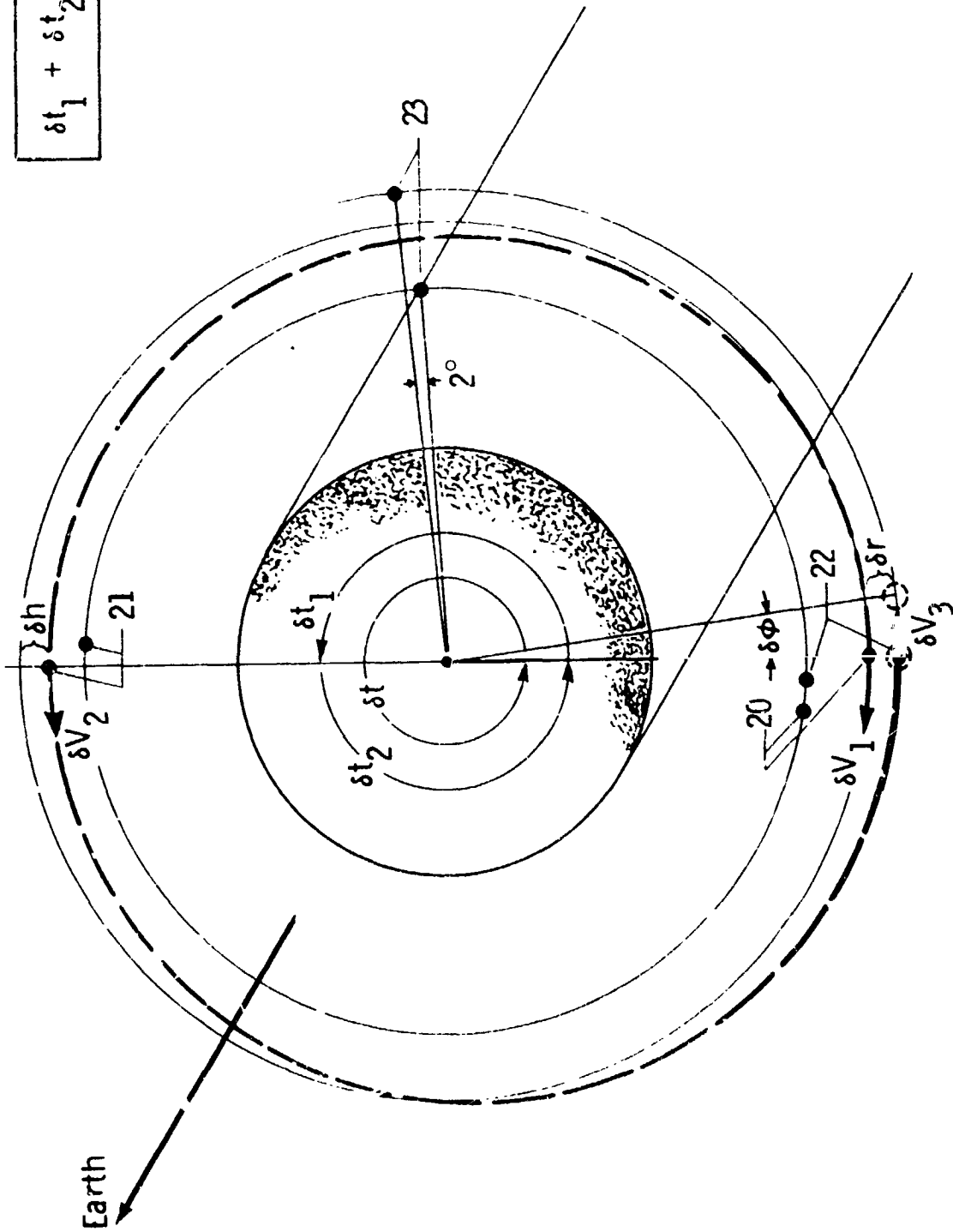


Figure III-7 Mission Phase #5 - Circular Trim Sequence Through 10th Occultation Exit

#22) After a fixed time  $\delta t_2$  later (nominally  $180^\circ$  after trim #2) the final (3rd) trim maneuver is performed to circularize the orbit at  $R_f$ --the desired final radius. Note that  $\delta h$  was computed so that  $\delta t_1 + \delta t_2 = \delta t$ . Where  $\delta t$  is the time required for the desired phasing point (dotted circle in Figure III-1) to cross the Orbiter line at  $\omega + TA$ .

#23) Immediately after trim #3 the vehicles are programmed to look along the relative position vector to establish rendezvous radar lock. The optimum phase angle of  $2^\circ$  is nominally achieved at the 10th MAV exit from the Earth occultation zone.

Discussion. The 3 maneuver circular trim sequence corrects the Orbiter radius error ( $\delta r$ ) in an amount of time ( $\delta t$ ) so that the phasing error ( $\delta \phi$ ) is also nulled. This is accomplished by iteratively solving the following equation for  $\delta h$ :

$$\frac{1}{2}P(a_1) + \frac{1}{2}P(a_2) = T(1 + \delta \phi / 360) \quad (7)$$

$$a_1 = a_0 + \delta h / 2; a_2 = a_1 + \delta r / 2; a_3 = R_f$$

In equation (7)  $P(a) = 2\pi(a^3/\mu)^{1/2}$  and  $T$  is the period of the desired final circular orbit of radius  $R_f$ .  $a_0$  is the initial semi-major axis (SMAA),  $a_1$  is the SMAA after  $\Delta V_1$ ,  $a_2$  is the SMAA after  $\Delta V_2$ , and  $a_3$  is the SMAA after  $\Delta V_3$ . The trim maneuvers are performed in-plane--no provision is made for removing out-of-plane error. This trim strategy is very similar to the Viking '75 Mission A strategy in that the purpose of trim #1 is to establish a prescribed phasing error at the time of trim #2 so that when trim #2 adjusts the radius a phase rate is produced which just cancels the phase error  $180^\circ$  later.

For dispersed cases the Orbiter position vector at nominal  $\omega + TA$  will not lie along the line of apsides. A small  $\Delta V$  is initially used to establish the velocity vector perpendicular to the position vector at  $\omega + TA$  prior to trim maneuver computations. Trim #1 then is actually the sum of  $\Delta V$  and the  $\Delta V_1$  computed for the 1st Hohmann maneuver in the trim sequence.

Results. The individual 99 percentile trim  $\Delta V$ s (Table III-14) indicate that considerably more  $\Delta V$  is expended correcting phase error (23.2 m/s, 20.2 m/s) than radius error (1.2 m/s). The 1.2 m/s velocity change produces  $\approx 8$  km of radius change.

Table III-14 Trim  $\Delta V_{STAT}$

	Nominal v	99% $\Delta V$	$\Delta V_{STAT}$
Trim #1	0.	23.2 m/s	23.2 m/s
Trim #2	0.	1.2 m/s	1.2 m/s
Trim #3	0.	20.2 m/s	20.2 m/s
Total	0.	42.6 m/s	42.6 m/s

Immediately after trim #3 the Orbiter and the MAV are programmed to acquire rendezvous radar lock. The line-of-sight accuracy at this point in the mission is  $4.6^\circ$  in-plane ( $6\sigma$ ) and  $1.9^\circ$  out-of-plane ( $6\sigma$ ). The  $3\sigma$  dispersions in the actual Orbiter state relative to the actual MAV state are shown in Table III-15. These represent the limit for the Earth-controlled portion of the mission. It has been shown that the automatic on-board system can start with these conditions and always effect a terminal rendezvous.

Table III-15 Dispersion Ellipse At  
10th Occultation Exit

$3 \sigma_u = 7.7 \text{ km}$	$3 \sigma_{\dot{u}} = 39.3 \text{ m/s}$
$3 \sigma_v = 71.7 \text{ km}$	$3 \sigma_{\dot{v}} = 2.9 \text{ m/s}$
$3 \sigma_w = 26.3 \text{ km}$	$3 \sigma_{\dot{w}} = 5.7 \text{ m/s}$

## B. NAVIGATION SENSITIVITY STUDIES

This section deals with the sensitivity of mission performance to various navigation parameters and techniques. The attempt here is to identify error sources and techniques that the mission performance is most sensitive to and then to suggest how they may be dealt with in order to enhance mission performance.

### 1. Approach Optical (TV) Guidance

On-board TV sightings of Deimos against a star background may be used to simultaneously solve for the spacecraft and satellite states. This technique has been used for Mariner 9 encounter O.D. and is planned as a backup navigation aid on Viking '75 (Ref. III-5). The sightings are taken from MOI-72 hrs to MOI-18 hrs (Figure III-8). Typical B-plane ellipse major axes for this type of data are of the order of 25 km. Minor axes reportedly may be as small as 12 km (Ref. III-6). This allows very accurate entry flight path control for any  $\theta_{AIM}$  approach angle. Since a Mariner TV system weighs at least 30 lbs it is also necessary to examine the tradeoff between corridor width reduction and increased Orbiter weight. Because a  $4^\circ$  corridor width ( $6\sigma_\gamma$ ) is attainable with radio (DSN) tracking only the above tradeoff was not considered in the scope of this contract. Figure III-9 shows, however, that optical approach guidance has a great capability for enhancing the approach O.D. Radio only  $\sigma_{|B|}$  capability (minor axis) is limited to ~ 25 km because of Mars ephemeris error. Radio + optical allows a  $2^\circ$  corridor width for any hyperbolic approach angle while radio-only affords  $4^\circ$  accuracy for a very restrictive approach angle (namely along the minor axis of the B-ellipse). A restrictive approach angle also means limited latitude accessibility. According to the approximate formula then (assumption #4 shown on Figure III-9) it may be concluded that a  $4^\circ$  corridor is attainable with radio only data (baseline design) and that to achieve a  $2^\circ$  corridor requires optical sightings.

### 2. DSN Data Type Evaluation for Relative State Estimation

This study evaluated the conventional Doppler range rate data type and an experimental interferometric tracking data type for relative state estimation in Mars orbit. The evaluation of data types was carried out by comparison of the root-sum of squares (RSS) of error components of estimation

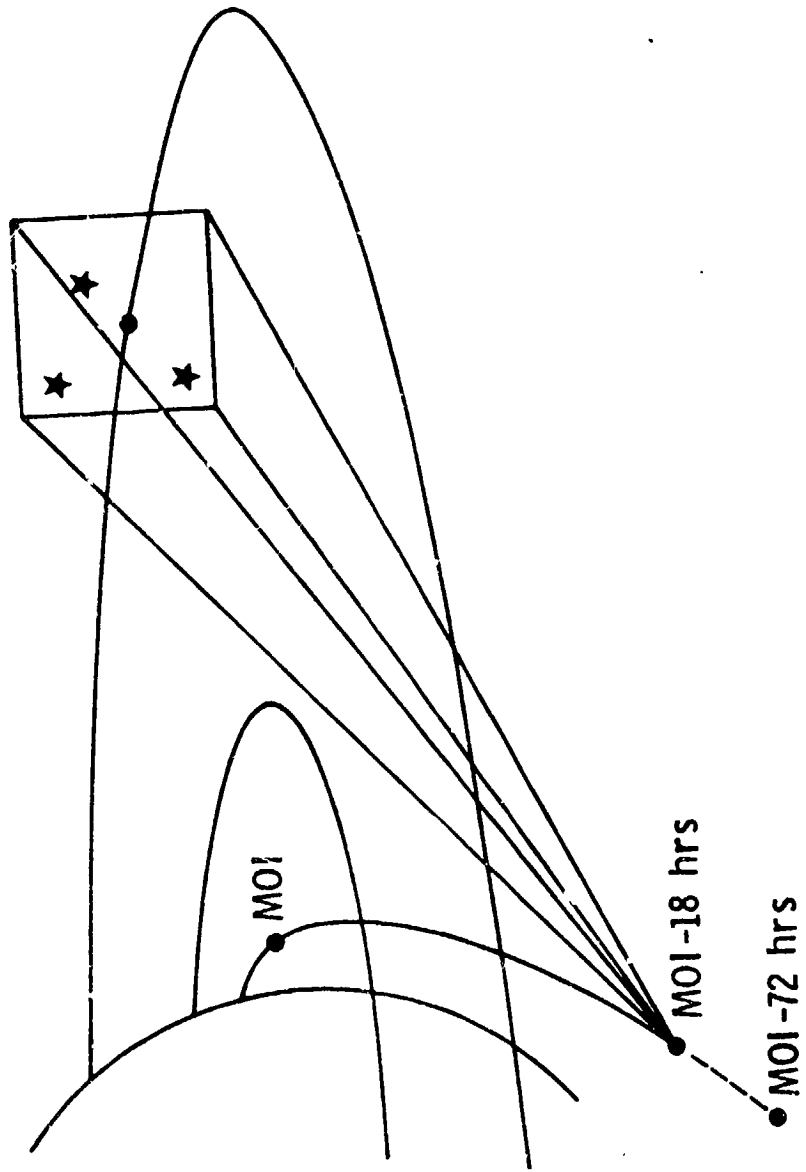


Figure III-8 "Knowledge" Data Type Deimos/Stars - Single Camera

Assumptions:

- 1) VAP 3.15
- 2)  $\gamma = -18.50$
- 3) At least 1 star in satellite background
- 4)  $\sigma_{\gamma} = R_E \sqrt{V_{\infty}^2 + 2\mu R_E} \sigma_{|B|}$
- RE = 5637.24
- 5)  $-V_{\infty} \text{ CSC } \gamma$
- Radio: E-30d E-12 hrs
- Optical: E-3d E-18 hrs } Deimos

Results:

	Radio Only		Radio + Optical
$\sigma_{ B }$	25 km	50 km	12 km
$1 \sigma_{\gamma}$	.67°	1.352°	.324
$6 \sigma_{\gamma}$	4.056°	8.112°	1.946

Conclusions:

- 1) Optical (TV) Sightings Required to Achieve 2° Corridor
- 2) 4° Attainable with DSN (optional QVLBI)
- 3) Results with Optical Independent of LD/ED

Figure III-9 Approach O.D.: DSN vs DSN + Optical

error covariance matrices. The analysis pointed out that indeed after four or five orbits of conventional Doppler range rate tracking the relative state of two vehicles is better known than either single vehicle state because the single vehicle errors become highly correlated.

The multi-vehicle interferometric data type, however, is intrinsically better because it measures directly a component of the relative velocity vector and hence yields a more rapidly converging solution. Relative state accuracies of  $\sim 1$  km and  $\sim 50$  cm/sec are expected.

The Viking Navigation Analysis Program (VNAP) (Ref. III-7) was used to compute estimation error covariance matrices for single vehicle orbit determination in Mars orbit. The MAV is in a 2200 km altitude circular orbit ( $P_1 = 3.53$  hrs) and the orbiter is in the 2250 km circular orbit ( $P_2 = 3.58$  hrs). The orbital inclination to the "plane-of-the-sky" (POS)\* was large ( $\sim 108^\circ$ ). This minimizes the effects due to uncertainty in the POS ascending mode. The VNAP was used in the sequential weighted least squares (WLS) mode with sets of gravity field ignore parameters corrupting the state estimate. The relative state covariance matrix (between the two vehicles) was computed from the single vehicle VNAP results as follows: the error in the single vehicle estimates is given by

$$\Delta X_{E1}^i = (A_1^T W A_1 + P_1)^{-1} P_1^{-1} \Delta X_{E1} + A_1^T W B_1 \Delta Z + A_1^T W n_1 \quad (8)$$

$$\Delta X_{E2}^i = (A_2^T W A_2 + P_2)^{-1} P_2^{-1} \Delta X_{E2} + A_2^T W B_2 \Delta Z + A_2^T W n_2 \quad (9)$$

In equations (8) and (9):

- $A_i$  = matrix of partial derivatives of measurements with respect to vehicle (N x 6)
- $B_i$  = matrix of partial derivatives of measurements with respect to ignore parameters (N x M)
- W = N x N data weighting matrix
- $P_i$  = 6 x 6 a-priori state covariance matrix for ith vehicle
- $\Delta X_{Ei}$  = a-priori error in ith vehicle state
- $n_i$  = measurement noise vector for ith vehicle
- $\Delta Z$  = vector of ignore parameter derivations
- N = number of data points in batch
- M = number of ignore parameters

\* Plane perpendicular to the Earth-Mars line.

These expressions written for batched WLS estimates are also valid for the sequential estimates at the end of the data arc.

The relative state estimate formed from the single vehicle states is in error by

$$\begin{aligned} \Delta \bar{X}'_{ER} &= \Delta X'_{E1} - \Delta X'_{E2} \quad \text{so that the error covariance matrix is} \\ P'_R &= \overline{\Delta X'_{ER} (\Delta X'_{ER})^T} = P'_1 + P'_2 - P'_{12} - P'_{21} \quad \text{with} \quad (10) \\ P'_{12} &= \overline{\Delta X'_{E1} (\Delta X'_{E2})^T}; \quad P'_{21} = \overline{\Delta X'_{E2} (\Delta X'_{E1})^T} \\ P'_1 &= \overline{\Delta X'_{E1} (\Delta X'_{E1})^T}; \quad P'_2 = \overline{\Delta X'_{E2} (\Delta X'_{E2})^T} \end{aligned}$$

The expression for  $P'_{12}$  in equation (10) as derived from equations (8) and (9) is:

$$P'_{12} = (A_1^T W A_1)^{-1} A_1^T W B_1 \overline{\Delta Z \Delta Z^T} (A_2^T W B_2)^T (A_2^T W A_2)^{-1}$$

assuming no a priori weighting and uncorrelated noise vectors  $n_1$  and  $n_2$ .

$P'_{12}$  may be computed from the VNAP quantities

$$P'_{12} = \overline{\Delta X'_{E1} \Delta X'_{E2}^T} \quad \text{and} \quad P'_{22} = \overline{\Delta X'_{E2} \Delta Z^T} \quad \text{by noting from equations}$$

(8) and (9) that

$$P'_{12} = (A_1^T W A_1)^{-1} A_1^T W B_1 \overline{\Delta Z \Delta Z^T} \quad \text{and} \quad P'_{22} = (A_2^T W A_2)^{-1} A_2^T W B_2 \overline{\Delta Z \Delta Z^T}$$

so that

$$P'_{12} = P'_{12} \overline{(\Delta Z \Delta Z^T)^{-1}} (P'_{22})^T$$

$P'_{12}$  and subsequently  $P'_R$  is computed by an auxiliary program named RELCOV.

Two sets of VNAP matrices are input to RELCOV for each  $P'_R$  computation time.

The relative state covariance matrices resulting from sequential filtering of multi-vehicle differential Very Long Baseline Interferometry (ΔVLBI) tracking data were computed with the MSTRAK program. This is a modified version of the PVTRAK program (Ref. III-4) developed for Pioneer Venus wind determination studies. The following capabilities were added to PVTRAK:

- 1) propagation of bus state covariance matrix;
- 2) addition of conic trajectory and propagation for second vehicle;
- 3) a tracking schedule consisting of any number of station pairs (input for any number of disjoint tracking intervals), and tracking interval start/stop times.

The multi-vehicle  $\Delta$ VLBI data type results from very long baseline interferometry on two coherent vehicle sources. The technique depends on counting interference fringes for a specified time period--the fringe rate being proportional to a component of the relative velocity vector. The data type may also be thought of as being the symmetric double difference of range changes of two spacecraft measured from two Earth-based tracking stations. In this analysis (MSTRAK) it is modeled as a measure of the component of relative velocity along the projection of the baseline vector in a plane perpendicular to the Earth-Mars line. When thought of as a double differenced range measurement it becomes clear that errors due to tracking station location, frequency biases and clock errors all cancel out and hence were not considered in this analysis. The only error source considered in the  $\Delta$ VLBI analysis was measurement noise. For an Earth-controlled rendezvous utilizing  $\Delta$ VLBI and conventional data (or QVLBI data) the ground orbit determination system will process both data types simultaneously and solve for both vehicle states (or a single vehicle state and the relative state) simultaneously.

The  $\Delta$ VLBI measurement noise is computed from Ref. III-3:

$$\sigma_{\Delta\text{VLBI}} = (b_p / r_{EM}) \sigma_{\dot{\rho}_p} = .034 \text{ mm/s}$$

where  $b_p$  is the projected baseline magnitude,  $r_{EM}$ , the Earth-Mars distance and  $\sigma_{\dot{\rho}_p}$  the uncertainty in projected velocity. For a  $1^\circ$  fringe resolution this quantity is equal to  $10 t^{-1}$  where  $t$  is the fringe integration time (i.e. the more fringes counted the more accurately is  $\dot{\rho}_p$  computed. Since the value computed is only an average for the interval  $t$ , the usefulness of a  $\dot{\rho}_p$  computed for too large an interval is questionable). The  $\sigma_{\dot{\rho}_p}$  used here was 2 m/s corresponding to  $t = 5$  sec. Table III-16 shows a comparison of relative state accuracies for conventional Doppler and  $\Delta$ VLBI data types. These single vehicle results are not for the same orbital geometry case as discussed earlier. These results are only to show that initially (after 1 rev) the RSS rel. error is simply the RSS of the single vehicle errors (i.e.,  $193.^2 = 168.3^2 + 88.6^2$  and  $139.4^2 = 130.7^2 + 57.7^2$ ) but that after 4 revs the RSS relative error is considerably smaller than either single vehicle errors. This effect is due to build-up of correlated single vehicle errors which cancel when the relative state is formed by subtraction.

Relative State Accuracy: Single Vehicle Doppler Tracking

Time	RSS S/C #1	RSS S/C #2	RSS REL
1 rev	168.3 km/10.7 m/s	88.6 km/57.7 m/s	193.0 km/139.4 m/s
2 revs	90.0 km/ 37.8 m/s	41.1 km/48.7 m/s	68.7 km/ 19.5 m/s
3 revs	63.0 km/ 14.9 m/s	37.0 km/ 6.1 m/s	28.7 km/ 4.3 m/s
4 revs	9.9 km/ 1.3 m/s	5.8 km/ .8 m/s	4.9 km/ .7 m/s

Relative State Accuracy: ΔVLBI Tracking

Time	$\sigma_x$ (km)	$\sigma_y$ (km)	$\sigma_z$ (km)	$\sigma_{\dot{x}}$ (m/s)	$\sigma_{\dot{y}}$ (m/s)	$\sigma_{\dot{z}}$ (m/s)	RSS
1/8 rev	24.7	29.3	15.8	6.3	9.1	2.7	41.5/11.4
1/4 rev	1.1	2.4	1.1	.6	1.0	.8	2.9/ 1.4
3/8 rev	.9	1.0	.8	.6	.7	.6	1.6/ 1.0
1/2 rev	.7	1.1	.7	.2	.5	.3	1.5/ .6
1 rev	.5	.5	.2	.1	.2	.1	.7/ .3

Table III-16 ΔVLBI vs Conventional Doppler

The second part of Table III-16 shows relative state uncertainty after ΔVLBI (DLBI) tracking. It can be seen that this data type provides a very accurate relative position and velocity determination with only a single orbit of data. The only added constraint on the mission plan is that simultaneous visibility of both vehicles must be provided.

### 3. Sensitivity of State Vector Prediction Accuracy to Orbital Altitude

Table III-17 shows the effect of predicting the state ahead a number of orbits after tracking for four orbits. Also shown is the resulting local uncertainty at the end of 6.6 orbits. This is merely to show that sufficient accuracy is available after only 4 orbits of data have been processed (.9 km, 1.4 m/s) but that additional data would further reduce the local uncertainty. The period of a 2200 km altitude orbit is 12700 secs or about 3.5 hrs. If it is assumed that 12 hrs of time must be allotted for O.D. and maneuver computation, then a prediction capability of 3 or 4 orbits is imperative. Table III-17 clearly shows a very gradual corruption of state accuracy with each additional orbit of prediction (about .3 km/orbit RSS position degradation and about .1 m/s/orbit RSS velocity degradation). The growth of position and velocity error is caused primarily by orbital period error as seen by the large increases in OMEGA (argument of periapsis) and  $T \neq TP$  (time of periapsis passage) uncertainties. This means that the RSS position error will be largely due to the downtrack component and the RSS velocity error due largely to the radial component since these two are highly correlated. Table III-17 results appear acceptable for 4 orbits of tracking and the required 4 orbits of prediction. For comparison purposes see Table III-18. In this case the orbital altitude is only 1725 km--475 km closer to the uncertain gravity field. Note that uncertainties are generally a factor of 2 worse than those of Table III-17. Seven orbits of data are required to reduce the uncertainty to 2.2 km and 3.5 m/s. It is interesting that the same degradation per orbit is found at 1725 km as was found at 2200 km, namely .3 km and .1 m/s. This is the case since the local 4 orbit and 7 orbit solutions have the same initial period error.

Table III-17 Prediction Capability for  $h_p = 2200$  Circular

REVS TRACKING	REVS PREDICTION	PER (SEC)	IP (KM)	INC (DEG)	NODE (DEG)	OMEGA (DEG)	TFT (SEC)	RSS POS (NM)	RSS VEL (M/S)
4	0	.254	.0311	.0264	.5032	1.804	63.83	.912	1.35
4	1	.233	.0206	.0264	.0047	2.028	72.10	1.248	1.406
4	2	.137	.0187	.0268	.0062	1.429	50.82	1.473	1.470
4	3	.197	.0295	.0267	.00776	1.932	68.62	1.633	1.506
4	4	.576	.0580	.0264	.00928	6.998	247.77	1.949	1.573
4	5	.969	.119	.0266	.0108	12.44	440.12	2.259	1.67
4	6	1.434	.2018	.0268	.0124	19.32	683.74	2.357	1.71
4	7	2.110	.337	.0264	.0140	32.66	1154.13	2.17	1.78
6.6	0	.2606	.0416	.0069	.0052	.679	23.79	.605	.265

Table III-18 Prediction Capability for  $h_p = 1725$  Circular

Revs Tracking	Revs Prediction	PP (sec)	HP (km)	INC (deg)	NODE (deg)	OMEGA (deg)	T # TP (sec)	RSS POS. (km)	RSS VEL (m/s)
7	0	.241	.111	.0672	.0063	3.791	116.6	2.18	3.52
7	1	.208	.122	.067	.0071	2.986	21.90	2.49	3.56
7	2	.296	.154	.068	.0081	1.807	55.2	2.73	3.60
7	3	.598	.191	.067	.0091	2.265	70.4	2.94	3.62
7	4	1.06	.257	.067	.010	6.37	198.1	3.22	3.65
7	5	1.65	.356	.067	.011	12.27	380.7	3.53	3.71
7	6	2.35	.500	.067	.012	19.71	611.0	3.77	3.75
7	7	3.25	.734	.067	.013	30.18	934.8	4.01	3.79

#### 4. Gravity Field Uncertainty and Drag

Perhaps the greatest challenge of an MSSR mission is orbit determination in the presence of an anomalous Mars gravity field. This field has been partially mapped by the Mariner 9 orbiter (Ref. III-2). The gravity harmonics solved-for from Mariner 9 data allow accurate state prediction for Mariner 9 class orbits but may not for MSSR type orbits. This is due to the non-uniqueness of harmonic solutions from a single type of orbit geometry. In this study it was assumed, however, that the Mariner 9 derived field was valid for MSSR orbits. This point of view was taken in the belief that gravity field parameters which allow accurate state prediction comparable to Mariner 9 would be determined during the MSSR mission. The 2nd order representation along with quoted uncertainties was used to generate baseline results for the rendezvous navigation analysis.

Since the MAV ascent orbit is not completely out of the Mars atmosphere (i.e. detectable atmosphere ends at  $\sim 243$  km altitude) it was necessary to determine the effect of drag uncertainty on the ascent orbit estimation accuracy. Atmospheric density uncertainty was modeled as drag coefficient ( $C_D$ ) uncertainty. A value of 10% (post-Viking '75 result) was used. In this section the sensitivity of O.D. results and  $\Delta V_{STAT}$  results to the higher order gravity terms and to drag is examined.

Table III-19 presents O.D. results for the 100 x 2200 km and 2200 x 2200 km orbits with different sets of systematic error parameters. (Gravity uncertainties were taken from Ref. III-2 and a 10%  $C_D$ , drag coefficient, uncertainty was assumed.) Note that 3rd order terms have a significant effect for both orbits.

Table III-19 MAV Orbit Determination Accuracies

Case	Local (7 Orbits Data)		Predicted (5 Orbits)		
	RSS X	RSS X	RSS X	RSS X	
A S C E N T C I R C  C-2	$\mu, J_2, C_{22}, S_{22}$	4.6 km	.9 m/s	3.2 km	1.8 m/s
	$\mu, J_2, C_{22}, S_{22}, C_D$	7.7 km	1.5 m/s	5.7 km	2.1 m/s
	$\mu, J_2, C_{22}, S_{22}, J_3, C_{31}, S_{31}, C_{32}, S_{32}, C_{33}, S_{33}, C_D$	14.7 km	2.8 m/s	9.9 km	5.7 m/s
	$\mu, J_2, C_{22}, S_{22}$	.9 km	1.4 m/s	1.9 km	1.6 m/s
	$\mu, J_2, C_{22}, S_{22}, C_{31}, S_{31}, C_{32}, S_{32}, C_{33}, S_{33}$	1.5 km	2.5 m/s	2.5 km	2.6 m/s

The individual component errors for the ascent and circular orbit updates are shown below. The ascent update includes 7 orbits of data and 5 orbits of prediction whereas the circular orbit case is for 4 orbits of data and 4 orbits of prediction. It is apparent that 3rd order effects are much more important in the ascent orbit than the circular orbit as expected. It is felt that even 4th order terms should be considered for the ascent orbit but not for the circular one.

		$\sigma_x$ (km)	$\sigma_y$ (km)	$\sigma_z$ (km)	$\sigma_{\dot{x}}$ (m/s)	$\sigma_{\dot{y}}$ (m/s)	$\sigma_{\dot{z}}$ (m/s)
A S	1st, 2nd Order	1.1	2.3	2.1	.6	1.0	1.3
C E	1st, 2nd Order + Drag	1.4	4.7	2.8	.5	1.7	2.6
N T	1st, 2nd, 3rd + Drag	3.5	6.8	6.5	2.0	3.1	4.3
C I	1st, 2nd Order	.8	1.3	1.3	.2	1.2	1.0
R C	1st, 2nd, 3rd Order	.7	1.0	.9	.4	1.7	1.8

Tables III-20 through III-23 present a comparison of mission performance parameters when O.D. accuracies are corrupted by the 2nd order gravity field and by the 3rd order field + drag. The effect on orbiter and MAV  $\Delta V_{STAT}$  loads is minimal (Tables III-20 and -21). The major effect is on the control dispersion ellipse at nominal TRI (Table III-22). The downtrack position dispersion is increased by 20%. Since downtrack dispersions are accounted for by varying the TRI time, this increase will not have an impact on terminal rendezvous propellant. Table III-23 shows that pointing accuracy after the 3rd trim maneuver is also significantly degraded by the degraded O.D. capability. However, results are still well within the radar beam width of  $20^\circ$ . This means that sufficiently accurate pointing commands can be computed before the trim sequence to allow radar acquisition after trim #3. Post-circularization MAV orbits were examined to see if somehow the poorly targeted CIRC burn might produce an unacceptable periapsis altitude. This was found to not be the case as all orbits were quite acceptable.

Table III-20 MAV  $\Delta V_{STAT}$  Sensitivity

	$\Delta V_{STAT}$ (m/s)	
	2nd Order Field	3rd Order Field
CIRC	39.3	39.5
RECIRC	17.9	21.6
Total	41.6	45.0

Table III-21 Orbiter Trim  $\Delta V_{STAT}$  Sensitivity

	$\Delta V_{STAT}$ (m/s)	
	2nd Order Field	3rd Order Field
Trim #1	23.2	24.1
Trim #2	1.2	1.9
Trim #3	20.2	21.1
Total	42.6	45.0

Table III-22 Dispersion Ellipse Sensitivity

	$\sigma_u$ (km)	$\sigma_v$ (km)	$\sigma_w$ (km)	$\sigma_{\dot{u}}$ (m/s)	$\sigma_{\dot{v}}$ (m/s)	$\sigma_{\dot{w}}$ (m/s)
2nd Order Field	7.7	71.7	26.3	39.3	2.9	5.7
3rd Order Field	10.2	90.0	26.4	46.8	2.7	8.7

Table III-23 Sensitivity of Pointing Accuracy To Gravity Field Errors

	2nd Order Field	3rd Order Field
$6\sigma$ In-Plane	4.6°	3.9°
$6\sigma$ Out-of-Plane	1.9°	3.4°

## 5. Trim Strategy Considerations

The Viking Mission A trim maneuver strategy and the MSSR circular trim strategy are very similar in nature. Viking trims #1, #2, and #4 compare very closely to MSSR trims #1, #2, and #3 (see Figure III-10). The circular trim sequence does not attempt to correct out-of-plane error resulting after circularization burn and hence there is no MSSR trim corresponding to Viking trim #3 (a pure inclination change produced at the nodal crossing). Planar corrections could be introduced into the circular trim sequence by choosing  $(\omega + TA)_{\text{NOM}} = 90^\circ$  for the 1st trim and adding an out of plane component to rotate the nodal line. At the new nodal crossing ( $90^\circ$  later) the inclination could then be adjusted with an additional trim similar to Viking. This strategy would work better for higher inclination orbits. For low inclination orbits the 1st trim should be placed so as to minimize the out-of-plane  $\Delta V$  component.

In the present trim strategy the orbiter "catches up" to the MAV by performing trim #1 (a Hohmann transfer) to produce a lower radius orbit (taking energy out of the orbit) and subsequently fires trim #2 to adjust the final circular orbit radius. It often turns out that trim #2 is a prograde maneuver, thereby putting the same energy back into the orbit. In cases like this, phasing corrections are wasteful of energy. If the orbiter post-circularization radius is biased sufficiently greater than 50 km above the MAV and sufficiently further ahead than  $45^\circ$ , it should be possible to require orbiter trim #1 to always be a catch up maneuver (retrograde) and trim #2 to always lower the final radius (also a retrograde maneuver). This procedure would cut trim  $\Delta V_{\text{STAT}}$  in half, thereby enhancing mission performance.

## 6. $\Delta V_{\text{STAT}}$ Sensitivity to Rendezvous Errors

Table III-24 presents 99 percentile  $\Delta V$  results for 8 different Monte Carlo cases, each of which considers an additional error source. Nomenclature is as follows:

$DV_{X1}$ ,  $DV_{X2}$ , and  $DV_{XT}$  denote the MAV circularization, trim and total  $\Delta V$ s, respectively.

$DV_{Y1}$ ,  $DV_{Y2}$ ,  $DV_{Y3}$ , and  $DV_{YT}$  denote the three orbiter circular trims and the total trim  $\Delta V$ , respectively.

**Viking '75 Mission A  
(Rendezvous with Landing Site)**

Maneuver	Maneuver Location	To Adjust
MOI	Periapsis	Apoapsis Alt. to Biased Value
Trim #1	Periapsis	Timing Error at Trim #2 to Desired Value
Trim #2	Periapsis	Apoapsis to Nominal
Trim #3	Nodal Crossing	Inclination
Trim #4	Apoapsis	Periapsis to Desired Value

**URDMO  
(Rendezvous with MAV)**

Maneuver	Maneuver Location	To Adjust
MOI	Periapsis	Apoapsis Alt. to Nominal
Phasing	Periapsis	Timing Error = 0 at Circularization
Circularization	Periapsis	Eccentricity to 0.
Trim #1	Periapsis/ Apoapsis	Timing Error at Trim #2 to Desired Value
Trim #2	Periapsis/ Apoapsis	Apoapsis/ Periapsis to Desired Value
Trim #3	Periapsis/ Apoapsis	Apoapsis/ Periapsis to Desired Value

Figure III-10 Comparison of Orbiter Maneuvers

Table III-24 Sensitivity of  $\Delta V_{STAT}$  to Initial Rendezvous Errors

#	Description	MAV						Orbiter						
		DV <sub>X1</sub>	DV <sub>X2</sub>	DV <sub>XT</sub>	$\Delta V_{STAT}$	DV <sub>Y1</sub>	DV <sub>Y2</sub>	DV <sub>Y3</sub>	DV <sub>YT</sub>	$\Delta V_{STAT}$	RMAG	STAT RMAG	VMAG	STAT VMAG
1	Nominal	337.3	3.4	340.7	-----	0.5	0.7	0.2	1.4	-----	207.3	-----	99.7	-----
2	MAV Ascent Dispersions	378.5	3.8	382.3	41.6	0.5	0.7	0.2	1.4	0.0	207.6	6.3	113.5	13.8
3	#2 + MAV Execution Error	376.5	21.1	382.3	41.6	0.6	0.7	0.5	1.4	0.0	213.3	6.0	112.8	13.1
4	#3 + MAV O.D. Error (All MAV Error)	376.6	21.3	382.3	41.6	3.4	0.8	2.6	6.5	5.1	211.2	3.9	112.8	13.1
5	#4 + Orb. Circ. Execution Error	376.6	21.3	382.3	41.6	23.4	1.5	20.3	43.8	42.4	222.8	15.5	113.5	13.8
6	#5 + Orb. Trim Execution Error	376.6	21.3	382.3	41.6	23.4	1.5	20.4	43.8	42.4	213.5	6.2	110.2	10.5
7	#6 + Orbiter O. D. Error	376.6	21.3	382.3	41.6	23.4	1.7	20.5	43.8	42.4	259.2	51.9	126.1	26.4
8	#7 + Orbiter/MAV Relative Error	376.6	21.3	382.3	41.6	23.6	1.9	20.4	44.0	42.6	255.5	48.2	122.5	22.8

RMAG is the 99 percentile relative orbiter/MAV position magnitude at 10th occultation exit where a phase angle of  $2^{\circ}$  is targeted for.

VMAG is the 99 percentile relative velocity magnitude at 10th occultation exit where a phase angle of  $2^{\circ}$  is targeted for.

The following can be noted from the table:

1. Statistical variation in the total MAV  $\Delta V$  (denoted  $\Delta V_{STAT}$ ) is due solely to ascent dispersions.
2. Injected MAV apoapsis dispersions cause a 14 m/s difference in orbiter/MAV circular velocities when a 50 km separation is maintained.
3. MAV execution error requires a trim maneuver ( $DV_{X2}$ ) which does not impact  $DV_{XT}$ .
4. Orbiter execution error in the circularization maneuver determines the orbiter  $\Delta V_{STAT}$  requirement.
5. Orbiter O.D. error determines RMAG, VMAG.

### C. ASSESSMENT OF NAVIGATION FEASIBILITY

The implications of navigation studies discussed in this chapter on mission feasibility are summarized below. Feasibility per se is demonstrated by results of the Monte Carlo ascent-to-rendezvous simulation which showed acceptable TRI control dispersions, maneuver  $\Delta V_{STAT}$  and antenna pointing accuracies. Important O.D. and maneuver characteristics lead to these results. Estimates of the initial MAV orbit (computed from conventional DSN range rate data) are accurate enough to target the MAV circularization maneuver which lifts the MAV out of the gravity well. The maneuver computation is not very sensitive to exact knowledge of the Mars gravity field. Orbit determination in the vicinity of 2200 km circular is quite adequate for rendezvous. As stated, MAV apopsis altitude may be better controlled to 2200 km by the use of S-band ranging measurements on the lander--although this is not required for the baseline.

The use of multi-vehicle  $\Delta VLBI$  tracking data will provide a very accurate relative state estimate for targeting the circular trim sequence. Viking Orbiter trim maneuver execution uncertainties have a negligible effect on relative state control error at TRI. Orbit dispersions introduced by the larger burns, however, do have to be taken out by the circular trim sequence.

## REFERENCES

1. "Functional Requirement Viking Orbiter 1975; Maneuver and Articulation System Accuracies," Viking Orbiter Design Handbook, No. V075-3-170, 16 February 1973.
2. "Gravity Field of Mars from Mariner 9 Tracking Data," Jack Loreil, et al, JPL and MIT, November 1, 1972. ICARUS 18, 304-316 (1973).
3. "Wind Speeds in Lower Atmosphere of Venus: Status Report on Possible Measurement via Differential VLBI Tracking of Entry Probes," I. I. Schapiro, Report to Pioneer Venus Science Steering Group, May 1972.
4. "Doubly Differenced Long Baseline Interferometry (DLBI) Analysis," 29 December 1972, D. V. Byrnes, A. L. Satin, MMC-D-72-48747-001.
5. "Navigation Analysis with Regard to Station Longitude Uncertainty Growth", C. Acton, N. Jerath, et al, JPL IOC #391.8-91, 10 September 1973.
6. Private communication from N. Jerath, JPL.
7. VNAP Users Manual (to be published by MMC).

#### IV GUIDANCE AND CONTROL ASPECTS OF ASCENT, RENDEZVOUS AND DOCKING

The primary advantage of the Mars orbital rendezvous mode is that it allows a drastic reduction in the spacecraft weight that is landed on, and ascended from the planet surface. However, this advantage can only be capitalized upon if the hardware and operational techniques required to perform the rendezvous sequence can be kept simple and reliable and if adequate control of off-nominal performance can be maintained.

The objective of this part of the study was to define guidance and control (G&C) equipment and strategies to support the MAV and orbiter navigation sequences described in Chapter III, and the terminal rendezvous, docking and sample transfer functions that follow them. The priorities for assignment of decision making functions and operational complexity were: Earth control center first; orbiter second; and, MAV last.

The MAV ascent to the initial 1 x 2200 km orbit, and the orbiter terminal rendezvous maneuvers are the only portions of the baseline MSSR mission profile that are done without Earth-based control. The study approach therefore was to keep the performance tolerances on these functions as loose as possible and the hardware requirements simple. The result, as described in this chapter is a G&C hardware and operational concept that features the following: 1) a simple, reliable, "forgiving" MAV G&C system that will deliver the vehicle to a safe, Earth trackable parking orbit; 2) a simple in-orbit G&C system for the MAV that combines pointing reference and command functions so the vehicle is always under the control of the Earth or the Orbiter; and, 3) G&C systems for the other vehicles (orbiter, lander and ERV) that will have been proven in the Viking and Pioneer Venus programs.

## A. PRELAUNCH OPERATIONS

The science guidelines followed in this study restricted the landed science operations to visual imaging of the sampling site and gathering the selected samples. The only other required activities during the 11 days between landing and MAV lift-off are updating the lander position and attitude and calculating the required launch orientation. These functions are performed on Earth using tracking and telemetry data from the lander.

The position of the lander on the surface, within the guaranteed Viking landing footprint of 650 x 1748 km, can be determined by DSN tracking or by on-board gyro compassing using the lander inertial reference unit. A lander S-band transponder similar to the one used on the MAV is baselined to provide direct DSN tracking capability. The lander position accuracy for each type of determination is shown below:

### Guaranteed Viking Footprint Accuracy

Latitude -  $10.97^{\circ}$  or 650 km ( $3\sigma$ )

Longitude -  $29.5^{\circ}$  or 1748 km ( $3\sigma$ )

### Gyro Compassing (Lander IRV)

Latitude -  $5^{\circ}$  (296 km -  $3\sigma$ )

Azimuth -  $5^{\circ}$  (296 km -  $3\sigma$ )

### Earth-based Tracking

Latitude -  $0.3546^{\circ}$  or 21 km, ( $3\sigma$ )

Longitude -  $0.03039^{\circ}$  or 1.8 km, ( $3\sigma$ )

Altitude - 984.24 ft or 0.3 km, ( $3\sigma$ )

The navigation simulation studies described in Chapter III used gyrocompassing accuracy in predicting the lander position. Even so, this conservative position accuracy assumption resulted in dispersions on the MAV - ascent orbit parameters that were acceptable.

The lander attitude or local orientation on the surface can be determined by using one of the MAV Sun sensors before the MAV is erected. The Sun position as a function of time as sensed by the Sun sensor, which has a known relationship to the Lander, and those data are telemetered back to Earth to calculate the lander attitude. Lander longitude can also be described from this information.

The lander position and attitude should be determined during the early portion of the landed phase to allow time for the calculation of the nominal launch orbit and any contingency orbits. Contingency orbits are alternatives to the nominal that might allow early launches (to avoid surface environmental effects) or back-up launch opportunities to a delayed launch.

The MAV is not erected until just before launch, so it can be kept within narrow temperature limits in the thermo-control canopy to guarantee the performance of the solid propellant motors. The MAV is erected to the correct attitude by predetermined and prestored commands calculated by Earth-based computers and verified by the Sun sensor system. A small and simple software program in the lander GCSC is used to automatically erect the MAV. The attitude of the erected MAV is verified by comparing the prestored position of the Sun at a certain time with that sensed by the Sun sensor system. The lander GCSC has a much greater capability than is required for these operations and can be used without modification to augment the on-surface operation by controlling and verifying these operations. The MAV is launched at the azimuth corresponding to the inclination of the orbiter orbit, and at a nominal initial pitch ramp angle of 54.8 degrees for the approximated gravity turn it will follow. The MAV is launched at a prestored and predetermined time with discretes from the GCSC.

More details on the hardware implementation for the prelaunch phase are provided on Paragraph E of this chapter.

## D. MAV LAUNCH, ASCENT AND ORBITAL OPERATIONS

During ascent, the MAV is guided autonomously by its own three-axis stabilized guidance and control (G&C) system to inject it into a rough, but safe, initial orbit. A study was conducted to consider whether a three-axis or spin-stabilized system is better for the Mars sample return mission. The three-axis stabilized system was selected because its weight was found to be only slightly greater than the spin stable system and its performance was generally superior for all phases of flight. Either type of stabilization can be used, but only if its weight advantage becomes more pronounced should a spin stabilized system be considered. The results of the study comparing the two types of stabilization are discussed in Section F of this chapter.

The MAV uses a simple open loop guidance system with a constant pitch-over rate to execute the ascent phase. The MAV pitch profile and its dynamic pressure during the flight are shown in Figure IV-1. The constant pitchover rate ( $\theta = 0.16t + 54.8$ ) that approximates a gravity turn, is also shown. The dynamic pressure reaches a maximum of  $515 \text{ kg/m}^2$  ( $105.3 \text{ lb/ft}^2$ ) at the end of the first stage burn.

Figure IV-2 shows the launch, ascent and Earth acquisition sequence of the MAV. The 54.8 degree initial pitch angle of the MAV must be held to an estimated pointing accuracy of  $\pm 1/2$  degree. During the ascent phase, the MAV executes a constant pitchover rate turn of 0.16 deg/sec with an estimated accuracy of 0.004 deg/sec, due to principally rate gyro bias errors. The description and the sources of derivation of the errors assumed in the simulation of the ascent phase are shown in Table IV-1. The numerical values of launch phase tolerances used in the simulation of the ascent phase are shown in Table IV-2 with their nominal values. The first stage burn takes 54.8 seconds and the MAV then coasts for 200.8 seconds (see Figure IV-2). The second stage is ignited with a time discrete from the on-board computer based on the transponder clock and injects the MAV into a 100 x 2200 km altitude orbit. The second stage burns for 31.2 seconds. Shortly after injection, the MAV is commanded by prestored and precalculated commands to point toward the Earth. The MAV attitude pointing

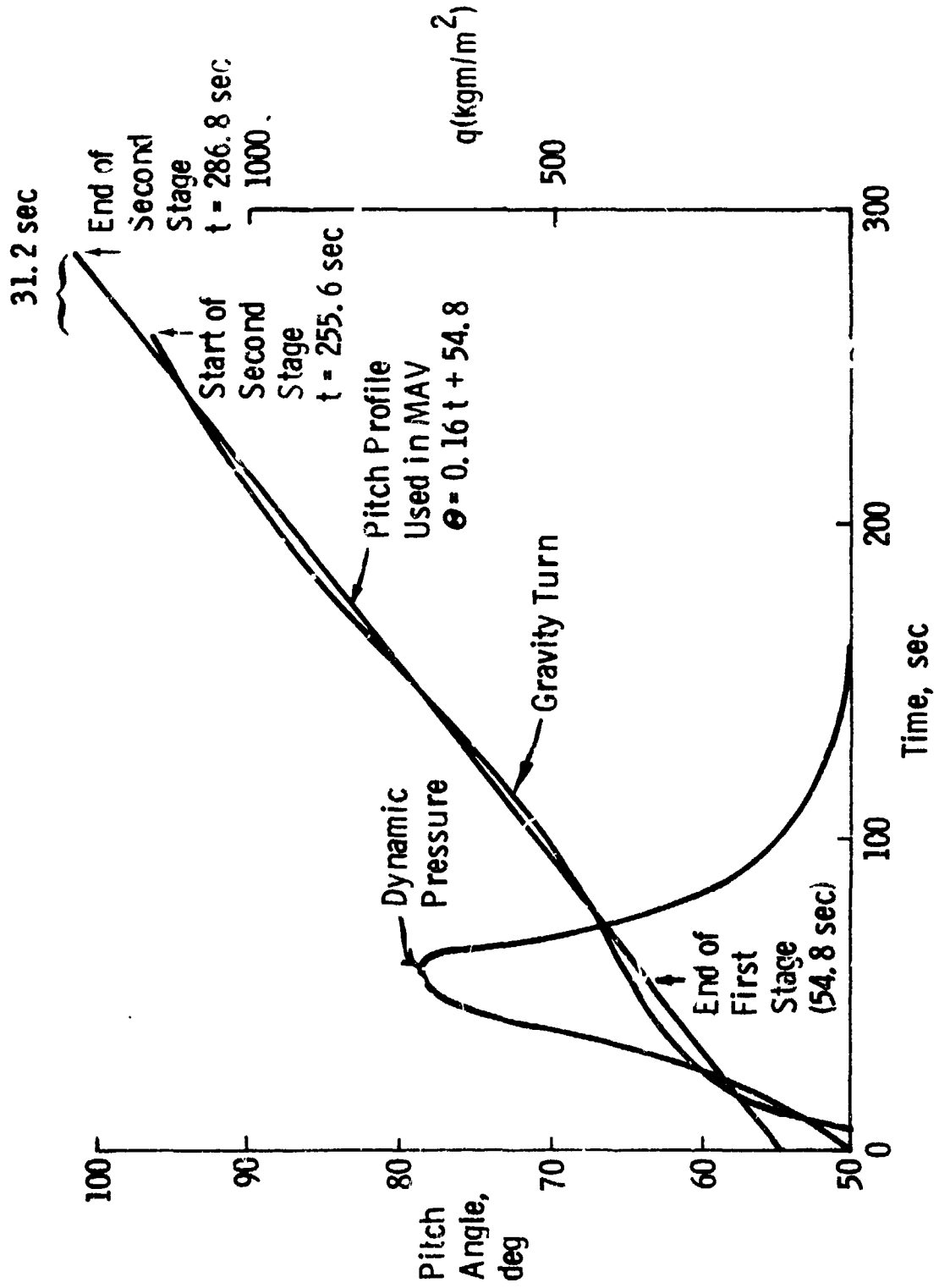


Figure IV-1 MAV Pitch Angle and Dynamic Pressure vs Time of Flight

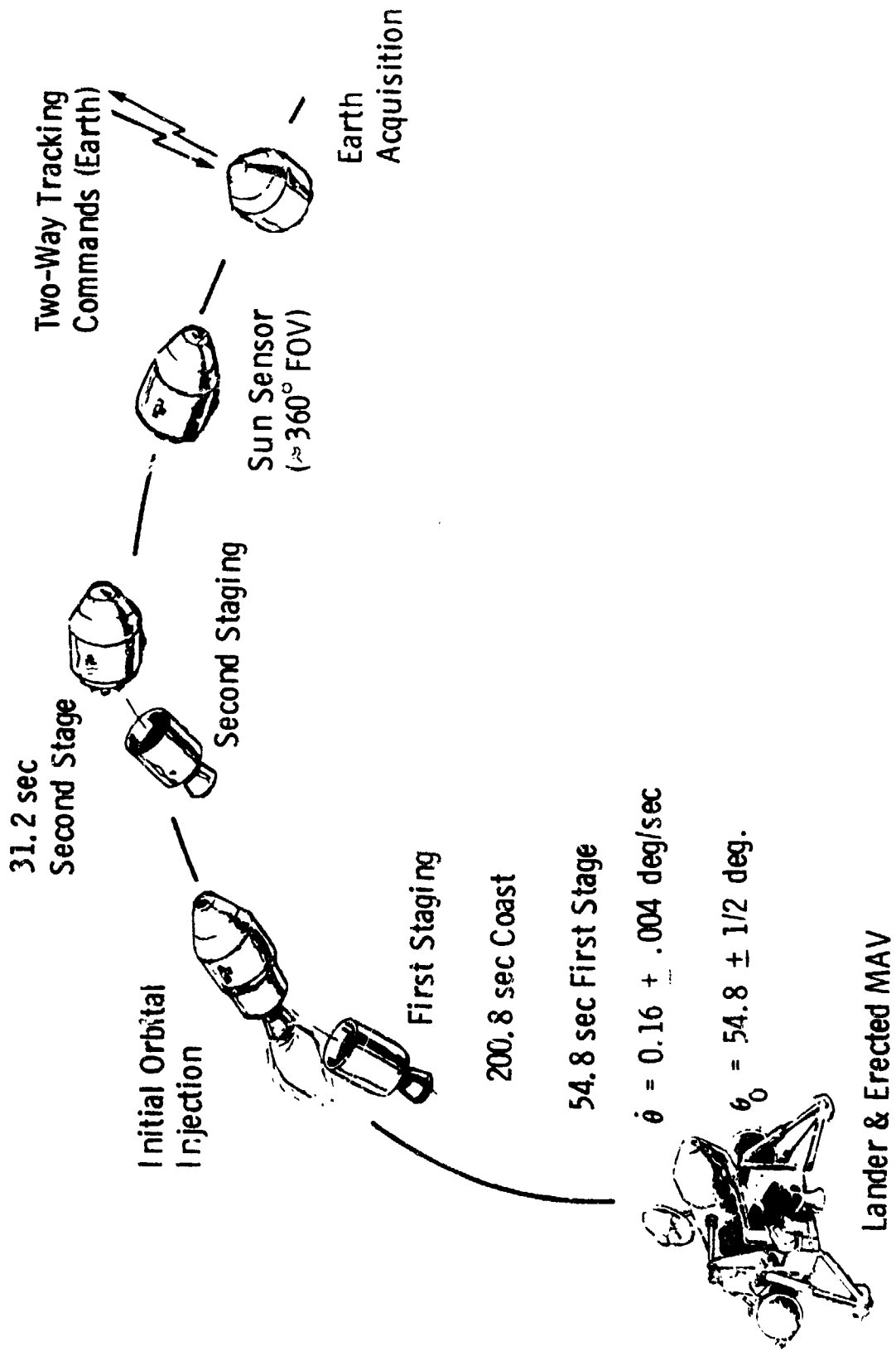


Figure IV-2 MAV Launch, Ascent, and Earth Acquisition

Table IV-1 Launch Phase Error Source

Error Source	Error
Pitch Rate	Gyro Bias Error
Liftoff Weight	0.3% ( $3\sigma$ )
Ramp Angle	MAV Sun Sensor ( $0.25^\circ$ )
J2 Gravity Coefficient	Viking '75 Environmental Specs
Central Gravity Coefficient	Viking '75 Environmental Specs
Launch Azimuth	MAV Sun Sensor ( $0.25^\circ$ )
Coast Time	Launch Thrust Ignition Errors
Launch Site Altitude	Based on Estimated Lander Position
Geodetic Latitude	5.0 deg ( $3\sigma$ )
Propellant Weight	0.25 ( $3\sigma$ )
Burn Time	4.0% ( $3\sigma$ )
Thrust	4.0% ( $3\sigma$ )
Impulse	0.75% ( $3\sigma$ )

Table IV-2 Launch Phase Errors

<u>Error Source</u>	<u>Nominal</u>	<u>Error (<math>1\sigma</math>)</u>
Pitch Rate (1)	0.16612 deg/sec	0.00416 deg/sec
Pitch Rate (2)	0.16612 deg/sec	0.00416 deg/sec
Liftoff Weight	290 kg (638 lbs)	0.25 kg
Ramp Angle	35.2 deg	0.25 deg <sup>-5</sup>
J2 Gravity Coefficient	0.00197	0.67 (10 <sup>-5</sup> )
Central Gravity Coefficient	42828.4 km <sup>3</sup> /sec <sup>2</sup>	0.467 km <sup>3</sup> /sec <sup>2</sup>
Launch Azimuth	----	0.250
Coast Time	200.8 sec	0.045 sec
Launch Site Altitude	----	608.3 m (1995.7 ft)
Geodetic Latitude	0 deg	5.0 deg
Weight Propellant (1)	128.4 kg (282.5 lbs)	0.266 kg
Burn Time (1)	54.8 sec	0.554 sec
Thrust (1)	6600 N (1500 lbs)	5.3 N
Weight Propellant (2)	81.6 kg (179.5 lbs)	0.243 kg
Burn Time (2)	31.2 sec	1.01 sec
Thrust (2)	6600 N (1500 lbs)	6.6 N
Impulse (1)	358892 N-sec	1643.3 N-sec
Impulse (2)	227921 N-sec	1500.0 N-sec

system, using the angle tracking system, acquires the DSN and uses that microwave signal to control its pitch and yaw attitudes. The roll attitude of the vehicle is measured by the Sun sensor system, and is used as input to the roll attitude system.

Earth acquisition represents the completion of the ascent phase and the start of the initial rendezvous phase. During the initial rendezvous phase, the MAV orbit is circularized and trimmed to a more accurate 2200 km circular orbit. The orbiter orbit, which is a loose 1000 x 100,000 km orbit initially, is circularized and trimmed to match the MAV orbit to be within rendezvous radar acquisition range in the 2200 km circular orbit. The vehicles are tracked between the orbital maneuvers so their orbits can be determined and the maneuvers necessary to inject the spacecraft into the next orbit can be determined.

Figure IV-3 shows how the MAV executes the Earth-controlled orbital maneuvers. At the start of an orbital maneuver, the MAV is Earth-oriented so it can communicate and receive commands from Earth which it can store in its minicomputer. The MAV is first commanded to execute a predetermined roll maneuver by stored command to place the AV maneuver direction in the pitch plane. This roll maneuver can be verified on board by comparing Sun sensor value to values calculated by Earth-based computers and prestored in the MAV minicomputer. These values can be verified back on Earth if time and power are available, since the vehicle is still pointed toward Earth. The MAV is then commanded, again by stored command, to execute a pitch maneuver until the vehicle has the correct orientation for the orbital maneuver. This maneuver can also be verified on board with a small software program in the minicomputer by comparing Sun sensor values to prestored values. The maneuver is executed and the engine is shut down based on time from the MAV clock. The MAV is then commanded back to the Earth pointing orientation and executes these maneuvers in the reverse order. The MAV is then commanded back into the automatic Earth pointing orientation control.

The MAV is inertially oriented except during ascent and when it is executing orbital maneuvers. The MAV has the capability of operating in three attitude control modes during its Earth-controlled orbital operations.

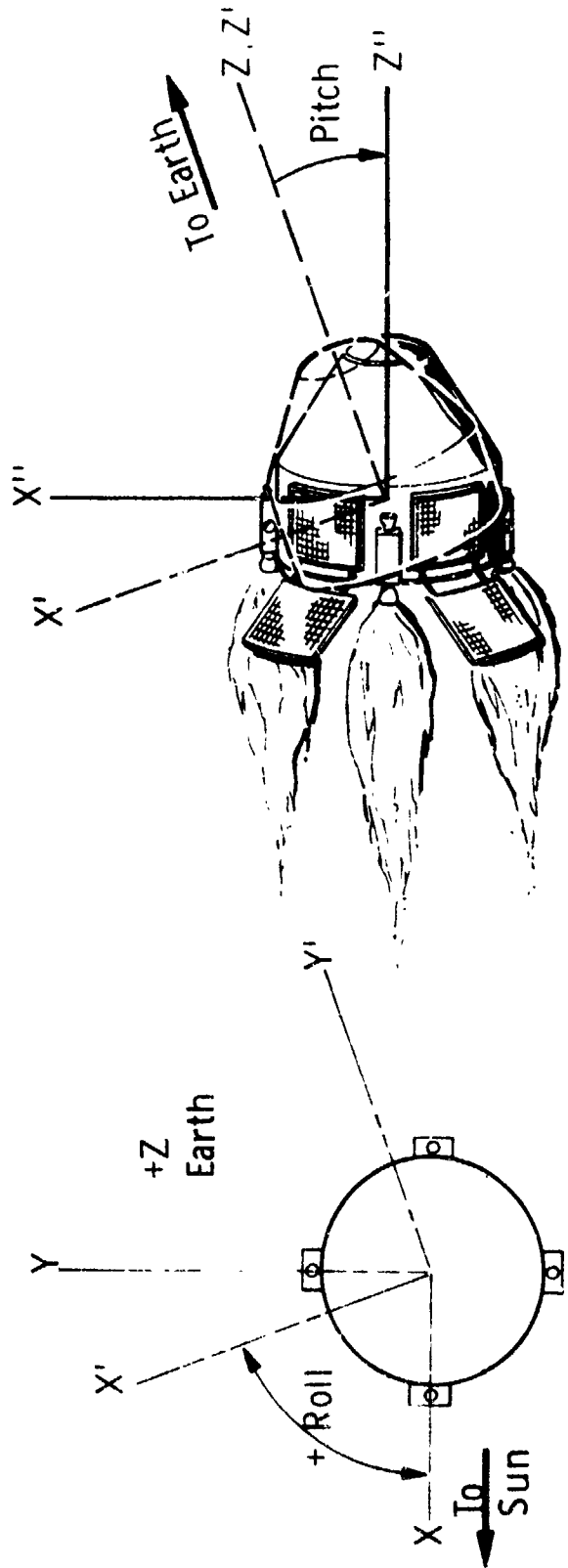


Figure IV-3 MAV Orbital Maneuvers

During ascent and during occultation of the Sun or Earth all the attitudes of the MAV are controlled by an on-board inertial reference system using rate gyros. When the vehicle is being tracked in orbit and no occultations occur it uses the Sun sensor system and the Earth-pointing angle tracking system to establish a celestial reference system. A third hybrid reference mode is available on command to save power which uses the pitch rate gyro and the Sun sensor system to control the vehicles' attitudes.

At the end of the initial rendezvous phase, the vehicles have executed maneuvers so they are well within rendezvous radar range and are celestially oriented as shown in Figure IV-4. The MAV has an Earth-Sun orientation and the orbiter has an Earth-Canopus orientation in the celestial mode. The vehicles are commanded to point at each other by stored commands calculated on Earth and telemetered to each vehicle. The rendezvous radar (RR) on the orbiter is then commanded on. As shown in Chapter III all predicted dispersions in relative position of the orbiter and MAV will be well within the maximum range (750 km) and antenna beam width ( $20^{\circ}$ ) of the orbiter rendezvous radar so that acquisition and lock-on will occur.

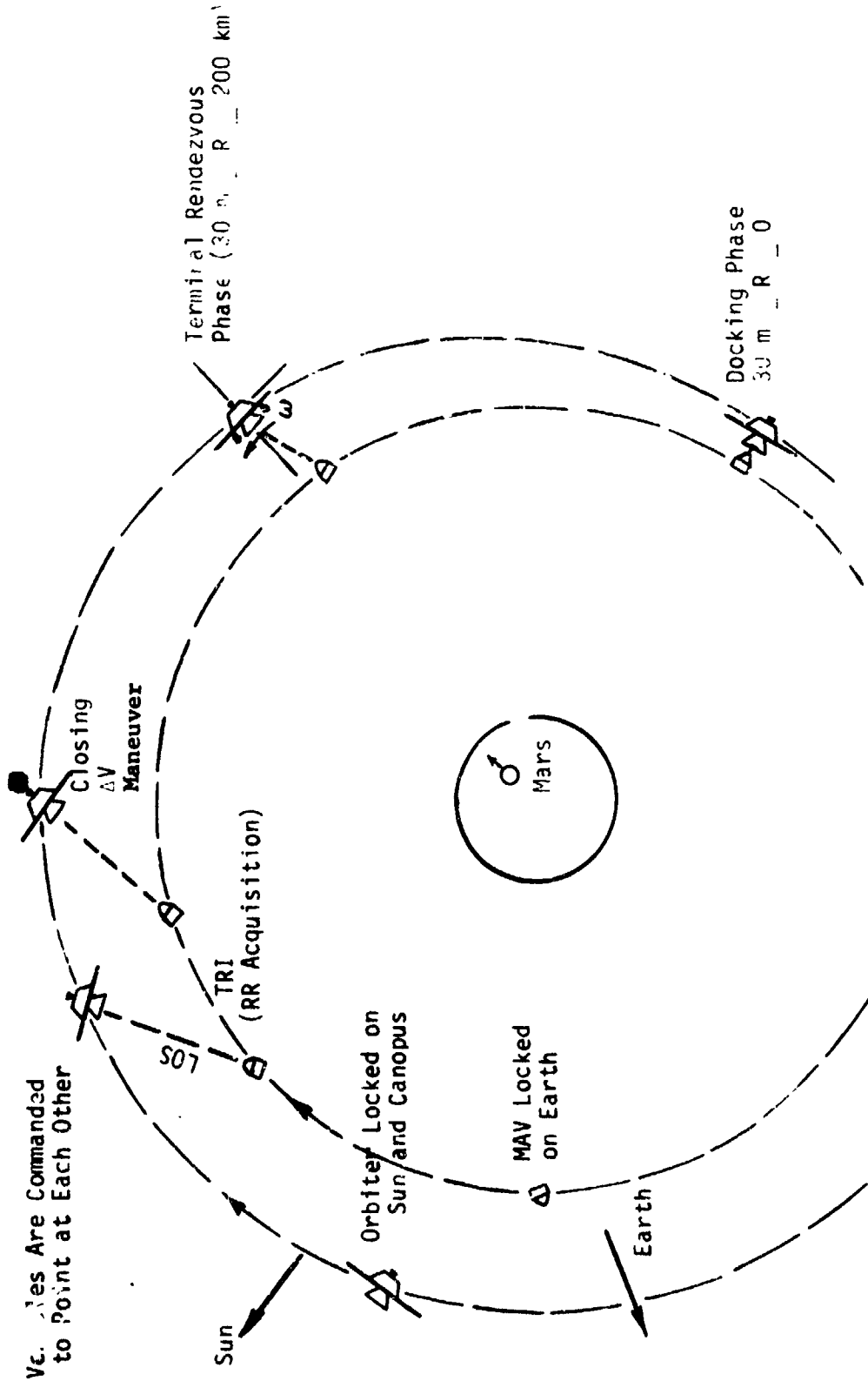


Figure IV-4 Terminal Rendezvous and Docking Phases

### C. TERMINAL RENDEZVOUS

Terminal rendezvous initiation (TRI) occurs when the rendezvous radar acquires the MAV. After terminal rendezvous initiation the orbiter attitudes are controlled by the RR and the MAV attitudes are controlled by the angle tracking system using the RR microwave signal to give angle pointing errors. Both vehicles are controlled to point along their mutual line of sight (LOS) throughout the terminal rendezvous and docking phases although this pointing is modified to control the LOS rotation rate during the closed loop terminal rendezvous phase. The MAV transponder turns around the RR microwave signal to implement a cooperative rendezvous system. The first maneuver in the terminal rendezvous phase is the initial closing  $\Delta V$ , executed by the orbiter when the relative range between the vehicles is reduced to 100 km as sensed by the RR. The closing  $\Delta V$  maneuver is executed along the LOS between the two vehicles to accomplish an approximate interception between the two vehicles.

From our rendezvous simulation studies and the way the terminal rendezvous phase was implemented, it appears that a fixed closing  $\Delta V$  magnitude cannot be used throughout the range of dispersions predicted by the navigation analysis. Either the magnitude of the closing  $\Delta V$  has to be calculated on board on the basis of the relative state between the two vehicles, as sensed by the RR, or the terminal rendezvous phase implementation has to be refined so that smaller  $\Delta V$ s are executed after the initial closing  $\Delta V$  to compensate for dispersions.

A variable  $\Delta V$  maneuver calculated as a function of the spacecraft's relative dispersions is the approach used in the Apollo space program and was baseline in this study.

One way to derive the closing  $\Delta V$  magnitude is to use sensitivity theory to derive a sensitivity coefficient, which is a constant in the orbiter control computer (CC) and is multiplied by the position dispersion from the RR to get the  $\Delta V$  magnitude. The rate of change of closing  $\Delta V$  magnitude required as a function of the dispersion must be close to linear to get an accurate determination, since linear perturbation theory is used. Further studies should be conducted in this area to determine the optimum method for executing the closing  $\Delta V$  maneuver.

After the closing  $\Delta V$  maneuver has been executed, the orbiter is commanded into the closed loop control portion of the terminal rendezvous phase where the vehicles are brought to within 30 m of each other for docking phase. A number of types of rendezvous and intercept guidance schemes were considered for the terminal rendezvous algorithm. The following types were considered as candidates:

- Pursuit Course
- Modified Pursuit Course
- Constant Bearing Course
- Proportional Navigation
- Optimum Guidance Schemes

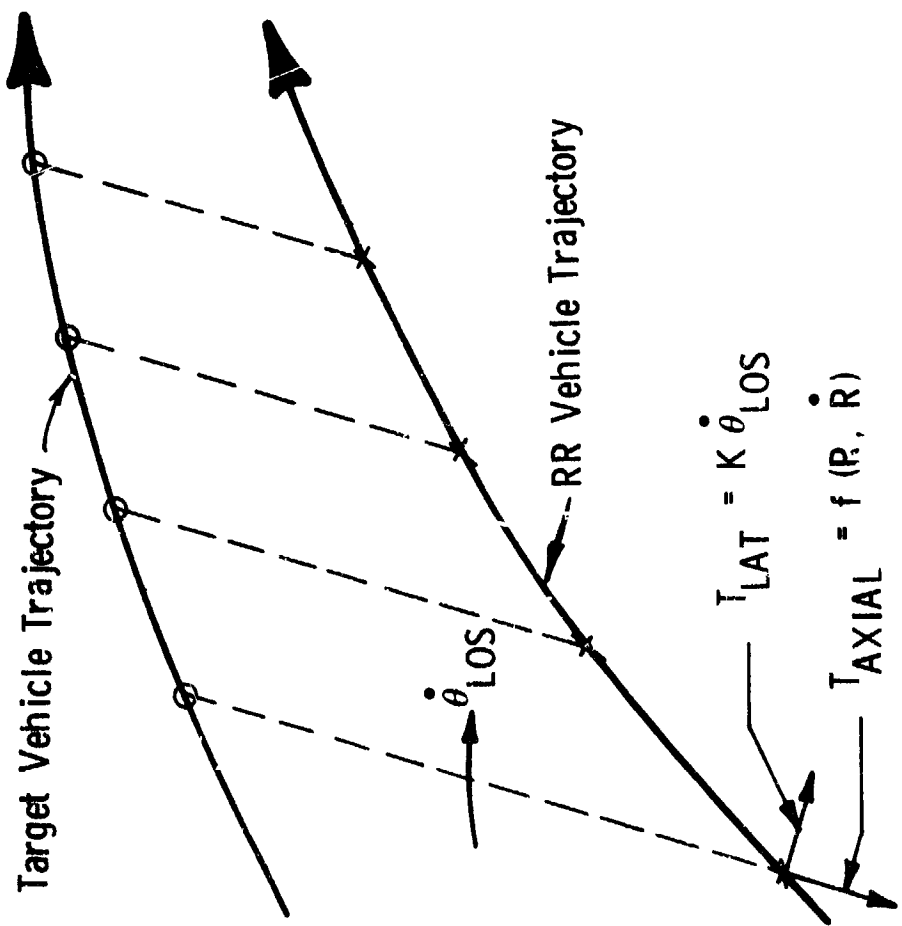
The rendezvous vehicle that uses a pursuit guidance utilizes a constant rate turn to pursue the target, but requires a very large lateral acceleration capability that is usually not available. The modified pursuit course leads the target and requires less thrust capability, but still requires large lateral accelerations. Constant bearing course (collision course) maintains a constant bearing--inertial orientation of LOS in space. Proportional navigation guidance is the most popular and a practical method of approximating a constant bearing type of guidance. The optimum guidance schemes used for terminal rendezvous involve complicated on board calculations of orbital parameters and require complex hardware and software implementation.

The proportional navigation guidance algorithm is the only type that has been implemented in previous U.S. or Soviet space programs and was therefore the first choice for the baseline in this study. The Gemini and Apollo spacecraft used this type of guidance to accomplish their rendezvous. In some cases, the terminal rendezvous was executed automatically (unmanned) in the Apollo space program. The United States has never demonstrated an autonomous (unmanned) docking. The Soviets demonstrated automatic rendezvous and docking between Cosmos 186 and Cosmos 188 as early as October 30, 1967, using a similar type of proportional navigation guidance (Ref. IV-1). They demonstrated it again with Cosmos 212 and Cosmos 213. Figure IV-5 illustrates the principal of proportional guidance.

If two vehicles are on an approximate intercept course and the LOS rate ( $\dot{\theta}_{\text{LOS}}$ ) is kept small, a rendezvous between two vehicles is accomplished when the relative range rate is driven to zero as the relative range goes to zero. An interception is defined as when the two vehicles positions are matched at the same time. A rendezvous is defined as when the two vehicles' positions and velocity are matched at the same time. The way that proportional navigation is generally implemented is to have separate lateral and axial engines. The lateral thrusters ( $T_{\text{LAT}}$ ) are used to keep the LOS rate small and the axial thrusters control the axial acceleration of the vehicle to match the vehicle's position and velocity. The axial and lateral thrust control laws are shown on Figure IV-5. The lateral control law is implemented like any attitude rate control system. The axial control law is implemented by axial thrust control curves which will be described later.

The proportional navigation guidance was implemented slightly differently in this study to simplify the orbiter and MAV propulsion systems and to allow a back-up option of having the MAV perform the rendezvous maneuvers in the event of an orbiter malfunction. In the approach used here the line-of-sight pointing control law is modified so that a component of the axial thrust is used to control the LOS rate.

Figure IV-6 shows the rendezvous propellant efficiency, which is proportional to the  $\Delta V$  requirement coefficient (ordinate) as a function of time of rendezvous in fractions of an orbital period shown on the abscissa. The angle  $\alpha$  is the initial angle at the terminal rendezvous between the LOS and the MAV velocity vector. If the orbiter is directly above or below ( $\alpha = 90^\circ$ ) the MAV, the rendezvous is most inefficient. If the orbiter is in back or front of the MAV ( $\alpha = 0$  or  $\alpha = 180^\circ$ ) at the start of the rendezvous, then the longer time that is taken the more efficient is the rendezvous. Although this method of rendezvous is the most efficient, it was not selected for this mission because possible ambiguities in the pointing direction would make the required field-of-view (FOV) of the rendezvous radar too large or would require a rendezvous radar search mode to acquire the MAV initially. In all cases, except when the MAV is in front of or back of the orbiter, the terminal rendezvous that takes one-half of an orbital period is the most efficient. A Hohmann transfer ( $\alpha = 90^\circ$ ) is a good example of the most efficient method of changing orbits by using a  $180^\circ$  transfer.



Proportional Navigation

$$T_{AXIAL} = f(R, \dot{R})$$

$$T_{LAT} = K \dot{\theta}_{LOS}$$

$$T_{LAT} = K \dot{\theta}_{LOS}$$

$$T_{AXIAL} = f(R, \dot{R})$$

Figure IV-5 Proportional Navigation

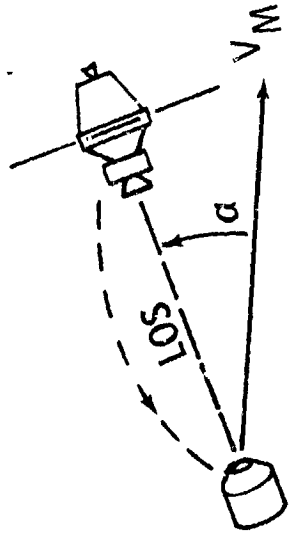
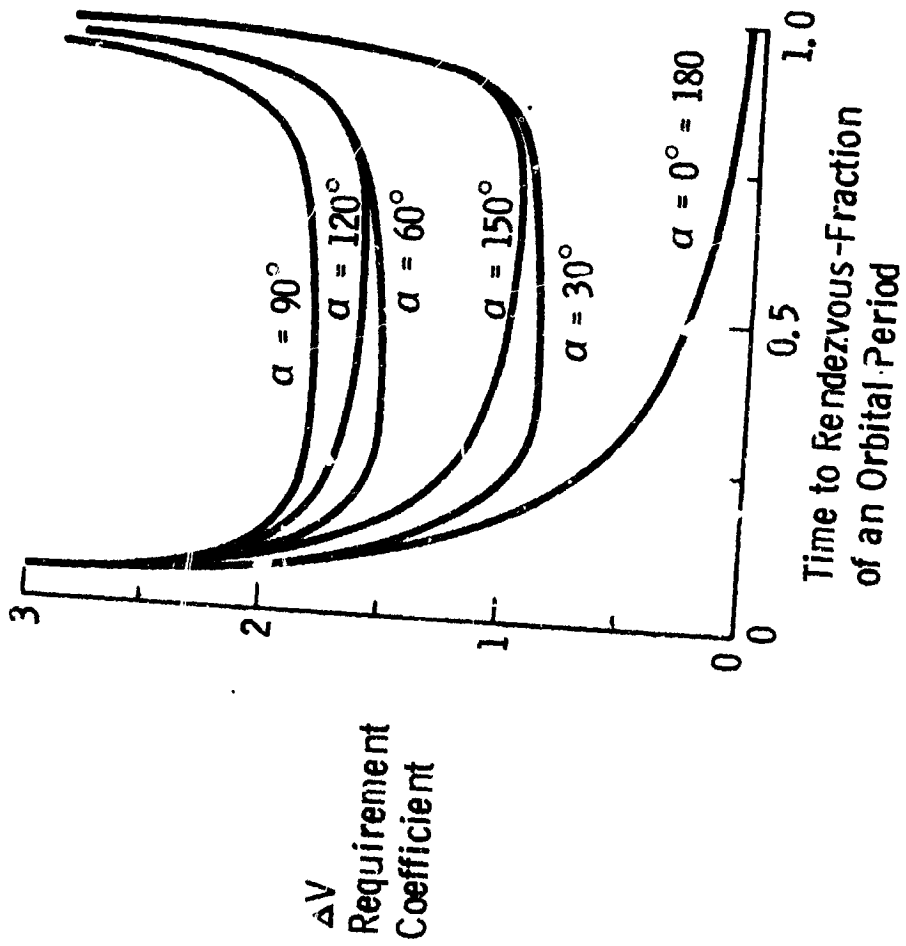


Figure IV-6 Rendezvous Propellant Efficiency

The terminal rendezvous phase was simulated on the digital computer to prove the feasibility of the approach and to understand the proportional navigation type of guidance. The digital computer simulation is described in the appendices. The following studies were conducted using the simulation tool:

1. Thrust control curve definition studies;
2. LOS rate gain studies;
3. axial thrust sizing studies;
4. terminal rendezvous initiation angle studies;
5. terminal rendezvous transfer angle selection studies;
6.  $3\sigma$  dispersion studies; and
7. interception sensitivity to closing  $\Delta V$  maneuver magnitude.

The results of these studies are discussed in more detail in the appendices.

Figures IV-7 through IV-13 show the results from the digital computer simulation of the nominal case and the  $3\sigma$  worst case (26 m out-of-plane error). The other  $3\sigma$  worst cases (7.7 km high and low) are described in the appendix. Previous simulation experience of the terminal rendezvous phase has shown that rendezvous propellant expenditure is much more sensitive to position dispersion than to velocity dispersions.

Figures IV-7 through IV-9 show the results from the simulation for the nominal case. Figure IV-7 shows the axial thrust control curves used to control the medium sized axial engines which control the relative range rate of the orbiter during terminal rendezvous phase. Two sets of control curves are shown, where one set is used above the gain change range (altitude) of 4.4 km (14,500 ft) and another set is used at closer ranges. In each set, the upper curves are the thrust-on control curves and the lower curves are the thrust-off control curves. The control curves are parabolas described by the following equations:

$$R = \frac{O(\dot{R})^2}{T/M} + R_K \quad \text{when } R \geq 4.4 \text{ km}^*$$

$$R = \frac{P(\dot{R})^2}{T/M} + R_K \quad \text{when } R < 4.4 \text{ km}^*$$

\* Determined by trial and error to minimize propellant consumption.

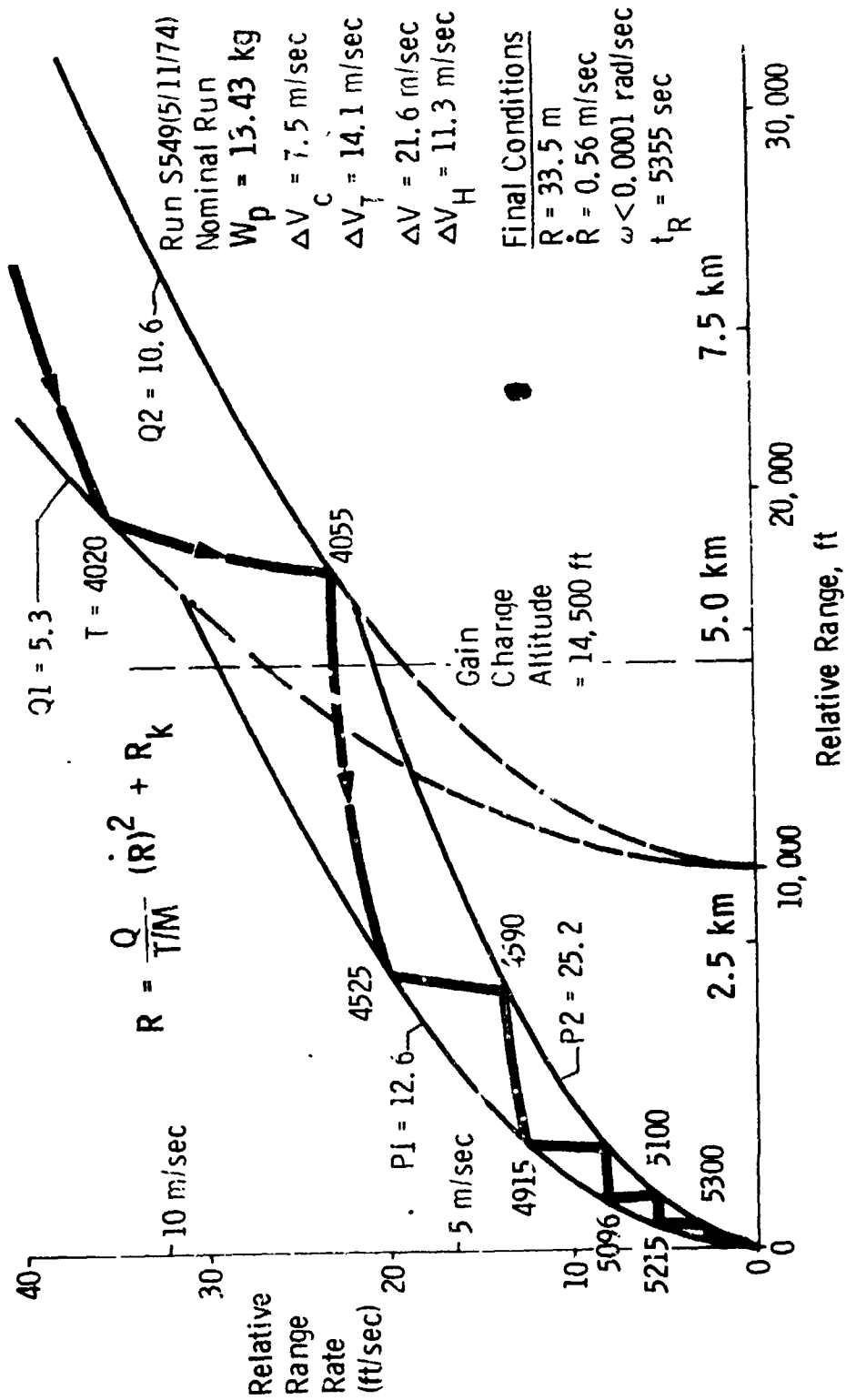
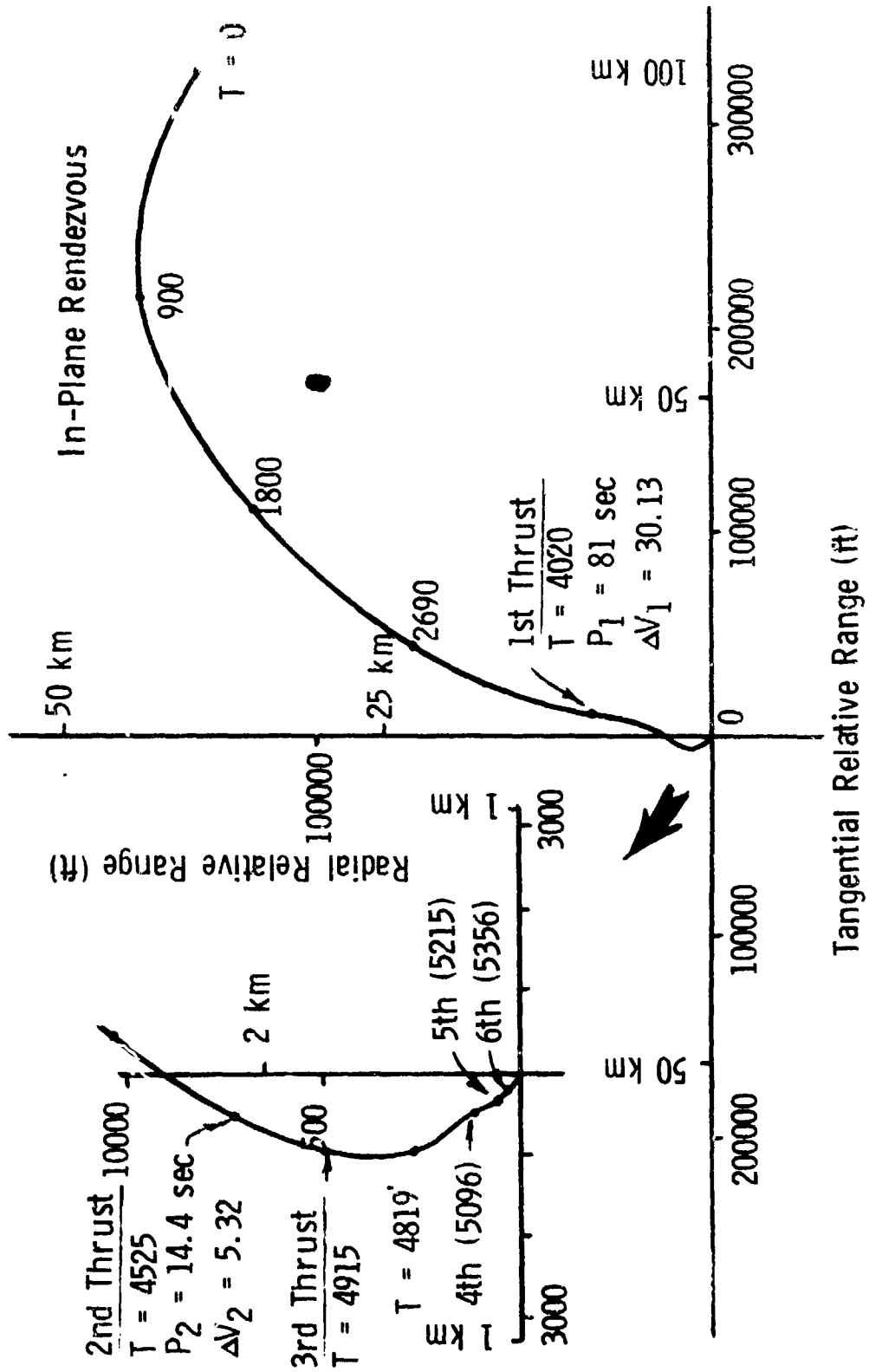


Figure IV-7 Axial Thrust Control Curves - Nominal Case



02-A1

Figure IV-8 Rendezvous Trajectory (Rotating Coordinates) - Nominal Case

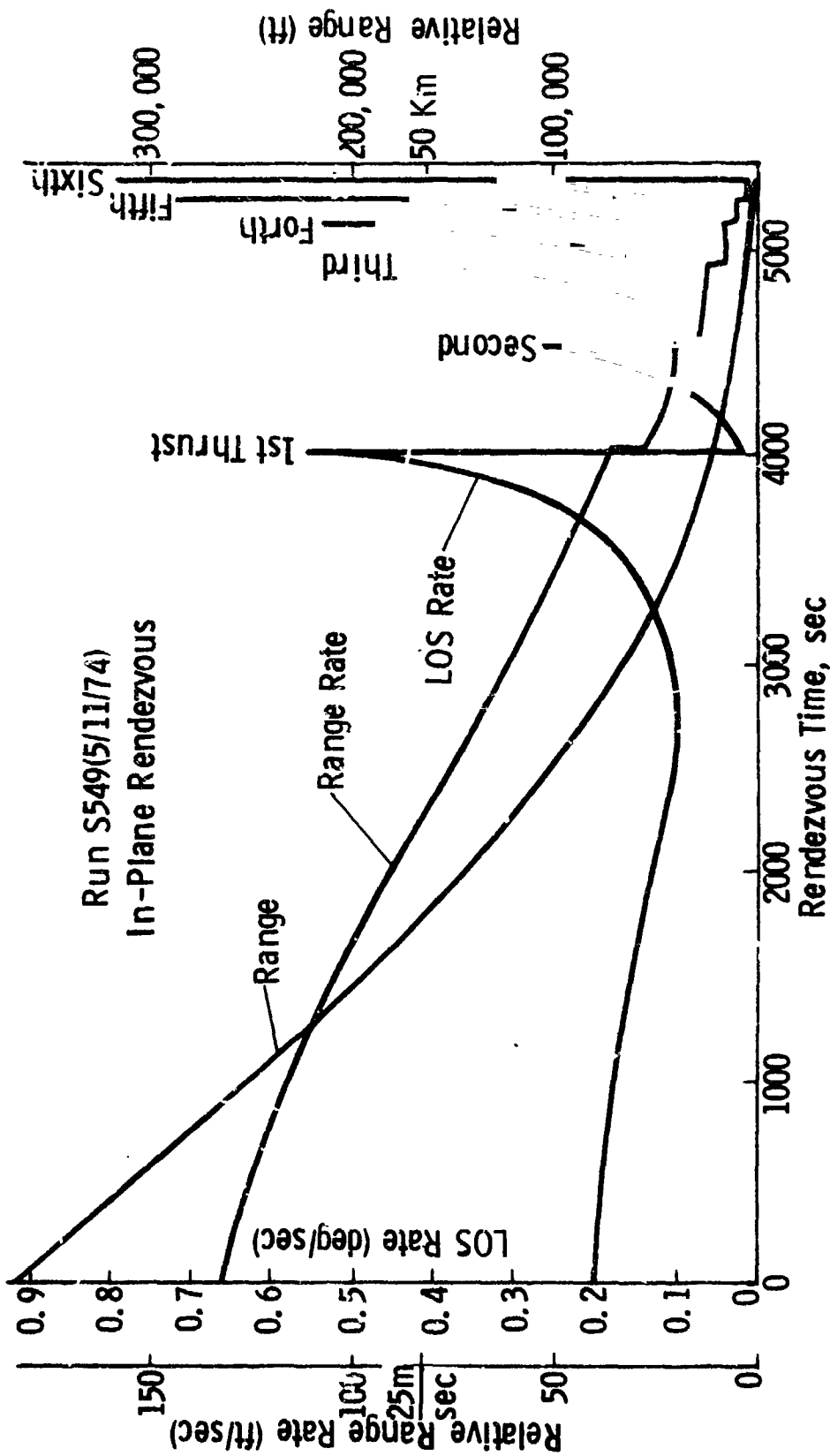


Figure IV-9 Range, Range Rate and LOS Rate vs Rendezvous Time - Nominal Case

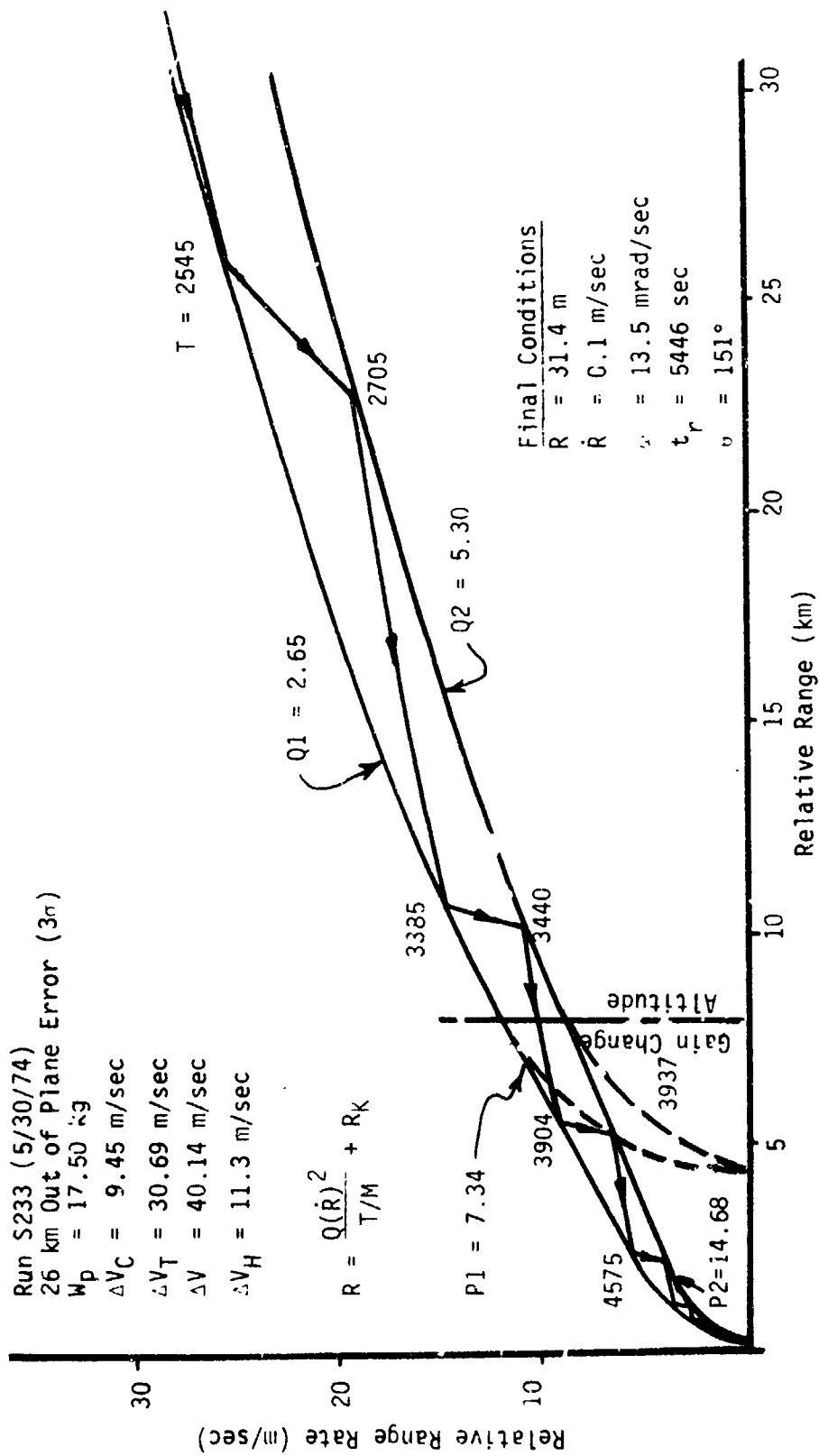


Figure IV-10 Axial Thrust Control Curves - 3-Sigma Dispersed Case

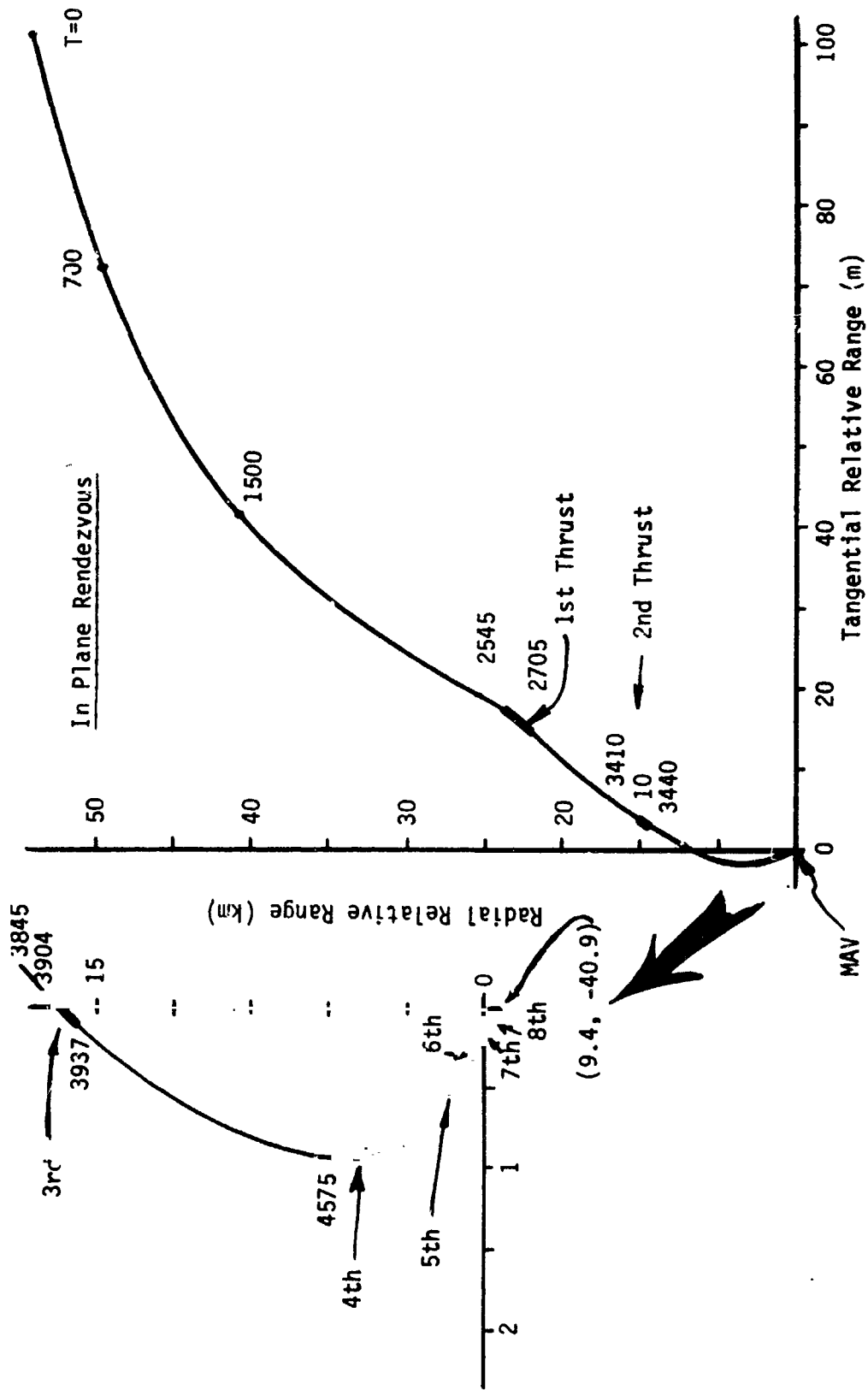


Figure IV-11 Rendezvous Trajectory (Rotating Coordinates) - 3-Sigma Dispersed Case

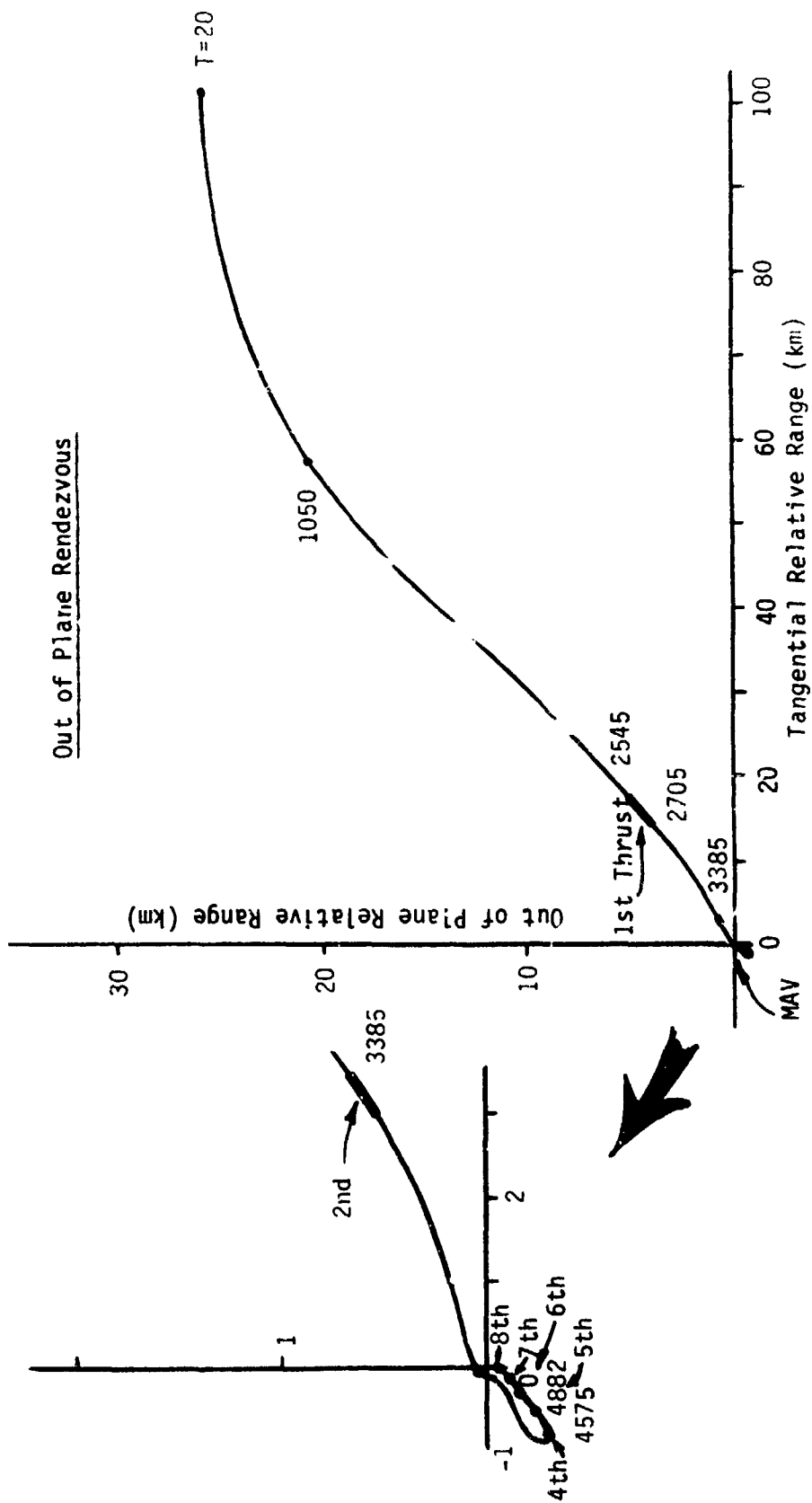


Figure IV-12 Rendezvous Trajectory (Out-of-Plane) - 3-Sigma Dispersed Case

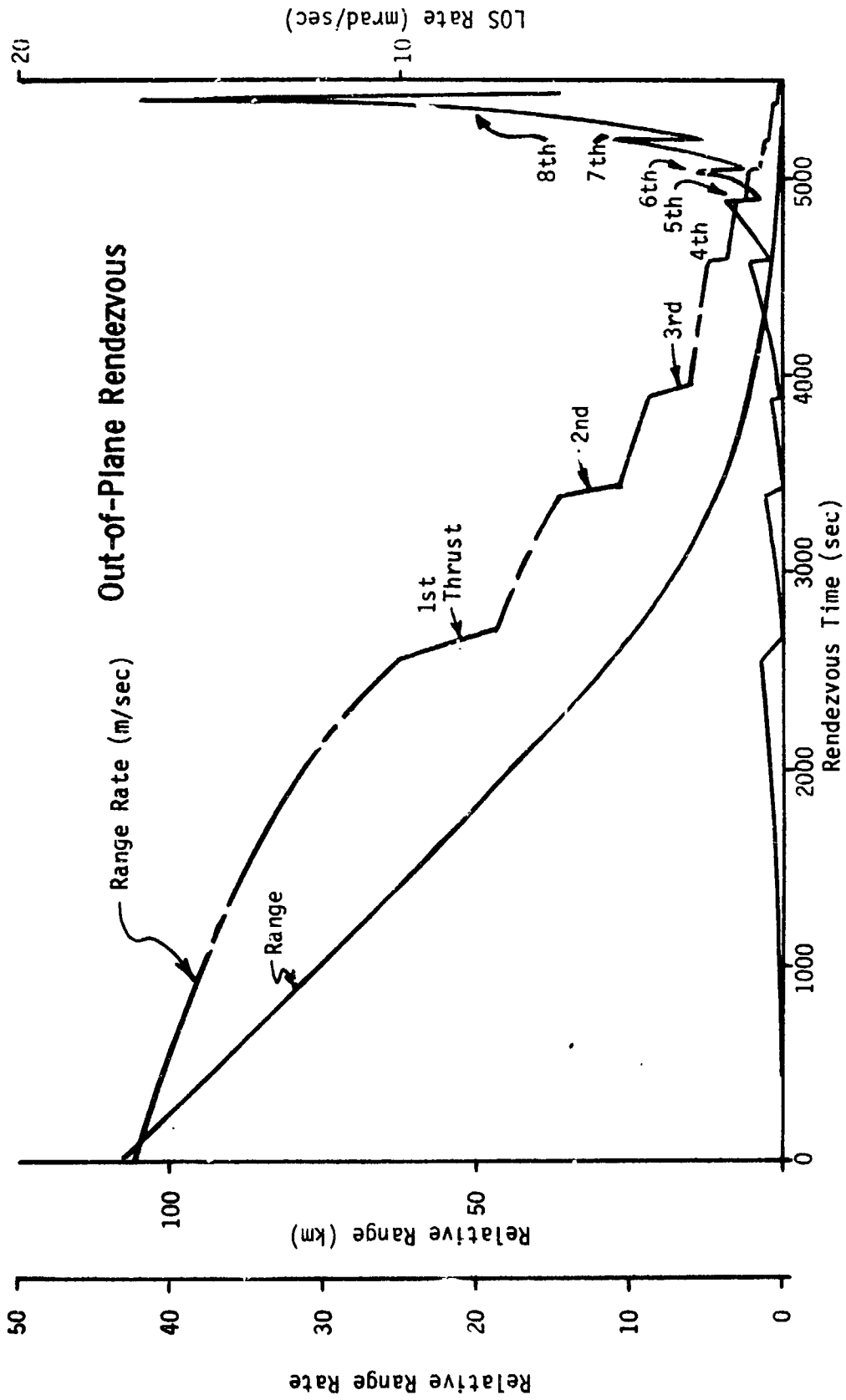


Figure IV-13 Range, Range Rate, LOS Rate vs Rendezvous Time - 3-Sigma Dispersed Case

where  $\bar{R}$  = relative range between vehicles (abscissa)  
 $\dot{\bar{R}}$  = relative range rate between vehicles (ordinate)  
 $R_K$  = asymptotic ranges  
 $Q1$  = control gain for thrust-on curve above 4.4 km  
 $Q2$  = control gain for thrust-off curve above 4.4 km  
 $P1$  = control gain for thrust-on curve below 4.4 km  
 $P2$  = control gain for thrust-off curve below 4.4 km  
 $T/M$  = average thrust-to-mass during TR phase

The orbiter coasts from the end of the  $\Delta V$  closing maneuver, when the vehicles are 100 km apart, until it meets the condition of the thrust-on curve shown in Figure IV-7. The medium-sized thrusters on the orbiter are fired to decrease the closing rate, until the conditions of the thrust-off curves are met. The axial thrusters are then shut off at 4055 seconds (time of flight is also indicated on this figure). The orbiter executes its second thrusting period, when the relative range is reduced to 2 km after 4525 seconds have elapsed in the terminal rendezvous phase. The relative range rate is reduced to about 4 m/sec after the second thrust period. The third, fourth, fifth and sixth thrust periods are executed at 4915, 5096, 5215, and 5356, respectively. The total  $\Delta V$  required was 21.6 m/sec where 7.5 m/sec was required for the closing  $\Delta V$  maneuver ( $\Delta V_C$ ) and 14.1 m/sec for the terminal rendezvous retro thrusting phase ( $\Delta V_T$ ). The propellant required for the terminal rendezvous was 13.43 kg. The Hohmann transfer  $\Delta V$  ( $\Delta V_H$ ), which is an optimum maneuver, is also shown for comparison purposes. These simulation results show that the rendezvous efficiencies achieved with proportional navigation algorithms are not optimum but the allowable propellant margins on board the orbiter are adequate to handle the estimated 3 worst cases. Further terminal rendezvous studies should be conducted to investigate and improve the efficiency of the terminal rendezvous phase.

The terminal rendezvous final conditions, which are also the initial conditions of the docking phase, are also shown in Figure IV-7. The final range, range rate and LOS rate are 33.5 m, 0.56 m/sec and less than 0.1 mrad/sec. respectively. The terminal rendezvous transfer angle is 151 degrees with a transfer time of 5355 seconds. Figure IV-8 shows the rendezvous trajectory in the MAV centered tangential coordinates, where

the ordinate is in the radial direction and the abscissa is tangent to the MAV orbit. The small insert shows the final phase of the terminal rendezvous. The orbiter accomplishes the final closure from above and behind the target vehicle. The thrust period time (P) and  $\Delta V$  are shown for earlier thrust periods. Figure IV-9 shows the range, range rate and LOS rate as a function of time during the terminal rendezvous phase. The range rate is driven to zero in steps as the range is reduced. The LOS rate builds up until it is reduced during the thrust period by the component of the thrust vector that is perpendicular to the LOS. The LOS rate is reduced below the threshold of 0.1 milliradian/second during the terminal rendezvous phase.

Figures IV-10 through IV-13 show the simulation results for the  $3\sigma$  worst case, which has a 26 km out of plane error. The terminal rendezvous trajectory in terms of range vs range rate is shown in Figure IV-10. The  $\Delta V$  and propellant requirement for the  $3\sigma$  worst case is shown, along with the terminal rendezvous final conditions. The propellant required on board to accomplish the worst case terminal rendezvous is 17.5 kg. A total  $\Delta V$  capability of 40.14 m/sec is required where about 25 percent (9.45 m/sec) is required in the orbiter main engine propulsion system. A total  $\Delta V$  capability of 80 m/sec was allotted on the orbiter in the baseline design to allow for malfunction and reinitiation options. The in-plane trajectory shown in Figure IV-11 is similar to the nominal case. Figure IV-12 shows the out-of-plane trajectory, where the orbiter starts with a 26 km out-of-plane error. The vehicle accomplishes the final phase of the rendezvous by closing from the other side of the orbit and looping over and under the MAV. The reason the rendezvous was accomplished in this way was to compensate for an off-optimum initial closing  $\Delta V$  maneuver.

#### D. DOCKING PHASE

The docking phase is initiated when the vehicles are within 30 m of each other and the sample canister has already been deployed (see Figure IV-14). The vehicles pointing will not be affected when the antenna beamwidth changes due to sample canister deployment.

During the docking phase, a different axial control algorithm is used to control the closing velocity lateral position and attitude of the orbiter. The small RCS engines on the orbiter are used as the propulsion element. The attitudes of both vehicles are controlled to point in the LOS direction during docking. The axial control algorithm commands the orbiter to close at a constant velocity of 0.3 m/sec along the LOS while LOS rate is reduced to below the threshold level of 5.0 milliradians/sec in the 100 second docking phase. The combination rendezvous and docking radar can sense range rate to an accuracy within 0.1 m/sec. The allowable sample canister angular misalignment tolerance of 1/2 degree should be easily realized and can consist almost entirely of alignment errors as the RR controlled pointing errors are very small (approximately 1.5 millirad or  $0.13^\circ$ ). An estimated range accuracy of 3 m (10 ft) can be obtained by the RR at 30 m range, but the range accuracy degrades as the range decreases. The absolute range between the two vehicles is used only to change the mission phases, and is never used at closer ranges than 30 m. The range calibration needed to reinitiate docking, in the event of a malfunction can be obtained by integrating the range rate from the RR, which is very accurate ( $\pm 0.1$  mps).

After the MAV is docked and the docking discrete is received by the orbiter control computer, the MAV can be commanded over the Orbiter-to-MAV command link to separate the sample canister and back the MAV away from the orbiter. The MAV can then back off as far as needed, provided it does not exceed the maximum range of the RR radar. The MAV is then commanded back to its Earth-pointing orientation to reacquire the DSN signal for attitude control. An orbital maneuver can be executed to place the MAV in a safe orbit.

If propellant is available, the terminal rendezvous and docking can be reinitiated as many times as needed. The terminal rendezvous relative state

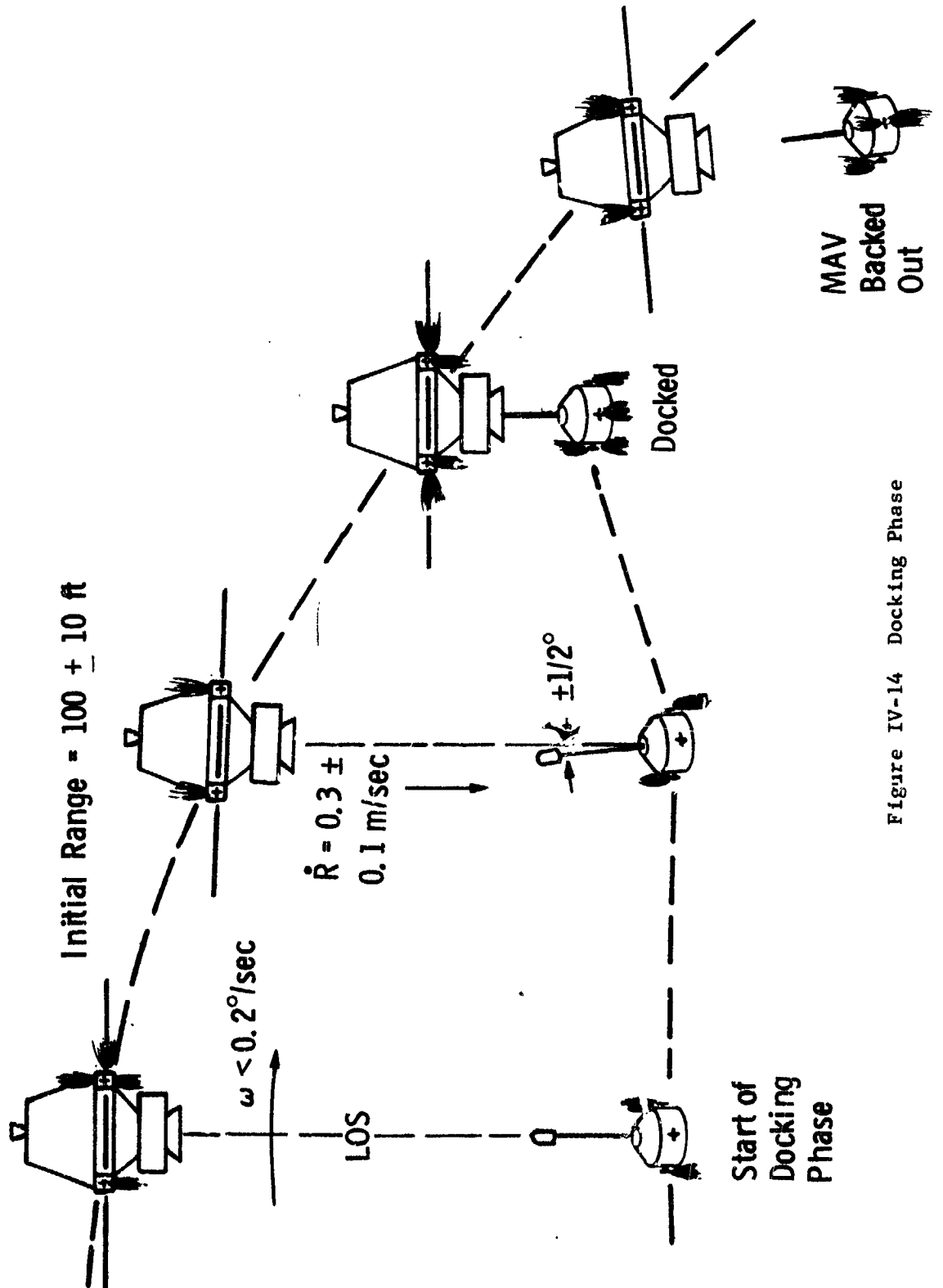


Figure IV-14 Docking Phase

as sensed by the RR can be compared from time to time to stored nominal state information to determine whether terminal rendezvous should be redone. If a docking discrete is not received after a few seconds from the expected time, the MAV can be commanded to back off a few feet and to reinitiate the final phase of docking. Propellant budgeting is discussed in Chapter VI-E.

Other malfunction options are available during the terminal rendezvous and docking phases. If the orbiter axial engines fail, the MAV can rendezvous or dock with the orbiter by calculating the MAV axial thrust commands with the orbiter CC and sending the commands over the Orbiter-to-MAV command link to be executed by MAV. Another malfunction option is available if the transmitter section of the MAV transponder fails; a passive cooperative rendezvous can be accomplished from a degraded range of 8.5 km. In this mode the orbiter rendezvous radar still tracks the MAV antenna while the MAV transponder receiver continues to angle track on the orbiter signal.

## E. G&C HARDWARE IMPLEMENTATION

A number of small studies were conducted early in this contract to define and understand the problems associated with designing and optimizing the G&C hardware used in the ascent, rendezvous and docking phases.

They involve:

1. launch and ascent error study;
2. selection of the MAV sensors;
3. spin vs 3-axis stabilization study;
4. methods to implement ascent guidance;
5. G&C baseline definition study;
6. terminal guidance selection study;
7. terminal guidance simulation study; and,
8. methods of implementing autonomous docking.

The first five of these studies were conducted before midterm to define the preferred baseline design. A study to define whether a spin or a three-axis stabilized system should be used was conducted early in this contract. This is described in the next section. The last three studies were conducted after the midterm to define the preferred implementation to execute the terminal rendezvous and docking.

After the three-axis stabilized system was selected, a study was conducted to define the best sensor implementation for that concept to:

1. determine the lander and the MAV attitudes on the surface;
2. determine the lander surface position more accurately;
3. support ascent guidance;
4. determine the MAV attitudes in orbit;
5. update the MAV position in orbit; and,
6. cooperate in the rendezvous and docking.

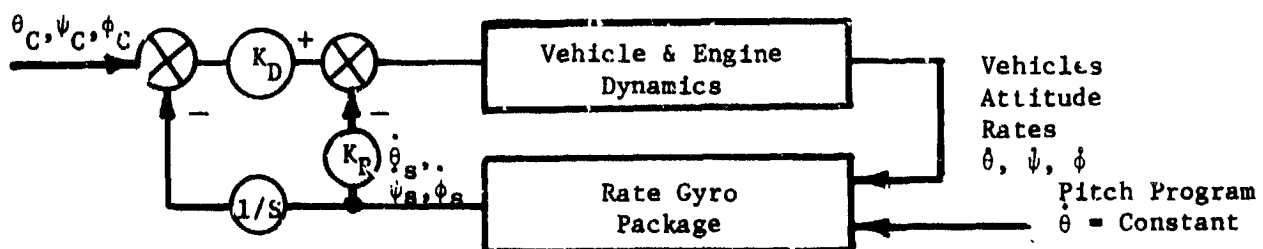
Body-mounted rate gyros were chosen as sensors to guide the vehicle during the ascent phase, during orbital maneuvers, and during Sun or Earth occultations. The rate gyros keep track of the spacecraft attitudes from the last inertial attitude update. A sensor system then had to be selected to get an inertial update by using a celestial reference. A Sun sensor system is the cheapest and simplest method to get one of the two references generally required to implement a celestial reference system. Another

sensor is needed to fully implement a celestial reference system and the best choice for this sensor is not obvious. Planet sensors, horizon sensors and star sensors were considered for this second sensor. Since the MAV also required an Earth tracking transponder to work with the DSN orbit determination, an attractive solution was found to using this Earth pointing direction as the second celestial reference. Thus with one multi-function transponder, the MAV can be tracked from Earth, can determine its own pointing reference, can receive and send commands and engineering data both ways, and also turn around the rendezvous radar microwave signal to implement a cooperative rendezvous. The multiple use concept also applies to the Sun sensor system which is also used to determine the MAV and lander attitudes on the surface of Mars. This sensor implementation seems to be the lightest and simplest way to mechanize the MAV G&C system to the required level of accuracy.

Once the MAV sensors and the method of vehicle stabilization have been chosen, the launch and ascent errors can be estimated on the basis of selected sensor specifications, method of lander update, and planet and vehicle physical parameters.

Our approach to defining the preferred G&C system implementation was to first select the simplest ascent guidance system and to then iterate to a more complex system only if it is needed and only when the sensitivity to this change is understood. An open loop guidance system utilizing a constant pitch-over rate to approximate a gravity turn is the simplest and was used in our first iteration. This type of guidance was simulated on the digital computer and the flight path dispersion analysis results indicated it to be an adequate design for this mission, obviating the need to examine a more complex guidance system.

The simple open loop guidance system used in the study baseline is shown below:



- $\theta$  = Pitch Attitude
- $\psi$  = Yaw Attitude
- $\phi$  = Roll Attitude

The pitch program, which is no more than a constant in the MAV minicomputer, is used to torque the pitch rate gyro. The indicated operations are performed on the rate gyro sensed output ( $\theta_s, \psi_s, \phi_s$ ) to form thrust commands ( $T_C$ ) from the attitude commands ( $\theta_c, \psi_c, \phi_c$ ). This is a very simple guidance system to implement in the MAV minicomputer. In the celestial modes, which are similar to those used on the Viking '75 orbiter, the celestial sensors are used to sense vehicle attitudes and the rate gyros can be used to sense attitude rates.

The total MAV guidance and control system mechanization is shown in Figure IV-15. The rate gyros are needed to guide the vehicle during the ascent phase and to stabilize the MAV during Sun or Earth occultation. During the normal celestial mode of operation, pitch and yaw attitude pointing errors are obtained from the Earth pointing system, while roll attitudes are obtained from the Sun sensor system. During the commanded power saving celestial mode of operation, roll and yaw attitudes are used from the Sun sensor system and pitch attitude is used from the pitch rate gyro.

Existing technology is needed to implement the MAV minicomputer which utilizes CMOS solid state (medium-scale) integrated circuits. The minicomputer was sized roughly to need a 1000 word random-access memory (RAM) and a 2000 word permanent read-only memory (PROM). A 10 bit word size was assumed. The minicomputer must be programmed to control, guide and sequence the MAV mission from launch to docking. The ACS logic, which is similar to the Viking Orbiter logic, must be mechanized in the MAV computer. The size of computer needed on the MAV was minimized by having the orbiter control computer and the Earth-based computers do the calculations whenever possible. Table IV-3 shows the estimated weight of the components of the MAV G&C system. The uncased weight for the G&C components are shown because all of the electronics are packaged together. CMOS technology is necessary, which is today's state-of-the-art, to operate the minicomputer on the power shown in Table IV-3. The other components were included in this table to compare the three-axis stabilized MAV to the spin stabilized MAV.

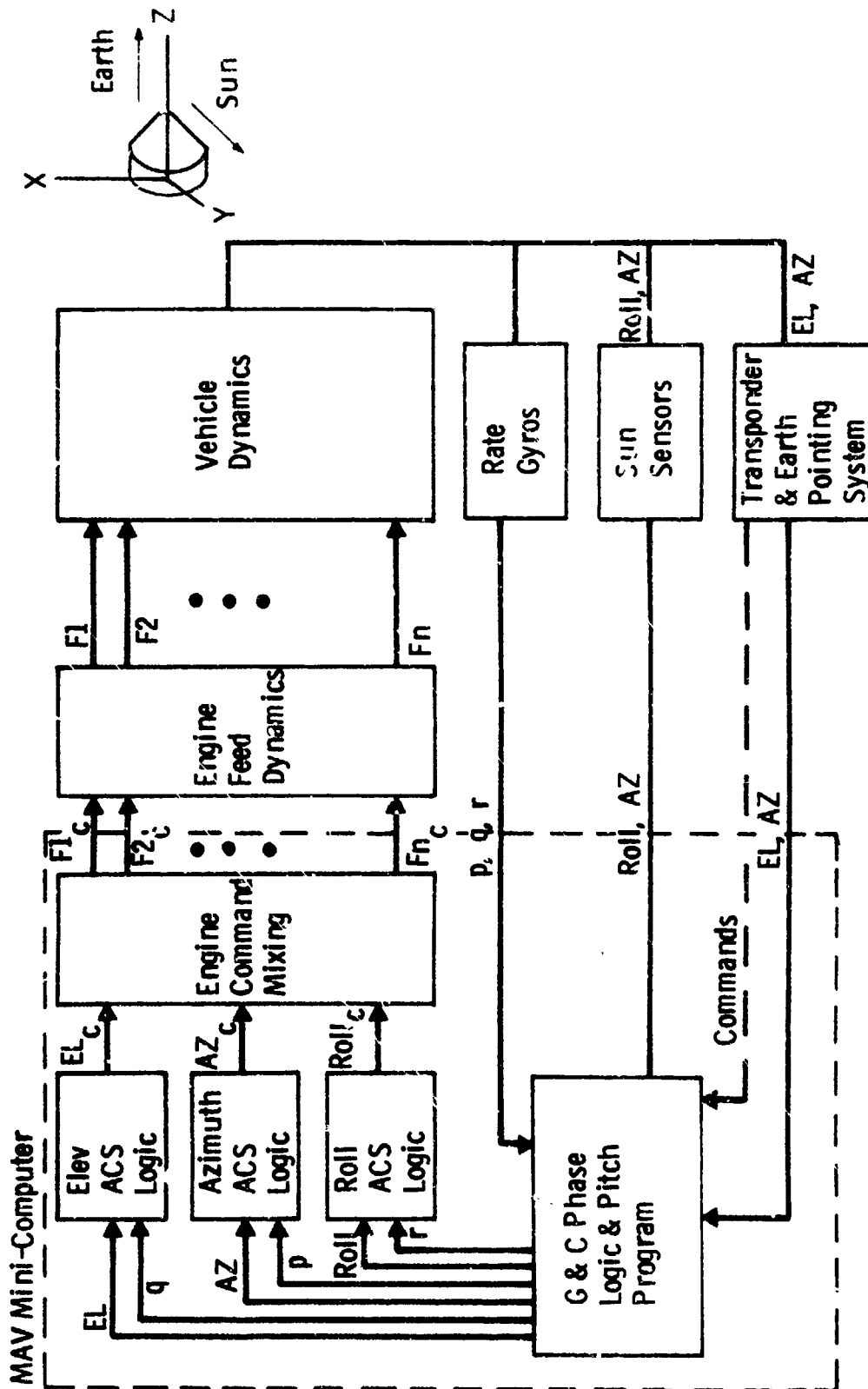


Figure IV-15 Orbiter G&C System Mechanization

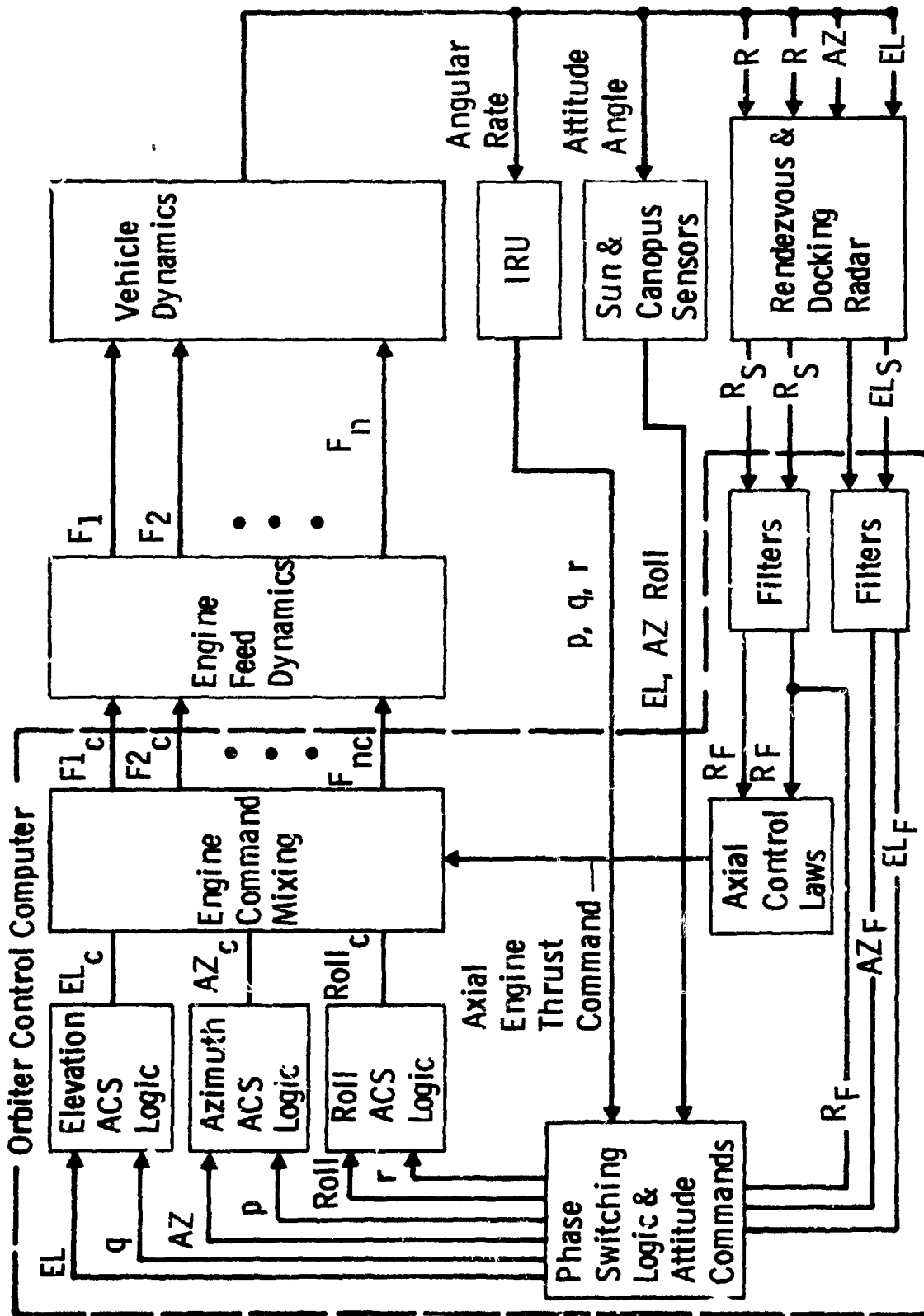


Figure IV-16 MAV G&C System Mechanization

Table IV-3 Three-Axis Stabilized MAV

<u>Components</u>	<u>Weight</u>	<u>Power</u>
4 ΔV and Launch ACS Engines	2.18 kg ( 4.8 lbs)	-----
8 ACS Engines	1.45 kg ( 3.2 lbs)	-----
1 Attitude Sun Sensor System	0.18 kg ( 0.4 lbs)	-----
3 Rate Gyros and Electronics	* 1.36 kg ( 3.0 lbs)	5.0 Watts
1 Computer and Sequencer	* 1.59 kg ( 3.5 lbs)	4.0 Watts
1 Transponder and Antenna Feed	* 1.59 kg ( 3.5 lbs)	20.5 Watts
1 Antenna Dish and Reflector	0.52 kg ( 1.2 lbs)	-----
	<hr/>	
	8.87 kg (19.6 lbs)	

ACS Propellant Required - 4.2 lbs (Isp = 235 sec)

44 N (10 lb) Ascent Engines for Thrust Offset and ΔV

\* Uncased

The orbiter G&C system mechanization as shown in Figure IV-16 is the basic Viking'75 hardware modified to accommodate the combination rendezvous and docking radar. The orbiter CC software must be modified and reprogrammed for this mission. Additional axial control laws are needed in the control computer to control the axial engines. The rendezvous radar filters are either mechanized in the digital computer by software or in the rendezvous radar by analog circuits. These modifications should be minor modifications to the existing orbiter G&C system.

## F. SPIN STABILIZED VS THREE-AXIS STABILIZED MAV

Initially, the performance characteristics of each method of vehicle attitude stabilization were considered to see if one selection was an obvious choice. Some of the more important attributes of each type of stabilization system are shown in Table IV-4. The estimated weight and power required for the components needed for each type of stabilization were then compared to see if an obvious choice emerged (see Tables IV-3 and IV-5). The attitude control propellant needed to accomplish this mission is also included in the tables for a fair comparison since the weight needed for the spin stabilized MAV is very sensitive to the number of maneuvers needed during the mission. Maneuvers to change the pointing direction, are very expensive in terms of propellant needed on the spin stabilized MAV because the vehicle is stiff due to spin stabilization and must be precessed to the maneuver attitude. The weight of the two systems are comparable if the maneuver propellant is included; the 3-axis stabilized system weighs 10.8 kg and the spin stabilized system weighs 9.1 kg. The weight comparison is even closer because the 1.9 kg of ACS propellant in the 3-axis stabilized design adds to its  $\Delta V$  capability during ascent. This close weight comparison might be surprising considering the relative simplicity of the spin stabilized system until it is recognized that:

1. this mission requires many maneuvers; and
2. the MAV G&C system must perform several functions other than stabilization.

The three-axis stabilized vehicle executes maneuvers more accurately because they are executed by a closed loop G&C system. Open loop maneuvers and vehicle precession during ascent, rendezvous and docking would degrade the performance of a comparable spin stable system to a point where mission feasibility could be impaired. The spin stabilized system would not be selected unless detailed system design weight calculations show a pronounced weight advantage. In that case performance risks would have to be thoroughly evaluated.

Table IV-4 Attributes of Three-Axis vs Spin Stabilized MAV

<u>Three-Axis Stabilized</u>	<u>Spin Stabilized</u>
Attitude maintained by slightly heavier subsystems that continually consume power.	Attitude maintained automatically at no expense of power on weight of auxiliary subsystems.
More efficient at attitude maneuvers.	Less efficient at attitude maneuvers.
Optimum system for missions requiring many attitude reorientations.	Optimum system for long missions requiring few attitude reorientations.
Less sensitive to dynamic imbalance.	More sensitive to dynamic imbalance.
Higher power requirements.	Probably lower overall power requirements.
Does not provide sensor scanning.	Does provide sensor scanning.
Less complex computations to determine inertial attitude.	Complex calculations required for attitude determination.
Closed loop maneuvers.	Open loop maneuvers.
Requires more complex thermal protection.	Good thermal characteristics.
C&C hardware for rendezvous and docking is simpler.	Maneuvers must be executed in a rotating coordinate frame.
Vehicle dynamics can be modeled simply; minimal cross coupling between equations of motion.	Mathematical modeling of vehicle dynamics is complex; requires sophisticated analysis and simulation of cross coupling effects.
ACS system must correct for thrust.	Minimizes thrust offsets.

Table IV-5 Spin Stabilized MAV

<u>Components</u>	<u>Weight</u>	<u>Power</u>
4 Pitch and Yaw Engines	0.73 kg ( 1.6 lbs)	-----
2 Roll Maintenance Engines	0.36 kg ( 0.8 lbs)	-----
1 Sun Sensor	0.09 kg ( 0.2 lbs)	-----
1 Computer and Sequencer	2.73 kg ( 6.0 lbs)	4.0 Watts
1 Transponder	1.81 kg ( 4.0 lbs)	4.0 Watts
1 Antenna	0.68 kg ( 1.5 lbs)	-----
	<hr/>	
	6.40 kg (14.1 lts)	

ACS Propellant Required - 6.0 lbs (Isp = 235 sec)

Maneuvers:

Launch	100°
Initial Rendezvous	480°
Terminal Rendezvous	100°
Contingency	<hr/> 60° (10%)
	720°

## G. TECHNOLOGY ASSESSMENT

The G&C systems for the Mars sample return mission can be implemented with current technology. Minor modifications are needed to the Viking orbiter G&C hardware to integrate the rendezvous radar as an additional sensor. It appears that no G&C hardware modifications are needed to the lander to use it as the delivery system to the surface. The computers on all the vehicles have to be reprogrammed for this mission.

The MAV is the only completely new vehicle that has to be developed and existing and off-the-shelf components proved to be adequate in most cases, to mechanize the G&C system. Table IV-6 shows the typical G&C components that were selected for the MAV mechanization. All the components are off-the-shelf and space qualified components except the Intel computer.

In order to meet the power and weight requirements of the MAV, this computer will have to be implemented with CMOS integrated circuitry. This technology exists today but has not been demonstrated in space qualified applications. Another option available is to use the current NMOS circuitry computer in an operating mode that has a lower power duty cycle.

Table IV-6 Guidance and Control Components (Typical)

<u>Components</u>	<u>Weight</u>	<u>Power</u>
1 All Attitude Sun Sensor System Adcole 14477 (Digital Sun Aspect Sensors) Resolution 1/4° FOV 128 x 128° Accuracy ± 6' Size 8.75 x 8.75 x 2.54 cm	0.45 kg (1.0 lb)	0.45 watts
3 Rate Gyros and Electronics U.S. Time (AC-AC) Full Scale 10°/sec Accuracy 0.01°/sec Drift 1/2°/hr Size 17.15 x 12.1 x 7.6 cm	1.36 kg (3.0 lb)	5.0 watts
1 Computer and Sequencer Intel SIM8-01 Memory 1 K x 8 RAM 2 K x 8 PROM 10-bit Parallel CPU Interrupt Capability	1.59 kg (3.5 lb)	4.0 watts

REFERENCE

IV-1 Legostayev, V. P. and B. V. Raushenbakh: Automatic Rendezvous in Space,  
December 1968. FTD-HT-23-1346-68.

## V RADAR SENSOR DESIGN FOR RENDEZVOUS AND DOCKING

This chapter discusses the rendezvous and docking sensor that performs the tracking function required for orbiter/MAV rendezvous. The design and expected performance of such a sensor is described and its interaction with the orbiter and MAV space vehicles is investigated.

### A. REQUIREMENTS

The orbiter/MAV rendezvous and docking sensor must be capable of providing accurate measurements of range, range rate and angle between the two vehicles during the final rendezvous and docking phase. The overall sample return mission dictates that the sensor size, weight, and power requirements be minimized and that the rendezvous sensor be effectively integrated into the sample transfer guide cone of the Earth return vehicle. Similarly, extreme restrictions on the size and weight of the MAV transponder suggest that the transponder perform multiple functions and that an integrated design capable of operating effectively in conjunction with the sample canister and sample transfer system be employed. The selected sample canister location is directly in front of the transponder reflector antenna and thus represents an important reference point in the design of the rendezvous system. Physical transfer of the sample canister occurs when the MAV and the Earth return vehicle are separated by 1 meter (distance between effective antenna aperture planes) or less. Accurate measurements of range rate and angle down to this range are, therefore, essential to the rendezvous and docking mission. Stringent weight and power requirements imposed on both the orbiter and MAV sensors suggest that the rendezvous and docking functions be incorporated into a single, integrated sensor. It was also felt desirable to allow the orbiter rendezvous system to operate in either a cooperative or non-cooperative mode. Thus, in case of failure of the MAV transponder, the system could be switched into the skin-track mode where the orbiter would be capable of tracking the MAV transponder antenna possibly out to ranges of approximately 8-10 km.

In addition to the above requirements, a command channel must be provided for the orbiter/MAV link and a telemetry channel for the MAV/orbiter link. These systems should be integrated into the rendezvous and docking system in order to achieve the smallest and lightest electronics package. The command system must function both before and after transfer of the

sample canister, so that in case of a locking malfunction the MAV vehicle can be commanded away from the docking cone prior to reinitiating the docking maneuver.

The parameter measurement limits and the parameter measurement accuracies required during rendezvous and docking were investigated and are listed in Table V-1. It is interesting to note that a range measurement during the final docking phase ( $R < 30$  m) is actually not required as long as accurate range rate and angle data can be maintained to impact.

Table V-1 Rendezvous and Docking Sensor Measurement Requirements

System Parameter	Measurement Limits	Measurement Accuracy
Range	30 m - 750 km	3 m ( $R = 30$ m)
Range Rate	0.3 m/sec - 50 m/sec	0.1 m/sec
Angle	$\pm 10^\circ$	3 mrad
Angle Rate	20 mrad/sec	0.1 mrad/sec

A number of possible implementations for the rendezvous, docking, and command system were considered. These included pulse, pulse/Doppler, and cw sensors. The requirements for a unified sensor system dictated the use of a cw system which has no inherent minimum range limitations and could, therefore, be employed for both rendezvous and docking functions. Furthermore, such systems are simple, lightweight, reliable, and require minimum power while still providing adequate long range performance.

## B. SELECTED SENSOR CHARACTERISTICS

### 1. Orbiter Elements

A simplified block diagram of the multi-tone FM/CW rendezvous and command system selected for incorporation in the orbiter is shown in Figure V-1. This system can be employed to acquire, track, and rendezvous with the MAV vehicle. It provides range, range rate, and angle data from a maximum unambiguous range of 750 km down to a minimum docking range of 3 meters. A phase comparison monopulse system utilizing four traveling wave antennas located in the sample transfer guide cone of the Earth return vehicle is employed to provide angle tracking in both the azimuth and elevation planes. The location of the four antennas along the guide cone permits the sample canister to be transferred beyond the effective aperture plane of the monopulse array. This allows the command system to function even after transfer of the sample canister. The antenna arrangement is illustrated in Figure V-2. The antenna array is fed by a monopulse beam forming network and produces a conventional sum pattern for ranging and an up-down and right-left difference pattern for angle tracking. The beam-forming network is located at the top of the cone to minimize transmission line lengths. The rendezvous system transmitter and receiver are also located in this region, thus providing a compact assembly. Rigid strip lines are employed to feed the four traveling wave antennas to minimize errors due to precomparator phase shifts. Array near field amplitude and phase distributions for a 1.36 meter aperture antenna are shown in Figure V-3 for various distances along the cone axis. The symmetry of the phase distribution in the near field indicates that the difference pattern null of the antenna pattern will be maintained during the orbiter/MAV docking phase where accurate angle and range rate information must be obtained.

The transmitter consists of a frequency synthesizer which generates all the fixed frequencies required for coherent signal transmission and reception. A VCO frequency of 19.1003 MHz is employed which is multiplied by 120 in a solid state varactor frequency multiplier chain providing high reliability and adequate power output at S-band. The ranging modulation consists of a sidetone ranging system utilizing 5 tones and capable of a maximum unambiguous range of 750 km. The minor tones are phase modulated on the 819.2 kHz subcarrier. The command signal is added to the modulated

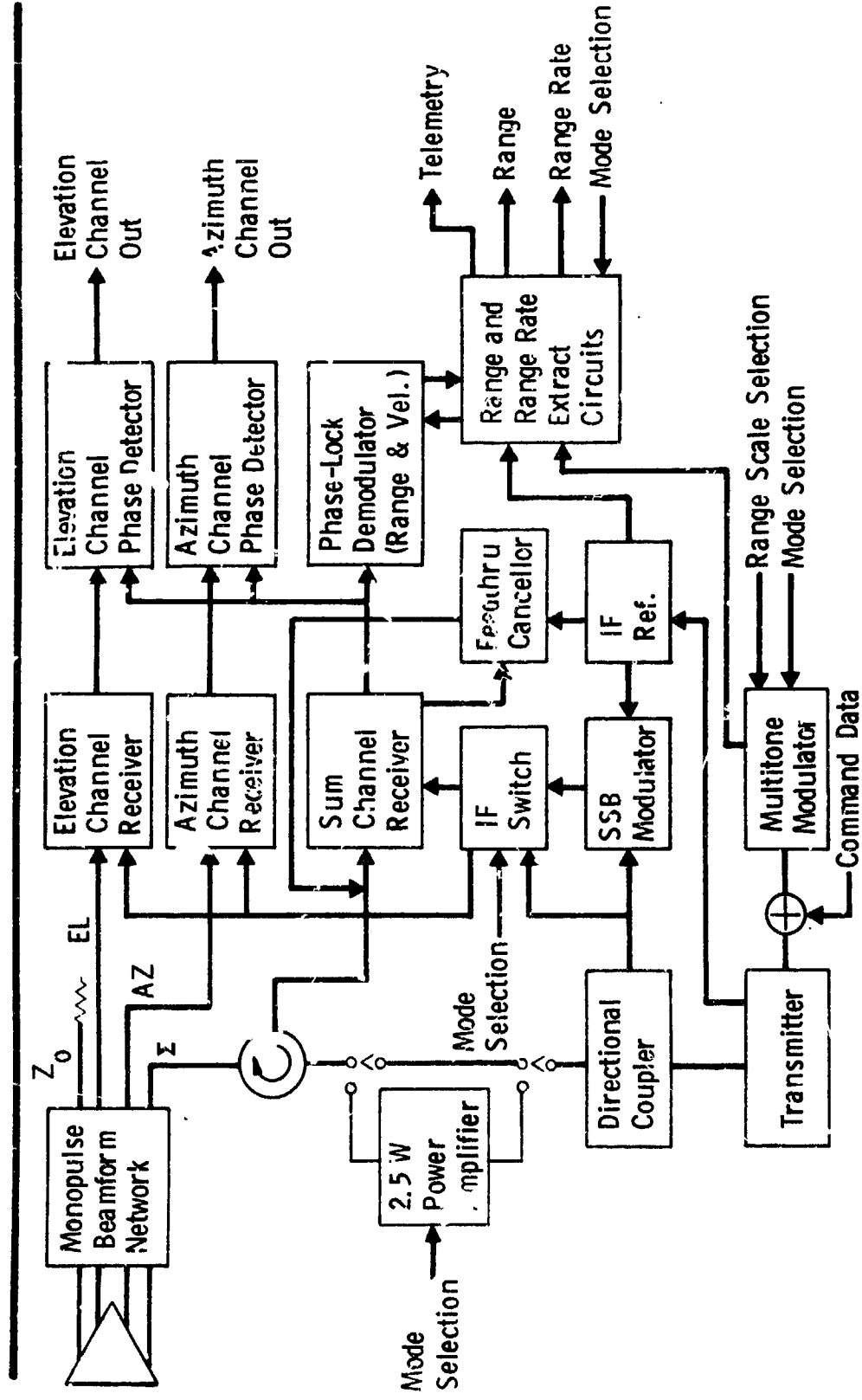


Figure V-1 Orbiter Rendezvous and Command System--Simplified Block Diagram

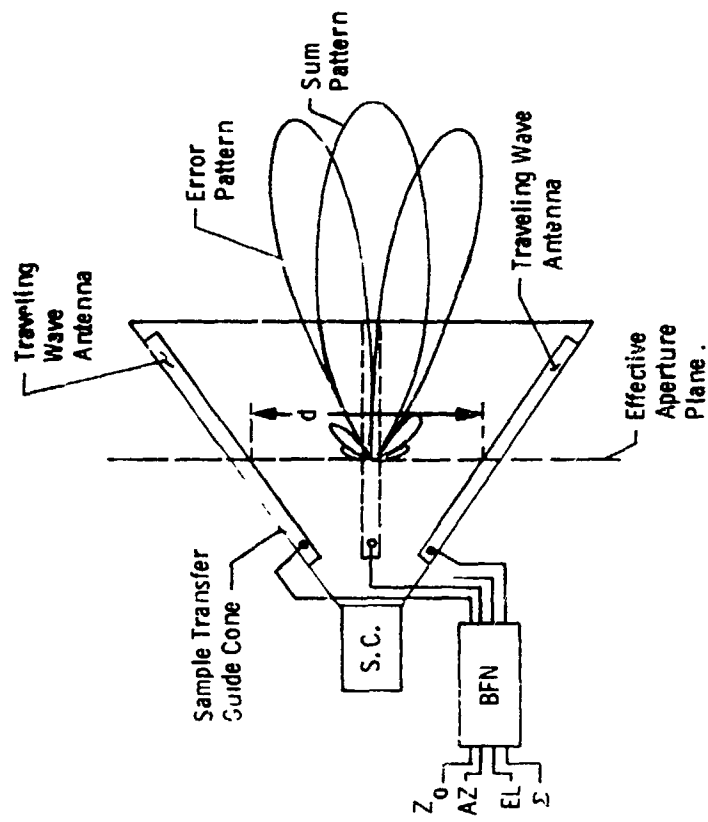


Figure V-2 Orbiter Rendezvous and Command System--System Antenna

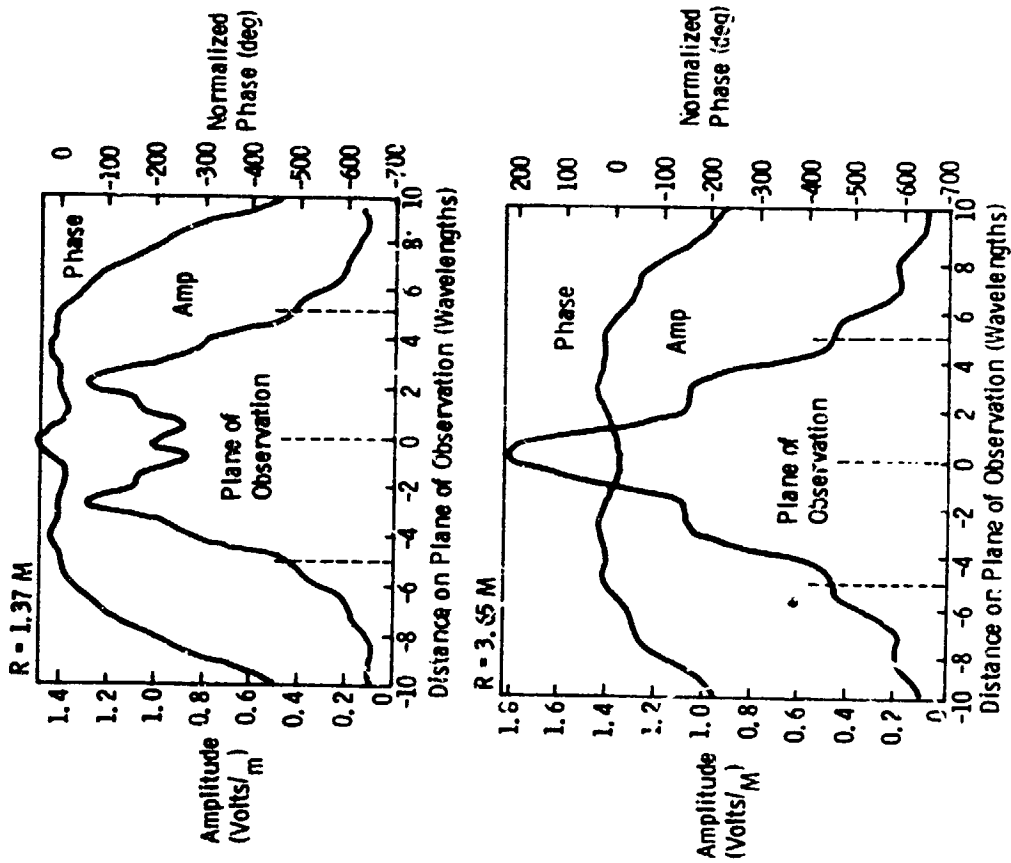


Figure V-3 Antenna Near-Field Amplitude and Phase Distributions

subcarrier to obtain a composite modulation signal which phase modulates the S-band transmitter. Dual mode operation of the rendezvous system is provided. In the normal transponder mode the transmitted S-band signal ( $120 f_0 = 2282.48$  MHz) is sent to the MAV transponder which coherently removes the modulation from the carrier, filters it, and remodulates the beacon transmitter. The coherence ratio is 220/239 so that the retransmitted frequency is 2101.03 MHz. When this signal is received at the rendezvous receiver, it is mixed with a sample of the transmitted signal coupled to the three receiver mixers through a directional coupler and power splitter. This transmitter signal is used as the local oscillator for the first mixer. A triple conversion receiver is employed for maximum sensitivity, and identical receivers are employed for the three channels. The local oscillator signals for the second and third mixers are provided by the frequency synthesizer. After I.F. amplification the sum channel signal is demodulated by a phase lock demodulator. This unit coherently removes the 819.2 kHz range subcarrier from the carrier and transfers it to the range unit which contains the range tracking circuits. The ranging unit receives the ranging subcarrier and minor tones, extracts the range data, and converts it to a 17-bit binary number. Range is determined by measuring the phase delay between the received and transmitted multi-tone modulation waveform. Range rate is obtained from a two-way Doppler measurement by measuring the received Doppler cycles for a unit of time. In order to determine the Doppler frequency it is essential to maintain frequency coherence of the orbiter rendezvous transmitter through the MAV transponder and back to the rendezvous receiver where it is compared against a sample of the transmitter frequency.

Angle tracking is achieved in both planes with the aid of a phase comparison monopulse system. A conventional three-channel system is employed to provide the sum and azimuth/elevation plane difference channels. In a phase comparison system the angle of arrival is obtained by comparing the phase of signals received by antennas separated a considerable electrical distance but having parallel boresight axes. Thus, it is possible to increase the angular accuracy of the rendezvous system by moving the four traveling wave antennas further up along the sample transfer guide cone which increases the electrical spacing between antennas. Furthermore, in such a system the required angular accuracy is achieved with less stringent mechanical tolerances than with an amplitude comparison system.

In the non-cooperative mode, which can be employed as a failure mode for ranges up to 8 km, the transmitted S-band signal remains at the same frequency ( $120 f_0 = 2282.48 \text{ MHz}$ ) but the local oscillator signals must be shifted in frequency to provide the correct I.F. frequencies for the triple conversion receiver. This is achieved by a single sideband modulator which offsets a sample of the transmitted signal received from a directional coupler by the appropriate I.F. frequency for use as the local oscillator signal. Transmitter feedthrough appears as a narrow band signal in the IF amplifier, but the delayed signal is phase modulated and occupies a wide spectrum. Feedthrough cancellor circuits are provided to null out this undesired feedthrough signal since the circulator isolation of 30 dB is insufficient to achieve a low enough feedthrough level. A synchronous notch filter is, therefore, employed to provide the additional isolation.

The sidetone ranging modulation system consists of a five-tone system where the four minor tones are phase modulated on a subcarrier. The subcarrier frequency is chosen so as to provide the highest frequency for a given bias error in the range measurement and must, therefore, be consistent with the docking requirements. The highest tone is used to determine the finest increment of range, and the lower frequency tones are used to remove range measurement ambiguities. The range tones are phased so that when the lowest frequency tone has a zero crossing, the higher frequency tones also have a zero crossing.

The frequency ratio between the tones should be high enough to allow implementation of a practical system with a minimum number of tones. Each tone must resolve the ambiguity in the next highest tone which equals 1 cycle of that tone. Assuming the r.m.s. phase errors are equal and independent for each tone, the frequency ratio must satisfy the inequality:

$$\sqrt{R^2 + 1} \sigma_T \leq \frac{\pi}{F}$$

where: F = confidence factor in resolving ambiguity

R = frequency ratio

For 99.9% probability of correct ambiguity resolution, the value of F = 3.7. The quantity,  $\sigma_T$ , consists of uncorrectable bias and random errors and is set at 3 m.

The simplest implementation requires the smallest number of tones or largest value of R. Past experience indicates that for reliable ambiguity resolution R should not exceed 8. Thus, starting with the highest tone of 819.2 kHz, the minor tones are given by: subcarrier = 819.2 kHz

1. Minor tone = 102.4 kHz
2. Minor tone = 12.8 kHz
3. Minor tone = 1.6 kHz
4. Minor tone = 200 Hz

This implementation yields a maximum unambiguous range of 750 km, which appears more than adequate for the MAV/orbiter rendezvous system.

The range tone spectrum as well as the command and telemetry subcarriers are shown in Figure V-4. The command channel is required for the orbiter to MAV link while the telemetry channel is needed for the MAV to orbiter link. The simplest mechanization of this system is illustrated in Figure V-5. The range extraction unit receives the detected range tones from the receiver and the 819.2 kHz tone and reference pulses from the tone generator. The time interval unit measures the time interval between the start and stop pulse which is proportional to range between the orbiter and the MAV. The range rate extraction unit determines Doppler by measuring the time required to count a fixed number of cycles of the two-way Doppler plus bias frequency. The time interval unit measures this time interval with the same method as is used for the range measurement.

## 2. MAV Elements

The primary mode of operation of the rendezvous system is the cooperative beacon mode. The MAV transponder will be required to provide the coherent rendezvous response and the MAV/DSN tracking function as well as an indication of the angle between the MAV and the Earth-based DSN transmitter. Thus, a monopulse receiver is also required for the MAV vehicle, even though the angular accuracy requirements are much less severe than those required for the orbiter rendezvous receiver. A phase comparison system is again employed for the angle measurements and provides an accuracy of  $\pm 1/4$  deg. The antenna consists of a 50 cm diameter dish fed by a 4 arm, dual mode, flat spiral antenna. Assuming an antenna efficiency of 65% and a mean carrier frequency of 2.2 GHz the unblocked antenna gain is 19.5 dB. Aperture blocking introduced by the sample canister and the steel rod will cause a reduction

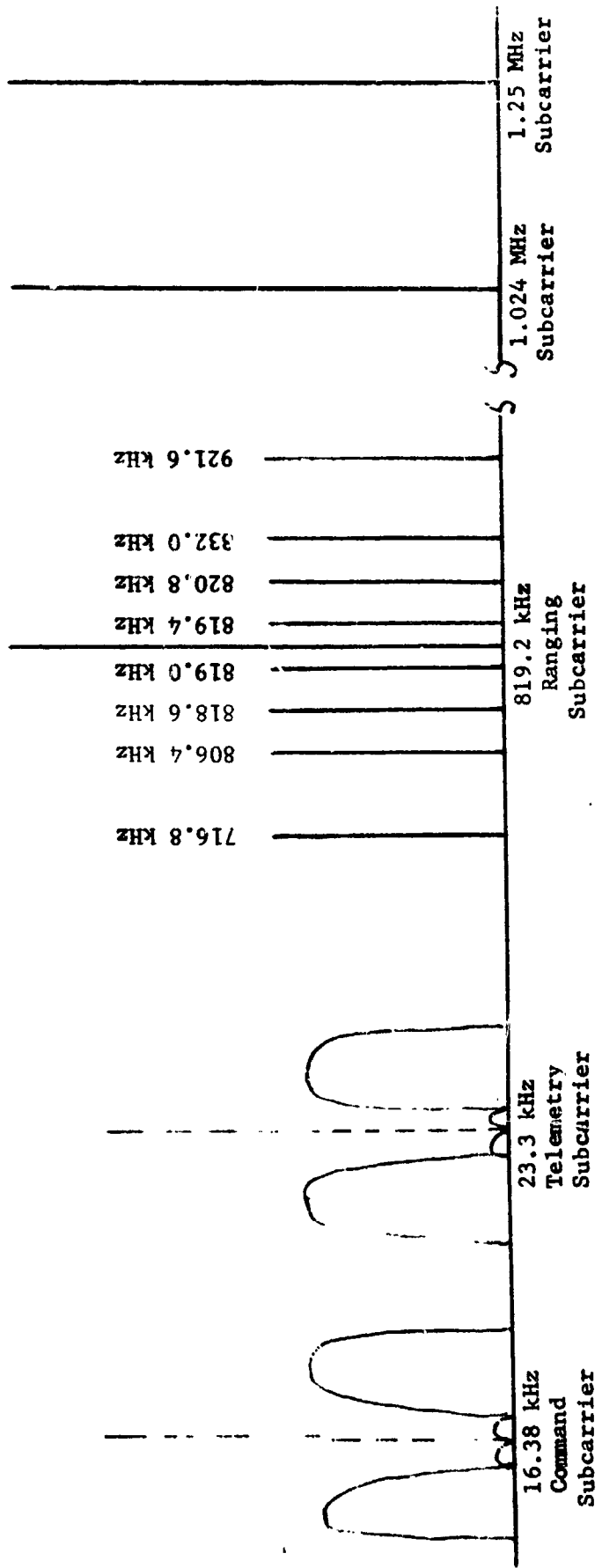


Figure V-4 Composite Signal Spectrum

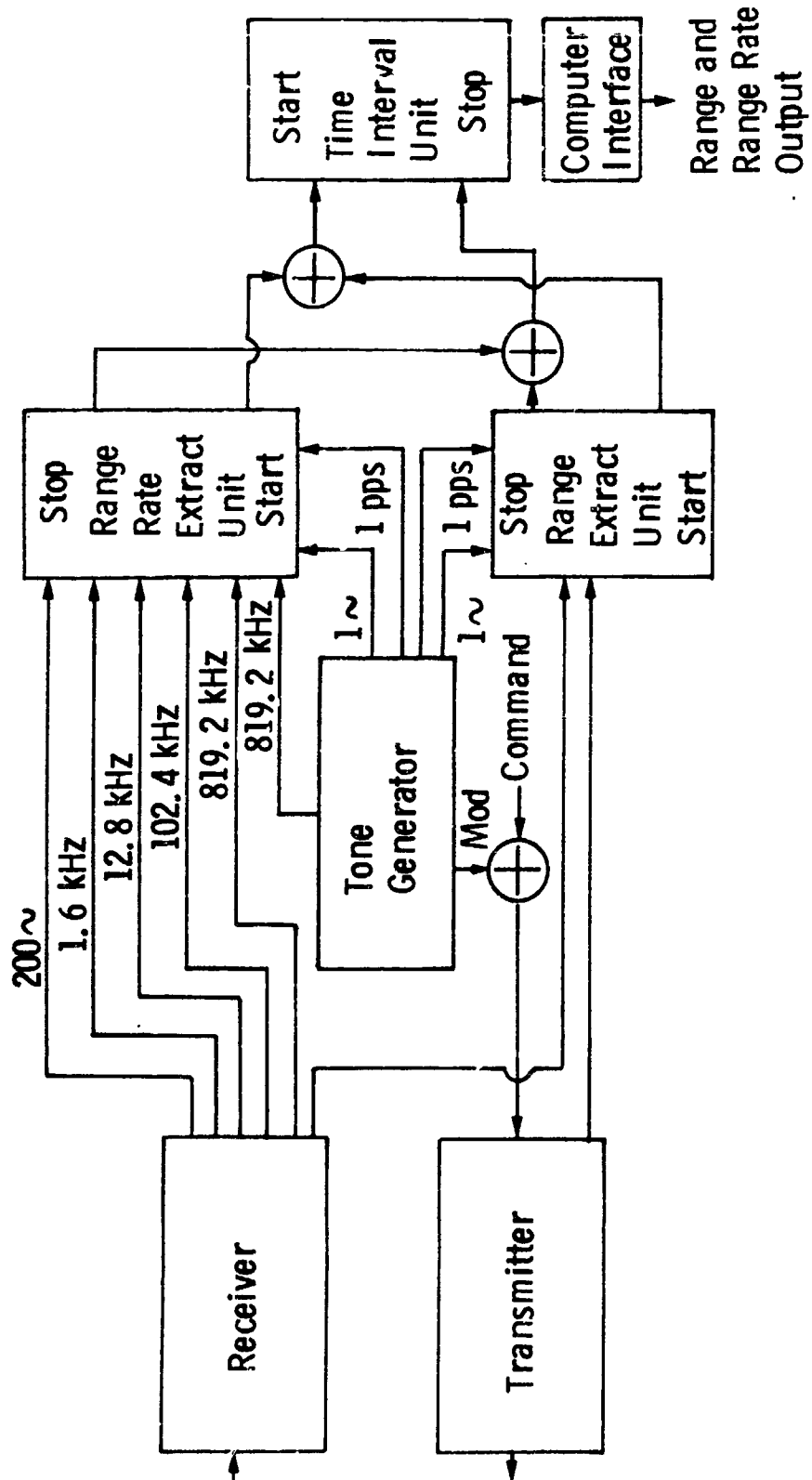


Figure V-5 Orbiter Rendezvous and Command System--System Block Diagram

in antenna gain, increase in antenna pattern sidelobe levels and pattern changes due to phase error effects. Another important consideration is the effect on the azimuth and elevation difference pattern nulls brought about by possible asymmetries in the location of the sample canister.

Two possible antenna mechanizations were considered:

- 1) Front-fed parabola
- 2) Cassegrain dual-reflector system

In the front-fed parabola, the dual-mode spiral antenna feed can be mounted on the bottom face of the canister and the element arm orientation takes the form shown in Figure V-6 below.

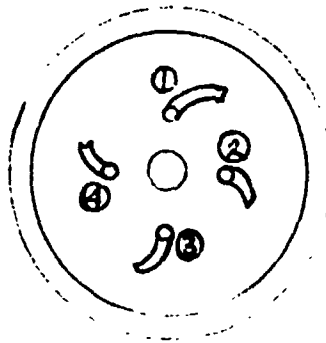


Figure V-6 Multi-mode Spiral Feed

The central portion of the dual-mode spiral feed antenna has been eliminated to allow room for the 1.27 cm diameter steel rod. The minimum  $F/D$  ratio for a front-fed design is about 0.4 which locates the spiral feed antenna 20 cm from the vertex of the parabola. To eliminate the need for long transmission lines between the spiral feed points and the beam forming network, it is desirable to mount the four strip line 180 deg hybrid junctions directly behind the spiral feed antenna. This prevents the introduction of differential phase shifts and losses that can become very critical in monopulse tracking systems. Another possibility is to include the sum channel and error channel mixers and the 1-IF preamplifiers in an integrated electronics package mounted directly behind the feed antenna. This can be accomplished with a minimum weight penalty and would require a minimum of four cables to be brought out to the feed. A disconnect system is required so that when the sample canister is removed the spiral feed system will stay in place unperturbed and allow the system to continue to function.

In the Cassegrain dual-reflector system, the dual-mode spiral antenna feed is located at the vertex of the parabola and hyperboloid subreflector is mounted on the bottom face of the canister. The minimum F/D ratio for this arrangement is about 0.3 which now locates the subreflector only 15 cm from the vertex of the parabola. Closer spacings are theoretically possible but other considerations dictate against such shorter distances. In general the feed aperture required for a Cassegrain antenna is larger than that required if the antenna system has the feed at the parabolic focus. This difference in size increases as the F/D ratio decreases. It is very difficult to increase the directivity of a 4-arm, dual-mode, spiral antenna, so that for a Cassegrain configuration it is essential to place the subreflector close enough to the feed antenna to prevent excessive amounts of forward spillover. The only other alternative is to place the spiral feed antenna inside a conical horn so that the aperture area and directivity of the horn will effectively control the illumination of the subreflector. This approach, although somewhat heavier due to the inclusion of the horn, will then allow larger F/D ratios to be employed. The principal advantages of the Cassegrain system are location of all RF components at the antenna feed system thus eliminating the need for long transmission lines, image feed reduction, and flexibility of the antenna parameters to accommodate different designs. Another important advantage in the MAV application is that no disconnect system is required so that the subreflector can be permanently attached to the sample canister package. After ejection of the sample canister, the rendezvous system, including the command channel, will continue to operate in a low-gain mode despite loss of the subreflector.

A preliminary design of the MAV Cassegrain antenna was carried out to determine the expected antenna performance and its dependence on the sample canister. Since the size of the sample canister determines the hyperboloid subreflector diameter and the resulting aperture blockage of the main dish, the antenna performance will be a function of the sample canister diameter. It is desirable to satisfy the minimum blockage condition with a reasonable main dish F/D ratio. Figure V-7 illustrates the minimum blockage condition and the MAV antenna/transponder assembly. Two possible implementations for the sample canister configuration were considered and are shown in Figure V-7:

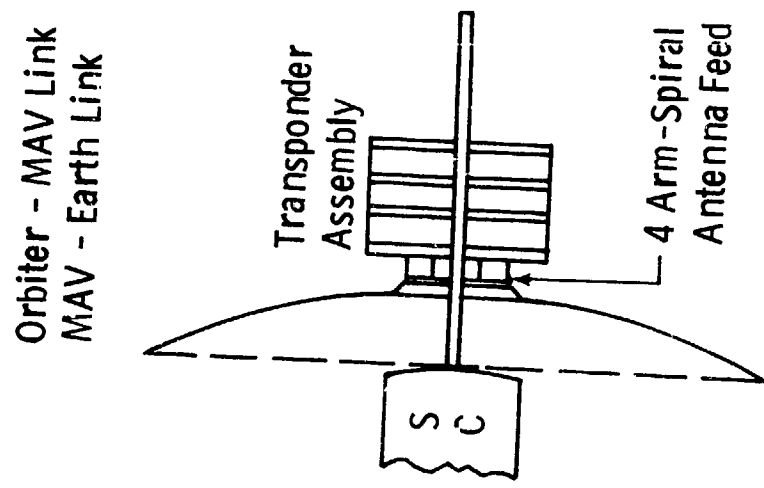
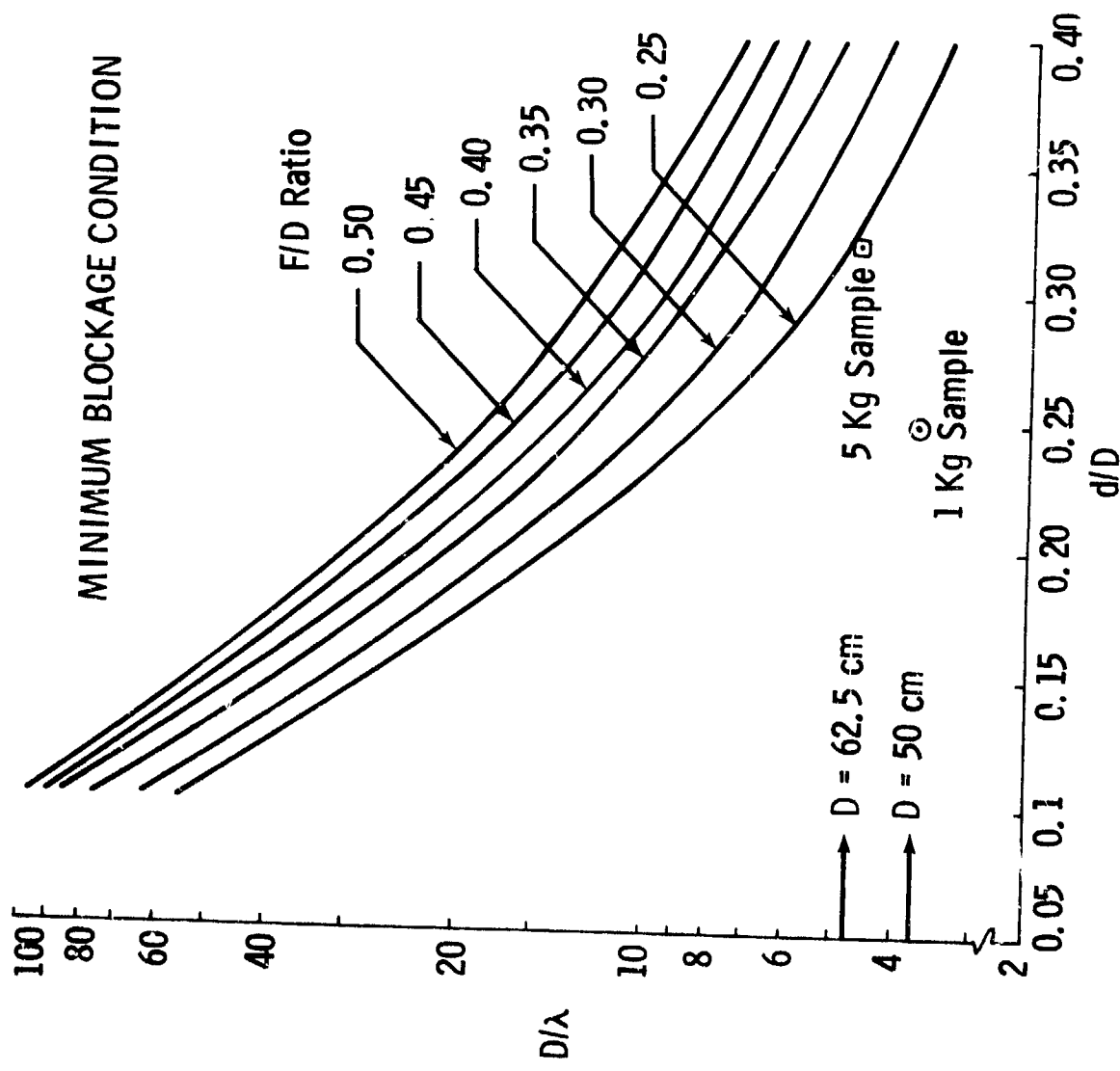


Figure V-1: MAV Angle Tracking Dual-Ratio Transponder--System Antenna

1 kg sample:  $D = 50$  cm;  $d/D = 0.250$

5 kg sample:  $D = 62.5$  cm;  $d/D = 0.325$

The minimum blockage curves indicate that the large diameter main dish design (5 kg sample) with the increased diameter sample canister will allow a higher main dish F/D ratio for the MAV antenna. One of the problems encountered with these designs is that the subreflector diameter as well as the main dish diameter are relatively small in terms of wavelengths at S-band. The effect of subreflector blockage on antenna gain and sidelobe level is shown in Figure V-8. For a sample canister diameter of 12.5 cm (1 kg sample) and a main dish diameter of 50 cm, the net antenna gain is 18 dB and the SLL = -11 dB. For a sample canister diameter of 20 cm (5 kg sample) and a main dish diameter of 62.5 cm, the net antenna gain is 19.3 dB and the SLL = -9 dB. The reduction in gain due to the subreflector appears to be tolerable despite the large blocking ratios. Another important consideration is the effect on the difference pattern nulls due to increased aperture blockage and possible asymmetries in the subreflector location.

The MAV dual function transponder block diagram is shown in Figure V-9. Single IF chain angle tracking is chosen over a conventional three channel receiver since it is lighter and contains much less equipment. The simplification occurs by replacing the error signal IF chains by a crystal filter, balanced modulator, and low frequency oscillator. Tradeoffs indicate for this system a reduction in size, weight, and power, and an increase in reliability. The price paid for this improvement is a 3 dB decrease in S/N ratio and reduction in sensitivity due to phase shifts of about 0.6 dB.

The error signals are converted in the first IF with mixers identical to those in the sum channel. Each error signal is then modulated with a distinct tone in the balanced modulator producing sidebands whose amplitude is proportional to the amplitude of the error signals. The error sidebands, which are outside the normal modulation sideband of the reference channel, are added to the sum channel. This composite signal after conversion to the second IF passes through a multiple crystal filter which places a narrow band pass about one of the sidebands of each error signal. The command and ranging signals are stripped off before these multiple filters. After amplification the error signals are detected in coherent amplitude detectors, which are basically phase detectors with reference signals which are in

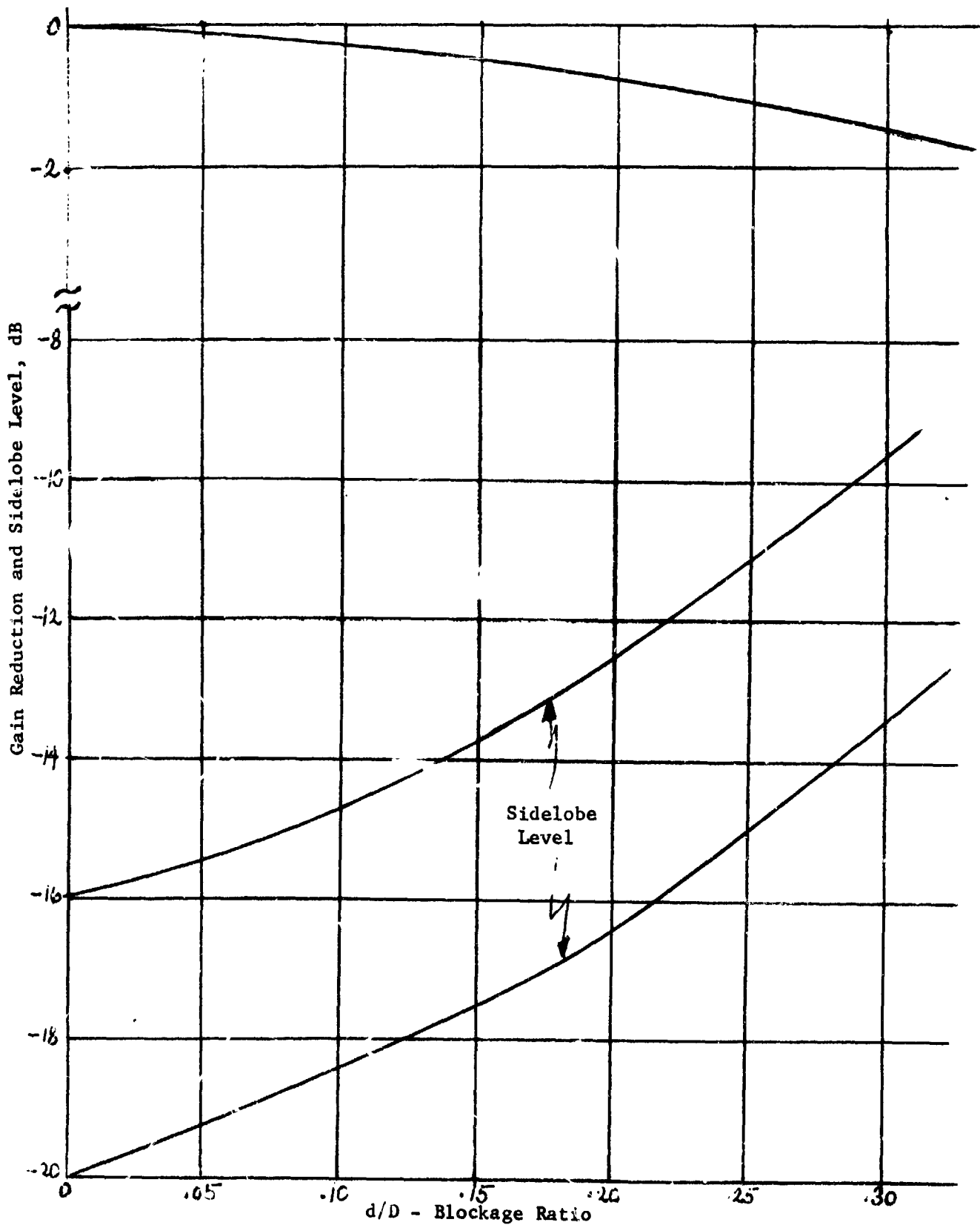


Figure V-8 MAV Antenna Gain Reduction and Sidelobe Level vs Blockage Ratio

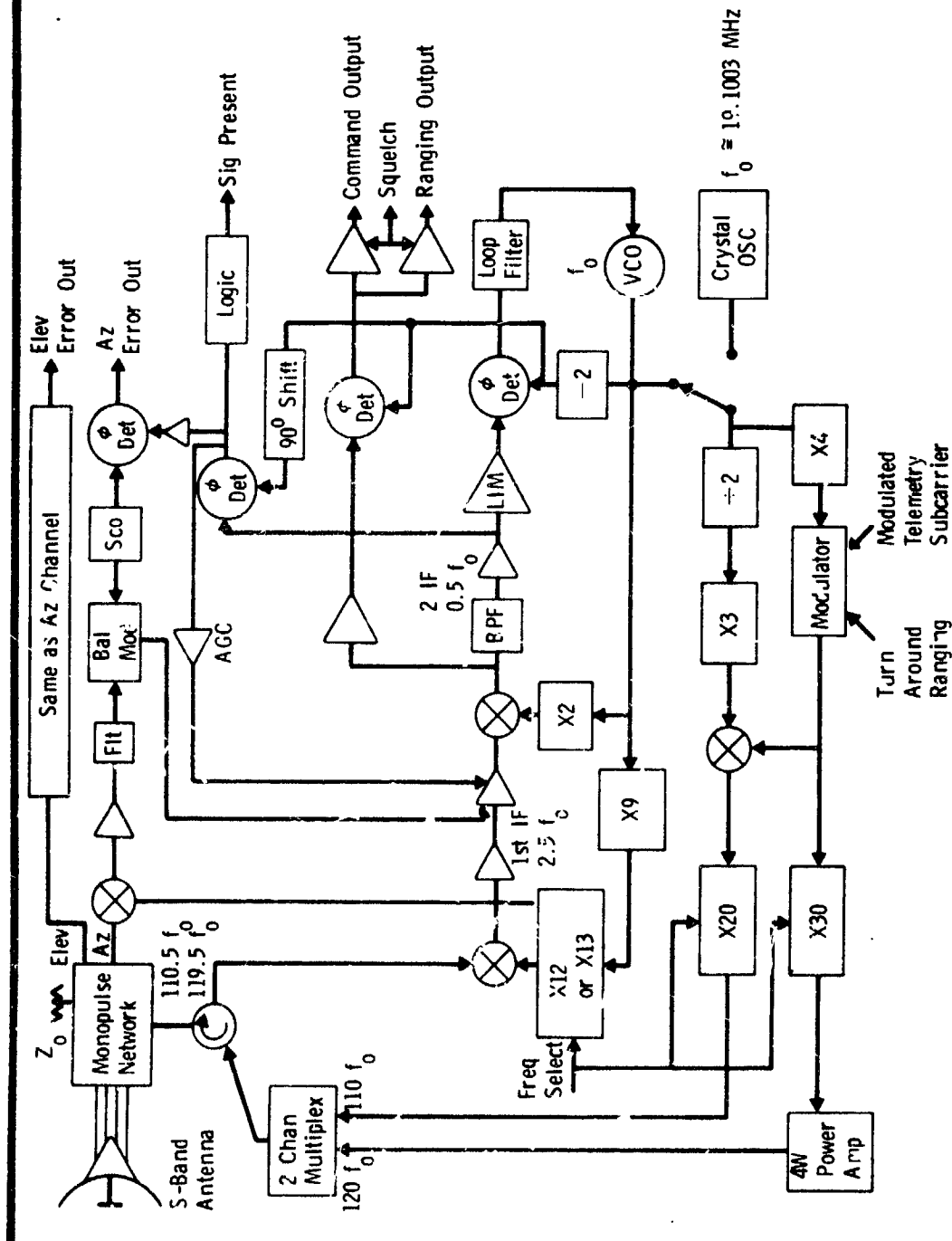
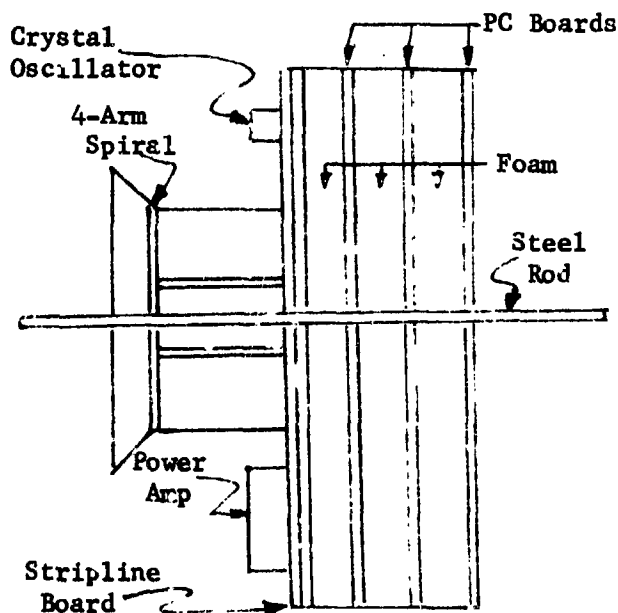


Figure V-9 MAV Dual-Ratio Transponder Block Diagram

phase with the carrier signal. The amplitude and phase of the error tones are then determined.

The dual-ratio transponder utilizes the sum channel from the monopulse antenna. The coherence ratio is 240/221 for the standard DSIF link and 220/239 for the rendezvous link with the orbiter. For a 220/239 transponder ratio, the transponder receives at  $119.5 f_0$  and transmits at  $110 f_0$  where  $f_0$  is the VCO frequency. For a 240/221 transponder ratio, the transponder receives at  $110.5 f_0$  and transmits at  $120 f_0$ . A system of mixing and multiplication is employed to achieve these ratios, and the appropriate chain is selected for either the DSN or rendezvous function.

It is essential to minimize the size and weight of the transponder assembly in order to meet the MAV weight restrictions. This can be accomplished by subdividing the transponder into eight subassemblies, in addition to the power amplifier and crystal oscillator. These subassemblies will occupy four circuit boards as shown below. The top circuit board is the strip line board which contains the RF subassembly and also serves as the ground plane for the antenna feed. The other three circuit boards are conventional PC boards. The complete assembly will be foamed to allow it to withstand the expected 11 g acceleration environment.



Based upon this concept the transponder weight including the antenna feed system has been estimated and is shown in Table V-1. The entire assembly fits directly behind the dish and provides an extremely compact transponder assembly.

Table V-1 MAV Transponder Mass

Printed Spiral Feed	0.22 kg
Feed Cavity	0.10 kg
P.C. Boards	0.55 kg
Crystal Oscillator	0.32 kg
Power Amplifier	0.12 kg
Rigid Coax Lines	0.13 kg
Connectors	0.10 kg
Case	0.59 kg
Transponder Mass	2.13 kg
Antenna Mass	0.9 kg
Total Mass	3.03 kg

### C. SENSOR SYSTEM CALCULATIONS

In order to assess the performance of the rendezvous system, it was decided to perform system calculations and to determine the range, range rate, and angle errors inherent with this system.

Link calculations were performed for both the orbiter/MAV and the MAV/orbiter links. Four traveling wave antennas were employed along the sample transfer guide cone in a phase comparison monopulse arrangement. The MAV transponder antenna consisted of a 50 cm Cassegrain dish as described before. Transfer of the sample canister during the docking stage of the rendezvous mission allows the beacon antenna to continue functioning in a low gain mode so that the command link will operate even after transfer of the sample canister.

#### Orbiter to MAV Link:

$$P_R = P_T - L_{FS} - L_{FI_1} - L_P + G_T + G_R - L_{FI_2}$$

$P_R$  = received power at MAV

$P_T$  = 300 mW = 24.8 dBm

$L_{FI_1}$  = orbiter circulator, BFN, cable losses = 2 dB

$L_P$  = polarization loss (linear to circular) = 3 dB

$L_{FS}$  = path loss =  $36.6 + 20 \log R + 20 \log (2282) = 103.3 + 20 \log R$

$R$  = orbiter to MAV range in miles

$G_T$  = transmitting antenna gain = 15 dB ( $l/\lambda \approx 3.5$ ,  $d/\lambda \approx 2$ )

$G_R$  = receiving antenna gain = 18.3 dB (50 cm dish; 12.5 cm subreflector)

$L_{FI_2}$  = MAV circulator and R.F. losses = 1 dB

$R$  =  $24.8 - 103.8 - 20 \log R - 2 - 3 + 15 + 18.3 - 1$

$P_R$  =  $51.7 - 2 \log R$

The modulation of the transmitted carrier is as follows:

- (a) Deviation of each minor tone on the 819.2 kc subcarrier:
  - 0.6 radian peak each
- (b) Deviation of the composite range tone spectrum on the carrier:
  - 1.0 radian peak

then:

(1) Carrier Power:  $P_c = J_0(1)^2 P_R = P_R - 2.3 \text{ dB}$

(2) Unmodulated Subcarrier Power:  $P_{SC(U)} = J_1(1)^2 P_R + 3 \text{ dB} = P_R - 4.1 \text{ dB}$

(3) Power in Minor Tones:

$$P_{MT} = [J_1(\beta_1)J_0(\beta_2)J_0(\beta_3)J_0(\beta_4)]^2 P_{SC(U)} + 3 \text{ dB} = P_R - 14.4 \text{ dB}$$

(4) Power in Modulated Subcarrier:

$$P_{SC(M)} [J_0(\beta_1)J_0(\beta_2)J_0(\beta_3)J_0(\beta_4)]^2 P_{SC(U)} = P_R - 7.3 \text{ dB}$$

The signal to noise ratio at the MAV transponder:

(1) Carrier Loop:  $\left(\frac{S}{N}\right)_c = \frac{P_R}{\eta(2B_L)} - 2.3 \text{ dB}$

$$\eta = -167.5 \text{ dBm/Hz}$$

$$2B_L = \text{loop two-sided noise bandwidth} = 1 \text{ kHz} = 30 \text{ dB}$$

$$\eta(2B_L) = -167.5 + 30 = -137.5 \text{ dBm}$$

Then:  $\left(\frac{S}{N}\right)_c = (-51.7 - 20 \log R) + 135.2$

(2) Ranging Channel: The range tones are filtered in the ranging channel and remodulated on the beacon transmitter. The bandwidth of the ranging channel is 300 kc since no ranging is being done in the DSN link.

Then:

$$\left(\frac{S}{N}\right)_{RU} = \frac{P_R}{\eta B} - 4.1 \text{ dB}$$

$$\eta = -167.5 \text{ dBm/Hz}$$

$$B = 300 \text{ kc} = 54.8 \text{ dB}$$

$$B = -167.5 + 54.8 = -112.7 \text{ dBm}$$

$$\left(\frac{S}{N}\right)_{RU} = (-51.7 - 20 \log R) + 108.6$$

From Figure V-10 it is clear that there is no suppression of the retransmitted range tone power up to an orbiter/MAV range of 1100 km. Maximum range of the rendezvous system is estimated at 750 km, although considerably longer ranges are possible.

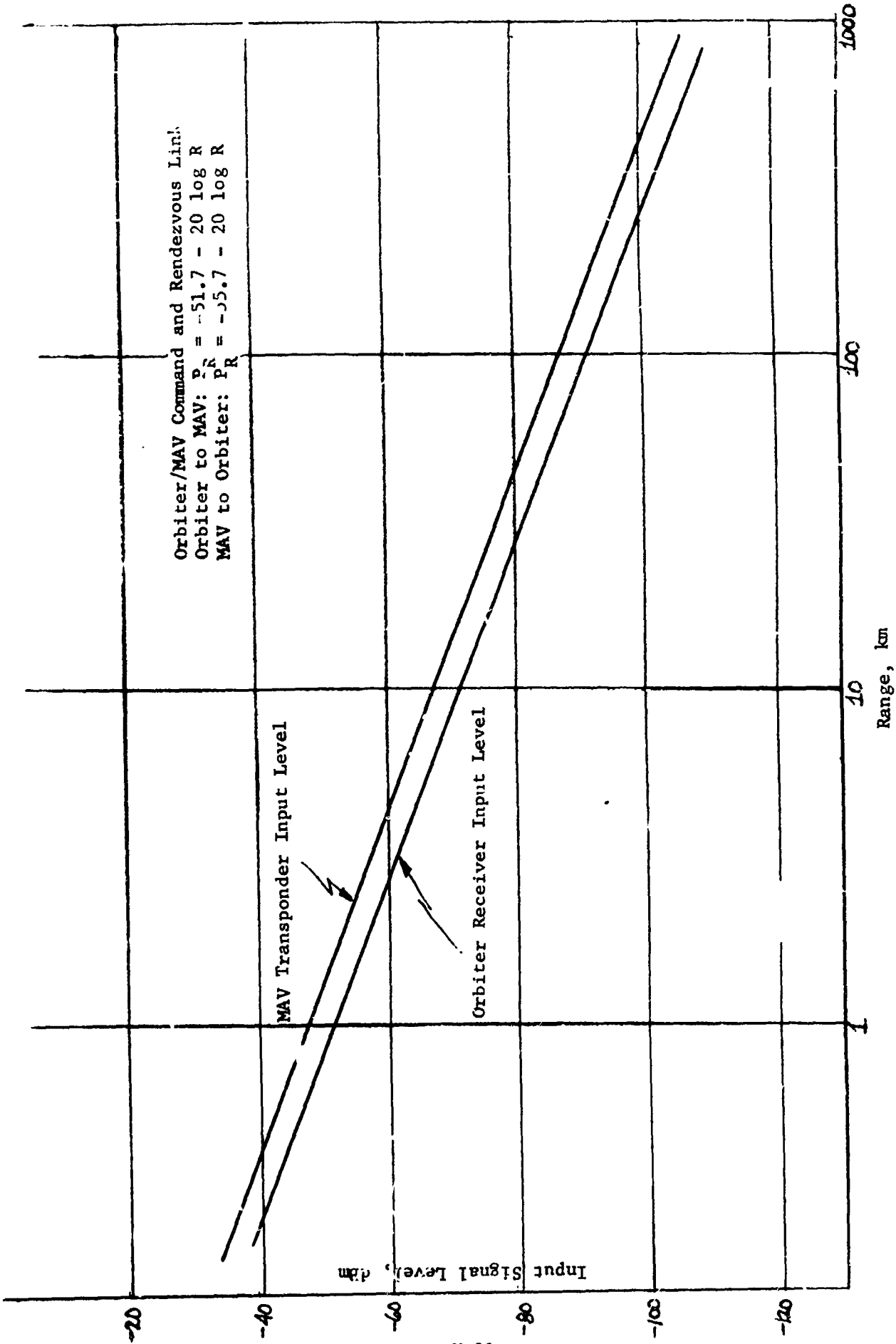


Figure V-10 Input Signal Levels vs Range

MAV to Orbiter Return Link:

$$\begin{aligned}
 P_R &= \text{received power at orbiter} \\
 P_T &= 150 \text{ mW} = 21.8 \text{ dBm} \\
 L_{FI_1} &= \text{transponder diplexer, circulator and BFN losses} = 2.5 \text{ dB} \\
 L_P &= \text{polarization loss (circular to linear)} = 3 \text{ dB} \\
 L_{FS} &= \text{path loss} = 36.6 + 20 \log R + 20 \log (2101) = 103.0 + 20 \log R \\
 G_T &= \text{transmitting antenna gain} = 18.3 \text{ dB} \\
 G_R &= \text{receiving antenna gain} = 14.7 \text{ dB} \\
 L_{FI_2} &= \text{orbiter R.F. losses} = 2 \text{ dB} \\
 P_R &= 21.8 - 103.0 - 20 \log R - 2.5 - 3.0 + 14.7 + 18.3 - 2 \\
 P_R &= -55.7 - 20 \log R
 \end{aligned}$$

After modulation of the beacon transmitter the range tones are retransmitted to the orbiter receiver. The signal to noise ratio at the orbiter receiver is then obtained as follows:

$$\begin{aligned}
 (1) \text{ Carrier Loop: } \left(\frac{S}{N}\right)_c &= \frac{P_R}{\eta(2B_L)} - 2.3 \text{ dB} \\
 2B_L &= 1 \text{ kc} = 30 \text{ dB} \\
 \eta(2B_L) &= -167.5 + 30 = -137.5 \text{ dBm} \\
 \left(\frac{S}{N}\right)_c &= (-55.7 - 20 \log R) + 135.2
 \end{aligned}$$

(2) Tone Filters: The composite modulation spectrum is demodulated by the orbiter rendezvous receiver. The 819.2 kHz tracking filter locks to the modulated subcarrier and demodulates the minor tones. The signal to noise ratio in the 819.2 kHz tone filter is then:

$$\begin{aligned}
 \left(\frac{S}{N}\right)_{RT} &= \frac{P_R}{\eta B} - 7.3 \text{ dB} \\
 B &= \text{filter bandwidth} = 10 \text{ Hz} = 10 \text{ dB} \\
 \eta B &= -167.5 + 10 = -157.5 \text{ dBm} \\
 \left(\frac{S}{N}\right)_{RT} &= (-55.7 - 20 \log R) + 150.2
 \end{aligned}$$

The signal to noise ratio in the tone filters of the minor tones is:

$$\begin{aligned}
 \left(\frac{S}{N}\right)_{R_{MT}} &= \frac{P_R}{\eta B} - 14.4 \text{ dB} \\
 B &= 10 \text{ Hz} = 10 \text{ dB} \\
 \eta B &= -157.5 \text{ dBm} \\
 \left(\frac{S}{N}\right)_{R_{MT}} &= (-55.7 - 20 \log R) + 143.1
 \end{aligned}$$

The various input signal levels and signal to noise ratios are plotted in Figures V-10 and V-11. The range tones consist of the 819.2 kHz subcarrier and minor tones of 102.4 kHz, 12.8 kHz, 1.6 kHz, and 200 Hz. At 200 Hz the maximum unambiguous range is 750 km, so that longer ranges can be considered.

In order to achieve a given range accuracy with a multitone ranging system it is necessary to consider both fixed and random errors in the range measurement.

Past experience with the Apollo/LM rendezvous radar indicates that phase can be maintained within  $3^\circ$  as a function of temperature, aging, etc. The basic phase relationship is given by:

$$(1) \quad \phi = \frac{2\pi}{\lambda} d = \left( \frac{2\pi f_T}{C} \right) d$$

where:  $f_T$  = highest tone frequency

$$\text{Then:} \quad \delta\phi = \left( \frac{2\pi f_T}{C} \right) \delta d$$

$$\text{And:} \quad f_T = \frac{C \delta\phi}{2\pi \delta d}$$

To achieve a bias error  $\delta d \approx 3$  meters, we can solve the above equation for  $f_T$ :

$$f_T = \frac{(3)(10^8)}{(3.06)} \left( \frac{3}{360} \right) = 818 \text{ kHz}$$

Thus, for a 3 m bias error the highest tone should be 818 kHz. For a five-tone ranging system with a maximum unambiguous range of 750 km, the highest tone then turns out to be 819.2 kHz.

The range measurement accuracy is also affected by random errors. The range measurement is basically obtained by a phase measurement on the highest frequency tone and range ambiguities are resolved by measuring the phase of succeeding lower tones. The rms phase error due to thermal noise is given by:

$$(2) \quad \sigma_\phi = \frac{1}{\sqrt{2(S/N)_T}} \quad (S/N)_T = \text{signal to noise ratio of tone}$$

The corresponding rms error in the range measurement is:

$$(3) \quad \sigma_R = C \left( \frac{\sigma_\phi}{2\pi f_T} \right) = \frac{C}{\sqrt{2(S/N)_T}} \left( \frac{1}{2\pi f_T} \right)$$

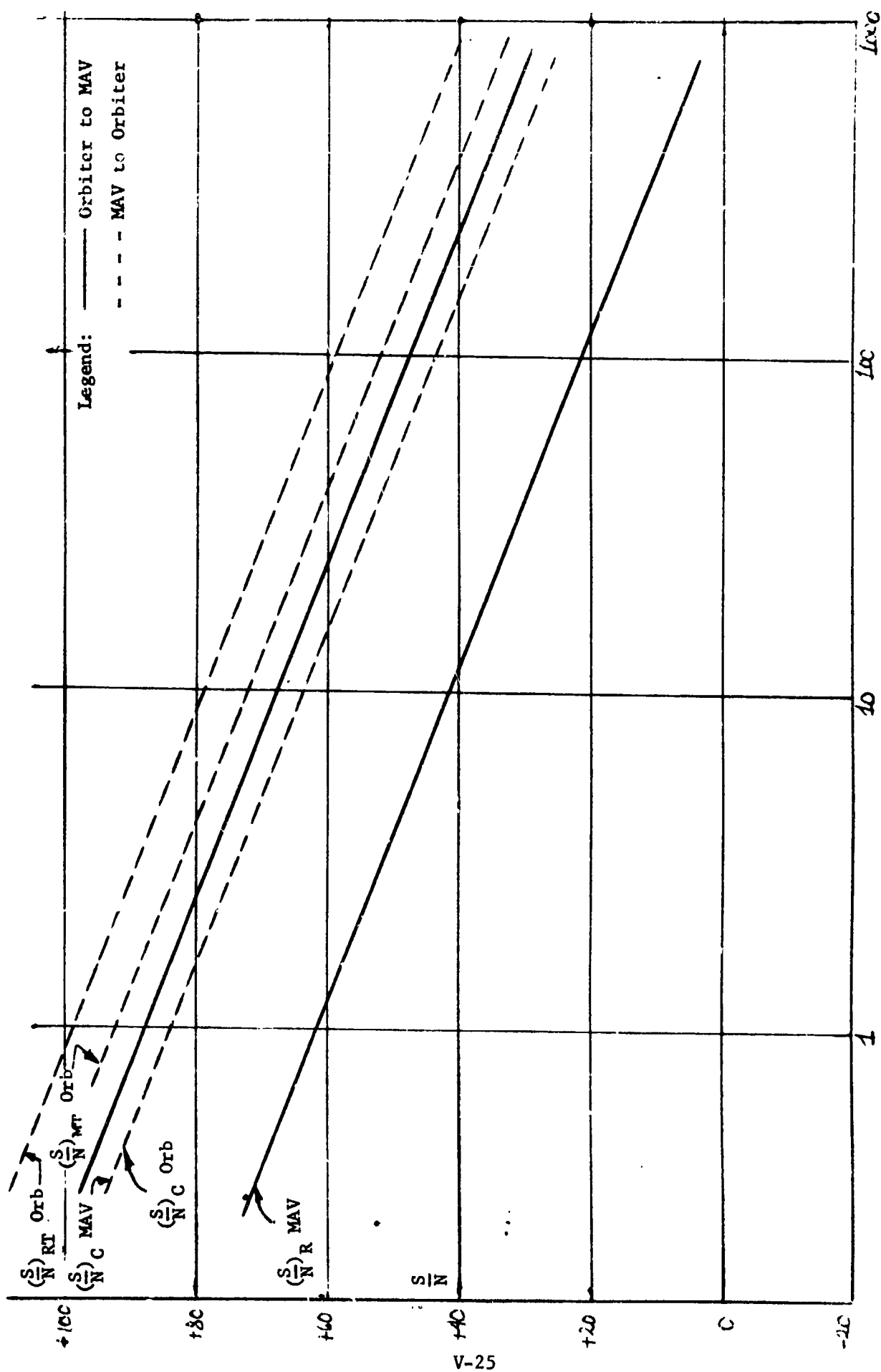


Figure V-11 S/N Ratio vs Range

To achieve a  $1\sigma$  random error of  $\sigma_R = 3\text{m}$ , then, it is now necessary to solve the above relation for the required signal to noise ratio. This becomes:

$$(4) \quad \sqrt{2(S/N)_T} = \frac{1}{\left(\frac{\sigma_R}{C}\right)(2\pi f_T)}$$

If the filter in the tracking loop has a bandwidth of  $B=10$  Hz, then the tracking loop time constant is 0.1 sec, and the improvement through integration becomes

$$(5) \quad n = f_T T_i$$

and  $\sqrt{2(S/N)_T n} = \sqrt{2(S/N)_T} f_T T_i = \frac{\sqrt{2(S/N)_T} f_T}{\sqrt{B}}$

where  $B$  = tracking loop bandwidth

Substituting in (4) we, then, obtain:

$$\sqrt{2(S/N)_T} f_T = \frac{\sqrt{B}}{\left(\frac{\sigma_R}{C}\right)(2\pi f_T)}$$

$$\sqrt{2(S/N)_T} = \frac{\sqrt{B}}{2\pi \left(\frac{\sigma_R}{C}\right) f_T^{3/2}}$$

For  $\sigma_R = 3$  m,  $B = 10$  Hz,  $C = 3 (10)^8$  m/s, and  $f_T = 8.19 (10)^5$  Hz, we get:

$$(S/N)_T = 2.24 (10^{-3}) = -26.5 \text{ dB}$$

Thus, as long as the signal to noise ratio is greater than -26.5 dB it is theoretically possible to achieve the required  $1\sigma$  random error of 3m with a tracking loop bandwidth of 10 Hz. The sidetone ranging system utilizes tones of 102.4 kHz, 12.8 kHz, 1.6 kHz, and 200 Hz in addition to the 819.2 kHz subcarrier. The  $1\sigma$  random error associated with these tones has been calculated using the same relationships employed above and the signal to noise results obtained from the link calculations. Then, for a maximum range of 250 km the random range error becomes 238 m and for a maximum unambiguous range of 750 km this error reaches a maximum of 754 m. The range error is plotted as a function of system range in Figure V-12. It is evident that although large random errors will be encountered at long ranges, the range accuracy at short ranges is quite excellent. In fact, Figure V-12 indicates that the random error can be kept at 3 m or below for ranges up to 65 km which should be more than sufficient for the intended rendezvous mission.

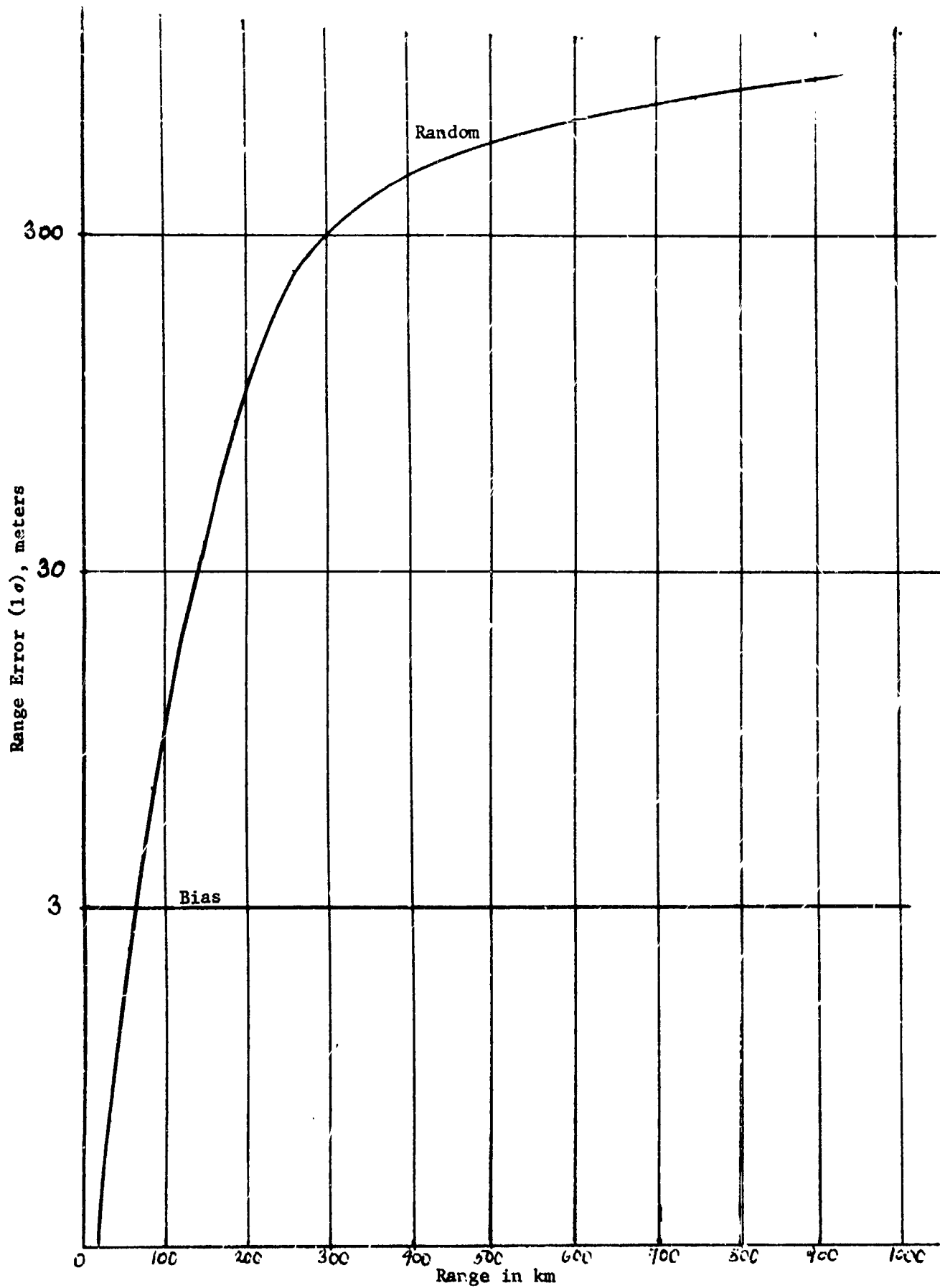


Figure V-12 Range Error vs Range

The lag error of the ranging system will depend both on the relative velocity and the integration time. For a system with a tracking loop bandwidth of 10 cps, the integration time is 0.1 seconds. Thus, if the lag error is not to exceed 3 m then the velocity must not exceed 30 m/s. If the velocity exceeds 30 m/s during the terminal phase of the rendezvous mission then the tracking loop time constant must be reduced where it appears that there is adequate signal margin.

The 819.2 kHz subcarrier is used to measure range. A time delay of one cycle of the 819.2 kHz subcarrier is equivalent to the range between the two terminals changing by 183.5 m. The 819.2 kHz subcarrier is demodulated and filtered by a phase locked tracking filter with a two-sided noise bandwidth of 10 Hz. The signal to noise ratio at a maximum range of 250 km is 51 dB and the signal to noise ratio at a maximum unambiguous range of 750 km is 41 dB. The r.m.s. phase jitter of a sine wave signal with additive noise is

$$\sigma = \tan^{-1} \sqrt{1/2(S/N)} \text{ rad.}$$

Thus, at the maximum unambiguous range the range error due to phase jitter is given by:

$$\begin{aligned} \sigma &= \tan^{-1} \sqrt{1/25,200} = \tan^{-1} 1/159 \text{ radians} \\ \sigma &= 0.361 \text{ degrees} \end{aligned}$$

The rms jitter in meters is then:

$$\sigma = (0.361/360) (183.5) = 0.184 \text{ meters}$$

Thus, it is clear that both the bias and random range errors will be greater than the errors introduced due to phase jitter.

Additional system error calculations have been performed and are given in Appendix E. These calculations include range rate and angle error calculations for the orbiter/MAV rendezvous sensor. A summary of all range, range rate, and angle error calculations is shown in Table V-2. This table also shows similar data extracted from measurements on LM/CSM rendezvous radars when these units were exposed to the vibration and thermal vacuum environment expected during the Apollo mission. The LM/CSM rendezvous system is also a sidetone ranging system and utilizes an amplitude comparison monopulse system for angle tracking. The data shown represents typical 1 $\sigma$  accuracies from production line units. It is interesting to note that the orbiter/MAV

Table V-2 Rendezvous Radar Error Summary

Radar Error	LM/CSM System	Orbiter/MAV System
Range Error (Bias)	48 m	3 m
Range Error (Random)	R < 65 km	< 3 m
	R = 750 km	750 m
Range Rate Error (Bias)	7.6 cm/sec	5 cm/sec
Range Rate Error (Random) R = 750 km	15 cm/sec	5 cm/sec
Angle Error (Bias)	1.7 mrad	1.5 mrad.
Angle Error (Random)	R < 10 km	< $5 \times 10^{-2}$ mrad.
	R = 750 km	1.1 mrad.

rendezvous system promises to yield comparable performance to the flight-proven LM/CSM system with the added advantage of providing useful radar data during the final docking phase.

#### D. SENSOR SYSTEM COMPARISONS AND COST CONSIDERATIONS

The rendezvous and docking sensor described in Sections A and B provides range, range rate, and angle data to the computer. An S-band, all solid state cw system was employed. Previous work in the area of rendezvous systems between space vehicles must be taken into account in assessing the development time and cost involved in the design of an orbiter/MAV rendezvous sensor. A comparison of four cw rendezvous sensors is shown in Table V-3. All of these sensors use sidetone ranging systems and three channel monopulse receivers for angle tracking. Although the Apollo rendezvous system operates at X-band, it is very similar to the orbiter/MAV system except that it was not designed for automatic docking. This similarity is illustrated in Table V-4 which shows a comparison of the major system parameters of the two rendezvous systems. Over \$20 M was spent during the LMRR development contract for design, development, and space qualification of the radar. This experience can be utilized in the design of the orbiter/MAV rendezvous sensor. In Table V-3, the non-recurring cost for the modified LM/CSM system proposed for Shuttle missions is thus very low because of the experience factor and the extent of the modifications.

The unified S-band system is a rendezvous sensor based on a system concept where the S-band equipment performs all tracking, command and communication functions in the Apollo system. It utilizes similar equipment in both the LM and CSM vehicles, and provides a substantial reduction in both system weight and power over the X-band systems. The orbiter/MAV system also performs all tracking, command, and telemetry functions and must operate in a fully automatic mode during rendezvous and docking. The stringent MAV weight restrictions and power constraints favor the use of a low-power S-band system based on proven tracking techniques developed for both the JPL-DSIF system and the Apollo rendezvous mission. Thus the orbiter/MAV system will provide a high reliability rendezvous link at very low cost. The costs shown in this table are based on realistic estimates of equipment development costs and space qualification costs, as well as past experience in the design of range and range rate sensors in the X-band, S-band, and VHF region of the EM spectrum. Utilization of advanced packaging techniques and increased use of microcircuit technology results in considerable reduction in size and weight of the S-band systems. Extensive use of integrated

Table V-3 CW Rendezvous Radar Sensor Characteristics

Rendezvous Sensor	Frequency	Radar Weight	Radar Power	Transponder Weight	Transponder Power	Non-recurring Costs	First Unit Cost	MTBF
Apollo/LM (Operational)	X	34 kg	160 W (Nominal)	6.6 kg	75 W (Nominal)	\$30 M	\$1.5 M	2000 hrs
Apollo/LM (Modified)	X	18 kg	80 W	4.1 kg	50 W	\$ 4.0	\$0.6 M	3000 hrs
Unified S-Band System	S	6.4 kg	13.5 W	6.1 kg	14 W	\$ 7.0 M	\$0.4 M	3000 hrs (Est.)
Orbiter/MAV System	S	7.3 kg	14 W	2.9 kg	11 W	\$ 8.5 M	\$0.3 M	3000 hrs (Est.)

NOTES

1. Non-recurring costs include cost of prototype unit, qualification unit, and qualification tests.
2. All sensors except the Orbiter/MAV system are rendezvous sensors only (R > 30 m).
3. Apollo/LM (modified) data are for a proposed rendezvous sensor for the Shuttle orbiter (active cooperative mode).
4. Orbiter/MAV cost estimates are based on past experience on space qualified rendezvous and tracking sensors.

Table V-4 Comparison of Apollo and URDMO Rendezvous Sensors

System Parameter	LM/CSM Rendezvous	Orbiter/MAV Rendezvous/Docking
Frequency	X-Band	S-Band
Radar Type	CW	CW
Radar Mode	Automatic and Manual	Automatic
Modulation	PM: 3 tones	PM: 819 kc - Subcarrier 4 Minor Tones
Radar Power	0.3 W (Solid State)	0.3 W (Solid State)
Maximum Range	750 km	750 km
Minimum Range	24 m	3 m
Radar Antenna	Cassegrain	Travelling Wave Array
Angle Track Method	Amplitude Monopulse	Phase Monopulse
Transponder Power	0.3 W (Solid State)	0.15 W (Solid State)
Transponder Antenna	Horn	Cassegrain
Coherence Ratio	240/241	220/239

circuits in both the rendezvous sensor and the transponder will, furthermore, improve system reliability and will account for the estimated increase in MBTF to 3000 hrs for the S-band systems.

### E. RENDEZVOUS SENSOR RELIABILITY AND FAILURE MODE OPERATION

The rendezvous sensor must be capable of operating under various environmental conditions and should have the capability to provide adequate performance in various failure modes. Calculations were performed to assess the range performance of the rendezvous system in the non-cooperative mode. In this situation, it was assumed that the orbiter antenna was pointed within  $\pm 1^\circ$  of the MAV transponder antenna axis and that the MAV antenna was matched to the transponder at the rendezvous transmitter frequency ( $\Gamma_R = 0$ ). The latter represents a worst case condition since any mismatch will contribute to the radar cross-section of the passive antenna target. The radar cross-section of the MAV antenna is then given by:

$$\sigma = \frac{G^2 \lambda^2}{4\pi} = .922 \text{ m}^2 \text{ at } \lambda = 13.2 \text{ cm}$$

At  $+9^\circ$  (3 dB pts) this would become  $\sigma = .23 \text{ m}^2$  and at  $\pm 1^\circ$  a good estimate is  $\sigma \approx .850 \text{ m}^2$ .

The system acquisition range is given by:  $R =$

$$R = \sqrt[4]{\frac{P_T G_A \sigma}{(4\pi)^2 k T_o B_n F_n (S/N)_{\min}}}$$

Let:  $k = 1.38 \times 10^{-23}$

$$T_o = 290^\circ \text{K}$$

$$B_n = 1 \text{ kHz}$$

$$A_e = .04385 \text{ m}^2$$

$$F_n = 6.3$$

Then: For  $S/N = 10 \text{ dB} \rightarrow R = 1.73 \text{ km}$

For  $S/N = 3 \text{ dB} \rightarrow R = 2.58 \text{ km}$

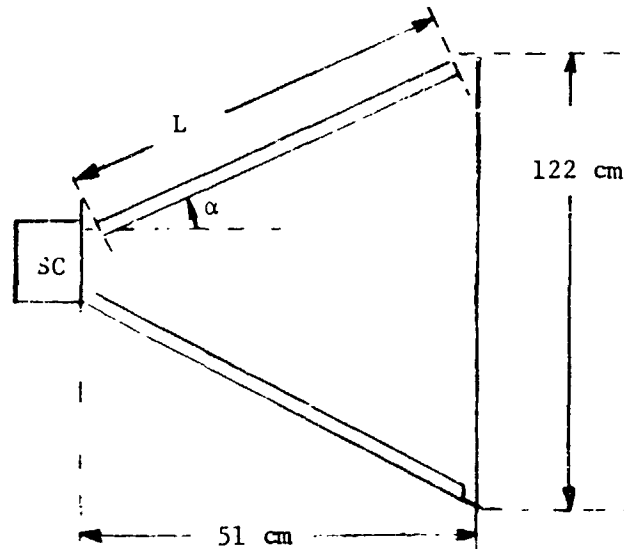
For the above calculations an antenna gain of 15 dB was assumed for the four antennas comprising the monopulse array. To achieve failure mode operation of the rendezvous sensor out to 8-10 km requires an antenna gain at S-band of 20 dB plus a 2.5 watt amplifier in the orbiter transmitter. For a system without failure mode operation, a 15 dB gain antenna would be sufficient, since system operation would be restricted to the cooperative mode. It was, therefore, decided to investigate the feasibility of increasing the antenna gain by utilizing alternate antenna designs. Current dimensions of the sample transfer guide cone are given in the sketch below.

$$\alpha = 45^\circ$$

$$\theta = \frac{\pi}{2} - \alpha = 45^\circ$$

$$\lambda = 13.6 \text{ cm}$$

$$L = 71.8 \text{ cm}$$



Using the above configuration, the maximum length of each array would be 71.8 cm or  $5.3\lambda$ . The peak of the array radiation pattern must occur at  $\theta = 45^\circ$  from broadside, so that if a conventional, scanned broadside array is employed, the gain will be reduced by 1.5 dB from the broadside gain. For a line source, the gain loss at  $45^\circ$  is only 0.4 dB if  $kL \approx 33$ . In this case, then, the antenna gain is given by:

$$G = 10 \log \frac{2nL}{\lambda} - 0.4 \text{ dB} = 9.3 \text{ dB}$$

In the sum mode, all four antennas are operated in phase and the total antenna gain is given by:

$$G_T = 9.3 \text{ dB} + 6 \text{ dB} = 15.3 \text{ dB}$$

It is, therefore, not advisable to employ a line source as the array element since insufficient gain is produced for failure mode operation.

If a traveling wave antenna is chosen as the array element, then " $\alpha$ " should preferably be smaller than  $45^\circ$ . For  $\theta = \alpha = 45^\circ$ , the following parameters have been calculated to guarantee that the traveling wave antenna contains only a single lobe:

$$d/\lambda = 0.58$$

$$L/\lambda g = 0.41$$

where  $d$  = element spacing of traveling wave antenna  
 $\lambda$  = feed line length between traveling wave antenna elements.

The propagation constants are given by:

$$k = \frac{2\pi}{\lambda} = \text{free space propagation constant}$$

$$\beta = \frac{2\pi}{\lambda_g} = \text{feed line propagation constant}$$

The main beam of radiation from the traveling wave antenna, occurring at angle  $\theta$ , satisfies the following relationship, if it is assumed that the elements are omni-directional:

$$kd \sin \theta - \beta l = 2n\pi$$

where  $n$  = integer (0, +1, +2, etc.)

The slant length of the cone is  $L = 5.3\lambda$  so that with  $d/\lambda = 0.58$  the maximum length array that could be accommodated would have 9 elements ( $N = 9$ ). This traveling wave antenna would, then, take up the full length of the cone, which represents an upper limit on the achievable gain from this antenna. The gain of the antenna is, then, obtained as follows:

$$G = 10 \log_{10} N - 1.5 \text{ dB} + 10 \log_{10} g_r(45^\circ, 0^\circ)$$

where  $g_r$  = element gain factor at  $\theta = 45^\circ$ ,  $\phi = 0^\circ$

The only practical elements which can be considered for the traveling wave antenna are either dipoles or slots, and these have a low element gain factor. Assuming a unidirectional cosine power pattern from these elements, we then get

$$g_r(45^\circ, 0^\circ) \approx 2.04 \approx 3.1 \text{ dB}$$

The traveling wave antenna gain is, then, given by:

$$G = 9.5 \text{ dB} - 1.5 \text{ dB} + 3.1 \text{ dB} = 11.1 \text{ dB}$$

Again, in the sum mode, all four antennas are operated in phase, and the total antenna gain is:

$$G_T = 11.1 \text{ dB} + 6.0 \text{ dB} = 17.1 \text{ dB}$$

While this is an improvement over the line source array, it still does not provide the desired 20 dB gain.

In the original design a surface wave antenna was proposed as a feasible array element for the monopulse antenna. Again assuming utilization of the full slant length of the sample transfer guide cone, we would get for this arrangement:

$$L = 5.3\lambda$$

Instead of using a traveling wave antenna structure, an array of top loaded monopoles on a ground plane fed by a dipole reflector combination could be designed. Experimental work on such antennas indicates that the relative phase velocity along the array for a maximum gain design should satisfy the following relationship:

$$\frac{C}{V} = \frac{\lambda}{\lambda_z} = 1 + \frac{\lambda}{3L} \quad (3\lambda < L < 8\lambda)$$

or

$$\frac{\lambda}{\lambda_z} = 1.063 \text{ for } L = 5.3\lambda$$

The gain of the surface wave antenna is then given by:

$$G \approx 10 \log_{10} \frac{10L}{\lambda} \approx 17.2 \text{ dB}$$

To avoid mechanical interference at the feed with the sample canister, it would be desirable to shorten the antenna and locate the feed point further up along the cone. This can be done by shortening the antenna length to  $L = 4\lambda$ , which then yields for the gain:

$$G \approx 10 \log_{10} 40 \approx 16 \text{ dB}$$

Again, in the sum mode, all four antennas are operated in phase, and the total antenna gain is:

$$G_T = 16.0 \text{ dB} + 6.0 \text{ dB} = 22.0 \text{ dB}$$

This would appear satisfactory for failure mode operation of the rendezvous system.

The above antenna options would require further experimental work to determine the actual performance of these arrays and to verify that these antenna gains can be achieved in practice.

If a 20 dB gain array can be achieved the non-cooperative acquisition range for a S/N = 10 dB is 3.08 km while the acquisition range for a S/N = 3 dB is 4.6 km. The actual signal to noise required for reliable acquisition

depends on the required detection probability and false alarm rate, as shown in the enclosed figure (Figure V-13). Typically for  $P_D = 90\%$  and  $P_{FA} = 10^{-3}$ , the required S/N = 10.7 dB. The lowest tone frequency is 200 Hz and the integration time is .1 sec (BW = 10 Hz). Hence the integration gain is given by:

$$N = [(200)(.1)]^{.7} = 20^{.7} = (8.1)^{.7} = 9.1 \text{ dB}$$

Then the required signal to noise ratio is given by:

$$(10.7 \text{ dB} - 9.1 \text{ dB}) + \text{margin} = 1.6 \text{ dB} + \text{margin}$$

The minimum margin is 3 dB, so that the S/N required is about 5 dB for  $P_D = 90\%$  and  $P_{FA} = 10^{-3}$ . This is the minimum S/N required which must be used in the range equation. The following acquisition ranges are then obtained:

$$\begin{array}{ll} \text{For } G = 15 \text{ dB} & R = 2.3 \text{ km} \\ G = 20 \text{ dB} & R = 4.1 \text{ km} \end{array}$$

To increase the range to 8-10 km would, further, require the inclusion of a power amplifier in the orbiter rendezvous transmitter as shown in Figure V-1. Thus, if the transmitter power output were increased from 300 mW to 2.4 watts, the acquisition range would increase from 4.1 km to 8.2 km. The power amplifier would be switched in only during transponder failure mode operation to provide the higher transmitter power levels required for non-cooperative tracking and docking with the MAV vehicle.

Further consideration was given to the reliability of the system components in the rendezvous sensor and the transponder. The only high power components in these assemblies are the 2.5 watt power amplifier in the rendezvous radar and the 4 watt power amplifier in the transponder. The former is only employed during failure mode operation, while the latter is essential to the MAV/DSN link. The normal procedure providing redundant transmitter power amplifiers was considered. This approach did not appear as attractive as designing the solid state amplifier to provide inherent redundancy and graceful degradation of output power by virtue of the basic amplifier circuit arrangement. This can be accomplished by providing a large number of amplifier stages in parallel with matched hybrids combining the outputs from these transistorized stages. Thus, the failure of one or two stages will not have a catastrophic effect on the output power of these systems. All circuitry in these assemblies is of the MIC variety on high

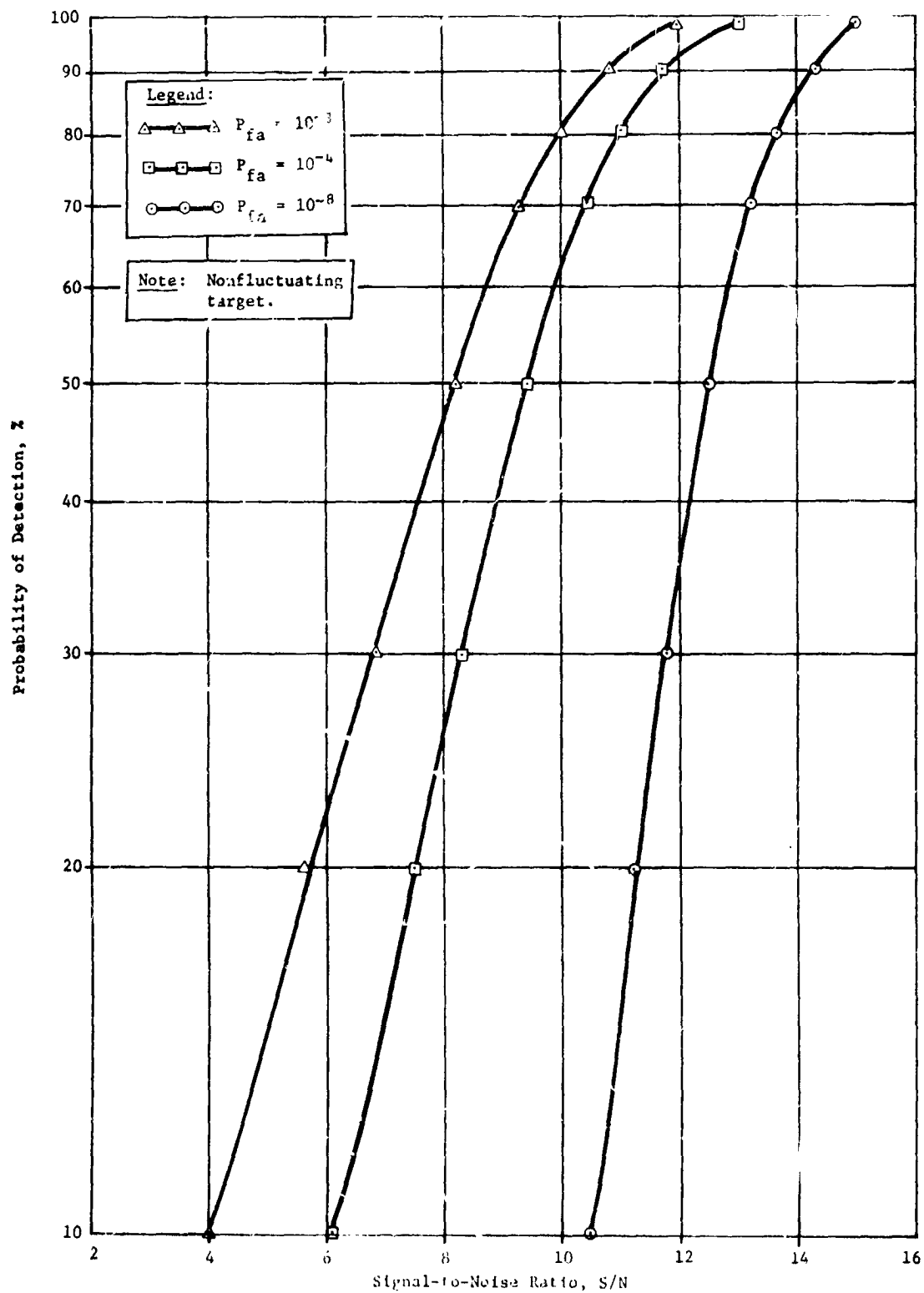


Figure V-13 Radar Detection Probability Curves

dielectric alumina substrates directly soldered, along with the devices, to a thin aluminum carrier to minimize weight. Conduction cooling of the amplifiers is accomplished by mechanical fastening of the stripline carrier to a suitable aluminum heat sink.

## F. NEW TECHNOLOGY DEVELOPMENT REQUIREMENTS

An assessment of the new technology requirements for the rendezvous and docking sensor was undertaken. The design of the orbiter/MAV rendezvous sensor is based on proven tracking techniques developed for Apollo and post-Apollo missions. Thus, new technology development work is required only in areas related to the Martian space environment and the orbiter/MAV rendezvous and docking mission. In particular, antenna designs required for the orbiter and MAV space vehicles must be developed to satisfy space vehicle and mission constraints. A phase-comparison monopulse system was selected because of its high on-axis gain, high boresight null sensitivity, and low probability of sidelobe tracking.

The design of both the orbiter antenna array and the MAV transponder antenna is greatly influenced by the presence of the sample canister and the mechanical sample transfer system. Thus, the monopulse antenna array must be integrated with the sample transfer guide cone to establish an effective aperture plane ahead of the sample canister well. Antenna development work is required on the traveling wave antenna and the monopulse array with emphasis on pattern stability and sidelobe reduction to assure that the system has only one stable tracking null. The MAV antenna requires an oversize subreflector to shield the sample canister from the antenna feed system. Development work is required to establish an optimum reflector surface and to come up with a suitable feed design. The Cassegrain antenna system has been selected for the MAV antenna because of the convenience of the mechanical arrangement whereby the feed and associated transmitter/receiver are close together and the system hardware can be easily packaged behind the dish. In such an arrangement the subreflector should be several wavelengths in diameter and normally would not block more than a small percentage of the main dish aperture. In the MAV design, neither of these conditions can be satisfied because of mechanical constraints and the choice of the S-band operating wavelength. It is, therefore, mandatory to investigate the performance of Cassegrain systems with oversize subreflectors where both the main dish diameter and subreflector are not large compared to the wavelength. The effect of large subreflector designs on both the sum channel and error channel patterns must be established. The MAV dual-ratio transponder operates as a standard DSIF transponder or as a rendezvous

transponder. Further development work is required on this unit as well as the angle tracking receiver, which utilizes a single IF channel to conserve weight and power and is an integral part of the MAV transponder package. A summary of this new technology development requirement is given in Table V-5.

Table V-5 New Technology Development Requirements

System	System Component	Important Factors
Orbiter Rendezvous Sensor	Antenna Elements	Sum-Pattern Gain Boresight Null Sensitivity
	Monopulse Array	Sidelobe Reduction Pattern Stability
	Beam Form Network	Phase Stability Broadband Performance
MAV Transponder	Cassegrain Antenna Antenna Feed Dual-Ratio Transponder Angle-Track Receiver	Reflector Surfaces Subreflector Symmetry Feed Spillover Sidelobe Control Diplexer Losses Error Channel Patterns

## VI SPACECRAFT SYSTEM DESIGN

This chapter includes tradeoff discussions, requirement summaries, and system configuration and performance descriptions for the MAV, lander and orbiter elements of the MSSR mission. It also contains the overall spacecraft mass properties derivation and mass margin allocation considerations. Other topics include a discussion of ERV candidates, failure modes discussions and a summary of the impact of the 1983/84 mission opportunity on the 1981 system designs.

### A. MARS ASCENT VEHICLE TRADEOFF AND SYSTEM DESIGN SUMMARY

#### 1. Tradeoffs

The major system level tradeoffs conducted in this study included the following:

- Number of ascent stages,
- Solid vs liquid propulsion,
- Rendezvous altitude and MAV sizing,
- 3-axis stabilized vs spin stabilized third stage,
- Size of soil sample,
- Method of sample transfer.

These tradeoffs are reviewed briefly followed by a description of the system design that evolved on the basis of the tradeoffs.

The primary driver in the case of the ascent staging tradeoff is maximizing the weight that can be launched into the rendezvous orbit for a given launch weight. In this tradeoff, discussed in Chapter II, it was found that almost three times the non-propulsive payload could be obtained with a 3-stage system than could be achieved with a two-stage launch vehicle. Also, the small size of the propulsion system required plus the thin Mars atmosphere (which results in very little drag or aeroheating penalties due to the high velocities attained with solids) combined to produce a clear cut advantage for the use of solids in the first two stages. This is the case even though the performance of the solids is somewhat degraded by the requirement for sterilization. This tradeoff, for which propulsion system details may be found in Chapter VII, included the evaluation of a liquid system to perform the functions of the second and third stages. However,

a monopropellant hydrazine 3rd stage system that provided both orbit circularization and attitude control during lower stage burns was found to be superior. One disadvantage of this 3-stage vehicle is its relatively large axial dimension. This requires stowing it in the horizontal position on the lander and then erecting it prior to launch. The squatier, all-liquid system or 2-stage solid/liquid system, could be integrated into the lander in a fixed vertical position. However, the mass fractions achievable with the liquid system simply do not result in enough non-propulsive system weight to support the functions that the MAV has to perform in ascent rendezvous and docking.

In the rendezvous orbit altitude tradeoff (Chapter II) it was found that a somewhat larger MAV (325 kg) could be landed than the baseline 290 kg MAV. This would have allowed more weight to be allocated to the MAV third stage which would in turn permit more capability for growth and thus be desirable from a cost standpoint. However, selecting the maximum weight MAV would also result in larger MAV dimensions and this would aggravate the integration of the MAV with the existing size Viking '75 Lander. Also, the increase in usable MAV third stage weight would not be as great as might be expected, i.e., the rendezvous altitude would have to increase (due to the added MAV weight having to be taken out of the orbiter propellant budget) and this added altitude would require more propellant in the MAV. Consequently the 2200 km orbit altitude, corresponding to the minimum practical MAV size (290 kg) was adopted.

Selection of a 3-axis stabilized vehicle over a spin stabilized one was based primarily on the finding in Chapter IV that the 3-axis vehicle would not be much heavier than the spin stabilized vehicle. In this situation, the 3-axis system is preferred since either docking with a spinning vehicle or despinning it just prior to docking would result in more complex operations than those required with a three-axis stabilized system. The primary reasons for the 3-axis system being almost as light as the spin stabilized vehicle are the relatively frequent attitude maneuvers required of the MAV which impose a greater penalty on the "stiffer" spin stabilized vehicle, and the fact that gyro system technology has advanced to the point that the traditional weight disadvantage of 3-axis vehicles relative to spin stabilized vehicles has been greatly diminished.

The impact of the surface sample size and location on the system design is discussed more fully later in this section. The findings are that a sample much bigger than 1 kg rapidly diminishes the available system weight margin due to the 10 to 1 relation between MAV launch weight and third stage payload. (This corresponds to a 13 to 1 ratio between Mars lander entry weight and MAV third stage payload weight.) This sensitivity to third stage payload weight, along with recommendations from the science community that a 1 kg sample would be adequate, see Appendix A, resulted in the selection of 1 kg as the baseline sample size for this study. Increasing the sample to 5 kg was found to require a large enough increase in landed weight to dictate a narrower entry corridor which in turn would necessitate optical guidance.

Finally, the method of transferring the sample from the ascent vehicle to the Earth return vehicle was studied and is reported in Section C of this chapter. It was determined early in that study that a hard docking scheme, as opposed to a toss and catch technique, was required to achieve sufficient reliability, and that to minimize back contamination, jettisonable docking aids should be employed. Within these constraints there is a choice between simply extending the sample canister from the MAV and capturing it with the orbiter (or ERV), versus fully mating the MAV with the orbiter and then internally transferring the sample to the ERV. Since the latter concept requires accurate positioning of the two vehicles in roll attitude in addition to lateral direction and pitch and yaw attitudes plus requiring an additional set of latches, it is the heavier and more difficult concept to accomplish. Also it presents somewhat more uncertainty in jettisoning the docking cone since it requires incorporating fairly elaborate latches and disconnects. Consequently, the simpler version was selected as the baseline for this study.

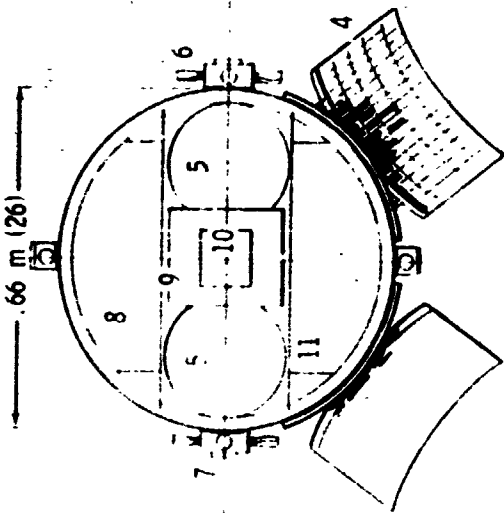
The results of the above tradeoffs along with the study guidelines and constraints identified in Chapter I comprise the system level requirements on the Mars ascent vehicle. The resulting system design is described next with detailed subsystem requirements and descriptions provided in Chapter VII (except for G&C and Rendezvous Radar Subsystems which are contained in Chapters IV and V).

## 2. MAV System Description

The selected configuration for the 2.1 meter high MAV is shown in the cutaway view of Figure VI-1. Spherical solid rocket motors, 56 and 48 cm in diameter respectively, make up the two booster stages that effect launch and injection into the initial 100 km x 2200 km elliptical orbit. Thrust levels for these stages are both 6672 Newtons. The tank and inter-stage skirt construction is of conventional design but the propellant formulation and grain support design will be a new development based on studies of sterilizable solids currently under way at JPL. Performance estimated for these motors are an Isp of 2795 N-sec/kg (285 sec) and a mass fraction ( $\lambda$ ) of 0.88. Thrust vector control during first and second stage burns is accomplished by the monopropellant hydrazine third stage thrusters.

The third stage is a very compact 3-axis stabilized spacecraft complete with all subsystems necessary for orbit circularization, attitude determination and control, Earth and orbiter communications, sample environmental control, and rendezvous and docking operations. This stage is 66 cm in diameter and 50 cm long. It has a non-propulsion system mass of 21 kg of which 2.0 kg comprize the sample and its container. The main features of this spacecraft include:

- 1) An 18.0 cm long by 13.7 cm diameter sample canister located flush with the nose cap of the vehicle and mounted on the antenna feed. The external surface of the canister cap may be coated with a thin layer of ablative material.
- 2) An extendible boom for transferring the sample canister to the ERV constructed similar to the Viking '75 soil sample boom.
- 3) A 40 degree half-angle conical nose fairing and radome constructed of RF transparent, reinforced plastic material.
- 4) A 50.8 cm diameter Cassegrain antenna with monopulse feed located in a fixed position on the vehicle centerline.
- 5) Two 0.815 sq meter solar panels utilizing violet cells that provide 10.5 watts of power in an attitude normal to the Sun line. Panels are hinged so that they may be deployed to an angle of 24 degrees to the body axis prior to orbital operations.



**Legend:**

- 1. Sample Canister
- 2. R/F Transparent Fairing
- 3. Antenna
- 4. Solar Panel
- 5. Stage III Propellant Tank (2)
- 6. ACS Motor Assembly (4)
- 7. Sun Sensor Assembly (4)
- 8. Flight Control Subsystems
- 9. Telecommunication System
- 10. Boom Drive Mechanism
- 11. Electrical

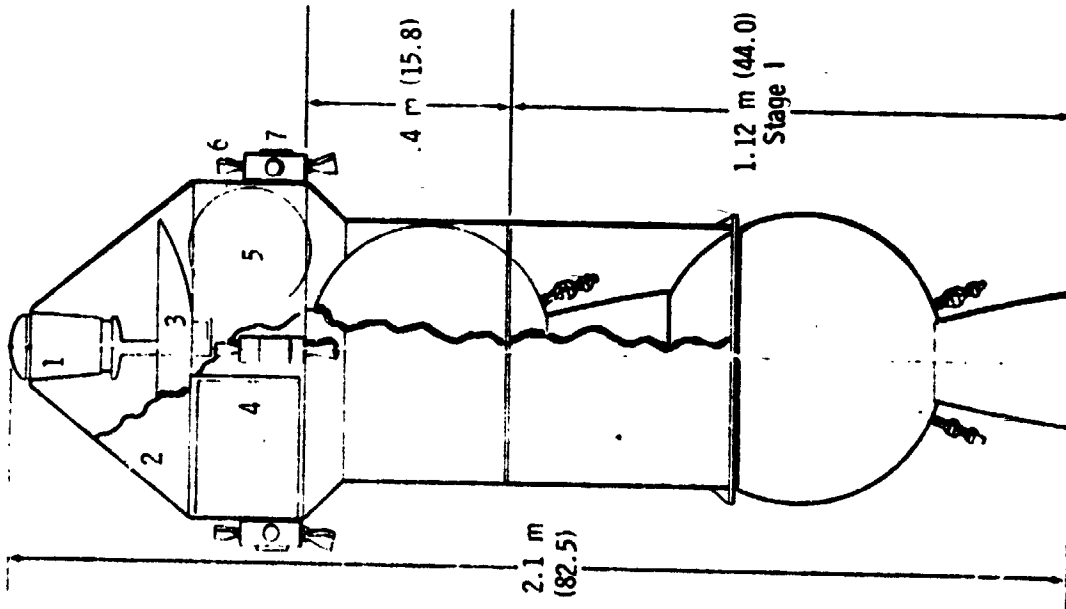


**Figure VI-1 Mars Ascent Vehicle**

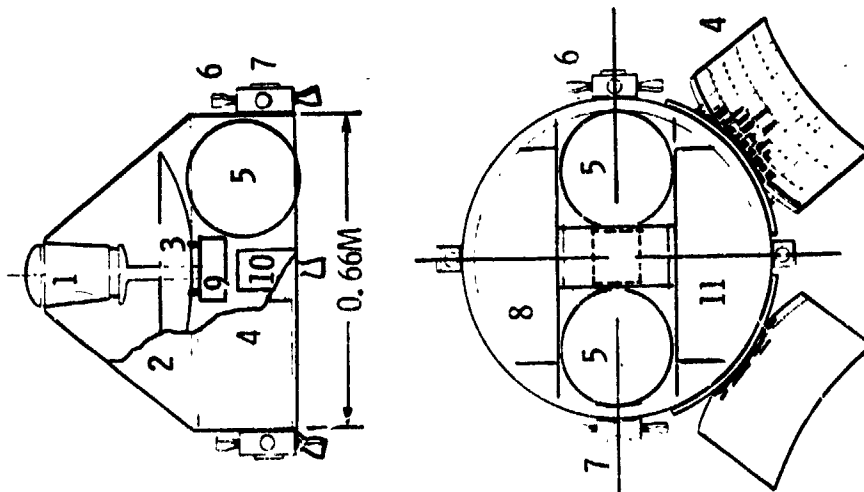
- 6) Sixteen nickel hydrogen battery cells providing 57 watt-hours of electrical power.
- 7) Two 23-cm diameter monopropellant hydrazine tanks.
- 8) Four RCS and orbit circularization thruster assemblies consisting of:
  - 4 aft facing 53 Newton thrusters;
  - 4 forward facing .4 Newton thrusters;
  - 4 tangential 1.8 Newton thrusters.
- 9) A flight control system that includes a sun sensor, 3 gyros and a small computer capable of controlling the open loop, constant pitchover rate turn in ascent, plus the Earth pointing maneuvers in orbit. The computer utilizes CMOS technology and is estimated to weigh approximately 1.59 kg. It will require 4 watts of power.
- 10) A telecommunications system containing, in addition to the Cassegrain antenna, an S-band angle tracking, dual ratio transponder; provisions for receiving Earth and orbiter-based command; and provisions for telemetering data to Earth or the orbiter. Maximum output of the transmitter is 4 watts.
- 11) Thermal control insulation, heaters and optical coatings for maintaining equipment and sample temperature limits during orbital operations.

The mass and inertia properties for the MAV are given in Table VI-1. Detailed mass properties for the total MAV can be found in Appendix F and further descriptions of subsystems in Chapters IV, V and VII.

Because of the relatively small size of the third stage, a close look was taken at the packaging of the propulsion system, communications and power systems, and the flight controls system. Figure VI-2 shows the volumes available compared to those estimated to comprise the various components and elements. In the packaging concept envisioned, the electrical, electronics, and G&C components are integrated into a single package arranged to fit around the propulsion tankage and sample canister extension mechanism. Component locations within the 3 volumes shown in this package are selected to minimize interconnections, and achieve a third stage center of gravity within 0.5 cm of the vehicle centerline. A reduction in component case mass over conventional packaging is achieved by essentially using the structure as the case.

Table VI-1 1981 MAV Mass Properties

<u>Element</u>		<u>Mass, kg</u>			
<b>Stage III</b>					
Structure and Mechanism		8.85			
Radio Frequency		1.63			
Telemetry Unit		In RF			
Guidance and Control		3.09			
Power		3.90			
Cabling		.77			
Propulsion Inerts		11.29			
Contingency, 10%		<u>2.90</u>			
Step 3 Burnout		32.43			
Propellant		<u>8.30</u>			
Delta V	6.49				
RCS	1.81				
Total Step 3		40.73			
Sample		<u>1.00</u>			
Stage III at Liftoff		41.73			
<b>Stage II</b>					
Skirt		3.95			
Propulsion Inert		11.11			
Propellant		81.55			
Total Step 2		<u>96.61</u>			
Stage II at Liftoff		138.34			
<b>Stage I</b>					
Skirt		5.67			
Propulsion Inert		17.51			
Propellant		128.41			
Total Step 1		<u>151.59</u>			
Stage I at Liftoff		289.93			
<b>MAV Center of Gravity and Inertia</b>					
		<u>Center of Gravity</u>		<u>Moment of Inertia, kg/m<sup>2</sup></u>	
	<u>Mass</u>	<u>Longitudinal cm</u> From Nose	<u>Lateral cm</u> From Centerline	<u>Roll</u>	<u>Pitch/Yaw</u>
Stage III	41.7	53.1	0.25	2.44	1.5
Stage II	138.3	80.8	0.25	5.63	9.1
Stage I	290.0	123.0	0	11.58	62.2



Item	Mass Kg	Vol cm <sup>3</sup>	Vol Avail cm <sup>3</sup>
1 Sample & Container	1.90	2200	2200
2 Radome	0.36	--	--
3 Antenna Dish	0.54	--	--
4 Solar Array	1.09	--	--
5 Propellant Tanks	2.0	(2600 Ea)	14700
6 Thrusters & Support	5.44	--	--
7 Sun Sensors	0.18	--	--
8 G&C Comp	(3.77)	(8575)	(19602)
Rate Gyro	1.36*	1575	
Electronics	1.59*	4500	
Inverter Converter	0.82*	2500	
9 RF&TM Package	2.08	2000	3200
10 Boom Drive Mech	1.00	1300	1400
11 Elect Comp	(2.67)	(5620)	(19602)
Battery	1.22*	1620	
Charger Control	1.45*	4000	

\*Uncased.

Figure VI-2 MAV Stage III Equipment Accommodations

RF and telemetry subsystems are located directly behind the parabolic antenna reflector. A hole through the center of the package allows the shaft of the canister extension mechanism to extend up to the canister. Integral to this package is the RF antenna feed which extends through the center of the antenna reflector. All KF and TM system components are mounted to four PC boards (see Chapter IV for details). The total package will be foamed for structural rigidity and tied to the third stage outer shell structure by side rails which also provide a heat sink for the power amplifier and crystal oscillator. With this arrangement and the use of a Cassegrain feed, no coax or waveguides are required.

Primary electrical components are located in the volume next to the solar arrays thus reducing the cabling length required. The  $\text{NiH}_2$  battery which consists of 16 cylindrical containers, the battery charger, power regulator, and power controller are located in this area. Hard wiring will be used throughout the third stage to avoid the weight and space penalty of connectors.

The volume on the opposite side from the electrical area contains all of the guidance and control components and the inverter/converter. The G&C electronic components are sized based on use of CMOS technology. Achieving the required size and weight can be done with today's off-the-shelf computers, but achieving the low power levels requires use of CMOS technology. Although this is essentially a state of the art technology, space-qualified units are not yet "off-the-shelf" items.

### 3. Impact of Canister Size and Location on System Design

The selected canister configuration is shown in Figure VI-3. The design is a can within a can with the inner one mounted on guides. The inner can is driven out to receive the sample then in again by means of an internally mounted, screw drive actuator. The canister is loaded while in the horizontal position and this concept minimizes the possibility of sample particles impairing the sealing process. A gold deforming seal was selected for this application. To avoid cycling the seal, the cover would never be completely seated until after sample loading has been completed. An additional seal will be installed inside the outer can to cover the opening used to fill the inner can. This seal is not nearly so critical as the

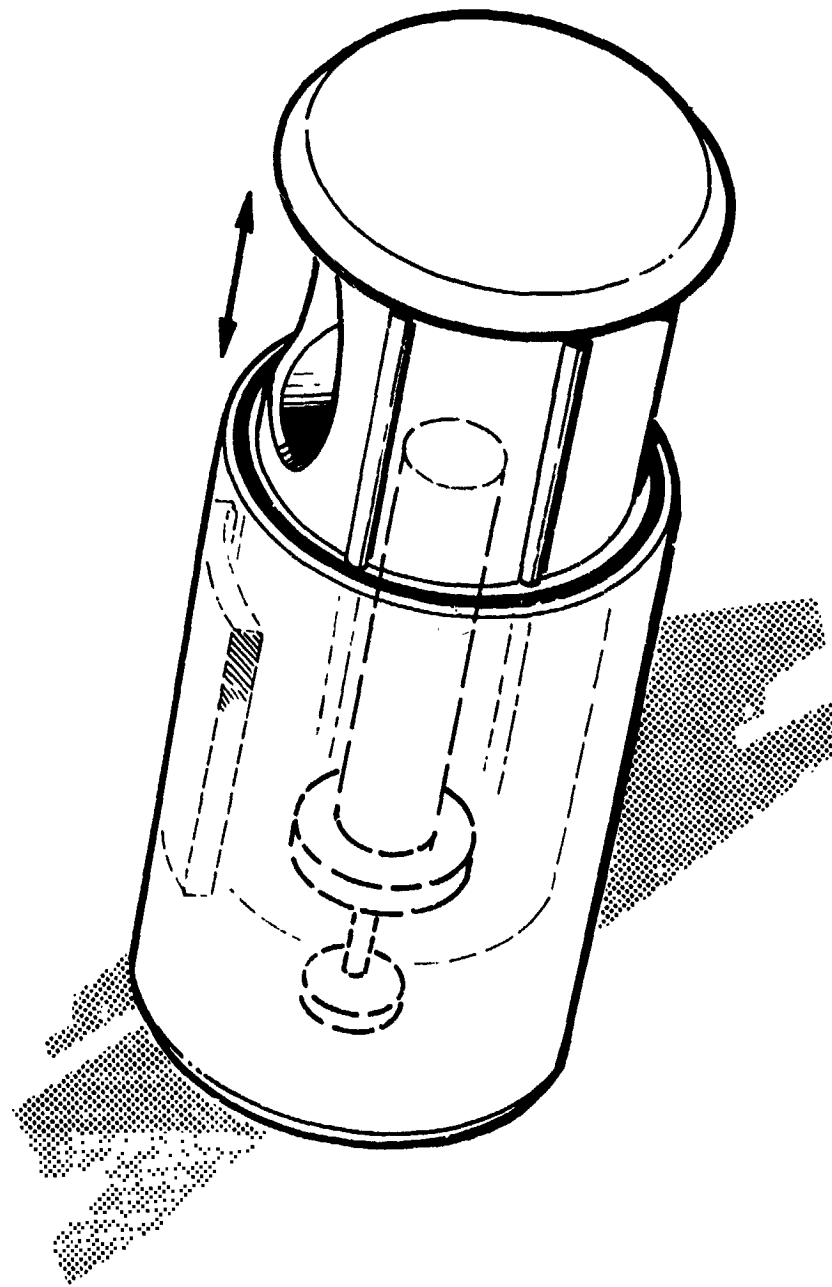


Figure VI-3 Sample Canister Concept

cover seal in that its purpose is simply to confine the sample and it is not involved in back contamination considerations.

The baseline sample canister was sized for a 1 kg sample. This sample was assumed to have a density of  $1.3 \text{ g/cm}^3$ , and a packing efficiency of 75% of the total volume was assumed to account for the "pouring" method of introducing the sample into the container.

The sample canister is located on the forward centerline to maintain the symmetry of the MAV third stage; for ease of sample loading; and to simplify the docking and sample transfer operation.

To examine the impact of increased sample size, a 5.0 kg sample was selected. The significant changes to the MAV third stage to accommodate this sample included increasing the canister diameter and length from 12.7 cm diameter x 18 cm long, to 20.3 cm diameter x 28 cm long, see Figure VI-4. While the necessary volume increase could have been achieved by other combinations of length and diameter increase, any greater increase in the length dimension would cause interference with the lander afterbody when the MAV is stored on the lander. Also, going to any larger diameter worsens the antenna blocking situation.

For the 20.3 cm diameter canister it is necessary to enlarge the antenna dish from 51 cm to 61 cm to compensate for the increased blockage. This in turn increases the fairing size and the length of the cylindrical structural skirt as shown in Figure VI-4.

Increases in Stage III mass required Stage III propellant and propellant tankage weight increases which are compared in Table VI-2.

As also shown in Table VI-2, the increased sample mass and Stage III changes influence the entire MAV system. Total mass for a MAV and launcher designed for a 5 kg sample exceeds the landing capability of the baseline landing system. However, there are several further lander modifications which could increase the landed weight capability to accommodate the larger sample. These include reducing the entry corridor ( $\Delta\gamma_E$ ) to  $2^\circ$  instead of  $4^\circ$ ; increasing parachute and/or aeroshell size; or increasing terminal engine thrust. Reducing the entry corridor requires the addition of an optical guidance system but this is feasible. The main disadvantages of

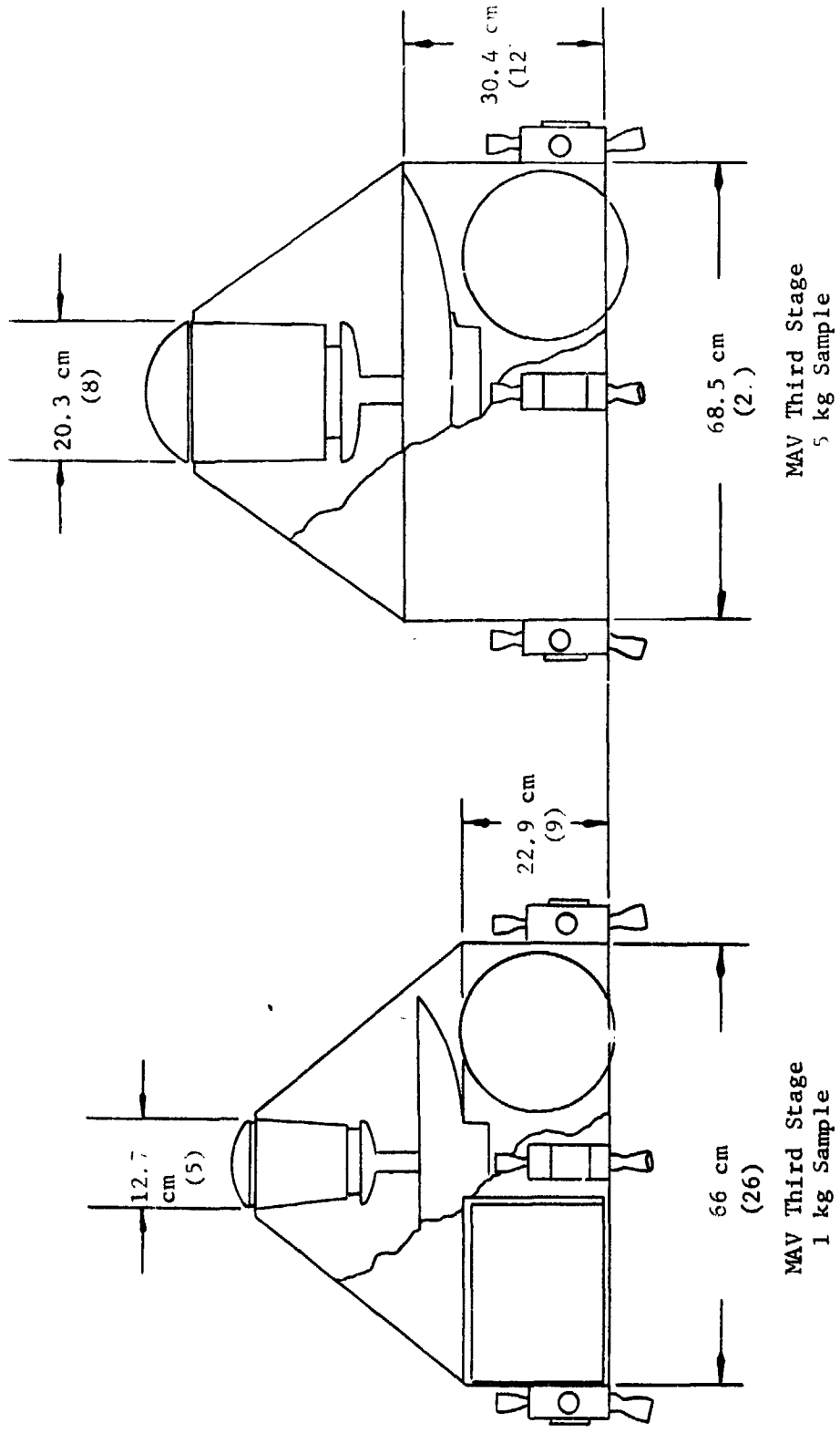


Figure VI-4 Impact of Increasing Sample Size from 1.0 kg to 5.0 kg

the increased sample size are that the dimensional growth of the MAV causes more distortion of the Viking '75 lander capsule shape than is desirable, and the system weight margin is decreased significantly.

Table VI-2 1 kg vs 5 kg MAV Mass Comparisons

	<u>1 kg Sample</u>	<u>5 kg Sample</u>
Sample	1.0	5.0
Stage III Non-propulsive	20.0	21.6
Stage III Propulsion	20.7	22.4
Stage II including Skirt	96.6	112.9
Stage I including Skirt	<u>151.6</u>	<u>117.2</u>
Total MAV	289.9	339.1
Launcher	<u>41.0</u>	<u>45.1</u>
Total MAV System	330.9	384.2

#### 4. Effect of Sterilization on MAV Components

Because the MAV vehicle contains many subassemblies and components which have not been qualified for the Viking sterilization requirements, a study was conducted to determine whether these systems could meet sterilization requirements and whether any increases in mass would result from making them compatible with such requirements. Because some of the subsystems involved are new designs, the approach used to evaluate their sensitivity to sterilization cycling was to examine the effect of sterilization on typical components and piece parts which have already been evaluated for the Viking program.

The results of this investigation relative to guidance and control and electronics components indicates that for selected MAV components weight increases due to sterilization will be negligible. Viking engineers responsible for testing, packaging, parts selection, and reliability all agreed that if Viking experience is followed in the design there will be no difficulty from sterilization. The following paragraphs summarize Viking sterilization findings and possible MAV impact.

Battery. The battery specialist indicated that for the selected Ni-Cad battery weight increase due to sterilization was negligible while for

the silver zinc batteries considered for Viking at one time some weight increase would be expected. The proposed URDMO battery is Ni-H<sub>2</sub> and a manufacturer of this type battery has indicated that if Ni-Cad can be sterilized then Ni-H<sub>2</sub> should be no problem.

Piece Parts. In general, any part which is based upon silicone technology such as transistors, diodes, ICs, etc., sees a temperature during manufacture higher than the sterilization temperature and therefore will be no problem. This applies to most of the electronics components selected for MAV including the computer memory. Conventional parts such as resistors, capacitors, etc., can be procured in sterilizable configurations. The series of components which gave the most trouble on Viking were wet slug tantalum capacitors which at first would not pass sterilization. This item which weighs between .003 and .018 pounds was redesigned to pass sterilization for approximately a 5% weight increase and is now a Viking standard.

PC Boards and Flat Flex Cable. It was found that if these components were top quality they passed sterilization tests. If, however, quality was marginal, failures frequently occurred after sterilization cycle.

Housing Material. The original magnesium alloy housings had a creep problem associated with sterilization. Parts were changed to magthorium or beryllium and slightly heavier flanges, resulting in small weight increases. MAV weight requirements depend upon lightweight electronic packaging which cannot be achieved using conventional Viking casing design, rather the structure will form the casing. Consequently, sterilization requirements will become another structural design requirement, and while it may limit the choice of materials and processes it should not add to system weight.

Parts Mountings. Because of sterilization it was found that mechanical fasteners required careful selection, special washers and torquing instructions. However, weight effect was negligible.

Gyros and Accelerometer. Viking Lander utilizes a similar gyro which has more stringent requirements than MAV. This gyro has successfully passed sterilization qualification testing. The only special consideration given to sterilization was to size the fluid bellows which is approximately  $\frac{1}{2}$  in. diameter x  $\frac{1}{4}$  in. long, large enough for the fluid volume over the full temperature range, a negligible weight item.

Solar Panels. A separate investigation was conducted on the sterilization effects on solar panels and is reported in Chapter VII-B. The conclusion of the investigation was that solar panels with proper mechanical design can be sterilized.

The conclusion of this investigation is that sterilization will not affect the MAV component weights. However, meeting sterilization requirements, in particular the testing required to qualify components will be a relatively costly proposition.

## B. LANDER SYSTEM DESIGN

### 1. Requirements Imposed on the Lander by the MSSR Mission

The lander requirements stem from the guideline to use as much of the existing Viking '75 lander system design as possible as well as from the results of the MAV systems trade-offs discussed earlier. These include requirements to:

- o Maintain the Viking lander capsule basic shape and size.
- o Retain existing aerodecelerator (parachute) and terminal descent engines.
- o Delete engineering and science components not required to support the MSSR mission and relocate other systems as necessary to prevent interference with the MAV.
- o Provide thermal control of MAV during cruise, entry and descent and during pre-launch operations on the surface.
- o Support the MAV structurally during Earth launch and Mars landing.
- o Remain stable during entry, descent, landing and MAV erection.
- o Provide power for pre-launch MAV operations.
- o Provide telemetry and command loop for pre-launch data transmission and for Earth based launch commands.
- o Provide an erection mechanism capable of controlling MAV azimuth and elevation to within .25 and .5 degrees respectively.

### 2. Lander Modifications

Figure VI-5 shows the major modifications to the Viking Lander Capsule. These include:

- o Beefing up the aeroshell and increasing heat shield thickness in order to survive direct entry.
- o Enlarging the after body bioshield cap, and aeroshell base cover.
- o Modifying the parachute support truss.

Also, a number of modifications are required on the Lander itself to accommodate the MAV and its erection mechanism and to permit proper alignment of the MAV for lift off. The basic geometry of the lander along with the landing leg assemblies remain unchanged. However, several of the

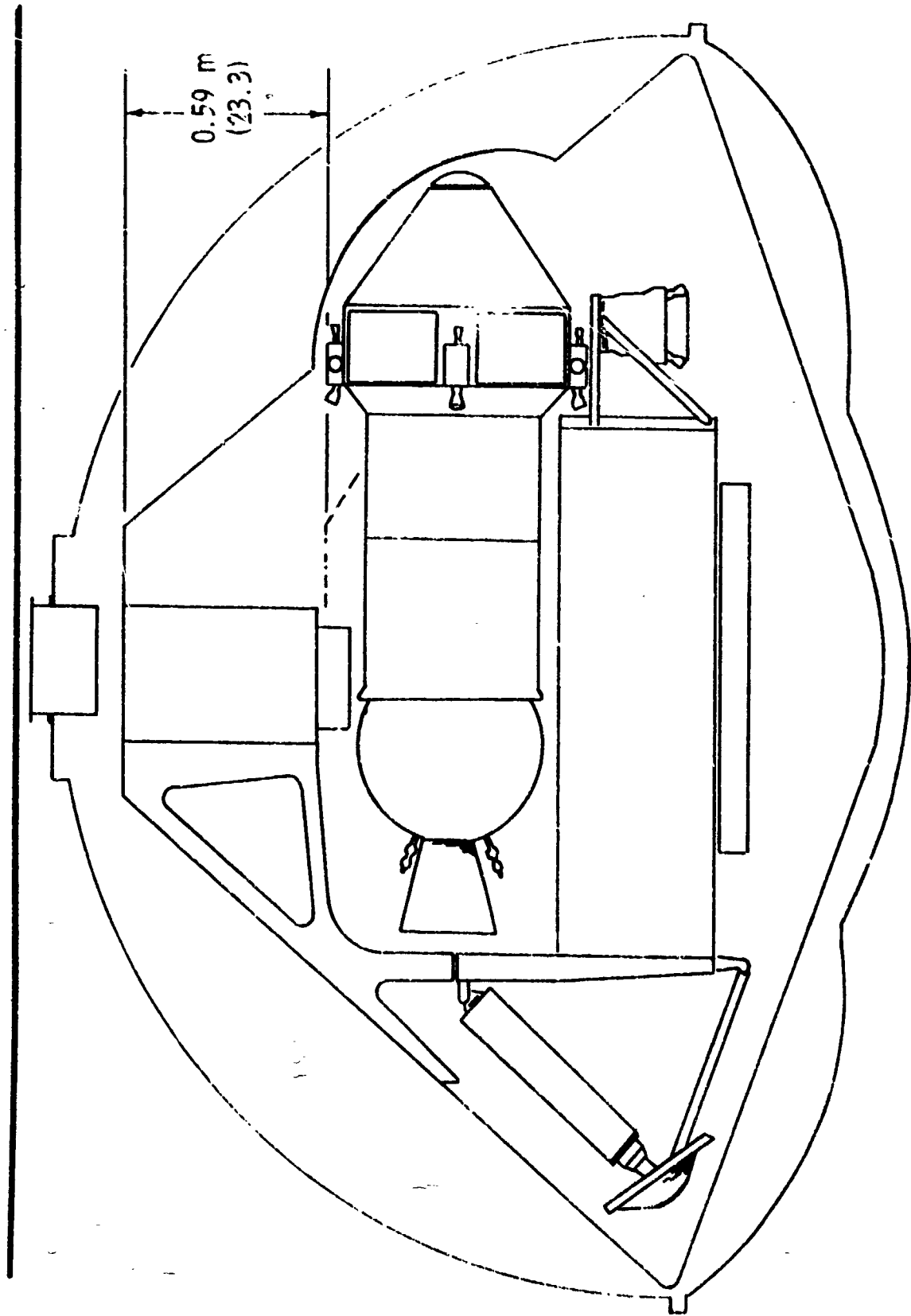


Figure VI-5 MAV Impact on Viking Lander Capsule

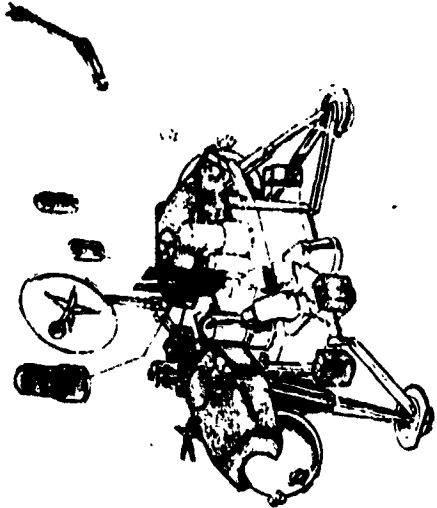
Viking components are not required for the sample return mission and will be deleted. These deletions are shown in Figure VII-6 and are:

- o UHF antenna with electronics
- o Seismometer
- o GCMS with processor
- o Biology with processor
- o X-ray fluorescence experiment
- o Meteorology
- o One camera

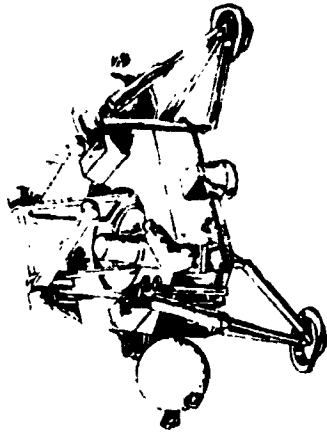
Other modifications include: replacing the 35 watt RTG's with smaller 20 watt units; deleting the thermal switches and adding heat pipes as defined in Chapter VII; relocating the surface sampler to facilitate interfacing the sample collector with the sample canister; modifying the S-band antenna mast so as not to interfere with the MAV erection and alignment; and incorporating a blow down terminal descent propulsion system to accommodate additional landed weight. In the proposed pressure regulated system one terminal decent tank would be replaced with a pressure sphere and the full propellant load would be carried in the other Viking tank. This solution is practical because the resulting center of gravity shifts during terminal descent can be tolerated by the RCS system.

To this stripped down and modified lander is added the MAV with its support and erection mechanism or launcher. The launcher is attached to and supported by the lander equipment mounting plate. The launcher incorporates a turn table or turret capable of rotating the MAV 360° in azimuth. Torque motors located at the top of each of the two support posts raise the elevation arms and produce the 75° elevation capability. Prior to erection the MAV is cradled at fore and aft support points on the lander body so located that Earth launch and Mars landing loads are transmitted directly into the lander side panels. These loads do not go through the launcher. Upon landing, the MAV is released from the cradle freeing it for the launch alignment process. The thermal short created by the launcher structure is a major contributor to the environmental control problem of survival on Mars surface. The proposed solution is

Viking '75 Lander



Modified Lander



Lander With MAHV



▨ Indicates Components Not Required for Sample Return Mission

Figure VI-6 Lander Modifications

to add a canopy to the lander that would enclose not only the MAV but the launcher mechanism as well and be heated by heat pipes whose heat source is waste heat from the RTG's. The construction of the canopy would be similar to the Viking RTG wind screens.

The thermal/mechanical interface of the lander/launcher/MAV is the most difficult design problem determined in this study. It stems primarily from the requirement for maintaining the MAV solid propellants above  $4^{\circ}\text{C}$  at lift off while the average daily temperature could be as low as  $-45^{\circ}\text{C}$ . This situation would be considerably alleviated if solid rocket propellants could be developed whose performance at lower temperatures was more repeatable. (Conventional motors have been fired successfully at very low temperatures but performance is variable.) However, the canopy approach appears to be a feasible solution and should be achievable within the 41 kg weight budget allocated as shown in Table VI-3.

Table VI-4 gives the mass properties breakdown for the modified lander. It is presented in two parts showing first the changes to the lander bus, and in the second a derivation of the total lander system. Data are presented in a sequential mass statement format showing those items taken directly from the Viking Lander System and noting changes required to achieve the URDMO system. Major changes are those associated with direct entry and providing space to carry the MAV.

More details on lander modifications are presented in Chapter VII subsystems discussions.

### 3. URDMO Landed Weight Capability

Greater landed weight is achieved in the URDMO mission than in the Viking '75 mission, 776 kg vs 590 kg, in spite of the higher entry velocity of the direct entry mode. The higher velocity and heavier vehicle require over 75 kg to be added to beef up the aeroshell and heatshield. However, the landed weight capability is still increased due primarily to three factors as shown in Figure VI-17. Changing the blowdown terminal descent propulsion system to a pressure regulated system provides the biggest portion of the increased performance. The higher average thrust

Table VI-3 Launcher and Thermal Canopy Mass

	<u>Kilograms</u>
Mechanism	10.43
Actuators	6.85
Support and Latches	6.35
Cabling	1.82
Canopy (4.46 m <sup>2</sup> )	11.79
Contingency	<u>3.72</u>
	41.05

Table VI-4 Lander Mass Derivation

<u>Part 1 Lander Derivation</u>	
	<u>Kilograms</u>
Viking Lander - Landed (2/19/74)	594.2
Remove UHF	- 5.85
Reduce RTG Size	-22.54
Remove One Battery (1/2 Package)	-11.47
Remove Data Storage	-13.83
Modify Thermal System	- 5.35
Remove Science (except one camera & soil sampler)	-60.55
Add Regulated Pressure System	+ 1.45
Modify Telemetry	- 6.58
Modify S-Band to MAV Components	-15.15
Remove Cabling	- 9.98
Beef-up Landing Struts	+ 2.07
Add MAV	+288.93
Add MAV Launcher (incl. Thermal Protection)	<u>+ 41.05</u>
URDMO Landed	776.40
<u>Part 2 Lander System Derivation</u>	
	<u>Kilograms</u>
Landed Mass	776.4
Landing Propellant	<u>70.8</u>
Terminal Ignition	847.2
Aero Decelerator Structure/Viking'75	65.8
Raise Parachute 55 cm	<u>8.7</u>
On Chute Aeroshell Separated	921.7
Aeroshell and Heat Shield/Viking'75	119.6
Deorbit System and Miscellaneous/Viking'75	66.8
Aeroshell Structure (Direct Entry)	50.0
Heat Shield (Direct Entry)	13.6
Remove Science	- 7.8
Less Heat Shield Ablated	<u>- 5.4</u>
On Chute Aeroshell Attached	1158.5
Parachute/Viking'75	41.2
Add Heat Shield Ablated	<u>5.4</u>
Entry	1205.1
Deorbit Propellant/Viking'75	72.0
Miscellaneous/Viking'75	<u>7.9</u>
Separated Lander System	1285.0

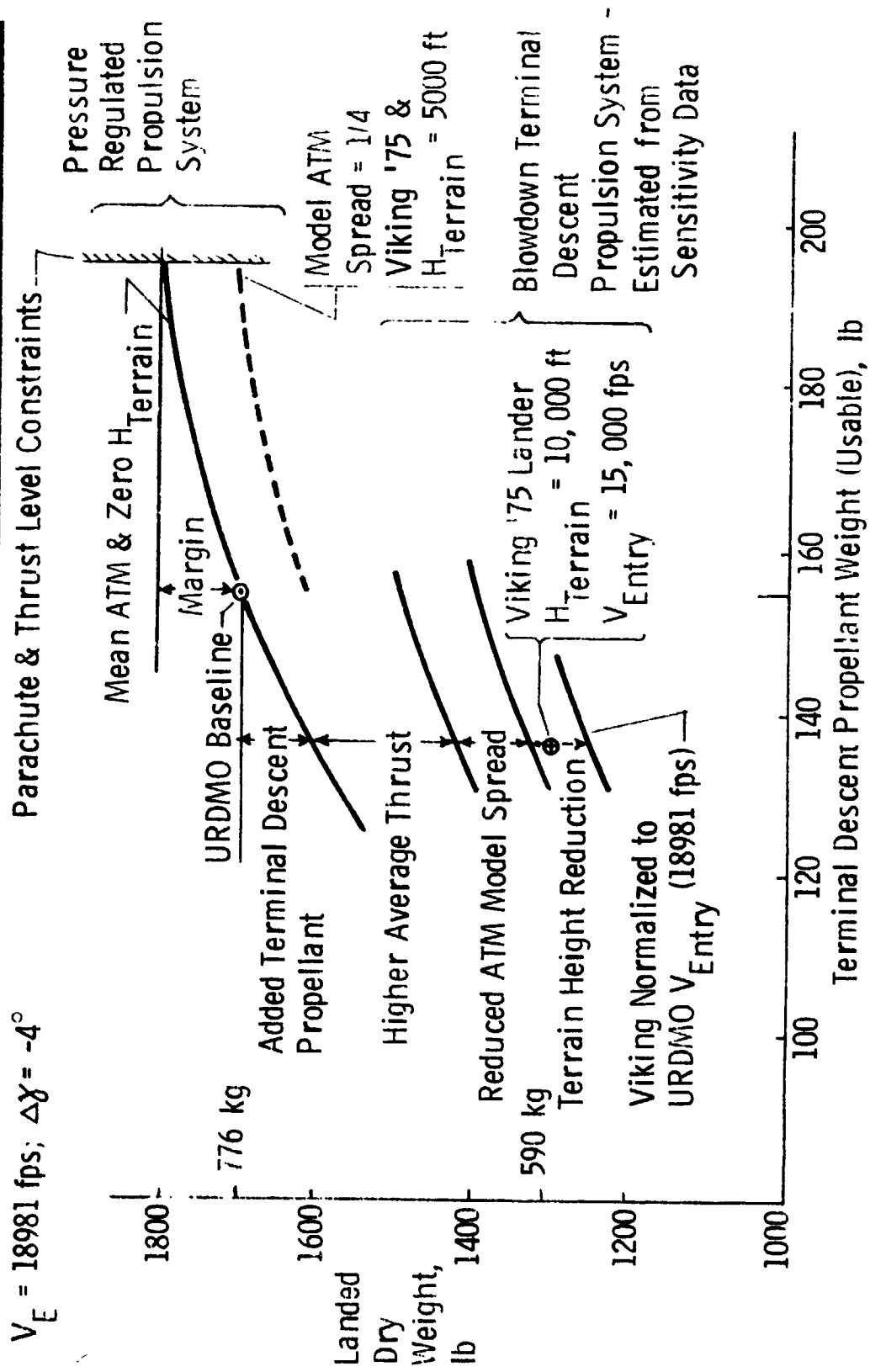


Figure VI-7 URDMO/Viking Landed Weight Relations

level it affords means a shorter burn time and thus more time for the parachute to reduce the descent rate. Also, more propellant can be carried without an increase in tank weight.

The other factors are the designation of a zero terrain height requirement and use of the mean atmosphere model instead of the large spread in atmosphere models used in Viking. These revised constraints used in the URDMO baseline are believed to be reasonable in view of the improvement in the knowledge of the atmosphere model and the planet radius (mean surface level) anticipated following the Viking mission. However, it is possible to select values for these constraints intermediate between Viking '75 and the URDMO baseline and still attain the required landed weight by further increasing the propellant loading, see the dashed curve in Figure VI-7.

#### 4. Lander Stability Study

Due to the 30% greater mass and the 6 inch higher CG of the URDMO lander, a landing impact study was conducted using the Viking '75 Dynamic Landing Analysis Computer program. Both "flat" landings and "steep slope" landings were evaluated. No attempt was made, however, to duplicate the hundreds of runs made in establishing the statistical performance of the Viking '75 landing gear system. Twelve cases were selected including those that were intuitively on the severe side. The touch down parameters shown below were drawn from Viking '75 specifications.

- o Vertical Velocity ( $V_V$ ) =  $8 \pm 3$  fps (e.g.,  $3\sigma = 11$  fps)
  - o Horizontal Velocity ( $V_H$ ) =  $0 \pm 4$  fps
  - o Roll Angle ( $\theta_R$ ) =  $0^\circ$  to  $360^\circ$  (Random distribution)
  - o Ground slope angle ( $\alpha$ ) = Per Mars Engineering model
  - o Direction of Slope Fall Line ( $\beta$ ) =  $0^\circ$  to  $360^\circ$  (Random distribution)
  - o Pitch and Yaw Angle ( $\theta_p$ ) =  $0^\circ$  to  $\pm 5^\circ$
  - o Attitude Rates, Engine Thrust
  - o Tail off Variation in Strut Loads
- } Not considered in this study

Results of the analyses are presented in Tables VI-5 through VI-7.

Conclusions from these analyses are summarized below:

Table VI-5 Results of Flat Landings Study

Conditions: Level Lander Attitude, Level Ground ( $\alpha = 0$ ),  $V_H = 0$ , Coefficient of Friction  $\mu = 0.20$  All Legs.  $V_V$  As Shown.

	$V_V = 11$ fps		$V_V = 8$ fps		$V_V = 5$ fps	
	URDMO	V'75	URDMO	V'75	URDMO	V'75
Max. Main Strut Stroke (in.)	7.51	6.68	4.74	4.22	2.73	2.45
Min. TDLR* Clearance** (cm)	17.6	21.8	26.5	29.1	33.5	35.2
Max. C.G. Accel. (Gs)	3.21	4.15	3.19	3.78	2.24	2.66

\* Terminal Descent Landing Radar.

\*\* Note - for comparison, V'75 statistical requirement is  $> 22$  cm. (Mean -  $3\sigma$ )

Table VI-6 Results of Nominal Descent Rate Landings on 20° Slopes (1)

Conditions:  $V_V = 8$  fps;  $V_h = 0$  fps;  $\alpha = 20^\circ$   
Coefficient of Friction = 1.0

Initial Lander Attitude - Level	URDMO	Viking '75
Leg 1 Uphill Stable?/Max Pitch Max. Limiter Deformation (2)	Yes/2.2° 2.5 in.	Yes/3.0° 2.2 in.
Leg 2 Uphill Stable?/Max. Pitch Max. Limiter Deformation (2)	Yes/3.3° 3.6 in.	-----
Leg 3 Uphill Stable?/Max. Pitch Max. Limiter Deformation (2)	Yes/3.3°	-----
Initial Lander Attitude - Uphill Leg Pitched Downhill 5°	URDMO	Viking '75
Leg 1 Stable?/Max. Pitch Max. Limiter Deformation (2)	Yes/3.3° 2.8 in.	Yes/3.9° 2.3 in.

(1) 20° slope is exceeded only 2% of the time in the Rough Martian Surface Distribution Model.

(2) Limiter Deflections greater than 3.3" require local redesign.

Table VI-7 Results of Max, Horizontal Velocity Landings on Steep Slopes

DOWNHILL LANDINGS:  $V_H = 4$  fps DOWNHILL

Conditions: Leg 1 Uphill, Coefficient of Friction = 1.0, $V_y = 8$ fps, Slope Angle $\alpha = -20^\circ$		
Initial Lander Attitude-Level	URDMO	Viking '75
Stable?/Max. Pitch Max. Limiter Deformation	Yes/2.6° 2.7 in.	Yes/1.7° 3.3 in.
Initial Lander Attitude-Up- hill Leg Pitched Down 5°	URDMO	Viking '75
Stable?/Max. Pitch Max. Limiter Deformation	Yes/2.7° 3.7 in.	Yes/1.5° 2.7 in.

UPHILL LANDINGS:  $V_H = 4$  fps UPHILL

Conditions: Leg 1 Uphill, Coefficient of Friction = 1.0, $V_y = 8$ fps		
Initial Lander Attitude-Level	URDMO	Viking '75
$\alpha = 20^\circ$		
Stable?/Max. Pitch Max. Limiter Deformation	Yes/4.9° 3.8 in.	Yes/2.0° 2.6 in.
Initial Attitude - Uphill Leg Down 5°	URDMO	Viking '75
$\alpha = 20^\circ$		
Stable?/Max. Pitch	No	Marginal/ 10.1°
Max. Limiter Deformation	4.6 in.	3.1 in.
$\alpha = 15^\circ$		
Stable?/ Pitch = -5° Max. Limiter Deflection	Yes/4.9° 4.1 in.	Yes/4.5° 2.8 in.

- o The greater mass of the URDMO lander does not cause crushable material in the legs to bottom out. A  $3\sigma$  (11 fps) flat landing does result in 4 inches less ground clearance and local beef-up of gear and attachment fittings will probably be required to maintain clearances.
- o Stability of URDMO vehicle in up slope and down slope landings does not appear to differ significantly from the Viking '75 lander.
- o Adaptation of Viking '75 system is feasible within weight constraints identified for URDMO.

### 5. Sample Acquisition

Comprehensive tradeoffs were not conducted since a single "grab" sample was considered adequate to meet mission requirements. This could be accomplished with the Viking '75 surface sampler thereby taking advantage of the resulting cost savings.

The baseline acquisition scheme involves scooping up some soil with the surface sampler and pouring it directly into the opening in the top side of the sample canister. The process is repeated as necessary to fill the canister. The physical relationship of the sampler to the MAV is shown in Figure VI-8. The entire loading process would be completed while the MAV is in the horizontal position on the lander to insure proper alignment between the canister and sampling unit.

A camera is included on the lander to provide the flexibility of being able to sample the most interesting portion of the sampling field. It would be desirable to use the existing Viking camera and this configuration is shown in Figure VI-8. However, due to limitations in the field of view seen by this camera (due to partial obstruction by the MAV and the surface sampler itself), a new camera design and/or relocation would better suit the requirements of this mission.

Sample acquisition methods other than the "grab" concept that could have application in this mission includes drills for subsurface core samples; chipper, brush, and abrader adapters for the Viking sampler; and concepts for segregating grab samples by encapsulation.

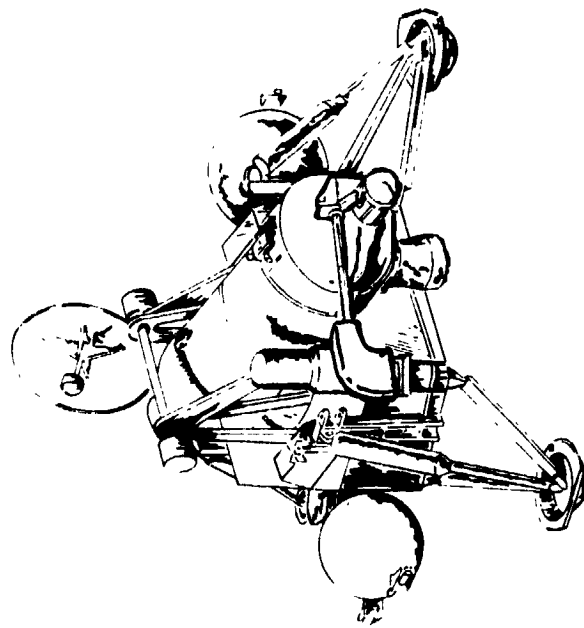


Figure VI-8 Sample Acquisition Operation

## C. ORBITER SYSTEM DESIGN

### 1. Requirements Imposed on the Orbiter by the MSSR Mission

The following requirements stem from adapting the existing Viking '75 Orbiter Design to carry the heavier URDMO Lander capsule along with an Earth Return Vehicle, and to achieve rendezvous, docking and sample transfer with the Mars Ascent Vehicle. These requirements include:

- o Physically mounting a 263 kg, spin stabilized Earth Return Vehicle and a 1285 kg Lander Capsule on the Orbiter such that after Lander Capsule separation, the ERV will be in a position that facilitates docking and sample transfer.
- o Providing additional Mars orbit insertion propellant to accomplish the  $\Delta V$  required by the 2200 km rendezvous orbit.
- o Providing an auxiliary propulsion system with forward facing rendezvous control thrusters.
- o Providing an attitude control system capable of orbiter translation in the docking phase and capable of handling the increased mass and inertia of the total spacecraft during trans-Mars cruise.
- o Providing a jettisonable cone for docking assistance and back contamination control.
- o Providing capability for commanding the MAV from the orbiter as a backup mode.
- o Providing an S-B CW range rate, and angle tracking system for tracking the MAV during terminal rendezvous and docking.
- o Providing the computer for implementing the rendezvous initial closing  $\Delta V$  and control law burns.
- o Removal of all science experiments and associated data handling, storage and transmission systems.
- o Providing for an additional 400 days of life while mated with the ERV in Mars orbit.

### 2. Orbiter Modifications

The physical arrangement of the orbiter with the other elements of the complete MSSR spacecraft is shown in Figure VI-9. The ERV, containing

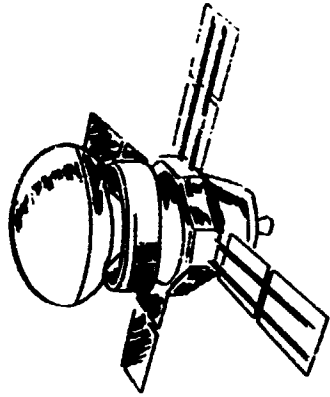
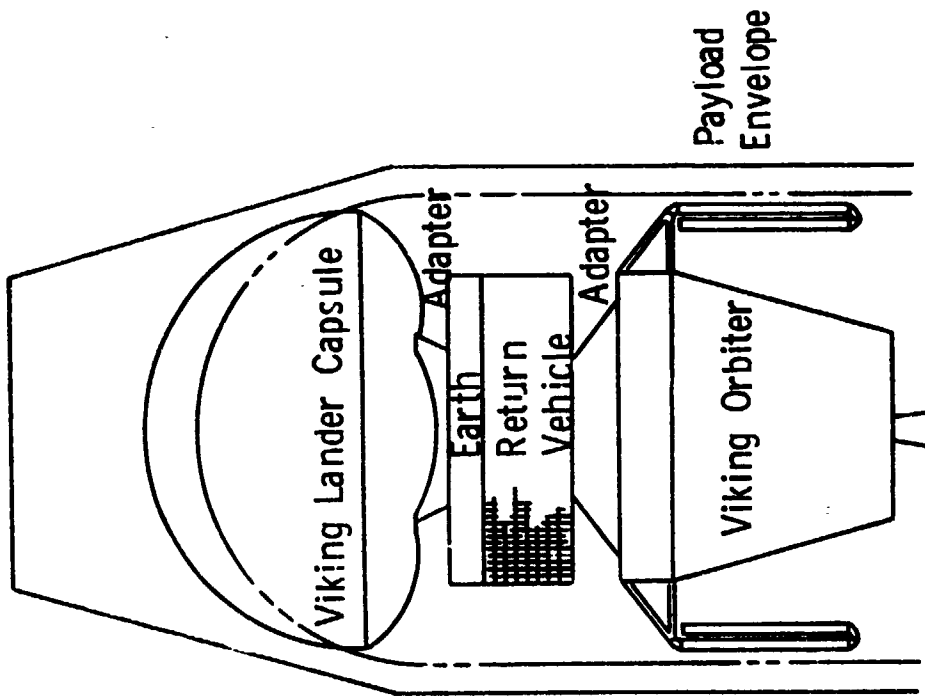


Figure VI-9 MSSR Elements in Earth Launch Arrangement

the Earth Entry Capsule, mounts to the orbiter and in turn supports the MSSR lander capsule. Attachment to, and separation from the ERV and orbiter is similar to the attachment and separation of the Viking '75 capsule and orbiter. However, a new conical adaptor is required to span the difference in diameter between the orbiter hard points and those of the Pioneer Venus derived ERV.

The most significant modifications to the orbiter are:

- o The removal of 87 kg of orbital science along with the 33 kg scan platform and 31 kg of associated data storage equipment,
- o Lengthening the barrel section of the main propellant tanks by 12 cm to accommodate the 15 percent increase in propellant required,
- o Replacement of the cold gas RCS system with a monopropellant hydrazine auxiliary propulsion system that provides both the RCS functions for the longer mission and the intermediate thrust levels, 140 N, required in the rendezvous and docking phase. (This system is similar to that planned for the MJS '77 spacecraft and could share components with that system),
- o Adding a 60 cm long, 90° included-angle docking cone containing an 18 db, three channel monopulse antenna and receiver. (These elements are not mounted directly to the orbiter but rather to the ERV),
- o Providing software changes to the existing orbiter computer to accommodate the flight controls requirements during rendezvous and docking.

Table VI-8 gives the mass distribution for the modified orbiter. Details of the above modifications can be found in the subsystems discussions in Chapters V and VII.

Table VI-8 Derivation of Modified VO'75 Orbiter for the MSSR Mission

	<u>Kilograms</u>
Viking Orbiter (Dry)	925.9
Remove Science	-87.0
Remove Scan Platform	-32.8
Remove Data Storage Sys.	-31.4
Remove Cold Gas RCS (Incl. Gas)	-46.2
Add Auxiliary Propulsion Sys. (Dry)	22.8
Main Propellant Tank Stretch	23.9
Add Docking Cone and Rendezvous Radar	<u>15.3</u>
Modified VO'75 Orbiter (Dry)	791.5
Auxiliary Propulsion Propellant	38.0
RCS	5.0
Terminal Rendezvous	33.0
	<u>33.0</u>
Orbiter Less Main Tank Propellant	829.5
Main Tank Propellant	1542.0
MOI	1534.0
Main Eng. Rendezvous	8.0
	<u>          </u>
Orbiter Post Midcourse	2371.5
Midcourse Propellant	<u>51.0</u>
Orbiter Pre Midcourse	2422.5

### 3. Sample Transfer Tradeoffs

The baseline sample transfer scheme is shown in Figure VI-10. A number of factors were instrumental in arriving at this design. Risks associated with a "toss and catch" concept were sufficient to quickly drive the design to a more positive transfer, but back contamination considerations still dictated a minimum of contact between the MAV and the ERV/EEC. The baseline configuration meets both these criteria by, first, not releasing the canister until it has been driven home into the ERV and second, all hardware on the ERV that comes into contact with the MAV is jettisoned prior to the return trip to Earth.

The sample canister is mounted on top of the antenna feed and is presented for transfer by an extendable boom similar to the Viking surface sampler. The extension is completed prior to final closure between the orbiting spacecraft and the MAV. The structural adapter cone that supports the Viking lander capsule also supports the inner cone that guides the canister into the receptacle in the EEC. As the canister is secured, a switch is activated which releases the extendable boom from the canister. After the Orbiter backs away from the MAV, the adapter cone is jettisoned.

With the sealing considerations shown in Figure VI-11, only the lid of the canister is exposed to the Martian environment and this lid is subjected to aero heating and skin friction forces during ascent thru the Mars atmosphere. Back contamination possibilities are thus minimized and as an additional safeguard, the canister receptacle in the EEC is sealed prior to the return trip.

Another consideration is the possibility of biota transfer from the MAV to the ERV prior to actual docking. As seen in Figure VI-12 the closest the ERV will get to the MAV before their orientation relative to each other is controlled will be 100 km. At this range, the chance of any soil particles that become dislodged from the MAV reaching the ERV is negligible. When the range between the vehicles has closed to 50 meters the jettisonable docking cone screens the ERV from line of sight traveling particles. This includes the instant of initial docking contact between the vehicles (in addition, such contact has been determined not

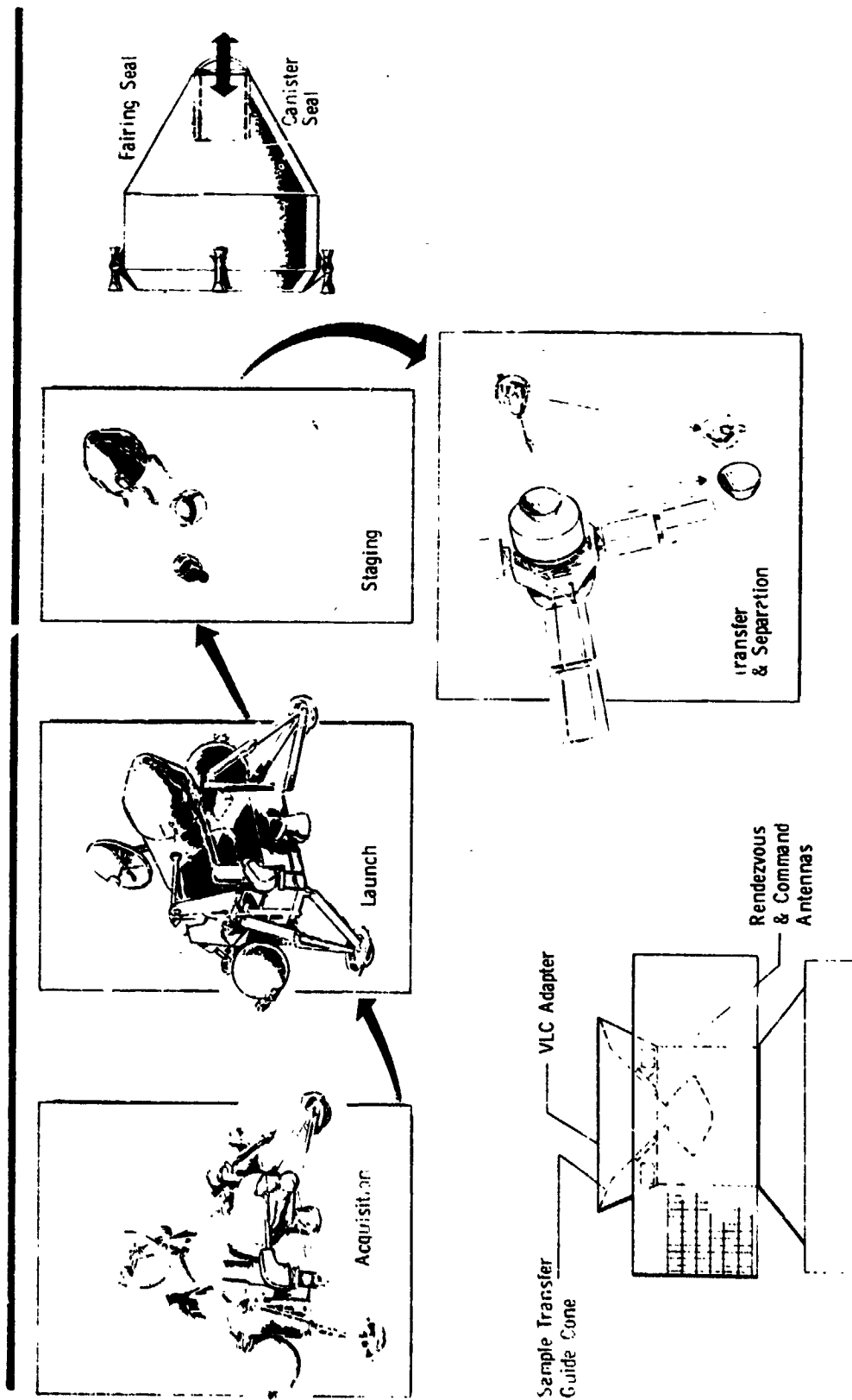


Figure VI-10 Sample Transfer and Contamination Control

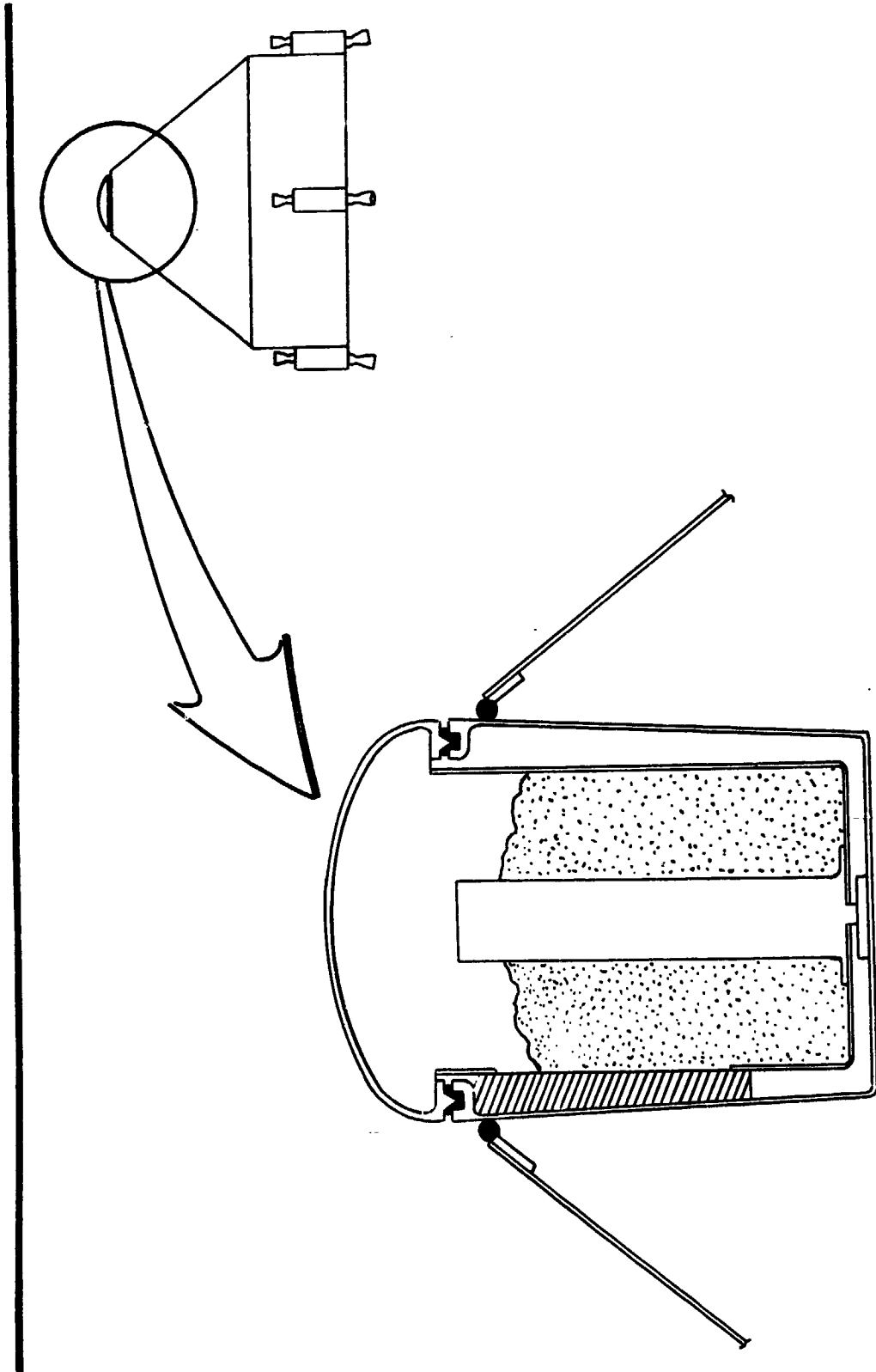
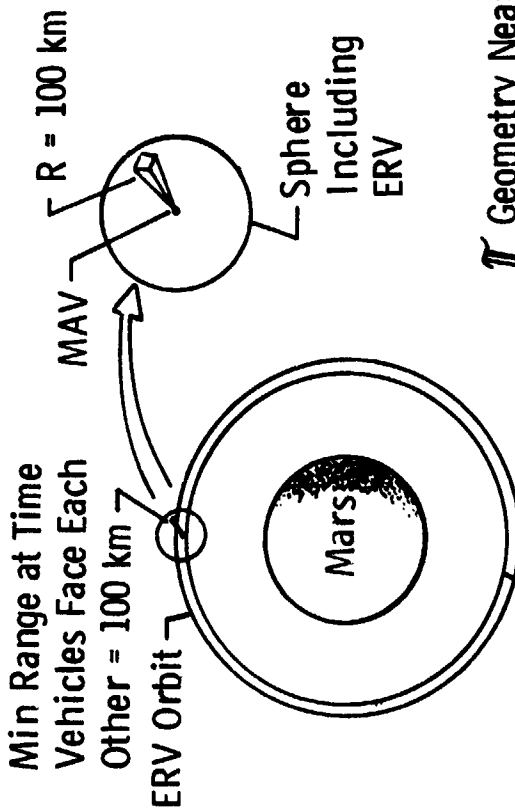


Figure VI-11 Sample Canister Sealing Concept

Geometry at Start of Rendezvous



Equivalent Area of ERV / Area of 100 km Sphere =  $10^{-10}$  i.e., Negligible Chance of Biota Transfer Prior to Vehicles Orienting Toward Each Other

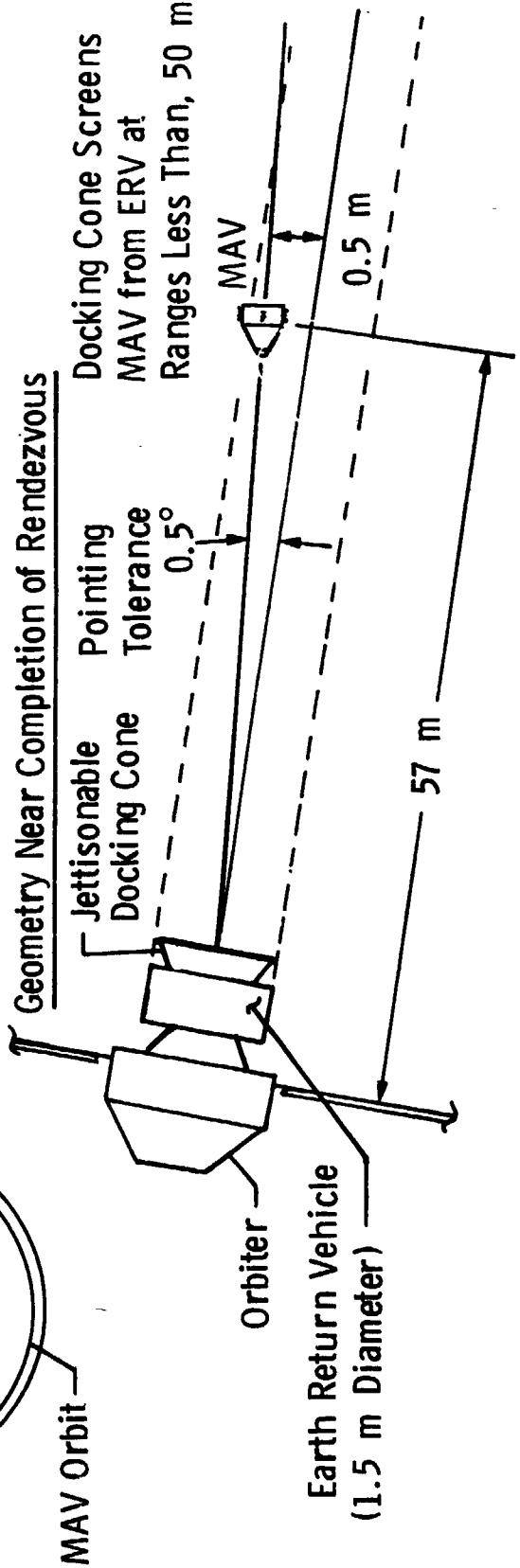


Figure VI-12 Earth Return Vehicle (ERV) Contamination Considerations

to be sufficiently energetic to cause particle dislodgement, see Appendix G). Between 50 meters and 100 km range some view factor will exist between the sides of the ERV and the surface of the MAV, however, considering the low population density probability of biota on the MAV, the very small fraction of ERV surface exposed until the range greatly exceeds 50 m, and the energy required to dislodge a soil particle (i.e., it takes a micrometeorite hitting the surface), it is concluded that biota transfer possibilities can be kept within acceptable limits.

Alternative sample transfer schemes utilizing Velcro, one-way petal, and the space bola capture concepts were investigated but did not meet the requirements for a positive transfer; maintaining a stable CG in the return vehicle; and minimizing the back contamination probability. With these requirements, there is relatively little flexibility as to the method used to transfer the sample; however, an alternative transfer concept that differed somewhat from the baseline design was evaluated. This concept involves docking the upper stage and the MAV with the orbiting spacecraft by means of a docking alignment aid as shown in Figure VI-13. This alternate approach requires exposing the entire sample canister on the nose of the MAV as the extendable boom is not a part of this design. For this reason, and due to the close proximity of the MAV and ERV during transfer, back contamination is of greater concern than with the baseline concept and the complexity involved is much greater.

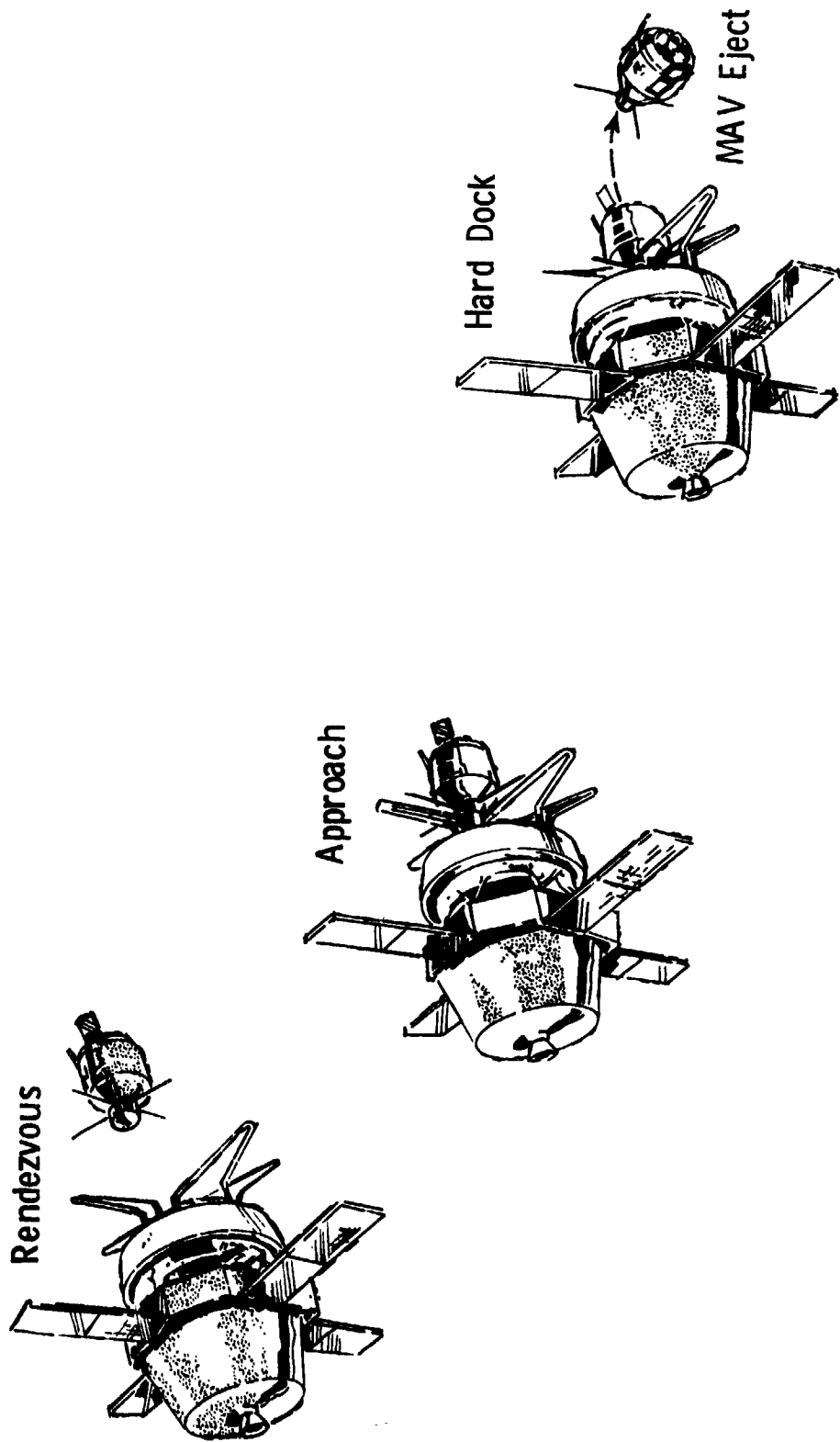


Figure VI-13 Alternative Sample Transfer Concept

#### D. EARTH RETURN VEHICLE CANDIDATES

Several possible Earth Return Vehicles have been examined briefly. Because of the long cruise phase and minimum maneuvers required of the ERV a spin stabilized spacecraft appears to be the most desirable vehicle. The ERV will carry the Earth Entry Capsule containing the Mars sample from Mars orbit to Earth encounter. The ERV itself does not enter the Earth's atmosphere or inject into Earth orbit.

The mission baseline assumes an ERV spacecraft with a dry mass of 105 kg and 130 kg of propellant. This spacecraft carries a 28 kg EEC, of which 2 kg is sample and container, for a total vehicle mass of 263 kg. Achieving the 263 kg mass requires major modifications to the existing Pioneer Venus spin stabilized vehicles which have grown from their originally planned size due to the selection of the Atlas Centaur launch vehicle for the PV mission. It is feasible, however, to derive a 263 kg vehicle by using most of the PV spacecraft components and designing a more compact structural framework.

If less modified versions of the PV vehicle are desired, to lower ERV costs, more of the MSSR mission margin could be allocated to the ERV. Preliminary mass estimates were conducted on two such configurations. The minimum modification design removes only those structural elements not required and adds a support for the Earth Entry Capsule (EEC). The maximum modification design reduces the spacecraft diameter from 2.54 m dia. to 1.8 m dia. This diameter still provides space for propellant tanks and the required solar array area. In each case the subsystem mass was derived by stripping those items not required for ERV from the Pioneer Venus estimate. Principal items removed were science and high gain antenna and their supporting components. Based upon reduced electrical load the solar panel area (even at the greater distance Mars is from the Sun) is  $3.35 \text{ m}^2$  a reduction of approximately  $2 \text{ m}^2$  from the Pioneer Venus probe bus.

The  $\Delta V$  schedule for Earth return is first burn 1044 m/sec, 2nd burn 22 m/sec and final burn 667 m/sec. It is proposed that the first burn use a solid propellant motor and the 2nd and 3rd burns use bipropellant

liquid propulsion systems. Bipropellant was chosen over monopropellant for reduced mass and volume. Four PV propellant tanks appear adequate for the bipropellant system including monopropellant hydrazine for RCS. Thus, the modification to the PV propulsion system would consist of adding two propellant tanks and bipropellant thrusters for an estimated 8 kg.

Summary mass statements for the two spacecraft are presented in Table VI-9. Version A could be flown on the baseline mission only if essentially all the weight margin were to be allocated to the EKV while with Version B the weight margin could be split between the lander/MAV system and the ERV. See also Figure VI-14.

Table VI-9 Candidate ERV Mass Summaries Based on Modified Pioneer Venus Spacecraft

<u>Element</u>	<u>Mass - kg</u>	
	<u>Version A (Min Mod)</u>	<u>Version B (Max Mod)</u>
Communications	10.50	10.50
Data Handling	7.44	7.44
Control	10.42	10.42
Structure	87.40	74.60
Power	25.20	25.20
Propulsion	19.60	19.60
Contingency 5%	<u>8.04</u>	<u>7.44</u>
Total ERV Dry	168.60	155.20
Earth Entry Capsule	<u>28.00</u>	<u>28.00</u>
Total ERV Dry + EEC	196.60	183.20
RCS Propellant	6.00	6.00
Liquid Propellant	50.30	46.90
Solid Rocket Motor	<u>138.80</u>	<u>129.60</u>
ERV Gross	391.70	365.70

E. TOTAL SPACECRAFT MASS DISTRIBUTION AND MARGIN CONSIDERATIONS

The physical arrangement of the Mars sample return system elements was shown in Figure VI-9. The 4408.9 kg throw mass capability of the Titan III Centaur establishes the mass of this total system and this section develops the mass distribution among the various elements.  $\Delta V$  budgets used to establish the system mass distribution are shown in Table VI-10 and the resulting orbiting system mass is shown in Table VI-11.

Table VI-10  $\Delta V$  Budget in M/Sec

	<u>Nominal</u>	<u>Statistical</u>	<u>Total</u>
Midcourse (Main Engine)		35	35
Orbit Insertion (Main Engine)			
MOI $\Delta V$	1098		
Hp $\Delta V$	22		
Circular $\Delta V$	1044		
Finite Burn	<u>56</u>		
	2220	37.5	2257.5
Initial Rendezvous Trim	0	50	50.0
Terminal Rendezvous & Trim			
Closing $\Delta V$ } (Main Engine)	7.5	2.0	9.5
Margin } (Main Engine)			<u>9.5</u>
			19.0
Terminal $\Delta V$ } (Auxiliary Engines)	14.1	16.6	30.7
Margin } (Auxiliary Engines)			<u>30.3</u>
			61.0
			2422.5
<u>RECAP</u>			
Midcourse (M/C)		35.0 M/Sec	
Total Main Engine (Less M/C)		2326.5 M/Sec	
Auxiliary Propulsion (Less ACS)		<u>61.0 M/Sec</u>	
		2422.5 M/Sec	

Table VI-11 Orbiting System Mass Derivation

Throw Mass		4408.9
Less: Launch Vehicle Peculiar	-104.3	
Adapter S/C to Booster	- 61.2	
Bioshield Cap	<u>- 53.7</u>	
	-219.2	<u>- 219.2</u>
Spacecraft Pre-Midcourse		4189.7
Less: Midcourse Propellant		<u>- 51.0</u>
Spacecraft Post-Midcourse		4138.7
Less: Adapter Orbiter to Lander	- 13.7	
Bioshield Base	- 73.3	
Separated Lander	<u>-1285.0</u>	
	-1372.0	<u>-1372.0</u>
Orbiting System Mass		2766.7

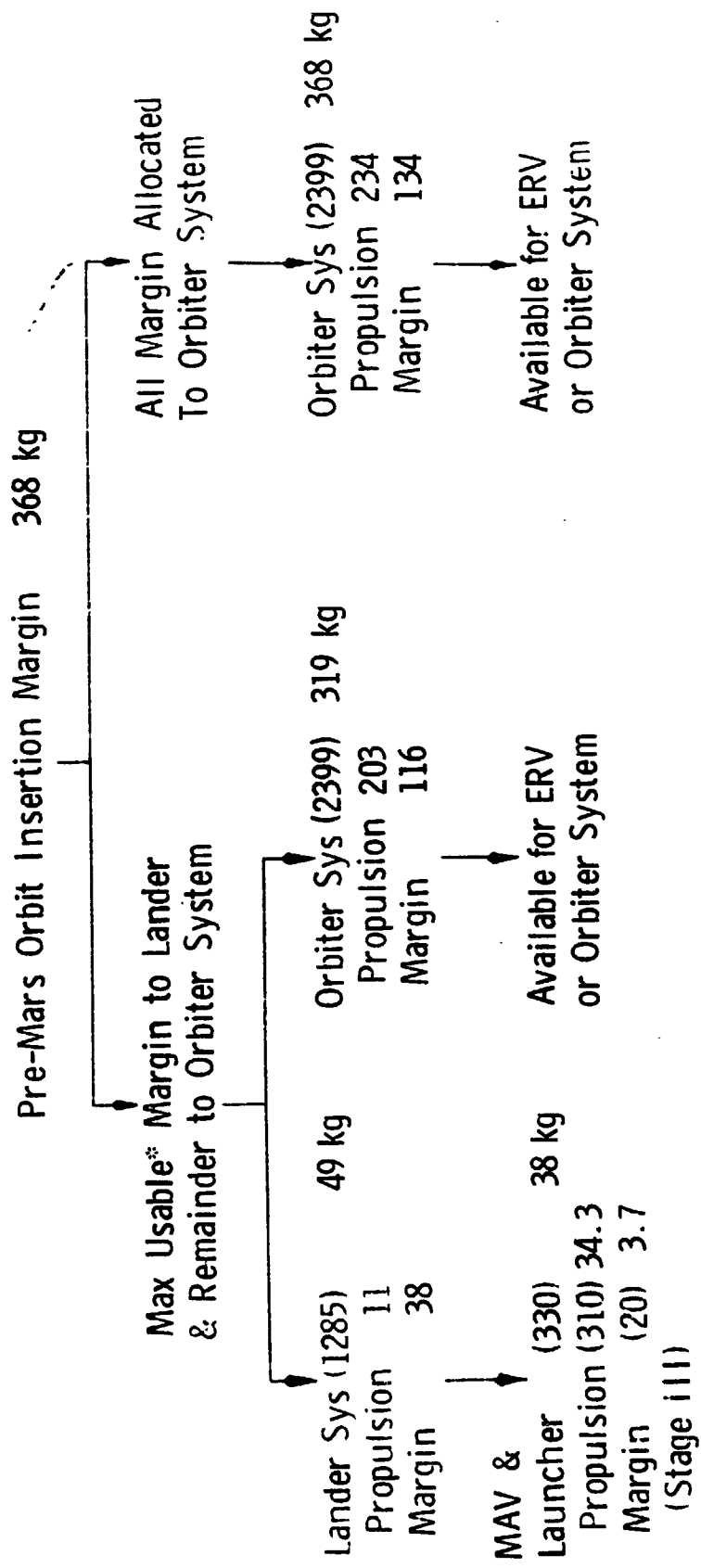
The orbital system is considered to consist of the modified VO '75 orbiter, the Earth return Vehicle (including the EEC but without the sample return canister). The orbiter propulsion system is sized to place the total orbiting system into Mars orbit and is assumed to remain as part of the total mass during rendezvous and docking.

Mass estimates have been made for all of the orbiting system elements and the difference between the sum of these elements and the mass which can be placed in orbit is considered as the system margin. This margin may be allocated throughout the system with various benefits. Determination of the magnitude of this margin in terms of additional nonpropulsion system weight which could be put into Mars orbit for the baseline configuration is given in Table VI-12.

Table VI-12 Determination of In-Orbit Margin for the  
Baseline Configuration

		<u>Kilograms</u>
Orbiter System Mass		2766.7
Less: Orbiter Post-Midcourse (Table VI-8)	-2371.5	
ERV (263 less 2 kg for sample and container)	- 261.0	
	-2632.5	<u>-2632.5</u>
Margin		134.2

Alternative margin allocations are identified in Figure VI-14. The calculations shown assume that the in-orbit margin derived above is reallocated to the pre-orbit insertion period. Thus the 134 kg of in-orbit margin becomes 368 kg (it took 234 kg to put the 134 kg into orbit) and this amount may be applied to the various system elements. Figure VI-14 shows several possible applications of this margin. The lander system can only be increased by 49 kg without exceeding its landed weight capability as constrained by use of the existing lander with the minimum modifications identified in section VII-B. Allocation of this maximum usable margin to the lander system results in a 3.7 kg margin in the MAV Stage III with 116 kg remaining as in-orbit margin. More extensive lander modifications could increase this MAV margin allocation. In-orbit margin may be applied either to the ERV or to the orbiter rendezvous propellant or hardware. However, the rendezvous  $\Delta V$  budget currently appears adequate and therefore some further allocation of margin to the ERV is practical.



\*Based on Viking '75 Lander as modified for baseline URDMO (parachute dia, aeroshell dia, terminal engines, and lander body size not changed).

( ) Current mass estimate without margin; however, a 10% contingency is included in new hardware estimates.

Figure VI-14 Alternative Margin Allocations

## F. FAILURE MODES AND BACKUP PROVISIONS

Due to weight constraints it was not deemed practical to build complete redundancy into all critical functions associated with the ascent, rendezvous and docking. However, the baseline system does provide many areas where failure of the primary system is compensated for by use of a backup mode. These are identified in Table VI-13. Additional redundancy features can be provided but a more comprehensive study is required to pinpoint the areas where the existing weight margin can be most effectively utilized.

The situation relative to potential single point mechanical system failures does not differ significantly from that for other space program missions, i.e., propulsion system failures, separation system failures, chute failures, etc., and it does not appear desirable to try to provide dual systems in all these areas.

## G. TRADEOFF CONSIDERATIONS RELATIVE TO KEEPING THE ORBITER AND ERV MATED DURING THE 400-DAY PARKING ORBIT AT MARS

The baseline design provides for not separating the Earth return vehicle until the approximately one-year duration stay in orbit is complete. This approach is based on the following considerations:

- o The orbiter has more comprehensive and sophisticated station keeping and telemetry subsystems.
- o The larger mass of the combined ERV/Orbiter does not cost significant attitude control propellant.
- o The ERV design is simplified in that only the trans-Earth cruise mode need be addressed.
- o The possible degradation of the orbiter systems that might compromise subsequent ERV separation is less of a concern than imposing a one-year-greater lifetime on the ERV systems.

Table VI-13 Failure Modes and Backup Provisions

<u>Event</u>	<u>Primary Mode</u>	<u>Potential Failure Mode</u>	<u>Back-up Mode</u>
MAV Elevation and Liftoff Command	Lander GCSC (Computer) Issues Discretes	Lander GCSC Fails	Earth Command Loop to MAV Computer That Bypasses GCSC (Still Use Lander Communications Link)
MAV Earth Pointing	Programmed Turn	Program Lost	Automatic Search Sequence Initiated
MAV Circularization	Earth Based Command (Update of Stored Nominal Command)	Can't Gain Access to MAV Computer (But Still Have Tracking Capability)	MAV Executes V per Pre-stored Nominal Command (Orbiter Adapts)
MAV and Orbiter Reorient to Face Each Other	Stored Command	Discrete(s) Fails to Occur	Send Command from Earth
Initiate Orbiter Closing V (Main Engine)	Stored Command	Discrete Fails	Reinitiate Firing Based on Onboard Accelerometer Data
Perform Rendezvous Control Law Burns	Stored Program - Uses Orbiter Axial Thrusters	Thruster Failure	Use MAV Axial Thrusters (Requires Additional Av Capability in MAV, 60 m/s Max or ~2 kg)
Relative Range, Range Rate and Angle Tracking	Cooperative Sensors Orbiter and MAV	MAV Transponder Fails	Within 10 km Range, Orbiter Can Achieve Rendezvous by Skin Tracking MAV
Docking	Signal from Sensor Confirms	No Docking Confirmation	Automatic Program for Back Out and Re-enter

#### H. FEASIBILITY OF PROVIDING FOR LANDER SURVIVAL AFTER MAV LAUNCH

The baseline mission was deliberately limited in science objectives to include only the accomplishment of a sample return. This was done to make it a minimum weight and cost mission. However, the question arises as to the impact on this system of performing additional science experiments after the ascent vehicle (MAV) has been launched. In our baseline design, an integration concept for the MAV and launcher was selected which was the best compromise between launcher operation and thermal control of the MAV while on the lander. With this concept it would be difficult but not impossible to return the entire lander to operating condition after launching the MAV. A substantial weight penalty would be incurred however if this were done. However, it would be possible to carry out some experiments after MAV launch by providing a separate compartment inside the lander which would be designed to survive MAV launch. These two approaches are summarized in Table VI-14. More ambitious experiments than could be contained within the lander body would suggest revising the baseline thermal/mechanical integration concept of the MAV. These have not been evaluated.

#### I. IMPACT OF THE 1983/84 MISSION OPPORTUNITY ON SYSTEM DESIGNS

In the 1983/84 opportunity, because of the increased entry velocity, several changes will be required of the lander system. Assuming the same landed weight of 776.4 kg, the following changes will be required:

Increased Terminal Propellant	1.8 kg
Increased Aeroshell	12.2 kg
Increased Heat Shield	<u>8.2 kg</u>
Total Increase	22.2 kg

This will result in a total lander system mass of 1307.2 kg.

Assuming the same launch vehicle is used as in the 1981 baseline design, the increased launch energy requirements, plus the larger MOI  $\Delta V$  requirement and the slightly increased lander mass result in a negative margin for the orbiting system. This indicates that a single launch in

Table VI-14 Requirements and Feasibility of Lander Survival After MAV Launch

Approach I Total Lander Survival

Requirement

Re-establish Thermal Control Canopy After Launch.  
Prevent Structural/Thermal Damage to Equipment Mounted on Top of Lander.

Impact on Baseline

1. Provide Structural Cover for Insulation Inside Canopy and Lander Side Panels.
2. Locally Protect Turntable and Launcher Hinges, Motors, Camera, RTGs, Heat Pipes and S-Band Antenna.
3. Provide Door in Canopy to Cover Opening Left by MAV.
4. Provide Retractable Panel in Canopy for Exhaust Escape.

Feasibility

Possible with Substantial Weight Increase. Appears a More Reliable and Lighter-weight Approach is to Provide Selective Protection as in Approach II Below.

Approach II Selective Protection

Requirement

Protect Only Communication System Components and Selected Experiments.

Impact on Baseline

1. Provide Separate Compartment Inside Lander to House Equipment That Must Survive. Use Electrical Heaters and Insulation Locally for Thermal Control.
2. Relocate External Sensors Away From Top of Lander. Provide Blast Proof or Retractable High Gain Antenna.

Feasibility

Feasible with Moderate Increase in Weight. (Magnitude Depends on Nature of Post Launch Science Desired).

1983/84 will require either a larger launch vehicle than the Titan III Centaur or that space storable propellants will have to be used for Mars orbit insertion. Another alternative would of course be a dual launch.

Assuming an adequate launch system and the '81 baseline orbiting system components, a further stretch of the VO '75 tankage would still allow the modified VO'75 orbiter to be used. In this case the total propellant required would be 1773 kg including midcourse and the tank stretch would be 26% or 22 cm.

The 1981 MAV design would not be affected since the landed weight would remain constant. ERV sizing would depend on whether the 1983/84 mission were flown with a larger launch vehicle (or dual launches) or with space storable MOI propellant. In the latter case the ERV situation would remain approximately the same as for 1981. In the case of a larger launch vehicle, perhaps a heavier, eg, a less modified Pioneer Venus spacecraft, could be flown.

## VII SUBSYSTEM DEFINITION FOR ALL MISSION PHASES

### A. COMMUNICATIONS

Subsystem requirements and a description of the proposed telecommunications subsystems for the MAV, Orbiter, and Lander are discussed in this section. Included are provisions for telemetry, command, and ranging as used during rendezvous and docking between the MAV/Orbiter. In all cases, the systems are compatible with the NASA Deep Space Network which utilizes S-band transmission. The MAV communications subsystems are described first.

#### 1. MAV and Orbiter Communications Subsystem

Several options were considered in providing communications for the Mars surface operations preceding the MAV launch. Commands and telemetry as required for collecting a surface sample and launching the MAV into its initial orbit could conceivably be provided using S-band equipment mounted in either the Lander or the MAV. Initial findings tend toward use of S-band on the Lander for surface operations to provide daily Earth contact, if required. A disadvantage of use of the MAV S-band equipment is the necessity for a high gain antenna that can be gimballed to track Earth and the need for an omni antenna for command backup. These, even though they could be separated from the MAV in the launch attitude, require extensive RF interface and impose weight penalties for the MAV. Thus, employment of S-band equipment in the Lander is preferred.

The need for an Earth reference for the MAV attitude and the requirement to determine the MAV orbit from Earth tracking leave little option for use of other than an S-band MAV/Earth communications capability. For a three-axis stabilized MAV, a monopulse type angle sensor and a typical DSN two-way Doppler, command and telemetry system appear to best fulfill the needs.

During rendezvous of the MAV and orbiter, the MAV S-band subsystem used for MAV/Earth communications and pointing error data during MAV orbit adjustment could serve the same functions in interfacing with the Orbiter as with the DSN by adding a ranging turnaround capability and providing a means for operating at appropriate frequencies. The alternative is to provide a separate rendezvous and docking subsystem which would result in weight,

power, and volume penalties. Consequently an angle tracking dual ratio S-band transponder has been selected that provides pointing, communication, and tracking capabilities when interfacing with either the DSN or the Orbiter in the MAV orbit and MAV rendezvous modes.

Requirements. Basic requirements for the MAV telecommunications subsystem are shown in Table VII-1. The requirements are based on the decision to integrate MAV/Earth direction sensing, rendezvous, and docking functional requirements into the telecommunications subsystem. Maximum range for Earth/MAV communications is  $257 \times 10^6$  km based on completing MAV/Orbiter rendezvous within 38 days after arrival at Mars as shown in Figure VII-1.

Subsystem Description. A block diagram of the selected MAV telecommunications subsystem is shown in Figure VII-2. The subsystem consists of a monopulse-fed 18 dB gain antenna, an angle tracking dual ratio transponder, command detector, command decoder and telemetry data handling circuitry packaged in an integrated case. Angle tracking errors are obtained by a cassegrain monopulse feed and frequency sharing of a common sum channel receiver by generating error channel sideband signals and frequency multiplexing the sum and error signals.

Telemetry and command are DSN compatible PCM/PSK/PM with two-way coherent Doppler. Turnaround ratio is 240/221 for DSN operation and tentatively 220/239 for Orbiter interfacing. Turnaround ranging is intended only for the MAV/Orbiter rendezvous. The command subsystem has a single channel using a sinewave subcarrier. Telemetry is a single-channel squarewave subcarrier. The 4-watt MIC power amplifier is sized for MSC 3005 transistors and 20 volts dc input.

The Guidance Control and Sequencing Computer (GCSC) provides the power turn-on control for the telecommunications except that an uplink receive signal enables turn on of the command detector and decoder. Low power designs are contemplated for all units.

Detail descriptions of the antenna and the transponder are given in Chapter V. The command detector and command decoder provide the same functions as the Viking '75 Lander command detector and command decoder but are to be designed for minimum weight, size, and power using technology available for a 1981 mission such as CMOS/LSI. An integrated package to include the transponder, the command detector, and command decoder functions

Table VII-1. MAV Telecommunications Functional Requirements

1. MAV on the Surface:

Multiplex and format engineering data, from the various MAV sub-systems, into a PCM data stream for transmission at 8-1/3 bps over the Lander-to-Earth S-band link.

2. MAV During Ascent from Mars Surface:

No telecommunications functions.

3. MAV During Orbital Operations Prior to Rendezvous Mode:

- a. Provide X and Y error signals indicating Earth pointing error magnitude and direction using S-band signal from Earth as point source. Accuracy of error signals are to be less than 0.5 degree within 8 degrees of boresight.
- b. Provide standard DSN 2-way Doppler using 240/221 transmit to receive frequency ratio.
- c. Provide 8-1/3 bps telemetry-to-Earth capability at bit error rate of better than 5 in  $10^3$  for telemetry.
- d. Provide single channel command detection and decoding capability at rate of 4 symbols/second and bit error rate of better than 1 in  $10^5$  (use Viking Lander format and subcarrier waveform)-- command subcarrier frequency must be high enough to fall outside the MAV transponder carrier loop under strong signal conditions during this and the rendezvous mode.
- e. Provide a capability for telemetering a read out of stored commands to Earth for verification of MAV maneuver command parameters.

4. MAV During Rendezvous and Docking:

- a. Provide a transponder transmit-to-receive frequency turnaround ratio of 220/239 for cooperative rendezvous with the Orbiter.
- b. Provide X and Y error signals for use in pointing the MAV toward the Orbiter using the Orbiter S-band range and rate transmission as a point source. Pointing error signal accuracies of 0.5 degree or less are required.
- c. Provide a ranging turnaround channel capability assuming a 819.2 kHz subcarrier and 300 kHz ranging signal bandwidth.
- d. Provide an engineering telemetry transmission and command channel reception capability identical to that provided during orbital operations prior to the rendezvous and docking mode.

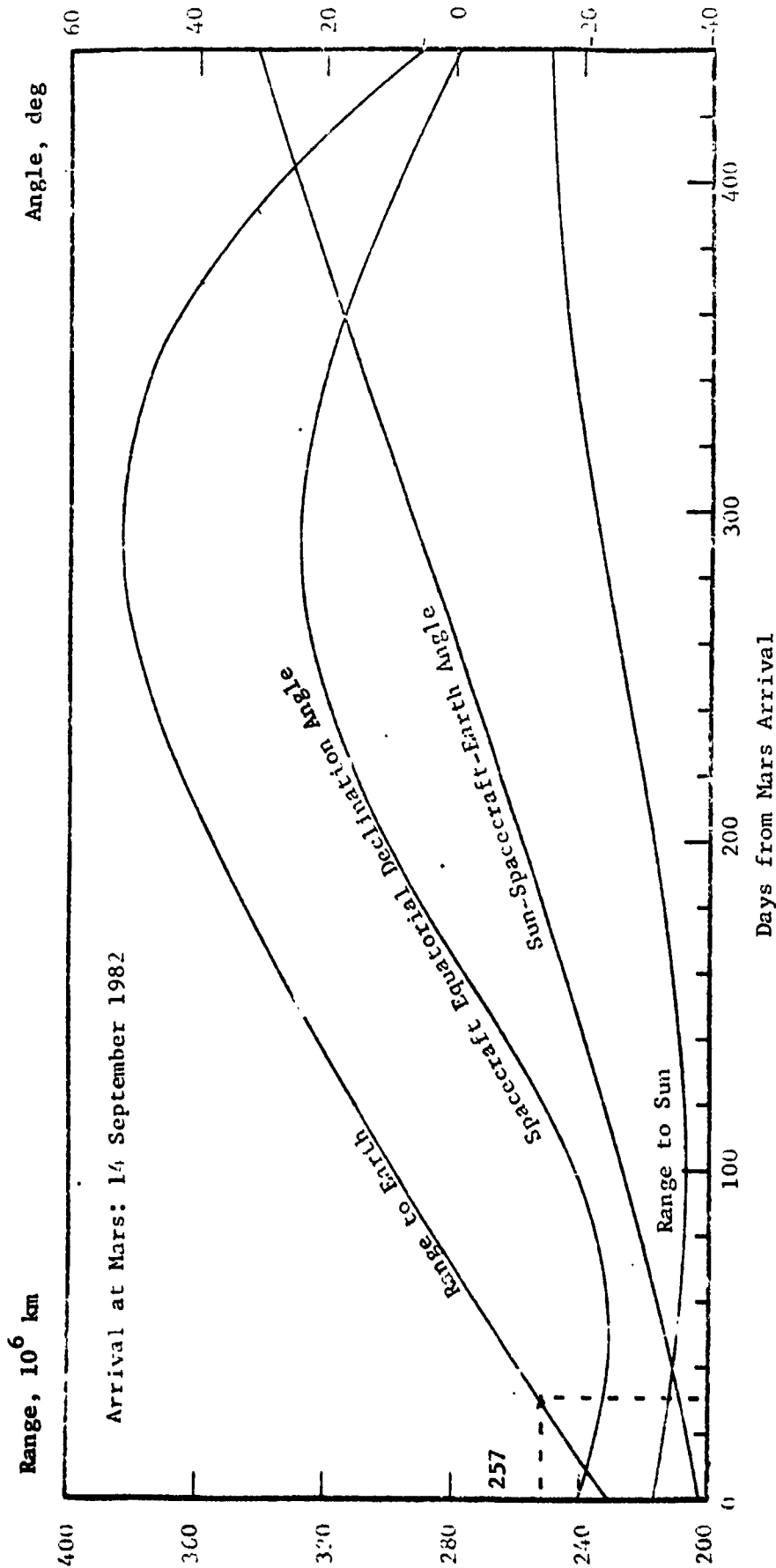
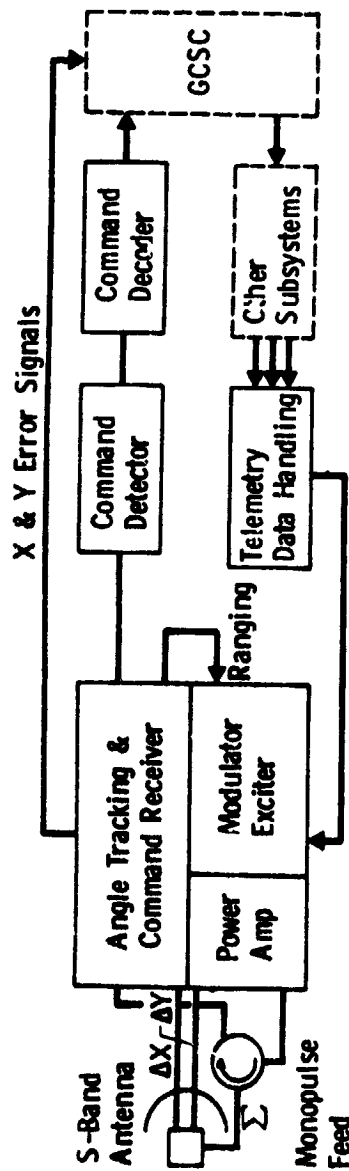


Figure VII-1. Geometries for Orbiter Phase of a 1981 URDMO Mission



Subsystem Data:

Weight 2.1 kg (4.7 lb) Uncased  
 Max dc Power 21.3 W  
 Min dc Power 3.5 W

Characteristics	DSN/MAV Link	Orbiter/MAV Link
Tracking	2-Way Doppler	Doppler, Ranging & Angle
MAV Attitude (Pointing)	S-Band Monopulse Feed & Single Channel Rec.	Same
Commands	Single Channel Subcarrier	Same
Telemetry	8-1/3 bps	Same
Transmitter Power Amp	4 Watts	4 Watts/150 mW
MAV Transmit Freq	2292.03 MHz	2101.03 MHz
MAV Receiver Freq	2110.58 MHz	2282.48 MHz

Figure VII-2. Proposed MAV Telecommunications Block Diagram

was designed. Table VII-2 shows physical properties of the subsystem. The total size (192 cu in.) is based on an electronic package density of 40 lb/cu ft.

Table VII-2. MAV Telecommunications Weight and Power Estimates

Quantity	Component	Average dc Power, watts	Uncased Weight, lbs	Size, cm <sup>3</sup> /in <sup>3</sup>
1	Antenna Feed and Hybrids		0.3	3160/192
1	Circulator		0.7	
1	S-band Power Amplifier	13.0	0.5	
1	* S-band Receiver	3.5	0.8	
1	* S-band Modulator/Exciter	2.3	0.6	
1	Command Detector	1.0	0.3	
1	Command Decoder	0.5	0.3	
1	Case for Above		1.0	
1	** Telemetry Data Handling Unit	1.0	<u>0.9</u>	
			5.4	
Note: * Integrated Package ** Packaged with G&C				

In the normal rendezvous and docking mode the MAV S-band transponder provides turnaround for a coherent ranging signal, demodulates a command subcarrier, and combines a PSK modulated subcarrier with the ranging for transmission to the Orbiter. Commands from the Orbiter will be required only in event the Orbiter cannot maneuver for rendezvous. In this case the MAV could be commanded to start or stop thrust. Thus, command is backup only. Telemetry from MAV-to-Earth via the Orbiter is an option available at additional cost and was not investigated.

The Orbiter must perform the rendezvous and docking maneuvering once it is in the desired orbit. To accomplish this, an S-band range, range rate, and angle tracking system is provided using an 18 dB monopulse antenna and receiver system, a 300 mW transmitter, and coherently generated range tones. The highest frequency tone is 819.2 kHz which provides a resolution of approximately 3 meters. Four additional tones are used for resolving range ambiguity for the maximum required range of 750 km. These

tones are modulated onto the highest frequency tone prior to transmission by the Orbiter and demodulated when received from the MAV turnaround.

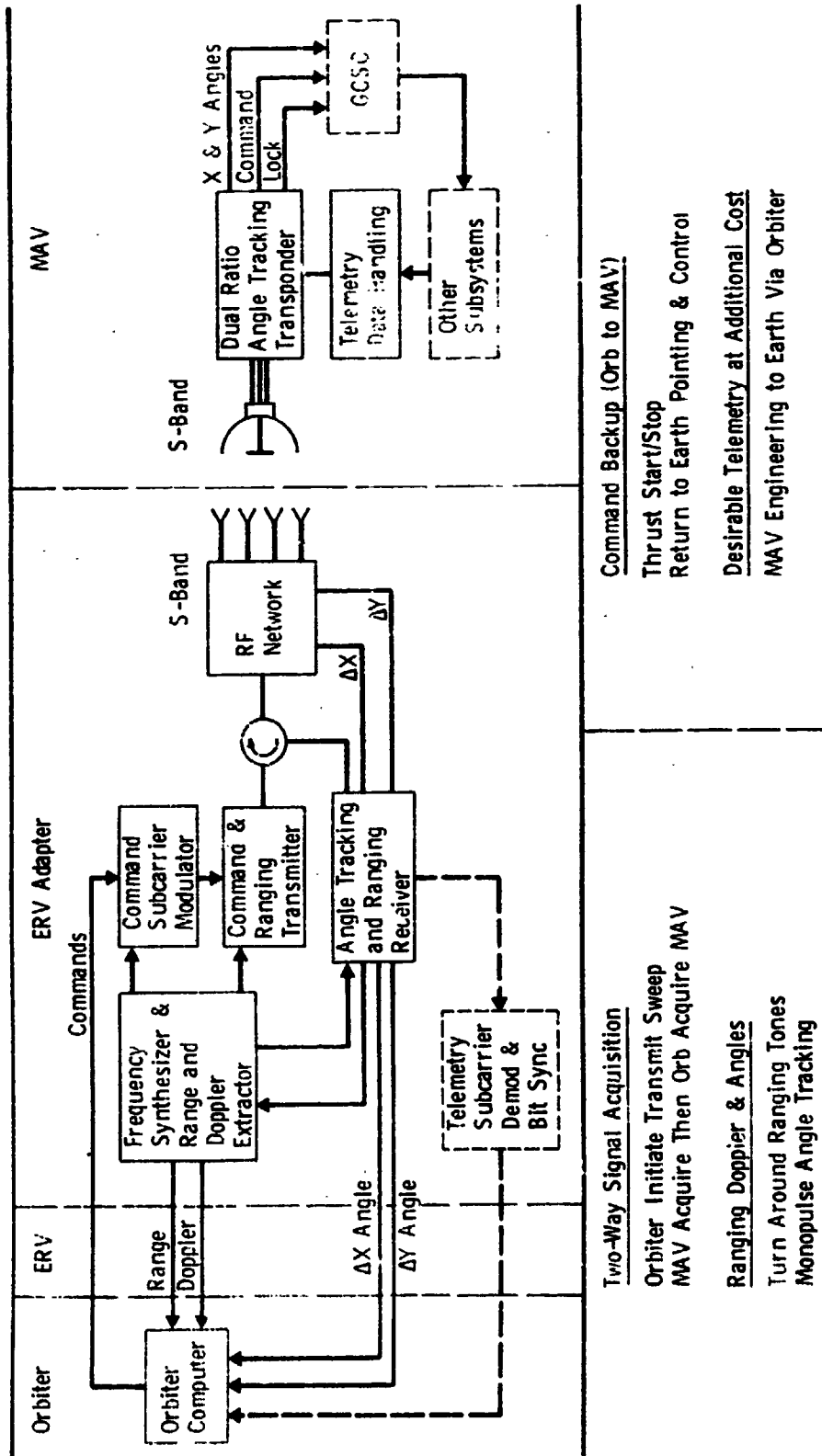
The presently conceived interface for the Orbiter equipment is to mount it near the sample transfer cone (using the cone to support surface traveling wave antenna elements) and carry power and digital signals through connector interfaces between the ERV and the Orbiter main body. After docking and transfer, the cone and S-band equipment may be jettisoned. A block diagram of the proposed Orbiter/MAV communications network is shown in Figure VII-3.

Telecommunication design control tables have been prepared for MAV/Earth command and telemetry links for purposes of sizing the transmitter power amplifier and antenna and assessing performance margins. Table VII-3 shows the major parameters of the telemetry link. Adequate margin is indicated at a range of  $2.57 \times 10^8$  km for an 8-1/3 bps uncoded data rate using a 4-watt transmitter, an 18 dB MAV antenna and the 64 meter DSN net when the MAV is pointed up to 10 degrees from the MAV Earth line. The range indicated is for the 1981 mission and is based on completing the MAV rendezvous within 38 days after Mars arrival as shown in Figure VII-1. The relative Mars/Earth geometry would be similar for the 1983 mission so the range would also apply to that mission.

Table VII-4 shows the link parameters for an Earth-to-MAV command link using the 64 meter DSN net and a 10 kW transmitter. Adequate margin is available to allow use of the 26 meter net for an Earth pointing reference in place of the 64 meter net but a downlink capability (MAV-to-Earth) is limited to the 64 meter net. Energy per symbol or bit and additional data channel losses (lines 20 and 22 of Tables VII-3 and VII-4, are estimated based on Viking design control tables for purposes of sizing the system.

MAV/Orbiter link calculations to determine range, range rate, and pointing accuracies during rendezvous and docking operations are discussed in Chapter V. The command and telemetry links between the MAV and Orbiter are, however, shown in Tables VII-5 and VII-6.

MAV Telemetry Requirements. The MAV subsystems were reviewed to determine parameters and events to be instrumented and transmitted to Earth via the telemetry link. Some of the data are relayed to Earth via the Lander



Two-Way Signal Acquisition  
 Orbiter Initiate Transmit Sweep  
 MAV Acquire Then Orb Acquire MAV

Ranging Doppler & Angles  
 Turn Around Ranging Tones  
 Monopulse Angle Tracking

Command Backup (Orb to MAV)  
 Thrust Start/Stop  
 Return to Earth Pointing & Control

Desirable Telemetry at Additional Cost  
 MAV Engineering to Earth Via Orbiter

Figure VII-3. Proposed Orbiter/MAV Communications

Table VII-3. MAV-to-Earth Communications Link With MAV in Orbit

No.	Parameter	Nominal Value	Adverse Tolerance	Notes
1	Total Transmitting Power (dBm)	+ 36.0	0.4	4 watts
2	Transmitting Circuit Loss (dB)	- 1.5	0.2	
3	Transmitting Antenna Gain (dB) 2292 MHz	+ 15.0	0.5	18 dB on Axis, Dish
4	Communications Range Loss (dB)	-267.9	0.0	257 x 10 <sup>6</sup> km
5	Atmospheric Absorption & Defocusing Losses (dB)	0	0	
6	Polarization Loss (dB)	- 0.3	0.3	
7	Multipath and Other Losses (dB)	0	0	
8	Receiving Antenna Gain (dB)	+ 61.5	0.4	64 Meter DSN
9	Receiving Circuit Loss (dB)	0	0	
10	Net Loss (dB) (2+3+4+5+6+7+8+9)	-193.2	1.2	
11	Total Received Power (dBm) (1+10)	-157.2	1.6	
12	Receiver Noise Spectral Density (dBm/Hz)	-184.2	0.5	25° Elev.
13	Total Received Power/ $N_0$ (dBm·Hz) (11-12)	+ 27.0	2.1	
<u>Carrier Tracking</u>				
14	Carrier Power/Total (dB)	- 1.7	0.4	0.613 Rad.
15	Additional Carrier Losses (dB)	+ 0.1	0	
16	Threshold Tracking Bandwidth - $2B_{LO}$ (dB)	+ 10.8	0	
17	Threshold SNR (dB)	+ 10.0	0	
18	Performance Margin (dB) (13+14+15-16-17)	+ 4.4	2.5	
<u>Data Channel</u>				
19	Data Power/Total (dB)	- 4.8	0.8	
20	Additional Data Channel Losses (dB)	- 2.9	0.3	
21	Data Bit Rate - bps (dB)	+ 9.2	0	8-1/3 bps
22	Threshold Energy Per Data Bit - $E_b/N_0$ (dB)	+ 5.2	0	Uncoded
23	Performance Margin (dB) (13+19+20-21-22)	+ 4.9	3.2	

- Conditions:
1. PCM/PSK/PM modulation.
  2. Maximum MAV-to-Earth range.
  3. 3-dB pointing loss included in No. 3.

Table VII-4. Earth-to-MAV Command Link with MAV in Orbit

No.	Parameter	Nominal Value	Adverse Tolerance	Notes
1	Total Transmitting Power (dBm)	+ 70.0	0	10 kW
2	Transmitting Circuit Loss (dB)	0	0	
3	Transmitting Antenna Gain (dB)	+ 60.4	0.7	64 Meter Net
4	Communications Range Loss (dB) 2110.58 MHz	-267.1	0	257 x 10 <sup>6</sup> km
5	Atmospheric Absorption & Defocusing Losses (dB)	0	0	
6	Polarization Loss (dB)	- 0.4	0	
7	Multipath and Other Losses (dB)	0	0	
8	Receiving Antenna Gain (dB)	+ 14.3	0.5	-3 dB Pointing
9	Receiving Circuit Loss (dB)	- 2.5	0.3	
10	Net Loss (dB) (2+3+4+5+6+7+8+9)	-195.3	1.5	
11	Total Received Power (dBm) (1+10)	-125.3	1.5	
12	Receiver Noise Spectral Density - (dBm/Hz)	-167.5	0.8	13000K
13	Total Received Power/N <sub>0</sub> (dBm·Hz) (11-12)	+ 42.6	2.3	
<u>Carrier Tracking</u>				
14	Carrier Power/Total (dB)	- 2.5	0.2	
15	Additional Carrier Losses (dB)	0	0	
16	Threshold Tracking Bandwidth - 2B <sub>L0</sub> (dB)	+ 12.6	0.5	18 Hz
17	Threshold SNR (dB)	+ 10.0	0	
18	Performance Margin (dB) (13+14+15-16-17)	+ 17.5	3.0	
<u>Data Channel</u>				
19	Data Power/Total (dB)	- 4.0	0.2	
20	Additional Data Channel Losses (dB)	- 1.5	0.2	
21	Symbol Rate - SPS (dB)	+ 6.0	0	4 SPS
22	Threshold Energy Per Symbol - E <sub>s</sub> /N <sub>0</sub> (dB)	+ 11.5	1.0	SER = 10 <sup>-5</sup>
23	Performance Margin (dB) (13+19+20-21-22)	+ 19.6	3.7	

Table VII-5. Telecommunications Design Control Table - Turn Around Ranging with MAV-to-Orbiter Telemetry

No.	Parameter	Nom. Value	Adverse Tolerance
1	Total Transmitter Power (dBm)                      300 mW	+ 24.8	0.5
2	Transmitting Circuit Loss (dB)	- 2.0	0.5
3	Transmitting Antenna Gain (dB)                      MAV Dish	+ 15.0	0.5
4	Transmitting Antenna Pointing Loss (dB)	- 1.0	0
5	Space Loss: F=2782 MHz; R=300 km (dB)	-148.4	0
6	Polarization Loss (dB)	- 3.0	0.2
7	Receiving Antenna Gain (dB)                      Orbiter	+ 18.3	0.5
8	Receiving Antenna Pointing Loss (dB)	- 1.0	0
9	Receiving Circuit Loss (dB)	- 1.0	0.3
10	Net Circuit Loss (dB)	-123.1	2.0
11	Total Received Power (dBm)	- 98.3	2.5
12	Receiver Noise Spectral Density (dBm/Hz) Noise Temperature ( <sup>o</sup> K)	-167.5 1300	0.7
13	Carrier Modulation Loss (dB)*	- 4.8	1.0
14	Received Carrier Power (dBm)	-103.1	3.5
15	Carrier APC Noise BW: $2 B_{LO} = 1 K \pm 2 \text{ Hz}$ (dB·Hz)	+ 30.0	0
16	Carrier SNR in $2 B_{LO}$ (dB)	+ 34.4	4.2
17	Carrier Threshold SNR in $2 B_{LO}$ (dB)	+ 10.0	0
18	Threshold Carrier Power (dBm)	-127.5	0.7
19	Performance Margin (dB)	+ 24.4	4.2
<u>Turnaround Ranging</u> (4 minor tones each modulating a 819.2 kHz tone at 0.6 Rad. peak)			
20	Ranging Modulation Loss: 1.1 Rad. $\pm$ 10% (dB)	- 6.4	1.0
21	Ranging Signal Power (dBm)	-104.7	4.5
22	Ranging Noise BW (dB·Hz)                      300 kHz	+ 54.8	0.8
23	SNR at Limiter Input (dB)	+ 8.0	5.3
24	Limiter Suppression (dB)	0	0.4
25	Radio Assembly Output Power (dBm)	+ 20.0	0.5
* Carrier modulated by ranging and command subcarriers each at 1.1 rad peak.			
- Continued -			

Table VII-5. Telecommunications Design Control Table - Turn Around Ranging with MAV-to-Orbiter Telemetry (continued)

No.	Parameter	Nom. Value	Adverse Tolerance
<u>Turnaround Ranging (concluded)</u>			
26	Transmitting Circuit Loss (dB)	- 2.5	0.5
27	Transmitting Antenna Gain (dB)                      MAV Dish	+ 18.3	0.5
28	Transmitting Antenna Pointing Loss (dB)	- 1.0	0
29	Space Loss: F=2103 MHz; R=300 km (dB)	-147.7	0
30	Polarization Loss (dB)	- 3.0	0.2
31	Receiving Antenna Gain (dB)	+ 15.0	0.5
32	Receiving Antenna Pointing Loss (dB)	- 1.0	0.5
33	Receiving Circuit Loss (dB)	- 2.0	0.5
34	Net Circuit Loss (dB)	-123.9	2.7
35	Total Received Power (dBm)	-103.9	3.2
36	Receiver Noise Spectral Density (dBm/Hz) Noise Temperature ( <sup>o</sup> K)	-167.5 3000	0.7
37	Carrier Modulation Loss (dB)	- 2.6	0.5
38	Received Carrier Power (dBm)	-106.5	3.7
39	Carrier APC Noise BW: $2B_{LO}=1$ kHz(+0,-20%)(dB·Hz)	+ 30.0	0
<u>Carrier Performance - Data Demodulation</u>			
40	Carrier SNR in $2 B_{LO}$ (dB)	+ 31.0	4.4
41	Carrier Threshold SNR in $2 B_{LO}$ (dB)	+ 10.0	0
42	Threshold Carrier Power (dBm)	-127.5	0.7
43	Performance Margin (dB)	+ 21.0	4.4
<u>Ranging Channel</u>			
44	Ranging Modulation Loss: 0.9 Rad. $\pm$ 12% (dB)	- 5.5	1.0
45	Total Ranging Suppression (dB)	- 5.5	1.4
46	Ranging Signal Level (Total) (dBm)	-109.4	4.6
47	Tone Subcarrier Modulation Loss (dB)	- 3.2	0.5
48	Received Subcarrier Power (dBm)	+112.6	5.1
49	Tone Subcarrier Loop BW (dB)                      10 Hz	+ 10.0	0.8
50	Required Loop SNR (dB)	+ 20.0	0
- Continued -			

Table VII-5. Telecommunications Design Control Table - Turn Around Ranging with MAV-to-Orbiter Telemetry (concluded)

No.	Parameter	Nom. Value	Adverse Tolerance
<u>Banging Channel (concluded)</u>			
51	Threshold Tone Power (dBm)	-137.5	1.5
52	Primary Tone Performance Margin (dB)	+ 24.9	6.6
53	Secondary Tone Modulation Loss (dB)	+ 10.2	1.5
54	Received Secondary Tone Power (dBm)	-122.8	6.1
55	Secondary Tone Noise Bandwidth (10 Hz) (dB)	+ 10.0	0.8
56	Threshold Secondary Tone SNR (dB)	+ 10.0	0
57	Threshold Secondary Tone Power (dBm)	-147.5	1.5
58	Secondary Tone Performance Margin (dB)	+ 24.7	7.6
<u>Telemetry Data Channel</u>			
59	Subcarrier Modulation Loss (dB)	- 10.0	1.5
60	Waveform Distortion Loss (dB)	0.	0
61	Loss Through Radio System (dB)	- 0.5	0.2
62	Subcarrier Demodulation Loss (dB)	- 0.1	0.1
63	Bit Sync Detection Loss (dB)	- 0.1	0
64	Received Data Power (dBm)	-114.6	5.0
65	Bit Rate (8-1/3 bps) (dB·bps)	+ 9.2	0
66	Received $ST_B/N_o$ (dB)	+ 43.7	5.7
67	Required $ST_B/N_o$ (dB) BER = $5 \times 10^{-3}$	+ 5.2	0
68	Threshold Subcarrier Power (dBm)	-153.1	0.7
69	Performance Margin (dB)	+ 38.5	5.7

Table VII-6. Telecommunications Design Control Table -  
MAV-to-Orbiter Command and Ranging Uplink

No.	Parameter	Nom. Value	Adverse Tolerance
1	Total Transmitter Power (dBm)      300 mW	+ 24.8	0.5
2	Transmitting Circuit Loss (dB)	- 2.0	0.5
3	Transmitting Antenna Gain (dB)      MAV Dish	+ 15.0	0.5
4	Transmitting Antenna Pointing Loss (dB)	- 1.0	0
5	Space Loss: F=2782 MHz; R=300 km (dB)	-148.4	0
6	Polarization Loss (dB)	- 3.0	0.2
7	Receiving Antenna Gain (dB)      Orbiter	+ 18.3	0.5
8	Receiving Antenna Pointing Loss (dB)	- 1.0	0
9	Receiving Circuit Loss (dB)	- 1.0	0.3
10	Net Circuit Loss (dB)	-123.1	2.0
11	Total Received Power (dBm)	- 98.3	2.5
12	Receiver Noise Spectral Density (dBm/Hz) Noise Temperature ( <sup>o</sup> K)	-167.5 1300	0.7
13	Carrier Modulation Loss (dB)*	- 4.8	1.0
14	Received Carrier Power (dBm)	-103.1	3.5
15	Carrier APC Noise BW: $2 B_{LO} = 1 K \pm 2 Hz$ (dB·Hz)	+ 30.0	0
16	Carrier SNR in $2 B_{LO}$ (dB)	+ 34.4	4.2
17	Carrier Threshold SNR in $2 B_{LO}$ (dB)	+ 10.0	0
18	Threshold Carrier Power (dBm)	-127.5	0.7
19	Performance Margin (dB)	+ 24.4	4.2
<u>Command Channel</u>			
20	Subcarrier Modulation Loss (dB)	- 6.4	1.0
21	Waveform Distortion Loss (dB)	0	0
22	Loss Through Radio System (dB)	- 1.5	0.2
23	Subcarrier Demodulation Loss (dB)	0	0
24	Bit Sync Detection Loss (dB)	0	0
25	Received Data Power (dBm)	-106.2	3.7
26	Symbol Rate (dB)      4 sym/sec	+ 6.0	0
27	Received $ST_{Sym}/N_o$ (dB)	+ 55.3	4.4
28	Required $ST_{Sym}/N_o$ (dB)      BER = $10^{-5}$	+ 11.5	1.0
29	Threshold Subcarrier Power (dBm)	-150.0	1.7
30	Performance Margin (dB)	+ 43.8	5.4

\* Carrier modulated by ranging and command subcarriers each at 1.1 rad peak.

telemetry link while the MAV is still attached. During docking with the ERV, the MAV is not oriented towards Earth and data are relayed to Earth via the ERV telemetry link. Except for these two times, the instrumented data will be transmitted to Earth by the MAV S-band telemetry system.

The total time from Lander separation to ERV docking is approximately 16 days. During this time the MAV is oriented towards Earth. The total time that Earth is in view of the MAV has not been determined; therefore, the total time available for data transmission has not been established. This will be required before a sample rate can be established for each measurement on the MAV. The present data transmission rate is 8-1/3 bps to Earth via the S-band DSN. This rate has not been verified since the establishment of symbol rates and formats are beyond the scope of this study.

Table VII-7 is the MAV measurement list for the subsystems. The events and parameters shown are necessary to monitor the MAV events during the 16-day period from Mars launch to rendezvous with the ERV. The list is preliminary with anticipated ranges. Final ranges can only be given after hardware requirements have been established. Data formats can be established after the ranges are finalized and the sample rates determined.

Frequency Allocations. The various telecommunications, command, tracking, and rendezvous/docking functions require a large number of links which must be coordinated under a unified frequency allocation plan. Basic telecommunications requirements for the Lander and MAV during surface operations, MAV in orbit, and MAV during rendezvous and docking with the Orbiter must be satisfied. Two-way links between the Orbiter and DSN and the Lander and DSN must be provided. The rendezvous and docking sensor and the MAV transponder include command and telemetry channels between the two vehicles. With the MAV in orbit, a tracking and command capability from Earth is required to circularize the orbit. Table VII-8 lists the various links, their respective functions, and the proposed frequency allocations. It is clear that the frequency separation between some links is extremely small and this needs to be further investigated before arriving at a firm, definitive frequency allocation plan. Furthermore, in the event of a dual launch where two orbiters and two landers are employed, it would be necessary to provide additional two-way links between the DSN and the second orbiter as well as the DSN and the second lander.

Table VII-7. MAV Measurement List

<u>Subsystem</u>	<u>Measurement Title</u>	<u>Range</u>	
Sample Canister	Canister Internal Temperature	-100 + 300°F	
	Canister Internal Pressure	2 mb + 1 bar	
	Canister Separation	1-Mated, 0-Separated	
	Canister Cover Lock	1-Mated, 0-Separated	
	Canister Weight	1-Empty, 0-Filled	
	Canister Boom Position	1-Stowed, 0-Extended	
Electrical	Solar Panels Deployed	1-Stowed, 0-Deployed	
	Solar Cell Voltage	0-30 V dc	
	Cell Array Current	0-1 A dc	
	Charge/Discharge Voltage	0-30 V dc	
	Battery Charge Current	0-1 A dc	
	Shunt Regulator Current	0-1 A dc	
	Battery Discharge Current	0-2 A dc	
	Load Bus Current	0-2 A dc	
	Battery Temperature	0-150°F	
Guidance and Command	Sun Sensor Roll and Yaw	0-360°	
	Mode Indication	1-Celestial, 0-Inertial	
	Computer Output	2 bps	
Transponder	Elevation Error Out	0-1 V	
	Azimuth Error Out	0-1 V	
	Signal Present	1-Present, 0-Absent	
	VCO Lockup	1-Locked Up, 0-Sweeping	
	Command Present	1-Present, 0-Absent	
	Decoder Output	0-1 V dc	
	Ranging Output	0-1 V dc	
	AGC Voltage	0-2 V dc	
	Power Amp Output	0-0.5 V	
	Oscillator Switch	1-On, 0-Off	
	Oscillator Temperature	50-200°F	
	Power Amp Temperature	50-200°F	
	Transponder Baseplate Temperature	50-200°F	
	Input Voltages	0-12 V dc 0-20 V dc 0-28 V dc	
		Telemetry Transmitter Power	0-4 W
		Telemetry Transmitter Drive Current	0-0.5 A dc
Data Handling Unit	A to D Reference Voltage	0-5 V dc	
	Baseplate Temperature	0-150°F	
Propulsion	Stage III Tank Pressure (2)	0-500 psia	
	Stage III Tank Temperature (2)	0-150°F	
	Stage III Nozzle Pressure (4)	0-200 psia	
	Stage II Solid Propellant Temperature	0-150°F	
	Stage II Separation	1-Mated, 0-Release	
	Stage II Ignition - Chamber Pressure	1-Burn, 0-Off	
	Stage I Solid Propellant Temperature	0-150°F	
	Stage I Separation	1-Mated, 0-Release	
Stage I Ignition - Chamber Pressure	1-Burn, 0-Off		

Table VII-8. UPLMO System Frequency Allocations

Link	Frequency, MHz	DSN Channel	Functions
DSN → MAV	2110.243	5 b	Command, 2-Way Doppler
MAV → DSN	2291.666	5 a	Telemetry, 2-Way Doppler
DSN → Orbiter	2117.746	27 f	Command, 2-Way Doppler
Orbiter → DSN	2299.814	27 e	Telemetry, 2-Way Doppler
DSN → Lander	2112.971	13 b	Command
Lander → DSN	2294.629	13 a	Telemetry
Orbiter → MAV	2282.480	----	Command, Rendezvous and Docking
MAV → Orbiter	2101.030	----	Telemetry, Rendezvous and Docking

Recommended Additional Studies. Two additional tasks related to MAV telecommunications are recommended for the next phase of work. Further consideration should be given to the possibility of having a stored ACS mode to search for Earth, if necessary, to bring the MAV to within 8 degrees of pointing toward Earth so that the DSN signal may be reacquired should the MAV lose it due to being off the proper attitude. An alternative is to provide an omni command link for the Earth/MAV link. Consideration should also be given to reliability tradeoffs since the baseline contains many single-string systems.

## 2. Lander Communications Subsystem

Requirements. Functional requirements of the Lander telecommunication subsystem were established assuming use of a direct S-band link between Earth and the Lander during operations on the Martian surface. These requirements are listed in Table VII-9.

Subsystem Description. A simplified block diagram of the Lander telecommunications subsystem is shown in Figure VII-4. Commands are initially received via the omni antenna and receiver. Once uplink command lock-up of the receiver/demodulator and decoder has been accomplished, the downlink transmitter and associated equipment can be activated for operation using the high gain antenna (HGA). The HGA and pointing control can be identical to the VO'75 equipment. Antenna pointing is under control of the GCSC. The balance of the telecommunications subsystem can be derived from the "light-weight" MAV telecommunications designs to save considerable weight, as compared to the present VL'75 designs. The 4-watt RF power amplifier is all solid state based on an MSC 3005 or 4005 output transistor operated at about 20 volts dc with an efficiency of 30%. The transponder (modulator exciter plus receiver) is the same as the MAV unit except for reduced carrier tracking loop bandwidth and without the receiver error channel equipment and the extra dual range frequency multiplier strings (needed only for MAV pointing and a 220/239 ratio needed only for MAV/Orbiter rendezvous). The two Lander receivers are identical. The command detector and decoder is identical with that of the MAV.

The telemetry data handling unit is assumed to be designed to accept both analog and digital inputs for multiplexing and formatting the downlink

Table VII-9. Lander Telecommunications Functional Requirements

1. Receive S-band transmissions from the Deep Space Network (DSN) while on the Martian surface and prior to MAV launch.
2. Transmit S-band signals to Earth with the transmit carrier coherently related to the receive signal by a ratio of 240/221 times the receive frequency (no transmission required after MAV launch).
3. Provide a capability for the following modes of communications at a maximum range of  $2.57 \times 10^8$  km (1.72 AU):
  - a. Receive commands from Earth at a rate of 4 symbols/second on an omni antenna to provide a Lander transmitter turn-on capability and means of controlling surface operations.
  - b. Using a high gain antenna to provide two-way Earth/Lander communications for the following:
    - 1) Simultaneous planetary ranging and engineering telemetry (8-1/3 bps was selected for engineering telemetry);
    - 2) Simultaneous command and downlink telemetry;
    - 3) Transmission of engineering data without ranging;
    - 4) Transmission of higher rate telemetry for scan camera or program storage readout (250 bps is the rate assumed).
4. Provide a telemetry subsystem capable of conditioning and multiplexing analog and digital inputs from Lander subsystems and MAV subsystems--the latter via an umbilical between MAV and Lander. A digital interface is assumed between MAV and Lander and between FAX camera and the telemetry subsystem.
5. Telemetry subcarrier and telemetry bit rate clocks are included in the telemetry data handling functions.
6. Provide a command subcarrier demodulation and decoding capability identical to Viking format and subcarrier waveforms. Command decoder output interface will be identical to Viking '75 for descriptive purposes.
7. Lander subsystems sequencing and power control functions will be provided by the Lander GCSC.
8. Storage of data for delayed telemetering, if required, will be provided as part of the GCSC function.



(to Earth) data. This unit can also be identical to the MAV unit for cost savings although the MAV as presently conceived transmits at a single data rate; therefore, this commonality approach would impose a slight weight penalty on the MAV. Weight, size, and power estimates for the telecommunications subsystem are given in Table VII-10 and are based on estimates of available 1981 technology.

In order to size the Lander transmitter and high gain antenna requirements, design control tables (link calculations) were prepared for telemetry, command, and ranging simultaneously with telemetry for the Lander/Earth link. In preparing these tables certain approximations were made in determining energy per bit requirements and losses due to subcarrier waveform, radio loss, bit sync loss and subcarrier demodulator loss. These were estimated based on VO-75 and Viking Lander link calculations and lumped rather than performing the detailed calculations for each item.

Table VII-11 is the design control table for the 250 bps Lander-to-Earth link based on a 4-watt S-band transmitter, the Viking Lander HGA and Viking Lander block coding (32, 6) using PCM/PSK/PM modulation. Performance margins exceed the sum of the adverse tolerances for both the carrier and data channels.

Table VII-12 is the design table for the Earth-to-Lander command link using the DSN 64 meter net, the 10 kW command transmitter, and the Lander low gain antenna. Performance margins exceed the sum of adverse tolerances by 2 to 3 dB. Coding and format are the same as for the Viking Lander.

Table VII-13 is the design control table for simultaneous ranging and 8-1/3 bps telemetry for the Earth/Lander up and downlinks using the 64 meter net, 10 kW DSN transmitter, and the Lander HGA. Margins are 5 dB or greater than the sum of the adverse tolerances for this mode of operation.

From the calculations in Tables VII-11, -12, and -13, one can conclude that the design is adequate for the required performance depicted in Table VII-14.

Table VII-15 lists the telecommunications equipment which must be powered during various phases of Lander operations. Related equipment on both the Lander and MAV are shown.

Table VII-10. Lander Telecommunications Physical Properties

Quan.	Component	Average dc Power watt	Weight, kg (lb)	Size, cm (in.)
1	Low Gain (Omni) Antenna		0.14 ( 0.3)	8.89 (3.5) dia.
1	High Gain Antenna (HGA) & Mast, same as Viking Lander		7.48 (16.5)	76.2 (30) dia.
1	Circulator/Diplexer		0.32 ( 0.7)	
1	S-band Power Amplifier	13.0	0.23 ( 0.5)	7.62x13.97x20.32 (3 x 5.5 x 8)
	S-band Receiver & dc/dc Conv.	3.5	0.36 ( 0.8)	
	S-band Modulator/Exciter	2.3	0.27 ( 0.6)	
	Command Detector	1.0	0.14 ( 0.3)	
	Command Decoder	0.5	0.14 ( 0.3)	
	Case for Above		0.50 ( 1.1)	
1	S-band Receiver (Omni Command)	3.5	0.54 ( 1.2)	7.62x13.97x10.16 (3 x 5.5 x 4)
1	HGA Drive (VL'75)	0.59	Incl. in Antenna	Note 1
1	HGA Controller (VL '75)	2.0	1.81 ( 4.0)	Note 1
1	Power Pre-regulator (85% eff)	4.0	1.45 ( 3.2)	
1	Telemetry Data Handling Unit	2.0	1.68 ( 3.7)	5.08x5.08x10.16 (2 x 2 x 4)
Note 1. Same as Viking circuitry.				

Table VII-11. Lander-to-Earth Telemetry Design Control Table - Surface Operations

No.	Parameter	Nominal Value	Adverse Tolerance	Notes
1	Total Transmitting Power (dBm)	+ 36.0	0.6	4 watts
2	Transmitting Circuit Loss (dB)	- 0.9	0.2	
3	Transmitting Antenna Gain (dB) (Viking Lander HGA)	+ 21.1	0.3	1 dB Pointing
4	Communications Range Loss (dB) 2292 MHz	-267.9	0	257 x 106 km
5	Atmospheric Absorption & Defocusing Losses (dB)	0	0	
6	Polarization Loss (dB)	- 0.1	0	
7	Multipath and Other Losses (dB)	0	0	
8	Receiving Antenna Gain (dB)	+ 61.1	0.4	64 Meter Net
9	Receiving Circuit Loss (dB)	0	0	
10	Net Loss (dB) (2+3+4+5+6+7+8+9)	-186.4	0.9	
11	Total Received Power (dBm) (1+10)	-150.4	1.5	
12	Receiver Noise Spectral Density (dBm/Hz)	-184.2	0.5	25° Elev.
13	Total Received Power/ $N_0$ (dBm·Hz) (11-12)	+ 33.8	2.0	
<u>Carrier Tracking</u>				
14	Carrier Power/Total (dB)	- 8.0	2.7	$\theta = 1.16$ Rad.
15	Additional Carrier Losses (dB)	- 0.1	0	
16	Threshold Tracking Bandwidth - $2B_{LO}$ (dB)	+ 10.8	0	
17	Threshold SNR (dB)	+ 10.0	0	
18	Performance Margin (dB) (13+14+15-16-17)	+ 4.9	4.7	
<u>Data Channel</u>				
19	Data Power/Total (dB)	- 0.8	0.5	$\theta = 1.16$ Rad.
20	Additional Data Channel Losses (dB)	- 2.0	0.3	Estimated
21	Data Bit Rate - bps (dB)	+ 24.0	0	250 bps
22	Threshold Energy Per Data Bit - $E_b/N_0$ (dB)	+ 3.0	0	WER = $10^{-2}$
23	Performance Margin (dB) (13+19+20-21-22)	+ 4.0	2.8	

Conditions: 1. PCM/PSK/PM modulation.

2. Block coding (32, 6), block decoding at the DSN.

3. Maximum Earth-Mars range used in No. 4.

4. Data channel losses (No. 20) include losses due to subcarrier waveform distortion, radio loss, bit synchronization loss, and subcarrier demodulator loss.

Table VII-12. Earth-to-Lander Command Design Control Table - Surface Operations

No.	Parameter	Nominal Value	Adverse Tolerance	Notes
1	Total Transmitting Power (dBm)	+ 70.0	0	10 kW
2	Transmitting Circuit Loss (dB)	0	0	
3	Transmitting Antenna Gain (dB)	+ 60.4	0.7	≈ 4 Meter Net
4	Communications Range Loss (dB)	-267.1	0	257 x 10 <sup>6</sup> km
5	Atmospheric Absorption & Defocusing Losses (dB)	0	0	
6	Polarization Loss (dB)	- 0.4	0	
7	Multipath. and Other Losses (dB)	0	0	
8	Receiving Antenna Gain (dB)	+ 1.3	0.5	LGA, Omni
9	Receiving Circuit Loss (dB)	- 1.3	0.2	-3.2 dB Pointing
10	Net Loss (dB) (2+3+4+5+6+7+8+9)	-207.2	1.4	
11	Total Received Power (dBm) (1+10)	-137.2	1.4	
12	Receiver Noise Spectral Density (dBm/Hz)	-167.5	0.8	
13	Total Received Power/N <sub>0</sub> (dBm·Hz) (11-12)	+ 30.3	2.2	13000 K
<u>Carrier Tracking</u>				
14	Carrier Power/Total (dB)	- 2.5	0.2	
15	Additional Carrier Losses (dB)	0	0	
16	Threshold Tracking Bandwidth - 2B <sub>L0</sub> (dB)	+ 12.6	0.5	
17	Threshold SNR (dB)	+ 10.0	0	
18	Performance Margin (dB) (13+14+15-16-17)	+ 5.2	2.9	
<u>Data Channel</u>				
19	Data Power/Total (dB)	- 4.0	0.2	
20	Additional Data Channel Losses (dB)	- 1.5	0.2	
21	Symbol Rate - SPS (dB)	+ 6.0	0	
22	Threshold Energy Per Symbol - E <sub>s</sub> /N <sub>0</sub> (dB)	+ 11.5	1.0	4 SPS
23	Performance Margin (dB) (13+19+20-21-22)	+ 7.3	3.6	SER = 10 <sup>-5</sup>

Table VII-13. Telecommunications Design Control Table - Planetary Ranging with Downlink Telemetry (Lander)

No.	Parameter	Nom. Value	Adverse Tolerance
1	Total Transmitter Power (dBm)                      10 kW	+ 70.0	0.0
2	Transmitting Circuit Loss (dB)	0.0	0.0
3	Transmitting Antenna Gain (dB)                      64-m DSN	+ 60.4	- 0.7
4	Transmitting Antenna Pointing Loss (dB)	0.0	0.0
5	Space Loss: $F=2110.6$ MHz; $R=257 \times 10^6$ km (dB)	-267.1	0.0
6	Polarization Loss (dB)	- 0.4	0.0
7	Receiving Antenna Gain (dB)                      VL HGA	+ 21.1	- 0.3
8	Receiving Antenna Pointing Loss (dB)	- 1.0	0.0
9	Receiving Circuit Loss (dB)	- 1.3	- 0.5
10	Net Circuit Loss (dB)	-188.3	- 1.5
11	Total Received Power (dBm)	-118.3	- 1.5
12	Receiver Noise Spectral Density (dBm/Hz) Noise Temperature ( $^{\circ}$ K)	-167.5 1360.0	+ 0.7 +240.0
13	Carrier Modulation Loss (dB)	- 8.6	- 1.4
14	Received Carrier Power (dBm)	-126.9	- 2.9
15	Carrier APC Noise BW: $2B_{LO} = 18 \pm 2$ Hz (dB·Hz)	+ 12.6	+ 0.5
<u>Carrier Performance</u>			
16	Carrier SNR in $2 B_{LO}$ (dB)	+ 28.0	- 4.1
17	Carrier Threshold SNR in $2 B_{LO}$ (dB)	+ 8.7	0.0
18	Threshold Carrier Power (dBm)	-146.2	+ 1.2
19	Performance Margin (dB)	+ 19.3	+ 4.1
<u>Turnaround Ranging</u>			
20	Ranging Modulation Loss: 1.19 Rad. $\pm 10\%$ (dB)	- 0.6	- 0.3
21	Ranging Signal Power (dBm)	-118.9	- 1.8
22	Ranging Noise BW (dB·Hz)	+ 61.8	+ 0.8
23	SNR at Limiter Input (dB)	- 13.2	- 3.3
24	Limiter Suppression (dB)	- 15.2	- 3.3
25	Radio Assembly Output Power (dBm)	+ 36.0	- 0.6
26	Transmitting Circuit Loss (dB)	- 0.9	- 0.2
27	Transmitting Antenna Gain (dB)                      VL HGA	+ 22.1	- 0.3
28	Transmitting Antenna Pointing Loss (dB)	- 1.0	0.0

- Continued -

Table VII-13. Telecommunications Design Control Table - Planetary Ranging with Downlink Telemetry (Lander) (continued)

No.	Parameter	Nom. Value	Adverse Tolerance
<u>Turnaround Ranging (concluded)</u>			
29	Space Loss: $f=2292$ MHz; $R=257 \times 10^6$ km (dB)	-267.9	0.0
30	Polarization Loss (dB)	0.0	0.0
31	Receiving Antenna Gain (dB) 64-m DSN	+ 61.3	- 0.5
32	Receiving Antenna Pointing Loss (dB)	0.0	0.0
33	Receiving Circuit Loss (dB)	0.0	0.0
34	Net Circuit Loss (dB)	-186.5	- 1.0
35	Total Received Power (dBm)	-150.5	- 1.6
36	Receiver Noise Spectral Density (dBm/Hz)	-183.8	+ 0.5
	Noise Temperature ( $^{\circ}$ K)	30.0	+ 3.9
37	Carrier Modulation Loss (dB)	- 4.1	- 1.2
38	Received Carrier Power (dBm)	-154.6	- 2.8
39	Carrier APC Noise BW: $2B_{LO}=12$ Hz(+0,-20%)(dB·Hz)	+ 10.8	0.0
<u>Carrier Performance - Data Demodulation</u>			
40	Carrier SNR in $2 B_{LO}$ (dB)	+ 18.4	- 3.3
41	Carrier Threshold SNR in $2 B_{LC}$ (dB)	+ 10.0	0.0
42	Threshold Carrier Power (dBm)	-163.0	+ 0.5
43	Performance Margin (dB)	+ 8.4	- 3.3
<u>Ranging Channel</u>			
44	Ranging Modulation Loss: 0.45 Rad. $\pm$ 12% (dB)	- 10.4	- 2.0
45	Total Ranging Suppression (dB)	- 25.6	- 5.3
46	Ranging Signal Level (dBm)	-176.1	- 6.9
47	Ranging SNR in 1 Hz (dB)	+ 7.7	- 7.4
48	Required SNR in 1 Hz (dB) (4.6 min.; $T_{ACQ}$ nom.)	- 6.0	0.0
49	Performance Margin (dB)	+ 13.7	- 7.4
50	Ranging Code Acquisition Time (sec) $T_{ACQ} = 70 / (\text{SNR}) \text{ 1Hz, (80 sec min)}$	+ 80.0	+ 80.0
- Continued -			

Table VII-13. Telecommunications Design Control Table - Planetary Ranging with Downlink Telemetry (Lander) (concluded)

No.	Parameter	Nom. Value	Adverse Tolerance
<u>Telemetry Data Channel</u>			
51	Subcarrier Modulation Loss (dB)	- 3.8	- 1.1
52	Waveform Distortion Loss (dB)	0.0	0.0
53	Loss Through Radio System (dB)	- 0.5	- 0.2
54	Subcarrier Demodulation Loss (dB)	- 0.1	- 0.1
55	Bit Sync Detection Loss (dB)	- 0.1	0.0
56	Received Data Power (dBm)	-155.0	- 3.0
57	Bit Rate (8-1/3 bps) (dB·bps)	+ 9.2	0.0
58	Received $ST_B/N_c$ (dB)	+ 19.6	- 3.5
59	Required $ST_B/N_o$ (dB) <span style="margin-left: 100px;">BER = <math>5 \times 10^{-3}</math></span>	+ 5.2	0.0
60	Threshold Subcarrier Power (dBm)	-169.4	+ 0.5
61	Performance Margin (dB)	+ 14.4	- 3.5

Table VII-14. Lander Telecommunications Performance

Command Error Rates	1 in $10^5$ bit errors
Science Error Rates	1 in $10^2$ word errors
Engineering Telemetry	5 in $10^3$ bit errors
Ranging Code Acquisition Time	4.6 minutes

Table VII-15. Lander/MAV Equipment Operating Sequence for Surface Operations

	Standby	2 Way Communications Science (TV)	2 Way Communications Lander Engineering and Lander Update	2 Way Communications MAV Engineering	2 Way Communications MAV Update	2 Way Communications MAV Launch Attitude	2 Way Communications MAV Checkout and Sample Acquisition
<b>LANDER EQUIPMENT</b>							
<u>Telecommunications</u>							
S-band Power Amplifier		X	X	X	X	X	X
S-band Receiver Transponder		X	X	X	X	X	X
S-band Mod/Exciter							
Command Detector	X	X	X	X	X	X	X
Command Decoder	X	X	X	X	X	X	X
S-band Receiver (Primary)	X	X	X	X	X	X	X
HGA Controller		X	X	X	X	X	X
HGA Drive		X	X	X	X	X	X
Power Freregulator		X	X	X	X	X	X
Telemetry Data Handling Unit		X	X	X	X	X	X
<u>Other</u>							
GCSC		X	X	X	X	X	X
TV Camera		X					
Other Subsystem Sensors			X			X	X
<b>MAV EQUIPMENT</b>							
Telemetry Data Handling (only)				X	X		X
All Telecommunications						X	0
<u>Other MAV</u>							
GCSC				X	X	X	X
Other Subsystem Sensors				X		X	0
X - Powered 0 - On During Checkout of that Subsystem							

Two other approaches were considered for Lander/MAV communications during surface operations. These were:

1. Use the MAV S-band equipment for surface communications with Earth thus eliminating Lander S-band equipment;
2. Use a UHF relay between Lander and Orbiter for surface communications with Earth.

The first option would require mounting an articulated HGA and LGA on the MAV for use while on the surface or tying the Lander HGA and LGA to the MAV S-band system. This equipment, even though it could be jettisoned if located on the MAV, would severely complicate the MAV telecommunications and would require additional 3rd stage MAV weight due to the RF interfaces. For these reasons the first option was discarded.

The second option (use of Viking '75 type UHF relay to Orbiter and add an Orbiter-to-Lander command link) was discarded due to the poor relay communications opportunities associated with an elliptical ( $10^3 \times 10^5$  km) Orbiter capture orbit (4-day period) as well as the limited range and complications of relaying data to and from Earth via the Orbiter.

Table VII-16 is a summary table of the telecommunications link margins for the four MAV conditions. The weakest RF link is when the MAV is on the surface. The 4-watt transmitter adequately handles 250 bps but 5 or 8 watts would improve this link. The command link is limited by the available SNR of the command receiver. The uplink transmitted power and antenna gain can not be increased; therefore, a lower receiver noise temperature must be achieved in order to improve the command link margin. The other telemetry and command links have satisfactory margins.

Recommended Additional Studies. Additional studies should be conducted before finalizing the telecommunications system for the Lander/MAV during surface operations. Additional thought should be given to Lander operations and timelines in considering time required to update the MAV (number of command words divided by rate capability, etc.) and to verify the command program stored in the MAV. Also time to check out the MAV prior to launch and to verify attitude should be estimated including any 2-way Earth-Mars time delays, etc., to verify timelines for trouble and for power profile verifications. While accomplishing this, one should verify that the bit rates are indeed adequate.

Table VII-16. MAV Telecommunications Link Margins

Link	MAV Condition	Function Rate	Nominal Margin for Data & Carrier, dB	Comment
DSN/Lander	MAV on Surface	Command 4 sps	7.3	Improve margin with better receiver
Lander/DSN		Telemetry 250 bps	5.2	
DSN/MAV	MAV in Orbit	Command 4 sps	4.0 4.9	Satisfactory
MAV/DSN		Telemetry 8-1/3 bps	19.6 17.5	
Orbiter/MAV	MAV in Rendezvous	Command 4 sps	4.5 4.4	More RF power would improve margin
MAV/Orbiter		Telemetry 8-1/3 bps	43.8 24.4	
DSN/Orbiter	MAV in ERV	Command 4 sps	38.5 21.0	Satisfactory
Orbiter/DSN		Telemetry 4 kbps	16.0 16.7	
			9.0 11.7	Satisfactory

## B. POWER

The two primary concerns of the power system evaluation portion of this study were to investigate the feasibility of supplying the power required by the Mars Ascent Vehicle (MAV) during ascent, rendezvous and docking, and to establish any modifications required to the orbiter. A design was defined for the MAV permitting power and energy needs to be identified. Also, equipment modifications to existing Viking Lander and Orbiter vehicles were identified. Based on these modifications and known power requirements for the 1975 Viking vehicles, it was possible to define new power totals for the MSSR mission. The Earth Return Vehicle is assumed to be based upon existing technology, but since the design was not detailed in this study, power requirements were not identified quantitatively.

### 1. Baseline Designs

Viking Orbiter (VO) 1975 Power Subsystem. This design utilizes arrays of photovoltaic cells arranged on four double-section, folding solar panels to furnish primary power for all sun-oriented operations. Two identical nickel-cadmium batteries are used as a secondary source of power for off-sun operations and to share the load when power demand exceeds the solar array capacity. Redundant power conditioning and distribution functions are provided with two battery chargers, two booster regulators, two 2.4 kHz inverters, two 400-Hz 3-phase inverters, two 30-Vdc converters, and associated power source logic and control and switching functions. The power subsystem provides the VO with 2.4 kHz single phase, 400-Hz three-phase, regulated dc (30 and 55.2 V) and unregulated dc power. Unregulated dc power is also provided to the Viking Lander Capsule.

It is expected that the VO'75 power system will be used without change for the URDMO mission except for modification of the distribution system to accommodate removal of the orbital science, the scan platform, data storage and the addition of a rendezvous radar requiring 14 watts.

Viking Lander Power Subsystem. Two radioisotope thermoelectric generators (RTGs) rated at 35 watts each provide prime power. Four 8 ampere hour nickel cadmium batteries provide energy storage to carry peak loads beyond the RTGs capability. The batteries are maintained in a discharged state during interplanetary cruise and charged using orbiter

supplied power prior to deflection into the Mars entry trajectory. The RTGs are shorted out and the Lander Capsule is supplied from the Orbiter until pre-separation checkout when the short is removed and power is transferred to the RTGs.

In order to obtain mass and volume allowances to permit installation of the Mars Scent Vehicle (MAV) for the URDMO mission it is necessary to reduce the rating of the Lander power subsystem. This was achieved by using only three out of the four 8 ampere hour batteries used for the 1975 mission and by replacing the two 35-watt RTGs by two 20-watt RTGs of higher specific output. Since 1968, the Atomic Energy Commission have sponsored a technology contract to develop a new high efficiency, high temperature material. One of these, TPM, is a selenide base material with a potential efficiency of twice that of presently used materials. A preliminary design has been described for a 20-watt generator operating with a moderate temperature of 800°C at the thermoelectric hot junction. This generator would develop an efficiency of 8 percent and have a mass of 5.5 kilograms.

Mars Ascent Vehicle Power Subsystem. The MAV is mass critical and emphasis is placed on holding power levels and every demands to a minimum and using advanced technology. Also, MAV components must be capable of undergoing dry heat sterilization prior to Earth launch. Due to the mission duration it is necessary from a mass optimization viewpoint to use a solar cell/battery system. High efficiency violet cells are incorporated into a 0.163 square meter (1.75 sq ft) solar array. These solar cells have an output of 12.14 watts at a solar distance of 1.44 AU. Sixteen 3-ampere hour nickel-hydrogen cells provide peak power capability. (The nickel hydrogen battery is under development, see the technology development discussion at end of section.) The shunt regulated circuit arrangement is shown in Figure VII-5. The shunt regulator acts as a variable load to control voltage and is enabled by the control unit when the array power exceeds load current and battery charging needs. When the bus voltage decreases slightly due to load demand exceeding array capability, the discharge regulator is enabled and the battery supports the bus through the step-up discharge regulator. Loads are supplied directly from the 28 volt bus except for the S-band power amplifier supplied from the converter and the rate gyros operating from the inverter.

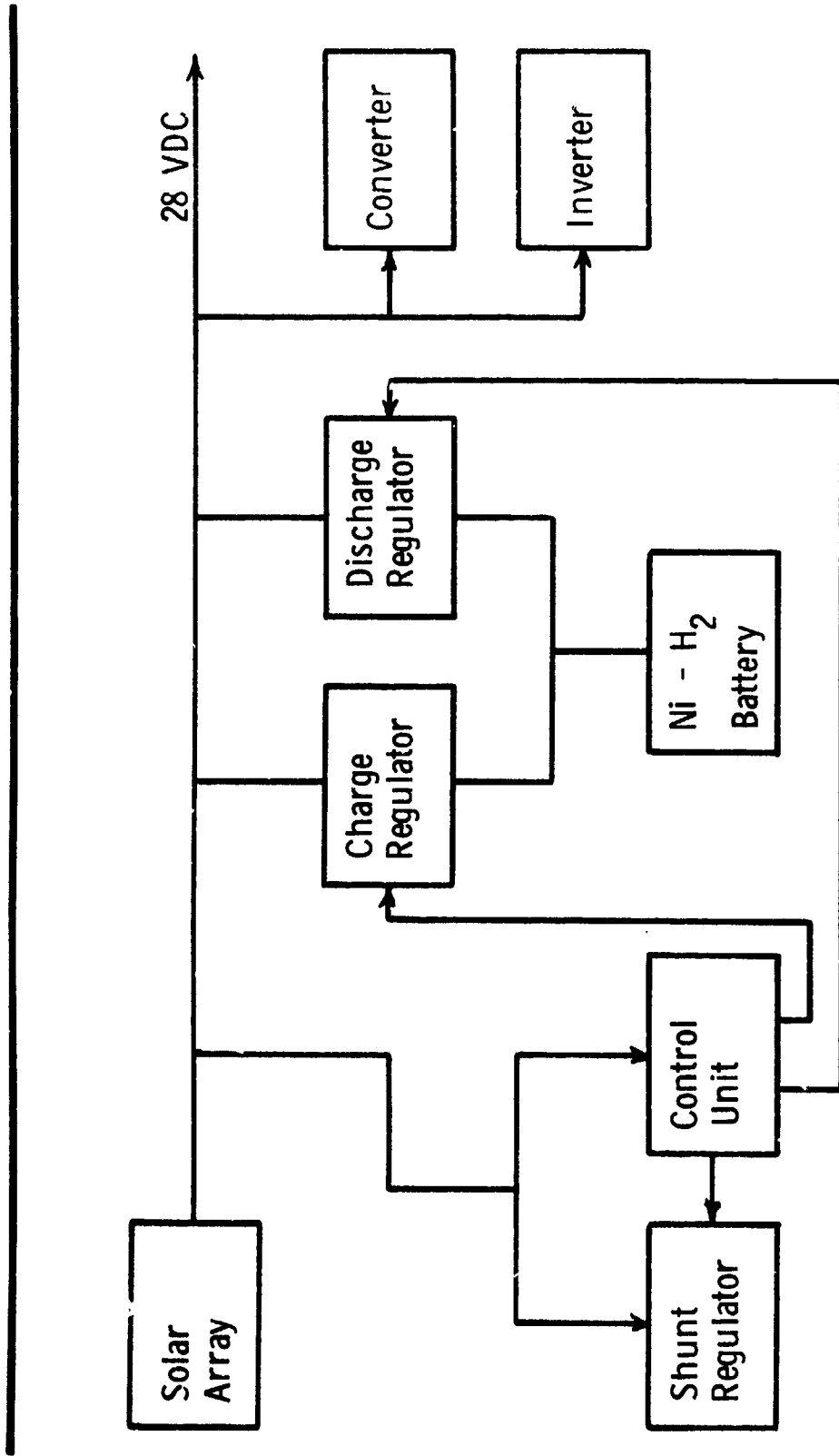


Figure VII-5 MAV Power Subsystem

Earth Return Vehicle Power Subsystem. Although specific requirements have not been established for the Earth Return Vehicle (ERV) it is expected to utilize a solar cells body-mounted on a spinning vehicle. The ERV will carry the Earth Entry Capsul (EEC) incorporating a power control unit and a beacon. Both of these devices require a battery supply which is discussed in Chapter IX.

## 2. Power and Energy Requirements

Viking Orbiter. Viking Orbiter modifications include removal of science associated items including all orbiter science, the scan platform, and the data storage system. This results in the following power needs during orbit cruise:

Table VII-17 Orbiter Power Allocation

<u>Item</u>	<u>Power (W)</u>
Engineering Loads	165.90
Science Loads	.00
Total 2.4 kHz Inverter Load	165.90
Inverter Efficiency	.902
Total 2.4 kHz Inverter Input	183.92
Total Booster Regulator Load	200.92
Booster Regulator Efficiency	.899
Total Booster Regulator Input	223.50
Total Unregulated Power	408.10
System Efficiency	.982
Total Raw Power	415.58

When adjustment is made for operation at two percent off the maximum, a power margin of 196.1 watts is attained. This is obtained from using the solar array's rating of 620 watts. For the 1981 mission the distance to the Sun is less than that for the 1975 mission; 1.44 AU vs 1.66 AU. This will result in a greater solar array capacity for the 1981 mission. 777.5 watts, giving additional margin.

During terminal rendezvous with the MAV a small radar is in operation. This requires 14 watts of power. During orbit insertions, orbit trim and terminal rendezvous, the solar panels of the Orbiter may lose their orientation to the Sun, necessitating operation from the battery system. Listed

below are energy requirements which may be imposed upon the battery together with the resulting margins.

Table VII-18 Orbiter Energy Requirements and Margins During Maneuvers

<u>Item</u>	<u>Battery (Wh)</u>	
	<u>Energy Needs</u>	<u>Energy Margins*</u>
Orbit Insertion Maneuver Turn	250.7	1651.3
Orbit Insertion Maneuver Burn	334.8	1567.2
Orbit Trim Sequence (3 burns, 3.5 hr Total Duration)	1127.5	774.5
Terminal Rendezvous (3.0 hr duration)	966.4	935.6

\* TN-3770004, Issue 23, Viking Orbiter Power Status Report, June 1, 1973, gives power and energy requirements for VO'75 for different operational modes. Adjustments of Operational Mode 29 (3.6 hr Solar Occultation) were used in setting values for the orbit trim sequence and terminal rendezvous.

The tabulation shows that less than one-half of the energy in the batteries (1902 Wh) is required for the first two operational modes. Thus, these operations can be carried out even if only one battery is connected. The load can be adequately provided with power for the last two operational modes if both batteries are on the bus. Whether the load could be carried in the event of failure of one battery and its removal from the bus will depend upon the amount of load sharing with the solar array. Determining this will require definition of panel orientation with respect to the Sun during maneuvers.

Mars Lander. Figure VII-6 shows the Lander power requirements during the time period from separation of the Lander from the Orbiter (-4.17 hours) to touchdown. Total energy requirements during the deorbit coast period amount to 624 watt hours of which 427 watt hours is allocated to the guidance and control subsystem. Energy available from the RTG/battery subsystem is 680 watt hours leaving a margin of 56 watt hours (based upon an allowable depth of discharge for the batteries of 75 percent). Landed operations are reflected by the power profile shown in Figure VII-7. Most of the energy (2532 watt hours) is required to maintain command capability for the Lander. Two-way communication, transmitting to Earth an image of the site from which

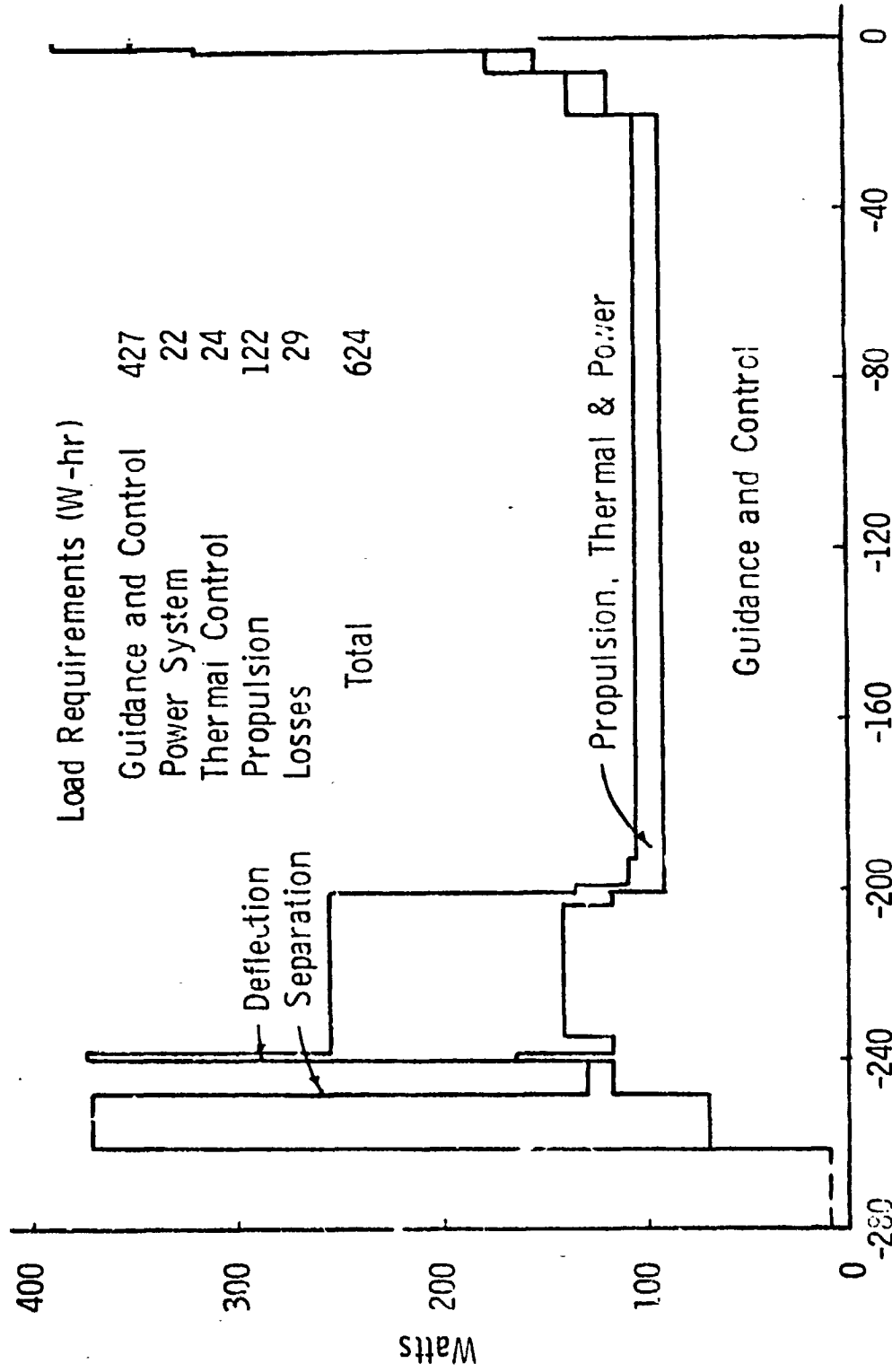


Figure VII-6 Lander Deorbit Coast Energy Allocation

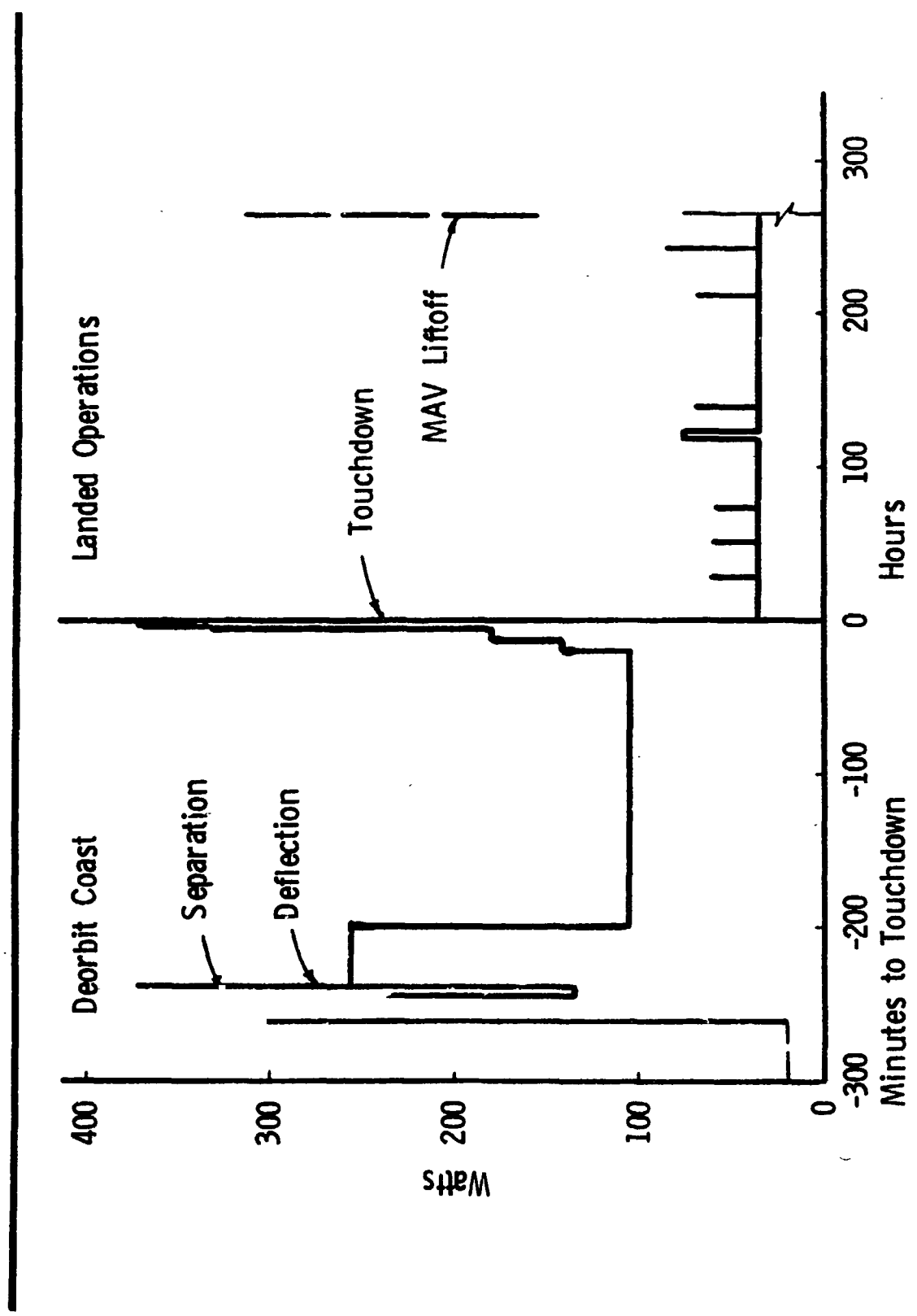


Figure VII-7 Lander Power Profile

the soil sample is to be taken, science and MAV positioning provide the balance of power needs during the 263.75 hours of landed operations. The total energy required for this period is 2744 watt hours giving an average load of 10.4 watts. These together with thermal control needs can be provided adequately by the two 20-watt RTGs.

Mars Ascent Vehicle. The major power requirement during the MAV mission is set by operation of the S-band transponder during doppler measurements used for trajectory corrections. This is illustrated in Figure VII-8. In order to operate within the capability of the power subsystem, limited in rating because of mass restrictions, equipment operates at high power during these periods for only 50 minutes of each 3.5 hour orbit. The battery supplements solar power during these tracking periods and is permitted a discharge depth of 75 percent prior to being recharged during the remainder of each orbit.

Rendezvous and docking with the orbiter is accomplished in approximately three hours from the time the MAV and orbiter are reoriented to point toward each other. During this period the solar cell panels may be displaced from their normal orientation to the Sun by an average of as much as 45 degrees, but the S-band power amplifier operates at reduced power lowering energy needs and the battery again supplements the solar array power. Table VII-19 lists the power utilization items and their power needs for both the orbit tracking and the rendezvous and docking modes of operation.

Table VII-19 MAV Power Utilization

<u>Item</u>	<u>Power Mode (Watts)</u>		
	<u>High</u> (In Orbit-During Dopple Tracking)	<u>Low</u> (Rendezvous & Docking)	<u>Standby</u> (In Orbit-Between Tracking Periods)
S-Band Power Amplifier	13.0	2.5	
S-Band Modulator Exciter	2.3	2.3	
S-Band Receiver	3.5	3.5	
Command Detector	1.0	1.0	
Command Decoder	0.5	0.5	
Telemetry Unit	1.0	1.0	
Sun Sensor	0.35	0.35	0.35
Valve Drive Amplifier	(15 W Peak)		
Rate Gyros (2)	3.3	3.3	
Rate Gyros (1)	1.7	1.7	1.7
Computer	4.0	4.0	0.5
Inverter Losses	<u>1.05</u>	<u>1.05</u>	<u>0.35</u>
	31.7	20.2	2.9

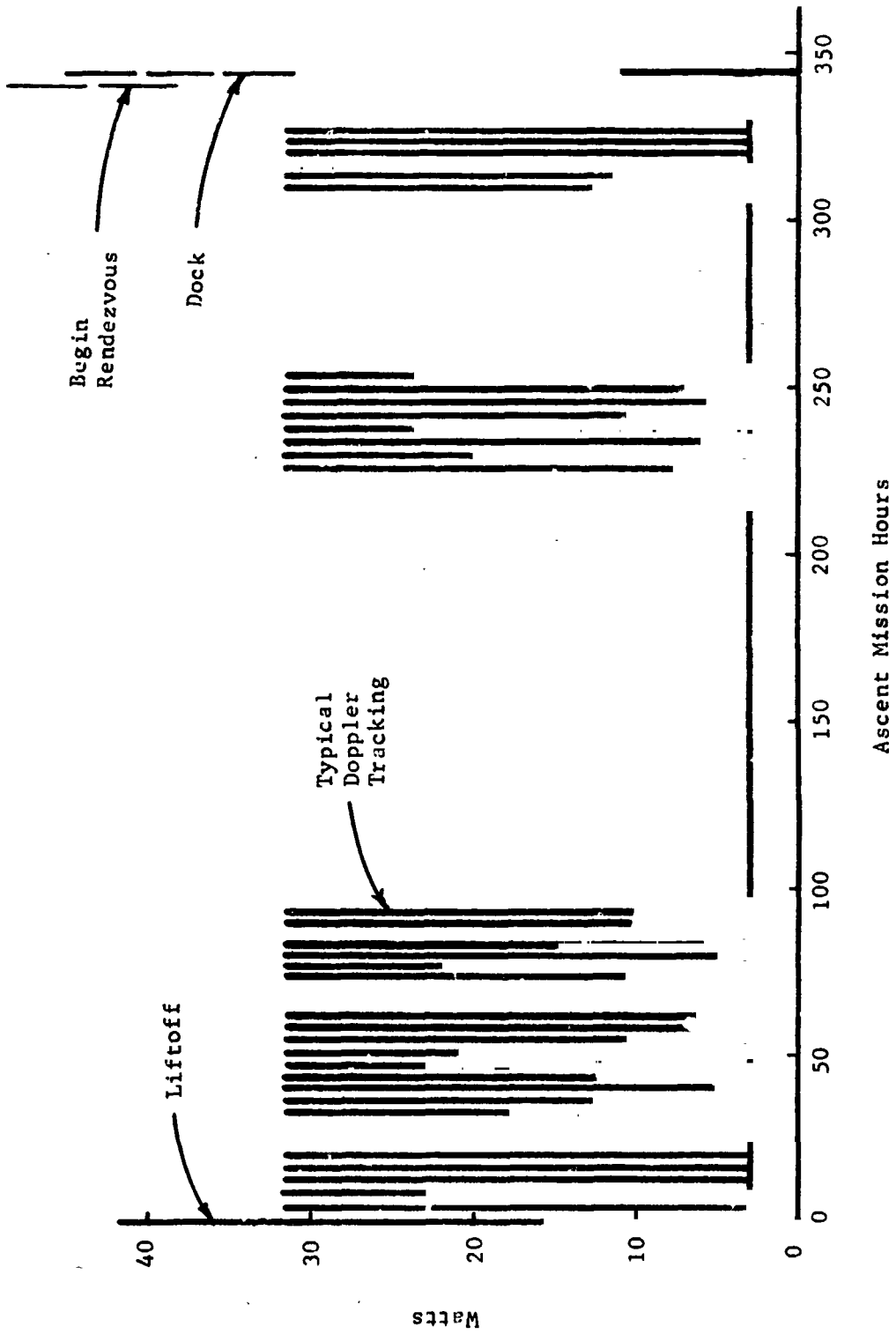


Figure VII-8 MAV Power Profile

3. Equipment Development Impacting System Availability. Although solar cells have been a key device in the space program, little improvement in efficiency occurred over a period of ten years. With the space program being virtually the only market for solar cells, production capacity has exceeded the demand. This has narrowed the solar cell producers from five to two companies and has limited research and funding. Recently as a result of independent work at COMSAT Laboratories, improvements in efficiency from 11 percent to 13 percent have been reported. This was achieved by extending the spectral response from 0.5  $\mu$ m to 0.3  $\mu$ m. The mechanisms involved were elimination of the highly damaged "dead layer" found on the surface of the conventional photocell and providing a fine electrode current collection geometry. This improved solar cell is called the "violet cell".

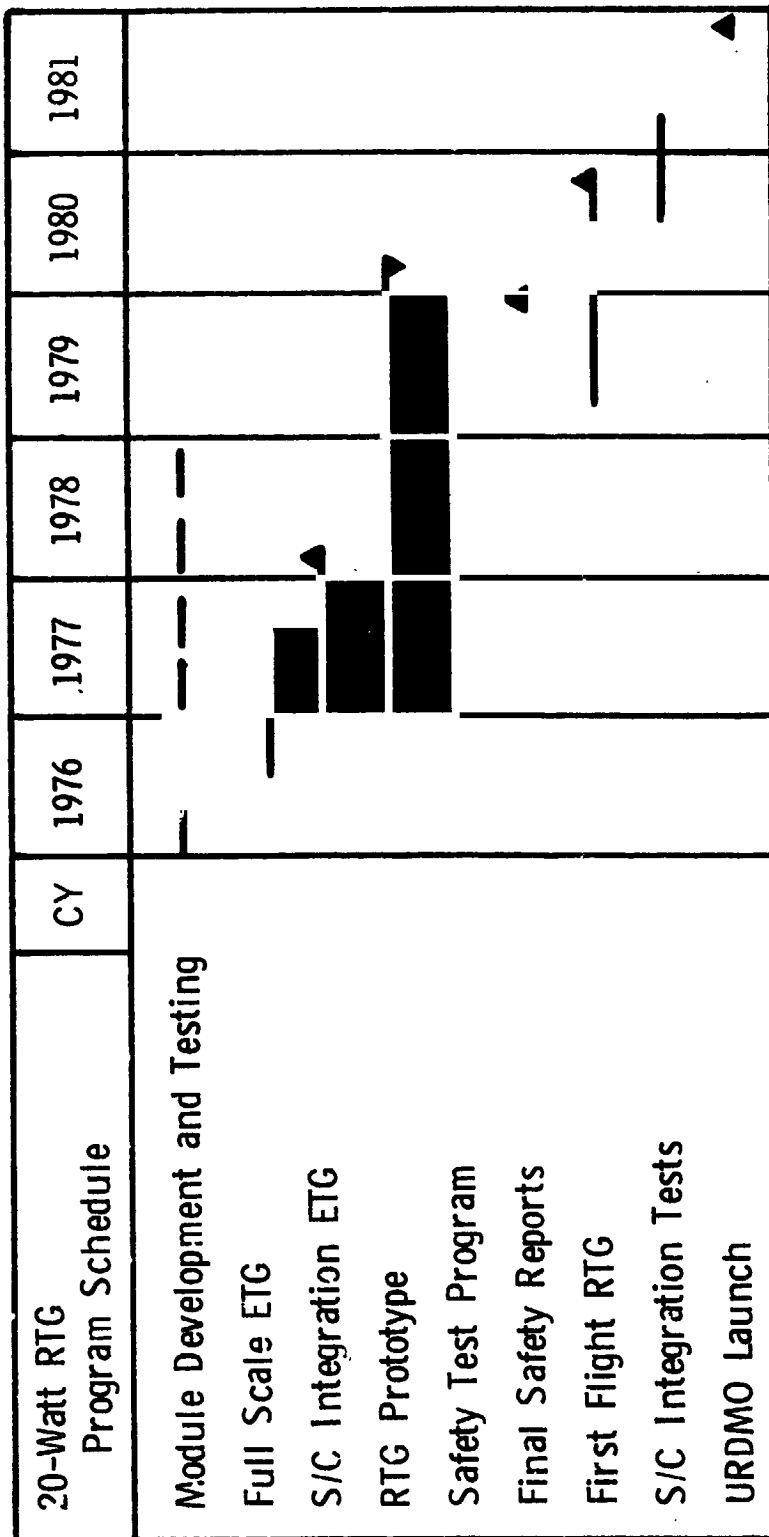
Progress has also continued in fabrication of lightweight arrays by use of thin coverslides and solar cells mounted on lightweight substrates. Solar cells having a titanium-palladium-silver contact system were resistance welded together using silver-plated molybdenum interconnections. Solar cell modules using this technique were fabricated and thermally shocked from  $-196^{\circ}\text{C}$  to  $+200^{\circ}\text{C}$  through 500 cycles. No failures were found upon completion of tests. The top limit far exceeds the  $125^{\circ}\text{C}$  level required for sterilization.

Work now underway by several manufacturers promise to make available two types of secondary batteries in addition to the widely used nickel cadmium. The new cells have an energy density capability between 55 and 150 W-hr/kg and will suffer no capacity loss with sterilization. The cells are built combining either a nickel or silver electrode with the long-life hydrogen fuel cell electrode. Hydrogen under pressure is consumed during discharge and released upon charging. The cell is not damaged by overcharge simplifying control. Work on the nickel-hydrogen cell has been sponsored by COMSAT for use on communications satellites.

In the RTG area a selenide base thermoelectric material, developed under AEC sponsorship, offers twice the efficiency of previous materials. Efficiencies to between 14 and 15 percent are predicted for these materials when operated at  $1000^{\circ}\text{C}$ . For a small generator, operation at  $800^{\circ}\text{C}$  with an 8 percent efficiency should be readily achievable.

The thermoelectric couple utilizing this material is composed of two selenide compounds. The p-leg of the couple is fabricated from copper selenide while the n-leg is made from gadolinium selenide. The materials have been under development since 1968 by the Minnesota Mining and Manufacturing Company (3M), working under a technology contract with the Atomic Energy Commission. The technology for the p-leg is well in hand but more effort is needed on the n-leg material to achieve full capabilities. The n-leg material is refractory in nature and is more difficult to bond than the p-leg. Tungsten is used as contacts on the hot junctions. Consequently at this stage of development it appears possible to build a generator using the selenides, which would operate at 800°C on the hot junctions and achieve 8 percent efficiency. This generator, however, would use pressure rather than bonded contacts on the hot side of the junctions. This arrangement was used on the SNAP-27 and other earlier generators. Later it is expected that technology will be developed to the point where generators yielding 10 percent efficiency and operating at 1000°C can be built.

The AEC currently holds contracts with 3M and Teledyne Isotopes to produce a 20-Watt converter module by the end of CY1974, together with designs for the isotope fuel capsule and systems engineering for the generator. Data from this program would give a firm basis for establishing requirements for a generator program such as the one outlined in Figure VII-9. Energy sources having long life in the inactive state are needed for the Earth Entry Capsule, described in Chapter IX, since three years will elapse from the time of launch until use during Earth entry. Two candidates have been considered: automatically activated silver-zinc batteries and primary cells utilizing lithium with an organic electrolyte. The latter is a new type, high energy battery now in production with a long shelf life. Energy density is as high as 270 watt hours per kilogram compared to 70 watt hours per kilogram for the self-activated silver-zinc battery. The stable electrochemistry is expected to yield a shelf-life as long as 10 years. Although the design is completely sealed and the cells have been used in high altitude balloons, they have not as yet been space qualified. Selection between the two types will depend upon establishing specific requirements including those for actuating pyrotechnic devices.



▲ Assembly/Delivery

▼ Disassembly

Figure VII-9 20-Watt RTG Program

## C. PROPULSION

### 1. Propulsion Requirements

Accomplishment of the Mars sample return mission requires the use of several major propulsion systems in addition to launch vehicle propulsion. These include the Viking Orbiter, Lander Deflection and Terminal Descent Systems, and the Mars Ascent Vehicle (MAV) propulsion. Of these only the MAV propulsion system was studied in considerable depth because it is a completely new system and its performance and associated weight impact critically on the feasibility of the mission. The other propulsion systems require some modifications to satisfy URDMO mission requirements, but in general these can be accomplished without major difficulties or excessive costs. These modifications were studied in sufficient depth to verify feasibility and evolve valid weight estimates.

The general requirements of each of these systems are qualitatively summarized in Tabl. VII-20 along with a brief description of the selected baseline designs. Pertinent quantitative parameters are defined in subsequent paragraphs. Major results evolving from the study are as follows:

- 1) Ascent from the Mars surface to the rendezvous orbit requires a completely new vehicle comprising three propulsive stages; the first two stages employ solid propellant motors to achieve an elliptical orbit, the third stage uses monopropellant hydrazine for orbit circularization and attitude control.
- 2) The Viking Orbiter main propulsion system must be modified by stretching the propellant tanks to provide a 14% increase in propellant load; The cold gas attitude propulsion system will be replaced with a new hot gas system that will provide rendezvous capability in addition to attitude control.
- 3) The Viking Deorbit propulsion system can be used without modification.
- 4) The Viking Terminal propulsion system must be modified to provide both additional impulse (14% increase in propellant load), and a higher average thrust level (achieved by replacing the blowdown pressurization system with a regulated GN<sub>2</sub> system).

Table VII-20 URDMO Propulsion Requirements

<u>Propulsion</u>	<u>Requirement</u>	<u>Baseline Design</u>
Orbiter (Main)	Midcourse $\Delta V$	
	Orbit Injection	
	Orbit Trim	VO '75 Bipropellant System 14% Stretched Tanks
	MAV Rendezvous (Initial Closing $\Delta V$ )	
(Auxiliary)	Attitude Control	New Hot Gas System (Replaces GN <sub>2</sub> APS)
	Rendezvous $\Delta V$ (Control law $\Delta V$ 's)	
Lander Deflection	Deflection $\Delta V$ for Direct Entry	VO '75 Deorbit Monopropellant Hydrazine System (Unmodified)
	Roll Control	
Lander Terminal Descent	Terminal Descent $\Delta V$ and Attitude Control	VO '75 Monopropellant Hydrazine with Regulated Pressurization 14% Propellant Increase
MAV	MAV Ascent Circularization and Attitude Control	Two Solid Propellant Stages Plus a Monopropellant Hydrazine 3rd Stage

## 2. MAV Propulsion System

General Characteristics. Propulsion requirements that evolve from the selected MAV mission profile consist of two large delta Vs (1654 and 2530 m/sec, respectively) to achieve a 100 x 2200 km orbit; a smaller delta Vs (391 m/sec total) for orbit circularization, trim, and rendezvous; and attitude control and stabilization throughout the entire MAV mission. To satisfy these requirements, a 3-stage baseline propulsion system has been selected consisting of two solid propellant motors to provide the two large delta Vs, and a single monopropellant hydrazine system to provide the smaller delta Vs in addition to the attitude control functions during all phases of the MAV mission. A two-stage vehicle employing a solid propellant first stage for Mars Ascent and a liquid bipropellant second stage for orbit insertion and circularization was also studied, but was eventually rejected because of poor overall performance (see Appendix H).

Solid motors were selected because of their superiority (high Isp and mass fraction) in the impulse range of interest to MAV. Of their major limitations: inflexible configuration, lack of restart capability, high thrust-to-weight ratio, and non-sterilizability, only the latter presents problems for the MAV application. Sterilizable solid propellents are not state-of-the-art, but are under development and should be available on a time scale compatible with the proposed Mars sample return mission as discussed subsequently.

Monopropellant hydrazine appears to be an ideal selection for the third stage propulsion system because of its comparative simplicity and high reliability, relatively high performance, and closely controllable impulse over an extremely wide range. It results in a relatively lightweight, compact installation.

Major features of the MAV propulsion system are shown in Figure VII-10, and are discussed in the following sections.

MAV Stage I and II Characteristics. Propulsion requirements for the MAV are summarized in Table VII-21. These comprise two large delta Vs to acquire a 100 x 2200 km orbit, followed by smaller delta Vs to circularize

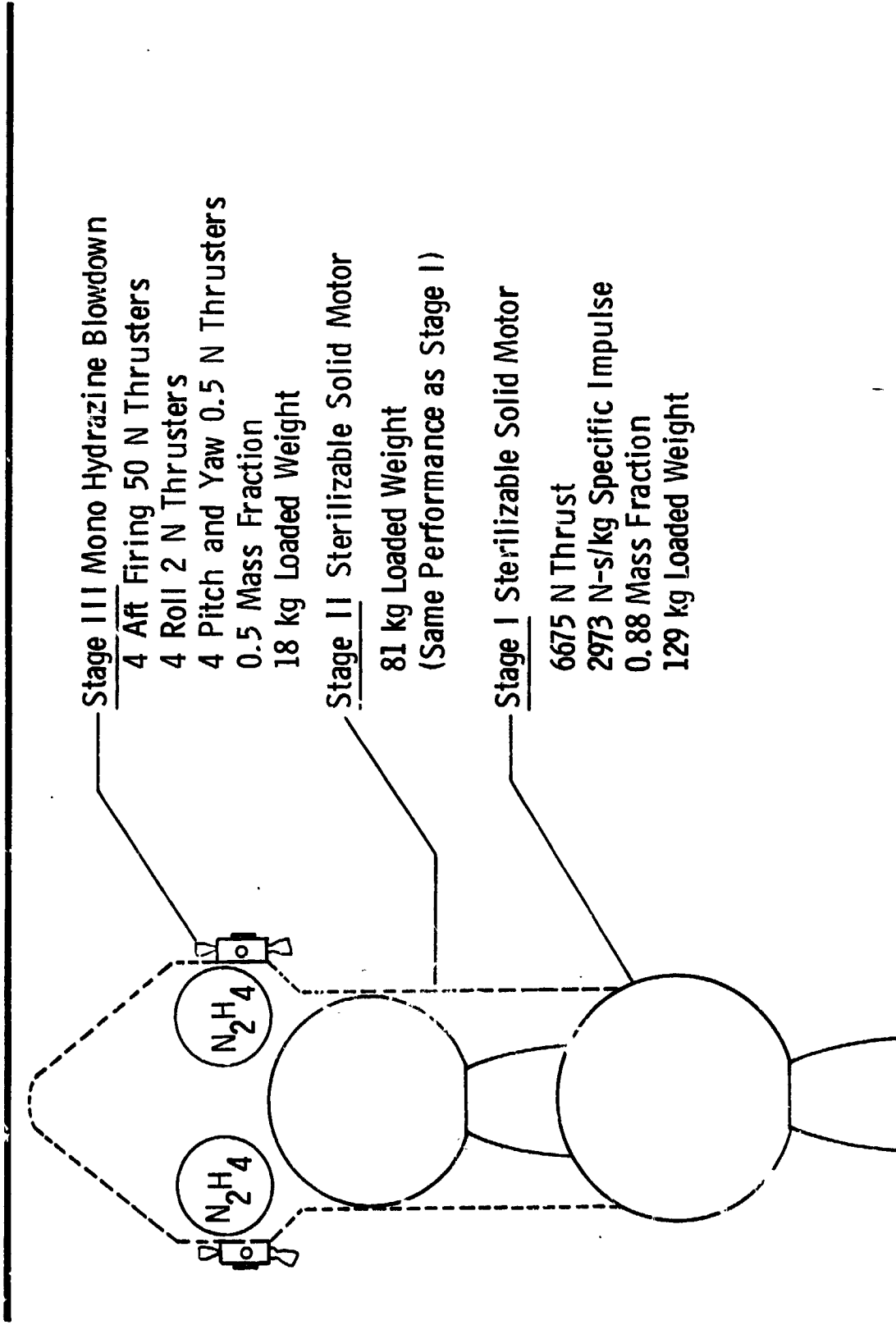


Figure VII-10 MAV Propulsion System

Table VII-21 MAV Propulsion System Characteristics

<u>Propulsion Requirements</u>	<u>Function</u>	<u>Baseline Selection</u>
<u>Delta V</u>		
$\Delta V_1$ 1654 m/s	Ascent to 100 km	Solid Motors (2) High Isp, High $\lambda$ Simple, Reliable
$\Delta V_2$ 2530 m/s	Transfer to 2200 km	
$\Delta V_3$ 341 m/s	Orbit Circularization	Monopropellant $N_2H_4$ Controllable Impulse Good Performance Simple, Reliable
$\Delta V_4$ 50 m/s	Trim/Contingency	
<u>Attitude Control</u>		
<u>During Burns</u>	Pitch Program Compensate Aero Moments Compensate Thrust Misalignment P, Y and R Stabilization	
<u>During Coasts</u>	Reorientation Maneuvers P, Y and R Stabilization	

and trim, plus the usual attitude control functions. From these requirements a three-stage vehicle has been evolved as an optimum configuration.

For a vehicle that has an initial gross weight in the range of 250 to 300 kg, and a propulsion system that provides a specific impulse of 2840 N-s/kg (achievable with conventional solid propellents or earth-storable liquid bipropellents), the quantity of propellant consumed in providing the initial 1654 m/sec  $\Delta V$  will be in the neighborhood of 125 kg. Likewise for a second stage burn providing a  $\Delta V$  of 2530 m/s it is found that 80 kg propellant will be consumed. Referring to Figure VII-11, it is seen that solid propellant motors appear to be the best choice to satisfy these requirements. The specific impulse provided by the solid motors is no better than that for liquid propellant liquids, but the mass fraction is considerably higher. Also, the solid motor is inherently simple, so it also may be expected to be more reliable. These motors do possess definite limitations regarding flexibility of configuration, thrust-to-weight ratio and impulse control, but these do not appear to be detrimental to the MAV application. One limitation that does present a problem is that state-of-the-art solid motors are not sterilizable, but this appears to be solvable. Recent R&D programs conducted by JPL and AGC have culminated in a successful firing (by AGC) of a full-scale solid propellant motor following (8) sterilization cycles to 125°C. Considerable additional effort in this area is required before flight qualified sterilizable motors will be available, but a major milestone has been passed and there is every reason to believe that the desired end goal will be reached. Because of the importance of this work to the proposed MAV design, a detailed discussion of it is included in Appendix I.

Although it is expected that sterilizable motors will be available on a time scale compatible with MSR mission requirements it will be noted that the sterilization requirement does impose some penalties. The propellant formulations are limited to a considerable degree by the thermal cycle requirement, and the motors are heavier due to the need for a unique flexible liner to support the propellant grain within the motor case. As a result the best that can be expected from sterilized motors is a specific impulse of 2795 N-s/kg and a mass fraction of 89. This is in comparison

to a specific impulse of 2840 N-s/kg and a mass fraction of .9 for the current generation of high performance motors in the 100 kg (propellant) class (Figure VII-11).

Following a number of iterations, the baseline MAV initial weight has been established at 289 kg, and the corresponding propellant loads for Stages I and II are found to be 129 and 81.3 kg, respectively. These are based on the values of Isp and  $\lambda$  cited above, and the  $\Delta V$ s previously given. The general configuration of the motors will be similar to the sterilized SVM-3 motor that was successfully fired by AGC (see Appendix J). Pertinent characteristics of each motor are summarized in Figure VII-12. The two motors are of identical configuration, having submerged nozzles with an area ratio of approximately 50:1 and being loaded with the same propellant formulation. Burning characteristics may be tailored to some degree to suit specific requirements, but it is proposed that both motors operate at an average chamber pressure of approximately  $414 \text{ N/cm}^2$  (600 psia) and produce a thrust of approximately 6675 N (1500 lbf). The first stage will be slightly larger in diameter (57 vs 48 cm) and slightly longer (81 vs 74 cm), and will have a longer burning time (55 vs 35 sec).

MAV Stage III Characteristics. Selection of a monopropellant hydrazine propulsion system to provide all propulsion requirements except the two initial large  $\Delta V$ s was arrived at primarily from considerations of the size of the system (quantity of propellant) and the need for a very flexible duty cycle. Solid propellant motors are out of the question because of the requirement for multiple burns and closely controlled impulses. Bipropellant systems are not appropriate because of the small quantity of propellant involved and the low thrust levels anticipated. Cold gas systems are not attractive because of their low performance capability and resultant high weight and volume requirements.

Using the Stage I and Stage II propellant weights and mass fractions cited previously, and assuming Stage I and Stage II skirt weights of 5.7 and 4.0 kg respectively, it is readily determined that the MAV weight following Stage II separation (initial Stage III weight) is 40 kg. Then assuming a propulsion system with a specific impulse of 2300 N-s/kg (achievable with monopropellant hydrazine catalytic thrusters), the

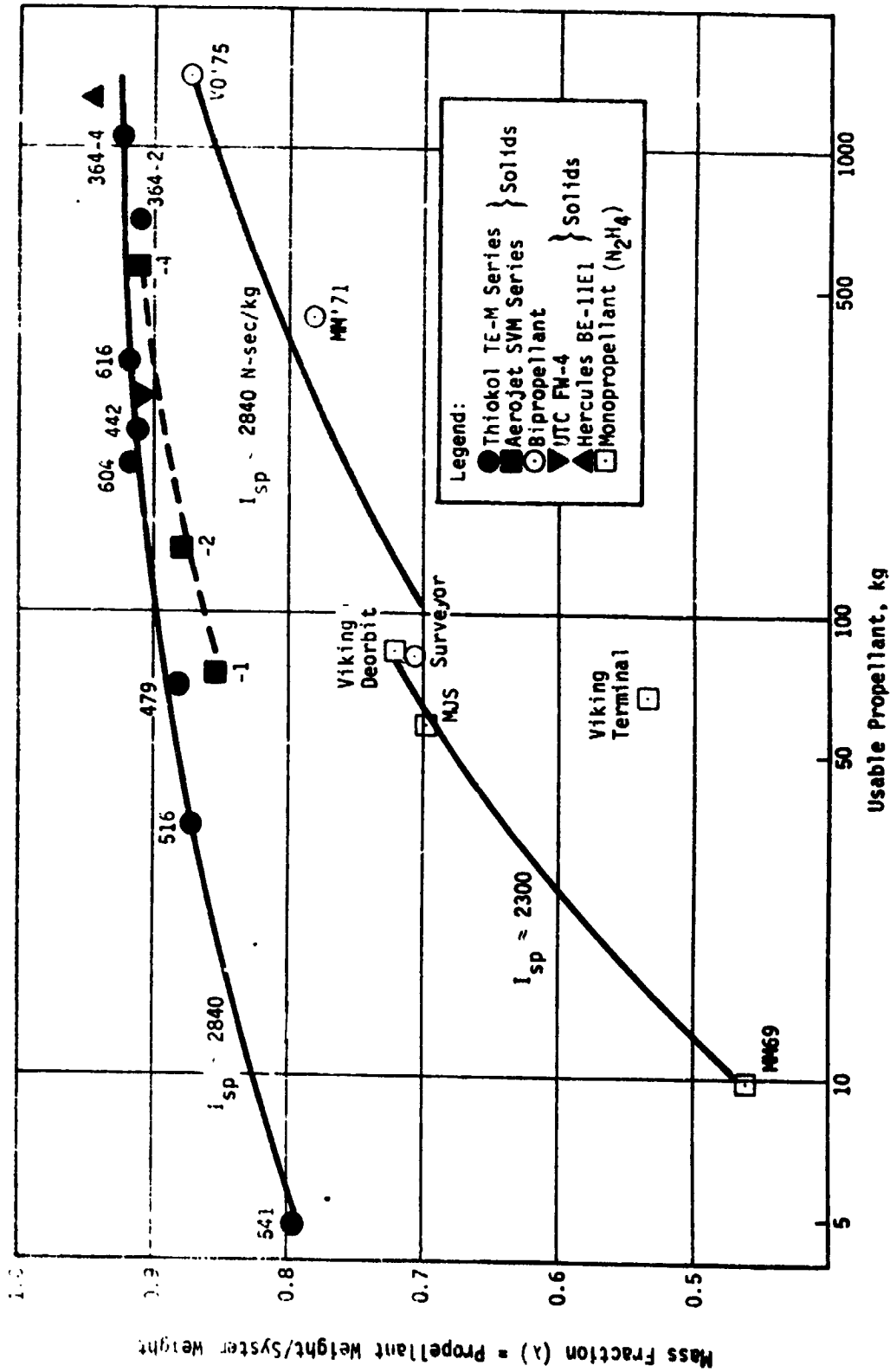
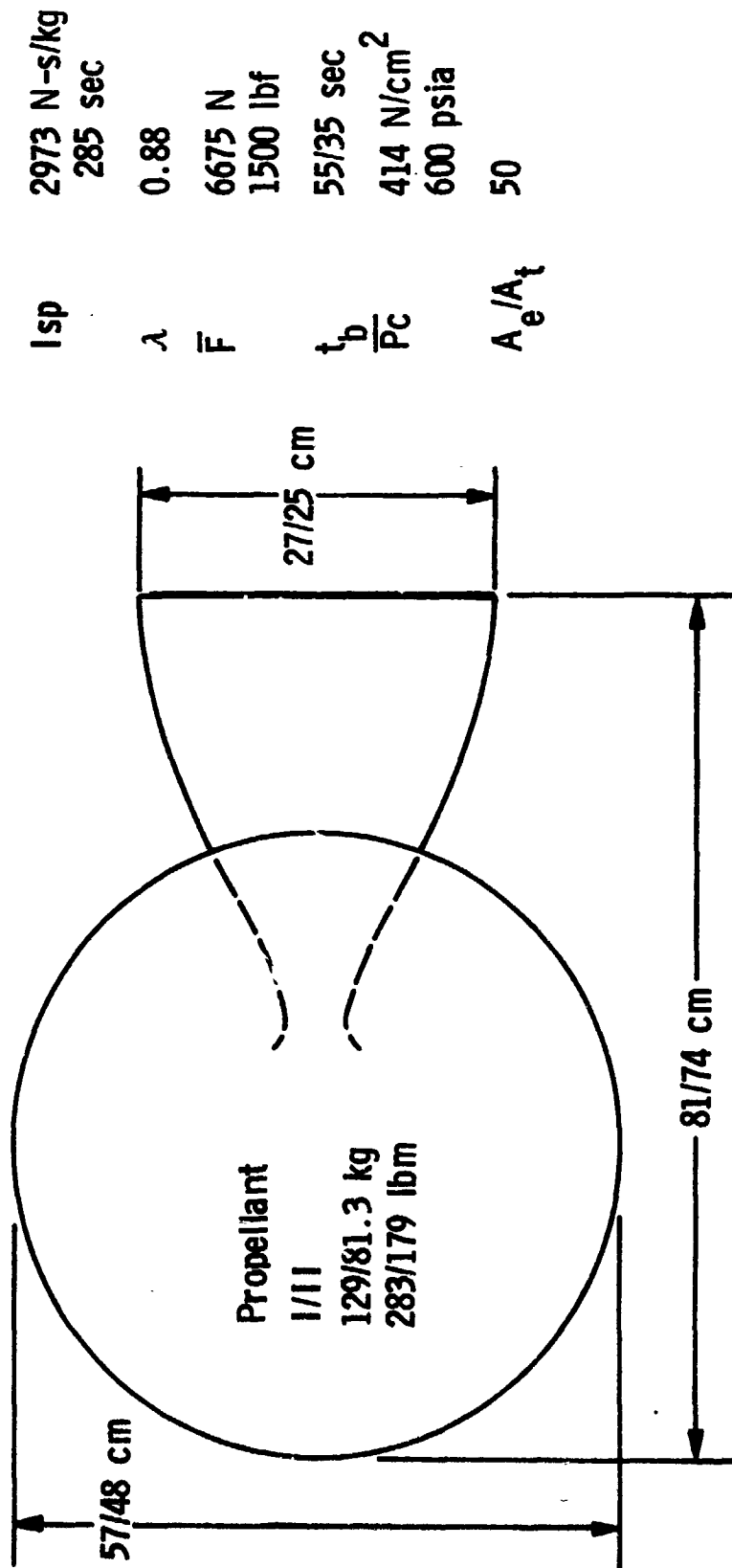


Figure VII-11 Typical Propulsion System Mass Fractions



VII-51

Figure VII-12 MAV Solid Propellant Motor Characteristics

quantity of propellant consumed to provide the remaining 391 m/s  $\Delta V$  is found to be 6.5 kg. If a cold gas system were selected in place of a monopropellant hydrazine system, the quantity of propellant needed would be in excess of 20 kg (specific impulse = 685 N-s/kg), and the total system weight would be in the order of 60 kg. This is greater than the allowable weight of the entire third stage, and it still doesn't account for propellant to be consumed in attitude control functions. Therefore, a liquid monopropellant system appears to be the best, probably the only, solution to the problem.

Thrusters. The MAV Stage III propulsion system has a number of functions to perform, but it has been concluded that these can be provided by a total of only twelve catalytic thrusters. Four of these are aft-firing thrusters located on the periphery of the MAV as shown in Figure VII-10. They perform the dual functions of attitude control during Stage I and Stage II solid motor burns, and orbit circularization for Stage III. They will pulse on as required to maintain proper attitude during the solid motor burns; they will operate essentially continuously during orbit circularization, except for occasional off-pulsing to maintain the desired MAV attitude. The nozzles will be canted outward approximately  $10^\circ$  to minimize impingement effects on the first two stages, and to provide an increased moment arm without entailing a significant loss in usable impulse.

Sizing of these four thrusters is based primarily on the requirement to compensate for solid motor thrust misalignments and upsetting aerodynamic forces. The latter is found to be the predominant effect, with maximum forces occurring at Stage I burnout (maximum q). The approximate level of force required to overcome these upsetting moments is found to be approximately 50 N (11 lbf) as shown in Appendix J. This leads to the selection of the Hamilton Standard Model REA 22-4 catalytic thruster as a logical candidate, though there may be others. This thruster is rated at 55 N (12 lbf) and weighs .7 kg.

Roll stabilization throughout the MAV mission is provided by four tangential firing thrusters arranged in opposing pairs  $180^\circ$  apart on the periphery of the Stage III vehicle. These must be large enough to overcome disturbing moments arising from aerodynamic effects and solid

propellant exhaust torques during Stage I and Stage II burns, but also must be capable of providing very small impulse bits during Stage III limit cycle operation.

Sizing of these thrusters is not straightforward because of the difficulty encountered in attempting to define the magnitude of the disturbing moments. The approach that was finally taken was to provide torques for MAV that are roughly equivalent to those that have been successfully applied in the Surveyor and Burner II programs, i.e., a roll torque of approximately .025 N cm per Newton of solid motor thrust. For MAV, which operates at a thrust level of 6675 N (1500 lbf) and has a roll moment arm of 35 cm, this evolves to a thrust level of approximately 2.4 N (.55 lbf) per thruster. The Hamilton-Standard Model Rea 17-6 thruster would satisfy this requirement.

Pitch and yaw stabilization during Stage III orbiting is provided by four forward-firing thrusters located just forward of the four aft-firing thrusters. These thrusters are not required to provide spacecraft Delta V, so they can be as small as practicable to assure a low propellant consumption during limit cycle operation. The thruster selected has a nominal output of .5 N (.1 lbf) thrust, the smallest size of catalytic thruster currently available. The Hamilton-Standard Model REA 10-14 thruster is representative of several candidates in this thrust range. To provide as small an impulse bit as possible, it is proposed to install a restrictor such as a Viscojet in series with each thruster. It is expected that this will permit impulse bits in the range of  $2.5(10)^{-3}$  N-s to be achieved.

Propellant Consumption. To determine the propellant requirement for the Stage III baseline propulsion system, the operation of the system has been studied in considerable detail. The MAV flight has been divided into seven major phases as identified in Table VII-22, and the consumption during each phase estimated as accurately as possible. The table also includes the approximate duration of each phase, and identification of the operating thrusters and their functions.

Table VII-22 MAV Stage III Propulsion System Duty Cycle

Event	Time Duration	Stage III Thruster Operation		Propellant kg (lbm)
		Thruster	Function	
1. Stage I Burn	55 sec	A* R	P-Y Control Roll Control	0.9
2. Coast	200 sec	A R	Orient/Hold P-Y Attitude Roll Stabilization	
3. Stage II Burn	35 sec	A R	P-Y Control Roll Control	0.3
4. Coast, Elliptical	33 hrs	F R	Earth Point/Hold, Reorient Roll Stabilization	0.2 0.1
5. Circularization Burn	100 sec	A A R	$\Delta V$ (341 m/s) P-Y Control Roll Control	5.8
6. Coast, Circular	310 hrs	F R	Earth Point/Hold Roll Stabilization	**
7. Rendezvous/Dock	3 hrs	F R	Orbiter Point/Hold Roll Stabilization	0.8
			Outage/Contingency	<u>0.8</u>
				8.9

\* A-Aft firing; R-Roll; F-Forward Firing

\*\* Included in 4. above.

The estimate of Stage III propellant consumption, during Stage I burn is based primarily on the requirement to overcome a solid motor thrust misalignment of .25 cm at the MAV center of gravity. It is found that the average Stage III thrust required to compensate for this misalignment is approximately 35 N (8 lbf), equivalent to one thruster operating two thirds of the time. Assuming a specific impulse of 2260 N-s/kg (230 sec) this evolves to a total consumption of .9 kg during the 55 sec Stage I burn. Aerodynamic moments are significant for only a few seconds near burnout, requiring only short duration thruster burns that do not add significantly to the propellant consumption. Consumption of the roll thrusters is based on the assumption of a 50% duty cycle to compensate for disturbing roll moments. Two 2.2 N (.5 lbf) roll thrusters will consume .1 kg propellant during a 55 second time period at this duty cycle.

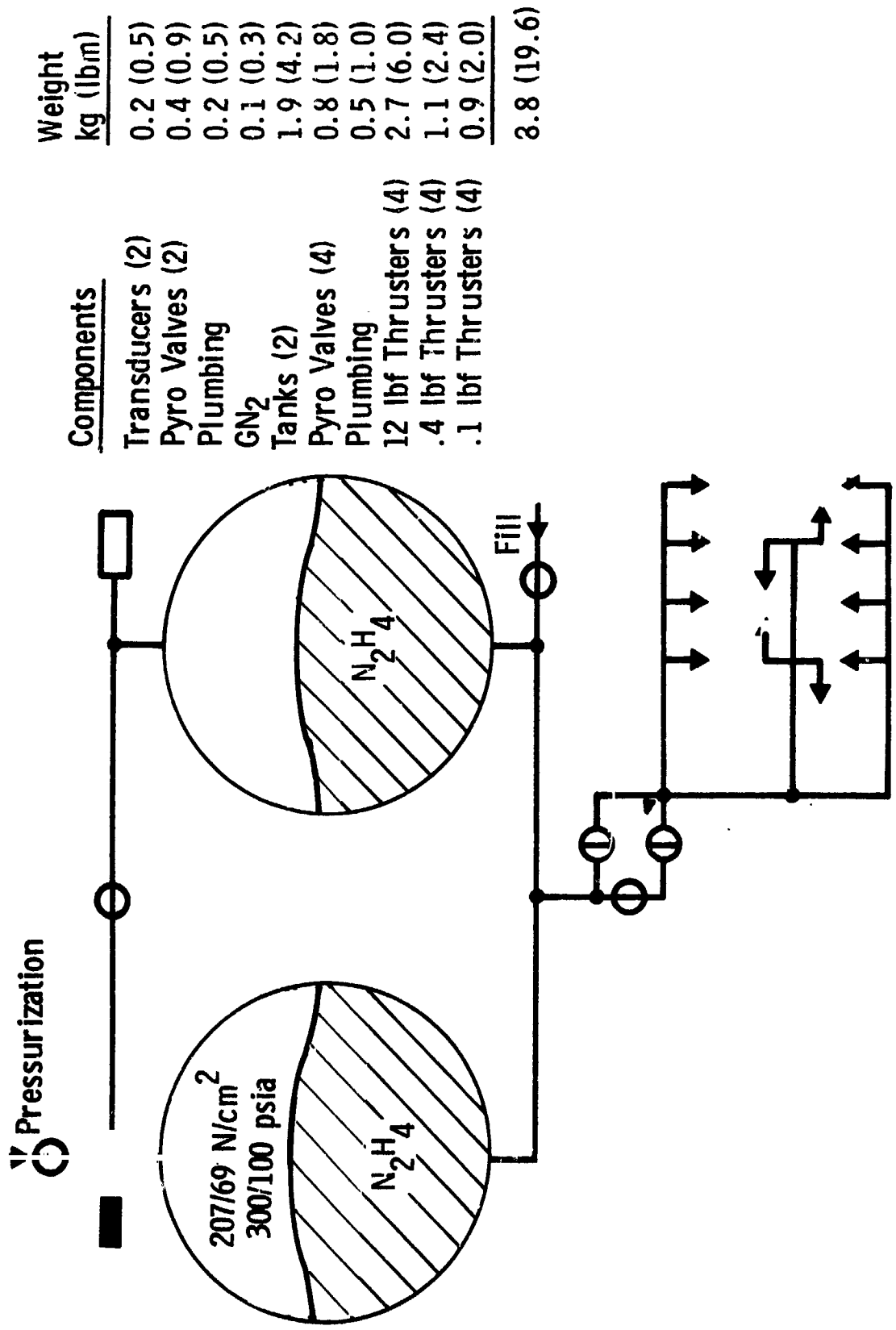
Stage III propellant consumption during Stage II burn has been estimated in a similar manner, but the results are different because of different moment arms and burn time. The average Stage III thrust required to overcome Stage II thrust misalignment is only 22 N (5 lbf), which results in a propellant consumption of only .3 kg during the 35 second Stage II burn.

Propellant consumption during the Delta V burns (combined orbit circularization and rendezvous) has already been shown to be 6.5 kg of which 5.8 kg is used for circularization and .7 kg is allocated to rendezvous. The propellant consumption rate of the roll thrusters during limit cycle operation (Stage III orbiting) is found to be approximately  $5.5(10)^{-8}$  kg/sec based on the size of the impulse bit previously cited and a wide half-angle deadband of .174 radians (see Appendix I). This evolves to a total consumption of about .1 kg during the MAV 400-hour orbital life. Similarly, the consumption rate of the pitch and yaw thrusters is also found to be approximately  $5.5(10)^{-8}$  kg/sec per axis, based on much smaller impulse bits, but also a much narrower deadband. Total consumption for the pitch and yaw axes combined is about .2 kg during the orbital life. Then allowing an additional 10% propellant for contingencies, the total requirement becomes approximately 9 kg for all Stage III operations.

System Characteristics. The major features of the baseline Stage III propulsion system are identified schematically in Figure VII-13. For packaging convenience two propellant tanks are provided, each approximately 23 cm in diameter, and weighing 1.0 kg. They are state-of-the-art design, fabricated from titanium alloy, and fitted with elastomeric bladders for effective propellant management. Blowdown pressurization is provided using  $\text{GN}_2$  as the pressurant. A propellant-to-tank volume ratio of 2:3 has been assumed, providing a high blowdown pressure ratio (3:1). This provides high available thrust levels early in the MAV flight when they are most needed, and low thrust levels near the end of the flight when low impulse bits are important. The tanks are designed to withstand the sterilization environment following loading. This does not impose a weight penalty because the tank wall thickness is limited by the use of minimum gage materials.

Propellant loading is accomplished through a pyro fill valve, then pressurization with  $\text{GN}_2$  is accomplished through a similar valve. An initial charge pressure of approximately  $207 \text{ N/cm}^2$  (300 psia) has been selected to provide the desired thruster outputs. Following pressurization, the tank ullage volumes are isolated from each other. Tank pressures are monitored throughout the MAV mission by means of the two pressure transducers shown on the schematic. These pressures will decay to a level of approximately  $69 \text{ N/cm}^2$  (100 psia) at the end of the mission.

The twelve thrusters are fed propellant through a set of pyro isolation valves as shown. The propellant will remain isolated from the thrusters until shortly before MAV liftoff. In the event of a thruster malfunction, the thrusters can again be isolated while the nature of the malfunction is being assessed. Then, assuming that a suitable solution to the problem has been found, the propellant system can be armed a second time. Redundant thrusters could be added to improve the reliability of the system, however, these are not included in the baseline design since a more comprehensive study is required to establish how to most effectively allocate the weight margin to the various components and subsystems of the MAV.



Components	Weight kg (lbm)
Transducers (2)	0.2 (0.5)
Pyro Valves (2)	0.4 (0.9)
Plumbing	0.2 (0.5)
GN <sub>2</sub>	0.1 (0.3)
Tanks (2)	1.9 (4.2)
Pyro Valves (4)	0.8 (1.8)
Plumbing	0.5 (1.0)
12 lbf Thrusters (4)	2.7 (6.0)
.4 lbf Thrusters (4)	1.1 (2.4)
.1 lbf Thrusters (4)	0.9 (2.0)
	<b>3.8 (19.6)</b>

VII-57

Figure VII-13 MAV Stage III Propulsion System

Component weights (included in Figure VII-13) are based on state-of-the-art designs and are believed to be realistic. Dry system weight is estimated to be about 9 kg, approximately the same weight as the propellant. This leads to a mass fraction of approximately .5, a relatively high value for such a small multi-purpose system.

### 3. Orbiter Propulsion System

General Requirements and Characteristics. To accommodate the Mars sample return mission, several modifications must be made to the Viking Orbiter propulsion system. These arise from the following requirements that are imposed on the orbiter by the MSR mission:

- 1) Additional propellant is required for orbit insertion because the MSR spacecraft is somewhat heavier than Viking '75.
- 2) An additional  $\Delta V$  of approximately 20 m/s is required of the main propulsion system to accommodate initial rendezvous.
- 3) An additional rendezvous  $\Delta V$  of approximately 60 m/s is also required, but with the thrust provided in the opposite direction from the main engine thrust, and of a much lower level (in the range of 200 to 250 N thrust).
- 4) A small  $\Delta V$  capability is needed for pitch and yaw translation during final rendezvous.
- 5) Pitch, yaw and roll attitude control is needed similar to that required of Viking '75, but for a longer period; i.e., 400 days following rendezvous.

Possibly a number of different solutions to these requirements could be found, but it appears that the best solution is to incorporate two basic modifications to the VO '75 as follows:

- 1) Enlarge the VO '75 propellant tanks to accommodate 14% more propellant that is required to accomplish orbit insertion for the heavier spacecraft and to provide the initial rendezvous  $\Delta V$ .

- 2) Replace the VO '75 cold gas attitude propulsion system with a completely new hot gas system that provides all necessary attitude control, plus the final rendezvous  $\Delta V$ . It is proposed that this system include (4) 50 N thrusters for final rendezvous  $\Delta V$  and (16) 1 N thrusters that provide 3-axis stabilization as well as a small translational  $\Delta V$  along the pitch and yaw axes.

Main Propulsion System. Schematically (Figure VII-14) the basic VO '75 system will remain unchanged. The major hardware change will be to the propellant tanks which will be enlarged by inserting a larger cylindrical barrel between the two hemispherical end domes. The barrel section will be lengthened 18 cm, extending the overall tank length from 140 cm to 158 cm. This degree of stretching of the tanks can be accommodated without necessitating major changes to the VO '75 structure. This modification will add 8 kg to the weight of each tank and will necessitate at least a partial requalification of the tank design.

Enlargement of the propellant tanks will also necessitate enlargement of the propellant management device by an equivalent amount. The basic design concept of the PMD will remain unchanged, but the redesigned PMD, like the propellant tanks, will undoubtedly require requalification. A weight increase of approximately 1 kg in the PMD is to be expected, bringing the total weight increase of the tank and PMD to 9 kg.

A 14% increase in the quantity of helium pressurant will also be required. If the bottle design pressure remained unchanged, the required 14% volume increase could be accommodated by increasing the bottle diameter from 63.5 to 67.3 cm. The resultant weight increase in the bottle would be approximately 5.5 kg, which added to the approximate 1.0 kg additional helium required, brings the total weight increase for the pressurant to approximately 6.5 kg. It should be noted, however, that final decision on the size of the helium bottle should be based on flow test results of the VO '75 propulsion system. Precise sizing of the pressurization system is very difficult due to the heat transfer accompanying the pressurization process, so it is conceivable that the existing bottle already has adequate capacity for the proposed MSR mission.

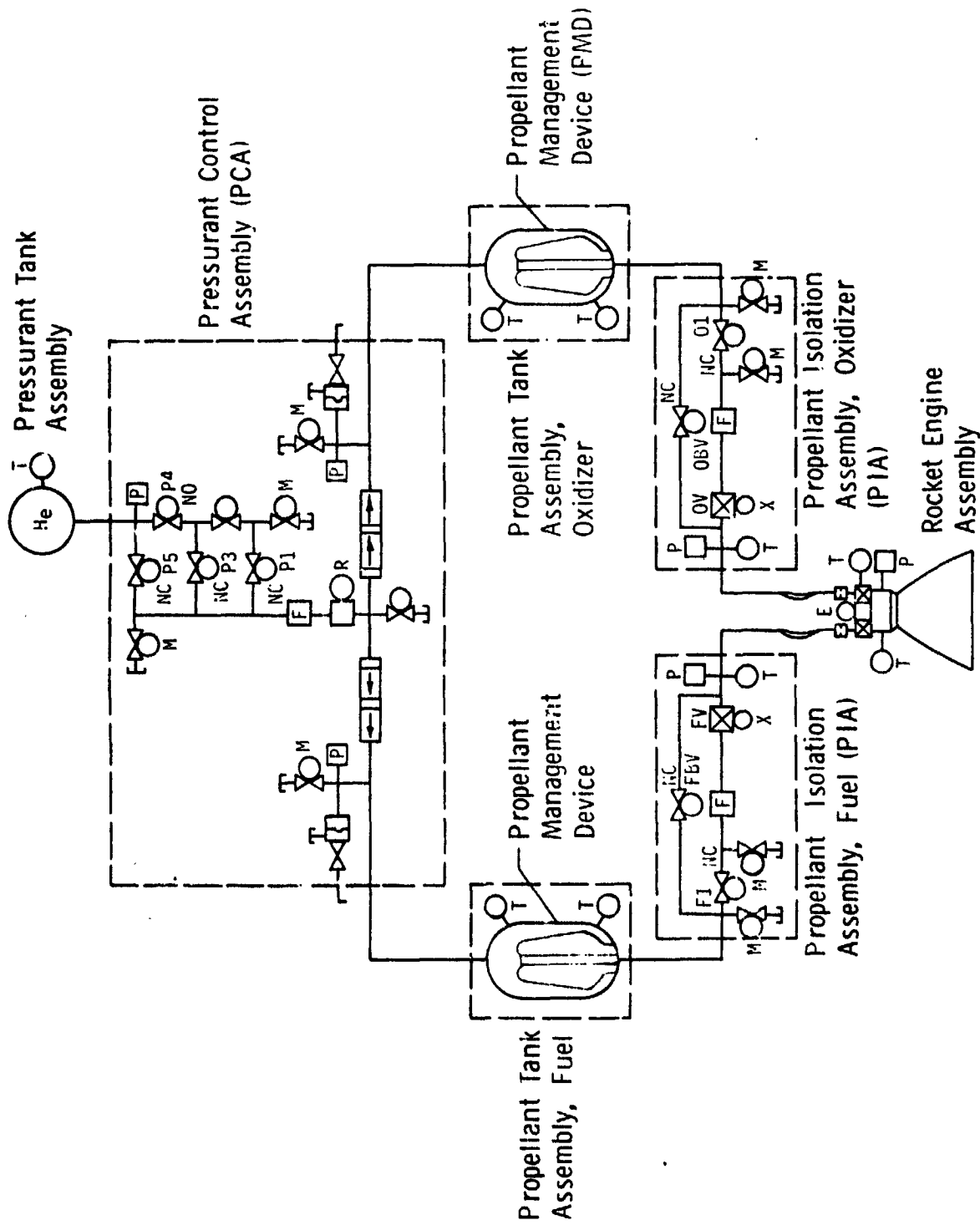


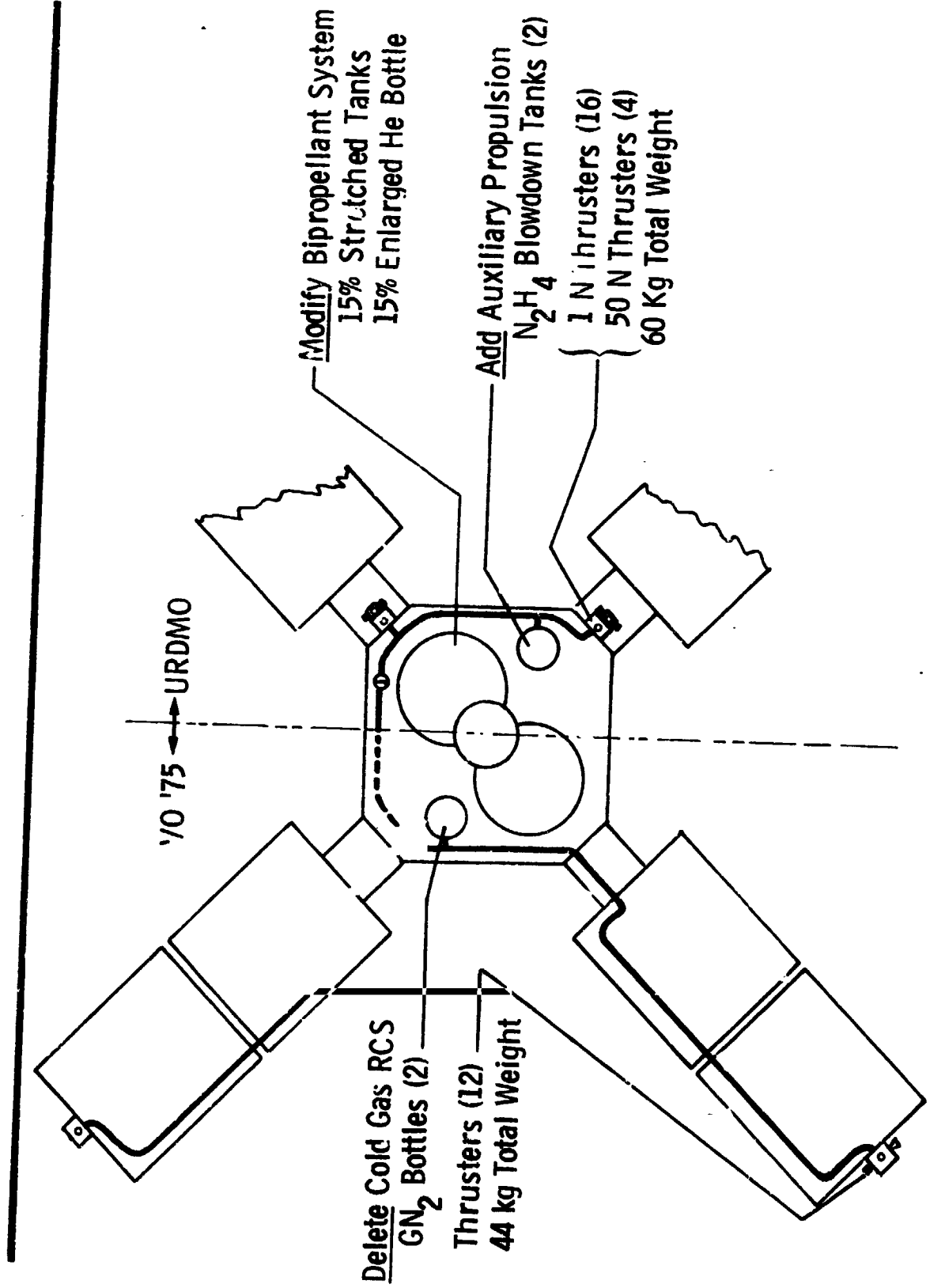
Figure VII-14 VO '75 Propulsion Subsystem

Components in the VO '75 flow system do not appear to require any modifications whatsoever, though they may have to be qualified for the longer life in orbit. The propellant isolation assemblies have the capability of an almost unlimited number of isolation cycles, so a modified engine duty cycle should present no problems. The engine itself will be required to provide a single burn of 52 minutes for orbit insertion instead of 45 minutes, and a total burn time of 62 minutes instead of 53 minutes to accommodate trim maneuvers and rendezvous. It is doubtful that any redesign of the engine will be required, but certainly requalification will be in order.

Orbiter Auxiliary Propulsion. The proposal to replace the cold gas attitude propulsion system with a hot gas system arises principally from the requirement for a  $\Delta V$  capability of 60 m/s for final rendezvous. It is readily determined that this requirement is best satisfied by a monopropellant hydrazine system, so it is logical to combine the attitude control requirements and this  $\Delta V$  requirement into a common monopropellant hydrazine system.

It is proposed that the  $\Delta V$  thrust requirement be provided by (4) 50 N monopropellant hydrazine thrusters, possibly the Model REA 22-4 thruster produced by Hamilton-Standard. These provide the proper level of thrust for the  $\Delta V$  maneuver, and they can be operated differentially for pitch and yaw control. An ideal location for them appears to be on the surface of the bus within the structure that supports the solar panels as shown in Figure VII-15. Assuming a specific impulse of 2250 N-s/kg, and a spacecraft weight of 1150 kg, the mass of propellant to be consumed by these thrusters in providing the 60 m/s  $\Delta V$  is computed to be 30 kg.

To provide the APS requirements, it is proposed to locate quads of 1 N thrusters on the bus surface in the vicinity of the 50 N thrusters, as shown in Figure VII-15. This location (on the bus) is necessary to minimize thermal control problems, but it tends to be inefficient insofar as propellant consumption is concerned because of the relatively small moment arm provided. The selection of 1 N thrust arises from the desirability of providing the same torque as the cold gas APS for spacecraft maneuvering. The moment arm of the hot gas thrusters will be only about



VII-62

Figure VII-15 Orbiter Propulsion System

1/3 that of the cold gas thrusters located on the tips of the solar panels, so the thrust level (1 N) must be approximately 3 times that of the cold gas thrusters (.3 N).

The use of a total of 16 APS thrusters is necessitated by the requirement to provide small translational  $\Delta V$ s along the pitch and yaw axes. The four sets of tangentially firing thrusters will be fired in pairs to provide this capability; two of these sets will be fired differentially to provide roll control. Arrangement of the thrusters in two strings, each protected by an isolation assembly, will permit isolation of one-half the thrusters in the event of an individual thruster failure (Figure VII-16). This will reduce the APS capability to that of providing only moments instead of pure couples, but this is no different from the capability to that of providing only moments instead of pure couples, but this is no different from the capability provided by the VO '75 cold-gas APS.

To precisely determine the propellant requirements for the APS entails extensive analysis which is beyond the scope of this study, but it is not difficult to compute the consumption in the limit cycle mode, a mode of operation that normally accounts for about one-third of the APS consumption. Computed consumptions (see Appendix C) are summarized below:

<u>Mode</u>	<u>Consumption Rate (lbm/sec)</u>	<u>Total Consumption (lbm)</u>
Cruise, Roll	.013(10) <sup>-6</sup>	.33
Cruise, p and y	.0029(10) <sup>-6</sup> (each axes)	.14 (both axes)
Orbit, Roll	.024(10) <sup>-6</sup>	.83
Orbit, p and y	.021(10) <sup>-6</sup> (each axis)	1.45 (both axes)
		<u>2.75 (1.25 kg)</u>

It is evident that the propellant consumption is low during the cruise phase when the spacecraft moments of inertia are large, but becomes significant during orbiting when the moments of inertia are small.

Assuming that the total propellant APS consumption for attitude control functions (exclusive of that for  $\Delta V$ ) is 3 times the limit cycle consumption (typical for this type of mission), a value of 3.75 kg is

obtained. Then adding this to the  $\Delta V$  consumption brings the grand total consumption to 33.75 kg. Allowing a 10% contingency factor, the total propellant requirement evolves to approximately 37 kg.

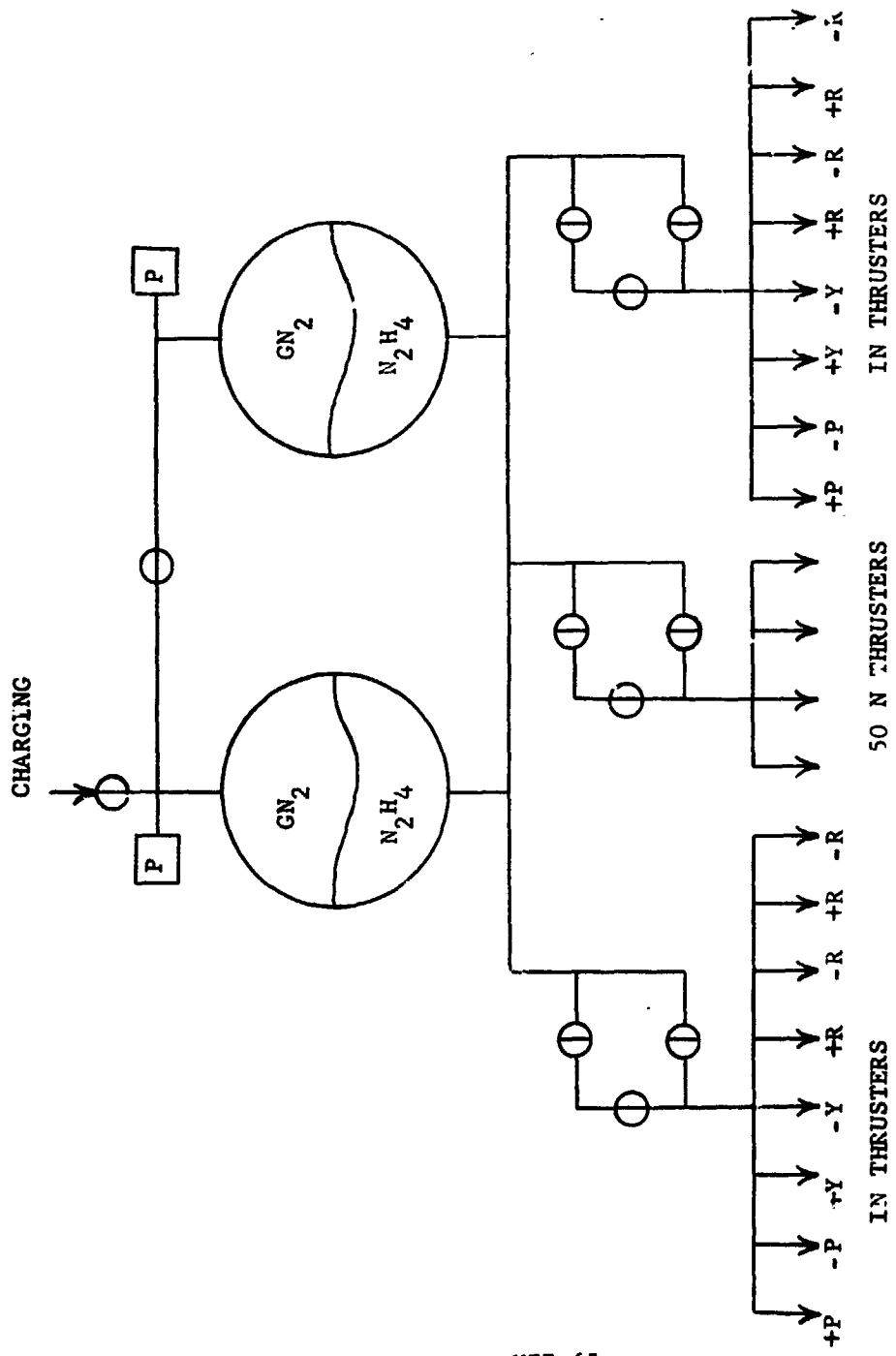
It will be noted that the propellant allowed for contingencies is much smaller than that provided for the VO '75 cold gas APS system. This is due to two factors; i.e., leakage is not significant with the hot gas system, and excessive propellant losses are prevented by prompt isolation of thrusters in the event of a fail-open failure (Figure VII-16). Also, it will be noted that even though there may be a large percentage error in the estimated propellant consumption for attitude control functions, this will have relatively little effect on the total propellant to be provided.

Assuming that the 37 kg propellant ( $N_2H_4$ ) will be contained in two spherical tanks, and that blowdown pressurization will be employed with a blowdown ratio of 2:1, the required volume of each tank is found to be approximately 37,000 cc, and the diameter is approximately 41 cm. It is proposed to install these tanks in place of the original cold gas pressure bottles, though the latter are slightly smaller in diameter. It is expected that minor repositioning of internal components will permit the slightly larger hydrazine tanks to be accommodated.

It is predicted that a mass fraction of 0.6 will be achievable with a hot gas propulsion system of this size, leading to a total system weight of 61.5 kg, or a dry system weight of 31.5 kg. This is in contrast to the VO '75 cold gas system which has a total weight of 44.8 kg, but carries only 14 kg propellant. The hot gas system weighs only 16.7 kg more than the cold gas system, but carries 23 kg more propellant.

#### 4. Lander Terminal Propulsion System

To accommodate the increased landed weight associated with the Mars sample return mission, it is necessary to modify the Viking '75 terminal propulsion system to provide both an increased total impulse and an increased thrust level. The need for increased impulse arises directly from the increase spacecraft weight to be decelerated; the increased thrust is needed to improve the propulsive efficiency so that the overall propellant consumption may be minimized.



VII-65

Figure VII-16 Orbiter Auxiliary Propulsion System Schematic

After considerable study it was concluded that the most attractive solution to the problem is to provide a regulated GN<sub>2</sub> pressurization system in place of the blowdown system used on Viking '75. This will permit the propellant feed pressure and thrust level to be maintained constant during terminal system operation (instead of decaying to approximately one-half the initial values), and will also permit a greater quantity of propellant to be loaded into the tankage. Maintaining the thrust level constant at slightly greater than 2670 N (600 lbf) results in a propellant requirement of 75.5 kg for the MSR mission, only 9.1 kg more than that required for Viking '75.

A number of possible options were considered for packaging of the propellant. The solution finally selected is to eliminate one of the propellant tanks and load all the required propellant into the remaining tank. The Viking '75 tanks are normally loaded to only about 30% of their capacity so that excessive pressure and thrust decay will not be experienced during blowdown. Loading the full 75.5 kg usable propellant into one of the tanks results in the tank being only about 70% full. Use of a single tank greatly simplifies the packaging problem on the lander, and at the same time eliminates a potential problem of cross flow and gas ingestion between tanks under the action of side loads, and simplifies the propellant feed system. The use of a single tank located some distance from the lander centerline does result in a shift in the center of gravity during system operation, but it appears that the lander guidance and control system can accommodate this shift without difficulty. The tank may require some redesign and requalification to accommodate the increased propellant load, but this does not present a major problem. Some additional weight saving presumably could be achieved by use of a somewhat smaller propellant tank, but it is doubtful that this is worth the additional development effort and cost involved.

The adoption of a regulated GN<sub>2</sub> pressurization system entails the addition of a high pressure bottle for storage of the GN<sub>2</sub>, and a pressure control assembly to regulate and control the GN<sub>2</sub> flow. Precise determination of the GN<sub>2</sub> requirements is somewhat difficult because of the complex nature of the heat transfer during system operation, but reasonably

accurate estimates can be made using simplified approaches. The approach that was used involved the assumption of a polytropic expansion of the  $\text{GN}_2$  in accordance with the equation  $PV^{1.3} = \text{constant}$ , and the assumption of instantaneous mixing of the gas in the propellant tank ullage volume, but no heat transfer between the gas and the propellant. An additional important assumption that entered into the sizing of the bottle was that the pressurization system is to be sterilized following  $\text{GN}_2$  loading. This requires that the bottle be loaded to a pressure level of only  $1550 \text{ N/cm}^2$  (2250 psia), when designed for a pressure level of  $2070 \text{ N/cm}^2$  (3000 psia), in order that the design pressure is not exceeded when the bottle is subjected to the sterilization environment ( $125^\circ\text{C}$ ).

Based on the above, it has been determined that the total quantity of  $\text{GN}_2$  required for pressurization is approximately 6.8 kg, of which 5.9 kg is initially stored in the bottle and .9 kg in the propellant tank. The bottle to contain this quantity of  $\text{GN}_2$  will be approximately 40 cm in diameter and will weigh approximately 9.5 kg. An approximate weight comparison between the unmodified Viking '75 terminal propulsion system and the modified system is presented in the table below.

	<u>System Weights (kg)</u>	
	<u>Viking '75</u>	<u>MSR</u>
Propellant Tanks	14.8	7.4
$\text{GN}_2$ Pressurant	6.5	6.8
Pressure Bottle		9.5
Pressurant Control Assy		4.1
Propellant Control Assy	<u>8.2</u>	<u>5.0</u>
Totals	29.5	32.8

The estimated dry weight of the modified system is seen to be only 3 kg greater than the unmodified system because the increased weight associated with the regulated pressurization system is nearly compensated by the weight saving in propellant tankage and the propellant feed system. One propellant tank is eliminated, and one propellant isolation assembly is eliminated, though the remaining isolation assembly may require some modification to reduce its flow resistance.

The modifications described above are summarized in Figure VII-17. One of the original propellant tanks remains on the lander in its normal location, the other one has been removed and replaced by the  $\text{GN}_2$  pressure bottle and its associated pressurant control valving. The number, sizes, and locations of the seven thrusters used in the Viking '75 terminal propulsion system remain unchanged.

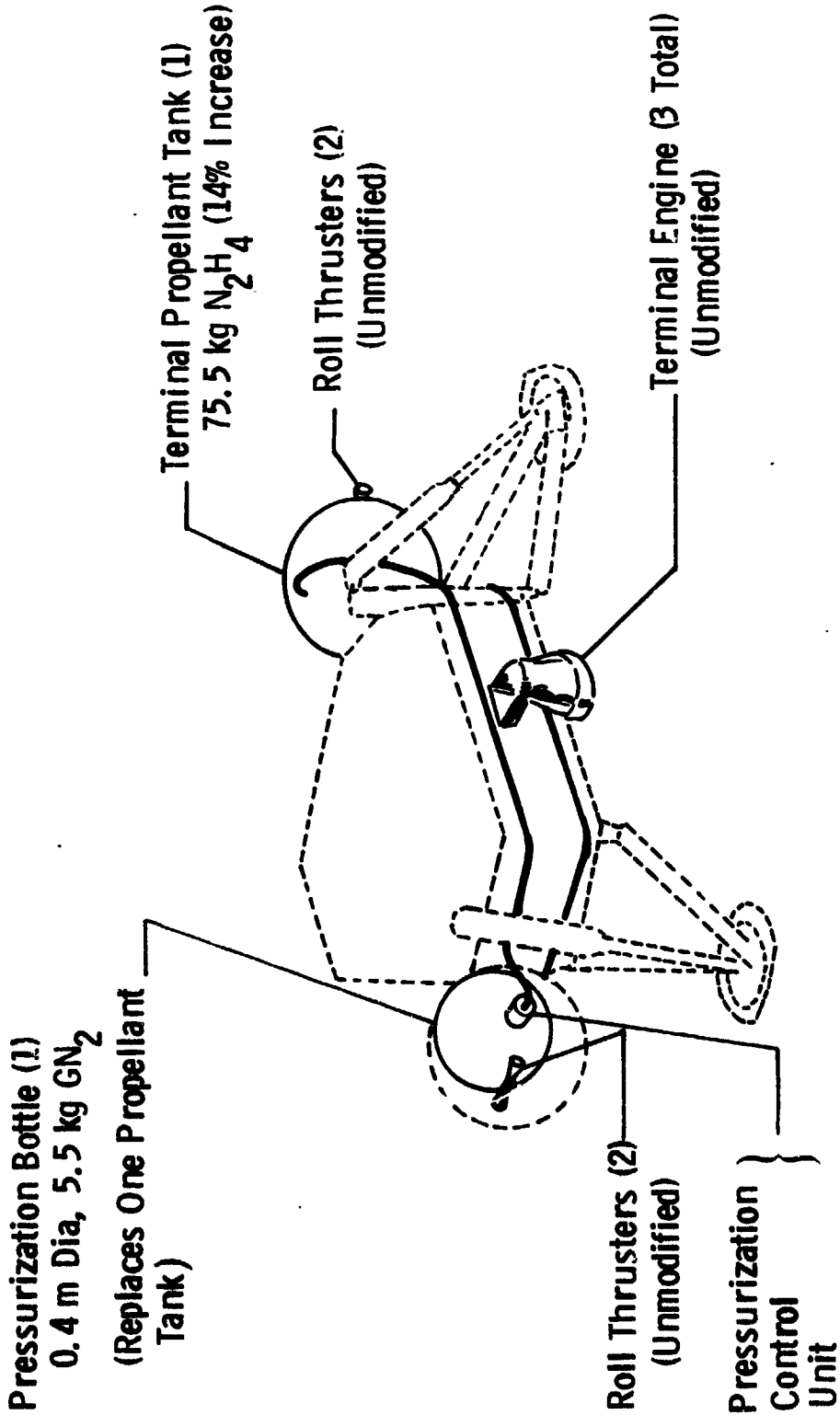


Figure VII-17 Terminal Propulsion System

## D. THERMAL CONTROL

The thermal performance of a space or planetary vehicle is uniquely determined by its temperature response to three sets of superimposed forcing functions: (1) the thermal configuration of the vehicle, i.e. the matrix of heat flow paths and thermal inertia provided by the structures and components (including thermal control); (2) the internal heat dissipation profiles; and (3) the external environments. These functions are time- and mission phase dependent, hence a valid assessment of thermal concerns and potential solutions of any given mission phase must take into consideration the total mission performed by the total spacecraft. In this section the thermal forcing functions of the MSSR Lander and MAV are examined in light of Viking'75 thermal technology, and the required modifications and new developments for the implementation of the MSSR mission are determined.

1. Sterilization-Through-Landing: The Viking'75 thermal control approach for these phases of the mission provides sufficient flexibility to assure adaptability to the MSSR mission, with modifications required at the detailed design level. The overall approach includes the use of a fluid loop for RTG temperature control during dry-heat sterilization, coupled with air conditioning during prelaunch operations; radiant distribution of RTG waste heat within the confines of the aeroshell and base cover for temperature-control of the lander and its external components during cruise; supplemental control of deorbit- and terminal propulsion systems by electrical heaters; the use of thermal inertia to maintain equipment temperatures during short transients, such as during boost, entry, parachute- and terminal descent, and midcourse maneuvers; and the use of coatings and insulation to control heat transfer through the capsule/environment interfaces. The requirements for modifications at the detailed design level are imposed primarily by two factors: the lower heat dissipation levels of the MSSR RTG's, and the configurational differences between the MSSR- and the Viking'75 landers.

2. Landed Operations: The most significant differences between the MSSR and Viking lander thermal characteristics occur during this phase of the mission:

(1) The presence of the MAV on the top of the MSSR lander increases the volume of the hardware requiring thermal control by a significant amount, the corresponding area of the lander/environment thermal interface being approximately three times that of the Viking '75 lander. The most significant problem associated with this thermal configuration is maintaining the MAV propellant temperatures within their required limits. The MAV propulsion system is characterized by bulky geometry, the absence of internal heat sources, narrow temperature limits, and low internal conductances. The supply and distribution of heat for thermal control of the MAV is, therefore, the central problem in the thermal control of the MSSR lander.

(2) Internal heat dissipation by equipment within the MSSR lander is approximately 25 to 30 percent, while total RTG heat dissipation is 40 percent of the Viking '75 levels.

(3) The environment on Mars during the MSSR mission is expected to be slightly warmer on the average, with somewhat narrower range of extremes, when compared with the Viking '75 mission. This is illustrated on Figure VII-18 which shows that for the initially assumed MSSR landing site accessibility latitudes of  $+30^{\circ}$  to  $-30^{\circ}$  the range of expected temperature extremes is in the order of  $22^{\circ}\text{C}$  (vs.  $56^{\circ}\text{C}$  for Viking), the "hot" extreme temperature being approximately  $5^{\circ}\text{F}$  warmer, than in the case of the '75 mission. The conditions for the specific latitude band identified in Figure II-8 of Chapter II will be somewhat less severe than those analyzed here.

The planned eight-day stay on Mars surface is too long to rely on the thermal mass of the propellants for temperature control. An analysis has indicated that the use of electrical heaters in combination with insulation as the principal means of maintaining propellant temperatures would be inconsistent with the weight and power limitations of the MSSR lander; the product of insulation weight and thermal watts required would range from 40 to 120 watt-power x kg insulation from hot to cold extreme situations, respectively. Because of the bulky nature of the propulsion system, and in view of the thermal configuration of the lander as described under (1) above, the thermal switch concept used on Viking '75 would be ineffective, when used to control MAV temperatures. In view of these considerations, a

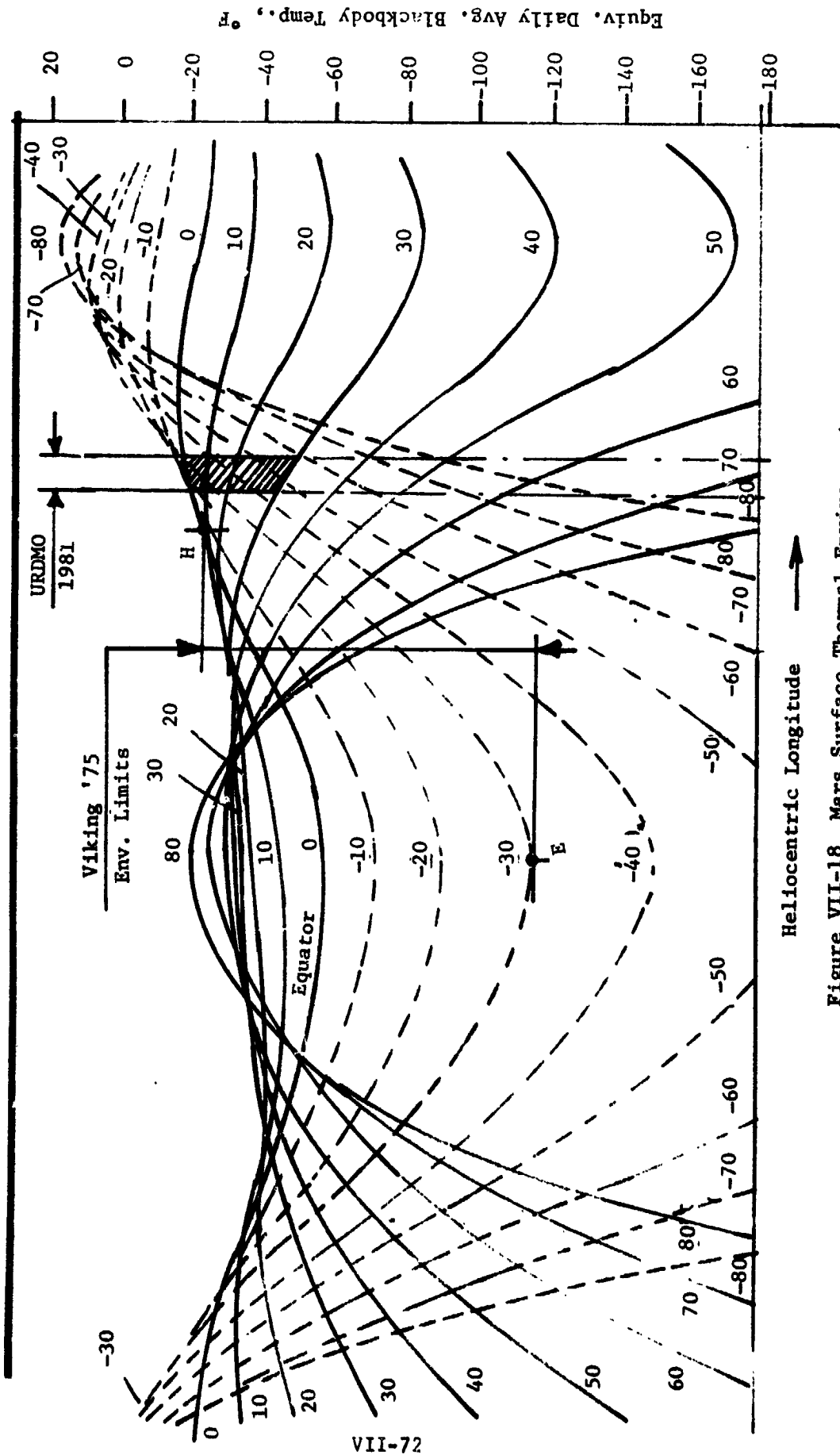


Figure VII-18 Mars Surface Thermal Environment

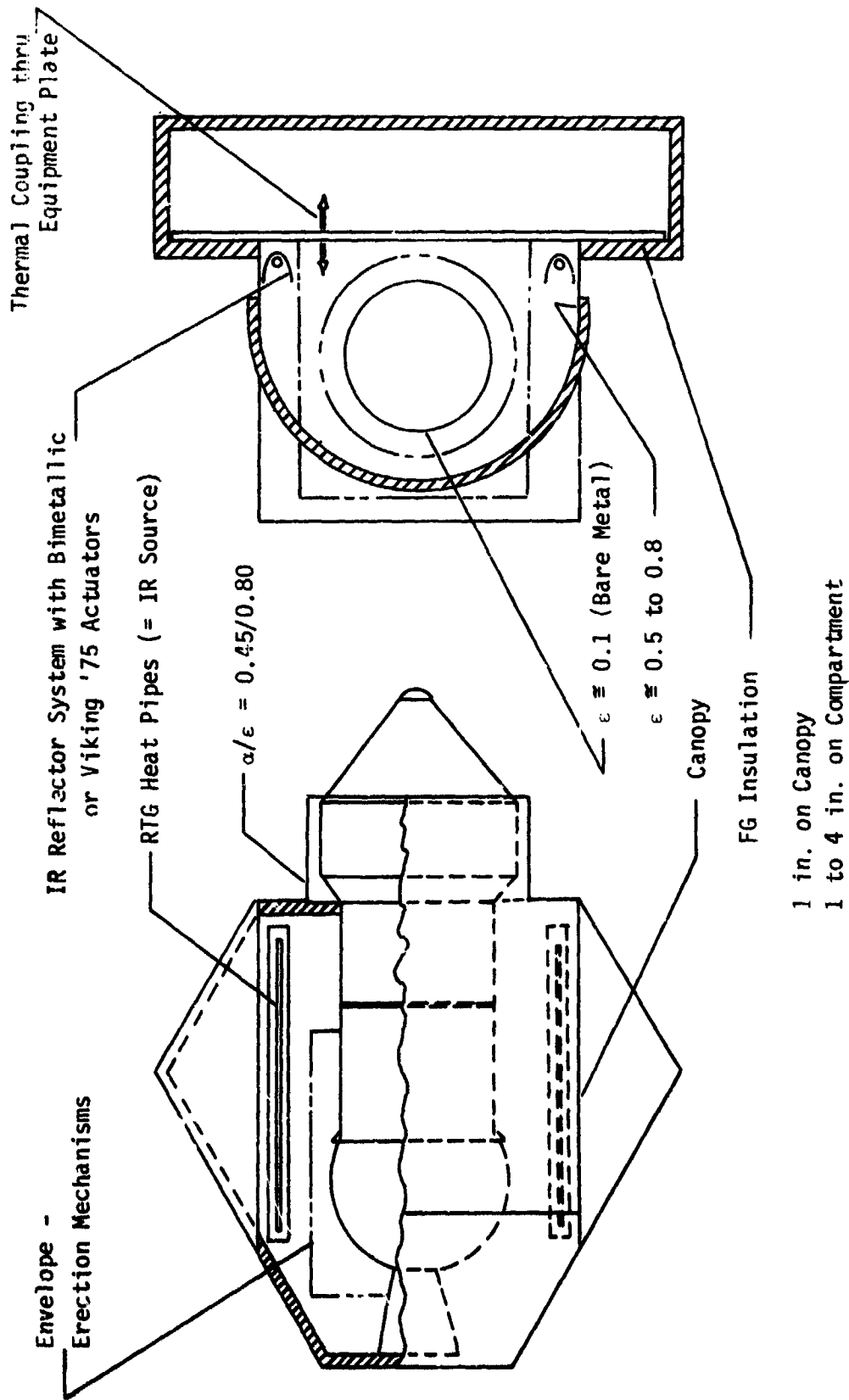
significant departure from Viking technology will be necessary in the thermal design of the MSSR lander/MAV configuration for Mars surface operations. The recommended approach is described below.

The baseline concept for Lander/MAV thermal control on Mars surface is depicted on Figure VII-19. The MAV is enclosed within a canopy on the top of the lander, which is thermally communicating with the lander equipment compartment through the equipment plate. The compartment and the canopy form an integrated thermal enclosure.

The "canopy" concept uses RTG waste heat as a source for thermal control, supplied in the form of "line-sources" via heat pipes. The heat pipe temperatures will be between 170 and 250°C. Radiant heat from the heat pipes will be directed essentially upward by IR reflectors (polished aluminum) as shown, and the radiation will be re-reflected and distributed around the MAV propulsion system by the reflective finish on the interior surfaces of the canopy. The "gap" between the canopy and the MAV serves as an insulator with effective conductivity = conductivity of Martian atmosphere + convective effects. Available experimental data indicate that the convective effects inside the canopy should be acceptable. A relatively thin layer of fibrous insulation is provided around the canopy to further aid in retaining the RTG waste heat inside the canopy, see Figure VII-19.

Control to accommodate hot and cold extremes is achieved in one or a combination of three possible ways: (a) rotation of the reflectors around the axes of the heat pipes via bimetallic actuators or equivalent; (b) size the system to survive the hot extreme, compensate for cold extremes by electrical heaters; (c) size the system for an appropriate nominal environment and qualify propulsion system for the hot and/or cold extremes.

The canopy will be terminated short of the tip of the conical nose of the MAV to provide access for sample acquisition (as shown), and supplemental electrical heating is provided to maintain the liquid propulsion temperatures within Stage III of the MAV. The upper portion of the canopy will be attached to the erection mechanism and will separate from the lander upon MAV erection prior to launch. For the baseline design no further thermal control of the lander is required after MAV launch.



VII-74

Figure VII-19 Current baseline Concept for MAV Thermal Control on Mars Surface

Functionally, the above baseline thermal control concept differs from Viking '75 lander thermal control in three essential aspects: (a) all of the RTG waste heat is dissipated inside a thermal enclosure; (b) the actively controlled part of RTG waste heat is the heat lost to the environment (as opposed to heat into the compartment); (c) heat distribution within the compartment is primarily by radiation channelling (vs. equipment plate conduction in the case of Viking '75).

MAV Ascent and Orbital Operations: Thermal control during this phase of the MSSR mission is accomplished by the use of standard methods, as depicted on Figure VII-20.

This concept takes advantage of the constant solar orientation of the MAV. Equipment compartment temperatures are maintained by passive thermal balance between the absorbed solar and emitted IR radiation through the "thermal window". The interior of the compartment is thermally coupled to the "window" by radiation, and it is thermally isolated from the rest of the spacecraft and from the space environment by multilayer insulation (except the window).

A similar concept is used to control the temperature of the sample container, with an absorptivity/emissivity ratio of  $a/e = 0.5$ , in order to maintain its temperature below  $0^{\circ}\text{C}$ . The solar angle was assumed constant at 35 degrees from the vehicle axis.

Thermal control of the shaded propulsion thrusters is achieved by insulation and thermostatically controlled electrical heaters.

Sample Container Thermal Control - Docking Through Earth Entry. During the approximately 730 days comprising Mars orbit- and Earth-return cruise, the sample container temperatures will be controlled as shown in Figure VII-21. Consideration was given to two types of anticipated requirements: a) the upper temperature limit of the sample is specified (e.g.  $0^{\circ}\text{C}$  as indicated on the figure), in which case thermal control can be achieved by passive means only; b) in addition, a relatively narrow range of controlled temperatures is also specified (e.g.  $-5$  to  $-25^{\circ}\text{C}$  as shown), which requires the addition of a 1 watt thermostatically controlled heater to minimize uncertainties associated with maintaining the lower temperature limit and the

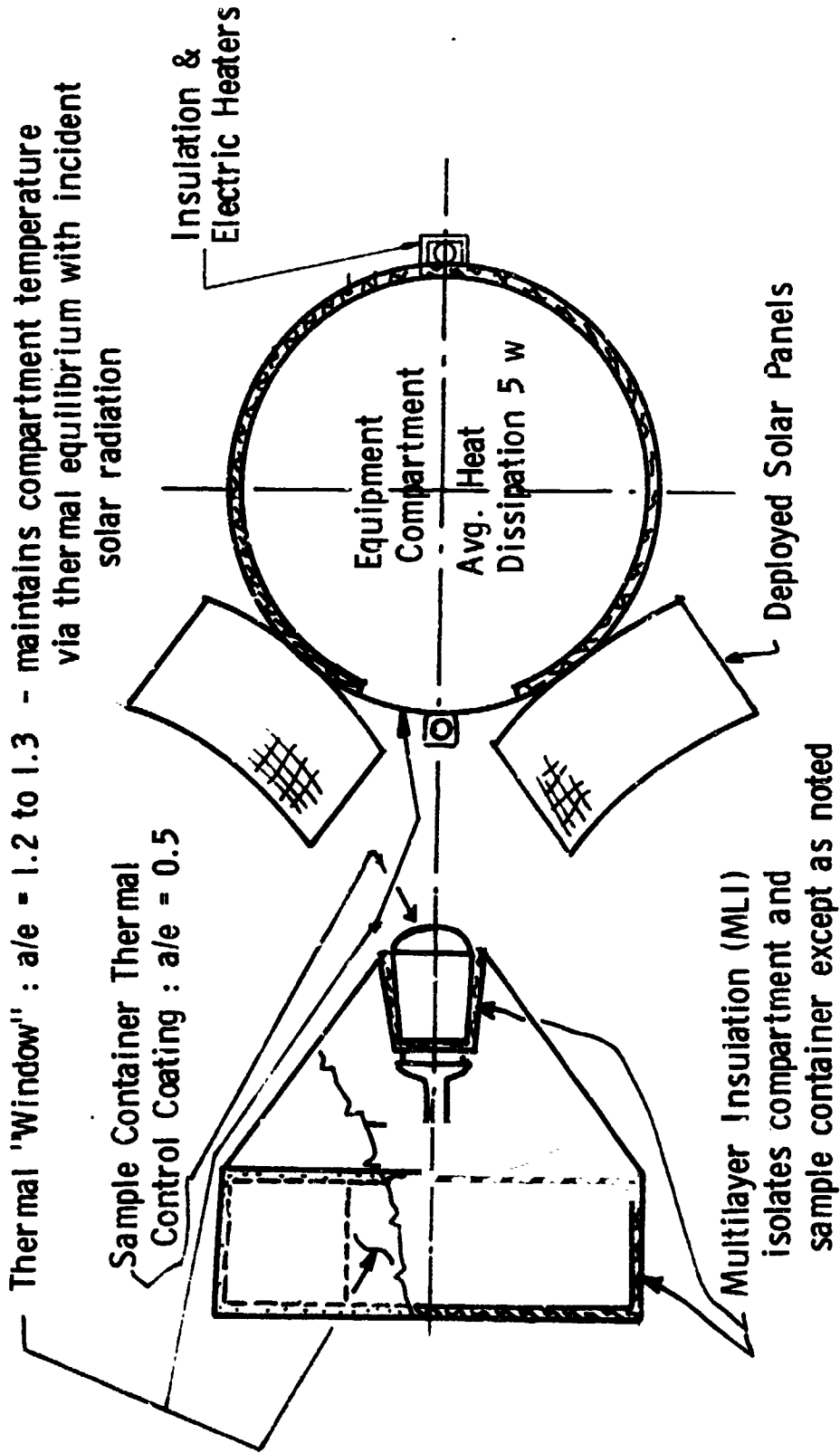


Figure VII-20 MAV Thermal Control During Orbital Operations

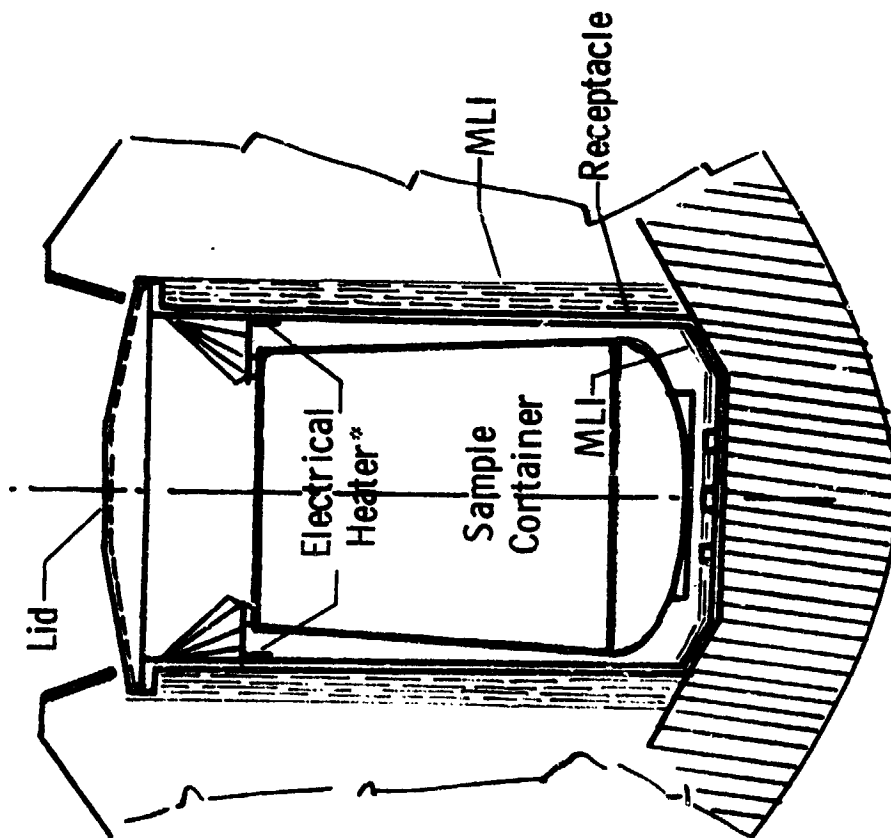
**Guideline: Maintain Sample Below 0°C (Say: -5 to -25°C)**

**Receptacle Lid: Thermal Radiator to Space (shaded from Sun except transients,  $\epsilon \approx 0.5$ )**

**Thermal Load to Lid: Internal Leakage = 2 watts; Controlled Electrical Heat = 0 to 1 watt\***

**Heat Leak Minimized by External and Internal Shielding (MLI), Titanium Receptacle (low k), Isolation Mounting of Container, Vacuum-Jacketed Configuration**

**Temperature Gradients through Sample Minimized by Aluminum (high k) Container, Isolation Mounting, "Cavity" Radiation Transfer**



\*For lower temperature limit control, if required.

Figure VII-21 Sample Container Thermal Control - Docking Through Earth Entry

required gradients through the sample. The requirement of maintaining the receptacle lid in the shade--except for short transients, such as during midcourse maneuvers--is consistent with current concepts of the mission profile.

## E. AERODYNAMICS

In this study the proposed configuration for the Mars Ascent vehicle has been evaluated from an aeroheating as well as from aerostability standpoint. Also, the modified Viking Lander Capsule was examined to confirm that the necessary cg shifts and after body shape changes were acceptable. The MAV is discussed first.

### 1. MAV Aerodynamics

A large amount of aerodynamic coefficient data for slender vehicles have been collected. Because for this type of vehicle the normal force coefficient variation with angle of attack is essentially linear up to about 25 degrees, this coefficient can be used for most purposes in derivative form with respect to angle of attack as a function of Mach number only. Also, the axial force coefficient and the center of pressure location are essentially invariant with angle of attack. Therefore, the aerodynamic coefficients can be presented in the simplified form shown in Figure VII-22.

The MAV center of gravity is located about 33 inches from the cone-cylinder juncture and the aerodynamic center of pressure is located very nearly at the juncture. Thus the vehicle is statically unstable, so that artificial stability (a reaction control system) is required unless tail fins are used. It has been estimated that cruciform fins with each panel having an area of about  $0.4 \text{ ft}^2$  would stabilize the MAV. However, it is not clear that positive stability is desired because in a strong cross wind the vehicle would tend to turn into the wind, whereas, without fins it would drift laterally with the ACS maintaining the desired attitude. Possibly, just enough fin area to provide neutral stability would result in a savings in ACS fuel. For the baseline however no tail is specified.

For the tailless vehicle, at the time shortly after liftoff, while the forward velocity is small, a cross wind would produce an angle of attack of 90 degrees. Under this condition the center of pressure occurs about at the centroid of the cross sectional area, just about coincident with the center of gravity. Thus the overturning moment would be essentially zero and the vehicle would gradually assume a lateral drift rate (relative to the ground) equal to the wind velocity.

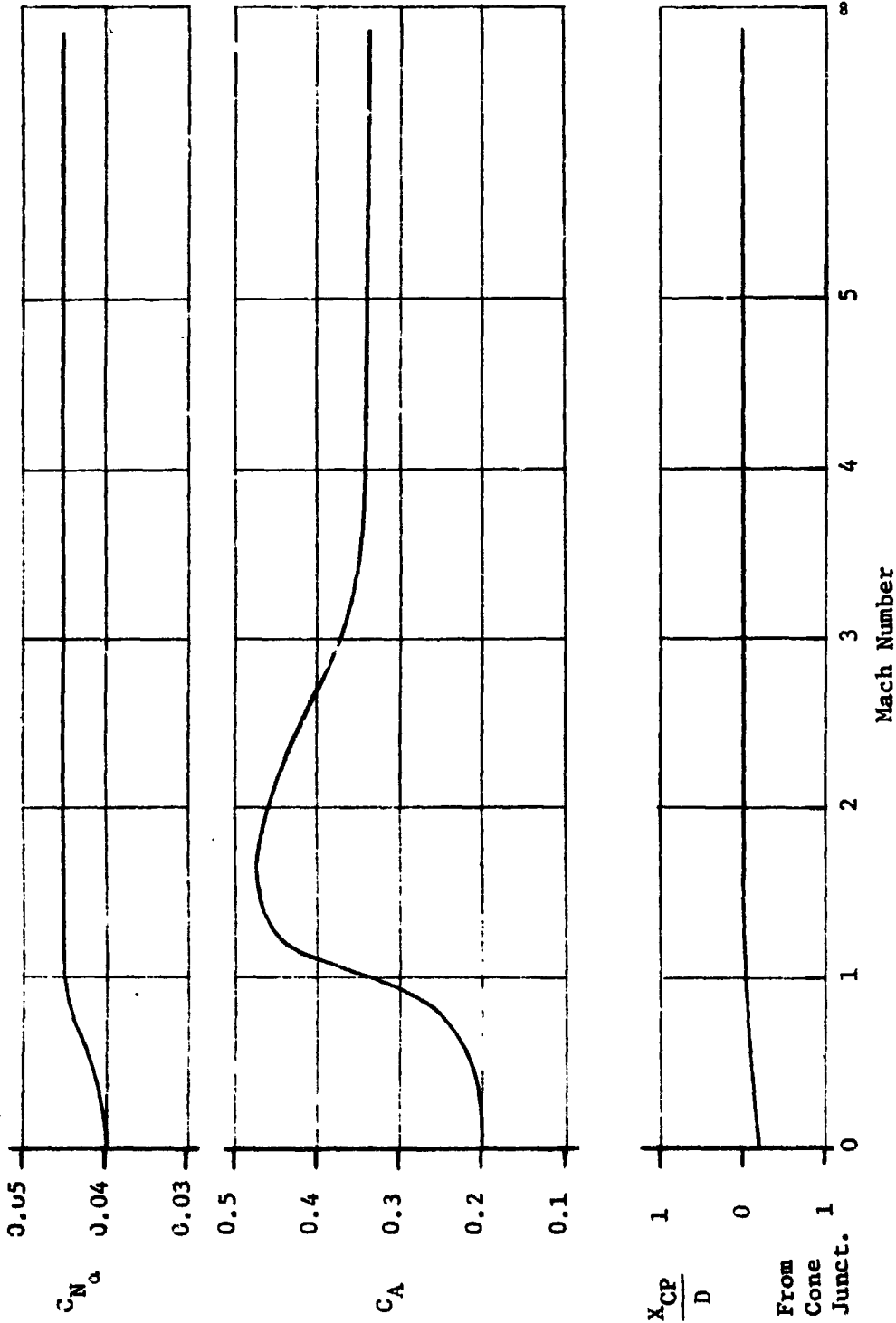


Figure VII-22 Aerodynamic Coefficients for the MAV

As the forward velocity increases, the center of pressure location will move toward the cone-cylinder juncture. Later in the trajectory the vehicle may be subjected to wind gradients. The NASA Mars Engineering Model specifies wind shears of 0.1 m/s/m up to 20 m/s. The peak value of 20 m/s is really insignificant. The gradient of 0.1 m/s is equivalent to an induced pitch rate of 0.1 rad/s. This is the disturbance which the ACS must be able to control. For the classical linear, spring-mass system the steady-state response to a ramp input is linear of the same magnitude with some time lag. This analogy is quite applicable to the MAV. Thus the control system will sense a pitch rate of 0.1 rad/sec and react accordingly. The rate of reaction, i.e., the torque required, will probably be established by the rendezvous accuracy requirements, since the rate of 0.1 rad/sec is small.

Because of the low atmospheric density on Mars' surface the dynamic pressure for a horizontal wind velocity of 90 m/s is only 2 psf. This pressure acting on the MAV in the upright position results in an overturning moment of only 106 ft-lb which is insignificant compared to the weight of the lander/MAV which produces a moment of 3946 ft-lb.

The cg of the lander/erection mechanism/MAV is 51 in. above the surface. This results in a tip over angle of 28 degrees. The wind effect on this angle is insignificant also.

Stagnation point heating rate as a function of time is shown in Figure VII-23 and the heating rate distribution for the MAV nose cone is given in Figure VII-24. This curve was obtained via a wind tunnel test in CO<sub>2</sub>. Candidate heat protection options are also shown in Figure VII-23.

## 2. MSSR Entry Vehicle Aerodynamic Stability

For the very blunt type of entry vehicle (EV) configuration, such as the Viking EV, the static aerodynamic characteristics are dominated by the forebody geometry. The nose radius, cone angle and edge radius are all important. The static stability, that is, the slope of the pitching moment curve,  $\frac{\partial C_m}{\partial C_n} = (x_{cp} - x_{cg})$ , is not strongly affected by longitudinal center of gravity location because the center of pressure is so far aft (well aft of the body) that small distances within the body are relatively insignificant. The center of pressure for the Viking EV as a function of Mach number is shown in Figure VII-25.

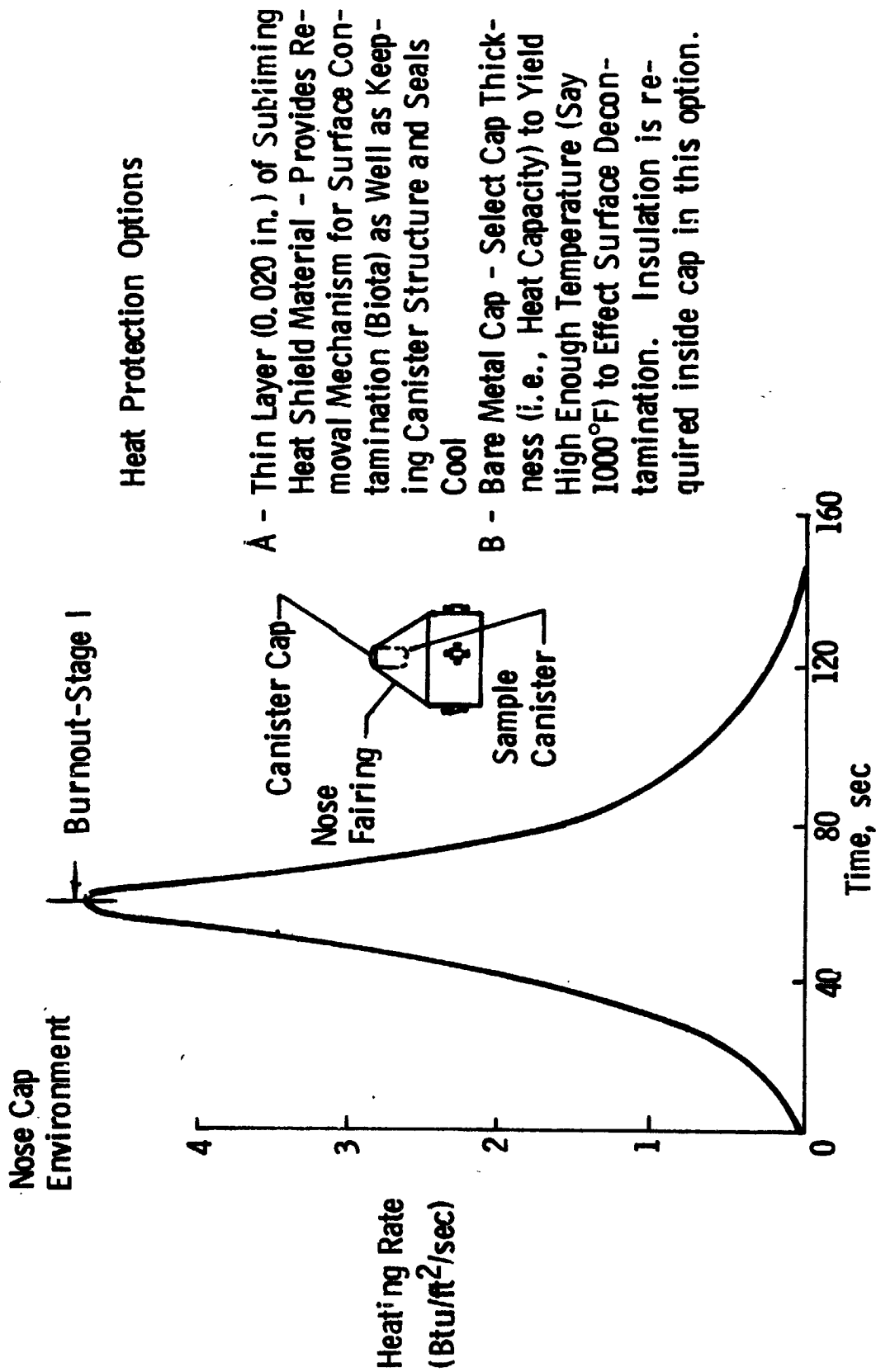


Figure VII-23 Aerodynamic Heating and Heat Protection Options During MAV Ascent

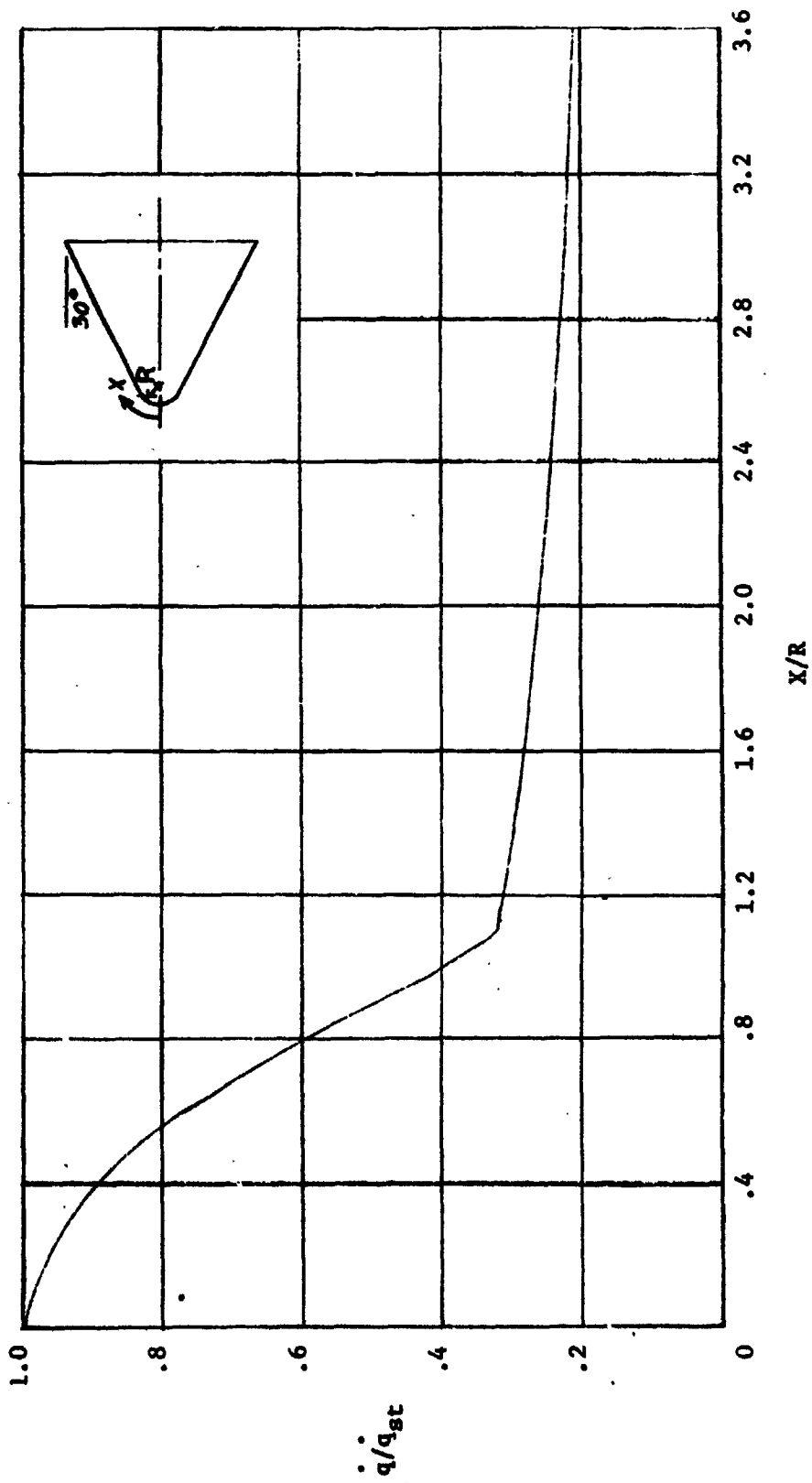


Figure VII-24 Aerodynamic Heating Distribution for the MAV Nose Cone

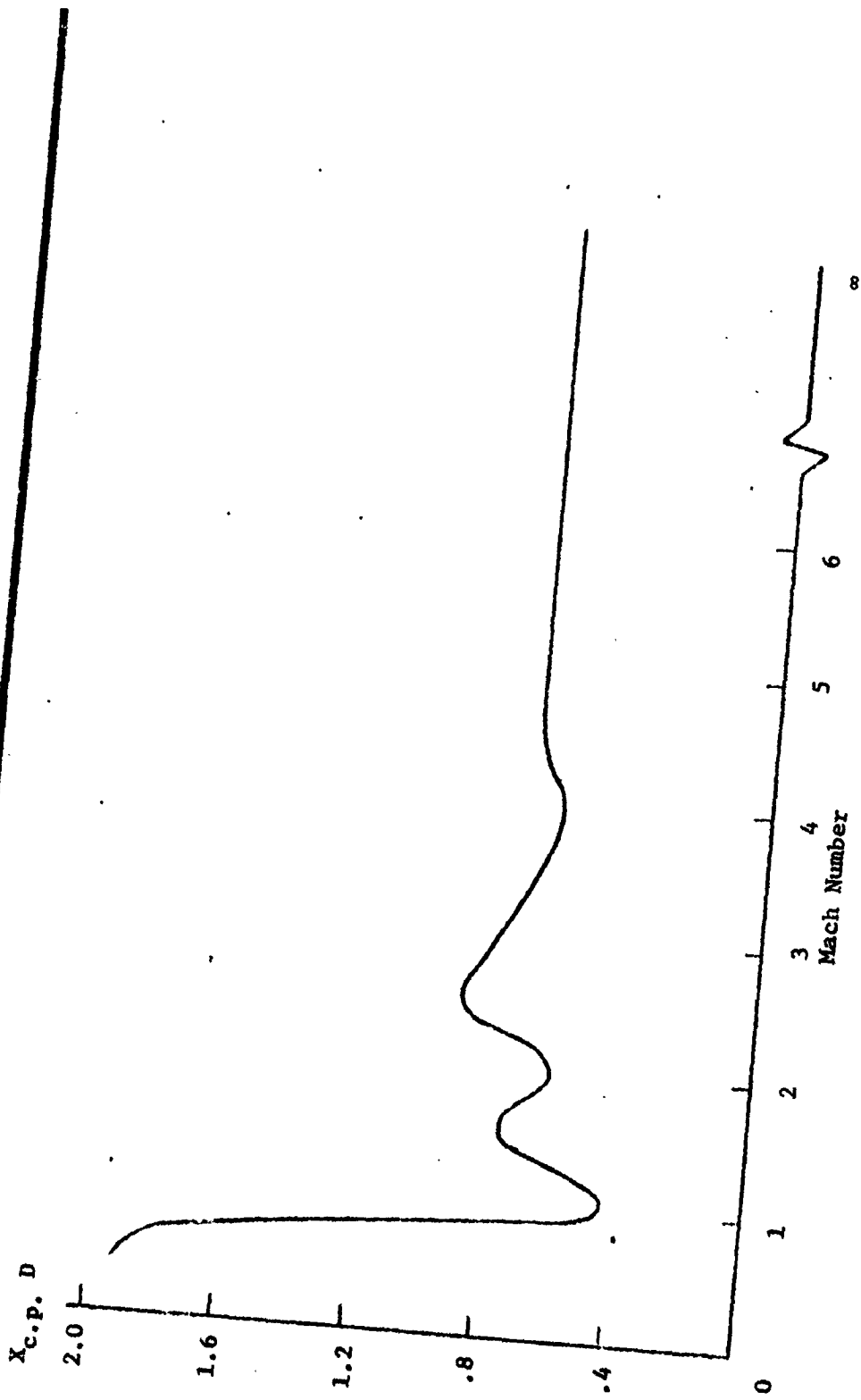


Figure VII-25 Center of Pressure Variation with Mach Number

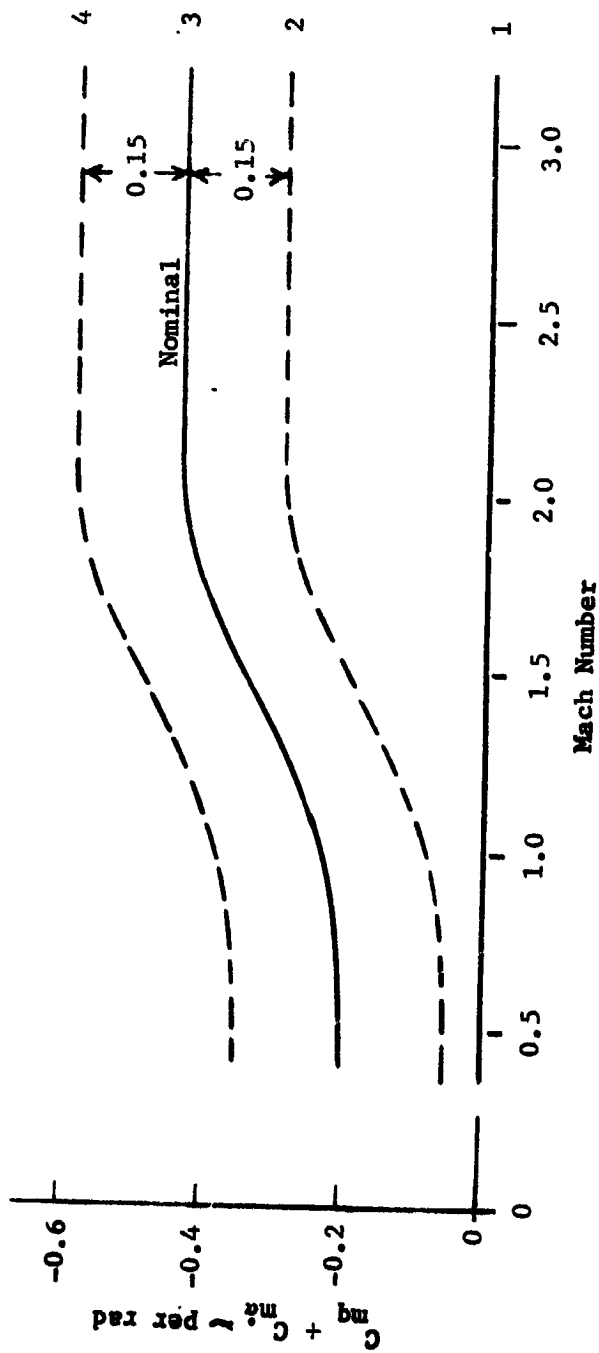
The dynamic stability is strongly dependent on the pitch damping coefficient derivative,  $C_{mq} + C_{m\dot{\alpha}}$ , which is very sensitive to c.g. location and afterbody geometry in addition to forebody geometry. Of particular importance is the angle of the afterbody just aft of the plane of maximum diameter. Another important parameter to dynamic stability is the ratio of body diameter to radius of gyration in pitch,  $D/\sigma_y$ . This ratio for high drag EV shapes must usually be greater than about 3.5. (The value for the Viking EV is about 5.3 because of the small, compact lander relative to the EV diameter. The reason for the importance of  $D/\sigma_y$  is that in the pitching equation of motion it appears as a squared multiplier on  $C_{mq} + C_{m\dot{\alpha}}$ .)

The aerodynamic coefficients for the Viking EV will apply for the URDMO vehicle if the geometry is not significantly different. Because with the presently conceived modifications the initial afterbody angle is not altered and the additional length is relatively small, it is believed that the Viking aerodynamic characteristics are quite applicable.

A slightly different degree of transverse c.g. offset ( $\bar{y}$  cg/D) is required for the MSSR entry capsule to achieve the same L/D since the axial c.g. location ( $x_{cg}/D$ ) is aft of that for the Viking entry capsule. However this amounts to only about an 0.12 inch change.

The pitch damping coefficients for the Viking EV have been determined through an extensive wind tunnel test program. First, a number of candidate shapes were studied and then the selected shape was thoroughly tested. The resultant coefficient which pertains in the range of the trim angle of attack is shown as a function of Mach number in Figure VII-26.

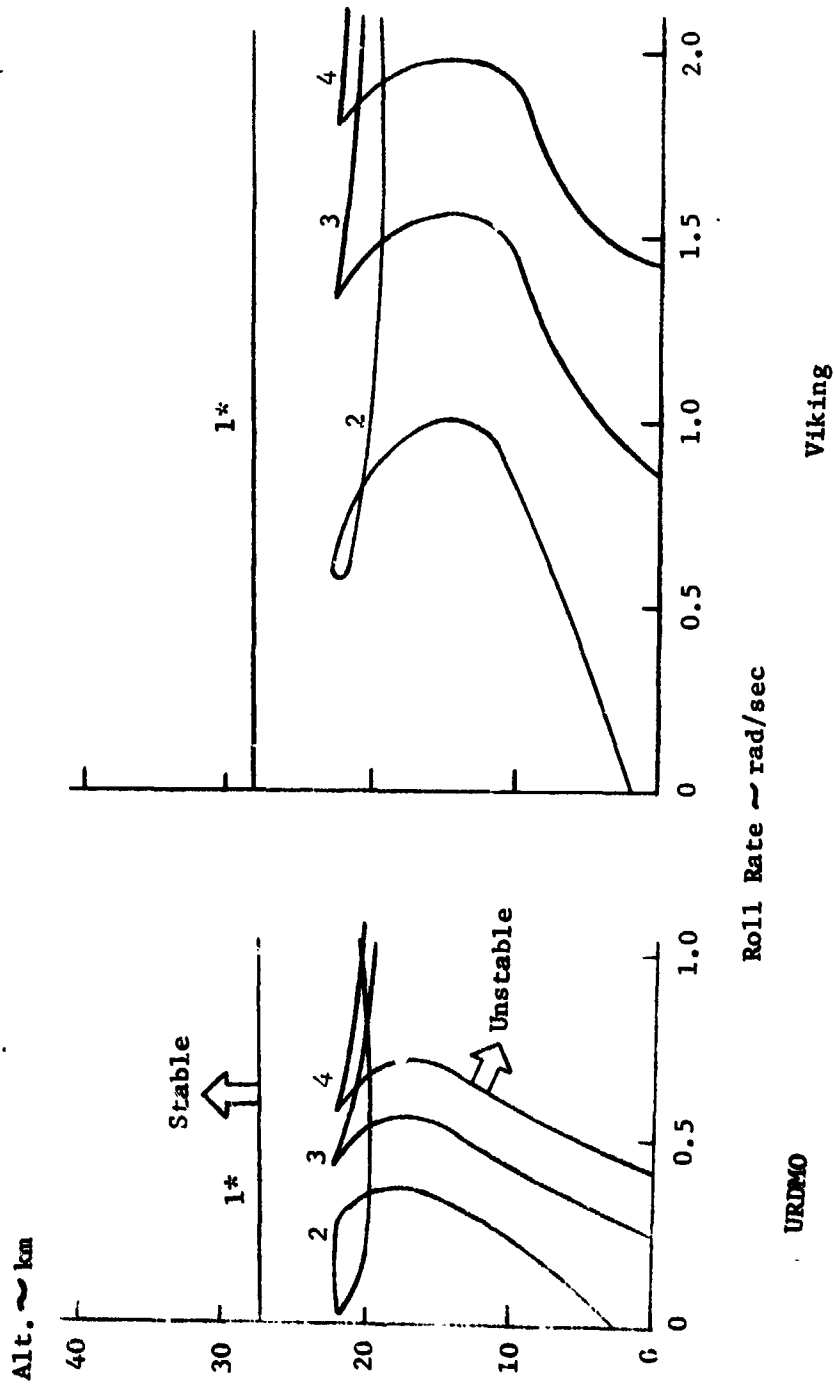
A brief study of the dynamic stability characteristics of our EV has been made by computing the Coakley stability criterion for various points along the entry trajectory using the four  $C_{mq} + C_{m\dot{\alpha}}$  functions shown in Figure VII-23 and various values of roll rate. A similar study has been made for the Viking EV for comparison. Although rolling is not intended for either mission it was deemed of interest to examine how close to roll resonance these configurations might be because in flight the roll control system will produce certain roll rates depending upon the severity of atmospheric disturbances experienced.



VII-86

Figure VII-26 Pitch Damping Coefficient Functions

The results of the study are shown in Figure VII-27 which delineates stability boundaries as functions of altitude and roll rate. By "stable" it is meant that an angle of attack disturbance will tend to converge. It is immediately apparent that for a value of  $C_{mq} + C_{m\dot{\alpha}}$  equal to zero, both vehicles become unstable below about 28 km during entry. This boundary corresponds to the destabilizing effect of the negative dynamic stability gradient subsequent to the passing of peak deceleration. It is apparent, since all of the boundary curves for the Viking EV occur at larger roll rates than our EV, that the Viking EV is somewhat more stable. This results mostly from the larger value of  $D/\sigma_y$ . At zero roll rate both vehicles become unstable at an altitude of about two kilometers with the number 2 damping coefficient curve. This is of no real significance because in both cases parachutes are deployed well above this altitude. For the MSSR EV with the number 2 curve the vehicle is very close to being passively unstable at about 21 km of altitude. It is quite possible that the vehicle would traverse this region before significant angle of attack divergence occurs even without its ACS system in operation. However with the Viking '75 ACS system in operation in the MSSR (URDMO) vehicle, stability is assured.



\*Number refers to  $C_{mq} + C_{m\dot{\alpha}}$  Function in Previous Figure

Figure VII-27 Pitch Damping Coefficient Functions

## F. STRUCTURE

The structural elements necessary to accomplish a sample return mission can, for the most part, be derived from existing hardware. The exceptions to this are the Mars Ascent Vehicle (MAV), the Earth Entry Capsule (EEC), and, to some degree, the Earth Return Vehicle (ERV). A Titan/Centaur with a Viking nose fairing was selected as the launch vehicle for the baseline mission. A modified Viking spacecraft would be used to accomplish the remainder of the mission. The Earth launched payload is shown in Figure VII-28.

Requirements: A significant portion of the structural design effort is as a result of the modifications that are required to existing hardware. These include stretching the orbiter propellant tanks and support truss; modifying the orbiter/VLC adapter structure to accommodate the ERV; enlarge bio-shield cap; enlarge base cover; redesign parachute support truss; and modify lander body to accept the MAV with its launcher.

MAV: The Mars Ascent Vehicle is a new-build item. Stages I and II consist of solid rocket motor assemblies with interstage skirts. The proposed motor assemblies would be spherical titanium tanks with nozzles constructed of low density carbon phenolic and glass phenolic. The skirts would be chem-milled aluminum cylinders with a ring frame at either end. Staging would be accomplished by using explosive nuts and the necessary fittings would be integrated into the skirts and frames. In addition, the Stage I skirt contains the fittings to interface the launcher mechanism.

Stage III of the MAV would be packaged as a single black box. The primary structure would be an aluminum cylinder with a transition section on the aft end to interface the smaller diameter Stg. II skirt. The nose fairing would be constructed of R/F transparent, glass reinforced, phenolic to allow operation of the antenna mounted inside the MAV. Subsystem components would be mounted on an aluminum rack which would also provide support for the titanium propellant spheres. Sealing the stage to protect the components from the martian environment is a major concern. The aft end, splice frames, propellant feed line and solar panel wiring penetrations, and the nose fairing interface with the sample canister, all would need to be sealed.

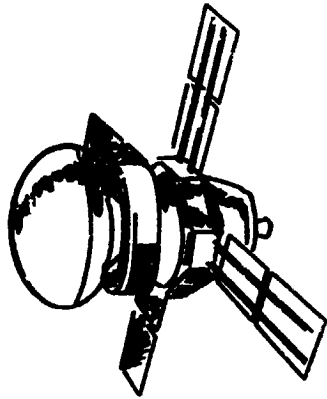
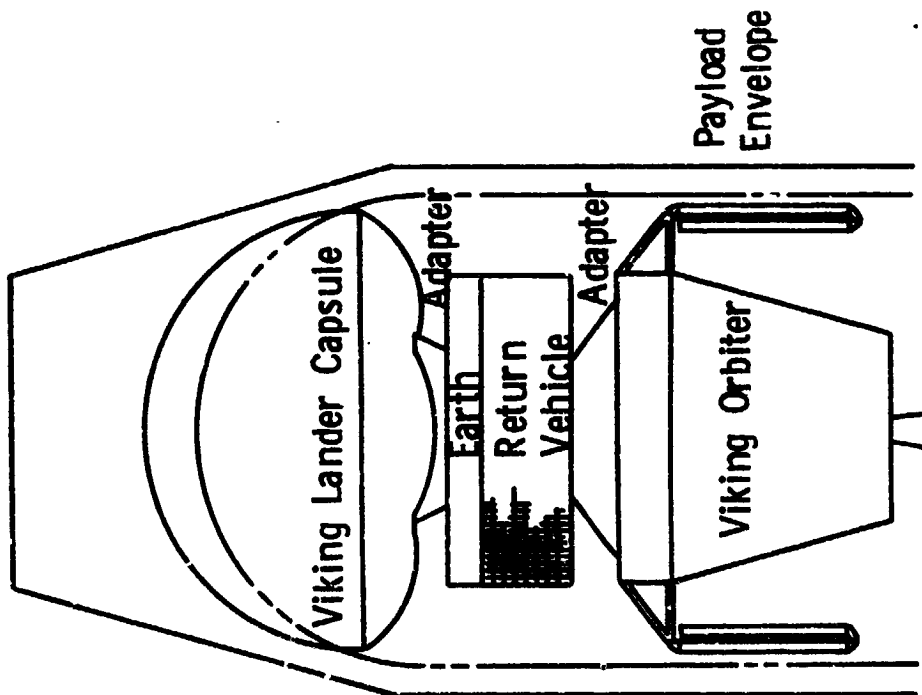


Figure VII-28 Earth Launched Payload

Mechanisms are required in Stage III to deploy the solar panels, open the canister to receive the sample, present the canister for transfer, and to release the canister following transfer. The solar panels would be solenoid released; the canister opened and closed by a screw drive actuator; the canister presented for transfer by a Viking type extendable boom, and a pyro release for the canister from the boom.

The sample canister is a can within a can. Again, aluminum alloy would be used to construct the can and a gold deforming seal would be employed to seal the container for the return trip.

Lander: The Viking lander body geometry, construction technique, and materials used would remain unchanged. The structure would be modified as required to accommodate component additions and/or deletions. The most significant of these is the addition of the MAV launcher which would be supported off the lander equipment plate. Enough components have been deleted from the plate to make this structurally feasible. By beefing up the landing leg load limiters, the leg assemblies appear adequate to land the increased weight imposed by the MAV based on analysis discussed in Chapter VI-B. The launcher would be turret mounted and provide a two point attachment with the MAV at its CG. It is capable of raising the MAV to desired elevation angle and rotating to the proper azimuth angle. Elevation angle movement would be provided by torque motors while the gear driven turret provides azimuth.

Installation of the MAV on top of the lander forces the parachute canister aft thus redesigning the parachute support truss and enlarging the base cover and bioshield cap accordingly.

Increased heat loads on the aeroshell/heat shield due to direct entry make it necessary to increase frame height and material gages on the aeroshell. The deletion of entry science in the aeroshell simplifies these mods.

Orbiter: The most significant structural change to the Viking orbiter is the stretch to the propellant tanks. The amount of propellant required is increased by 15% over the Viking'75 and this could best be accomplished by increasing the length of the tank barrel sections by approximately 12 cm and modify the thermal blanket accordingly. The remainder of the primary orbiter structure would not be affected except for addition and deletion of component brackets.

ERV: A major change to the Viking spacecraft is the addition of the Earth Return Vehicle between the orbiter and the Viking lander capsule. A Pioneer Venus derivative was assumed to be the ERV design. A conical adapter skirt of skin-stringer construction with a frame at either end would be used to transfer loads from the ERV to the orbiter. On the other end of the ERV is another conical adapter to attach the VLC to the ERV. This skirt serves two purposes in that it contains a liner that is used to guide the sample canister into the receptacle in the EEC. The skirt interfaces the existing VLC support points and the ERV thrust cylinder. The adapter will have the capability of being jettisoned from the ERV following sample transfer.

The ERV would contain the Earth Entry Capsule. To do this it would be necessary to relocate the Pioneer Venus antenna installation in order that the EEC could be installed on the vehicle centerline. Details of this antenna relocation were not worked under this study and should be a part of a future assessment of the entire Earth Return Vehicle. The Earth Entry Capsule would be clamped into the ERV so as to allow separation for Earth entry.

## VIII MISSION PROFILE/OPERATIONS

Part A of this section presents a detailed timeline for the MSSR mission. The timeline is the result of an exercise in the scheduling of mission activity carried out to uncover potential problems.

Part B deals with identification of Mission Opportunity Dependent quantities and their impact on the mission timeline presented above.

### A. 1981 DETAILED MISSION TIMELINE

Table VIII-1 contains a detailed profile of the MSSR mission as conceived in this study. Particular emphasis is placed on the orbital rendezvous, docking and sample transfer phases. The purpose here is to:

- 1) Delineate key computations (i.e. show what computations are made and when they are required in the mission)
- 2) Show where computations are performed (i.e. either in the mission control center or onboard one of the S/C)
- 3) Display the sequence of operations
- 4) Point out DSN tracking arcs in terms of number of orbits and type of data
- 5) Distinguish various maneuver types (i.e. pure attitude changes vs. thrust through center of gravity)

Certain groundrules and assumptions were used in establishing the timeline. These are:

- 1) Twelve hours allowed for O.D. and maneuver computation
- 2) One hour for attitude maneuvers after CMD reception
- 3) MAV has power for 50 minute tracking per orbit
- 4) Continuous CMD capability for vehicles in orbit

The busiest periods of mission control activity occur prior to MAV liftoff and prior to initiation of orbiter circular trim sequence. Most liftoff quantities can be computed once the MAV position and attitude have been determined (within three days of landing). Only the launch time and azimuth computations must be deferred until the final orbiter state is available.

Table VIII-1 MSSR Mission Detailed Timeline

Time (hours)	Total S/C Event	Mission Control Activity
Trans-Mars Injection (TMI)		
TMI (6 Dec. 1981)	* TMI * Begin Doppler TRK .....	Monitor Trans-Mars Injection (TMI)
TMI + 228.00	End Doppler TRK	Compute S/C State & 1st MCC with PQ Bias XMT CMDS for MCC #1
TMI + 239.00	Load CMDS Attitude Man.	
TMI + 240.00	* 1st MCC *	
Mars Encounter Phase: MOI - 720 hours = TMI + 272 days		
MOI - 720	Begin Doppler TRK .....	Begin O.D. for MCC, MOI and deflection .....
MOI - 252	Last Data Pt. for MCC .....	Compute S/C state and 2nd MCC maneuver without PQ bias. .....
MOI - 241	Load CMDS Attitude Man. .....	XMT Commands for MCC#2 .....
MOI - 240	* 2nd MCC * ..... TRK .....	Begin MCC Verification .....



Time (hours)	Orbiter Event	Lander Event	Mission Control Activity
LND + 0.5		End Xmission	Select HR TV Site. Generate CMD Seq. Process sun sensor data, determine Lander attitude.
LND + 24.6	TRK (~1.5 orbits)	Load CMDS Begin HR TV Xmission (250 bps) S-Band Ranging	XMT CMD SEQ.
LND + 25.1		End Xmission	Select Sample Site Compute Surface Sampler (S.S.) CMD Seq.
LND + 49.2		Load CMDS Open Sample Canister Obtain Sample Verify With HR TV	XMT S.S. CMD SEQ.
LND + 49.7		S-Band Range End 1st Sample Period	Select 2nd Sample Site
LND + 73.8		Load CMDS Repeat Sample Acquisition Cycle	XMT S.S. CMD SEQ Compute Lander Position From Ranging Data (Lat., Long., Alt.) Compute Orbiter State and Plane Change Man. XMT S.S. CMD SEQ to LNDR
LND + 146.25	End Doppler TRK	Load CMDS Repeat Sample Acquisition Cycle	
LND + 148.1			
LND + 156.25	Load CMDS Attit. Man.		XMT CMDS for Plane Chng.
LND + 158.25	* Plane Change *		

Time (hours)	Orbiter Event	Lander Event	Mission Control Activity
LND + 197.8	Begin Doppler TRK ..... TRK (~1.0 Orbit) ..... End Doppler TRK	Complete All Sample Acquisition Activity Close Canister	Verify Sample Canister Closed
LND + 251.8		Load CMDS Erect MAV	Compute MAV Ascent Parameters: • Liftoff Time (Biased) • Launch Azimuth • Pitch Rate • Elevation Angle • Burn Times • Coast Times • Time to Seek Earth XMT CMDS to MAV/Lander
LND + 261.75		MAV Event Verify/Correct Ascent Attit.	
MAV Ascent (ASC) to Rendezvous Phase: ASC = LND + 263.75 hours			
ASC	* Apopsis * Passage Begin Doppler TRK .....	* MAV Liftoff * (100 x 2200 km) P <sub>MAV</sub> = 2.58 hrs.	

Time (hours)	Orbiter Event	MAV Event	Mission Control Activity
ASC + 20.25		Seek Earth	Begin MAV O.D. Determine Best Data Processing for Prediction of Apoapsis State
ASC + 31.25		Lock-up Begin Doppler TRK (50 min/rev)	
		End Doppler TRK	
ASC + 32.25		Load CMDS Attit. Man. * MAV Circ. * (2200 x 2200) P MAV = 3.53	Compute MAV State and Circ. Maneuver CMDS; Time to Seek Earth XMT CMDS to MAV
	TRK (~1.5 orbits)	Seek Earth Lock-up Begin Doppler TRK	
		(50 min/rev) (~12 revs)	
ASC + 62.61		End Doppler TRK	Begin Final MAV O.D. and Recirc. Trim Computations; Also Time to Seek Earth XMT Recirc. CMDS to MAV
ASC + 73.61		Load CMDS Attitude Man. * Recirc Trim *	
ASC + 74.61	TRK (1.0 rev)	Seek Earth Lock-up Begin Doppler (50 min/rev) (~5½ revs)	
			MAV Orbiter O.D.

Time (hours)	Orbiter Event	MAV Event	Mission Control Activity
ASC + 93.5	End Doppler TKK	End Doppler TKK	Final Computation of Orbiter & MAV States and Orbiter Periapsis Adjust (HP) Maneuver; XMT HP CMDS to Orbiter
ASC + 104.5	Load CMDS Attitude Man.		
ASC + 105.5	* Periapsis * Adjust (2250x100,000) P Orb = 107.4 Begin Doppler TKK (~ 1.5 Orbits)		
ASC + 226.36	.....	Begin Doppler TKK ..... (50 min/rev) (~8 revs) End Doppler TKK	Final Computation of Orbiter and MAV States and Orbiter Phasing Maneuver XMT Phasing CMDS to ORB.
ASC + 254.6	End Doppler TKK		
ASC + 265.6	Load CMDS Attitude Man.		
ASC + 266.6	* Phasing * Maneuver (2250 x 5904) P Orb = 5.5 hrs Begin Doppler TKK .....		

Time (hours)	Orbiter Event	MAV Event	Mission Control Activity
ASC + 298.2	(~8.0 Orbits) ..... End Doppler TRK		Final Computation of Orbiter State and Orbiter Circ. Maneuver XMT CMDS to Orbiter
ASC + 309.2	Load CMDS		
ASC + 310.2	Attitude Man. *Circularization*		
	Begin Doppler/ AVLBI	Begin AVLBI TRK	
	(~4 Orbits) .....	(~4 Orbits) .....	
	End Doppler AVLBI	(50 min/rev) ..... End AVLBI	Compute MAV and Orbiter States, Orbiter Trim Maneuvers, $\Delta V_1$ , $\Delta V_2$ , $\Delta V_3$ , Maneuver Times, and MAV Orbiter Look Attitudes
ASC - 326.47			XMT CMD SEQ to Orbiter
ASC + 336.42	Load CMDS		
ASC + 337.42	Attitude Man.		
ASC + 338.42	* $\Delta V_1$ *		
ASC + 339.18	Attitude Man.		
ASC + 340.18	* $\Delta V_2$ *		
ASC + 340.94	Attitude Man.	Load CMDS	XMT Look CMDS to MAV
ASC + 341.94	* $\Delta V_3$ *		
	Seek MAV	Seek Orbiter	

Time (hours)	Orbiter Event	MAV Event	Mission Control Activity
ASC + 342.25	Radar Lock (LOS Lock) Compute Closing ΔV Maneuver Attitude Man.	Radar Lock (LOS Lock) ..... Attitude Hold ..... LOS Lock ..... Extend Sample Canister Boom	
ASC + 343.25	* Closing ΔV * LOS Lock Auto MCC Based on R, R Control Curves	* Hard Dock * Canister Release * Undock *	Verify Sample Transfer
ASC + 344.89 (100 secs)	Begin Docking Phase (Range = 30 meters)		
ASC + 344.92	* Hard Dock *		
ASC + 348.5	* Undock * Close EEC Cover (Seal Canister) Jettison Docking Cone	(Available as Aid for Mapping of Gravity Field Prior to ERV Departure.)	Verify Closing of EEC (Plan MAV Mission Based on Remaining Fuel Load)
Pre-Trans-Earth Injection (TEI) Phase: TEI - 384 hours = ASC + 393 days			
TEI - 384.0	Begin Doppler TRK ..... (-4 revs) .....		

Mission Control Activity
Compute Orbiter State and ERV Maneuver Attit XMT CMDS for Sep. Attit.
Compute ERV Orbit and Maneuver (HA) to Raise Apoapsis XMT CMDS for HA to ERV
Compute ERV State and Maneuver (HP) to Lower Periapsis XMT CMDS for HP to ERV

ERV Event
ERV * Separation Begin Doppler TRK . . (~4 Orbits) . . End Doppler TRK
Load CMDS *Raise Apoapsis* (2250x100,000) P <sub>ERV</sub> = 107.3 hrs Begin Doppler TRK . . (~1.5 Orbits) . . End Doppler TRK
Load CMDS Attitude Change

Orbiter Event
End Doppler TRK
Load CMDS Attitude Change
ERV * Separation (Available as Aid for Mapping of Gravity Field Once ERV Has Departed)

Time (hours)
TEI - 369.60
TEI - 357.60
TEI - 343.20
TEI - 331.20
TEI - 170.25
TEI - 159.25

Time (hours)	ERV Event	Mission Control Activity
TEI - 158.25  TEI - 12.00 TEI - 1.00 TEI (28 Nov. 1983)	Lower * * Periapsis Begin Doppler TRK . . . (~1.5 Orbits) . . . End Doppler TRK Load CMDS Attitude Change * TEI *	Compute ERV State and TEI Maneuver XMT CMDS for TEI
Trans-Earth Injection Phase		
TEI + 228.04  TEI + 240.0 TEI + 170 Days	Begin Doppler TRK . . . End Doppler TRK Load CMDS Attitude Change * MCC #1 * Begin Doppler TRK . . . End Doppler TRK	Compute ERV State and 1st MCC Maneuver XMT CMDS for 1st MCC  Compute ERV State and 2nd MCC Maneuver

Time (Days)	Earth Entry Interface (EI) Phase: EI - 60 Days = TEI + 247 Days		ERV Event	Mission Control Activity
TEI + 199.97			Load CMDS	XMT CMDS for 2nd MCC
TEI + 200			Attitude Change * MCC #2 *	
EI - 60 Days			Begin Doppler TRK : : :	
EI - 30.5 Days			End Doppler TRK	Compute ERV State and 3rd MCC Maneuver
EI - 30 Days			Load CMDS	XMT CMDS for 3rd MCC & EEC Separation Time
EI (1 Oct. 1984)			Attitude Change * MCC #3 * *Separate EEC* *Deflect ERV* * EEC Entry * *EEC Air Snatch*	

The busiest onboard activity period starts with circular trim sequence and ends with hard dock. Control is entirely with the orbiter. Guidance and control requirements for this period have been examined. With present Viking orbiter maneuvering (attitude rate) capability enough time is available for all events as presented.

No periods of activity (for either S/C or mission control) have been found to be too complex or busy to rule out this MSSR mission mode.

## B. MISSION OPPORTUNITY DEPENDENT QUANTITIES

The following mission opportunity dependent quantities are identified:

- 1) Encounter O.D. accuracies
- 2) In-orbit O.D. accuracies
- 3) Landing site latitude
- 4) Orbiter capture maneuver and plane change for return
- 5) Lander position determination accuracy
- 6) S/C CMD opportunities
- 7) ERV TEI requirement

Maneuver related quantities will limit the MSSR launch/encounter space but have little or no effect on the sequence of events presented in part A. Tracking requirements on the other hand will change the time between events depending on how much data is needed to produce a desired level of O.D. accuracy. Single vehicle Quasi Very Long Baseline Interferometry (QVLBI) data may be used to keep this variation to a minimum. During the encounter phase approach O.D. accuracies will impact the likely period of the inserted orbiter. This in turn will effect the period of the phasing orbit, etc. None of these quantities above, however, will change the ordering or contents of the sequence of events presented earlier.

## IX EARTH ENTRY CAPSULE STUDY

The Earth Entry Capsule Design Study was added to the MSSR Study after the mid-term review. Its inclusion was prompted by the results of a study of the potential failure modes which could cause contamination of the Earth in the Earth Entry Capsule method of sample return and recovery. That study, conducted by L. A. Manning, Ref. IX-1, indicated that an unacceptably low probability of successful sample recovery existed for the initially proposed capsule design because of the total dependance on successful parachute deployment. (Other capsule failure modes such as entering at angles steeper than the aeroshell/heatshield design corridor were found to have acceptably low probabilities of occurrence.) Contamination of Earth by the impacting bus (ERV) was also identified as a concern in the Reference IX-1 study and providing a propulsion system on the Entry Capsule to permit a capsule deflection mode was suggested. However, for purposes of this study the bus deflection was specified so that the emphasis in the capsule design could be placed on enhancing the entry, descent and especially the impact survival aspects of the capsule design. Task descriptions, ground rules and criteria for the study are presented in Section A and B with system descriptions and performance data in Section C. Recommendations for further enhancing the reliability of sample recovery are also provided.

### A. TASK DESCRIPTION

This study task is comprised of three subtasks: 1, definition of a capsule which has the capability of surviving entry and protecting the 1 kg sample canister from impact damage in the event of parachute failure plus providing a locator beacon system and flotation provision that function under normal conditions, i.e., successful parachute operation; 2, evaluation of extending the impact protection to include the beacon and flotation systems; and 3, evaluation of expanding the sample size to 5 kg.

As it became apparent very early in the study that the second version of the capsule, the complete system impact protection version, was not appreciably heavier or more complex than the sample-only protected version, it was adopted as the "baseline" in establishing the subsystem designs. The other versions were also examined and the results are reported herein.

## B. GUIDELINES

The assumptions and groundrules for the conduct of the Entry Capsule Study are summarized below:

1. Sample Payload 1.0 kg and 5.0 kg.
2. Nominal Entry Angle,  $\gamma$ , =  $-10^{\circ}$ .
3. Design Entry Angle Corridor =  $-6^{\circ}$  (skipout) to  $-15^{\circ}$ .
4. Parachute deployment altitude and capsule descent rate on the parachute will be based on Air Force Aerial Recovery Criteria.
5. For one version of the capsule the sample canister shall be designed not to fail if the entry capsule impacts the surface at terminal velocity in the event of parachute failure. For the other version of the capsule design, the surface impact protection shall be extended to include the beacon/flotation system as well as the sample canister.
6. The ERV, or bus, is assumed to provide all functions during Mars/Earth flight including deflecting the bus after capsule separation, i.e., the capsule has no deflection propulsion system on board.

### C. CONFIGURATION TRADEOFFS

Since the requirements for this entry capsule are somewhat different from those of previous earth or other planetary entry vehicles, it is appropriate to review some new configurations as well as existing entry vehicle shapes. For example, a sphere would provide the simplest arrangement and would be the most fool-proof from the standpoint of entry and earth impact survival. However, it would also be by far the heaviest design due both to the increased heat shield weight and the higher impact velocity caused by its low drag coefficient. The impact g's and hence the thickness of impact limiting material would be 5 or more times as great for the sphere. The sphere would also create a very difficult docking and sample transfer in Mars orbit, i.e., a heat shield cap would have to be emplaced and sealed after transfer, see Fig. IX-1, and the reliability of the primary aerial pickup mode would suffer due to difficulties in deploying a parachute through the heat shield from a tumbling vehicle. For these reasons the sphere was dropped from further consideration in this study.

The other class of vehicles considered all depend on achieving a prescribed orientation during entry, and also during earth impact in the event of parachute failure, by means of their aerodynamic shape and/or an active attitude control system. The Apollo shape has very well known characteristics and can be designed to have the mildest entry and earth impact conditions of any of the shapes due to its high drag coefficient. However, this shape requires an active attitude control system to maintain its orientation and is thus inherently less reliable and more expensive to build than a shape that is passively stable. Shapes which are passively stable in both the hypersonic entry regime and the subsonic terminal velocity descent regime include the family of spherically blunted  $45^{\circ}$  to  $70^{\circ}$  half angle cones being developed for planetary entry probes. Consequently these shapes were determined to be the most appropriate for the Earth Entry Capsule.

From this family of shapes, the  $60^{\circ}$  half angle cone was selected as representing the best compromise between high drag (low impact velocity and low entry heating), and passive stability (ability to damp out pitch and yaw disturbances). Also considerable aerodynamic coefficient and aeroheating data exist for this shape from Viking and pre-Viking studies, and a

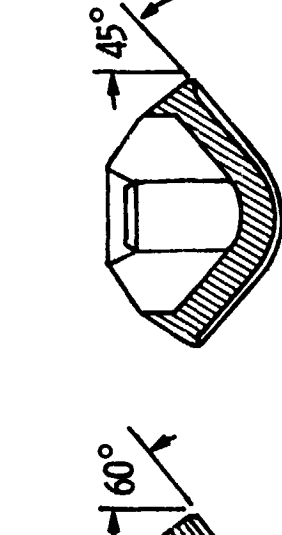
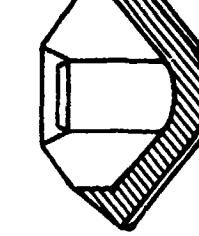
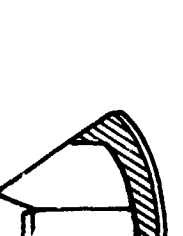
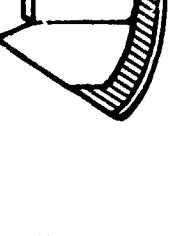
<p><b>Sphere</b> Heat Shield Sample Container Impact Limiter (Crushable Material)</p> 	<p><b>Apollo Shape</b></p> 	<p><b>Preferred Shape</b> 60° Half Angle Blunted Cone</p> 	<p><b>Preferred Shape</b> 45° Half Angle Blunted Cone</p> 	<p><b>No Requirement to Maintain Orientation During Entry &amp; Descent</b> <b>Thick Heat Shield and Impact Limiter Required</b> <b>Difficult Sample Transfer and Parachute Deployment</b></p>	<p><b>Requires ACS System to Maintain Proper Orientation</b> <b>Minimum Heat Shield and Impact Limiter Requirement</b></p>	<p><b>Orientation Maintained Passively</b> <b>Minimum Heat Shield and Impact Limiter Requirement</b></p>	<p><b>Orientation Maintained Passively</b> <b>Moderate Heat Shield and Impact Limiter Requirement</b></p>
---	---	---	---	--	--	--	---

Figure IX-1 Candidate Earth Entry Capsule Shapes

series of  $60^\circ$  cone scale model vertical wind tunnel tests were conducted at Langley Research Center as a part of the MMC Venus Probe Phase B Study, see Ref. IX-2. Based on these data, it is estimated that limit cycle pitch oscillations for this shape in terminal descent will be small,  $< 15^\circ$ , and that the impact limiting material can therefore be concentrated in the forebody area. (All-around protection is discussed as part of an Enhanced Probability of Recovery Capsule in part H of this chapter.) Afterbody shape is important from both a stability and aeroheating standpoint and data from the above studies were used to establish the geometry of the selected shape.

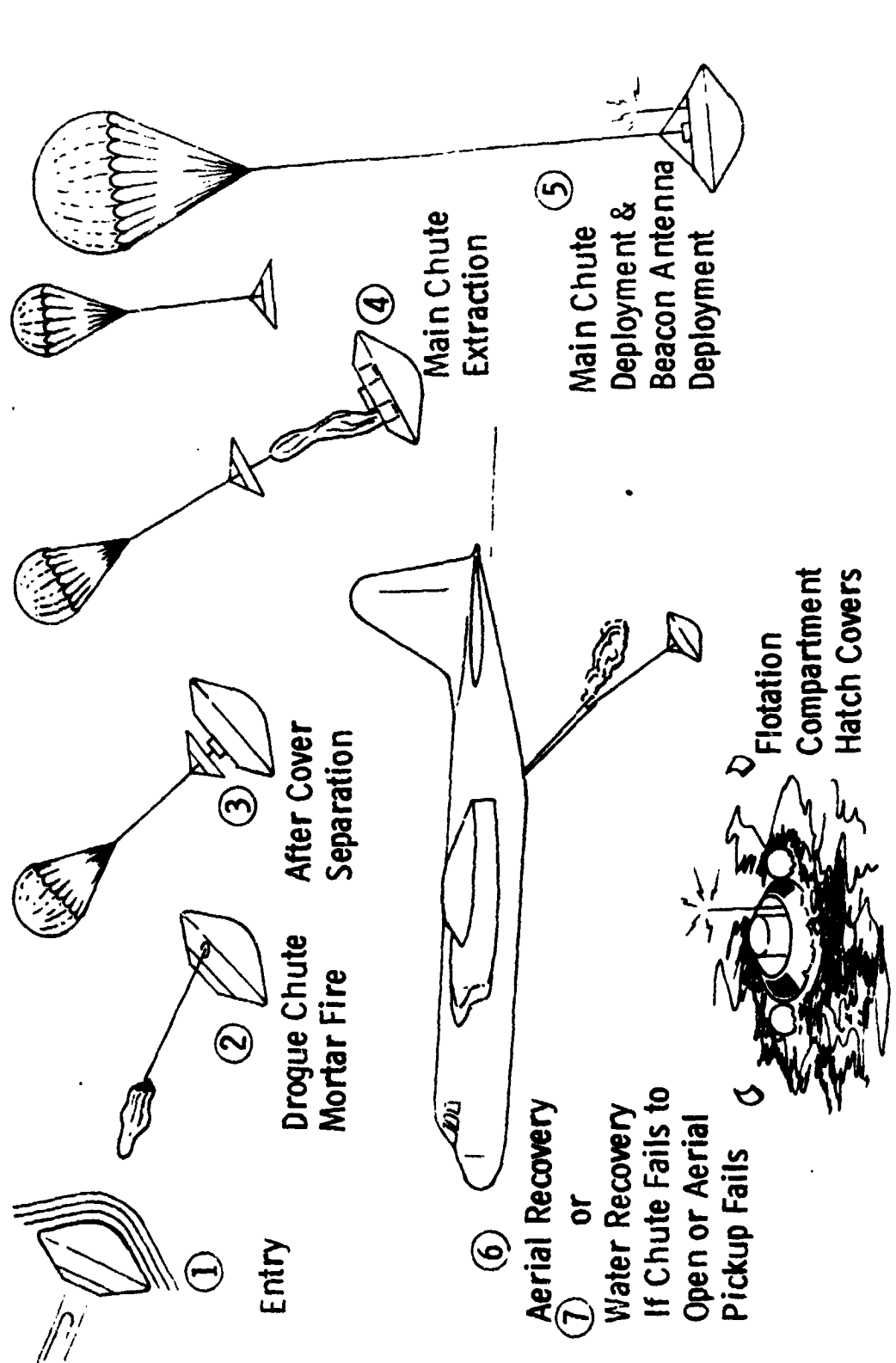
#### D. SEQUENCE OF EVENTS

The capsule events from Earth entry on are depicted in Figure IX-2, culminating in recovery either by air snatch or pick-up from the water or land surface. Approximately 6 hours prior to entry, the capsule is separated from the spinning ERV. This separation takes place at a capsule attitude (established by the ERV) such that the angle between the capsule body axis and the capsule flight path, the angle of attack, is zero at entry. This capsule attitude is maintained during the 6 hour coast period by the spin momentum imparted to the capsule by the spinning spacecraft (spin rate is 5 rpm. This imposes a constraint on the capsule (which is met by the selected configuration but not be the configurations with half cone angles less than  $45^{\circ}$ ) that the spin axis moment of inertia be greater than the moment of inertia about the pitch/yaw axes.

The entry heat pulse lasts for 50 seconds and the heat is dissipated by the half inch thick layer of ablative material. Heat soak through to the sample is prevented by providing sufficient ablator to keep the peak temperature of the back face of the heat shield (the outer face of the aeroshell structure) to less than  $360^{\circ}\text{F}$  and providing multilayer insulation between the structure and the sample receptacle. At approximately 15,200 meters (50,000 feet) altitude the drogue chute is mortared out through the afterbody cover. Upon inflation the drogue pulls the pyrotechnically released afterbody cover free of the capsule exposing the main chute and then extracts the main chute. The dynamic pressure and Mach number at this point are  $864 \text{ N/m}^2$  (18 psf) and 0.3 respectively, which are very mild in terms of existing parachute design experience.

An antenna is also deployed at this point and the rescue beacon is activated.

After 20 minutes, at approximately 3050 meters (10,000 feet) altitude, the descent velocity is 7.6 m/s (25 fps) and the aerial recovery aircraft engages the parachute with grappling hooks and reels it on board. This operation involving a number of planes can continue if necessary down to within a few hundred feet of the surface. If aerial pickup fails, the capsule impacts at 6 m/s (19 fps) and three flotation buoys are deployed to stabilize the vehicle and keep it afloat. Impact velocity is 35 m/s (116 fps) if the



① Entry

② Drogue Chute Mortar Fire

③ After Cover Separation

④ Main Chute Extraction

⑤ Main Chute Deployment & Beacon Antenna Deployment

⑥ Aerial Recovery or Water Recovery If Chute Fails to Open or Aerial Pickup Fails

⑦ Flotation Compartment Hatch Covers

Figure IX-2 Earth Entry Capsule Recovery Sequence

parachute system has failed to deploy, but the crushable impact limiter material causes the deceleration forces to remain within levels that the sample canister and its seals and the flotation/beacon systems can withstand, 1250 g's. The beacon system has an auxiliary battery capable of 30 day life. Its nominal range is 300 miles.

If impact occurs on land, the forebody impact material is still sufficient to maintain the integrity of the sample and capsule subsystems. However, if land recovery is desired as the primary mode of recovery, the capsule should be modified to include some impact limiting material in the afterbody area to cushion against secondary shock caused by rolling or tumbling after the initial impact. Also, a pair of internally flush mounted rescue beacon antennas, one facing forward and one aft, would replace the pop-up antenna used in the water recovery version. These modifications would result in approximately a 10% to 15% weight increase.

## E. DESCRIPTION OF BASELINE CAPSULE

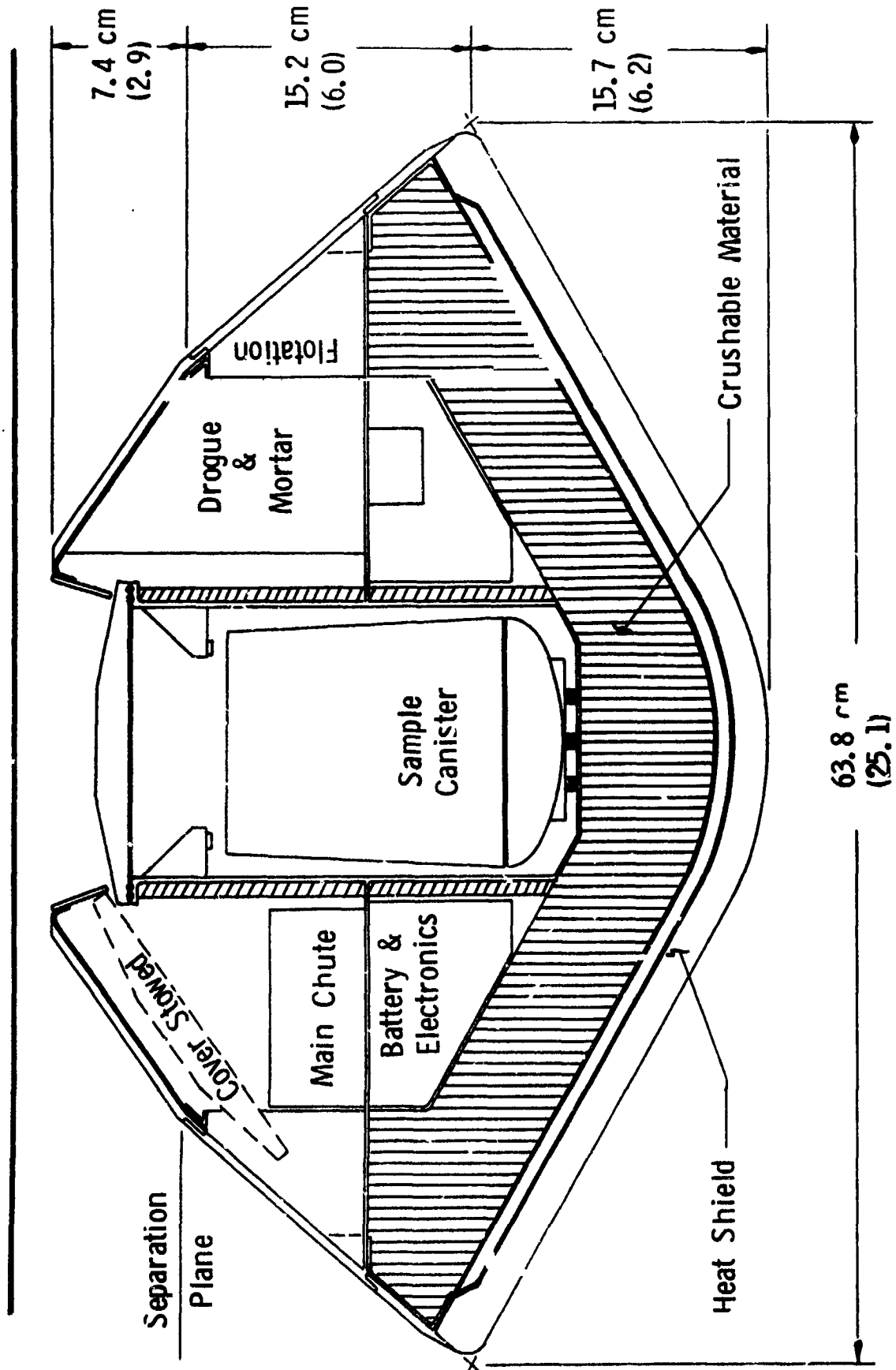
### 1. General Arrangement

The baseline capsule, shown in Figures IX-3 and IX-4, is arranged to facilitate insertion of the sample canister into a very sturdy cylindrical receptacle; to seal this receptacle in a positive manner; and to provide impact protection for both the sample and the flotation/beacon system in the form of crushable honeycomb. Reliable sample insertion during automatic docking with the Mars Ascent Vehicle in Mars orbit dictates the aft centerline location for the sample receptacle. Providing room to stow the receptacle lid and to install a motor driven linkage to move the lid into place establishes, in part, the afterbody dimensions. The other considerations in sizing the capsule are impact limiter thickness and parachute packaging design. The two-plus inches of crushable honeycomb stem from the assumption that the electronics equipment g-limits are of the order of 1000-1250 g's. This corresponds to the capability of existing aircraft search beacon systems and is slightly greater than the 900 or so g's that the more sophisticated Pioneer Venus Probe electronics will have to withstand during entry. Higher values might be achievable with special development.

The toroidal shape for the parachute container results from an attempt to keep the capsule as compact, and thus as light, as possible based on the sample occupying the aft centerline location as described earlier. This arrangement results in somewhat unconventional chute packaging and bag stripping operations as well as requiring an offset drogue mortar. These features, however, have been studied extensively (Ref. IX-2) and are believed to be sound. Further parachute design discussion is presented in part 3 of this section.

The lid which seals the sample canister also closes off the afterbody of the capsule, i.e., it forms an aerodynamic seal where it presses against the flexible ring surrounding the opening on the aft centerline. A small amount of heat shield, 0.10 inches, is provided on the outside surface of the lid as well as the other external surfaces of the afterbody.

Separate components house the flotation system and the beacon system with its power supply. The beacon used will probably be a standard Air



IX-10

Figure IX-3 Earth Entry Capsule (1 kg Sample)

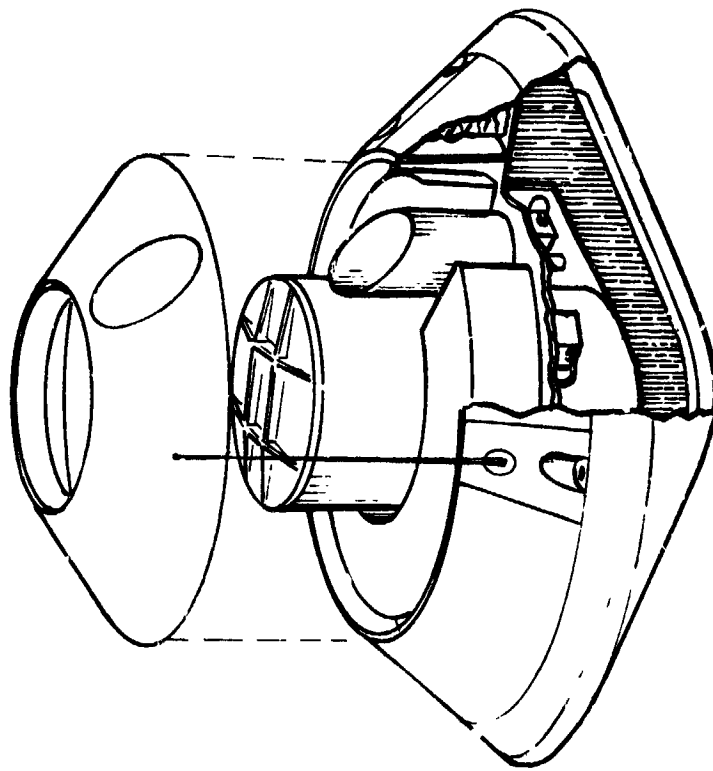


Figure IX-4 Earth Entry Capsule

Force recovery beacon with the addition of primary cells utilizing lithium with an organic electrolyte.

Structural elements are sized for the 1250 g's and in the case of the aeroshell for the entry dynamic pressures also. These loads, however, do not require very heavy gages due to the small dimensions and relatively light-weight components. One of the areas which appears to require some development is the separation hardware required at the afterbody cover/afterbody interface. The volume available in this region is too small for standard explosive nuts or pinpullers. Also the sample receptacle seals, which are the main line of defense against the exposure of the capsule to any biota contained on the surface of the sample canister, are also a development item. They are conceived as one-time actuated, deformable metal seals.

A summary of the characteristics of the key subsystems is given in Figure IX-5 and a complete weight statement is contained in Table IX-1. More detailed information on the individual elements of the capsule is provided in the following paragraphs.

## 2. Heat Shield Design

The severity of the entry heating conditions for this capsule falls between the conditions that existed for the Apollo vehicle and those predicted for the planned Pioneer Venus probes. The entry velocity of 12.8 km/sec or 47,000 fps (which corresponds to the highest velocity in the 1981-1984 opportunity period) is greater than the 36,000 fps for the Apollo and Venus entry situations. This velocity difference plus the smaller nose radius and steeper entry angle for the Earth Entry Capsule cause the peak convective heating rate to be about 4 times that for Apollo while radiative heating rates are comparable. Since in addition to convective heating rates, surface pressure gradients and shear stresses are also several times greater than Apollo, the relatively low specific gravity (0.5), ablative material used on Apollo cannot be used for this capsule.

Relative to the Venus Entry Probe conditions, however, the much shallower entry angle of the Earth Entry Capsule,  $-15^{\circ}$  max vs  $-60^{\circ}$ , results in convective heating rates that are less than 1/2 the Venus probe values and radiative

<u>Subsystem</u>	<u>Description</u>	<u>Mass (kg)</u>
Heat Shield	0.5 Inches Quartz Nitrile Phenolic (60 lb/ft <sup>3</sup> ) Critical Condition is Max Total Heat Case, 6.5° Entry (Skip Out Border)	5.8
Main Parachute	15 ft Diameter (D <sub>0</sub> ) Ring Slot Parachute Deployed by Drogue @ 52000 ft Altitude; Mach .32; Dynamic Pressure, 15 psf - Provides 25 fps Sink Speed at 10,000 ft.	2.3
Drogue Parachute	4 ft Diameter (D <sub>0</sub> ) Ribless Guide Surface, Mortar Deployed - Pulls Main Chute Out	0.5
Impact Limiting Material	Aluminum Honeycomb 2.4 in. Thick. Limits Capsule to <1250 gs in Event Chute Fails--Also Serves as Core for Aeroshell Structure.	1.1
Soil Sample Receptacle and Internal Support Structure	Aluminum Alloy - .040 Inch Wall Thickness (Max) Provides Resistance to Buckling at 1250 gs.	2.8
Beacon/Flotation System	Standard AF Satellite Recovery Beacon - CO <sub>2</sub> Inflated Flotation Bags (3); Dual Antennas	6.1

Table IX-1 Baseline Earth Entry Capsule Mass Distribution Estimate  
(1 kg Sample)

	<u>Mass Kilograms</u>
Structure	8.14
Sample Receptacle	1.86
Aeroshell Structure (incl. 2.5# Crush Material)	3.91
Inner Structure	.93
Upper Frustum	.61
Lower Frustum	.83
Ablator	5.76
Parachute System	3.54
Flotation System	1.36
Power and Cabling System	1.81
Electronics	2.95
Pyrotechnics	.91
Contingency 5%	<u>1.53</u>
	26.00
Sample and Container	<u>2.00</u>
	28.00

rates that are even less severe. Consequently one of the lower-density versions of the candidate materials for Pioneer Venus appears to be a good choice.

Table IX-2 summarizes the conditions for several entry angles and body locations for a ballistic coefficient of  $74 \text{ kg/m}^2$  (which is slightly greater than the  $59 \text{ kg/m}^2$  of the baseline capsule). Figure IX-6 illustrates the time history of the nominal entry angle heat pulses.

The response of the selected heat shield material, quartz nitrile phenolic with a specific gravity of 0.98, is shown in Figure IX-7. Thermal properties were taken from tests conducted in both MMC and Ames Research Center combined convective and radiative heating facilities in connection with the study of Reference IX-2. As indicated in Figure IX-6, approximately 1/3 of the 0.5 inch thick forebody heat shield is ablated away during entry. The structure behind the heat shield does not start to increase in temperature until after dynamic pressure loads have subsided to low levels. Peak structural temperature is maintained below  $350^\circ \text{F}$  with the 0.5 inch ablator thickness which is well below allowable adhesive bond line temperatures. Depending on the overall conductance of the crushable layer and internal insulation layers it may be possible to further reduce the heat shield thickness, however the 0.5 inch thick heat shield provides a comfortable margin on both recession and temperature soak-through and is recommended for the baseline design. It represents about 20% of the total entry weight.

### 3. Parachute Design

The Air Force has been successful in recovering satellites by deploying a parachute from the entry capsule and engaging the parachute with hooks suspended from an aircraft flying by with a sink speed equal to that of the descending capsule. Consequently this approach was selected as the primary recovery mode for the MSSR Earth Entry Capsule.

The two major requirements that the main chute has to meet are: 1) provide a descent rate of 25 fps or less at 10,000 feet altitude and 2) be deployed for 20 minutes prior to reaching the 10,000 ft level. In addition, the chute must be reinforced to withstand the air snatch loads and have a canopy/riser/bridle design that minimizes oscillations during descent. The ring slot

Table IX-2 Critical Entry Environment Results for the Earth Entry Capsule

Entry Angle (Deg)	Ballistic Coefficient (m/C <sub>D</sub> A)E (kg/ft <sup>2</sup> )	Surface Shear Force τ <sub>p</sub> (KN/m <sup>2</sup> ) (lb/ft <sup>2</sup> )	Location on Cone (R/R <sub>b</sub> )	Peak Convective Heating Rate q <sub>p</sub> (MW/m <sup>2</sup> ) (kBtu/ft <sup>2</sup> s)	Time-Integrated Convective Heat Input Q <sub>C</sub> (MJ/ft <sup>2</sup> ) (kBtu/ft <sup>2</sup> )	Peak Gas Cap Radiative Heating Rate q <sub>p</sub> (MW/m <sup>2</sup> ) (Btu/ft <sup>2</sup> s)	Time-Integrated Radiative Heat Input Q <sub>R</sub> (MJ/m <sup>2</sup> ) (Btu/ft <sup>2</sup> )
-10	74	0.60 (12.5)	0.00	17.9 (1.58)	351 (30.90)	1.23 (108)	8.48 ( 746)
			0.54	10.9 (0.96)	209 (18.40)	-	-
			1.00	6.55 (0.58)	136 (12.00)	-	-
-20	74	1.21 (25.3)	0.00	25.1 (2.21)	222 (19.50)	3.96 (349)	13.2 (1150)
			0.54	14.7 (1.30)	136 (12.00)	3.35 (295)	11.8 (1040)
			1.00	13.9 (1.22)	112 ( 9.85)	1.25 (110)	4.39 ( 386)
-30	74	1.83 (38.3)	0.00	30.8 (2.71)	191 (16.80)	6.65 (585)	15.0 (1320)
			0.54	17.2 (1.52)	124 (10.90)	-	-
			1.00	23.2 (2.04)	106 ( 9.32)	-	-

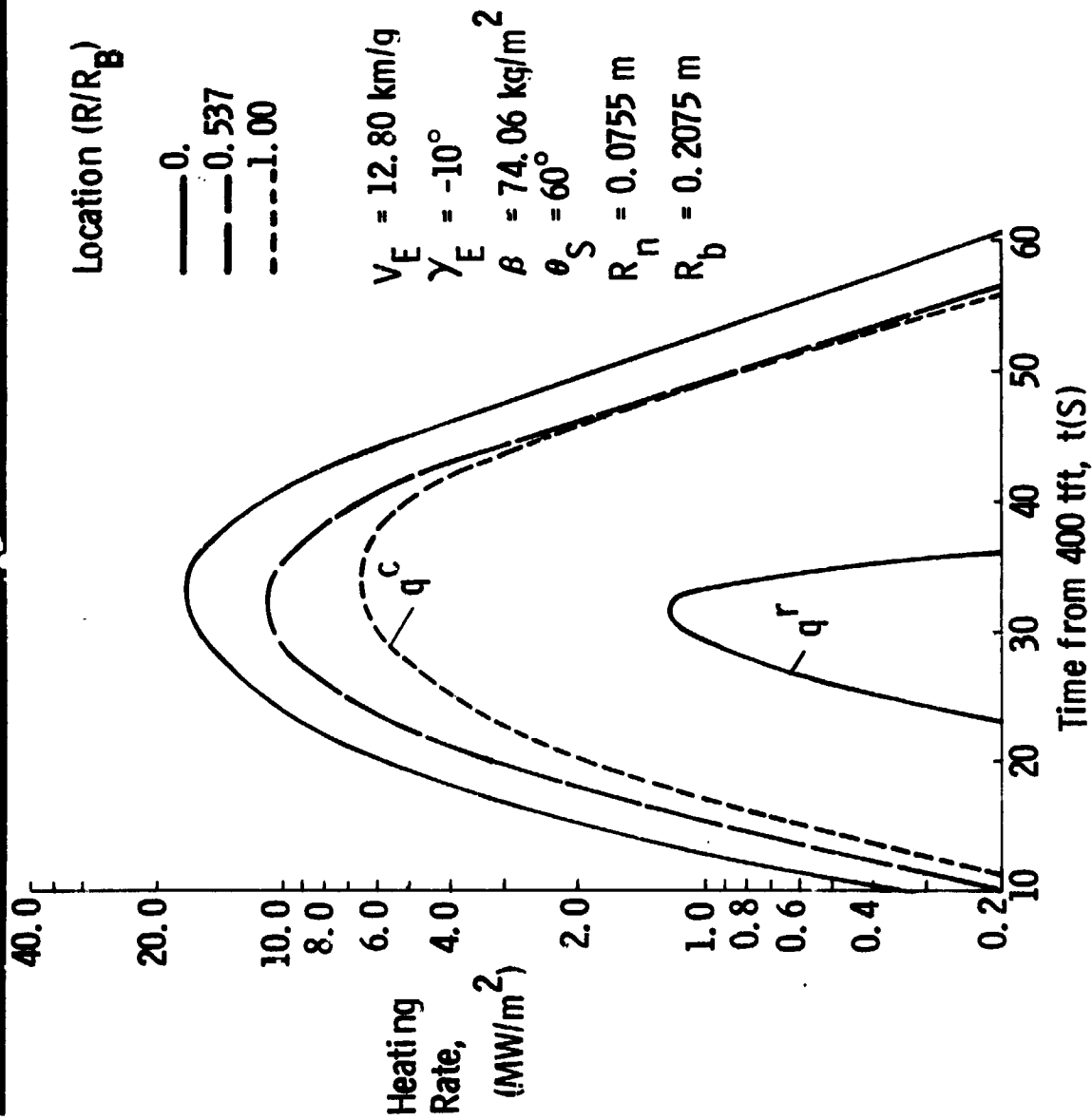
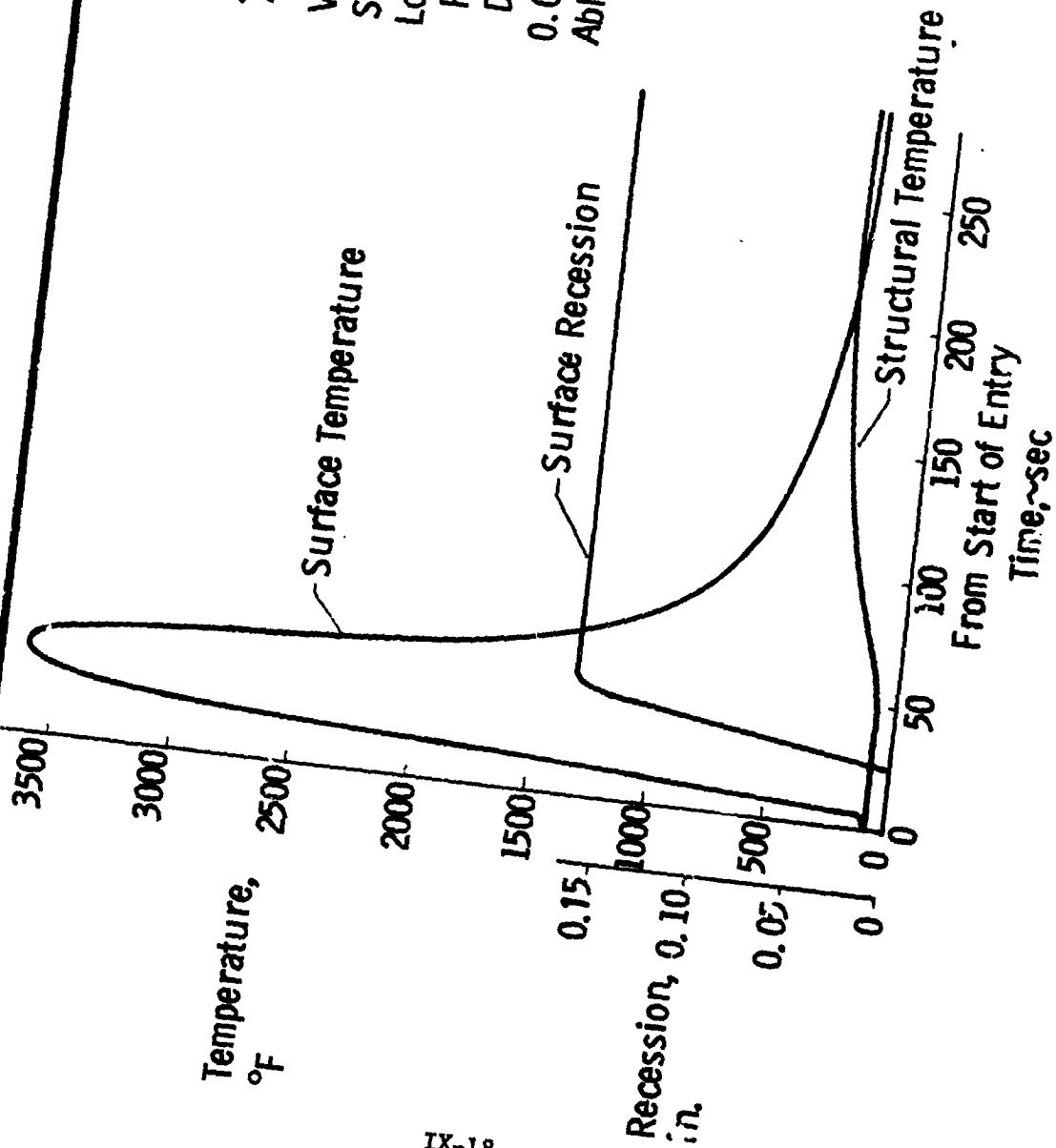


Figure IX-6 Typical Convective & Radiative Heating Rate Histories for the Earth Entry Capsule

Conditions Analyzed  
 $\gamma_E = -6^\circ$ ,  $M/C_D A = 74 \text{ Kg/ft}^2$   
 $VE = 12.8 \text{ ft km/s}$   
 Stagnation Point  
 Low Density Quartz Nitrile  
 Phenolic Ablative,  
 Density =  $60 \text{ lb/ft}^3$   
 0.050 Titanium Structure  
 Ablator = 0.50 in.



IX-18

Figure IX-7 Earth Entry Capsule Heat Shield Performance

canopy configuration has become a standard for this application and is the basis for our preliminary parachute system design in this study.

Chute Sizing - The uninflated diameter of the chute,  $D_o$ , is set by the 25 fps terminal velocity descent rate requirement at 10,000 ft, i.e.,

$$\frac{W_{CAPSULE}}{(C_D S)_{CHUTE}} = 1/2 \rho_{10000} V_{10000}^2 = 1/2 .001755 (25)^2$$

$$\frac{W_C}{C_D S} = .548$$

where:  $W_C = W_E - W_{H/S ABLATED} - W_{AFT COVER} - W_{DROGUE CHUTE}$

$$= (61 - 5 - 1 - 1) = 54 \text{ lb}$$

$C_D = .55$  for ring slot chute

$$S = \frac{\pi D_o^2}{4}$$

substituting

$$\frac{54}{.55\pi D_o^2/4} = .548$$

Thus  $D_o = 15.1 \text{ ft (4.6 m)}$

The velocity profile for this chute is shown in Figure IX-8. From this plot the lowest allowable deployment altitude, based on the 20 minute elapsed time requirement between 10,000 ft and deployment, is seen to be 52,000 ft. (15900 m).

An analysis of the influence of the entry angle on conditions at the deployment altitude was also conducted and the results are shown in Figure IX-9. These results show that below 70,000 ft (21400 m) the Mach number and deceleration (or dynamic pressure) are invariant with entry angle and consequently that a single design will work for any entry angle in the prescribed corridor. The final selection of a deployment altitude would be based on staying close to the minimum allowable altitude to minimize the Mach number and dynamic pressure and facilitate simulating the conditions in test flights, while still providing some margin on the 20 minute time period required by the recovery squadron.

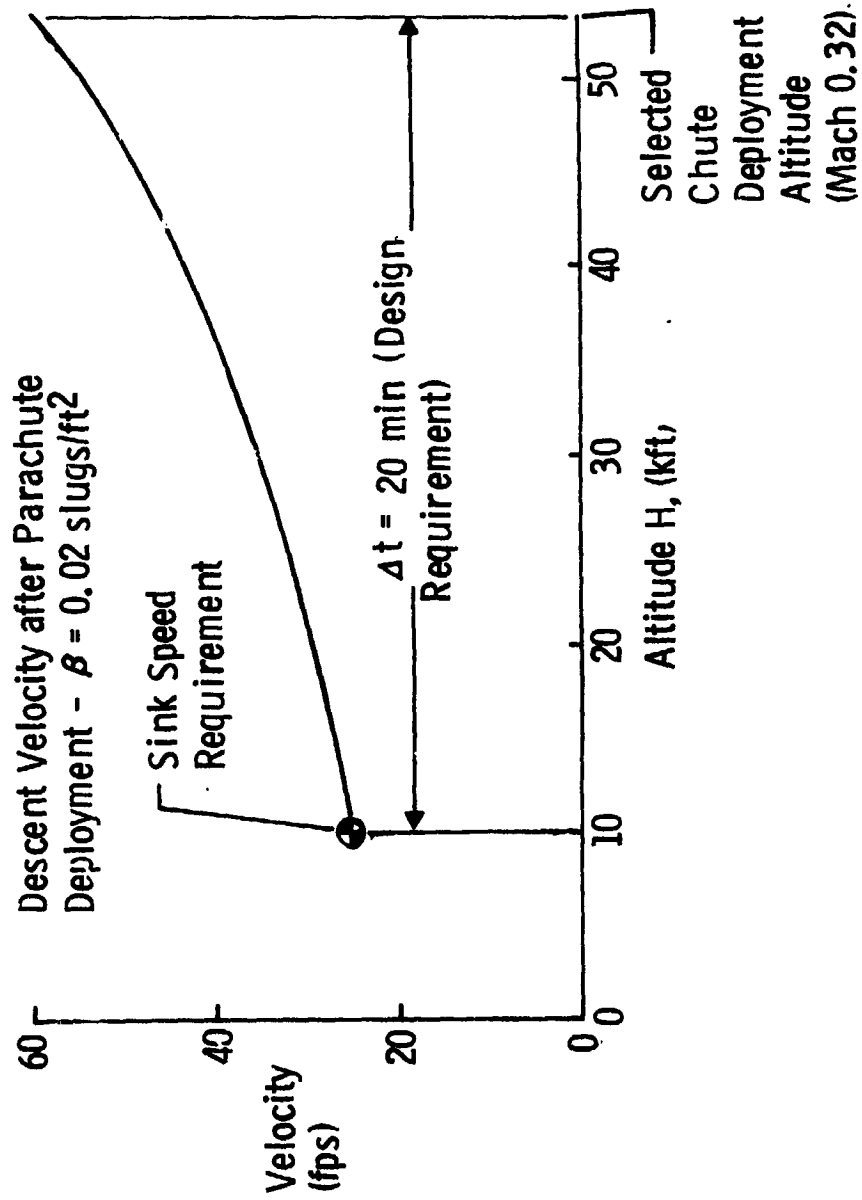


Figure IX-8 Earth Entry Capsule Descent Velocity Profile

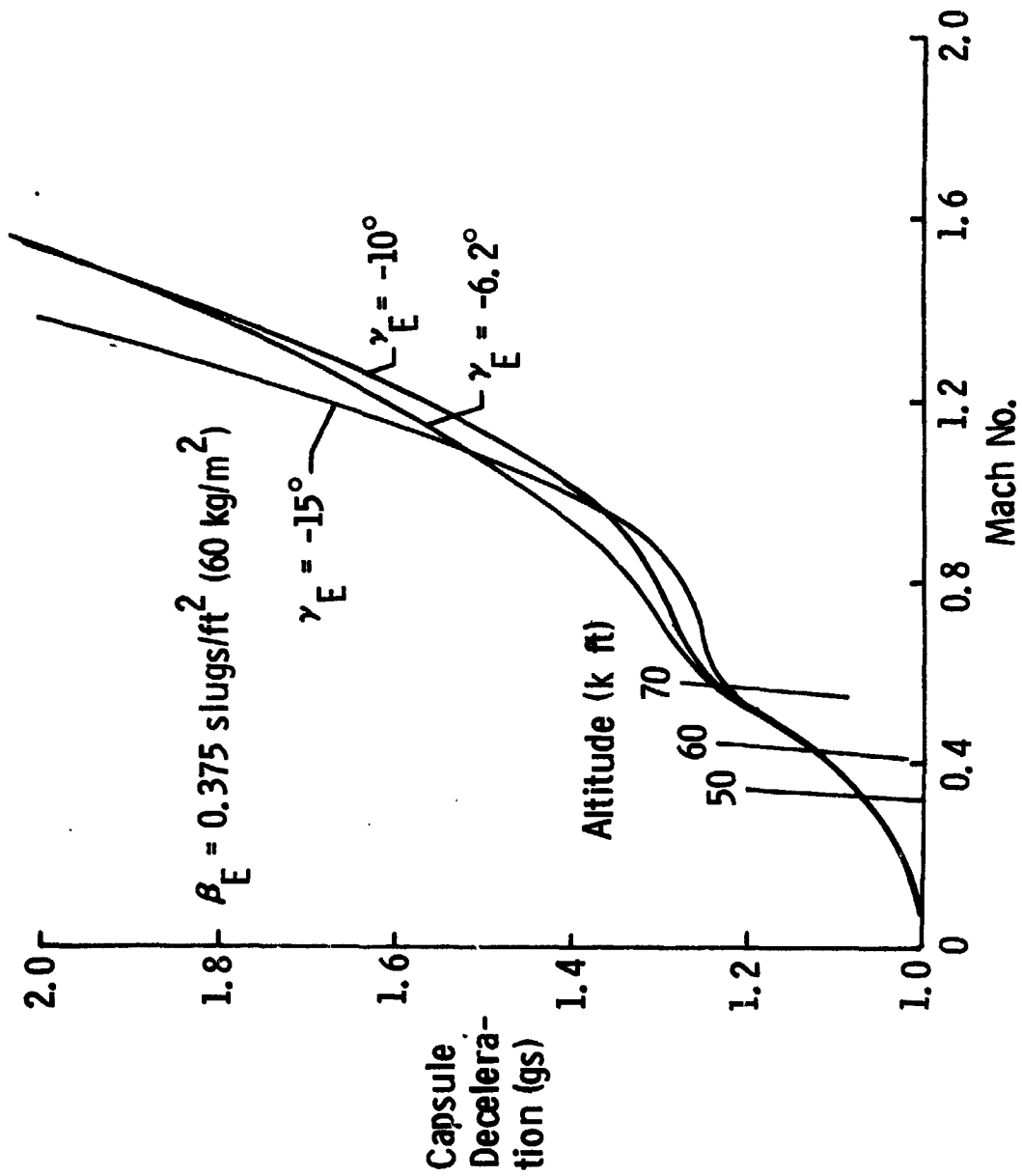


Figure IX-9 Entry Capsule Deceleration as a Function of Entry Angle

Packaging and Deployment Considerations - The ideal arrangement for deploying the main chute would be to mortar it out of a cylindrical container located on the aft centerline. A cylindrical container for the 15 foot (4.6 m) diameter chute would have to be about the same size as the sample receptacle, however, and it could not be packaged in this manner without substantially enlarging the capsule beyond the size required to house the sample canister.

Since weight and volume are critical, an alternative packaging and deployment technique was adopted based on preliminary design work accomplished in Ref. IX-2. This arrangement utilizes the volume around the sample receptacle and aft of the beacon and flotation system compartments for the parachute system. The main chute, folded into a bag, is stowed in this nearly toroidal volume as shown in Figure IX-4. A small 4 ft (1.22 m) diameter drogue chute and mortar are packaged in a cylindrical container mounted vertically along side the sample receptacle. Lines from the drogue chute are tied to the aft cover and a second set of lines from the aft cover are tied to the bag containing the main chute. When the drogue becomes taut, the aft cover is pyrotechnically released and the main chute is extracted by the drag force of the drogue. When the main chute lines become taut, the bag is stripped from the main chute canopy; the drogue and aft cover float free; and the main chute inflates.

A calculation was made to determine the allowable distance the drogue chute can be offset from the capsule center line without inducing unacceptable pitching moments when it is mortared out. For a 50 fps mortar velocity, the allowable distance is 7 inches which indicates the proposed design will not experience undesirable pitch rates.

#### 4. Electrical System Design

Electrical requirements for the Earth Entry Capsule (EEC) are derived from the groundrules established for the capsule. The capsule must be self-contained and have a timer, control logic, command capability, ordnance initiation, and a locator beacon. Environmental requirements will define certain hardware selection and packaging techniques.

A functional block diagram of the EEC electrical system is shown in Figure IX-10. The Power Control Unit (PCU) is powered by a 12 V battery and contains the pyro firing circuits, command sequencer, a coast timer, and power control circuits. The timer operates for 6.5 hours from ERV separation until the EEC is retrieved. The g-switches are redundant and sense entry deceleration and water impact and provide inputs to the sequencer as intelligence in the logic sequence.

A dual redundant hot-wire system is used for ordnance initiation with a mechanical S/A relay and SCR firing relay. The relays operate on 12 V and the squib firing circuit requires 5 A at 5 V for 10 ms. The power cartridges are the standard 1 A, 1 W no-fire for 5 min. with two bridge-wires in a single case. This design provides a simple, lightweight system with high reliability and dual redundancy. A set of two 2.8 V cells are provided for the redundant squib firing circuits.

The PCU provides commands to the mortar, aft lid cover, flotation, and antenna via the appropriate ordnance initiation circuitry. An electrical command is issued via a relay to energize the beacon to an "on-only" condition so that it can not be turned off once energized. This removes the dependency of the beacon upon the PCU or 12-V battery after initial execution. A backup g-switch is also included in the transmitter package to sense water impact and deploy the second antenna. The power control unit is powered by two lithium primary batteries, one for the electronic circuits and the other for firing the pyro squibs. The first battery will be composed of two parallel strings of 8-Ahr cells with five cells in series in each string. The second will consist of two cells of the same rating. Each cell has a nominal operating voltage of 2.8 and mass of 83 g resulting in a total cell mass of 996 g (2.2 lb). Each cell is in the shape of a standard D-size (6.1 x 3.3 cm dia.) battery.

The locator beacon transmitter is energized by command after the EEC is on the parachute at approximately 15.3 km (50,000 ft) altitude. The antenna is a "pop-up" STEM monopole antenna (61 cm long) actuated by an ordnance-initiated lid-release switch. If an air recovery is not executed, a second antenna will be deployed after water impact with a g-switch to act

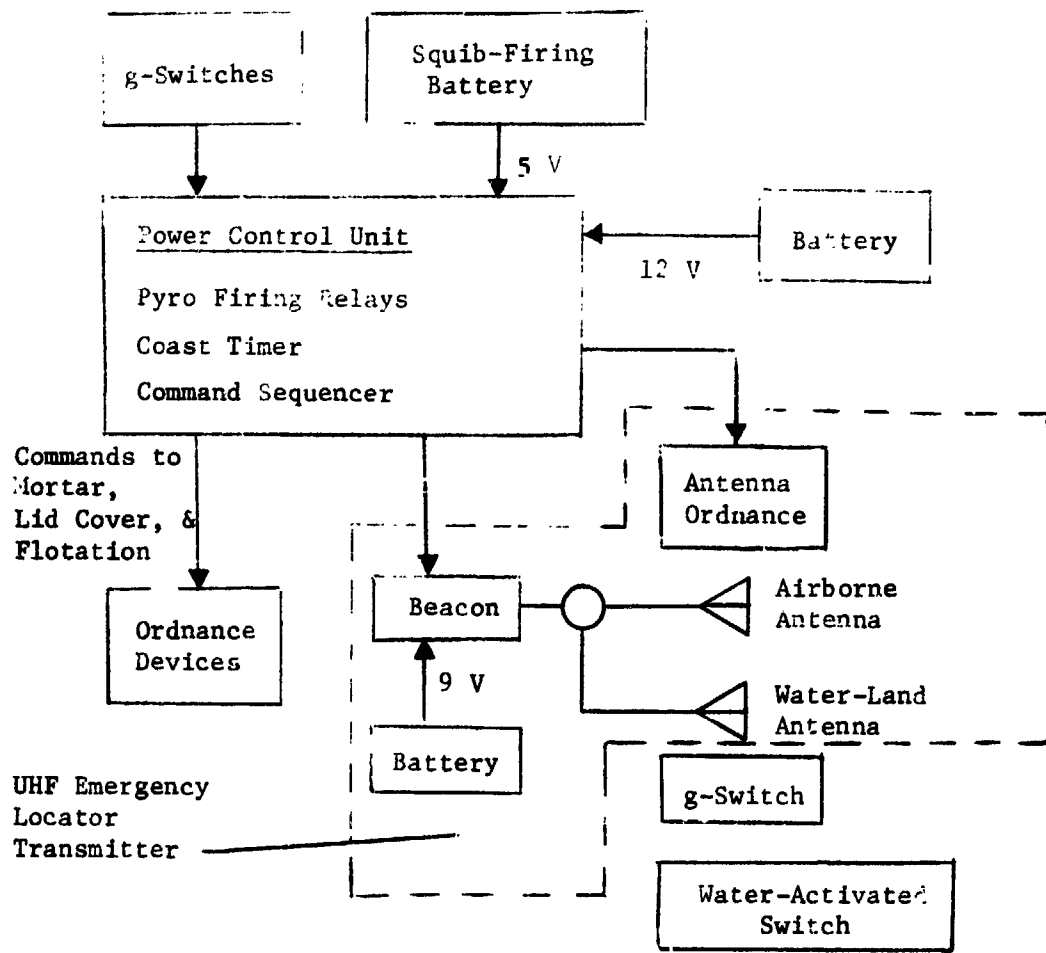


Figure IX -10 Earth Entry Capsule Electrical Functional Diagram

as a backup in case the first antenna does not survive the shock of water impact. The second antenna will be deployed by a mechanical lid-release switch operated in conjunction with the g-switch. A water-activated switch could also be used as a backup for the second antenna. The beacon requires an input power of 18 mA with 9 V from a separate battery and operates continuously for 30 days. The beacon operates on the emergency rescue frequencies of 121.5 and 243 MHz simultaneously and the beacon has an RF output level of 300 mW with a range of 480 km (300 miles). The beacon/battery pack is waterproof and is insulated to prevent the structural temperature of 350°F (176°C) due to Earth entry from damaging the components.

The beacon battery consists of two strings of four primary lithium cells in series. Each cell has an 8-A hr capacity and provides 2.8 V. 13 A-hr is required to operate the transmitter for 30 days. With this arrangement, 16 A-hr of energy is available. The mass of the cells used in the battery is 664 g (1.45 lb).

Physical properties of the hardware that comprises the electrical system of the EEC are listed in Table IX-3. The 12 battery cells include the 12 and 5 V sources of power. The antenna network includes two STEM antennas, a coaxial circulator, coaxial cable, and two lid-release switches.

Table IX-3 Physical Properties of the EEC Electrical System

<u>Electrical Hardware</u>	<u>Component Size, cm</u>	<u>Total Mass</u>	
		<u>kg</u>	<u>lb</u>
Power Control Unit	20 x 20 x 20	2.11	4.6
g-Switches (3)	4 x 2.5 dia.	.45	1.0
Batteries (12 cells)	6.1 x 20 x 6.9	1.00	2.2
Beacon Transmitter	9 x 4.5 x 4	.45	1.0
Beacon Battery (8 cells)	6.1 x 13.2 x 6.9	.66	1.4
Water Switch	4 x 4 x 4	.09	0.2
Ordnance Power Cartridges (4)	2.6 x 1.6 dia.	.04	0.1
Antenna Network	7.6 x 6.3 dia.	.76	1.7
Wiring		<u>.13</u>	<u>0.3</u>
Total		5.69	12.5

### 5. Mechanical/Structural Design

One of the main objectives of the capsule design study was to provide a capsule capable of withstanding impact on a nonyielding surface in the

event of parachute failure. The terminal velocity for this situation is 35 m/s (115 fps).

While it is possible to design a boilerplate container for the sample itself that would not rupture under this impact, insuring the integrity of the biota-barrier seals, or the beacon system electronic components, requires reducing the deceleration forces in a more controlled manner. In the manned Earth entry programs, Mercury, Gemini, and Apollo and in studies of hard landers for Mars, the approach has been to provide a layer of crushable material such as aluminum honeycomb to attenuate the impact g forces. This appears to be the best approach for this capsule as well.

The relation between impact g's and the thickness of the crushable layer is given in Figure IX-11 which was taken from a Hexcel Corporation design handbook. From this figure it is apparent that bringing the g levels down to a hundred or so requires unacceptably large thicknesses. However, the g levels do not need to be this drastically reduced. Commercial aircraft rescue beacons can withstand about 1000 gs and the more complex electronic packages on the Pioneer Venus probes will have to withstand similar levels during entry deceleration. Consequently a value of 1250 g's was selected as a reasonable design value for sizing the crushable layer. The resulting design has a thickness of 2.4 inches (6.1 cm).

The density of the crushable material is established by equating the kinetic energy of the capsule to the work done in crushing the honeycomb.

The structural framework that comprises the sample receptacle and the electronic and parachute support structure is seen from Figure IX-12 not to require particularly heavy gages to withstand the 1250 g's that result from use of the crushable honeycomb. In addition the honeycomb can be used as the core in a sandwich construction aeroshell, as in the Apollo command module design. These factors substantially reduce the weight penalty incurred in the crushable material approach.

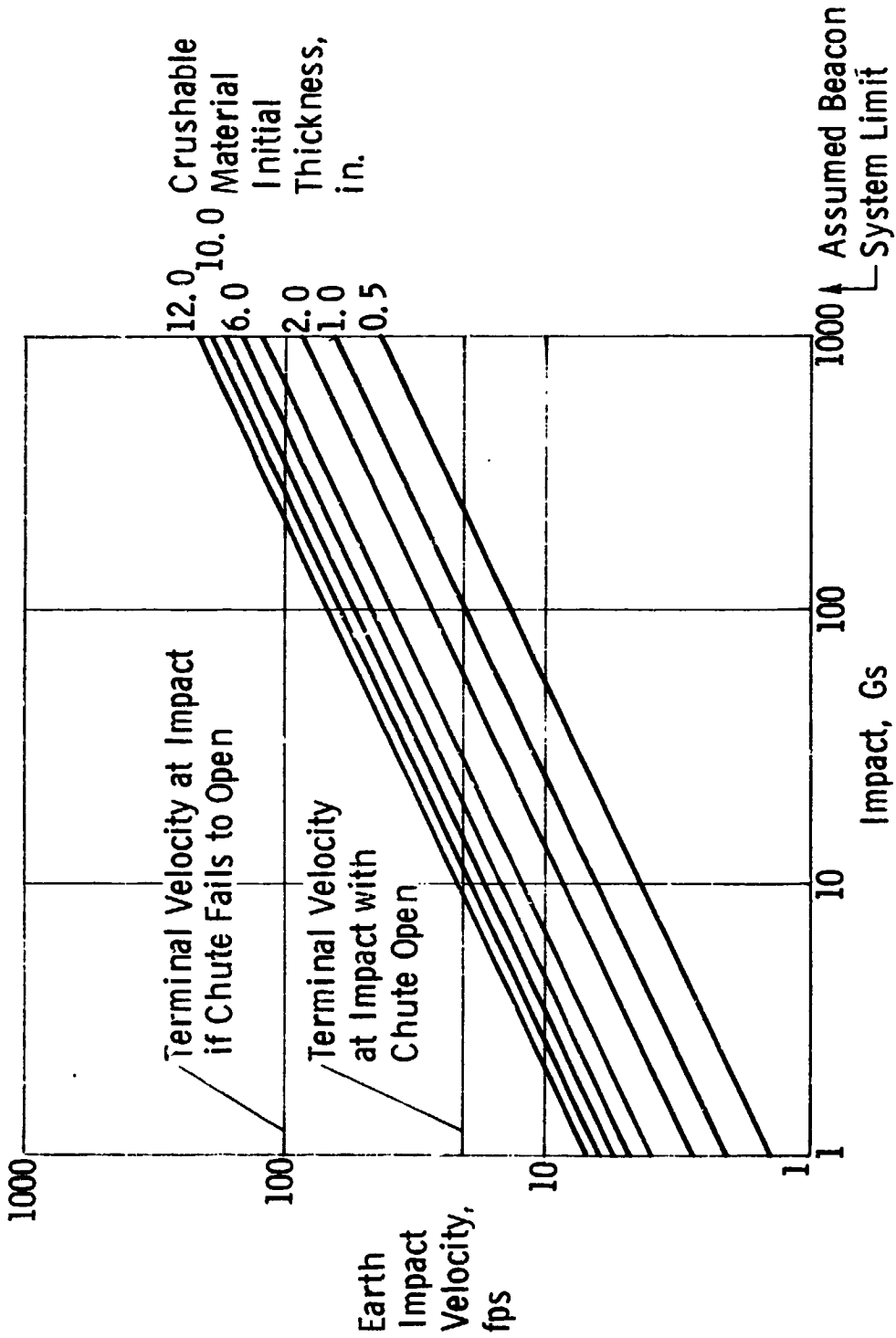
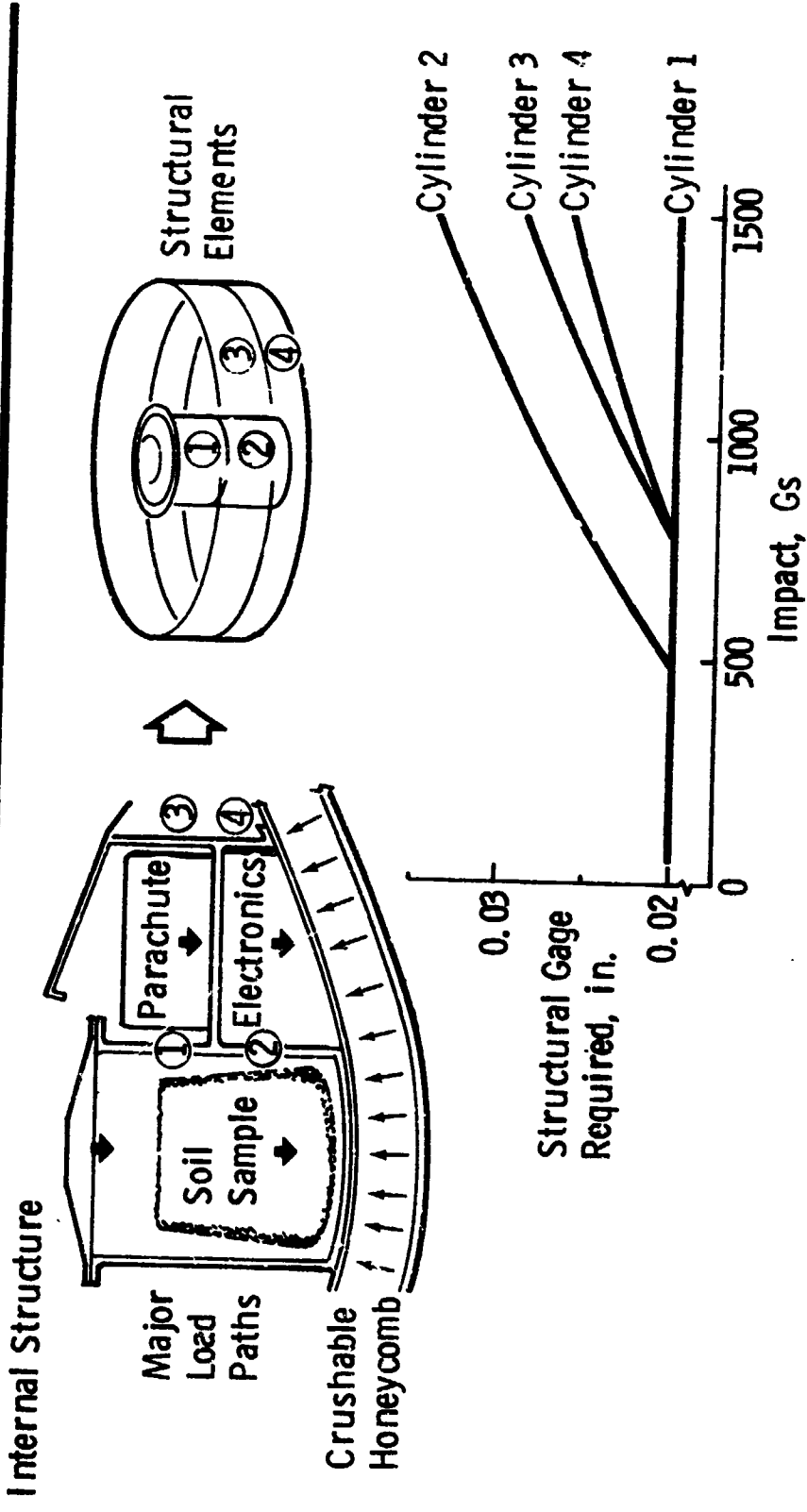


Figure IX-11 Impact Limiter Requirements-Earth Entry Capsule



**Aeroshell**

For maximum entry angle in corridor,  $\gamma = -15^\circ$ , Titanium sandwich with 0.050" faces 1/4" deep core would be sufficient. However using 2.4 in. deep crushable Honeycomb as the core for the aeroshell structure gives added  $\gamma$  capability with no additional weight.

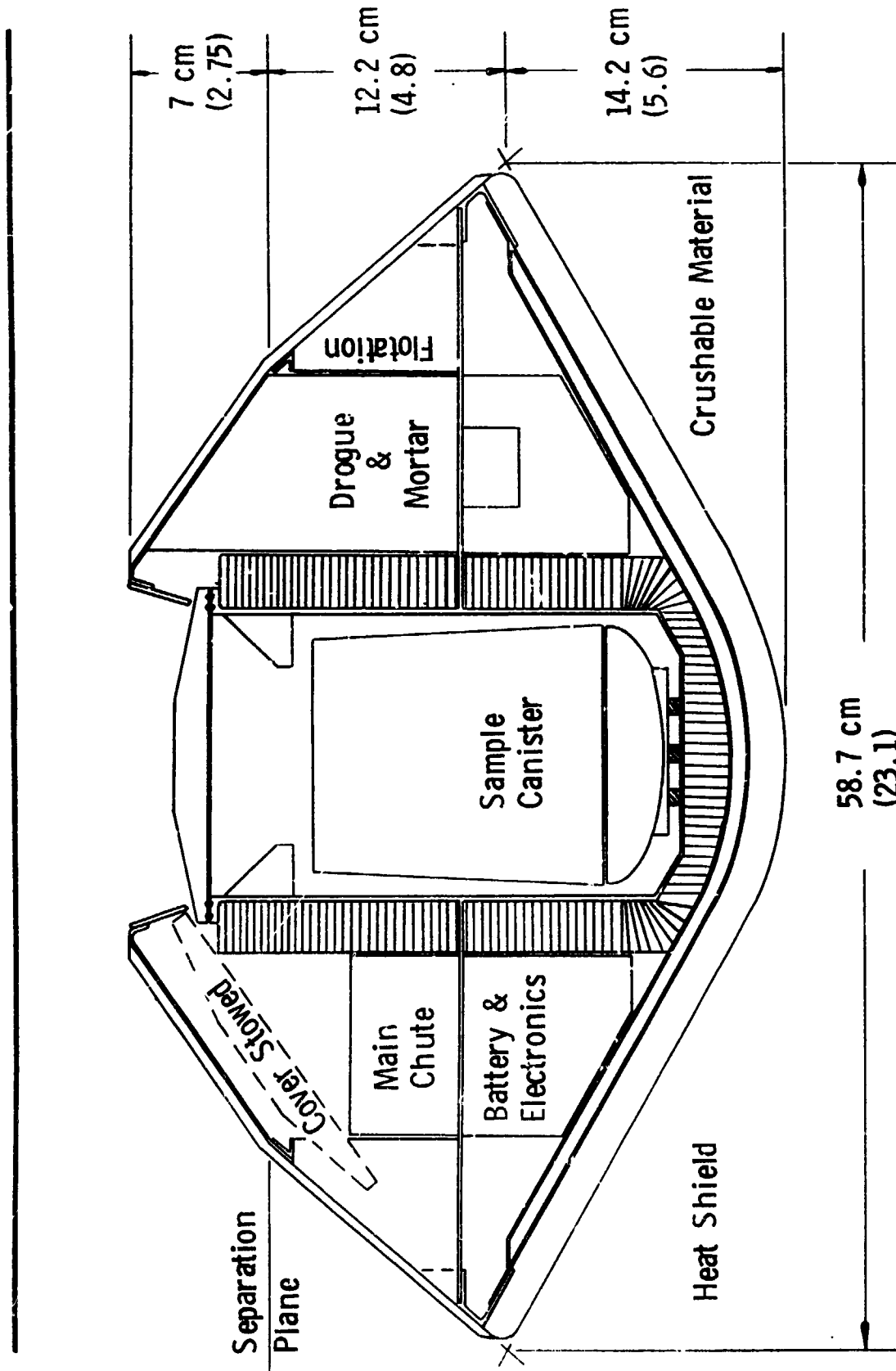
Figure IX-12 Earth Entry Capsule Design - Structural Considerations

#### F. SAMPLE-PROTECTION-ONLY CAPSULE DESIGN

The minimum capsule design is one in which only the sample canister is protected from impact damage. Even in this case, however, there is a requirement to maintain the integrity of the seal between the sample receptacle and its lid since presumably the outside surface of the sample canister may be contaminated. Again the use of crushable material is indicated to achieve a controlled g level. However, now the g level can be several times the 1250 level selected as the max allowable in the beacon-protected version. The crushable material is placed around the receptacle, 0.8 inch thick on the forward end and 1.2 inches thick on the sides where the masses of the supporting equipment could impose locally high inertia loads on the sample receptacle. For this version a considerably heavier-gage sample receptacle cylinder is required, see Figure IX-12, but the reduction in crushable material thickness allows the capsule diameter to be reduced from 25.1 inches (63.8 cm) to 23.1 inches (58.7 cm). This version of the capsule is depicted in Figure IX-13.

The net mass reduction, primarily due to the heatshield and aeroshell structural area reductions, is approximately 10% (25 kg vs 28 kg).

The mass reduction does not appear warranted in view of the fact that if the capsule is not recovered due to loss of the beacon or flotation system there is a likelihood that the initially intact sample container will ultimately undergo sufficient degradation to permit interaction of the contents with the earth's atmosphere or oceans.



IX-30

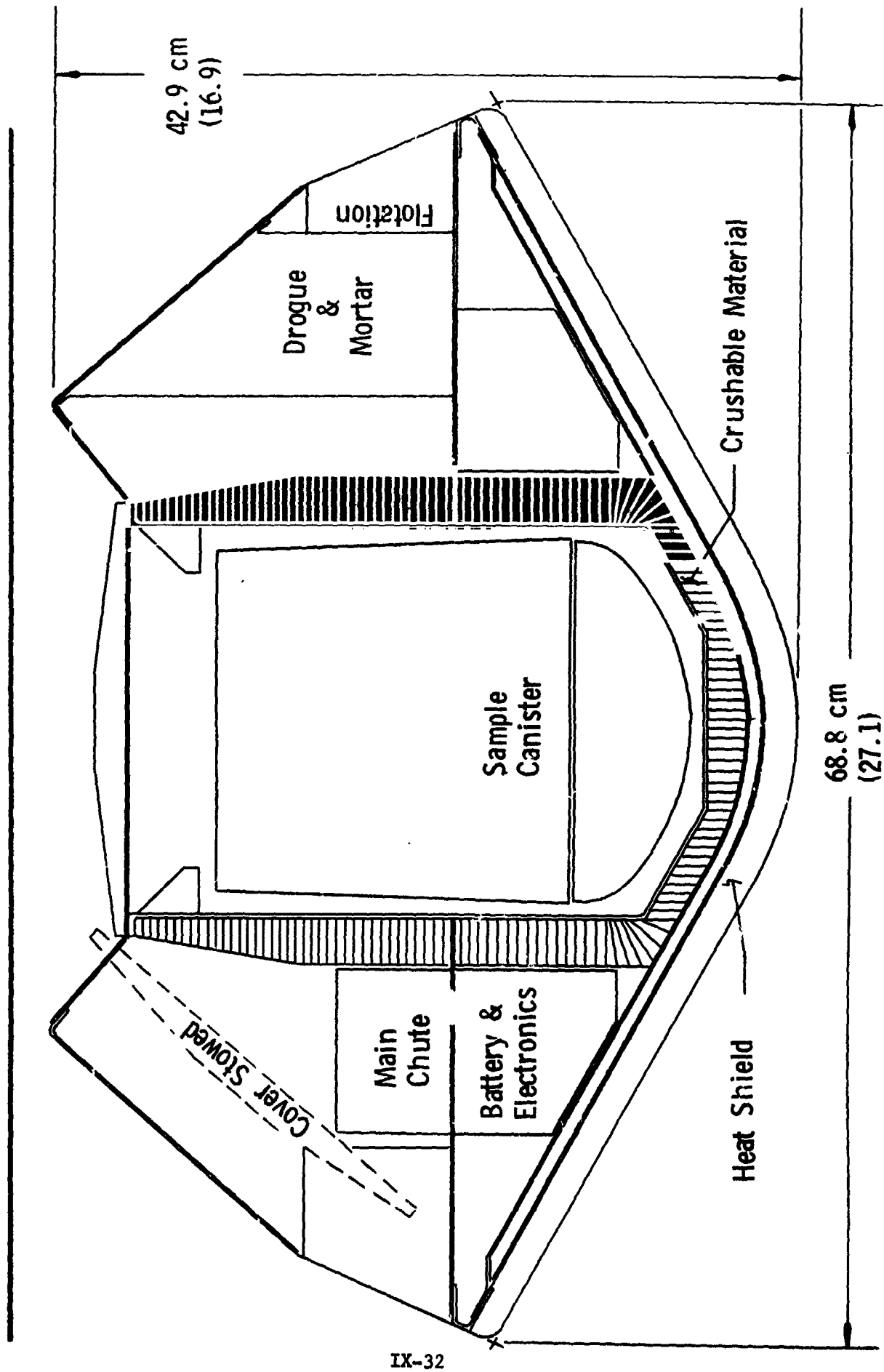
Figure IX-13 Earth Entry Capsule (Canister Survivability Only)

#### G. 5-kg SAMPLE CAPSULE DESIGN

To evaluate the impact on the Entry Capsule Design of increasing the sample size from 1 kg to 5 kg, the 5 kg sample canister developed in Chapter VI, Section A3 was used as the basis. This canister configuration was designed to facilitate integration into the Mars Ascent Vehicle, i.e., to minimize blockage of the rendezvous radar sensor and to cause as little growth in size and weight of the MAV as possible. This is significant in that without these constraints the larger weight and volume samples could be contained in a broader, shallower canister which would have less effect on the overall dimensions and weight of the Earth Entry Capsule.

Comparing first the sample-protected only versions it was found that the capsule diameter had to grow from 23.1 inches (58.7 cm) to 27.1 inches (68.8 cm), the overall length from 13.2 inches (33.4 cm) to 16.9 inches (42.9 cm). The mass would increase from 25 kg to 37 kg. Figure IX-14 shows this 5 kg sample capsule configuration.

For the capsules designed with impact protection for the beacon and flotation systems as well as the sample canister, the capsule entry weight increases from 28 kg to 41 kg to provide the 5 kg sample capacity.



IX-32

Figure IX-14 Earth Entry Capsule (5 kg Sample)

## H. ENHANCED-PROBABILITY-OF-SUCCESS CAPSULE DESIGN

Keeping weight and volume to a minimum was one of the major ground-rules in establishing the baseline capsule described earlier. Within these constraints, features were incorporated that significantly increased the probability of successful sample recovery over that of an earlier capsule design that was totally dependent on successful parachute operation. However, still further improvement is possible if more weight is available. The added weight could be obtained by assigning a portion of the margin identified in Chapter VI to the Entry Capsule, or it might be obtained by going to a dual launch or by the use of space storable propellants in the Orbiter main propulsion system.

A brief study was therefore conducted to assess what changes might be made if additional weight were allocated and to estimate cost trends accompanying these changes. The results are summarized in Table IX- and discussed in the following paragraphs.

The first column of Table IX-4 reiterates the design features of the baseline version of the capsule and characterizes what might be called a normal development and qualification test program for that design. In the first level of an enhanced success probability capsule, column II, a change is made to a more conventional, but bulkier, main chute packaging arrangement. This increases the reliability of the system since more direct benefit is derived from the many successful satellite recoveries by parachute as well as the series of successful manned flight entry vehicle recoveries and the Viking program parachute development work. This change, however, requires a substantial increase in capsule volume, diameter, and surface area since a main chute package in the form of a cylinder would be about the size and shape of the 1 kg sample receptacle. This change is estimated to require a 25% larger capsule diameter and consequently a heavier aeroshell, heat shield and main parachute. The total impact on system weight is estimated to be 12 kg.

This version of the capsule also incorporates an active attitude control and RCS system which functions both in the initial entry phase, to insure proper orientation of the heat shield at entry, during the pre-parachute deployment descent phase, and in the event of unsuccessful parachute operation, in the terminal descent phase as well. The biggest benefit of this

Table IX-4 Cost Trends as a Function of Probability of Successful Sample Recovery

	I Baseline System	II Enhanced Success Probability System ( $\Delta$ Weight I)	III Ultimate System ( $\Delta$ Weight II 50%)
<u>Design Aspects of Earth Entry Capsule</u>			
System Characteristics	Single Parachute with Most Compact Configuration. Passively Stable Vehicle Normal Factors on Structure and Heat Shield 30 Day Beacon Life	Change Chute to Conventional Packaging (Requires Larger Capsule) Add Active Attitude Control System and Crushable Material Double Factors on Structure and Heat Shield	Two Independent Chute Systems Two Independent Beacon Systems Extend Beacon Life to 150 Days
<u>Development and Qualification Aspects</u>			
Heat Shield	Plasma Arc Coupon Tests	Large Scale Component Plasma Arc Tests	Full Scale Earth Entry and Descent Flight Test - All Systems Functioning
Parachute and Capsule Aerostability	Wind Tunnel - Aircraft Drop Tests	Same as I	
Structure	Static/Dynamic Lab Tests	Aircraft Drop Tests	
Beacon/Flotation	Functional/Environmental Lab	Same as I	
Cost Factor - Capsule System Only	1.0	1.7	3.0

feature is that the possibility of a failure occurring due to the capsule impacting on the relatively unprotected afterbody (which conceivably could happen in severe wind storm conditions) is effectively reduced. An alternative to adding an active ACS that also attacks this problem would be the provision of impact-limiting material on the afterbody. This approach would not improve the entry heat protection system reliability (as would the active ACS approach) and it would adversely affect the parachute deployment reliability and the sample transfer reliability unless omitted over the aft centerline. However, being passive in nature, the added afterbody protection approach would not be subject to failure of electrical or propulsion devices as would the ACS/RCS system approach. The weight penalty for adding an ACS system plus impact limiter material on the afterbody, except over the canister and parachute, is estimated to be of the order of 10 kg.

Another feature of this version of the capsule is the use of larger than normal factors of safety in the design of the heat shield and aeroshell structure, e.g., 2.0 instead of 1.5. The weight increase would be almost proportional to the safety factor increase, or about 6 kg.

This makes the capsule weight increase in version II due to all of the above changes approximately a factor of 2.0, or an increase from 28 kg to 56 kg.

Associated with these design changes in Table IX-4 for costing purposes are some steps that could be undertaken in the development and qualification of the capsule to enhance its recovery reliability. Foremost of these is a series of capsule drop tests from an aircraft or helicopter which would include all possible capsule attitudes, pitch and roll rates, lateral velocities, surface slopes, surface hardness and wind conditions. These tests would include functional operation of the beacon and antenna systems. They would be relatively expensive in that after each drop the crushable material would have to be replaced. The overall relative contractor costs of the design changes and the enlarged development and qualification test program are estimated to be a factor of 1.7 greater than those for the basic capsule. The enhancement in reliability is impossible to state quantitatively, but would be very substantial.

The last column of Table IX-4 represents what might be done if weight and cost were of no concern. It is not obvious how completely redundant subsystems could be accomplished, particularly in the area of the parachute, but assuming this could be done, it would up the reliability by a large amount. Likewise, if a full-scale Earth entry descent and impact test were made a part of the capsule qualification or proof test program, the overall reliability would go up sharply. A very crude weight and cost estimate for this case was made and Table IX-4 lists the results.

## REFERENCES

- IX-1. "Preliminary Analysis of the Probability of an Accidental Exposure of a Mars Sample for a Direct Return Mission," by Larry A. Manning, NASA Ames Research Center.
- IX-2. Pioneer Phase B Study Final Report, June 1973, Martin Marietta Corp.

## X TECHNOLOGY AND PROGRAMMATIC ASSESSMENT

The results of this study support the conclusion that the rendezvous, docking and sample transfer operations required in the MSSR MOR mode can be implemented with existing technology. At no point were specific technical problems encountered for which solutions have not been at least demonstrated in current technology development programs.

There are a number of areas, however, where further technology development work will be required to: 1) evaluate the application of current space qualified technology to the specific conditions imposed by the MSSR mission; or, 2) extend needed technology that has been demonstrated but not space qualified.

### A. TECHNOLOGY DEVELOPMENT REQUIRED

Table X-1 summarizes the technology development items identified in this study. The following paragraphs provide a brief assessment of each of them. More details on technology requirements are provided at the end of appropriate chapters in this volume.

1. Sterilizable Solid Rocket Motor. The high impulse to weight ratio and compactness of solid motors proved to be a distinct advantage in the selection of the baseline MAV configuration. The motors defined in this report were based on current development work being directed by JPL. This program has been highlighted by the successful firing of a 67 cm diameter motor containing 360 Kg of propellant that had been subjected to eight 53-hour sterilization cycles at 125°C. (See Appendix I.) The continuation of this work would definitely enhance the MSSR mission.

A related development, listed in table X-1 as Lower Temperature Solid Rocket Motor, would accomplish a calibration of the sterilizable MAV motors to relieve the thermal control constraints on the MAV during landed operation prior to launch. In the current baseline the motors have to be held within a temperature range of 4°C to 32°C to guarantee their spec performance. If data were available on the performance characteristics at lower temperatures, then MAV temperatures could be allowed to go lower and the actual values telemetered back to Earth to be used in launch elevation and coast time calculations.

Table X-1 Technology Assessment

	<u>Related Development Currently Underway</u>
<u>Development Required for Baseline System</u>	
Sterilizabile Solid Rocket Motor	Yes - JPL/AGC
Sterilizabile Solar Panels	No, But Technique is Known
Sterilizabile NiH Battery	No, But Technique is Known
20 Watt RTG	Yes - AEC/Teledyne
Rendezvous Radar System - Multipurpose	No
CMOS Electronics	Yes - Industry Wide
<u>Development That Would Enhance Mission</u>	
Optical Guidance	Yes - JPL
Space Storable Propellant	Minimal - JPL
Lower Temperature Solid Rocket Motor	No
Advanced Soil Sampling Device	Yes - MMC (Viking '79)

2. Sterilizable Solar Panels. Actual exposure of solar panels to sterilization cycles has not been demonstrated but a number of related tests have provided assurances that both current and advanced panels can withstand the requirement. JPL has tested Mariner type panels to 125°C for as much as 1000 hours in storage evaluations. Advanced panels using resistance welded interconnects have been thermally shocked from -196°C to +200°C through 500 cycles without failure.

3. Sterilizable NiH Battery. The development of long life NiH cells has been stimulated by the Comsat Corp and a number of commercial firms are now producing them. These cells have an energy density capability between 55 and 150 W-hr/kg. The ability to withstand sterilization cycles has not been demonstrated but the manufacturers have expressed confidence that there will be no problems.

4. 20 Watt RTG. The RTG selected for the lander in this baseline use a selenide base thermoelectric material developed under AEC sponsorship by Teledyne Corp. A demonstration of this technology in an RTG is planned for February 1975. Current development plans provide for flight articles to be available in time to meet a 1981 MSSR opportunity.

5. Rendezvous Radar Systems - Multipurpose. The orbiter rendezvous radar defined for this baseline is based on technology used in the Apollo rendezvous radar. The transponder used in the MAV is also based on current technology and available parts and components. However, a number of features of the system as used in the MSSR rendezvous should be evaluated in a development program. These include: a) the five-tone ranging system used in the orbiter radar; b) the orbiter traveling wave antenna array built into the docking cone; c) the multiple functions of the MAV transponder (Earth tracking, telecommunications, command, angle tracking and rendezvous radar turnaround); d) the pointing accuracy of the MAV and orbiter systems at close range; and e) the interaction of the MAV and orbiter antenna patterns at close range. This development program should start early, i.e., FY75 or FY76 for the 1981 opportunity, and be conducted in conjunction with the development of the rendezvous algorithm discussed below.

6. CMOS Electronics. The MAV guidance and control computer will benefit greatly by the availability of space qualified, low power CMOS circuitry. This technology has been widely demonstrated and proven but space qualified computers have not yet been developed. Because of the traditional problems involved in Spacecraft computer development, work on the MAV computer should start early, even though its design requirements are relatively simple.

7. Distribution of Waste Heat by Radiation/Convection. This item refers to the thermal control system defined in the baseline configuration to keep the MAV solid motors within the required temperature limits (see item 1 above). The technique selected uses the RTG waste heat, distributed through heat pipes into a thermal control canopy that covers the MAV prior to launch. It appears to be an attractive design solution that is simple and workable. However, as in most thermal control designs proof of principle can only be established by test. A rather simple test program using a space simulation chamber would establish confidence in this approach.

8. Soil Sample Container Seals. The sample canister must be sealed to at least "air tight" conditions after the sample is loaded and the seal integrity must be maintained throughout the remainder of the mission. The Earth entry capsule receptor must have a similar seal. Work has been done by Martin Marietta on gold deforming seals for an advanced Mars biology instrument that must meet much more stringent leakage tolerances than MSSR requirements. This effort has been sponsored by the Ames Research Center. Additional development should be conducted on seals of the size required on the MSSR mission and on methods for preventing soil particles from interfering with the sealing action.

9. ΔVLBI Tracking Techniques. This technique for determining the relative position and velocity of two spacecraft by Earth based tracking is described in chapter III of this volume. It involves the simultaneous tracking of both vehicles by two separate Earth tracking stations and the processing of the data by double differencing interferometry techniques. ΔVLBI will be experimented with as the Viking 75 mission and will be used in the Pioneer Venus mission in 1978 (for wind drift measurements on the probes).

A parallel effort should be maintained to factor these developments and any other evolving information into the MSSR rendezvous design.

10. Rendezvous Algorithm. This is probably the most significant analytical development item identified in this study. The development of optimum strategies and control factors for executing the terminal rendezvous and docking phases is a complex procedure that involves a great deal of trial, iteration and refinement. Methods for optimizing the initial closing  $\Delta V$  maneuver, the subsequent range rate and line of sight control, and the docking algorithm must be analyzed and then demonstrated in computer and physical simulations. Such work should commence immediately (i.e., FY 75/76).

11. Optical Guidance. This item relates to the onboard guidance techniques used by the orbiter to target the direct entry lander to a narrower entry corridor than that used in the baseline mission ( $2^\circ$  vs  $4^\circ$ ). While not directly related to the rendezvous and docking phase, it will allow greater lander weight performance which could in turn enhance the performance of the MAV. JPL has investigated a number of onboard optical navigation techniques and the one most appropriate to the MSSR mission should be examined for this application.\* If the option to increase the baseline sample size from 1 to 5 kg is selected, the  $2^\circ$  entry corridor will be required, necessitating the use of optical guidance.

12. Space Storable Propellants. In order for the baseline mission described in this report to be performed in the 1983/84 opportunity, additional orbiter propulsion capability will be required. One alternative, and the one that will still permit the use of a single Titan IIIE/Centaur launch, is the conversion of the orbiter to high energy space storable propellants. Space storable propulsion system development has been going on at JPL for a number of years. Continuation of this work to include specific application to the Viking orbiter configuration would enhance the MSSR mission.

13. Advanced Soil Sampling Device. The guidelines of this study specified the return of a single bulk sample. However, discussions with members of the science community have produced recommendations that more sophisticated

\*Optical guidance was demonstrated in the Mariner 9 mission, as an experiment, using the satellites of Mars imaged against a star background.

sampling techniques may be desirable. Techniques for selecting specific fragment sizes by raking or sieving, segregating and separately sealing samples taken from different locations, and taking separate atmosphere samples should be among the things investigated and developed.

#### B. CONCERNS REQUIRING FURTHER STUDY

Although the baseline spacecraft and mission concept described in this report does appear to be a feasible approach to carrying out the MSSR mission, there are several areas that should be evaluated in more detail before a final concept is chosen. Three of these areas are: 1) evaluation of weight margins to make certain that major development and programmatic problems are not being built in by margins that are too small; 2) review of science objectives to identify any additional science instruments that might be required on the lander or the orbiter; and 3) further assessment of the sample transfer technique used in orbit so as to define the safest, most reliable concept.

APPENDIX A SCIENCE CONSULTANTS' RECOMMENDATIONS - MSSR SEMINAR  
(Denver, Colorado: May 9, 1974)

1. How much sample is required and what would be the allocations to biology, organic analysis, inorganic analysis, pathogenic evaluation and reserve for future analysis?

Inorganic Analysis - in sorting or sieving can be done to guarantee that sample particles are between 2 and 10 mm in size, then 100 grams per sampling site is adequate. If no sorting can be done, 500 grams will be required. Sorting is strongly recommended.

Organic Analysis - this group doesn't have the competence or experience to define this requirement. An intuitive feel says the sample should be a few hundred grams.

2. What types of sampling are desirable, e.g., surface, subsurface, loose rocks, bedrock chips, and atmosphere?

No strong requirement for core sampling partly because of the difficulty in accurately identifying the levels from which the parts of the sample came. If mobility is available the required variety of sample can probably be obtained by going horizontally instead of vertically. (Layered terrain will expose different stratifications.) The ability to take samples from the bottom of trenches of various depths was considered desirable. Biological and organic analysis samples should be fines. Inorganic analysis samples should be 2-10 mm sized particles. There was no support for a pure atmosphere sample.

3. From what location on the planet should the sample be taken?

The objective is to obtain samples from as many geological regimes as possible. If only one sampling point is available it would be desirable to have it at the mouth of a channel or stream bed.

4. How valuable would a rover be on the sample return mission for:  
a) collecting the sample to be returned; and b) operating after the ascent vehicle has launched and during the one-year wait period?

There is strong support for a rover. This would allow more different geological regimes to be sampled. Each additional geological regime sampled is equivalent in value to another mission. As described in the Mutch report, a rover could provide sampling from five geological regimes.

5. How should the sample be segregated, sealed and environmentally controlled during the return?

Sample should be sieved to 2-10 mm in size and mechanically segregated into packages for each sampling site. Segregation into separately controlled environments is not necessary. Loss of  $H_2$  in the sample should be minimized by properly coating the interior of the sample containers, e.g., with gold. Temperature should be kept as close to the Mars environment as possible but this can be done roughly. No extraordinary thermal control capability should be added. Temperatures below the freezing point of  $H_2O$  are probably not necessary, but temperatures as little as 10-15° above the maximum Mars day time levels could alter the sample adversely.

6. What sort of, if any, documentation of the sample and its setting are required, e.g., fax camera picture, film camera picture, atmospheric temperature and pressure, humidity, time of day, etc?

A camera to help select the sample is recommended. It would also indicate how deep a sampling trench is, etc. Sensing other environmental conditions such as temperature, pressure and humidity was not considered to be important. It would be desirable, if possible, to record the temperature of the soil when a subsurface sample was being taken.

7. What is the recommended back contamination control concept:

- a) direct entry return, sealed and protected sample;
- b) capture in Earth orbit for pathogenic evaluation;
- c) sterilize sample?

The two aspects that characterize the back contamination issue are scientific and political. Scientifically speaking, back contamination poses no major uncontrollable problems. Politically, however, one or two vocal people can always keep the issue firmly in the picture, so we must be prepared to live with some constraints. The obvious solution seems to be to capture the sample in Earth orbit and examine it in a shuttle delivered laboratory. The problem in outfitting and operating this lab will not be trivial, however. Viking '75 results may influence opinions on the criticality of the back contamination issue. From the viewpoint of the organic and bio chemist the unsterilized sample could be as much as 5 orders of magnitude more valuable than a sterilized one.

8. What other science is desirable on the lander and orbiter as part of the MSSR mission other than that required to directly support the sample return?

The major objective of the MSSR mission is and should remain to bring back samples. The only additional science recommended is that that can be accommodated easily within weight and cost budgets. Some thought should be given to providing science that will make use of the wait time at Mars and that will provide some scientific return in the event the sample does not get back to Earth. These activities could be on the Lander, the Orbiter or both. There was some question as to the value of the XRFs or alpha backscatter spectrometer from a geochemistry point of view. Others, however, thought such instrumentation could support the sample return mission and provide some education transferrable to the next mission.

9. At this time, does logic seem to weigh in favor of a 1981 MSSR mission, a 1983/84 mission, or a later one?

There are two basic strategies: 1) fly a precursor mission, then an MSSR mission; and, 2) go right to the MSSR mission. For strategy 1, 1983/84 is probably the earliest opportunity for MSSR. For strategy 2, MSSR could go in 1981. This group expressed general support for strategy 1. The value of the precursor would be to: 1) survey the surface composition on a global basis (with an orbiting gamma ray spectrometer); 2) survey the local terrain at high resolution (appearance and size of particles, inhomogeneity at small scale, soil compaction, etc.). The alternatives for the precursor mission in order of preference were: 1) Viking '79 with a rover; 2) Viking '79 without a rover; 3) an orbiter with gamma ray spectrometer; and 4) an actual MSSR mission with a rover in which the surface characterization would be done at the same time the sample was being sought.

10. Other Comments.

Some of the group thought that the support for the MSSR mission may not be as wide-spread as it now appears. People whose budgets will be threatened by MSSR allocations can be expected to fight it.

It was suggested that a good article on the scientific value of MSSR in a journal such as Science would be useful in coalescing more general and better informed support for the mission.

A Viking '79 rover mission repeated with a subsequent MSSR mission was suggested as a possible cost effective way of improving the sampling capabilities of the MSSR. The rover could be targeted to attempt an overland rendezvous with the MSSR lander.

Consultants in Attendance

Dr. A. W. England (USGS, Denver)  
Mr. H. Masursky (USGS, Flagstaff)  
Dr. W. Phinney (NASA, JSC)  
Dr. B. C. Clark (Martin Marietta, Denver)  
Dr. M. B. McElroy (Harvard)  
Dr. J. S. Lewis (MIT)  
Dr. T. M. Donahue (Univ. of Pittsburg)  
Mr. H. J. Allen (NASA-ARC, Ret.)  
Dr. R. E. Vogt (Cal Tech)  
Dr. D. M. Hunten (Kitt Peak National Observatory)  
Dr. G. H. Pettengill (MIT)  
Dr. C. Ponomperuma (Univ. of Maryland)

## APPENDIX B DESCRIPTION OF ASCENT TO RENDEZVOUS SIMULATION

The simulation described here was devised to test the mission design and maneuver strategies for trajectories dispersed by random maneuver execution and orbit determination (O.D.) error. The effect of these errors on mission performance is simulated by carrying along an "actual" and an "estimated" state ( $X_A$  and  $X_E$  respectively) for each spacecraft. The deviation between these two, the so-called knowledge error ( $\Delta X_E$ ), is initially determined at an update time by randomly sampling an appropriate O.D. error distribution characterized by a six dimensional position and velocity covariance matrix. (Samples are constructed from the eigenvalues and eigenvectors of the covariance matrix.) The state estimate is used to compute maneuver targets and a commanded  $\Delta V_C$ . Randomly drawn samples of execution error corrupt  $\Delta V_C$  to produce an actual  $\Delta V_a$  for implementation. After an impulsive maneuver then, the best estimate of state is given by

$$X'_E = X_E + \begin{bmatrix} 0 \\ \Delta V_C \end{bmatrix} \quad \text{whereas the actual state is}$$
$$X'_A = X_A + \begin{bmatrix} 0 \\ \Delta V_a \end{bmatrix}$$

The estimate will be improved at the next O.D. update time.

Simulation outputs of particular interest are 99 percentile  $\Delta V_a$  requirements (for each maneuver and for the sum of maneuvers), orbital dispersions, relative state dispersions and pointing errors.

### 1. Functional Flow Diagram

The MAV active portion of the simulation is relatively straightforward and need not be explained here. Note in the \*MAV active\* flow however that the elements in the dashed box are equated to the operation "Use  $\Delta V_C$  to compute  $\Delta V_a$ ." This expression will represent those operations later on. The \*orbiter active\* portion of the simulation begins with computation of the post-circularization orbiter estimate as would be available pre-circularization. This state  $YEO$  is a function of the MAV state estimate  $XEO$ .

Note that

- YEØ (1) = semi-major axis (a)
- YEØ (2) = eccentricity (e)
- YEØ (3) = inclination (i)
- YEØ (4) = argument of periapsis (ω)
- YEØ (5) = longitude of ascending node (Ω)
- YEØ (6) = true anomaly (TA)

Before circularization the orbiter orbit was adjusted so that, to the best "knowledge", the inclination and longitude of ascending node matches the estimated MAV values. The two period estimates, PXE and PYE, are used to compute the phase angle PHIØ desired at the first MAV occultation after orbiter circularization. The actual orbiter state after circularization is then computed using the matrix of sensitivity PARINS. Where

$$\text{PARINS} = \frac{\partial(\text{YAØ})}{\partial(\alpha, \beta, \text{TI}, \text{TA})} \quad \text{a } 6 \times 4 \text{ matrix.}$$

The assumption of zero pre-circularization phase error (i.e. at the first occultation exit (O.E.) the orbiter would lead the MAV by exactly PHIØ if the circularization maneuver were performed perfectly) now allows the computation of the MAV actual and estimated states immediately after orbiter circularization. The phase angle when the MAV is actually at O.E. (i.e.  $\phi_A$ ) is obtained by propagating all vectors forward by DTXA and then computing the included angle between position vectors. The error in that angle is the difference between  $\phi_A$  and the PHIØ which would be computed from PXA and PYA. The elapsed time from first O.E. is kept track of by TTOTAL.

After the ΔVLBI update is performed at TA = TAYY-YAØ(4) the desired orbiter state vector, YED, is computed from the new XE and YE. All vectors, YE, YA, XE, XA, YED are then propagated forward to the orbiter TA = TATRMI -YEØ(4). Here the commanded circular trim sequence ΔV<sub>1C</sub>, ΔV<sub>2C</sub> and ΔV<sub>3C</sub> and times Δt<sub>12</sub>, Δt<sub>23</sub> are computed. These are then executed in the simulation and actual and estimated states updated appropriately after each maneuver. Immediately after the third trim the estimated line-of-sight (LOS) components are computed in the U, V, W system defined by the actual relative state and stored in the SAVE3 array. The error in the relative state at this time is also computed and stored in the SAVE4 array while the actual relative

state is stored in SAVE5. The actual time from trim number three to 10th MAV occultation exit will vary with each Monte Carlo cycle. This time to go (TGO) is computed as shown using TTOTAL. Vectors are propagated forward by TGO and pertinent output quantities are stored. When NCASE cycles have been processed, statistics on the stored quantities are computed. These are basically sample means and variances and ordered sample sequences from which sample size percentiles may be ascertained.

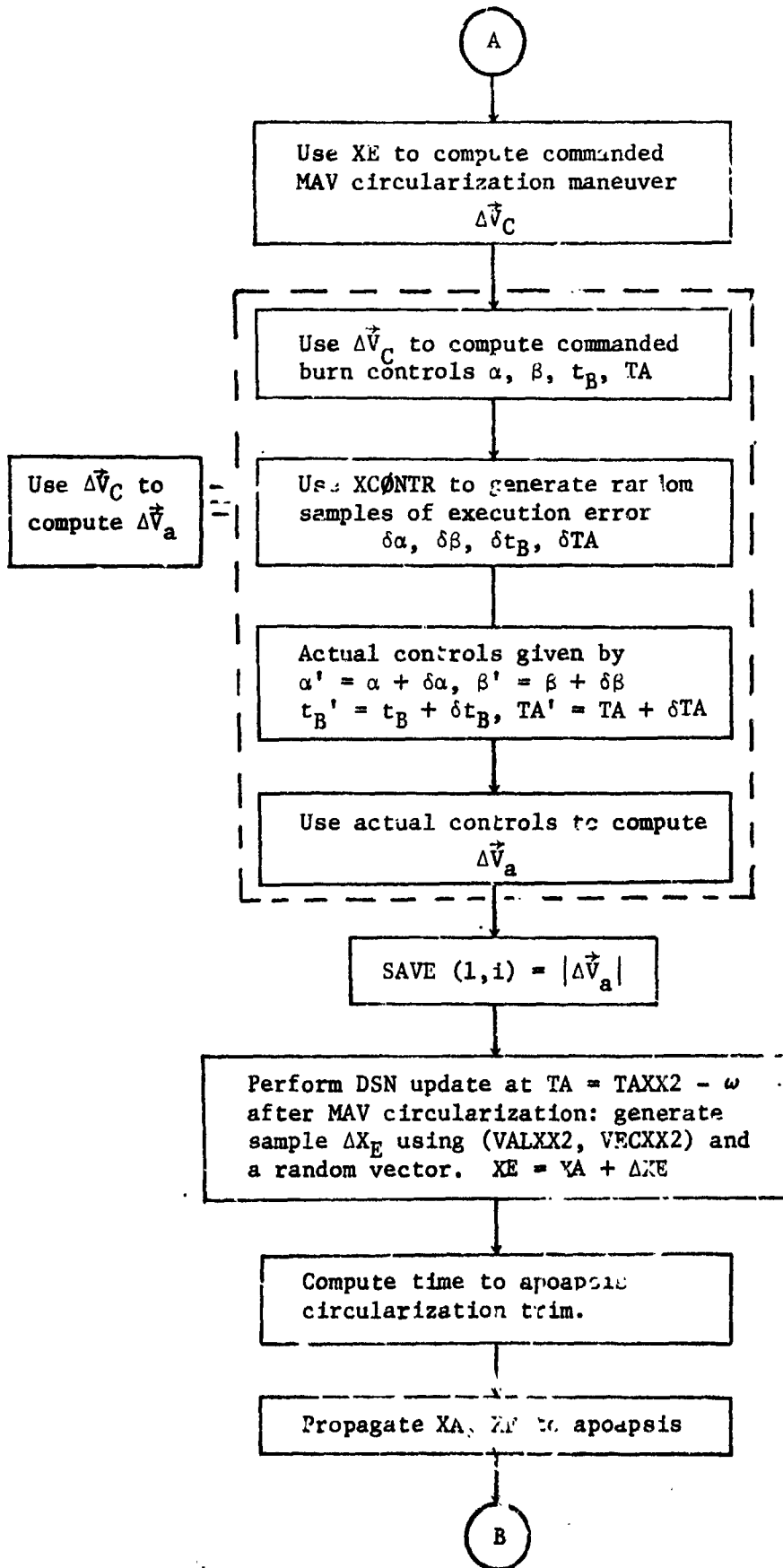
## 2. Input Description

<u>Variable</u>	<u>Definition</u>
XRO	Kepler elements for reference MAV ascent orbit
TAXX1, TAXX2, TAXX3	True anomalies of the three O.D. updates for MAV
TAYY	True anomaly of the O.D. update for the orbiter
XCONTR, YCONTR	Vector of MAV and orbiter execution error standard deviations
NCASE	Number of Monte Carlo cases
XJD	Julian date of encounter
VALXX1, VECXX1	Vector of eigenvalues and matrix of eigenvectors of covariance matrix for first MAV update
VALXX2, VECXX2	Vector of eigenvalues and matrix of eigenvectors of covariance matrix for second MAV update
VALXX3, VECXX3	Vector of eigenvalues and matrix of eigenvectors of covariance matrix for third MAV update
VALXX, VECXX	Vector of eigenvalues and matrix of eigenvectors of MAV ascent injected covariance matrix
VALXY, VECXY	Vector of eigenvalues and matrix of eigenvectors of covariance matrix for $\Delta$ VLBI update
VALYY, VECYY	Vector of eigenvalues and matrix of eigenvectors of covariance matrix for orbiter update
SIGA( $\sigma_\alpha$ ), SIGB( $\sigma_\beta$ )	Standard deviations of orbiter pointing errors during circularization
SIGTI( $\sigma_{t_B}$ )	Standard deviations of orbiter burn time errors during circularization

Variable

SIGTA( $\sigma_{TA}$ )	Standard deviations of orbiter initial TA error during circularization
PARINS	Matrix of partial derivatives of post-circularization state with respect to execution errors
DCA	Desired closest approach distance @ NOE <sup>th</sup> occultation exit
NOE	Number of occultation exits to TRI
TATRM1	Nominal argument of latitude, $(W+TA)_{NOM}$ , for orbiter circular trim number one





B

Compute commanded MAV  
circularization trim  $\Delta\vec{V}_C$

Use  $\Delta\vec{V}_C$  to compute  $\Delta\vec{V}_a$ .

Execute actual MAV circulari-  
zation trim  
$$X_A = X_A + \begin{bmatrix} 0 \\ \Delta\vec{V}_a \end{bmatrix}$$

SAVE (2,i) =  $|\Delta\vec{V}_a|$   
SAVE (3,i) = SAVE (1,i) + SAVE (2,i)

Perform DSN update at TA = TAXX3 -  $\omega$   
after circularization trim: generate  
sample  $\Delta XE$  using (VALXX3, VECXX3) and  
random vector.  $XE = X_A + \Delta XE$

Transform Cartesian MAV state  
XE to Kepler elements  $XE\phi$ :  
Compute estimated MAV period  
PXE

\* \* ORBITER \* \* \* \* \* \* \* \* \* \* \* \* ACTIVE \* \* \*

Initialize Orbiter Estimate  
At Circularization  
Targeted orbiter state post-  
circularization:  
 $YE\phi(1) = XE\phi(1) + 50.$   
 $YE\phi(2) = .001$   
 $YE\phi(3) = XE\phi(3)$   
 $YE\phi(4) = 258.68$   
 $YE\phi(5) = XE\phi(5)$   
 $YE\phi(6) = 0.$

C

C

Compute estimated orbiter period PYE and targeted phase angle  
 $PHI\phi = NOE * [(PYE - PXE) / PYE] * 360. + [DCA / XE\phi(1)] * 180 / \pi$

Using SIGA, SIGB, SIGTI, SIGTA  
Compute random 4-vector, RVEC,  
of orbiter circularization  
execution error.

Compute dispersed post-circ.  
orbiter state:  
 $\delta YA\phi = PARINS * RVEC$   
 $YA\phi = YE\phi + \delta YA\phi$

Transform actual orbiter Kepler  
state  $YA\phi$  to Cartesian YA

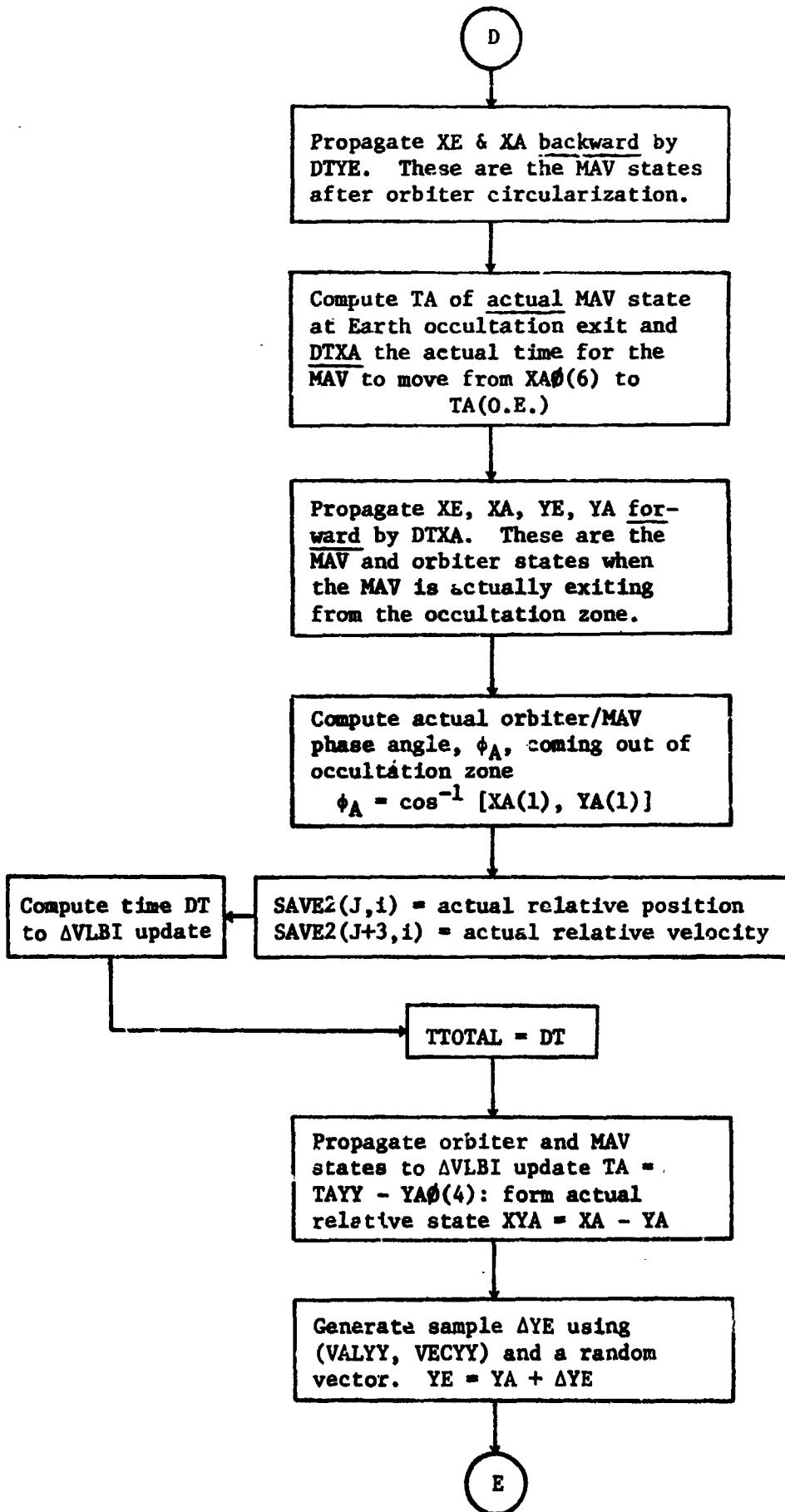
Compute TA of estimated orbiter  
state at Earth occultation exit  
(O.E.) +  $PHI\phi$ : i.e., compute  
 $TA(O.E. + PHI\phi)$

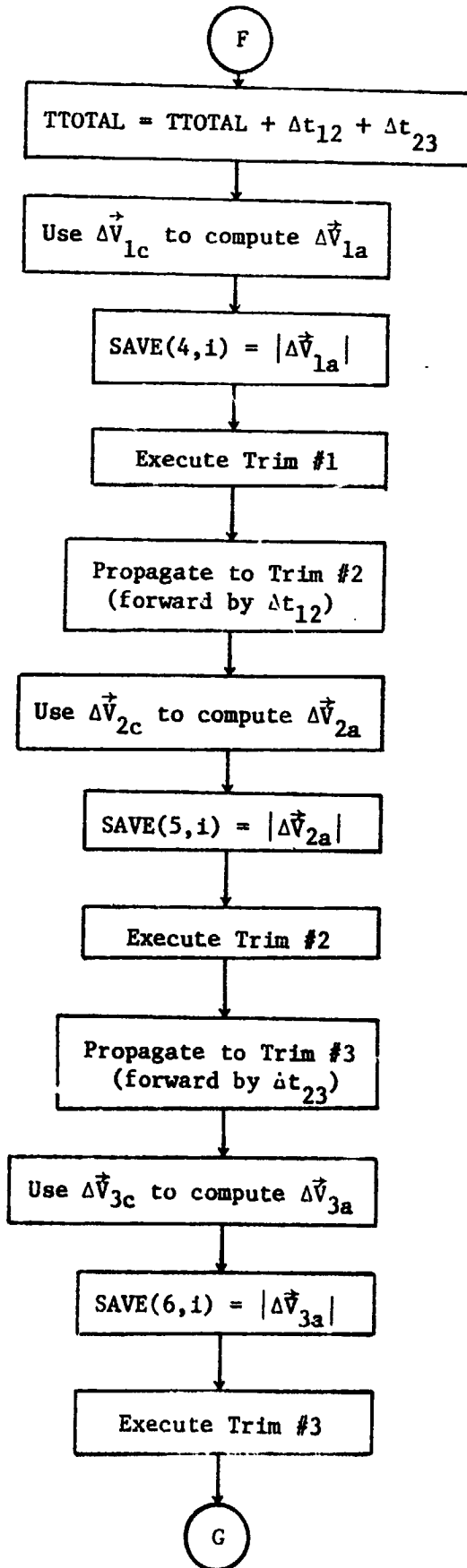
Compute estimated time, DTYE,  
for orbiter to move from  
 $TA = 0$  to  $TA(O.E. + \phi_0)$

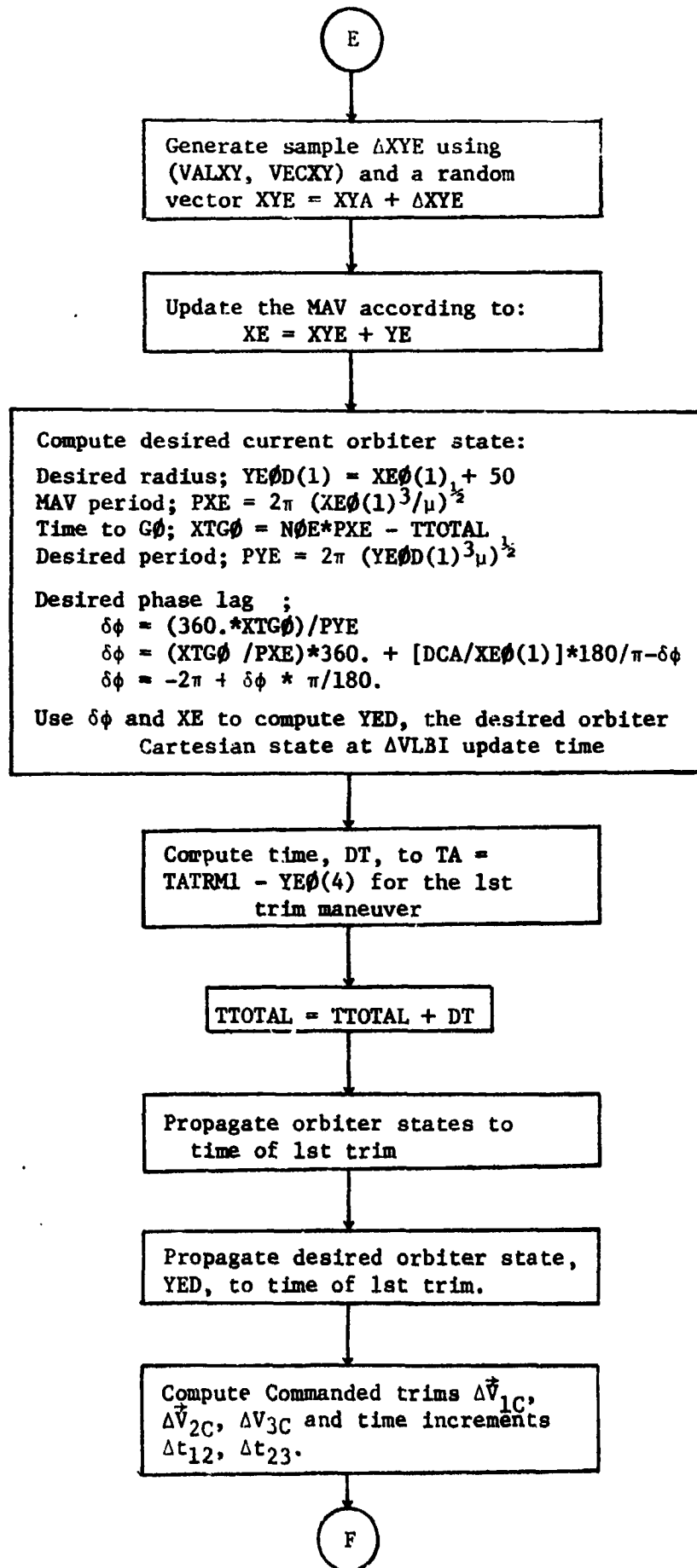
Compute  $TA(O.E.)$  for estimated  
MAV state and DTXE the esti-  
mated time for the MAV to move  
from  $XE\phi(6)$  to  $TA(O.E.)$

Propagate XE & YA forward by  
DTXE

D







G

Compute components  $XY1$  of estimated LOS in U,V,W coordinate system defined by the actual LOS.  $SAVE3(J,i)=XY1,(J),J=1,3$

Compute the error in the estimate of the relative state  $DXYE$   
 $SAVE4(J,i)=DXYE(J),J=1,6$

Compute the actual relative state  $XYA$ .  
 $SAVE5(J,i)=XYA(J),J=1,6$

Compute actual time to go ( $TG\phi$ ) for MAV to cross occultation exit for 10th time:  
 $TG\phi = N\phi E * PXA - TTOTAL$

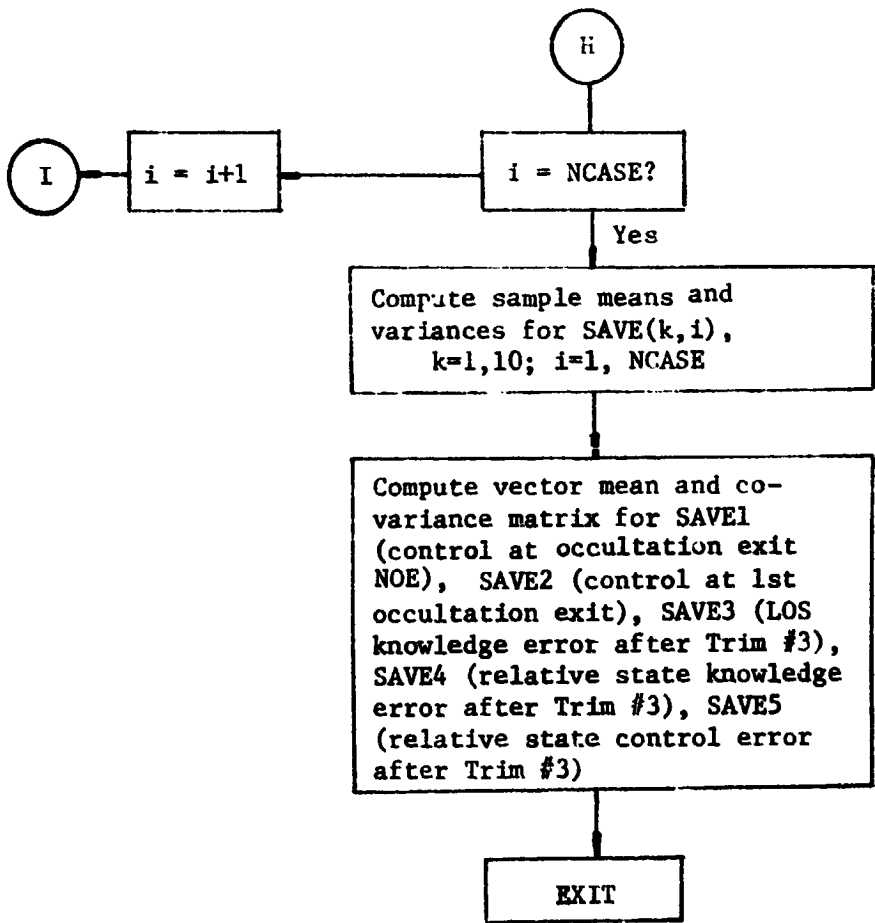
Propagate  $XE, XA, YE, YA$  forward by  $XTG\phi$

Compute actual MAV/orbiter phase angle at TRI  
 $\phi = \cos^{-1}[YA(1),XA(1)]$   
 $SAVE(8,i) = \phi$

Compute absolute magnitude of actual separation and velocity  
 $RMAG = YA(1) - XA(1)$   
 $SAVE(9,i) = RMAG$   
 $VMAG = YA(4) - XA(4)$   
 $SAVE(10,i) = VMAG$

Compute actual relative state  
 $XYA = YA - XA$   
 $SAVE1(J,i) = XYA(J),J=1,6$

II



## APPENDIX C RENDEZVOUS DIGITAL COMPUTER PROGRAM

A digital computer program was developed to simulate the initial and terminal rendezvous phases. This program is a six degree-of-freedom simulation with three translational coordinates. It assumes perfect dynamic control of the rendezvous vehicle attitudes, i.e., a perfect control system. The vehicles orbits are determined by their initial conditions and the planets gravitational field. The program has the capability of using one type of rendezvous scheme (Type II Guidance) for initial rendezvous maneuvers, and another type (Type I) for the terminal rendezvous phase. Guidance errors can also be included in both phases.

Type II guidance uses approximate guidance equations to command and execute impulsive maneuvers, so the rendezvous vehicle will intercept the target vehicle. This type of rendezvous scheme requires target ephemeris data and the angles between the LOS vector and the spacecraft velocity vector. Up to two corrective thrust periods can be used to bring the relative positions between the spacecrafts to within the range of the rendezvous radar, where the Type I rendezvous is used for the final closure.

The terminal rendezvous is accomplished by causing the relative velocity and relative position between the spacecrafts to converge to zero between two optimum switching curves. A new set of switching curves are required for each spacecraft design. A different set of switching curves is required for ranges closer than  $R_M$  to optimize the vehicle rendezvous trajectory at both are and close ranges.

Each set of switching curves consists of thrust-on and thrust-off parabolas that are selected for a near optimum rendezvous. These control curves are mechanized in the rendezvous vehicle control computer and are implemented to control the axial thrust of the vehicle.

The flow block diagram of the digital computer mechanization of the rendezvous program called RENDZ is shown in Figure C-1. The symbols used on this figure are defined below:

REPRODUCIBILITY OF THE ORIGINAL PAGE IS POOR

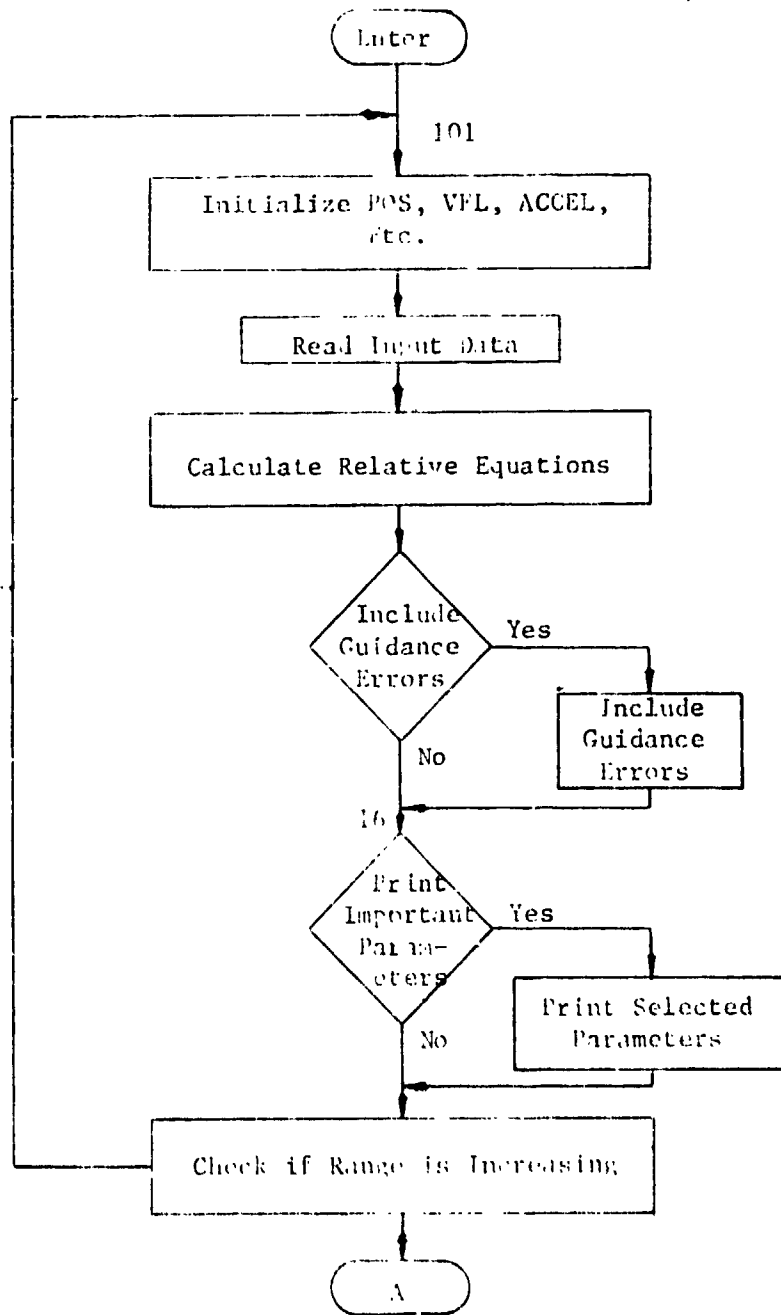


Figure C-1 RENZ Digital Computer Flow Diagram



REPRODUCIBILITY OF THE ORIGINAL PAGE IS POOR

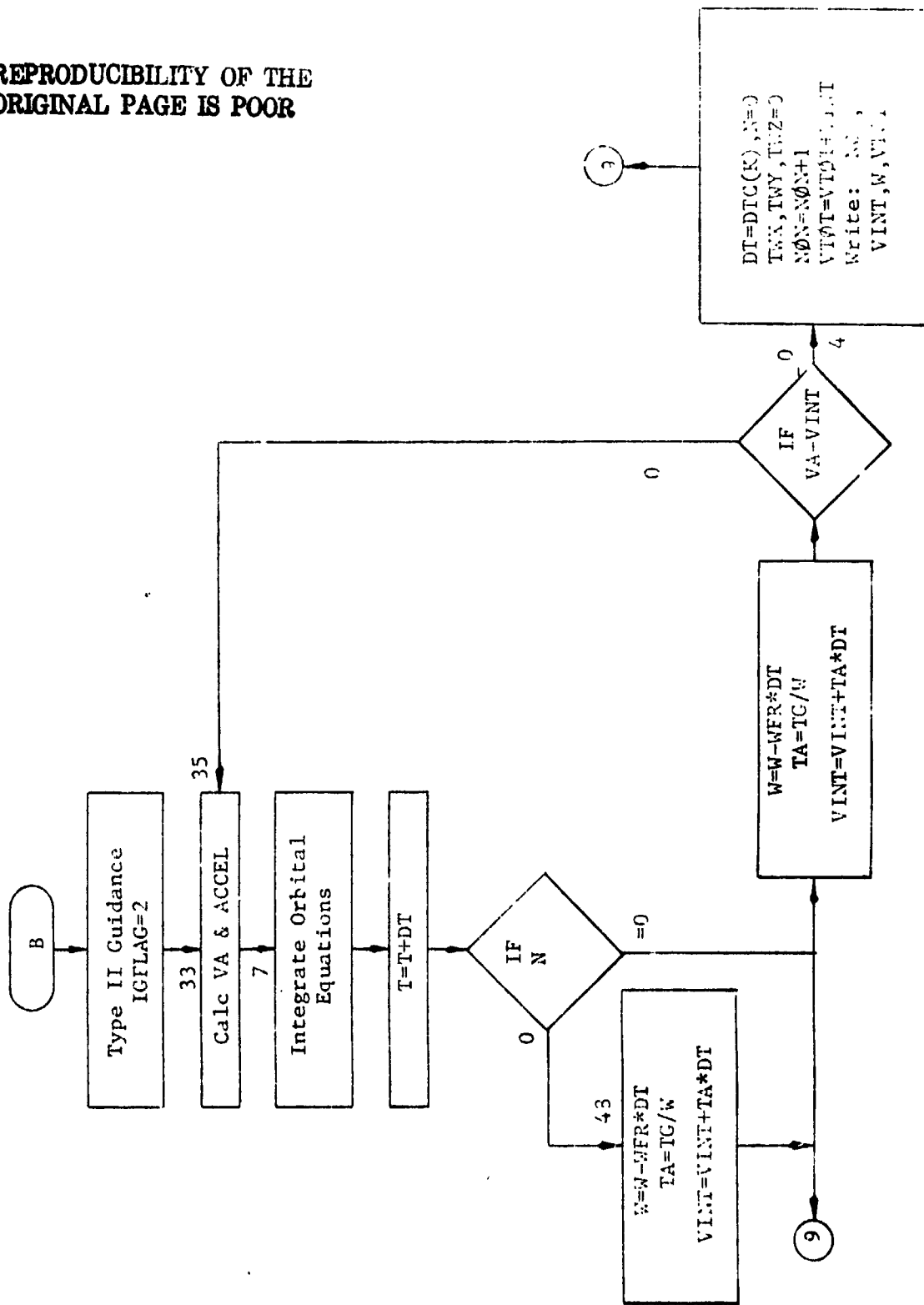


Figure C-1 (continued)

DRM	Range rate used in program
DT	Time increment
DTC(K)	Time increment for phase K
IGFLG	Type of guidance flag
F	Phase indicator
L	Range flag
M	Indicator of no. of maneuvers during Type II guidance
NØN	No. of engine thrusts
Q	Rate gains
Q1, Q2	Control gains
RB	Gain change altitude
RM	Range at start of Type I guidance
RR	Range
RRM	Range used in program
T	Time
TA	Thrust-to-Mass
TG	Vehicle thrust-to-weight
T/M	Vehicle average thrust-to-Mass
TWX, TWX, TWZ	Vehicle thrust
V <sub>A</sub>	Total velocity
VINT	Accumulated velocity
VRM	Relative velocity in program
VM	Vehicle velocity
VR	Relative velocity
VTØT	Total $\Delta V$
W2	Vehicle total LOS rate
W2M	Total LOS rate in program
W	Vehicle weight
WFR	Engine total flow rate

## APPENDIX D ADDITIONAL RENDEZVOUS STUDY RESULTS

A number of studies were conducted using a digital computer simulation of the terminal rendezvous phase to define a good design and size the terminal rendezvous system. The digital computer simulation called RENDZ of the terminal rendezvous phase is described in Appendix C. The following studies were conducted to define the terminal system:

1. LOS rate gain studies,
2. Axial thrust sizing studies,
3. Control curve definition studies,
4. Terminal rendezvous initiation angle studies,
5. Terminal rendezvous transfer angle selection studies,
6.  $3\sigma$  dispersion studies, and
7. Interception sensitivity to closing  $\Delta V$  maneuver magnitude.

The LOS rate gain sizing studies determined the bit rate gain to control the LOS rate of the vehicle. Rate gains of 10 and 3 were determined to be optimum for the far and close ranges respectively. These gains reduced the maximum LOS rate during the terminal rendezvous phase. These gains were the smallest rate gains that could be used and still control the LOS rate during the TR phase. Small rate gains did not control the LOS rates of the vehicle adequately. High rate gains did not decrease the LOS rates.

Axial thrust sizing studies were conducted to determine the optimum size thrust to execute the TR phase. The amount of thrust seemed to effect principally the  $\Delta V$  required for rendezvous. A vehicle using a smaller thrust required considerable more  $\Delta V$  to accomplish the terminal rendezvous. Axial engines with 132 newtons (30 lbs) of thrust seemed to be the optimum thrust level for the orbiter. Higher thrust levels than this did not improve the efficiency during TR phase, but reduced the pointing angles needed to control the LOS rates.

The control curve definition study defined reasonable control curves to execute the terminal rendezvous phase. The control curve design approach used was imperial. Additional study is required to develop theoretical techniques. The control curves can be changed by

raising the control gain, gain change altitude and position of curves. In the studies conducted during this contract, only the position of the curves and the gain change altitude was varied to determine the best ones to be used. The control curve gains were determined from formulas determined from previous studies. These formulas may not be optimum for this mission and should be further evaluated in future studies.

The optimum terminal rendezvous initiation angle selection is inter-related with the selection of the terminal rendezvous transfer angle. The initial relative velocity, which is a function of the initiation angle, affects the control curve design, and the time and angle of transfer. A discontinuity is produced due to keeping the LOS inertial attitude constant throughout long transfers. Terminal rendezvous transfer angles greater than 155 degrees could not be implemented due to large initiation angles used. The interrelation between the initiation angle and the terminal rendezvous transfer angle should be studied further to try to get 180 degree transfers, which should be the most optimum.

The control curves were designed initially for the nominal case, but did not accomplish the rendezvous in the worst 30 cases. The  $3\sigma$  initial condition dispersions were too large to use the nominal control curves for the worst cases, i.e., resulting intercept errors were too large. Consequently, control curves had to be designed that initiated maneuvers at very long ranges. However, these caused the initial terminal rendezvous maneuvers to be too large. Two approaches were considered to handle the  $3\sigma$  dispersions. One approach would be to limit the size of the early closed loop maneuvers by putting a constraint on the  $\Delta V$  burns as a function of range. The other approach is to change the closing  $\Delta V$  magnitude as a function of the dispersed state between the two vehicles. The latter approach was baselined for this mission and a method to process this algorithm on board the orbiter was devised. Further study of both approaches would be pursued to determine the best method to accomplish the approximate intercept. The closing  $\Delta V$  maneuver is designed so the orbiter lags the MAV when the orbiter crosses the MAV orbit. The closed loop maneuvers take out this lag and ultimately match the velocities between the two vehicles by trimming the orbits in progressively smaller

thrust periods. The sensitivity of interception range to in-plane and out-of-plane errors was studied to find a method to calculate the closing  $\Delta V$  on board. The sensitivity of the closing  $\Delta V$  magnitude to in-plane and out-of-plane dispersions was determined by perturbing the values of closing  $\Delta V$ . The sensitivity so determined was multiplied by the  $3\sigma$  dispersion (which would be sensed by the rendezvous radar) to get the required closing  $\Delta V$  maneuver magnitude. Terminal rendezvous was accomplished in all the  $3\sigma$  dispersed cases when the  $\Delta V$  maneuver magnitude calculated in this manner was used. The same axial control curves were used as in the nominal case.

Figures D-1 through D-4 show the results of the digital computer simulation of the  $3\sigma$  dispersed cases where the orbiter is 7.7 km higher than the nominal orbit. The terminal rendezvous propulsion system requirement was established by this case since this is the worst case found in terms of the propellant required. A factor of two was applied to the propellant allocation to allow for malfunction and reinitiation options. Eight thrust periods are needed to accomplish the closed loop portion of the terminal rendezvous as shown in Figure D-1, which shows the range rate vs range trajectory. The weight of propellant required for the terminal rendezvous phase for this case is shown on the figure. The terminal rendezvous phase final conditions or the docking phase initial conditions are also shown in this figure. Figures D-2 and D-3 show the rendezvous trajectories in tangential and inertial coordinates respectively. Figure D-4 shows the range rates and LOS rates as a function of rendezvous time. The thrust period times are also shown on this figure. A maximum LOS rate of 2.6 mrad/sec is reached before the end of the TR phase.

Figures D-5 through D-8 show the results of the digital computer simulation where the orbiter is 7.7 km lower than the nominal attitude -- a  $3\sigma$  position dispersed case. The  $\Delta V$  for each phase, required weight and final conditions for terminal rendezvous are shown in Figure D-5. The rendezvous trajectory in tangential and inertial coordinates is shown in Figures D-6 and D-7 respectively. Figure D-8 Shows how the relative range rate and LOS rate vary during the terminal rendezvous phase.

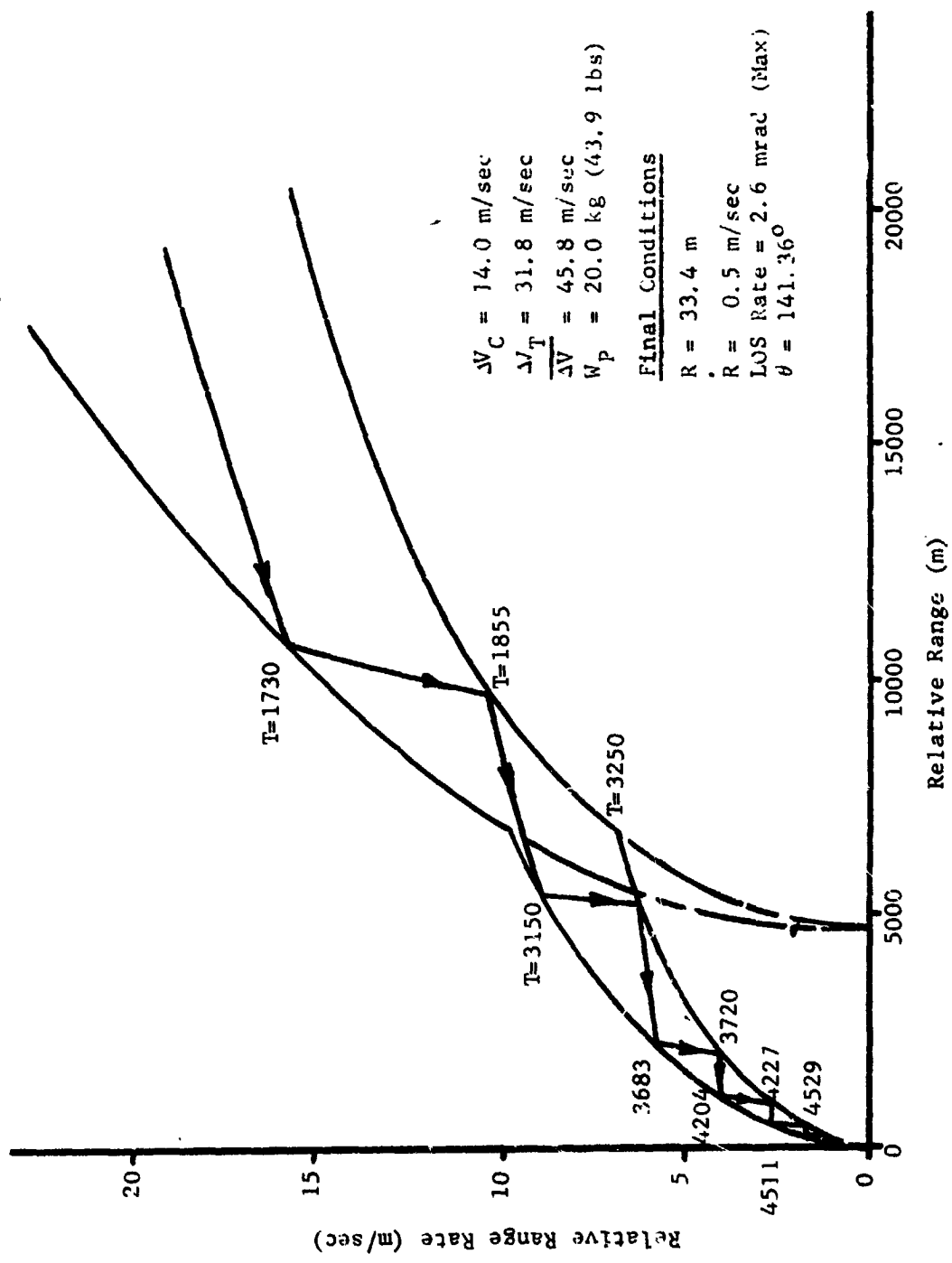


Figure D-1 Axial Control Curves (7.7 kr High - 3σ)

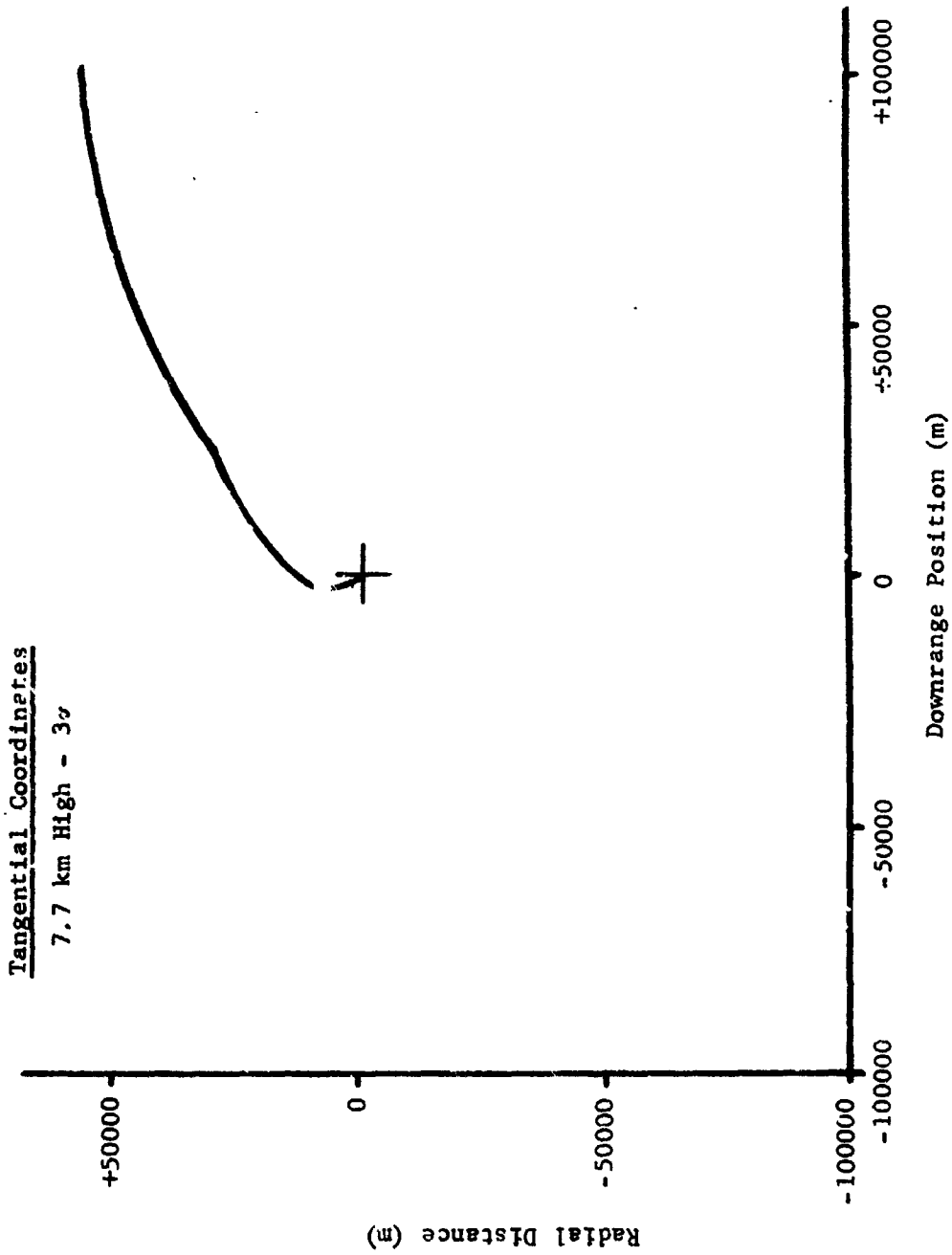


Figure D-2 Rendezvous Trajectory (Tangential Coordinates)

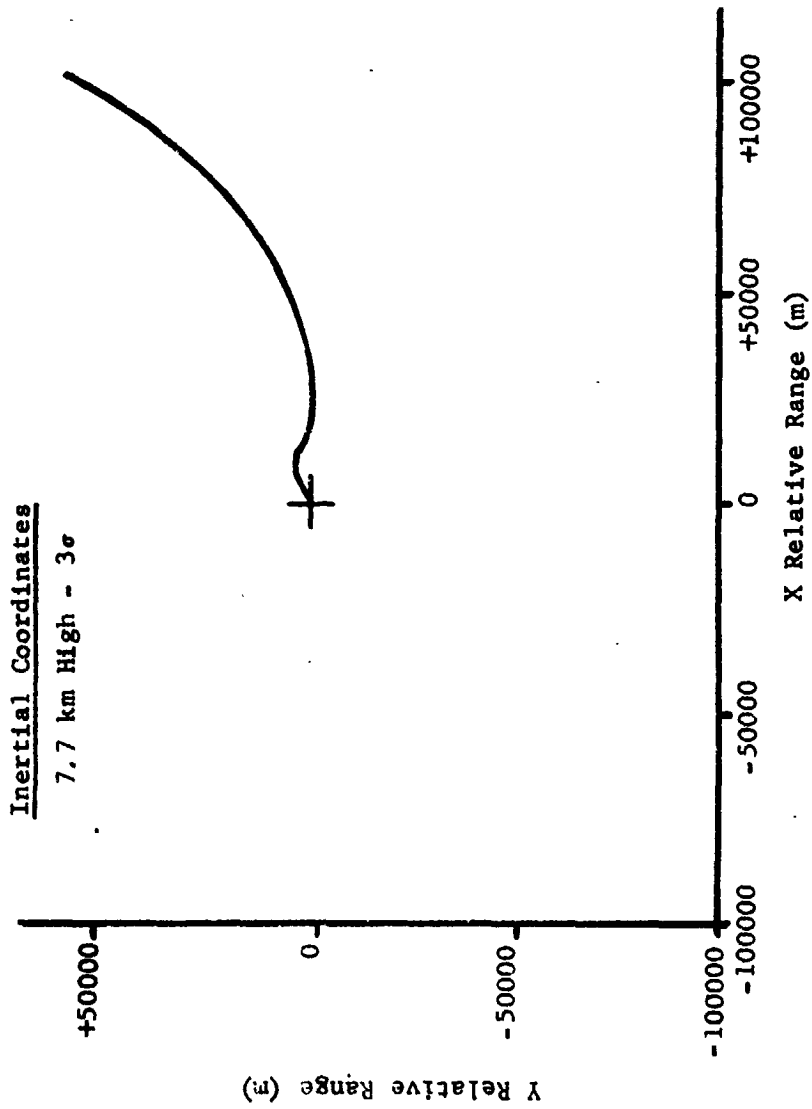


Figure D-3 Rendezvous Trajectory (Inertial Coordinates)

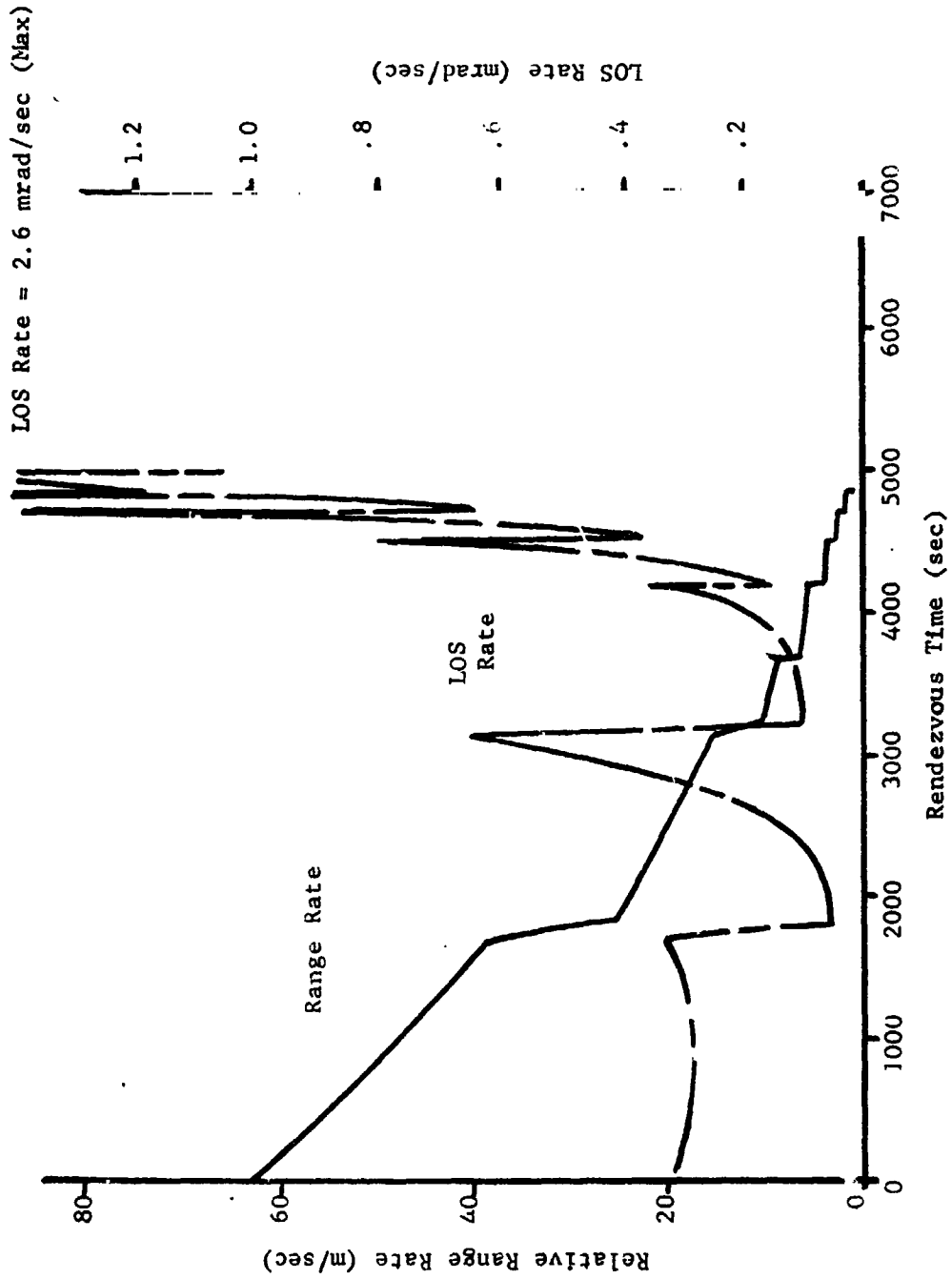


Figure D-4 Relative Range Rate, LOS Rate Vs Time

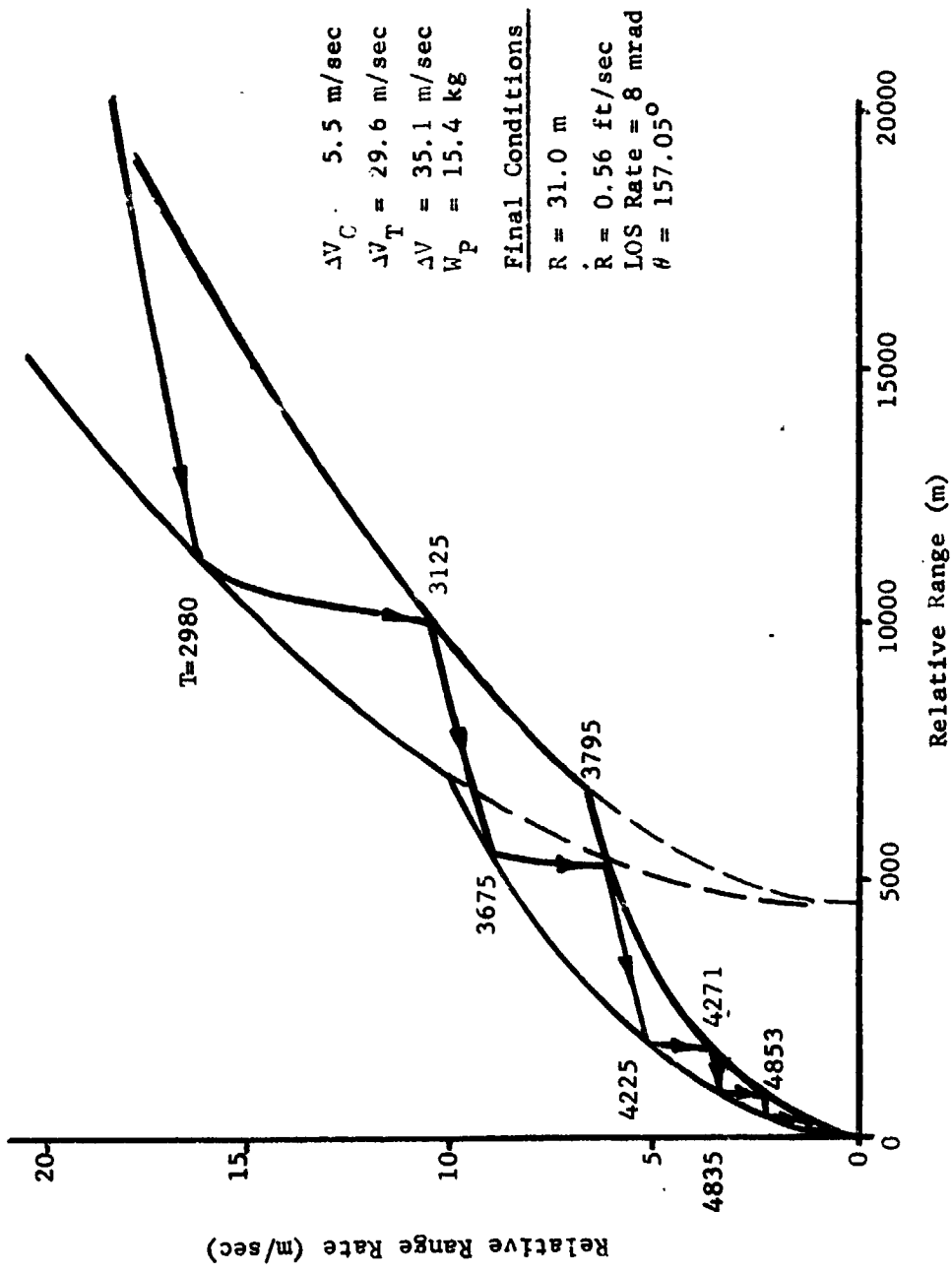


Figure D-5 Axial Control Curves (7.7 km Low -  $3\sigma$ )

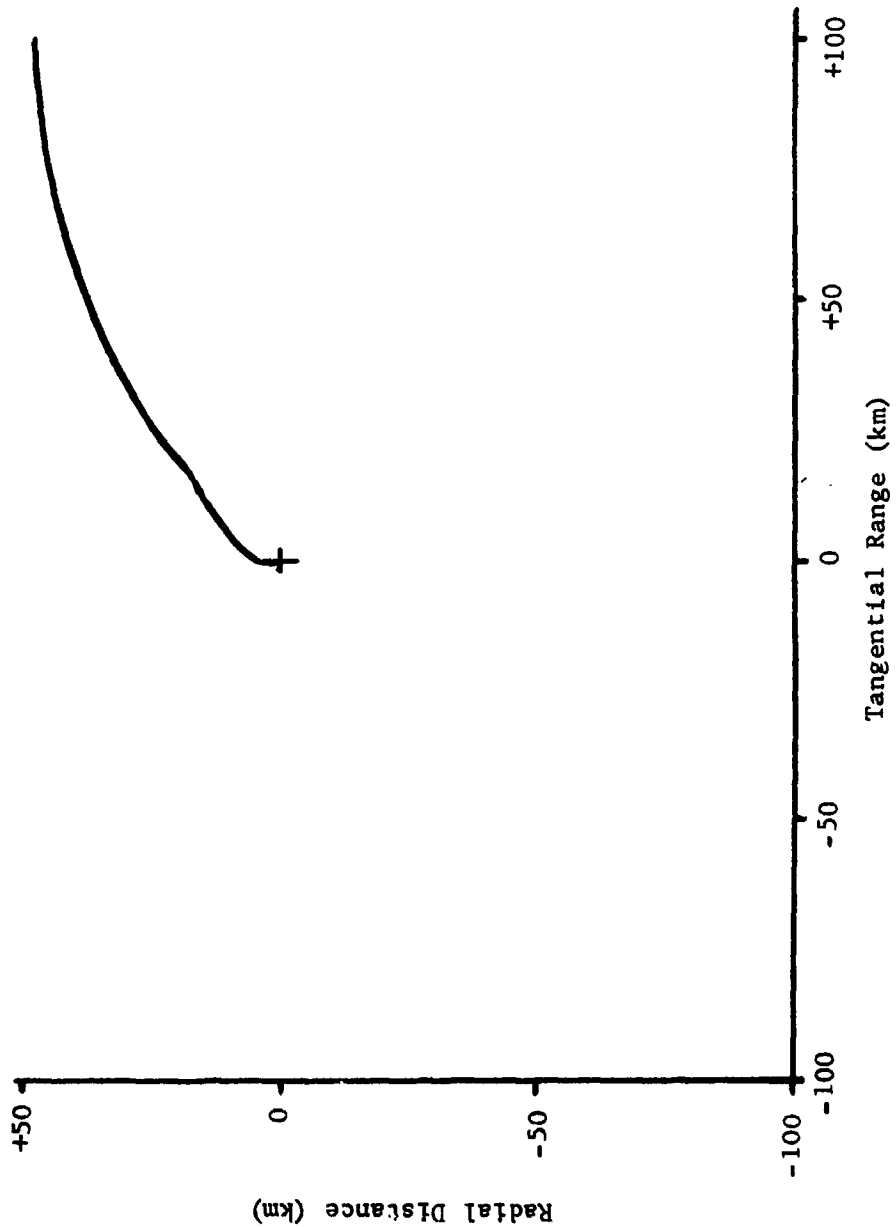


Figure D-6 Rendezvous Trajectory (Tangential Coordinates)

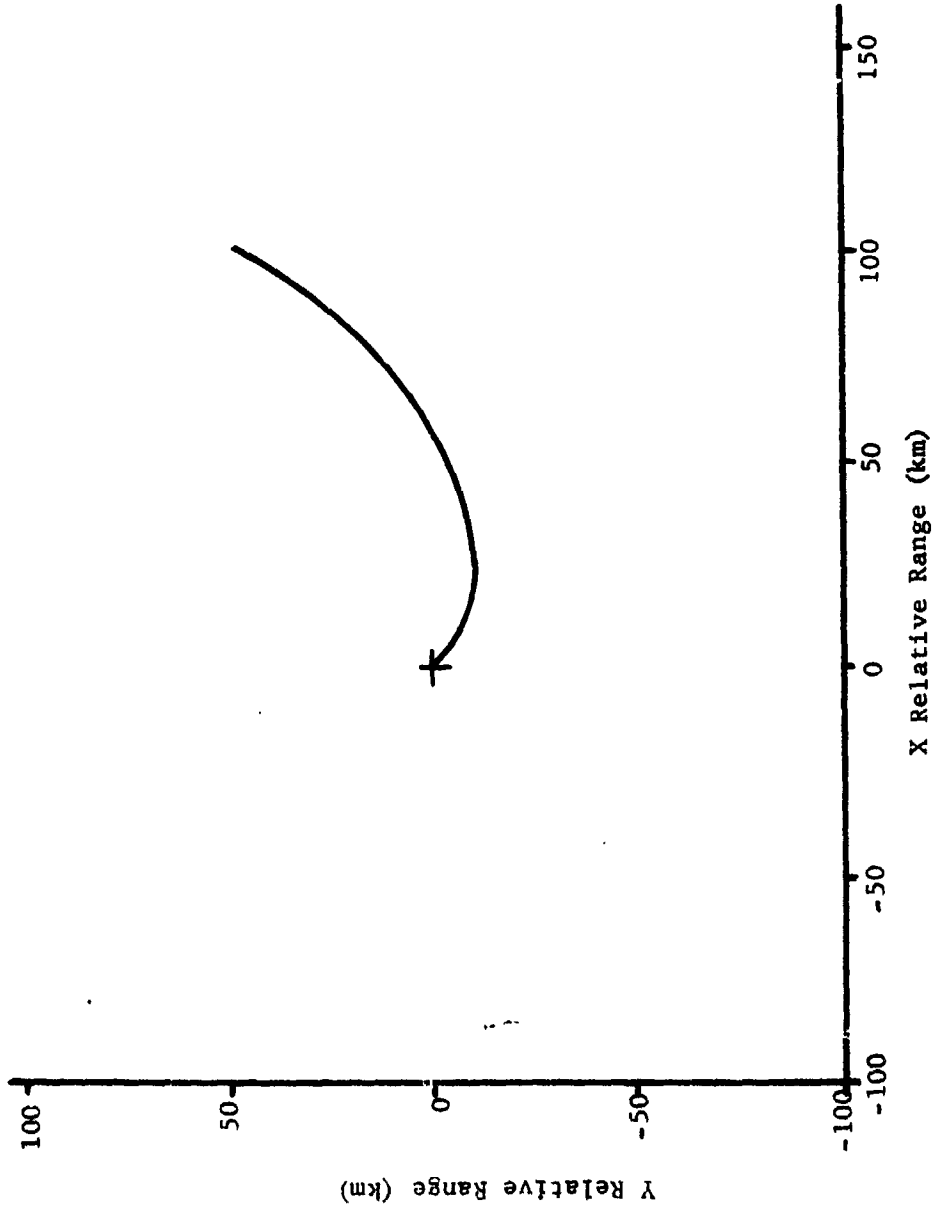


Figure D-7 Rendezvous Trajectory (Inertial Coordinates)

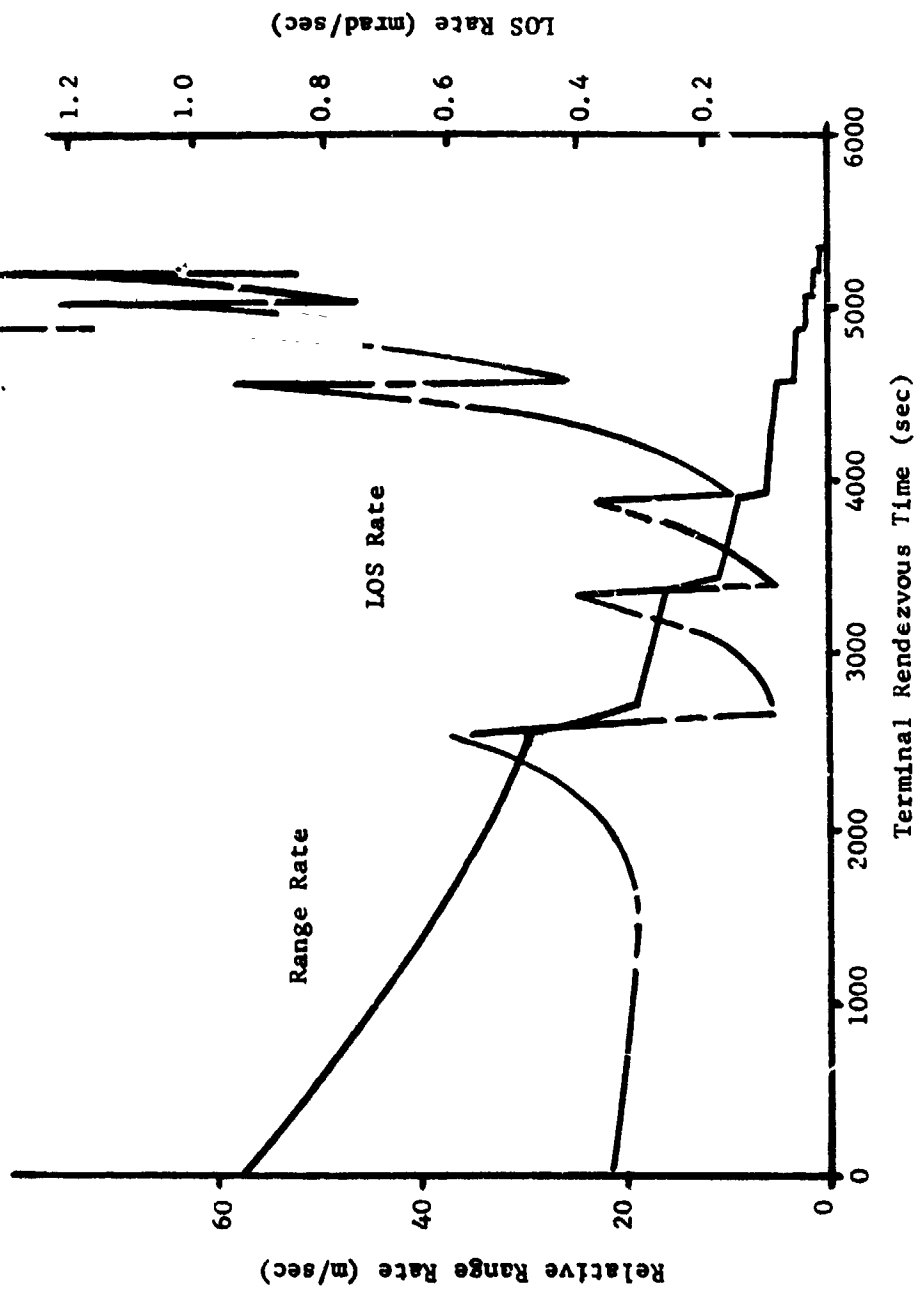


Figure D-8 Relative Range Rate and LOS Rate Vs Time

## APPENDIX E RENDEZVOUS SENSOR ERROR CALCULATIONS

System calculations to determine the range performance of the rendezvous sensor were performed in Section VB. These calculations included an assessment of bias and random range errors inherent with a sensor employing a sidetone ranging system. Additional calculations were performed to determine the range rate and angle measurement accuracy of such a system and these calculations are described in this Appendix.

The Doppler shifts on the carrier and the range tones were determined. Let the maximum range rate = 122 m/s.

$$\begin{aligned} f_c &= \text{transmitted carrier frequency} \\ f_c &= 2282.48 \text{ MHz (Orbiter to MAV)} \\ f_c &= 2101.03 \text{ MHz (MAV to Orbiter)} \\ f_d &= (2v/c) f_c = 8.14 \times 10^{-7} f_c \end{aligned}$$

Then:

$$\begin{aligned} f_d &= 1.855 \text{ kHz (Orbiter to M.V)} \\ f_d &= 1.708 \text{ kHz (MAV to Orbiter)} \end{aligned}$$

The Doppler shifts on the range tones are the Doppler shifts at the range tone frequencies. These are given by:

819.2 kHz tone	0.666 Hz
102.40 kHz tone	0.0833 Hz
12.8 kHz tone	0.0104 Hz
1.6 kHz tone	$1.3 \times 10^{-3}$ Hz
200 Hz tone	$1.63 \times 10^{-4}$ Hz

The Doppler measurement accuracy must be determined. The two-way frequency shift will be the difference between the transmitted reference and the received signal and is obtained as follows:

- (1) Transmitted frequency =  $120 f_o = (120) (19.1003) (10^6)$
- (2) Received frequency at MAV =  $120 f_o (1+v/c)$
- (3) Transmitted frequency by MAV =  $120 f_o (1+v/c) (220/239)$
- (4) Received frequency at orbiter =  $120 f_o (1+v/c)^2 (220/239)$
- (5) VCO frequency in orbiter receiver =  $(120/110.5)(220/239)(1+2 v/c)$

This frequency appears at the output of the carrier VCO, is multiplied by 4, and, then mixed with  $4 f_o$  to yield:

$$f_m = 4 f_o [1 - K (1 + 2 v/c)]$$

Where:  $K = (120/110.5)(220/239) = 0.99964$

The bias is then given by:

$$4 f_o (1-K) = (4)(19.1003)(10^6)(3.597)(10^{-4}) = 27.38 \text{ kHz.}$$

The maximum expected Doppler shift is then given by

$$4 f_o (2v/c) = (4)(19.1003)(10^6)(800/9.83 \times 10^8) = \pm 62 \text{ kHz.}$$

The Doppler measurement is obtained by counting  $f_o$  cycles for a period of time equal to 512 cycles of  $f_m$ . This period is:

$$T = 512/f_m = 512/4 f_o [1 - K(1 + 2v/c)]$$

The time for one count of  $4 f_o$  is  $T_o = 1/4 f_o$

The number of counts of  $f_o$  per period of T is then given by

$$T/T_o = N = 512/[1 - K(1 + 2v/c)]$$

The range rate counter, then, contains a bias count of

$$N = 512/1-K = 512/(3.597)(10^{-4}) = 1.425 \times 10^6 \text{ under zero Doppler conditions.}$$

The signal to noise ratio of the velocity measurement will be dependent upon the phase jitter in the phase locked loop. This phase jitter is given by:

$$\Delta \theta = \sqrt{1/2(S/N)}$$

The signal to noise ratio at maximum range is about 36 dB, so that  $\Delta \theta \approx .013 \text{ rad} \approx .725 \text{ degrees}$ . However, a degradation of 12 dB in S/N ratio must be taken so that the actual S/N ratio at maximum range is 24 dB for which  $\Delta \theta \approx .0456 \text{ rad} \approx 2.62 \text{ degrees}$ . The phase jitter at  $4 f_o$  is then 0.0238 degrees, and the effect of the jitter is to increase or decrease the counts by an amount equal to  $0.0238/360$  or  $6.61 \times 10^{-5}$  of a cycle. Since counts of the reference signal are accumulated for 512 cycles of the  $4 f_o - f_m$  difference, the r.m.s. error in any reading is given by:

$$(6.61)(10^{-5})/512 (\sqrt{2}) = 1.835 \times 10^{-7}$$

This corresponds to  $(1.835 \times 10^{-7})N$  or 0.26 counts at zero Doppler. Since a count at zero doppler is equivalent to 0.0536 m/s, it is concluded that at a range of 250 km the range rate error will not exceed .05 m/s. If the maximum range is extended to 750 km the signal to noise ratio will drop to

14 dB which is an r.m.s. error of  $5.69 \times 10^{-7}$  corresponding to 0.81 counts at zero Doppler. Thus, it is clear that even at this maximum range the rendezvous system will provide extremely accurate range rate measurements.

The signal to noise ratio in the error channels of the rendezvous receiver must be determined. The gain in the error channels relative to the gain in the sum channel affects the signal to noise ratio at the error output of the receiver. For a phase comparison monopulse system the error channel gain is approximately 2.6 dB below the sum channel gain. Hence, the increased power at the rendezvous receiver error channel antennas is given by:

$$P_R = -55.7 - 20 \log R - 2.6 = -58.3 - 20 \log R$$

The signal to noise ratio required for a given angle error is given by:

$$(S/N)_e = 1/8 [\lambda/\theta_e \pi d]^2$$

Taking a nominal spacing between surface wave antenna phase centers of  $d/\lambda \approx 2$ , we, then, have:

$$(S/N)_e = 3.17 \times 10^{-3} / \theta_e^2$$

where  $\theta_e$  = angle error in radians

This relationship has been plotted in Figure E-1. Taking the above relationship for the received power at the error channel antennas, the angle error (" $\theta_e$ ") is shown in Figure E-2 as a function of range.

Additional calculations were performed to ascertain errors introduced in the rendezvous sensor by the monopulse antenna array. There are three general sources of phase and amplitude imbalances in the antenna system:

1. Inequalities of transmission lines and antenna elements due to thermal gradient, radiation and vibration.
2. Inequalities of radiating elements.
3. Mechanical alignment.

These error sources will be briefly analyzed to assess their effects on the system.

#### 1. Transmission Line and Component Errors

The major errors introduced here are due to thermal expansion of

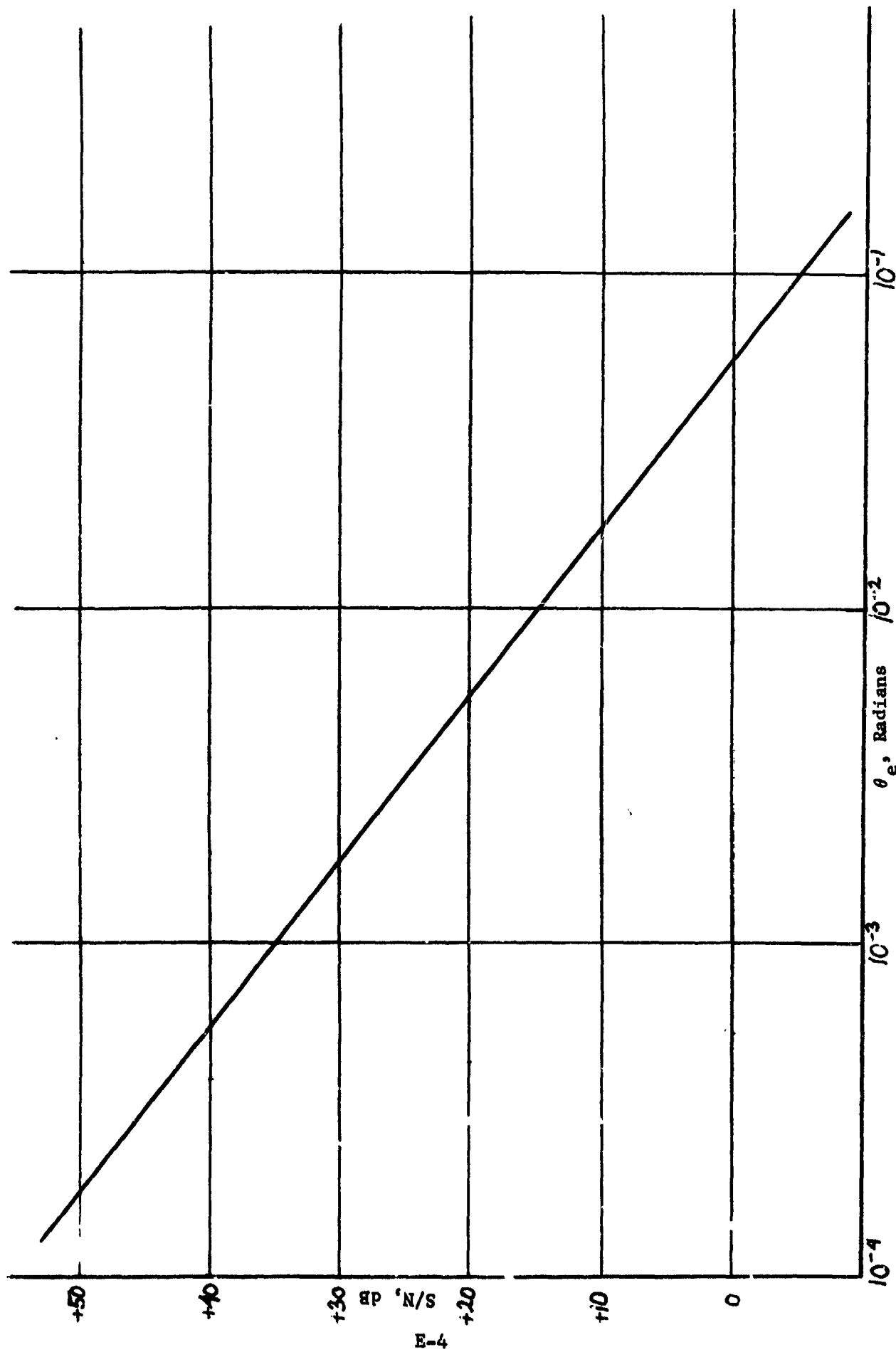


Figure E-1 S/N Ratio vs  $\theta_e$ ,  $d/\lambda \approx 2$

E-4

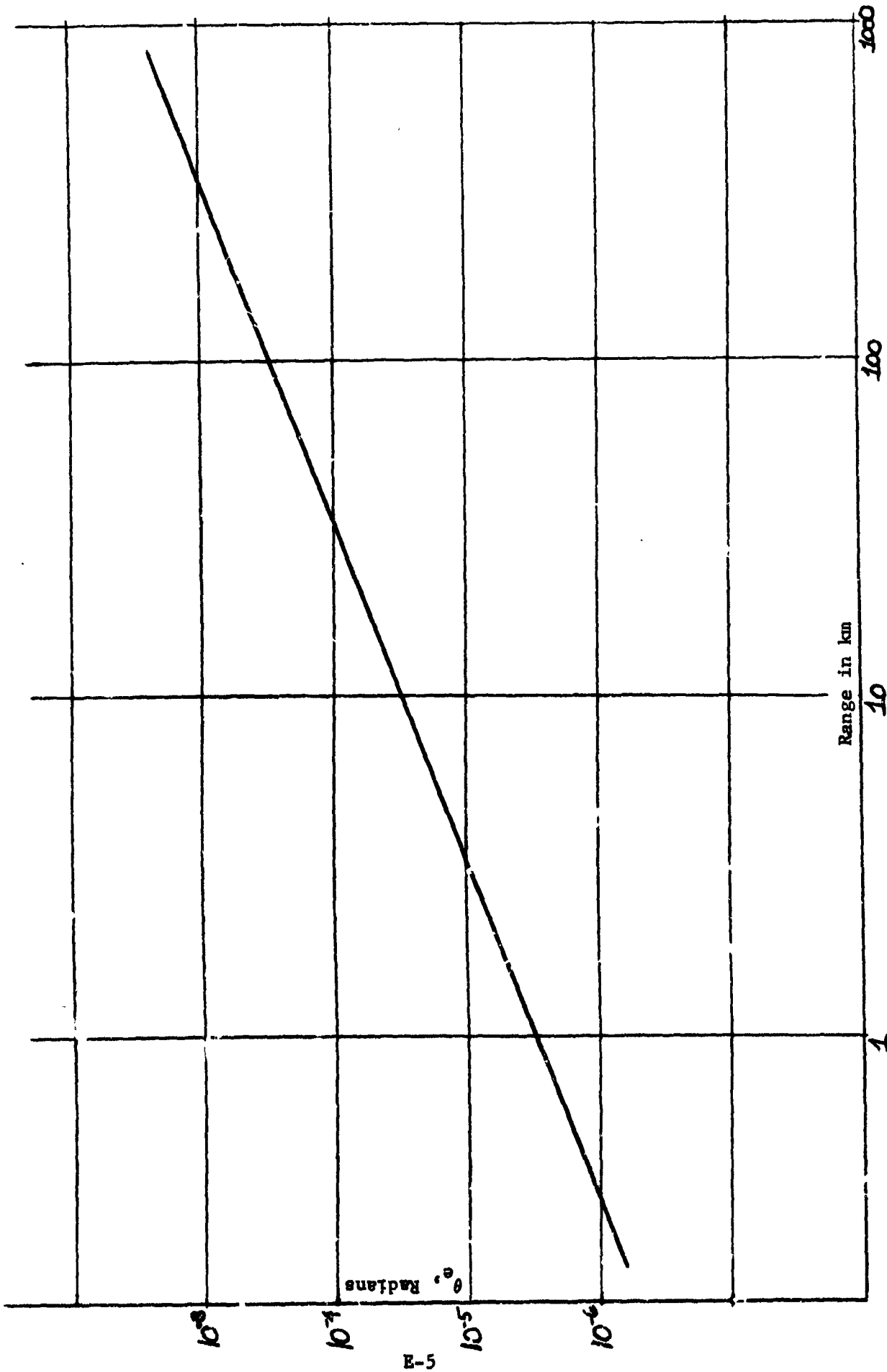


Figure E-2 Angle Error vs Range, MAV/Orbiter Rendezvous Link,  $d/\lambda \approx 2$

transmission lines feeding the traveling wave antennas. This can be counteracted by symmetrical mechanical design, careful thermal design, and use of identical rigid transmission lines feeding the four antennas. Differential precomparator phase shifts can also be introduced by the sun illuminating one traveling wave antenna while the others are shaded thus creating an unavoidable thermal gradient. In this case the differential phase shift introduced is given by:

$$\psi = \frac{2\pi(L_1 - L_2)}{\lambda} = \frac{2\pi\Delta L}{\lambda}$$

Assume a thermal gradient:  $\Delta T = 250^\circ\text{F}$

Assume a transmission line coefficient of expansion:

$$\gamma = 1.1 \times 10^{-5} \text{ units/unit}/^\circ\text{F}$$

Then:

$$\Delta L = L_1 - L_2 = (L)(\Delta T)(\gamma)$$

where:  $L_1, L_2 =$  precomparator transmission line length

$\lambda =$  wavelength

The shortest line lengths are achieved if the beam-forming network is placed at the base of the cone with its four outputs in line with the travelling wave antenna elements. This allows the employment of rigid striplines for the four transmission lines and minimizes the number of fittings and discontinuities between the BFM and the antennas. Under these conditions the maximum transmission line length will be approximately 30 cm and the BFM, transmission lines, and antenna elements can all be aluminum stripline construction. This appears to be a near optimum design and will yield the following errors:

$$\Delta L = (30)(250)(1.1 \times 10^{-5}) = 0.01 \text{ cm}$$

$$\psi = \frac{2\pi(0.01)}{13.61} = 0.0039 \text{ rad.} = 0.332 \text{ degrees}$$

The angular error corresponding to this differential phase shift is then:

$$\phi_e = \frac{\pm\psi}{\frac{2\pi d}{\lambda}} = \frac{0.0039}{6\pi} = \pm 0.0002/\text{rad.} = \pm 0.012 \text{ deg.}$$

We shall next assume that, in addition to the transmission lines, the antenna elements themselves are subject to thermal gradients producing differential phase shifts. Utilizing the same procedure we can combine

the transmission line errors with the antenna element errors, which would yield:

$$\begin{aligned}\Delta L_T &= 0.025 \text{ cm} \\ \psi &= 0.012 \text{ rad.} \\ \phi_e &= \pm 0.036 \text{ degrees}\end{aligned}$$

## 2. Inequality of Antenna Arrays

If the reflection coefficient of the 4 traveling wave antennas is different, then both amplitude and phase imbalances will occur which could affect the angular error. The magnitude of the reflection coefficient is related to the VSWR by:

$$|p| = \frac{\text{VSWR}-1}{\text{VSWR}+1}$$

When the VSWR is less than about 1.5, as it is expected to be for the traveling wave array, the fluctuations in "p" will be about half the fluctuations in VSWR, and:

$$\Delta|p| \approx \frac{1}{2}(\Delta\text{VSWR})$$

The expected value of the fluctuating imbalance between antennas would, then, be:

$$(\Delta\phi)^2 = \frac{[\Delta\text{VSWR}]^2}{2}$$

This assumes that the angle of the reflection coefficient is a random variable, and that each antenna is subject to independent fluctuations in reflection coefficient. The resulting angular error due to reflection coefficient imbalance is then:

$$\phi_e = \frac{\frac{\Delta\text{VSWR}}{2}}{\left(\frac{2\pi d}{\lambda}\right)} = \frac{\Delta\text{VSWR}}{12\pi} \text{ rad.} = 1.52 (\Delta\text{VSWR}) \text{ deg.}$$

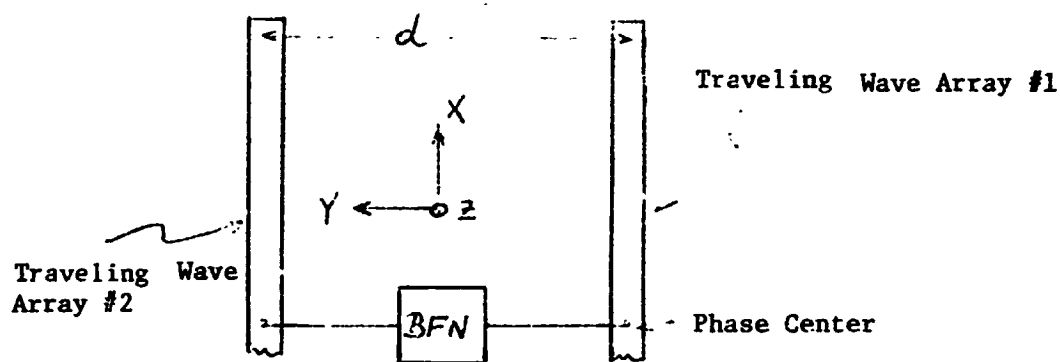
For a 9 element traveling wave array a change in VSWR of the order of  $\pm 0.03$  due to thermal gradients and mechanical changes appears a good assumption from past experience. This variation then yields:

$$\phi_e = (1.52)(\pm 0.03) = \pm 0.045 \text{ degrees}$$

### 3. Mechanical Alignment

Displacement of the traveling wave antennas with respect to each other will result in both amplitude and phase errors. Precomparator phase shifts are introduced by such motions and their magnitudes must be evaluated. We assume the geometry shown in Figure E-4 below:

Figure E-4 Antenna Array



This figure shows only 2 of the 4 traveling wave arrays, since the up-down and right-left channels are identical. The difference pattern of the angle tracking channels is given by:

$$\Delta(\phi) = E_1(\phi) e^{j\frac{2\pi}{\lambda}(x\cos\phi + y\sin\phi)} - E_2(\phi) e^{-j\frac{2\pi}{\lambda}(x\cos\phi + y\sin\phi)}$$

where  $x$ ,  $y$ , are the coordinates of the antenna phase centers of the traveling wave antennas.

Lateral motion (motion in the  $y$ - $z$  plane) introduces a precomparator phase shift given by:

$$\psi = \frac{2\pi}{\lambda} (y_1 + y_2) \sin\phi = \frac{2\pi}{\lambda} (y_1 + y_2) \phi$$

The antenna spacing "d" is the physical distance between antenna phase

centers. Then:  $y_1 = d/2 + \Delta_1$

$$y_2 = -d/2 + \Delta_2$$

And:

$$\psi = \frac{2\pi}{\lambda} (\Delta_1 - \Delta_2) \phi$$

Obviously for broadside operation lateral motion will produce zero phase errors, but in reality the actual boresight will differ slightly from zero. Mechanical tolerances and the rigidity of the antenna system determine the values of  $\Delta_1$  and  $\Delta_2$ . Although the values of  $\Delta_1$  and  $\Delta_2$  are not known at this time, we shall assume that the traveling wave antennas are allowed to move laterally due to misalignment so that:

$$\Delta_1 = \Delta_2 \cong \pm 0.13 \text{ cm}$$

Then, for  $\phi = 1^\circ$ , we get:

$$\psi = \frac{2\pi}{13.61} [0.13 - (-0.13)] (1.0) = 0.116 \text{ degrees}$$

Longitudinal motion, i.e., motion along the X-axis, will introduce a pre-comparator phase shift given by:

$$\psi = \frac{2\pi}{\lambda} (X_1 - X_2) \cos \phi = \frac{2\pi}{\lambda} (X_1 - X_2)$$

Again, there is little knowledge at this time of the actual values of  $X_1$  and  $X_2$  to be expected from an actual design. However, due to the symmetry of the cone it is reasonable to assume that the maximum longitudinal displacement should be considerably less than the maximum lateral displacement and, we assume that we have:

$$X_1 = X_2 \cong \pm 0.025 \text{ cm}$$

Then, we get:

$$\psi = \frac{2\pi}{5.36} [0.025 - (-0.025)] = .023 \text{ rad.} = 1.34 \text{ degrees}$$

Now, it is important to realize that the only misalignment errors that need to be considered here are errors introduced after the array has been boresighted, i.e., errors which may be introduced by environmental exposure, so that the maximum values chosen here certainly do not appear unreasonable. It is, also, clear that induced phase shifts due to longitudinal displacements have a much greater effect than those due to lateral displacements so that a rigid cone design is to be preferred to minimize such errors.

The expected angular accuracy of the radar due to these antenna errors can now be calculated by treating each of the foregoing sources of error independent of each other. We, then, obtain:

$$\psi_T = \sqrt{(0.996)^2 + \frac{(0.030)^2}{2} + (0.116)^2 + (1.34)^2}$$

$$\psi_T = \sqrt{2.8} = 1.675 \text{ deg.} = 0.0293 \text{ rad.}$$

The corresponding total RSS angular error is, then, given by:

$$\phi_{e_T} = \frac{\psi_T}{\left(\frac{2\pi d}{\lambda}\right)} = \frac{0.0293}{6\pi} = 0.00156 \text{ rad.} = 0.089 \text{ degrees}$$

A summary of all the system errors associated with the rendezvous sensor is given in Section VB.

APPENDIX F

1 kg Sample M<sup>A</sup> / Detail Mass Derivation (Mass in kilograms)

Structure		8.85
Return Capsule		.91
Outer Can and Lid	.45	
Inner Container	.23	
Opening Mechanism	.23	
Canister Deployment Unit		1.0
R.F. Transparent Cone (.030 Fibre Glass)		.36
Antenna Dish and Reflector		.54
Dish Honeycomb .23 m <sup>2</sup> @ 1.95 kg/m <sup>2</sup>	.45	
Reflector Dish	.09	
Body Structure		2.81
Upper Ring	.36	
Lower Ring	.36	
Interface Ring	.23	
Outer Shell .63 m <sup>2</sup> @ 1.59 kg/m <sup>2</sup> (O20 Outer shell)	1.00	
Inner Structure	.68	
Miscellaneous	.18	
Equipment Packages (.25xwt. Equip't.)		2.08
RF Package 1.63 x .25 =	.41	
Elect Box 3.00 x .25 =	.77	
G&C 3.6 x .25 =	.90	
Insulation and Paint		.45
Solar Panels Substrate and Deployment (.163m <sup>2</sup> @ 2.44 kg/m <sup>2</sup> for mechanism)		.68
Radio Frequency System and TM Package		1.63
G&C		3.09
Rate Gyros (3)		1.35
Sun Sensors (4)		.16
Valve Drive Amplifier (uncased)		.68
Computer (Hybrid CMOS Technology - uncased)		.90
Electrical		3.9
Solar Array 1.75 .163 m <sup>2</sup> @ 2.45 kg/m <sup>2</sup>	.41	
Battery Ni-H <sub>2</sub> 57.6 watt-hour	1.22	

Battery Charger (uncased)	}	1.45
Power Regulator (uncased)		
Power Control (includes Pyro Function)		
Inverter Converter		.82
Cabling		.77
Contingency 10%		<u>1.81</u>
Total Nonpropulsive Stage III		20.04
Propulsion Derivation Stage III		20.04
Payload = Nonpropulsive		20.04
Sample 1 kg		<u>1.0</u>
		21.04

Preliminary calculations indicated propellant required approximately 6.58 kg plus 1.81 kg for ACS.

Check Propellant initial wt. = Payload	21.04
Prop. Inerts	<u>12.38</u> (below)
	33.43

$$\Delta V = 391 \text{ m/sec}$$

$$\Delta V / I_{sp} = 391 / 2206 = .177 \quad e^{\Delta V / I_{sp}} = 1.194$$

$$W_p = (W_I) e^{\Delta V / I_{sp}} - 1 = 33.43 \times .194 = 6.48$$

Propulsion Components

Thrusters (Ham. Std. Units)	3.99
12# Thrust (REA 22-4) 4 @ .544 = 2.18	
.4# Thrust (REA 17-6) 4 @ .272 = 1.09	
.1# Thrust (REA 10-14) 4 @ .181 = .72	
Valves and Piping	1.9
Tanks 2 @ 1.0	2.0
Tank Supports 2 @ .72	1.45
Engine Mounts 4 @ 0.8	1.45
Residual Gas .1 Propellant .4	.5
Contingency 10%	<u>1.09</u>
Total	12.38

Propellant $\Delta V$ =	6.48
RCS =	<u>1.81</u>
Total Stage III Propulsion	20.67
Nonpropulsive Weight (p. 2)	<u>20.04</u>
Total Stage III Empty	40.73
Sample	<u>1.00</u>
Total Stage III	41.73

#### Derivation of Stage II

Skirt		3.94
Area $50.8 \times 33 = .527 \text{ m}^2$		
Mass = $.527 \text{ m}^2 \times 5.86 \text{ kg/m}^2$	3.08	
Cabling Connectors, etc.	.86	
Stage P/L Weight = Stage III	41.73	
Skirt	3.94	
RCS for Stage I and II	<u>-1.31</u>	
	44.36	

Solid Motor = .88 Isp = 2795 n-sec/kg

$\Delta V = 2530 \text{ m/sec}$

$\Delta V \text{ Used} = 2530 - 5 \text{ m/sec for RCS During Stage II} = 2525$

Sizing Equation

$$M_P = (W_{P/L} + (1-.88/.88) W_P) e^{\Delta V} - 1$$

$$M_P = (44.36 + .136 W_P) e^{2525/2795} - 1$$

$$= (44.36 + .136 W_P) 1.47$$

$$.80 M_P = 65.21$$

$$M_P = 81.51 \quad M_t + 179.7/.88 = 92.63 \quad M_{\text{CASE}} = 11.12$$

$$\text{Check } M_P = (44.36 + 11.12) 1.47 = 81.55$$

#### Derivation of Stage I

Skirt

$$\text{Area } 50.8 \times 45.72 = .73 \text{ m}^2 \quad 5.67$$

$$\text{Weight} = 7.85 \times 6.35 \text{ kg/m}^2 = 4.63$$

$$\text{Cabling Connectors, etc.} \quad .45$$

$$\text{Errector Fittings} \quad .59$$

Stage Payload Weight

Stage II P/L	44.36
Skirt	5.67
Stage II Prop	81.51
Propulsion Inert	11.12
RCS for Stage II	<u>.36</u>
	143.02

$$\Delta V = 1654 \text{ m/sec or } 5426 \text{ ft/sec}$$

$$\Delta V \text{ Used} = 1654 - 7 \text{ m/sec for RCS during Stage I}$$
$$= 1647$$

$$M_p = (143.02 + (1 - .88 / .88) W_p) e^{1647 / 2795} - 1$$

$$M_p = (143.02 + .136 W_p) .8$$

$$.891 M_p = 114.40$$

$$M_p = 128.39 \quad W_T = 145.51 \quad W_{\text{CASE}} = 17.51$$

$$\text{Check } W_p = (143.0 + 17.5) .8 = 128.39$$

Total Weight

P/L Stage I	143.02
Propellant	128.39
Propulsion Inert	<u>17.51</u>
	288.92
RCS Propellant Stage I and II	<u>.95</u>
Total Liftoff	289.87

## APPENDIX G

The attached report was prepared by Dr. J. F. Vandrey as part of our Feasibility Study of Unmanned Rendezvous and Docking in Mars Orbit (JPL Contract 953746).

Dr. Vandrey did the analytical work on the Viking Project to predict the probability that Earth organisms on the unsterilized Viking Orbiter could contaminate the Lander. He has applied this background plus his wide ranging scientific acumen to the potential problem of bringing Mars biota back to Earth on the Earth Return Vehicle (external to the sample canister).

### Step 1. Probable Number of Viable Organisms in Martian Soils

The existence of any life on Mars is uncertain at the present time. Should it, however, exist at all, it is very difficult to imagine that these Martian organisms could be active in more than very few particularly favorable locations, such as in the vicinity of perhaps existing still active or recently extinct volcanoes where there may be some liquid water in the ground. Estimating that these areas total a few  $10^3 \text{ km}^2$  on the planetary surface seems to be realistic, may even be generous.

Everywhere else on the Martian surface, the conditions are less favorable to life as we know it than in high-altitude terrestrial deserts, e.g., in some parts of the Andes, or also in some valleys of the Antarctic. Any viable Martian organisms could then exist over the greatest part of the Martian surface only in dormant forms, not unlike the "spores" of terrestrial bacteria.

In order to attempt an educated guess of the number of Martian microorganisms we may at most expect at an "average" landing site on the planet, we can use as guidance some data on the abundance of viable organisms in the most unfavorable terrestrial locations: While normal "garden soil" contains the order of  $10^9$  organisms per gram, the average bacteria count in the "bare" regions of the Antarctic is between the orders of  $10^2$  and  $10^3$  per gram, and some bare Antarctic valleys, some parts of the High Andes deserts, and of the Sahara appear even to be practically sterile, which means that they contain less than e.g. one viable spore per gram of soil.

Important for us here is that this "practical sterility" of a desert soil can exist in locations only a few hundred kilometers (or even less) from other locations which contain great numbers of microorganisms in their soils, and in the presence of an atmosphere which can transport all sorts of spores readily from place to place.

Using this admittedly meager information as a guide, although it may not quite apply to the life forms which may (or may not) have evolved on Mars, the writer would like to suggest that a number of Martian organisms two orders of magnitude less than the average of the Antarctic, or

$$n \sim 10^0 \text{ to } 10^1 \text{ organisms/gram} \quad (1)$$

is about the greatest one could reasonably expect at some distance from the very few and very small locations where an active life might be possible at the present time.

Before accepting this estimate as valid for most of the Martian surface, we have to consider again as well as possible in a very "nebulous" situation, a different remotely conceivable origin of the "dormant microorganisms" at an "average location" on Mars: Since there is some evidence in recently obtained pictures of the Martian surface that there was more water there in the distant past, these organisms could be dormant remnants of a much more abundant local population which have remained viable over a very long time. If this would be so, there might well be more than an average of 1 to 10 "spores" per gram of Martian soil at a randomly selected landing site.

It is, of course, impossible to say anything definite against this suggestion. The writer would, however, consider it as very unlikely that this could have happened, if the hypothetical Martian life forms are in any way similar to the terrestrial ones. His reason is that some of the presently practically sterile terrestrial soils are in locations which have seen a quite appreciable life activity in the geologically not so very distant past. The Sahara Desert, for instance, is geologically quite young. As recently as during the last Ice Age, much if not all of it was in a warm and moist zone, and it dried out only after the Central European Ice Sheet melted away, probably less than 30,000 years ago.

### Step 2. Estimate of the Dust and Biota Load of the Lift-off Rocket at Take-off

This will have to depend on test results in simulated Martian dust storms. Very roughly, the exposed surface of the rocket is of the order of  $1 \text{ m}^2$ , it may collect something of the order of 1 g of dust from dust storms and smaller events such as dust devils (if they can occur). The collection of dust on the (preferably very smooth) surface is likely to be somewhat selective, smaller particles will stick to the surface more easily than larger ones.

This has some bearing (although perhaps not very much) on the biota load of the rocket surface. Supposing that the Martian "spores" are of similar size as here on Earth, i.e., typically a few microns\*, it is likely that most of the Martian "spores" will adhere to small dust and sand particles in the soil, and also in a dust storm, so that those attached to the larger dustgrains would have a smaller chance to be deposited on the rocket surface, and to be taken aloft with it.

Supposing that this selective deposition is not too important, we can make the educated guess that the biota load of the rocket at take-off is probably on the average only a few spores, somewhere between 1 and 10 (?).

### Step 3. Estimate of Biota Losses During the Ascent of the Rocket through the Atmosphere

There are two mechanisms which can lead to a loss of Martian biota during the ascent of the rocket through the atmosphere:

1. they may be blown off by the relative wind;
2. they may be killed by aerodynamic heating.

For an analysis of both cases, one has to have a knowledge of the boundary layer over the surface of the rocket throughout the ascent through the sensible atmosphere, and particularly through its supersonic part.

According to estimates of aerodynamic separation which the writer has done a few years ago for another purpose, the separation of individual spores from the surface is much more difficult than the separation of larger particles to

---

\* This is not unreasonable, but by no means certain. The only justification the writer can give for this contention is that, according to Rasheoski's studies in Mathematical Biophysics, a growing cell would become dynamically unstable (and tend to divide) at about the same size of a few microns at which we normally observe it to occur.

which these spores may be attached. Depending on the way one accelerates the rocket upward, one may, for instance, blow off all particles of sizes 30 microns or larger, most of the particles between 20 and 30 microns, and very few of the smaller particles. To convert this into an estimate of the biota loss, one has to have a model of the size distribution of the dust load, supplemented by an assumption such as that the biota are "uniformly distributed over the total surface area of all the dust grains."

How much help one can get from this possible aerodynamic separation is difficult to say, but the writer would be surprised, if this mechanism could be shown to reduce an initial biota load to less than  $\frac{1}{2}$  of its initial value.

Aerodynamic heating, on the other hand, may be an effective way to reduce the biota load, if the surface temperature of the rocket becomes high enough. How high it should be is again difficult to say. One would clearly hesitate to say that the customary spacecraft sterilization temperature of  $135^{\circ}\text{C}$  (which kills all known terrestrial spores within 24 hours) is high enough for the few minutes of significant aerodynamic heating of the ascending rocket. On the other hand, it is difficult to imagine that even very hardy dormant organisms (of presumably very similar chemical composition as here) could stand the typical "deep-frying temperatures," such as  $185\text{-}195^{\circ}\text{C}$  for doughnuts, more than a few seconds, since the brown color of a baked doughnut indicates the thermal decomposition of important organic materials (polysaccharides). Some definite criterion on this will, of course, have to be established by the NASA Office of Planetary Quarantine. It seems, however, to the writer that a value such as  $200^{\circ}\text{C}$  will not meet very much opposition.

As an afterthought: We have become accustomed to building vehicles which will be subjected to severe aerodynamic heating as blunt-nosed. In the present case, however, we may well want a little more surface heating for killing any Martian organisms, and might then look at less blunted nose configurations. It might also be mentioned that turbulent boundary layers are more favorable for both heat transfer and aerodynamic separation of attached particles than laminar ones, so that one may consider an artificial induction of turbulence into the boundary layer, should this be needed.

Step 4. Transfer Probability of Martian "Spores" from the Ascent Rocket to the Earth Return Vehicle

Some years ago, the writer had made a study of the possible release mechanisms of small particles from the surface of a spacecraft in an orbit around Mars, with the result that suggested electrostatic and other effects could not lead to an ejection of attached particles, and that the only way in which this could occur was by the shockwave which is produced in the spacecraft surface material by the impact of a micrometeorite.

Even this has a rather modest effect. A micrometeorite of mass  $m$  can "clear" a circular area of radius

$$r < 4.8 \times 10^6 \sqrt{\gamma d m \rho_p / \rho_s} \text{ [cm]} \quad (2)$$

of particles of diameter  $d$  and density  $\rho_p$  from a surface with the density  $\rho_s$ , where  $\gamma \leq 1$  and usually  $\ll 1$  is a coupling factor for the energy transfer between the particle and the shockwave. Assuming, for instance, a typical grain diameter of 10 microns =  $10^{-3}$  cm for the dustgrains to which the presumably smaller Martian "spores" are attached, and a typical micrometeorite mass of  $10^{-11}$  g as in the writer's earlier work, we obtain with the maximum value of  $\gamma = 1$  and  $\rho_p / \rho_s \sim 1$  a value of  $r < 5$  mm, or a cleared area of less than  $1 \text{ cm}^2$ .

This is less than  $10^{-4}$  of the total surface area of the ascent rocket which is of the order of  $1 \text{ m}^2$ .

We assume now an original biota load of 10 organisms, and a loss of e.g. half of them during the ascent through the atmosphere because of aerodynamic heating and/or blowing off. The probability of one of the remaining five then becoming separated from the surface by a single micrometeorite impact is then

$$p_{\text{sep}} = 5 \times 10^{-4} = \frac{1}{2000} \quad (3)$$

Micrometeorite impacts are, however, rather rare occurrences, we expect an average of no more than one per day on a square meter in a Martian orbit. Assuming then that the docking maneuver takes about 2 hours  $1/10$  day, we conclude that the probability of separation of a single spore during this critical time is only one-tenth of this, or  $1/20,000$ .

Separation does, however, not yet mean that the spore hits the Earth Return Vehicle, and sticks to it. Without going into the details which will depend on the relative geometries of the rocket and the vehicle, we can say that it will not be very difficult to achieve a further reduction of the contamination probability by at least an order of magnitude, i.e., to 1/200,000, and that an even much better result can be achieved with a suitable design and a more detailed and careful analysis.

#### Concluding Remarks and Recommendations

The preceding example illustrates that the contamination probability of the Return Vehicle is in any case a very small one, even if one assumes an, in the opinion of the writer, unrealistically high initial biota load of the Ascent Rocket.

By its very nature, however, the precedingly outlined analysis of the contamination hazard for the return vehicle has to be based on a number of assumptions which should be discussed in detail with the NASA Office of Planetary Quarantine and with a number of interested and qualified scientists (Drs. Lederberg, Sagan, and Horowitz, for instance).

In particular, the writer would like to recommend such a discussion for the basic question of the probable biota content of Martian soils, and then of the surface temperature at which one can assume that all Martian "spores" will be killed by aerodynamic heating. Furthermore, one should discuss which probability of contamination would be acceptable as a design criterion, e.g.  $10^{-6}$ , or more, or less.

As a result of these discussions, the Office of Planetary Quarantine could then establish a basis for the analysis of the Return Vehicle Contamination Problem which is as good as we can make it at the present time.

It is, of course, to be expected that we shall know more about the question of life on Mars after a successful completion of the first Viking mission. A positive outcome of its biological experiment may force us to correct the assumption of the biota contents upwards, and a negative outcome may permit a drastic downward correction, although not necessarily to absolute zero.

## APPENDIX H ALTERNATIVE MAV BIROPELLANT STAGE

One MAV propulsion concept that appeared attractive and was studied in considerable depth was a two-stage propulsion system using a solid motor first stage, but a bipropellant second stage that combines the functions of this baseline second and third stages. This concept appeared attractive for two reasons; i.e., the use of a liquid second stage provides packaging flexibility that is not available with solid propellant motors, and the bipropellant liquid performance (delivered specific impulse) is slightly higher than that of solid motors, though the mass fraction is lower. The liquid system can be packaged to provide a relatively short squat MAV that conceivably could be contained in the lander in a vertical position so that elevation prior to launch would not be required.

To permit a direct comparison of the two-stage vehicle with the baseline three-stage vehicle, the same gross weight was assumed for both (250 kg at this stage in the study), and identical first-stage solid motors were assumed. The bipropellant stage was assumed to use  $N_2O_4$  and  $N_2H_4$  as propellants. These earth storable provide a high specific impulse, and also permit small monopropellant thrusters (for attitude propulsion) to be fed directly from the main fuel tanks. For optimum packaging, a total of four propellant tanks was assumed, these being pressurized by a regulated helium pressurization system. Four thrusters were selected to provide the desired packaging configuration, and also to permit pitch and yaw attitude control by off-pulsing of individual thrusters. The proposed system is shown schematically in Figure H-1; the proposed arrangement of major system components is shown in Figure H-2.

Considerable effort was devoted to the accurate determination of component sizes and weights so that the system mass fraction would be accurately known. A mass fraction of .7 was initially assumed for performance calculations. This permitted the propellant requirement to be determined (from the known gross weight and Delta V of the stage), from which the tank sizes were established and all component sizes and weights estimated. Pertinent results are summarized in Table H-1 which lists the components, their capacities in terms of pressures, volumes and thrust levels, the

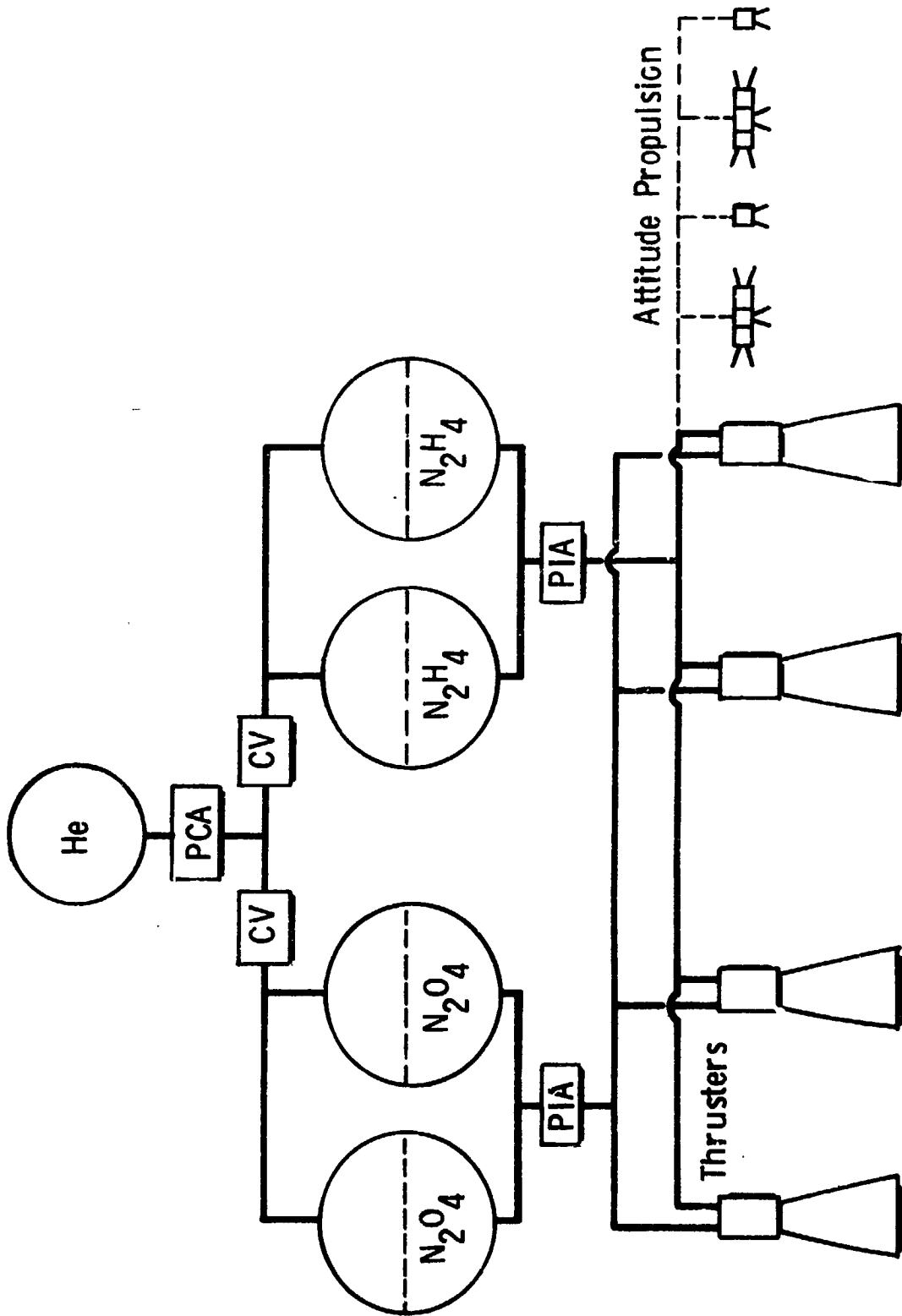


Figure H-1 MAV Bipropellant System Schematic

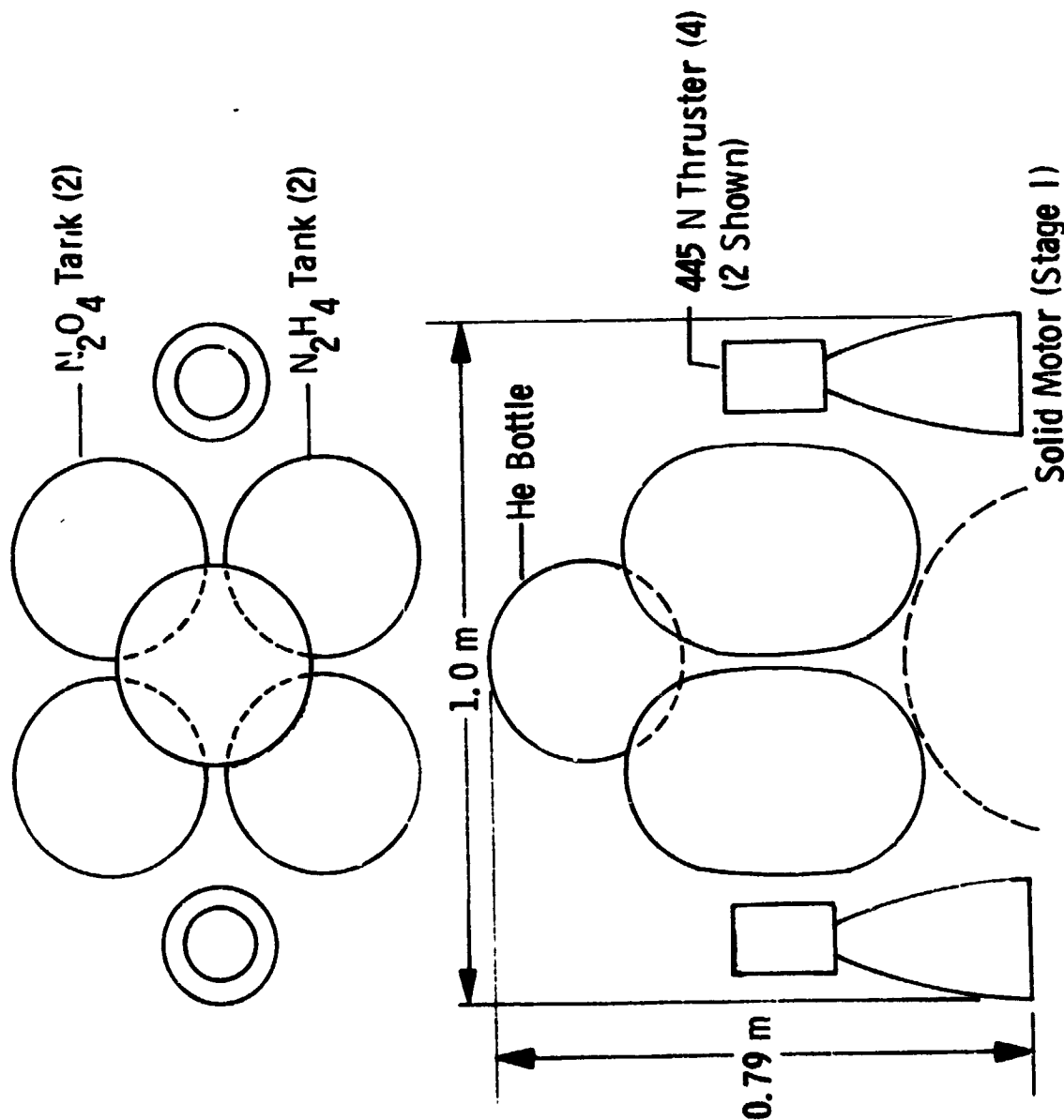


Figure H-2 Candidate Second Stage Bipropellant System-Considered in Tradeoff of 2 Stage vs Selected 3 Stage MAV

Table H-1 MAV Bipropellant Stage Weights

Component	Capacity	Basis for Selection	Weight kg (lbm)
Propellant Tank (4)	207 N/cm <sup>2</sup> ; 28,000 cm <sup>3</sup> (ea) 300 psia; 1710 in <sup>3</sup>	Apollo RCS, with Bladder	12.7 ( 28.0)
Pressurant Tank (1)	2620 N/cm <sup>2</sup> ; 9190 cm <sup>3</sup> (ea) 3800 psia; 560 in <sup>3</sup>	VO'75 (9.210 <sup>6</sup> N/cm <sup>2</sup> cm <sup>3</sup> /kg tank) (370,000 psi in <sup>3</sup> /lbm tank)	2.7 ( 6.0)
Thruster, Primary (4)	445 N (ea) 100 lbf	Apollo RCS (SM/LM)	9.1 ( 20.0)
Thruster, ACS (8)	2.2 N (ea) 0.5 lbf	H-S REA 17.6	2.2 (4.8)
PCA (1)		MM'71 (minus 2 pyros)	4.8 ( 10.5)
Check Assembly (2)		MM'71	2.2 ( 4.6)
PIA (2)		MM'71 (minus 4 pyros)	8.2 ( 18.0)
Tubing/Fittings		MM'71 + VO'75	<u>6.4 ( 14.0)</u> 48.3 (105.9)
Propellant (N <sub>2</sub> O <sub>4</sub> /N <sub>2</sub> H <sub>4</sub> )	113.5 kg (usable) 250 lbm		
Propellant Residuals		MM'71 (2.5%)	2.8 ( 6.2)
Helium		VO'75 (He = 13% Press. Tank)	<u>0.4 ( 0.8)</u> 3.2 ( 7.0)

$$\lambda = \frac{113.5}{113.5 + 48.3 + 3.2} = 0.69$$

space program providing the needed component technology, and the estimated component weights. The weight of required propellant is seen to be 113.5 kg, leading to the selection of propellant tanks with a volume of 1710 in<sup>3</sup> each. These are fitted with bladders for effective propellant management. The associated helium pressurant tank requires a volume of 560 in<sup>3</sup> when designed for a pressure 3800 psia. The size of the thrusters was not firmly established, but a thrust level of approximately 500 N (each) appears to be optimum. At greater thrusts the propulsive efficiency improves somewhat, but at the expense of additional inert weight. At lower thrusts the thruster weight decreases, but this is compensated by a loss in propulsive efficiency. The most significant result to be noted is that the computed mass fraction is .69, approximately the same as the value originally assumed. Therefore, it is concluded that this value can be used with confidence in computing MAV performance and inert weights.

A performance comparison between the two-stage and the baseline three-stage MAV is summarized in Table H-2. The definite superiority of the baseline MAV is immediately apparent. The baseline design provides a payload weight (non-propulsive) of 20 kg, whereas the two-stage concept provides only 2.7 kg. Obviously the slightly higher specific impulse delivered by the bipropellant system does not adequately compensate for the relatively low mass fraction that must be accepted.

In an effort to improve the performance of the two-stage vehicle, the stages were reapportioned so that the first (very efficient) stage would provide a greater percentage of the total Delta V requirement. Several cases were studied, including those in which the first stage weight exceeded 200 kg, but the largest payload that could be realized was approximately 8 kg, less than one-half that obtained with the baseline configuration. Therefore, the concept of a bipropellant second stage was abandoned in favor of the three-stage baseline design which uses two solid propellant stages to provide the required ascent Delta V.

Table H-2 MAV Performance Comparison

	Baseline MAV			Biprop. Stages II/III	
	Stage I	Stage II	Stage III	Stage I	Stage II/III
Propellant	Solid	Solid	N <sub>2</sub> H <sub>4</sub>	Solid	N <sub>2</sub> O <sub>4</sub> /N <sub>2</sub> H <sub>4</sub>
Isp. Nsec/kg (sec)	2795 (285)	2795 (285)	2300 (235)	2795 (285)	2892 (295)
Mass Fraction ( $\lambda$ )	0.88	0.88	0.50	0.88	0.70
$\Delta V$ , m/sec	1350	2865	491	1350	3356
Weight, kg (lbm)	113.0 (249)	104.5 (230)	32.2 (71.0)	113.0 (249)	137.0 (301.0)
Propellant	96.0 (211)	87.7 (193)	6.1 (13.5)	96.0 (211)	94.0 (206.5)
Prop. Inerts	13.2 ( 29)	12.2 ( 27)	6.1 (13.5)	13.2 ( 29)	40.3 ( 88.5)
Payload			20.0 (44.0)		2.7 ( 6.0)

## APPENDIX I STERILIZABLE SOLID PROPELLANTS FOR MAV

The baseline configuration selected for the MAV propulsion system comprises three stages, the first two of which use solid propellant motors. This selection of solid motors was made primarily because MAV weight is extremely critical, and the solid motor offers definite weight advantages over liquid propellant system in the size (total impulse) range applicable to MAV.

It is the purpose of this discussion to present a summary of sterilizable propellant state-of-the-art, and finally, a prediction of performance to be expected from propellant to be available in the future.

Sterilization Requirements. To assure adequate biological sterilization of planetary landers, it has been determined that the hardware must be subjected to a sterilization cycle involving exposure to dry heat for an extended period of time. The particular combination of time and temperature specified by the Viking Project for Flight Acceptance Tests is  $233 \pm 3^{\circ}\text{F}$  ( $112^{\circ}\text{C}$ ) for a period of 54 hours. Then to assure that each type of component can successfully withstand this sterilization environment with a high degree of confidence, a component Qualification Test requirement has been evolved consisting of the following:

- 2 - 54 hours cycles at  $254 \pm 3^{\circ}\text{F}$  ( $123 \pm 2^{\circ}\text{C}$ ), and
- 4 - 40 hours cycles at  $254 \pm 3^{\circ}\text{F}$  ( $123 \pm 2^{\circ}\text{C}$ ).

Since this combination of time and temperature refers to the coldest portion of the hardware, it is evident that the sterilization cycle will subject some portions of the hardware to an even more severe environment than that specified. This sterilization requirement poses a formidable challenge for the solid propellant chemist because solid propellants are not ordinarily required to withstand temperatures greater than 120 to  $140^{\circ}\text{F}$ .

Sterilization Effects. The two principal adverse effects of the heat sterilization process on solid propellants are:

- a) Decomposition due to long exposure at high temperature, and
- b) Mechanical failure (cracking, etc) due to overstressing.

Therefore, to satisfactorily withstand the sterilization environment, the propellant must possess:

- a) Extremely high thermal stability, and
- b) Excellent physical properties over a wide range of temperatures.

The importance of propellant thermal stability is readily apparent when consideration is given to the chemist's "rule of thumb" that reaction rates approximately double for each  $10^{\circ}\text{C}$  temperature increase. Therefore, at a sterilization temperature of  $123^{\circ}\text{C}$ , chemical reaction rates may be expected to be  $(2)^{7.3} \approx 150$  times as great as those at a typical propellant maximum temperature of  $\sim 50^{\circ}\text{C}$ . Degradation of performance or formation of gas bubbles and propellant voids that might not be detectable as a result of exposure at  $50^{\circ}\text{C}$  may become major problems when the propellant is exposed to temperatures of  $123^{\circ}\text{C}$ . Void formation presents an extremely serious problem because it results in increased burning surface which can readily lead to catastrophic failure of the rocket motor case.

The importance of good propellant physical properties becomes evident when one considers the stresses imposed on the propellant by differential thermal expansion as the temperature is varied over a wide range. An especially difficult problem is presented by the widely different coefficients of expansion exhibited by the propellant and the motor case. The end result is often the formation of cracks within the propellant or separation of the propellant from the liner, both of which introduce additional propellant burning surface with resultant possible catastrophic failure. In addition, it is necessary that the propellant possess a sufficiently high modulus at high temperature that it is not subject to deformation by plastic flow.

### 1. Early Investigations

Because of consideration given to the possible use of solid propellant motors on Viking, there was considerable activity beginning  $\sim 1965$  regarding the development of sterilizable solid propellants. This work was conducted principally by five different organizations; i. e., JPL, NASA Langley, Aerojet, Thiokol, and UTC. The investigations conducted

were concerned principally with propellant research focused on the critical problems of propellant thermal stability and enhancement of mechanical properties. No large scale motors were ever fired, but considerable progress was made in evolving a class of propellants that could withstand heat sterilization. These programs are summarized briefly in the following paragraphs.

JPL. Some of the earliest significant work in the area of sterilizable solid propellants was performed by JPL. Work began ~1965 and continued for several years. Of several candidate propellant formulations considered, saturated binder propellants (binder containing a saturated secondary hydroxyl terminated polybutadiene prepolymer chain extended with tolylene diisocyanate and cross-linked with trimethylol propane) exhibited excellent thermal stability and mechanical properties, and were selected for as many as ten sterilization cycles (56 hours at 275°F), and small 2 lbm motors were loaded and successfully fired. However, attempts to load 12" diameter motors were unsuccessful because of the many voids that formed in the propellant. Ultimately, it was concluded that the primary factor influencing void formation was the oxidizer (ammonium perchlorate). The relative effects of particle size, age, and moisture content on thermal stability eventually were well characterized, but the effort did not proceed to the point that a completely satisfactory propellant formulation was evolved. Detailed documentation of this work is presented in Ref. I-1 and I-2.

Thiokol. During the late 1960's, Thiokol was engaged in both in-house and contractual work in the area of sterilizable propellants. The latter effort (JPL contract 951405) consisted of a design study only and did not proceed to an experimental phase. This work was completed in mid-1966 and is reported in Ref. I-2.

Thiokol in-house investigations were concentrated on a propellant formulation designated TP-H-4002, using a saturated hydrocarbon binder in combination with a total solids content of 83%, of which 15% was aluminum. This formulation displayed some changes in physical properties and a measurable weight loss when subjected to the heat sterilization cycle, but these did not prove detrimental. It was found that void for-

mation could be minimized by use of an aziridine additive and by careful control of the oxidizer purity and particle size. Testing of inert liner and insulation materials resulted in identification of several different promising candidates. Ultimately, Thiokol successfully subjected 3" x 3" propellant cubes to seven sterilization cycles at 275°F with no evidence of void formation. Also, small motors containing this propellant formulation were successfully fired to determine ballistic characteristics, but loading of full-scale motors was never attempted.

NASA, Langley. Langley Research Center was involved in the sterilizable propellant program for a period of at least five years, but primarily as a technical monitor of contractual work. Langley sponsored early contractual efforts by both Aerojet and UTC, and attempted for a time to continue an in-house effort after the contractual work was completed. Finally, in 1972 NASA responsibility for the sterilization program was assigned to JPL, so Langley is no longer involved. It was not possible to uncover any of the results from work done in Langley's in-house program, so none are presented here. The contractual work of UTC and Aerojet is summarized below.

UTC. UTC was awarded a sizable contract by NASA Langley in the mid-1960's to develop a sterilizable solid propellant, but the program appears not to have produced results pertinent to this mission. Therefore, no attempt was made to uncover detailed information concerning their program. Numerous problem areas were identified by UTC, but in telephone conversations, UTC personnel have displayed considerable optimism regarding their capability to produce a sterilizable propellant (given additional time and money).

Aerojet. Aerojet was awarded a contract (NAS1-10086) in the late 1960's to "demonstrate the heat sterilizability of an integrated solid propellant rocket motor system". This initial effort was not intended to demonstrate sterilizability with full-scale motors, but rather to demonstrate the technology through the use of selected propellant specimens. Preliminary investigations were conducted with free standing specimens 2 1/2 x 2 1/2 x 5" in size. Then tests were conducted of 2.75" strain

motors; i.e., 3" dia. aluminum tubes into which the propellant was loaded and bonded.

Numerous propellant formulations were evaluated, as well as liner materials and bonding techniques. The sterilization cycle employed was essentially the same as that used by other investigators; i.e., (6)-53 hour cycles at 135°C. Considerable progress was made in identifying the problem areas and their potential solutions, but failures (in the form of cracks) occurred frequently in the strain cylinders. Eventually, it was concluded that a more flexible support system was required to attach the propellant to the motor case. This led to the evolution of Aerojet's concept of the "stress relieved motor" in which the propellant is loosely supported within the motor case so that differential thermal expansion does not cause excessive stresses to be transmitted between the case and the propellant.

## 2. Current Programs

Currently, investigations to evolve sterilizable propellants are being conducted by only two organizations; i.e., JPL and Aerojet. Aerojet's current program is being conducted under contract NAS1-10861, initially sponsored by NASA Langley, but currently monitored by JPL. In addition, JPL is conducting an in-house program to evolve a sterilizable solid propellant. These programs are described briefly in the following paragraphs.

Aerojet. The current Aerojet program, defined by the contract Statement-of-Work (Ref. I-4) has as its primary objective the "design, development, manufacture, and testing of two solid propellant rocket motors (exclusive of nozzle and igniter) capable of reliable operation after exposure to dry heat sterilization". Secondary objectives are "that the propellant exhibit reasonable performance, and the materials exhibit acceptable margins of physical properties following the required (6) sterilization cycles". Objectives are to be achieved through the use of "the 18-inch spherical SVM-3 rocket motor case and nozzle" (Fig. I-1).



The propellant formulation selected for the demonstration motor (designated ANB-3438) was evolved during the earlier propellant investigations conducted by Aerojet. It contains 84% solids and should be capable of producing a specific impulse of ~285. It is supported inside the motor case by the liner concept previously referred to as the "stress relieved motor". This liner is relatively heavy and results in a mass fraction penalty of about .02. In addition, the nozzle being used in the demonstration motor is very heavy, so that the resultant motor mass fraction is only about .84.

During the past few months the contract has been brought to a successful conclusion. Thermal cycling of the two motors was begun in the fall of 1973, and completed early in 1974. One motor was subjected to six 53-hour sterilization cycles at 135°C (10°C greater than the temperature required for Viking component qualification), with X-raying accomplished between cycles to detect any evidence of propellant deterioration. The motor successfully completed three cycles, but showed evidence of a small flaw after the fourth cycle. The flaw grew and broke through the inner surface of the grain during the fifth cycle but didn't develop further during the sixth cycle. As a result of this small surface crack, it was decided that the motor would not be fired, though the probability of catastrophic failure was very low.

The other motor, lagging the first one approximately one week in thermal cycling, was subjected to eight 53-hour cycles at 125°C. It successfully completed all eight cycles with no evidence of any flaws whatsoever. Consequently, it was committed to static firing which was successfully accomplished on 21 February 1974. Thus, a major milestone in the state-of-the-art of sterilizable propellants was passed. Performance (specific impulse) was approximately 2.5% lower than expected, but otherwise, results appear to have been entirely satisfactory. Detailed results are contained in an AGC final report soon to be published.

It is tentatively planned to extend the AGC contract to permit shock and vibration testing of the first motor to typical qualification levels. If this test is also successfully passed, it will do much to enhance the

probability that operational sterilizable solid propellant motors will be available for the MAV application. On the other hand, the current funding level is very low, and considerable additional funding will have to be provided if the desired end goal is to be reached.

JPL. The JPL in-house program is being conducted somewhat along the same lines as the AGC program, but only one motor is involved, and it is not to be statically fired. The JPL motor, however, is much larger than the AGC motor, so it will provide evidence of the sterilizability of very large propellant grains. The motor case, a surplus ATS Apogee motor, is 28" in diameter and accommodates a propellant load of 800 lbm. The propellant is a "saturethane" formulation evolved from JPL's earlier investigations. It contains only 81% solids so would be capable of delivering a specific impulse of only about 275. The grain is not bonded to the case, but is free to expand and contract independently from the case, the same as it would be if it were supported by one of the "stress-free" liner concepts. It will be noted that although the motor is not designed to be fired, the ability of the grain to withstand the sterilization cycles will be adequately proved by the X-raying to be accomplished.

Loading of the motor was completed early in 1974, but cycling and X-raying are proceeding very slowly due to conflicts in the use of the temperature conditioning facilities at EAFB. Only two sterilization cycles had been completed as of May 1974, and there was no firm schedule for completing the additional six cycles.

### 3. Conclusions

Based on the work accomplished to date, and forecasts of key personnel who have been active in the investigations of sterilizable solid propellants, the following conclusions have been evolved:

- a) Sterilizable propellant technology will be sufficiently advanced by the late 1970s that a highly reliable solid motor design can be assured for the MAV application, provided that funding is available to support continued development during the next few years.

- b) The best solid propellant specific impulse that can be expected for the MAV application is 285 to 287 sec. It is technically feasible to increase this value by  $\sim 15$  sec by substituting beryllium for aluminum in the propellant formulation, but the associated toxicity hazards are probably not acceptable.
- c) The solid propellant motor mass fraction that will be attainable for the MAV application is only about .87 because of the heavy liner required. This could probably be increased to .88 if an advanced design carbon nozzle were used in place of a more conventional nozzle.
- d) Igniters appear to present no problems whatsoever with regard to effects of the sterilization environment.
- e) Life requirements imposed by the MSR mission should be easily satisfied by the new generation of sterilizable solid propellants, because they have much greater chemical stability than conventional propellants.
- f) Effects of long term exposure to space vacuum (if any) are readily circumvented by applying a hermetically sealed closure to the nozzle exit.

#### REFERENCES

- I-1. "Heat Sterilizable Solid Propellants", by Robillard, Dowler, Shafer and Udlock; JPL Technical Report 32-1187, October 1, 1967 (Confidential).
- I-2. "Development of Saturethane Propellants", JPL Technical Report 32-1406, November 3, 1969 (Confidential).
- I-3. "Final Report, Design Study of Heat Sterilizable Solid Rocket Motors for Space Application", Contract 951405, Thiokol Chemical Corporation Report E15-66, June 27, 1966.
- I-4. "Statement of Work, Demonstration of a Sterilizable Solid-Propellant Rocket Motor", Langley Research Center, April 19, 1971.

## APPENDIX J THRUSTER SIZING AND PROPELLANT CONSUMPTION

### 1. Aft-Firing Thruster Size

During Stage I and Stage II solid motor burns, the aft-firing Stage III thrusters must be capable of maintaining the proper attitude of the MAV by providing moments that offset those arising from aerodynamic forces and solid motor thrust misalignments. The maximum disturbing moment is found to occur at Stage I burnout when aerodynamic forces are highest (max q). During Stage II burn, the atmospheric density is very low so that aerodynamic forces do not present a problem.

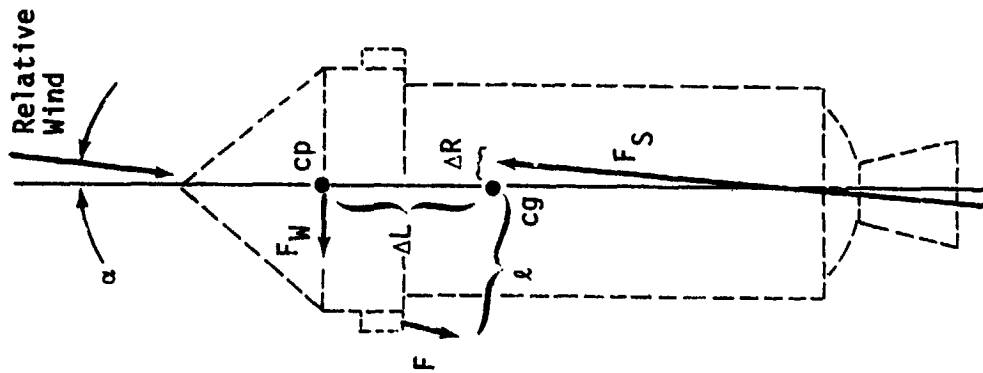
Pertinent forces acting on MAV during solid motor burns are shown on the diagram presented at the left in Fig. J-1; the numerical assumptions and pertinent computations are included at right. It will be seen that for additive moments due to thrust misalignment (.1 in at the center of gravity), and aerodynamic forces ( $1/3^{\circ}$  maximum angle of attack), the disturbing moment is 174 lbf in and the required thruster force is 10.9 lbf. Therefore, the selection of a 12 lbf thrust is realistic.

Shortly after liftoff, the aft-firing thrusters are also required to provide a moment for the pitchover maneuver, but this is found to be a negligible value compared to the above. For the assumed maximum pitch acceleration of .02 rad/sec the required moment is only about 11 lbf in, less than 10% of the maximum aerodynamic moment.

### 2. Limit Cycle Propellant Consumption

Determination of propellant consumption in the limit cycle mode is of considerable importance in the URDMO study because of the proposed use of hot gas thrusters for most attitude control functions. The thrusters tend to have high consumption rates in this type of application because the spacecraft moments of inertia are often low (particularly, for MAV), the thrust levels are relatively high (.5 N minimum), and the moment arms are small (the thrusters are located on the spacecraft surface to simplify thermal control problems).

Objective: Provide Adequate Moments for P-Y Control During Stage I & II Solid Motor Operation



Moments - Max q

Aero  $M_W = C_N \alpha q S \Delta L$   
 $= 87.4 \text{ lbf in.}$

Misalign  $M_S = F_S \Delta R$

$= 150 \text{ lbf in.}$

Resultant  $M_{py} = (M_W^2 + M_S^2)^{1/2}$

$= 174 \text{ lbf in.}$

Required  $F = \frac{M_{py}}{L}$

$= 10.9 \text{ lbf}$

Moments - Pitch Over

Inertial  $M_I = I_O \alpha_{max}$

$= .94 \text{ lbf ft.}$

$= 11.3 \text{ lbf in.}$

Misalign  $M_S = 150 \text{ lbf in.}$

Resultant  $M_{py} = 150.4 \text{ lbf in.}$

Assumptions

$C_N = .045 \text{ deg}$

$\alpha = 1/3 \text{ deg}$

$S = 3.7 \text{ ft}^2$

$q = 105 \text{ psf}$

$L = 15 \text{ in.}$

$F_S = 1500 \text{ lbf}$

$\Delta R = .1 \text{ in.}$

$\lambda = 16 \text{ in.}$

$I_O = 47 \text{ slug ft}^2$

$\alpha_{max} = .02 \text{ rad/sec}$

Figure J-1 Thruster Sizing - Aft Firing

The symmetrical limit cycle propellant consumption rate is computed from the equation:

$$\dot{w} = \frac{r(I_t)^2}{4\theta I_o I_{sp}} \quad \text{lbm/sec}$$

where  $r$  = thruster moment arm ft

$I_t$  = minimum impulse bit (two thrusters, if providing couples), lbf sec

$\theta$  = deadband (are half-angle) radians

$I_{sp}$  = specific impulse (in limit cycle mode, sec)

$I_o$  = spacecraft moment of inertia, slug ft<sup>2</sup>

Then the total consumption is determined by multiplying the rate by the appropriate time interval, and by the number of axes as applicable.

For the case of the Stage III MAV in roll, the assumed conditions are:

$$r = 1.167 \text{ ft}$$

$$\theta = 10^\circ = .174 \text{ rad.}$$

$$I_o = 1.758 \text{ slug ft}^2$$

$$I_{sp} = 120 \text{ sec}$$

$$I_t = .004 \text{ lbf sec (obtained at low feed pressure)}$$

Substituting these in the above equation yields a consumption rate of  $12.6(10)^{-8}$  lbm/sec [ $5.7(10)^{-8}$  kg/sec], or a total consumption less than .1 kg for the MAV 400 hour orbital life.

For the case of the Stage III MAV in pitch and yaw, the assumed conditions are:

$$r = 1.167 \text{ ft}$$

$$\theta = 1/4^\circ = .00436 \text{ rad.}$$

$$I_o = 1.16 \text{ slug ft}^2$$

$$I_{sp} = 120 \text{ sec}$$

$$I_t = .0005 \text{ lbf sec (throttled thrusters)}$$

Substituting these in the above equation yields a consumption rate of  $12(10)^{-8}$  lbm/sec [ $5.5(10)^{-8}$  kg/sec] for each axis, or a total consumption of approximately .2 kg (both axes) during the MAV 400 hour orbital life.

For the case of the Viking Orbiter attitude propulsion system the assumed conditions are:

$$\begin{aligned}
 r &= 4 \text{ ft} \\
 \theta &= .004 \text{ rad.} \\
 I_{sp} &= 120 \text{ sec.} \\
 I_t &= .0004 \text{ lbf sec.} \\
 I_o &= 2500 \text{ slug ft}^2 \text{ (cruise, roll)} \\
 &= 10,600'' \text{ (cruise, p and y)} \\
 &= 1360'' \text{ (orbiting, roll)} \\
 &= 1560'' \text{ (orbiting, p and y)}
 \end{aligned}$$

Substituting these values in the above equation, four consumption rates are determined. Then the total consumption during the entire mission is determined by accounting for the time interval for each phase of the mission; i. e., 300 days of cruise and 400 days of orbiting. Results of these calculations are tabulated below:

<u>Mode</u>	<u>Consumption Rate (lbm/sec)</u>	<u>Total Consumption (lbm)</u>
Cruise, Roll	$.013(10)^{-6}$	.33
Cruise, p and y	$.0029(10)^{-6}$ (each axis)	.14 (both axes)
Orbit, Roll	$.024(10)^{-6}$	.83
Orbit, p and y	$.021(10)^{-6}$ (each axis)	1.45 (both axes)
		<u>2.75 (1.25 kg)</u>